THE MOLECULAR MECHANISMS OF SYNAPTIC PLASTICITY IMPAIRMENTS IN ALZHEIMER'S DISEASE

EDITED BY: Gong-Ping Liu, Zhifang Dong, Yongjie Zhang, Peng Lei and Shupeng Li

PUBLISHED IN: Frontiers in Cell and Developmental Biology

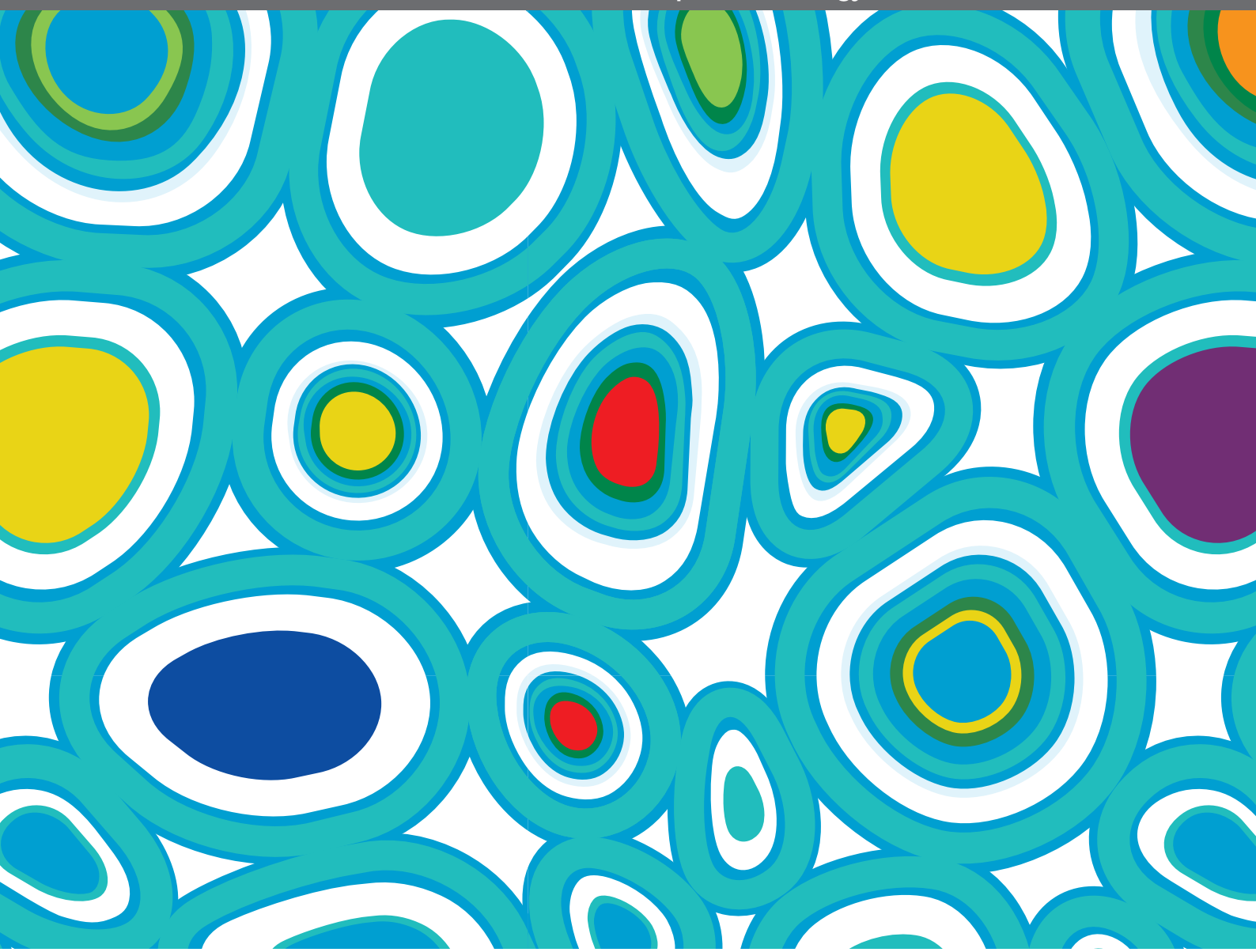

frontiers Research Topics

frontiers

ISSN 1664-8714
ISBN 978-2-88974-484-8
DOI 10.3389/978-2-88974-484-8

About Frontiers

Frontiers is more than just an open-access publisher of scholarly articles: it is a pioneering approach to the world of academia, radically improving the way scholarly research is managed. The grand vision of Frontiers is a world where all people have an equal opportunity to seek, share and generate knowledge. Frontiers provides immediate and permanent online open access to all its publications, but this alone is not enough to realize our grand goals.

Frontiers Journal Series

The Frontiers Journal Series is a multi-tier and interdisciplinary set of open-access, online journals, promising a paradigm shift from the current review, selection and dissemination processes in academic publishing. All Frontiers journals are driven by researchers for researchers; therefore, they constitute a service to the scholarly community. At the same time, the Frontiers Journal Series operates on a revolutionary invention, the tiered publishing system, initially addressing specific communities of scholars, and gradually climbing up to broader public understanding, thus serving the interests of the lay society, too.

Dedication to Quality

Each Frontiers article is a landmark of the highest quality, thanks to genuinely collaborative interactions between authors and review editors, who include some of the world's best academicians. Research must be certified by peers before entering a stream of knowledge that may eventually reach the public - and shape society; therefore, Frontiers only applies the most rigorous and unbiased reviews.
Frontiers revolutionizes research publishing by freely delivering the most outstanding research, evaluated with no bias from both the academic and social point of view. By applying the most advanced information technologies, Frontiers is catapulting scholarly publishing into a new generation.

What are Frontiers Research Topics?

Frontiers Research Topics are very popular trademarks of the Frontiers Journals Series: they are collections of at least ten articles, all centered on a particular subject. With their unique mix of varied contributions from Original Research to Review Articles, Frontiers Research Topics unify the most influential researchers, the latest key findings and historical advances in a hot research area! Find out more on how to host your own Frontiers Research Topic or contribute to one as an author by contacting the Frontiers Editorial Office: frontiersin.org/about/contact

THE MOLECULAR MECHANISMS OF SYNAPTIC PLASTICITY IMPAIRMENTS IN ALZHEIMER'S DISEASE

Topic Editors:
Gong-Ping Liu, Huazhong University of Science and Technology, China
Zhifang Dong, Chongqing Medical University, China
Yongjie Zhang, Mayo Clinic Florida, United States
Peng Lei, Sichuan University, China
Shupeng Li, Peking University, China

Citation: Liu, G.-P., Dong, Z., Zhang, Y., Lei, P., Li, S., eds. (2022). The Molecular Mechanisms of Synaptic Plasticity Impairments in Alzheimer's Disease. Lausanne: Frontiers Media SA. doi: 10.3389/978-2-88974-484-8

Table of Contents

frontiers in Cell and Developmental Biology

EDITORIAL
published: 21 January 2022
doi: 10.3389/fcell.2022.832728

Editorial: The Molecular Mechanisms of Synaptic Plasticity Impairments in Alzheimer's Disease

Gong-Ping Liu[1,2]*, *Peng Lei*[3], *Zhi-Fang Dong*[4] *and Shu-Peng Li*[5]

[1]Key Laboratory of Ministry of Education of China and Hubei Province for Neurological Disorders, Department of Pathophysiology, School of Basic Medicine, The Collaborative Innovation Center for Brain Science, Tongji Medical College, Huazhong University of Science and Technology, Wuhan, China, [2]Co-Innovation Center of Neuroregeneration, Nantong University, Nantong, China, [3]Department of Neurology and State Key Laboratory of Biotherapy, West China Hospital, Sichuan University, Chengdu, China, [4]Ministry of Education Key Laboratory of Child Development and Disorders, Chongqing Key Laboratory of Translational Medical Research in Cognitive Development and Learning and Memory Disorders, National Clinical Research Center for Child Health and Disorders, Children's Hospital of Chongqing Medical University, Chongqing, China, [5]School of Chemical Biology and Biotechnology, Peking University Shenzhen Graduate School, Shenzhen, China

Keywords: Alzheimer's disease, synaptic plasticity, spine, dendritic plasticity, cognition

Editorial on the Research Topic

The Molecular Mechanisms of Synaptic Plasticity Impairments in Alzheimer's Disease

Synaptic plasticity, which is directly related to memory and learning processes, is determined by morphological and functional modifications of synapses. Long-term potentiation and long-term depression are two main manifested forms of synaptic plasticity. Dendritic spines are small, highly dynamic protruding structures in the dendritic membrane, which have specialized subdomains with specific functions in synaptic transmission and plasticity, including scaffolding proteins, ion channels, cytoskeleton components, signal transduction molecules, and postsynaptic density (a complex mainly consisted by AMPAR and NMDAR) (Saneyoshi et al., 2010; González-Burgos, 2012). Structural changes, such as spines elongation and contraction, shape variations, spine distribution/density and functions mediate synaptic plasticity (Chidambaram et al., 2019). Impairments of synaptic plasticity, such as spine shape and density alteration, lead to synaptic dysfunction and cognitive impairment, which is found in many neurodegenerative diseases, including Alzheimer's disease (AD). Aberrant synaptic structure/morphology and decreased spine density in the hippocampus and neocortex is an early event and a major change, correlated with cognitive deficits in AD (Scheff et al., 1990; Scheff and Price, 2003), which usually appear well before neuronal loss. However, questions about the details and mechanisms of synaptic plasticity dysfunction in AD still warrant further studies, as in contrast with the well documented synaptic dysfunction elicited by pathological factors of accumulated phosphorylated tau and amyloid β peptide (Aβ). This topic focused on "*The Molecular Mechanisms of Synaptic Plasticity Impairments in Alzheimer's Disease*," and there were 21 manuscripts to be expected, 13 manuscripts actually submitted and 10 manuscripts accepted.

In this issue of frontiers, Mahaman et al. reviewed the role of STriatal-Enriched protein tyrosine phosphatase (STEP) in dendritic plasticity impairments in AD, whose level and activity are increased in AD *via* Aβ. STEP dephosphorylated and inactivated synaptic proteins *via* kinases such as Fyn, Pyk2 and ERK1/2 (Venkitaramani et al., 2009; Li et al., 2014), and it also led to the internalization of synaptic receptor complexes like GluN2B/GluN1 and GluA2/GluA1 subunits of NMDA and AMPA receptors, respectively (Poddar et al., 2010; Zhang et al., 2010). Furthermore, STEP dephosphorylated SPIN90 to dissociate from cofilin, and activated cofilin to depolymerize F-actin to G-actin. Together, increase of STEP led to synapse loss and dendritic plasticity impairments, and ultimately, resulting in

OPEN ACCESS

Edited and reviewed by:
Ramani Ramchandran, Medical College of Wisconsin, United States

***Correspondence:**
Gong-Ping Liu
liugp111@mail.hust.edu.cn

Specialty section:
This article was submitted to Molecular and Cellular Pathology, a section of the journal Frontiers in Cell and Developmental Biology

Received: *10 December 2021*
Accepted: *06 January 2022*
Published: *21 January 2022*

Citation:
Liu G-P, Lei P, Dong Z-F and Li S-P (2022) Editorial: The Molecular Mechanisms of Synaptic Plasticity Impairments in Alzheimer's Disease. Front. Cell Dev. Biol. 10:832728. doi: 10.3389/fcell.2022.832728

cognitive deficits in AD. Transmembrane protein 59 (TMEM59) reported to associate with AD was introduced by Meng et al. They showed that TMEM59 haploinsufficiency rescued memory defects and synaptic plasticity dysfunction in 5×FAD mice, which overexpressing human APP and PSEN1 transgenes with a total of five AD-linked mutations: the Swedish (K670N/M671L), Florida (I716V), and London (V717I) mutations in APP, as well as M146L and L286V mutations in PSEN1, and rapidly developing severe amyloid pathology and presenting synaptic degeneration. The authors found that overexpression of TMEM59 in the hippocampus caused memory deficits and had a trend to induce synaptic plasticity impairment in wild-type mice, which suggesting its neurotoxic role. Interestingly, while TMEM59 overexpression had no effect on worsening synaptic defects and impaired memory in the 5×FAD mouse model of AD, though it significantly exacerbated AD-like pathologies by increasing levels of detergent-insoluble Aβ and Aβ plaques. They proposed that, due to a mild impact on cognitive and synaptic function impairments, overexpressing TMEM59 may not be able to further worsen the quickly degenerative phenotypes in 5×FAD mice.

As one of the main pathophysiologic markers in AD, hyperphosphorylated tau led to the dissociation of Tau/Fyn/PSD-95/NMDAR complex, the disruption of synaptic potentiation required for LTP (Frandemiche et al., 2014), and the reduction of functional dendritic spine number (Tracy and Gan, 2018). Overexpressing tau decreased NMDAR level by activation of STAT1 and inactivation of STAT3 (Li et al., 2019; Hong et al., 2020). Jiang et al. found that, PINK1 overexpression ameliorated the decreased dendritic spine density *via* autophagy activation to decrease total and phosphorylated tau. In addition to abnormal aggregated tau or Aβ, multiple other risk factors, such as aging, oxidative stress, calcium signal dysregulation, neuroinflammation, genetic and environmental factors, could induce synaptic plasticity defects. In this issue of frontier, a study demonstrated that maternal lead (Pb) exposure induced synaptic plasticity impairment of offspring by reducing GLUT4 protein level in the cell membrane as well as glucose uptake via the PI3K-Akt signaling pathway.

Mitochondrial dysfunction is a well-established early etiological event in AD, which decreases ATP production, changes cytoplasmic calcium concentrations, and increases ROS/NO production, consequently leading to synaptic plasticity abnormalities. Huang et al. and Chen et al., respectively, found that, tetramethylpyrazine or dauricine, the extract from the rootstock of traditional Chinese medicine, modified the mitochondrial protein profile of AD animal models to increase ATP production and some synapse-related protein expression, and ultimately, improved synaptic plasticity and cognition.

Most of the accepted articles in this research topic contributed to expand and deepen our understanding of the risk factors and its mechanisms for synaptic plasticity damage in AD, and we understand that gestational Pb exposure could induce synaptic plasticity impairment of offspring, and etramethylpyrazine and dauricine ameliorate synaptic plasticity, which both are not reported previously. However, some questions, which we have a lot of interest in, are missing in this topic. For example, is LTP impairment caused by directly reduced synapse numbers or decreased synaptic transmission efficiency? What are the inherent molecular mechanisms underlying the aberrant spine number loss (synaptic-associated protein loss, microglia-mediated synapse elimination, neuroinflammation, neuron apoptosis or death)? We hope that the articles in this topic will be of interest to a broad range of researchers working in dendritic plasticity in AD, stimulating experimental work relating to the mechanisms of synaptic plasticity impairments and therapeutic strategies. In a future topic collection, we would like to see more articles about new molecular strategies directly targeting to promote synaptic plasticity.

AUTHOR CONTRIBUTIONS

G-PL wrote a draft of the Editorial that was revised by the other authors.

ACKNOWLEDGMENTS

We hereby thank a lot all the authors that participated in this Research Topic.

REFERENCES

Chidambaram, S. B., Rathipriya, A. G., Bolla, S. R., Bhat, A., Ray, B., Mahalakshmi, A. M., et al. (2019). Dendritic Spines: Revisiting the Physiological Role. *Prog. Neuro-Psychopharmacology Biol. Psychiatry* 92, 161–193. doi:10.1016/j.pnpbp.2019.01.005

Frandemiche, M. L., De Seranno, S., Rush, T., Borel, E., Elie, A., Arnal, I., et al. (2014). Activity-dependent Tau Protein Translocation to Excitatory Synapse Is Disrupted by Exposure to Amyloid-Beta Oligomers. *J. Neurosci.* 34, 6084–6097. doi:10.1523/JNEUROSCI.4261-13.2014

González-Burgos, I. (2012). From Synaptic Transmission to Cognition: an Intermediary Role for Dendritic Spines. *Brain Cogn.* 80, 177–183. doi:10.1016/j.bandc.2012.03.002

Hong, X.-Y., Wan, H.-L., Li, T., Zhang, B.-G., Li, X.-G., Wang, X., et al. (2020). STAT3 Ameliorates Cognitive Deficits by Positively Regulating the Expression of NMDARs in a Mouse Model of FTDP-17. *Sig Transduct Target. Ther.* 5 (1), 295. doi:10.1038/s41392-020-00290-9

Li, R., Xie, D.-D., Dong, J.-h., Li, H., Li, K.-s., Su, J., et al. (2014). Molecular Mechanism of ERK Dephosphorylation by Striatal-Enriched Protein Tyrosine Phosphatase. *J. Neurochem.* 128, 315–329. doi:10.1111/jnc.12463

Li, X. G., Hong, X. Y., Wang, Y. l., Zhang, S. J., Zhang, J. F., Li, X. C., et al. (2019). Tau Accumulation Triggers STAT 1-dependent Memory Deficits by Suppressing NMDA Receptor Expression. *EMBO Rep.* 20 (6), e47202. doi:10.15252/embr.201847202

Poddar, R., Deb, I., Mukherjee, S., and Paul, S. (2010). NR2B-NMDA Receptor Mediated Modulation of the Tyrosine Phosphatase STEP Regulates Glutamate Induced Neuronal Cell Death. *J. Neurochem.* 115, 1350–1362. doi:10.1111/j.1471-4159.2010.07035.x

Saneyoshi, T., Fortin, D. A., and Soderling, T. R. (2010). Regulation of Spine and Synapse Formation by Activity-dependent Intracellular Signaling Pathways. *Curr. Opin. Neurobiol.* 20, 108–115. doi:10.1016/j.conb.2009.09.013

Scheff, S., and Price, D. A. (2003). Synaptic Pathology in Alzheimer's Disease: a Review of Ultrastructural Studies. *Neurobiol. Aging* 24, 1029–1046. doi:10.1016/j.neurobiolaging.2003.08.002

Scheff, S. W., DeKosky, S. T., and Price, D. A. (1990). Quantitative Assessment of Cortical Synaptic Density in Alzheimer's Disease. *Neurobiol. Aging* 11, 29–37. doi:10.1016/0197-4580(90)90059-9

Tracy, T. E., and Gan, L. (2018). Tau-mediated Synaptic and Neuronal Dysfunction in Neurodegenerative Disease. *Curr. Opin. Neurobiol.* 51, 134–138. doi:10.1016/j.conb.2018.04.027

Venkitaramani, D. V., Paul, S., Zhang, Y., Kurup, P., Ding, L., Tressler, L., et al. (2009). Knockout of Striatal Enriched Protein Tyrosine Phosphatase in Mice Results in Increased ERK1/2 Phosphorylation. *Synapse* 63, 69–81. doi:10.1002/syn.20608

Zhang, Y., Kurup, P., Xu, J., Carty, N., Fernandez, S. M., Nygaard, H. B., et al. (2010). Genetic Reduction of Striatal-Enriched Tyrosine Phosphatase (STEP) Reverses Cognitive and Cellular Deficits in an Alzheimer's Disease Mouse Model. *Proc. Natl. Acad. Sci.* 107, 19014–19019. doi:10.1073/pnas.1013543107

Conflict of Interest: The authors declare that the research was conducted in the absence of any commercial or financial relationships that could be construed as a potential conflict of interest.

Publisher's Note: All claims expressed in this article are solely those of the authors and do not necessarily represent those of their affiliated organizations, or those of the publisher, the editors and the reviewers. Any product that may be evaluated in this article, or claim that may be made by its manufacturer, is not guaranteed or endorsed by the publisher.

frontiers in Cell and Developmental Biology

ORIGINAL RESEARCH
published: 28 October 2020
doi: 10.3389/fcell.2020.596030

TMEM59 Haploinsufficiency Ameliorates the Pathology and Cognitive Impairment in the 5xFAD Mouse Model of Alzheimer's Disease

Jian Meng[1†], Linkun Han[1†], Naizhen Zheng[1†], Hui Xu[1], Zhaoji Liu[1,2], Xian Zhang[1], Hong Luo[1], Dan Can[1], Hao Sun[1], Huaxi Xu[1] and Yun-wu Zhang[1,3]*

[1] Fujian Provincial Key Laboratory of Neurodegenerative Disease and Aging Research, Institute of Neuroscience, School of Medicine, Xiamen University, Xiamen, China, [2] Department of Neurology, Zhongshan Hospital Xiamen University, Xiamen, China, [3] Department of Neurology, The First Affiliated Hospital of Xiamen University, Xiamen, China

Alzheimer's disease (AD) is a progressive neurodegenerative disease associated with cognitive deficits and synaptic impairments. Amyloid-β (Aβ) plaque deposition, dystrophic neurite accumulation and neurofibrillary tangles are pathological hallmarks of AD. TMEM59 has been implicated to play a role in AD pathogenesis; however, the underlying mechanism remains unknown. Herein, we found that overexpression of TMEM59 in the hippocampal region led to memory impairment in wild type mice, suggesting its neurotoxic role. Interestingly, while TMEM59 overexpression had no effect on worsening synaptic defects and impaired memory in the 5xFAD mouse model of AD, it significantly exacerbated AD-like pathologies by increasing levels of detergent-insoluble Aβ and Aβ plaques, as well as dystrophic neurites. Importantly, haploinsufficiency of TMEM59 reduced insoluble Aβ levels, Aβ plaques, and neurite dystrophy, thereby rescuing synaptic plasticity and memory deficits in 5xFAD mice. Moreover, the level of TMEM59 in the brain of 5xFAD mice increased compared to wild type mice during aging, further corroborating its detrimental functions during neurodegeneration. Together, these results demonstrate a novel function of TMEM59 in AD pathogenesis and provide a potential therapeutic strategy by downregulating TMEM59.

Keywords: Alzheimer's disease, amyloid-β, cognitive deficits, neurite dystrophy, synaptic plasticity, TMEM59

OPEN ACCESS

Edited by:
Peng Lei,
Sichuan University, China

Reviewed by:
Robert Vassar,
Northwestern University, United States
James Duce,
University of Cambridge, United Kingdom

***Correspondence:**
Yun-wu Zhang
yunzhang@xmu.edu.cn

† These authors have contributed equally to this work and share first authorship

Specialty section:
This article was submitted to Molecular Medicine, a section of the journal Frontiers in Cell and Developmental Biology

Received: *18 August 2020*
Accepted: *05 October 2020*
Published: *28 October 2020*

Citation:
Meng J, Han L, Zheng N, Xu H, Liu Z, Zhang X, Luo H, Can D, Sun H, Xu H and Zhang Y (2020) TMEM59 Haploinsufficiency Ameliorates the Pathology and Cognitive Impairment in the 5xFAD Mouse Model of Alzheimer's Disease. Front. Cell Dev. Biol. 8:596030. doi: 10.3389/fcell.2020.596030

INTRODUCTION

Alzheimer's disease (AD) is the most common age-related neurodegenerative disorder characterized by abnormal accumulation and deposition of various amyloid-β (Aβ) peptides derived from amyloid-β precursor protein (APP), formation of neurofibrillary tangles containing hyperphosphorylated tau, synaptic dysfunction, neuroinflammation, neuronal death, and cognitive decline (Crews and Masliah, 2010; Huang and Mucke, 2012; Guerreiro and Bras, 2015; Kocahan and Dogan, 2017; DeTure and Dickson, 2019). So far no effective therapies are available to cure this devastating disease (Yu et al., 2019). Since social and financial burdens for AD have become enormous as our population ages, there is an urgent need to elucidate the detailed molecular mechanisms underlying AD pathogenesis, so that new targets may be identified for therapeutic development.

Transmembrane protein 59 (TMEM59) (also known as dendritic cell-derived factor 1, DCF1) is a type I transmembrane glycoprotein ubiquitously expressed in various tissues.

One study found that TMEM59 overexpression in cells induced APP retention in the Golgi, thereby inhibiting APP cleavage by α- and β-secretases at the plasma membrane and in the endosomes, respectively, resulting in reduced Aβ production (Ullrich et al., 2010). In addition, the *TMEM59* gene promoter region was found to be hypomethylated in postmortem frontal cortex of late-onset AD patients compared to controls; and methylation at this site was functionally associated with *TMEM59* mRNA and protein levels (Bakulski et al., 2012). Microarray data analysis also revealed that *TMEM59* gene expression was higher in AD patients than in controls (Guttula et al., 2012). Very recently another study reported that overexpression of TMEM59 reduced the cleavage of APP C99 fragment by γ-secretase and promoted learning and memory in drosophila expressing APP C99 (Li et al., 2020). All these studies suggest that TMEM59 is associated with AD. However, the exact role of TMEM59 in AD has yet to be fully determined.

In the current study, we explored the effects of TMEM59 on AD-associated phenotypes in mice and found that TMEM59 overexpression impaired memory in wild type (WT) mice and exacerbated Aβ and neurite pathologies in the 5xFAD mouse model of AD (Oakley et al., 2006). Importantly, TMEM59 haploinsufficiency rescued memory and synaptic plasticity deficits and reduced Aβ and neurite pathologies in 5xFAD mice. Moreover, we observed that TMEM59 expression was increased in the brain of 5xFAD mice.

MATERIALS AND METHODS

Animals

Tmem59 conditional knockout (*Tmem59*^{floxflox}) mice were generated using a traditional homozygous recombination strategy with service provided by Cyagen Biosciences. Briefly, a homology region covering mouse *Tmem59* exon3 to exon6 was subcloned into the targeting vector. One Loxp site was introduced into *Tmem59* intron3, and another Loxp site together with a modified Rox-flanked Neo cassette was introduced into *Tmem59* intron5 (**Supplementary Figure 1A**). After linearization, the targeting vector was transfected into C57BL/6 background mouse embryonic stem cells. After G418 selection and confirmation of successful homologous recombination of the targeting vector, positive clones were injected into mouse blastocysts, which were then implanted into pseudo-pregnant females. Born chimeric mice (F0) were crossed with C57BL/6 mice to generate F1 mice carrying the recombined allele. The Neo cassette flanked by modified Rox sites was self-deleted during mouse production, with a confidential design by Cyagen Biosciences. *Tmem59*$^{+/-}$ mice were generated by crossing *Tmem59*$^{flox/flox}$ mice with Zp3-Cre mice (kindly provided by Haibin Wang) (Cheng et al., 2018).

The PCR primers used for genotyping were as follows:

Tmem59$^{flox/flox}$, forward-5′-GAGTAGATGATGCTGACATAGAC-3′,
reverse-5′-CCTCTAAGGAGCTTTCTAAGTG-3′;
Zp3-Cre, forward-5′-CAGATGAGGTTTGAGGCCACAG-3′,
reverse-5′-TTCTTGCGAACCTCATCACTC-3′;
Tmem59$^{+/-}$, WT-forward-5′-GAGTAGATGATGCTGACATAGAC-3′,
KO-forward-5′-GTAAGAAACTAGAACTGGGCTTGAGC-3′,
reverse-5′-CCTCTAAGGAGCTTTCTAAGTG-3′.

5xFAD mice (Oakley et al., 2006) were crossed with *Tmem59*$^{+/-}$ mice to generate 5xFAD; *Tmem59*$^{+/-}$ mice. All mice were maintained and bred at Xiamen University Laboratory Animal Center. Mouse experimental procedures were performed in accordance with the National Institutes of Health Guide for the Care and Use of Laboratory Animals and approved by the Animal Ethics Committee of Xiamen University.

Stereotactic Injection of Lentivirus

For TMEM59 overexpression in the hippocampus, WT and 5xFAD mice at 2 months of age were anesthetized, placed on a stereotaxic frame, and injected bilaterally with Lentivirus-EGFP control or Lentivirus-TMEM59-Flag (1×10^9 v.g./mL, OBiO Technology) into the hippocampal region at the following coordinates: anterior posterior, −2.0 mm; medial lateral, ±1.5 mm; and dorsal ventral, −2.0 mm using an automated stereotaxic injection apparatus (RWD Life Science). Two μL lentivirus was delivered at 0.20 μL/min to each lateral. After each injection, the syringe was left for 10 min and then withdrawn slowly.

Behavioral Tests

Mice at 6–7 months of age were subjected to behavioral tests including open field, *Y* maze and Morris water maze. Habituation was done in the testing room for more than 30 min at the beginning of each test day. All tests were carried out by researchers blinded to mouse genotype. Data were recorded and analyzed using Smart 3.0 video tracking system (Panlab, Harvard Apparatus).

For open field test (Tatem et al., 2014), each test mouse was placed in the center of the square box [40 cm (L) × 40 cm (W) × 40 cm (H)] and allowed to explore freely for 10 min. Time spent in the center and total distance of movement were measured.

For *Y* maze test (Miedel et al., 2017; Lachance et al., 2019), each test mouse was placed in the center of a "*Y*" shaped chamber [30 cm (L) × 6 cm (W) × 15 cm (H)] and allowed to enter into each arm freely for 5 min. The sequence of arm entries and total numbers of arms entered by each mouse was recorded. The percentage of alternation was calculated as the ratio of consecutive specific arm entries to the total arm entries.

The Morris water maze test (Vorhees and Williams, 2006; Bromley-Brits et al., 2011) was performed in a large circular pool (120 cm in diameter) filled with opaque water, in which a platform was hidden 1 cm below the water surface. Mice were subjected to two training trials per day for six consecutive days; and they were placed into the water facing the sidewalls of the pool from different start positions across trials. The time spent to reach and climb onto the platform (escape latency) was recorded. If a mouse failed to find the platform within 60 s, it was guided

to the platform and allowed to stay on the platform for 10 s. On day 7, the platform was removed and a probe test for the mice was performed for 60 s. The time spent in each quadrant and the numbers of platform region crossings were recorded.

Electrophysiology

LTP was recorded as previously described (Penn et al., 2017). Briefly, mice were anesthetized with isoflurane. After decapitation, the brain was rapidly transferred into an ice-cold solution (64 mM NaCl, 2.5 mM KCl, 10 mM glucose, 1.25 mM NaH_2PO_4, 10 mM $MgSO_4$, 26 mM $NaHCO_3$, 120 mM sucrose, and 0.5 mM $CaCl_2$). The acute hippocampal slices (400 μm thick) were cut using a vibratome (VT1200S, Leica). Slices were allowed to recover for 1 h at 32°C and incubated for at least 1h at room temperature before recording in artificial cerebrospinal fluid (aCSF: 126 mM NaCl, 3.5 mM KCl, 1.25 mM NaH_2PO_4, 1.3 mM $MgSO_4$, 2.5 mM $CaCl_2$, 26 mM $NaHCO_3$, and 10 mM glucose). All solutions were saturated with 95%O_2/5%CO_2 (volume/volume). fEPSPs were induced in the Schaffer collateral pathway with a two-concentrical bipolar stimulating electrode (FHC, Inc.). LTP was induced by two trains of stimuli at 100 Hz for 1 s with 30 s interval. fEPSP response was recorded for 1 h after tetanic stimulation. Data were acquired with Clampex 10.6 (Molecular Devices) and analyzed using Clampfit 10.6 software (Molecular Devices).

Western Blotting

Mouse hippocampal and cortical tissues were homogenized and lysed in RIPA lysis buffer (25 mM Tris–HCl [pH 7.6], 150 mM NaCl, 0.1% SDS, 1% sodium deoxycholate, and 1% Non-idet P-40) supplemented with the Complete Protease and Phosphatase Inhibitor Cocktail (Roche). Protein concentrations were determined by a BCA Protein Assay Kit (Thermo Fisher Scientific) following the manufacturer's instruction. 25 micrograms of total protein lysates were resolved using SDS-polyacrylamide gel electrophoresis and transferred to PVDF membranes. After blocking in 5% milk in 0.1% PBS/Tween-20, membranes were immunoblotted with indicated primary antibodies overnight at 4°C, and then incubated with appropriate horseradish peroxidase (HRP)-conjugated secondary antibodies for 1 h at room temperature. The antibodies used were: anti-TMEM59 (ABclonal, WG-03224D, 1:4000), anti-APP (22C11, Millipore, MAB348, 1:1000), anti-APP Carboxyl-terminus (369, 1:1000) (Xu et al., 1998), anti-Flag (Proteintech, 20543-1-AP, 1:1000), anti-α-tubulin (Millipore, MABT205, 1:5000), anti-β-actin (Cell Signaling Technology, 8457S, 1:2000), and HRP-conjugated secondary antibodies (Thermo Fisher Scientific, 31460 or 31430, 1:5000). Protein band intensity was quantified using the ImageJ software (National Institutes of Health).

Immunostaining

Mice were anesthetized and intracardially perfused with ice-cold PBS and 4% paraformaldehyde. Brains were harvested and post-fixed for 2–4 h at 4°C. Brains were washed in PBS and cryoprotected in 30% sucrose in PBS. Coronal sections (15 μm thick) were collected with a freezing microtome (Leica). The sections were washed in PBS and then blocked in blocking buffer (5% BSA and 0.2% Triton X-100) for 1 h at room temperature, and then subsequently incubated with primary antibodies against human Aβ (6E10, BioLegend, 803014, 1:400) and LAMP1 (Abcam, ab24170, 1:200) overnight at 4°C, and appropriate fluorescence-conjugated secondary antibodies (Thermo Fisher Scientific, A-11008, A-11005 or A-31577, 1:500) for 1 h at room temperature in the dark. Confocal images were acquired using the A1R (Nikon) or FV1000MPE-B (Olympus) confocal microscope. All images were processed with ImageJ to calculate the area of Aβ plaques and dystrophic neurites.

Aβ ELISA Assays

Hippocampal tissues of treated 5xFAD mice were sequentially extracted with Tris-buffered saline (TBS), TBS containing 1% Triton X-100 (TBSX), and guanidine-HCl (GuHCl) supplemented with the Complete Protease Inhibitor Cocktail (Roche) as described previously (Youmans et al., 2011). Aβ40 and Aβ42 levels were measured using Human Aβ40 and Aβ42 ELISA Kits (Thermo Fisher Scientific, KHB3481 for Aβ40 and KHB3441 for Aβ42), following the manufacturer's instructions.

Oxygen Consumption Rate Measurement

Oxygen Consumption Rate (OCR) was studied using the Seahorse XF Cell Mito Stress Test Kit (Agilent, Santa Clara, CA, United States), with measurement on the Seahorse XFe 96 Extracellular Flux Analyzer (Agilent). Briefly, primary neurons from mice at embryonic day 16.5 (E16.5) were isolated and cultured for 7–10 days. 8–10 × 10^4 neurons per well were plated on a Seahorse XF 96 cell culture microplate. After baseline detection, 1 μM oligomycin, 1.5 μM FCCP, and 1 μM rotenone-antimycin A were injected sequentially into the assay micro-chambers. Data were analyzed using the Seahorse Wave 2.2.0 software package (Agilent).

Statistical Analysis

Statistical analysis was performed using GraphPad Prism 8 software. Data in figures were presented as mean ± SEM. Comparison of the mean values for multiple groups was performed using a one-way ANOVA or two-way ANOVA. Comparison of two groups was performed using unpaired *t*-test or Mann Whitney test. Exact sample sizes and statistical test used for each comparison were provided in corresponding figure legend. $p < 0.05$ was considered to be statistically significant.

RESULTS

TMEM59 Overexpression Causes Memory Deficits in Mice

To ascertain whether TMEM59 dysregulation influences AD pathology, we delivered lentivirus expressing either TMEM59 (Lenti-TMEM59, tagged with Flag) or EGFP as a control (Lenti-Control) into the mouse hippocampus bilaterally at 2 months of age (**Figure 1A**). Exogenous TMEM59 expression was confirmed in these mice at about 8 months of age,

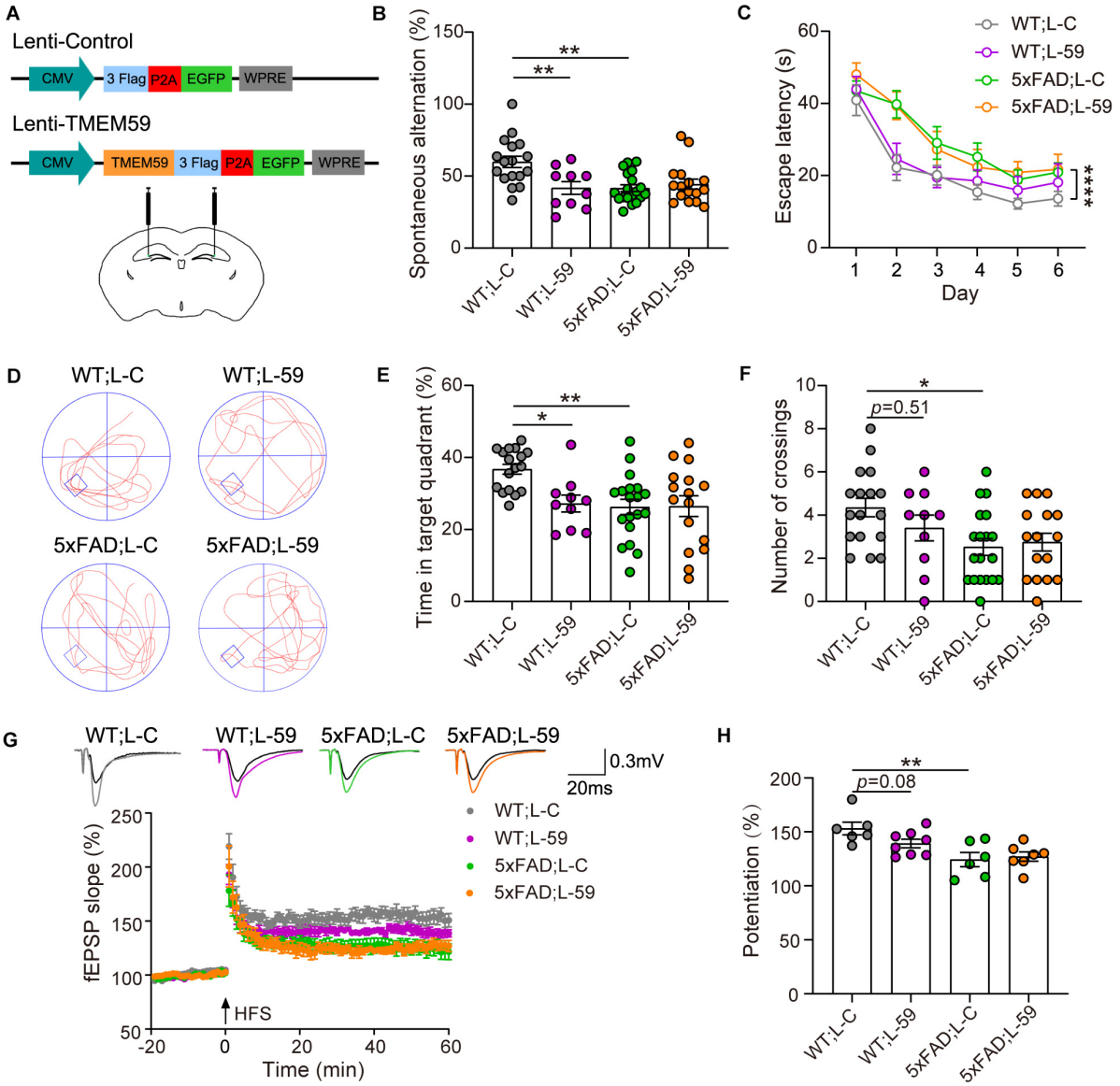

FIGURE 1 | Overexpression of TMEM59 causes memory deficits in mice. **(A)** The schematic diagram of lentivirus constructs expressing TMEM59 (Lenti-TMEM59, L-59) or control (Lenti-Control, L-C) (upper panels), and their stereotactic injection into the hippocampal region (lower panel). **(B)** In Y maze tests, spontaneous alternation percentage of WT; L–C (n = 17), WT; L-59 (n = 10), 5xFAD; L-C (n = 19), and 5xFAD; L-59 (n = 16) mice were calculated for comparison. One-way ANOVA followed by Tukey's *post hoc* test. **(C–F)** In Morris water maze tests, escape latencies during a 6-day training were recorded **(C)**. Representative swimming paths **(D)**, time spent in the target quadrant **(E)** and numbers of platform region crossings **(F)** during the probe test were also recorded. Comparisons were carried out for WT; L-C (n = 17), WT; L-59 (n = 10), 5xFAD; L-C (n = 19), and 5xFAD; L-59 (n = 16) mice. Two-way ANOVA followed by Tukey's *post hoc* test for comparisons in **(C)**, and one-way ANOVA followed by Tukey's *post hoc* test for comparisons in **(E,F)**. **(G)** Time course of fEPSP slopes in the hippocampal CA1 region in acute slices from WT; L-C, WT; L-59, 5xFAD; L-C, and 5xFAD; L-59 mice were recorded. **(H)** Quantifications and comparisons of average synaptic potentiation from the last 10 min shown in **(G)**. n = 6 slices for WT; L-C, n = 8 slices for WT; L-59, n = 6 slices for 5xFAD; L-C, and n = 7 slices for 5xFAD; L-59 from 4 to 5 mice per group, Mann Whitney test. Data represent mean ± SEM. $^{*}p < 0.05$, $^{**}p < 0.01$, $^{****}p < 0.0001$.

and had no significant effect on endogenous TMEM59 levels (**Supplementary Figures 2A,B**). At 6–7 months of age, we found that overexpression of TMEM59 in WT and 5xFAD mice did not affect their total moving distance and time spent in the center during open field tests, suggesting that TMEM59 overexpression has no effect on mouse locomotor activity and anxiety (**Supplementary Figures 2G,H**). It has been reported that 5xFAD mice display reduced anxiety only at 9–12 months of age in open field tests (Jawhar et al., 2012). Here our results also confirmed that 5xFAD mice had no anxiety change at 6–7 months of age.

As expected, 6–7 month-old 5xFAD mice showed short-term working memory deficits compared to WT mice in *Y* maze tests (**Figure 1B**). Interestingly, overexpression of TMEM59 impaired

short-term working memory in WT mice without further deteriorating the deficits in 5xFAD mice (**Figure 1B**). In Morris water maze tests, 5xFAD mice showed impaired spatial learning and memory with decreased escape latency during the training and reduced time spent in the target quadrant and numbers of platform region crossings during the probe test compared to WT controls (**Figures 1C–F**). While TMEM59 overexpression had no effect on altering these behaviors in 5xFAD mice, its overexpression in WT mice significantly reduced time spent in the target quadrant during the probe test (**Figure 1E**).

We next recorded LTP to test the effect of TMEM59 overexpression on synaptic plasticity (**Figure 1G**). We found that LTP was impaired in 5xFAD mice compared to WT controls. Moreover, TMEM59 overexpression moderately reduced LTP in WT mice without further compromising LTP deficits in 5xFAD mice (**Figure 1H**). Together, these results suggest that overexpression of TMEM59 leads to memory and synaptic plasticity impairments.

TMEM59 Overexpression Exacerbates Aβ Deposition and Neurite Dystrophy in 5xFAD Mice

We also studied the impact of TMEM59 overexpression on Aβ plaque formation in 5xFAD mice. Immunofluorescence staining revealed that total Aβ plaque areas were dramatically increased in TMEM59-overexpressing 5xFAD mice compared to controls (**Figures 2A,B**). Total LAMP1-positive areas indicative of dystrophic neurites, as well as LAMP1-positive areas around each Aβ plaque were also markedly increased upon TMEM59 overexpression (**Figures 2A,C,D**). To further determine the effect of TMEM59 overexpression on Aβ, we carried out ELISA to measure Aβ levels in TBS-soluble, TBSX-soluble, and GuHCl-soluble extractions from mouse hippocampus, of which the formal two represent soluble or newly generated Aβ and the latter one represents detergent-insoluble deposited Aβ (Youmans et al., 2011). TMEM59 overexpression had no effect on Aβ40 and Aβ42 levels in TBS- and TBSX-soluble extractions (**Figures 2E,F**). However, Aβ40 and Aβ42 levels in the GuHCl-soluble fractions were significantly higher in TMEM59-overexpressing 5xFAD mice than in controls (**Figure 2G**). These findings reveal that TMEM59 upregulation exacerbates Aβ plaque deposition and neurite dystrophy in AD. One previous study showed that TMEM59 overexpression reduced APP glycosylation and Aβ generation (Ullrich et al., 2010). However, here we found that TMEM59 overexpression in the mouse hippocampus had no effect on levels of total APP, glycosylated APP, and APP processed α- and β-carboxyl-terminal fragment (CTF) (**Supplementary Figures 2A,C–F**).

TMEM59 Haploinsufficiency Reverses Memory and Synaptic Plasticity Deficits in 5xFAD Mice

To further evaluate the involvement of TMEM59 in AD, we first generated *Tmem59* conditional knockout (*Tmem59*$^{flox/flox}$)

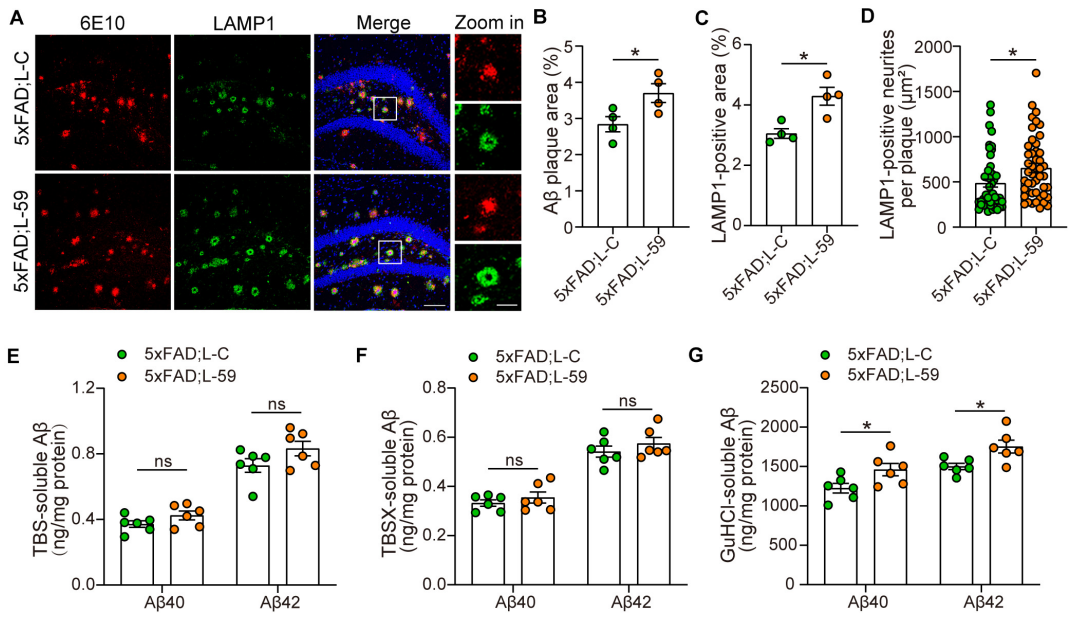

FIGURE 2 | Overexpression of TMEM59 exacerbates Aβ plaque deposition and neurite dystrophy in 5xFAD mice. **(A)** Z-stack confocal images of Aβ plaques (in red) and dystrophic neurites (indicated by LAMP1, in green) in the coronal sections from 6 to 7 month-old 5xFAD; L-C and 5xFAD; L-59 mice. Original magnifications are 20×, scale bar, 100 μm. Zoom-in images are on the right, scale bar, 30 μm. **(B,C)** Quantifications and comparisons of the total area of Aβ plaques **(B)** and LAMP1-positive dystrophic neurites **(C)** shown in **(A)**. $n = 4$ mice per group. **(D)** Quantifications and comparisons of the area of Aβ-associated LAMP1-positive dystrophic neurites per plaque shown in **(A)**. 48 plaques from four 5xFAD; L-C mice and 47 plaques from four 5xFAD; L-59 mice were studied for analysis. **(E–G)** The levels of Aβ40 and Aβ42 in the hippocampus of TBS-extractions **(E)**, TBSX-extractions **(F)**, and GuHCl-extractions **(G)** from 8 month-old 5xFAD; L-C and 5xFAD; L-59 mice were measured by ELISA and compared. $n = 6$ mice per group. Data represent mean ± SEM. $^*p < 0.05$, ns: not significant. Unpaired *t*-test.

mice. By crossing them with Zp3-Cre mice, we obtained *Tmem59* knockout (*Tmem59*$^{-/-}$) mice (**Supplementary Figures 1A–C**). Crossing heterozygous *Tmem59* knockout (*Tmem59*$^{+/-}$) mice with 5xFAD mice resulted in the generation of WT, *Tmem59*$^{+/-}$ (59$^{+/-}$), 5xFAD, and 5xFAD; *Tmem59*$^{+/-}$ (5xFAD; 59$^{+/-}$) mice (**Figure 3A**). As expected, 6–7 month-old 59$^{+/-}$ and 5xFAD; 59$^{+/-}$ mice showed reduced TMEM59 protein levels in the hippocampus compared to respective controls (**Supplementary Figures 3A–B**). The time spent in the center and total moving distance in open field tests of 59$^{+/-}$ and 5xFAD; 59$^{+/-}$ mice were comparable to respective controls (**Supplementary Figures 3G,H**), suggesting that TMEM59 haploinsufficiency did not affect mouse locomotor activity and anxiety at this age. However, TMEM59 haploinsufficiency had a moderate effect on rescuing short-term working memory deficits in 5xFAD mice in *Y* maze tests (**Figure 3B**). In Morris water maze tests, TMEM59 haploinsufficiency in 5xFAD mice significantly increased their time spent in the target quadrant and numbers

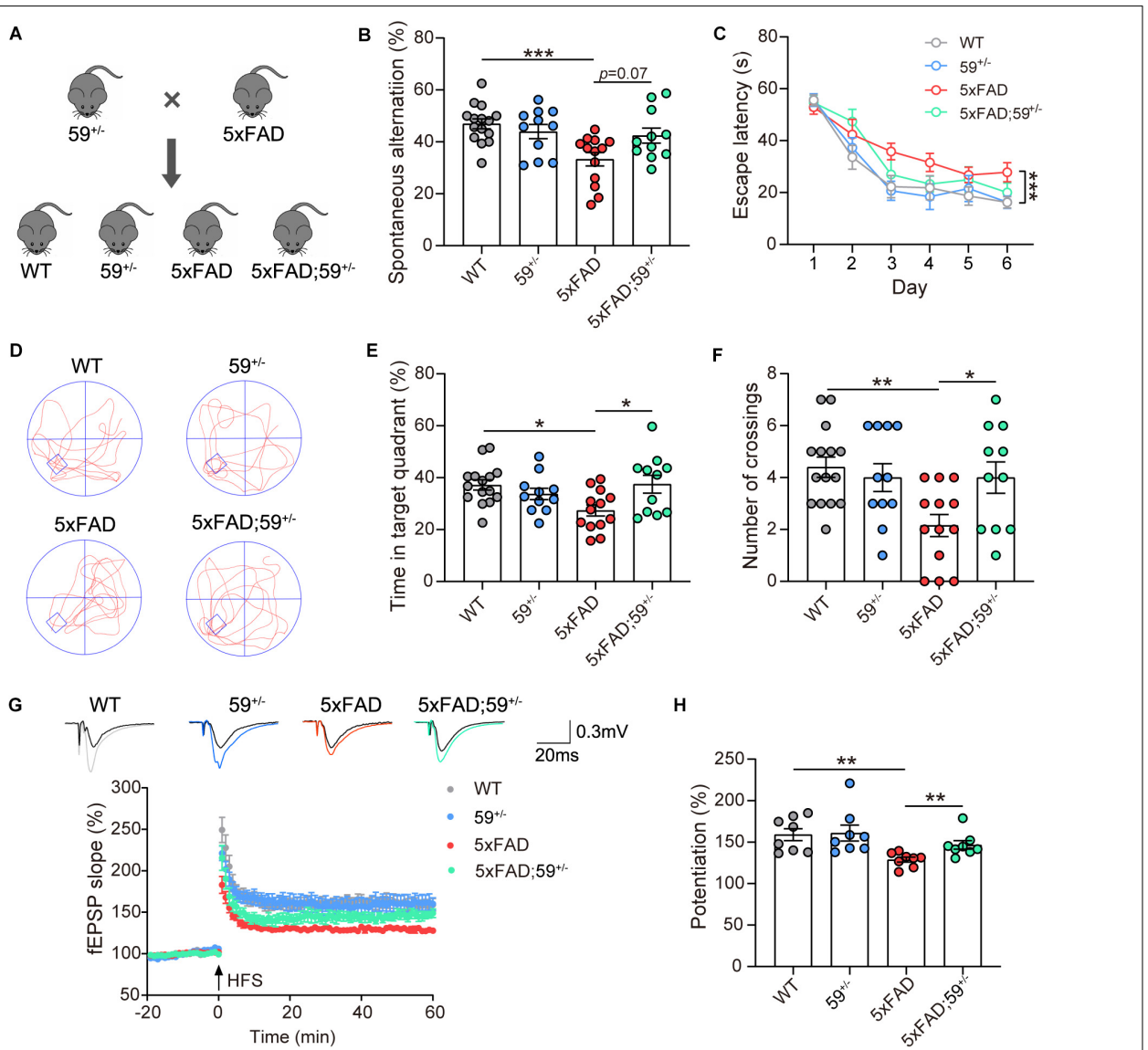

FIGURE 3 | TMEM59 haploinsufficiency attenuates memory and synaptic plasticity deficits in 5xFAD mice. **(A)** Schematic diagram for generating 5xFAD mice with TMEM59 haploinsufficiency. **(B)** In Y maze tests, spontaneous alternation percentage of WT (n = 15), 59$^{+/-}$ (n = 11), 5xFAD (n = 13), and 5xFAD; 59$^{+/-}$ (n = 11) mice were calculated for comparison. One-way ANOVA followed by Tukey's *post hoc* test. **(C–F)** In Morris water maze tests, escape latencies during a 6-day training were recorded **(C)**. Representative swimming paths **(D)**, time spent in the target quadrant **(E)** and numbers of platform region crossings **(F)** during the probe test were also recorded. Comparisons were carried out for WT (n = 15), 59$^{+/-}$ (n = 11), 5xFAD (n = 13), and 5xFAD; 59$^{+/-}$ (n = 11) mice. Two-way ANOVA followed by Tukey's *post hoc* test for comparisons in **(C)**, and one-way ANOVA followed by Tukey's *post hoc* test for comparisons in **(E,F)**. **(G)** Time course of fEPSP slopes in the hippocampal CA1 region in acute slices from WT, 59$^{+/-}$, 5xFAD, and 5xFAD; 59$^{+/-}$ mice were recorded. **(H)** Quantifications and comparisons of average synaptic potentiation from the last 10 min shown in **(G)**. n = 8 slices from 4 to 5 mice per group, Mann Whitney test. Data represent mean ± SEM. *p < 0.05, **p < 0.01, ***p < 0.001.

of platform crossings during the probe test (**Figures 3C–F**). Moreover, TMEM59 haploinsufficiency rescued impaired LTP in 5xFAD mice (**Figures 3G,H**). Together, these results suggest that TMEM59 haploinsufficiency can ameliorate memory and synaptic plasticity deficits in 5xFAD mice.

TMEM59 Haploinsufficiency Reduces Aβ Plaque Deposition and Neurite Dystrophy in 5xFAD Mice

We next studied the impact of TMEM59 haploinsufficiency on Aβ plaques in 5xFAD mice and found that Aβ plaque areas were reduced in 5xFAD; $59^{+/-}$ mice compared to 5xFAD mice (**Figures 4A,B**). Total dystrophic neurites and dystrophic neurites surrounding individual Aβ plaque, indicated by LAMP1-positive staining, were also decreased in 5xFAD; $59^{+/-}$ mice compared to controls (**Figures 4A,C,D**). We further measured Aβ levels by ELISA in sequential hippocampal extractions. Although not altered in TBS- and TBSX-soluble fractions, Aβ40 and Aβ42 levels were significantly decreased in GuHCl-soluble extractions in 5xFAD; $59^{+/-}$ mice compared to controls (**Figures 4E–G**). These results suggest that TMEM59 haploinsufficiency reduces Aβ plaque deposition and dystrophic neurite accumulation in 5xFAD mice. We also explored APP glycosylation and processing in mice with TMEM59 haploinsufficiency. The results showed that glycosylated APP levels were slightly increased in 5xFAD; $59^{+/-}$ mice compared to controls, whereas total APP and APP α-/β-CTF levels were not altered with TMEM59 haploinsufficiency (**Supplementary Figures 3A,C–F**).

TMEM59 Protein Levels Are Elevated in the Brain of 5xFAD Mice During Aging

Some previous studies reported that TMEM59 expression was increased in the brain of AD patients compared to controls (Bakulski et al., 2012; Guttula et al., 2012). Herein, we also observed that TMEM59 protein levels were elevated in 6–7 month-old 5xFAD mice compared to WT controls (**Supplementary Figures 3A,B**). To further determine the change of TMEM59 in AD, we studied TMEM59 levels in 5xFAD mice at different ages. We found that although hippocampal TMEM59 protein levels were comparable between 5xFAD mice and their littermate WT controls at 1.5 months of age, hippocampal TMEM59 levels were significantly elevated in 5xFAD mice compared to WT controls at 4 and 8 months of age (**Figures 5A,B**). Similarly, although TMEM59 protein levels in the cortex of 5xFAD mice were not altered at 1.5 and 4 months of age, they were significantly elevated at 8 months of age compared to WT controls (**Figures 5A,C**). These results indicate a correlation between TMEM59 elevation and AD and aging, and further support a detrimental role of TMEM59 elevation in synaptic functions and learning and memory.

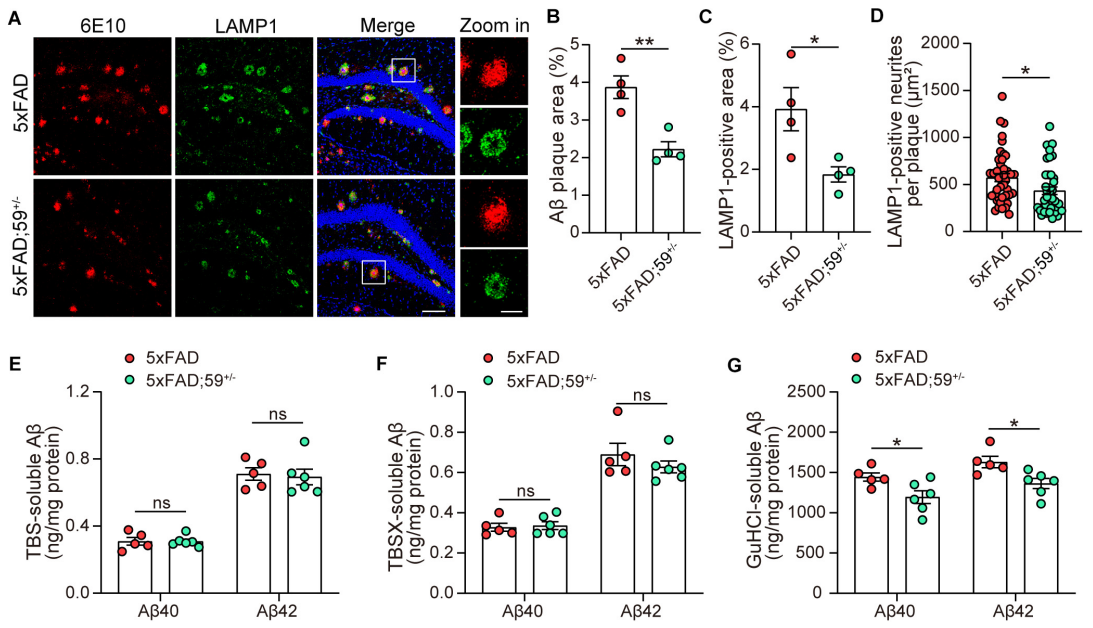

FIGURE 4 | TMEM59 haploinsufficiency reduces Aβ plaque deposition and neurite dystrophy in 5xFAD mice. **(A)** Z-stack confocal images of Aβ plaques (in red) and dystrophic neurites (indicated by LAMP1, in green) in the coronal sections from 6 to 7 month-old 5xFAD and 5xFAD; $59^{+/-}$ mice. Original magnifications are 20×, scale bar, 100 μm. Zoom-in images are on the right, scale bar, 30 μm. **(B,C)** Quantifications and comparisons of the total area of Aβ plaques **(B)** and LAMP1-positive dystrophic neurites **(C)** shown in **(A)**. $n = 4$ mice per group. **(D)** Quantifications and comparisons of the area of Aβ-associated LAMP1-positive dystrophic neurites per plaque shown in **(A)**. 43 plaques from four 5xFAD mice and 40 plaques from four 5xFAD; $59^{+/-}$ mice were studied for analysis. **(E–G)** The levels of Aβ40 and Aβ42 in the hippocampus of TBS-extractions **(E)**, TBSX-extractions **(F)**, and GuHCl-extractions **(G)** from 8 month-old 5xFAD and 5xFAD; $59^{+/-}$ mice were measured by ELISA and compared. $n = 5$ mice for 5xFAD, $n = 6$ mice for 5xFAD; $59^{+/-}$. Data represent mean ± SEM. $^{*}p < 0.05$, $^{**}p < 0.01$, ns: not significant. Unpaired *t*-test.

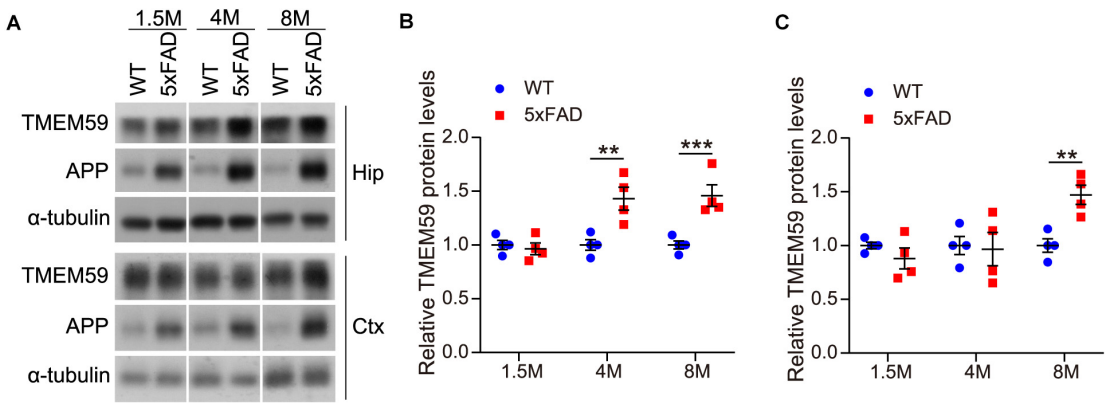

FIGURE 5 | TMEM59 protein levels are increased in 5xFAD mice during aging. **(A)** Protein lysates of hippocampal (Hip) and cortical (Ctx) tissues from WT and 5xFAD mice at different ages were subjected to western blotting to detect proteins indicated. **(B,C)** Hippocampal **(B)** and cortical **(C)** TMEM59 protein levels in **(A)** were quantified and compared to respective controls (set to 1.0). Data represent mean ± SEM, $n = 4$ mice per group. $^{**}p < 0.01$, $^{***}p < 0.001$. Two-way ANOVA followed by Bonferroni's *post hoc* test.

DISCUSSION

TMEM59 has been implicated to play a role in AD (Ullrich et al., 2010; Bakulski et al., 2012; Guttula et al., 2012). However, whether TMEM59 indeed modulates the pathology of AD, especially in animal models resembling AD phenotypes has yet to ascertained. In the present study, we observed that TMEM59 protein levels were significantly elevated in 5xFAD mice during aging; and this is consistent with the previous reports of high *TMEM59* expression levels and low DNA methylation in the *TMEM59* promoter region in AD patients compared to controls (Bakulski et al., 2012; Guttula et al., 2012), strengthening the correlation between TMEM59 and AD.

Cognitive impairment is regarded as a typical feature of AD in clinical diagnosis (McKhann et al., 2011). Herein, we found that lentivirus-mediated TMEM59 overexpression in the hippocampal region was sufficient to cause memory deficits and had a trend to impair synaptic plasticity in WT mice, implying that increased TMEM59 expression contributes to AD progression. However, TMEM59 overexpression did not exacerbate learning and memory and synaptic plasticity deficits in 5xFAD mice. One possible explanation is that the impacts of TMEM59 overexpression on cognitive and synaptic function impairments are mild and may not be able to further worsen the quickly degenerated phenotypes in 5xFAD mice. It is well-known that 5xFAD mice develop AD-like phenotypes very fast and such an aggressive phenotype in some ways is unphysiological to the human disease. Further study using models with relatively slow disease progression such as APP/PS1 and Tg2576 mice may be able to fully ascertain the contribution of TMEM59 elevation to AD progression.

Aβ is considered to be a prime culprit for AD pathogenesis and derived from APP through sequential cleavages by β-secretase and γ-secretase (Hardy, 2006; Zhang et al., 2011; Haass et al., 2012; Long and Holtzman, 2019). Aβ40 and Aβ42 are two major neurotoxic species among various Aβ species, with Aβ42 being more prone to aggregate into oligomers, fibrils and amyloid plaques in AD patients (Jarrett et al., 1993; Iwatsubo et al., 1994; Tu et al., 2014; Long and Holtzman, 2019). Interestingly, we found that TMEM59 overexpression exacerbated Aβ deposition in the brain of 5xFAD mice. We also studied Aβ40 and Aβ42 levels in 5xFAD mouse hippocampal fractions after sequential extraction by TBS, TBSX, and GuHCl, of which the formal two represent soluble or newly generated Aβ and the latter one represents detergent-insoluble deposited Aβ (Youmans et al., 2011; Zhong et al., 2019). Consistently, both Aβ40 and Aβ42 levels in GuHCl-soluble fractions were increased upon TMEM59 overexpression. However, TMEM59 overexpression had no effect on Aβ40 and Aβ42 levels in TBS- and TBSX-soluble fractions, implying that TMEM59 overexpression may not affect Aβ generation. This finding is in contrast to previous studies showing that TMEM59 overexpression could inhibit APP glycosylation and cell surface expression, as well as the cleavage of APP to generate Aβ in HEK293 cells (Ullrich et al., 2010), and that TMEM59 overexpression could reduce the γ-cleavage of APP C99 fragment and promote learning and memory in C99 transgenic drosophila (Li et al., 2020). Although our finding that APP glycosylation was increased in 5xFAD mice with TMEM59 haploinsufficiency is consistent with the observation that TMEM59 overexpression inhibited APP glycosylation (Ullrich et al., 2010), TMEM59 haploinsufficency had no effect on levels of total APP, APP α-/β-CTF, and soluble Aβ *in vivo*. One possibility for this discrepancy is that TMEM59 may have different effects on APP/Aβ metabolism in immortalized non-neuronal cell lines and animal models.

The formation of dystrophic neurites is also one pathological trait in AD (Holcomb et al., 1998; Guo et al., 2020). Many previous studies have demonstrated that LAMP1, a lysosomal marker for endo-lysosomal and autophagic vesicles, is enriched in dystrophic neurites and accumulates around Aβ plaques in AD mouse models (Condello et al., 2011; Gowrishankar et al., 2015; Yuan et al., 2016) as well as in AD patients (Terry et al., 1964;

Barrachina et al., 2006; Hassiotis et al., 2018). Therefore, LAMP1 staining has been used as a marker for dystrophic neurites. Herein, we also found that TMEM59 overexpression resulted in increased staining of LAMP1, emphasizing the pathologic contribution of TMEM59 elevation on neurite dystrophy in AD.

One research group reported that complete knockout and nervous system-specific knockout of *Tmem59* resulted in memory impairments in mice (Liu et al., 2018; Wang et al., 2019). In contrast, we found that TMEM59 haploinsufficiency had no effect on learning and memory and synaptic plasticity in WT mice. Importantly, TMEM59 haploinsufficiency reverses memory and synaptic plasticity deficits in 5xFAD mice. Consistently, TMEM59 haploinsufficiency reduces Aβ deposition, detergent-insoluble but GuHCl-soluble Aβ42 levels, as well as dystrophic neurites in the brain of 5xFAD mice. Therefore, downregulation of TMEM59 can provide protection in AD. We recently demonstrated TMEM59 deficiency in microglia resulted in elevated phagocytosis and mitochondrial respiration (Liu et al., 2020). Herein, we also found the basal respiratory capacity of mitochondria was enhanced in primary neurons derived from TMEM59 knockout mice when compared to controls (**Supplementary Figures 4A,B**). Therefore, one potential mechanism for TMEM59 haploinsufficiency to exert protection in AD is that TMEM59 haploinsufficiency increases microglial phagocytosis of Aβ and promotes cellular health.

In summary, our study demonstrates that an elevation of TMEM59 can exacerbate the pathological progress during aging, whereas downregulation of TMEM59 can ameliorate cognitive and synaptic deficits and pathologies in AD model mice. These findings strongly support the notion that TMEM59 plays an important role in AD pathogenesis and may provide a potential strategy for AD treatment.

DATA AVAILABILITY STATEMENT

All datasets presented in this study are included in the article/**Supplementary Material**.

ETHICS STATEMENT

The animal study was reviewed and approved by Animal Ethics Committee of Xiamen University.

AUTHOR CONTRIBUTIONS

JM and YZ designed the experiments. JM and LH performed most molecular and animal experiments. NZ carried out electrophysiological experiments under supervision by HS. HiX and ZL helped with animal experiments. XZ, HL, and DC provided technical supports. JM, LH, HaX, and YZ interpreted the data and wrote the manuscript. YZ supervised the project. All authors reviewed the manuscript.

FUNDING

This work was supported by grants from The National Natural Science Foundation of China (U1705285 and 81771377 to YZ), National Key Research and Development Program of China (2016YFC1305903 and 2018YFC2000400 to YZ), and Fundamental Research Funds for the Central Universities (20720180049 to YZ).

ACKNOWLEDGMENTS

We thank Dr. Haibin Wang for providing Zp3-Cre mice.

SUPPLEMENTARY MATERIAL

The Supplementary Material for this article can be found online at: https://www.frontiersin.org/articles/10.3389/fcell.2020.596030/full#supplementary-material

REFERENCES

Bakulski, K. M., Dolinoy, D. C., Sartor, M. A., Paulson, H. L., Konen, J. R., Lieberman, A. P., et al. (2012). Genome-wide DNA methylation differences between late-onset Alzheimer's disease and cognitively normal controls in human frontal cortex. *J. Alzheimers Dis.* 29, 571–588. doi: 10.3233/JAD-2012-111223

Barrachina, M., Maes, T., Buesa, C., and Ferrer, I. (2006). Lysosome-associated membrane protein 1 (LAMP-1) in Alzheimer's disease. *Neuropathol. Appl. Neurobiol.* 32, 505–516. doi: 10.1111/j.1365-2990.2006.00756.x

Bromley-Brits, K., Deng, Y., and Song, W. (2011). Morris water maze test for learning and memory deficits in Alzheimer's disease model mice. *J. Vis. Exp.* 53:2920. doi: 10.3791/2920

Cheng, Y., Wang, Z. M., Tan, W., Wang, X., Li, Y., Bai, B., et al. (2018). Partial loss of psychiatric risk gene Mir137 in mice causes repetitive behavior and impairs sociability and learning via increased Pde10a. *Nat. Neurosci.* 21, 1689–1703. doi: 10.1038/s41593-018-0261-7

Condello, C., Schain, A., and Grutzendler, J. (2011). Multicolor time-stamp reveals the dynamics and toxicity of amyloid deposition. *Sci. Rep.* 1:19. doi: 10.1038/srep00019

Crews, L., and Masliah, E. (2010). Molecular mechanisms of neurodegeneration in Alzheimer's disease. *Hum. Mol. Genet.* 19, R12–R20. doi: 10.1093/hmg/ddq160

DeTure, M. A., and Dickson, D. W. (2019). The neuropathological diagnosis of Alzheimer's disease. *Mol. Neurodegener.* 14:32. doi: 10.1186/s13024-019-0333-5

Gowrishankar, S., Yuan, P., Wu, Y., Schrag, M., Paradise, S., Grutzendler, J., et al. (2015). Massive accumulation of luminal protease-deficient axonal lysosomes at Alzheimer's disease amyloid plaques. *Proc. Natl. Acad. Sci. U.S.A.* 112, E3699–E3708. doi: 10.1073/pnas.1510329112

Guerreiro, R., and Bras, J. (2015). The age factor in Alzheimer's disease. *Genome Med.* 7:106. doi: 10.1186/s13073-015-0232-5

Guo, T., Zhang, D., Zeng, Y., Huang, T. Y., Xu, H., and Zhao, Y. (2020). Molecular and cellular mechanisms underlying the pathogenesis of Alzheimer's disease. *Mol. Neurodegener.* 15:40. doi: 10.1186/s13024-020-00391-7

Guttula, S. V., Allam, A., and Gumpeny, R. S. (2012). Analyzing microarray data of Alzheimer's using cluster analysis to identify the biomarker genes. *Int. J. Alzheimers Dis.* 2012:649456. doi: 10.1155/2012/649456

Haass, C., Kaether, C., Thinakaran, G., and Sisodia, S. (2012). Trafficking and proteolytic processing of APP. *Cold Spring Harb. Perspect. Med.* 2:a006270. doi: 10.1101/cshperspect.a006270

Hardy, J. (2006). Alzheimer's disease: the amyloid cascade hypothesis: an update and reappraisal. *J. Alzheimers Dis.* 9(3 Suppl.), 151–153. doi: 10.3233/jad-2006-9s317

Hassiotis, S., Manavis, J., Blumbergs, P. C., Hattersley, K. J., Carosi, J. M., Kamei, M., et al. (2018). Lysosomal LAMP1 immunoreactivity exists in both diffuse and neuritic amyloid plaques in the human hippocampus. *Eur. J. Neurosci.* 47, 1043–1053. doi: 10.1111/ejn.13913

Holcomb, L., Gordon, M. N., McGowan, E., Yu, X., Benkovic, S., Jantzen, P., et al. (1998). Accelerated Alzheimer-type phenotype in transgenic mice carrying both mutant amyloid precursor protein and presenilin 1 transgenes. *Nat. Med.* 4, 97–100. doi: 10.1038/nm0198-097

Huang, Y. D., and Mucke, L. (2012). Alzheimer mechanisms and therapeutic strategies. *Cell* 148, 1204–1222. doi: 10.1016/j.cell.2012.02.040

Iwatsubo, T., Odaka, A., Suzuki, N., Mizusawa, H., Nukina, N., and Ihara, Y. (1994). Visualization of a-Beta-42(43) and a-Beta-40 in senile plaques with end-specific a-beta monoclonals - evidence that an initially deposited species is a-beta-42(43). *Neuron* 13, 45–53. doi: 10.1016/0896-6273(94)90458-8

Jarrett, J. T., Berger, E. P., and Lansbury, P. T. Jr. (1993). The carboxy terminus of the beta amyloid protein is critical for the seeding of amyloid formation: implications for the pathogenesis of Alzheimer's disease. *Biochemistry* 32, 4693–4697. doi: 10.1021/bi00069a001

Jawhar, S., Trawicka, A., Jenneckens, C., Bayer, T. A., and Wirths, O. (2012). Motor deficits, neuron loss, and reduced anxiety coinciding with axonal degeneration and intraneuronal Abeta aggregation in the 5XFAD mouse model of Alzheimer's disease. *Neurobiol. Aging* 33, 196.e29–196.e40. doi: 10.1016/j.neurobiolaging.2010.05.027

Kocahan, S., and Dogan, Z. (2017). Mechanisms of Alzheimer's disease pathogenesis and prevention: the brain, neural pathology, N-methyl-D-aspartate receptors, tau protein and other risk factors. *Clin. Psychopharmacol. Neurosci.* 15, 1–8. doi: 10.9758/cpn.2017.15.1.1

Lachance, V., Wang, Q., Sweet, E., Choi, I., Cai, C. Z., Zhuang, X. X., et al. (2019). Autophagy protein NRBF2 has reduced expression in Alzheimer's brains and modulates memory and amyloid-beta homeostasis in mice. *Mol. Neurodegener.* 14:43. doi: 10.1186/s13024-019-0342-4

Li, W., Li, Y., Gan, L., Ma, F., Zhang, S., and Wen, T. (2020). Dcf1 alleviates C99-mediated deficits in drosophila by reducing the cleavage of C99. *Biochem. Biophys. Res. Commun.* 530, 410–417. doi: 10.1016/j.bbrc.2020.05.063

Liu, Q., Feng, R., Chen, Y., Luo, G., Yan, H., Chen, L., et al. (2018). Dcf1 triggers dendritic spine formation and facilitates memory acquisition. *Mol. Neurobiol.* 55, 763–775. doi: 10.1007/s12035-016-0349-6

Liu, Z., Ning, J., Zheng, X., Meng, J., Han, L., Zheng, H., et al. (2020). TMEM59 interacts with TREM2 and modulates TREM2-dependent microglial activities. *Cell. Death Dis.* 11:678. doi: 10.1038/s41419-020-02874-3

Long, J. M., and Holtzman, D. M. (2019). Alzheimer disease: an update on pathobiology and treatment strategies. *Cell* 179, 312–339. doi: 10.1016/j.cell.2019.09.001

McKhann, G. M., Knopman, D. S., Chertkow, H., Hyman, B. T., Jack, C. R. Jr., Kawas, C. H., et al. (2011). The diagnosis of dementia due to Alzheimer's disease: recommendations from the National Institute on Aging-Alzheimer's Association workgroups on diagnostic guidelines for Alzheimer's disease. *Alzheimers Dement.* 7, 263–269. doi: 10.1016/j.jalz.2011.03.005

Miedel, C. J., Patton, J. M., Miedel, A. N., Miedel, E. S., and Levenson, J. M. (2017). Assessment of spontaneous alternation, novel object recognition and limb clasping in transgenic mouse models of amyloid-beta and tau neuropathology. *J. Vis. Exp.* 123:55523. doi: 10.3791/55523

Oakley, H., Cole, S. L., Logan, S., Maus, E., Shao, P., Craft, J., et al. (2006). Intraneuronal beta-amyloid aggregates, neurodegeneration, and neuron loss in transgenic mice with five familial Alzheimer's disease mutations: potential factors in amyloid plaque formation. *J. Neurosci.* 26, 10129–10140. doi: 10.1523/JNEUROSCI.1202-06.2006

Penn, A. C., Zhang, C. L., Georges, F., Royer, L., Breillat, C., Hosy, E., et al. (2017). Hippocampal LTP and contextual learning require surface diffusion of AMPA receptors. *Nature* 549, 384–388. doi: 10.1038/nature23658

Tatem, K. S., Quinn, J. L., Phadke, A., Yu, Q., Gordish-Dressman, H., and Nagaraju, K. (2014). Behavioral and locomotor measurements using an open field activity monitoring system for skeletal muscle diseases. *J. Vis. Exp.* 91:51785. doi: 10.3791/51785

Terry, R. D., Gonatas, N. K., and Weiss, M. (1964). Ultrastructural studies in Alzheimer's presenile dementia. *Am. J. Pathol.* 44, 269–297.

Tu, S., Okamoto, S., Lipton, S. A., and Xu, H. (2014). Oligomeric Abeta-induced synaptic dysfunction in Alzheimer's disease. *Mol. Neurodegener.* 9:48. doi: 10.1186/1750-1326-9-48

Ullrich, S., Munch, A., Neumann, S., Kremmer, E., Tatzelt, J., and Lichtenthaler, S. F. (2010). The novel membrane protein TMEM59 modulates complex glycosylation, cell surface expression, and secretion of the amyloid precursor protein. *J. Biol. Chem.* 285, 20664–20674. doi: 10.1074/jbc.M109.055608

Vorhees, C. V., and Williams, M. T. (2006). Morris water maze: procedures for assessing spatial and related forms of learning and memory. *Nat. Protoc.* 1, 848–858. doi: 10.1038/nprot.2006.116

Wang, Y., Liu, Q., Xie, J., Feng, R., Ma, F., Wang, F., et al. (2019). Dcf1 affects memory and anxiety by regulating NMDA and AMPA receptors. *Neurochem. Res.* 44, 2499–2505. doi: 10.1007/s11064-019-02866-6

Xu, H., Gouras, G. K., Greenfield, J. P., Vincent, B., Naslund, J., Mazzarelli, L., et al. (1998). Estrogen reduces neuronal generation of Alzheimer beta-amyloid peptides. *Nat. Med.* 4, 447–451. doi: 10.1038/nm0498-447

Youmans, K. L., Leung, S., Zhang, J., Maus, E., Baysac, K., Bu, G., et al. (2011). Amyloid-beta42 alters apolipoprotein E solubility in brains of mice with five familial AD mutations. *J. Neurosci. Methods* 196, 51–59. doi: 10.1016/j.jneumeth.2010.12.025

Yu, D., Yan, H., Zhou, J., Yang, X., Lu, Y., and Han, Y. (2019). A circuit view of deep brain stimulation in Alzheimer's disease and the possible mechanisms. *Mol. Neurodegener.* 14:33. doi: 10.1186/s13024-019-0334-4

Yuan, P., Condello, C., Keene, C. D., Wang, Y., Bird, T. D., Paul, S. M., et al. (2016). TREM2 haplodeficiency in mice and humans impairs the microglia barrier function leading to decreased amyloid compaction and severe axonal dystrophy. *Neuron* 92, 252–264. doi: 10.1016/j.neuron.2016.09.016

Zhang, Y. W., Thompson, R., Zhang, H., and Xu, H. (2011). APP processing in Alzheimer's disease. *Mol. Brain* 4:3. doi: 10.1186/1756-6606-4-3

Zhong, L., Xu, Y., Zhuo, R., Wang, T., Wang, K., Huang, R., et al. (2019). Soluble TREM2 ameliorates pathological phenotypes by modulating microglial functions in an Alzheimer's disease model. *Nat. Commun.* 10:1365. doi: 10.1038/s41467-019-09118-9

Conflict of Interest: The authors declare that the research was conducted in the absence of any commercial or financial relationships that could be construed as a potential conflict of interest.

frontiers in Cell and Developmental Biology

ORIGINAL RESEARCH
published: 28 January 2021
doi: 10.3389/fcell.2020.631460

Fecal Fungal Dysbiosis in Chinese Patients With Alzheimer's Disease

Zongxin Ling[1†], Manlian Zhu[2†], Xia Liu[3†], Li Shao[4,5†], Yiwen Cheng[1†], Xiumei Yan[2†], Ruilai Jiang[2] and Shaochang Wu[2]*

[1] State Key Laboratory for Diagnosis and Treatment of Infectious Diseases, Collaborative Innovation Center for Diagnosis and Treatment of Infectious Diseases, National Clinical Research Center for Infectious Diseases, The First Affiliated Hospital, School of Medicine, Zhejiang University, Hangzhou, China, [2] Department of Geriatrics, Lishui Second People's Hospital, Lishui, China, [3] Department of Intensive Care Unit, The First Affiliated Hospital, School of Medicine, Zhejiang University, Hangzhou, China, [4] Institute of Hepatology and Metabolic Diseases, Hangzhou Normal University, Hangzhou, China, [5] Institute of Translational Medicine, The Affiliated Hospital of Hangzhou Normal University, Hangzhou, China

Gut bacterial dysbiosis plays a vital role in the development of Alzheimer's disease (AD). However, our understanding of alterations to the gut fungal microbiota and their correlations with host immunity in AD is still limited. Samples were obtained from 88 Chinese patients with AD, and 65 age- and gender-matched, cognitively normal controls. Using these samples, we investigated the fungal microbiota targeting internal transcribed spacer 2 (ITS2) rRNA genes using MiSeq sequencing, and analyzed their associations with the host immune response. Our data demonstrated unaltered fungal diversity but altered taxonomic composition of the fecal fungal microbiota in the AD patients. The analysis of the fungal microbiota was performed using 6,585,557 high-quality reads (2,932,482 reads from the controls and 3,653,075 from the AD patients), with an average of 43,042 reads per sample. We found that several key differential fungi such as *Candida tropicalis* and *Schizophyllum commune* were enriched in the AD patients, while *Rhodotorula mucilaginosa* decreased significantly. Interestingly, *C. tropicalis* and *S. commune* were positively correlated with IP-10 and TNF-α levels. In contrast, *C. tropicalis* was negatively correlated with IL-8 and IFN-γ levels, and *R. mucilaginosa* was negatively correlated with TNF-α level. PiCRUSt analysis revealed that lipoic acid metabolism, starch and sucrose metabolism were significantly decreased in the AD fungal microbiota. This study is the first to demonstrate fecal fungal dysbiosis in stable AD patients at a deeper level, and to identify the key differential fungi involved in regulating host systemic immunity. The analysis of the fungal microbiota in AD performed here may provide novel insights into the etiopathogenesis of AD and pave the way for improved diagnosis and treatment of AD.

Keywords: Alzheimer's disease, *Candida*, fungal microbiota, sequencing, TNF-α

OPEN ACCESS

Edited by:
Gong-Ping Liu, Huazhong University of Science and Technology, China

Reviewed by:
Jiaming Liu, Wenzhou Medical University, China
Yi Hao, Huazhong University of Science and Technology, China

***Correspondence:**
Shaochang Wu
shaochang_wu@163.com

† These authors have contributed equally to this work

Specialty section:
This article was submitted to Molecular Medicine, a section of the journal Frontiers in Cell and Developmental Biology

Received: *20 November 2020*
Accepted: *31 December 2020*
Published: *28 January 2021*

Citation:
Ling Z, Zhu M, Liu X, Shao L, Cheng Y, Yan X, Jiang R and Wu S (2021) Fecal Fungal Dysbiosis in Chinese Patients With Alzheimer's Disease. Front. Cell Dev. Biol. 8:631460. doi: 10.3389/fcell.2020.631460

INTRODUCTION

Alzheimer's disease (AD) is a neurodegenerative disorder characterized by a slow progression, which starts with mild memory loss and culminates in severe impairment of executive and cognitive functions. During the last decades, the prevalence of AD has been rapidly increasing due to the rise in life expectancy worldwide (Scheltens et al., 2016; Gaugler et al., 2019; Alzheimer's Association, 2020). It is estimated that by 2050, one in every 85 people will be living with AD (Brookmeyer et al., 2007). However, at present there are no mechanistic therapies or

disease-modifying therapies available for AD (Honig et al., 2018). As a result, a diagnosis of AD has become one of the most devastating that patients and their families can receive. The financial burden imposed by AD is formidable due to the care needed by the growing number of patients with AD and other dementias. Given the clinical and financial burdens of the disease, AD should be regarded as a global public health priority.

Increasing evidence recognizes AD as a multifactorial and heterogeneous disease with multiple contributors to its pathophysiology, which is not restricted to effects on the central nervous system, but also includes strong interactions with external factors such as the gut microbiota. At autopsy, AD is characterized by amyloid-beta (Aβ) plaques and neurofibrillary tangles (LaFerla et al., 2007; Kinney et al., 2018; Sepulcre et al., 2018; Chen et al., 2020; Wan et al., 2020). Recently, a genome-wide spatial transcriptomic analysis identified an amyloid plaque-induced gene network, suggesting that Aβ plays active roles in the development of AD (Chen et al., 2020). In fact, in the last decades, the progress made by accounts of AD etiopathology focusing on the nervous system remains limited. Recent studies of the gut–brain axis have highlighted the potential roles of the gut microbiota in the development of various brain diseases, including AD. Several studies have found an altered gut microbiota in AD patients, suggesting that the gut microbiota may be involved in AD pathogenesis (Vogt et al., 2017; Zhuang et al., 2018; Liu et al., 2019). Our group has also previously demonstrated that *Clostridium butyricum* and its metabolite butyrate can regulate the expression of Aβ, leading to an amelioration of cognitive deficits and neurodegeneration via modulation of the gut microbiota; these can therefore be considered to be potential psychobiotics (Sun et al., 2019a,b; Sun J. et al., 2020). Furthermore, a phase 3 clinical trial conducted in China by another group found that administering oligomannate led to a solid and consistent improvement in cognition in AD patients, suppressing gut dysbiosis and the associated phenylalanine/isoleucine accumulation, harnessing neuroinflammation, and reversing cognitive impairment (Wang et al., 2019). These findings indicate that gut dysbiosis can promote neuroinflammation during the progression of AD, while restoration of the gut microbiota may be a novel strategy for treating AD.

The gut microbiota is composed of a variety of microorganisms, including bacteria, viruses, fungi, and archaea. However, previous studies have mainly focused on the bacterial diversity and composition of the gut microbiota, while the fungal microbiota has not been explored extensively. Fungi are suggested to influence intestinal health and disease by suppressing the outgrowth of potential pathobionts, promoting immunoregulatory pathways, and modulating host metabolism (Huseyin et al., 2017; Ni et al., 2017; Sam et al., 2017; Chin et al., 2020). Several clinical studies have identified a distinct fungal microbiota dysbiosis in inflammatory bowel disease (IBD), primary sclerosing cholangitis, asthma, type 2 diabetes mellitus, chronic liver diseases, Parkinson's disease and other neurological diseases, and even colorectal cancer (Hoarau et al., 2016; Sokol et al., 2017; Forbes et al., 2018; Coker et al., 2019; Cirstea et al., 2020; Jayasudha et al., 2020; Jiang et al., 2020; Lemoinne et al., 2020; Qiu et al., 2020; van Tilburg Bernardes et al., 2020; Ventin-Holmberg et al., 2020). Studies of animal models have found that commensal fungi can activate host-protective immune pathways related to epithelial barrier integrity, but can also induce reactions that contribute to events associated with IBD (Iliev and Cadwell, 2020). In addition, by interacting with the bacteriome and/or virome, the gut fungal communities appears to be a cofactor in inflammation and in the host immune response, and therefore may contribute to various disease progression. Therefore, alterations to the fungal microbiota might actively contribute to the development of AD. In this study, we employed fungal-specific internal transcribed spacer (ITS) amplicon sequencing of a cross-sectional AD cohort to investigate associations between the fungal gut microbiota and AD using the 16S rRNA high-throughput gene MiSeq platform. Furthermore, we performed correlation analysis between fungal taxa and clinical indicators to decipher their possible roles in the pathogenesis of AD.

MATERIALS AND METHODS

Subject Enrollment

A total of 88 Chinese patients with well-controlled AD, whose diagnoses were based on the criteria of the National Institute of Neurological and Communicative Diseases and Stroke/AD and Related Disorders Association, were recruited from Lishui, Zhejiang province (China) from February 2019 to November 2019, along with 65 cognitively normal subjects as controls. The cognitive and functional status of each subject was scored using the Mini-Mental State Examination (MMSE, Chinese version), the current version in the Wechsler Adult Intelligence Scale series (WAIS-IV, published in 2008), and the Barthel Index of instrumental activities of daily living. Each participant was scanned using magnetic resonance imaging (MRI), with all AD patients diagnosed as showing brain atrophy. The detailed demographic data and medical history (including hypertension, diabetes mellitus, hypercholesterolemia, coronary heart disease, diarrhea, and constipation) were collected using a set of questionnaires. Exclusion criteria included: family history of dementia; any kind of other neurodegenerative disease such as Parkinson's disease; confirmed mental illness such as schizophrenia; any kind of tumor; antibiotic, prebiotic, probiotic, or synbiotic administration during the previous month; known active infections such as viral, bacterial, or fungal infections; and other diseases such as inflammatory bowel disease, irritable bowel syndrome, or other autoimmune diseases. The protocols for the study were approved by the Ethics Committee of Lishui Second People's Hospital (Zhejiang, China) and written informed consent was obtained from each of the subjects or their guardian before enrollment.

Fecal Sample Collection and DNA Extraction

Approximately 2 g of fresh fecal sample was collected from each subject in a sterile plastic cup, and stored at −80°C after preparation within 15 min, until its subsequent use. Metagenomic

DNA was extracted from 300 mg homogenized feces using a QIAamp DNA Stool Mini Kit (QIAGEN, Hilden, Germany) according to the manufacturer's instructions, with additional glass-bead beating steps performed using a Mini-Beadbeater (FastPrep; Thermo Electron, Boston, MA, United States). The amount of DNA was determined using a NanoDrop ND-1000 spectrophotometer (Thermo Electron). The integrity and size were verified by electrophoresis on a 1.0% agarose gel containing 0.5 mg/ml ethidium bromide. All DNA samples were stored at −20°C prior to further analysis.

Amplicon Library Construction and Sequencing

Amplicon libraries were constructed using Illumina sequencing-compatible and barcode-indexed fungal PCR primers ITS3 (5′-GATGAAGAACGYAGYRAA-3′) and ITS4 (5′-TCCTCCGC TTATTGATATGC-3′), which target ITS2 rRNA genes (Degnan and Ochman, 2012). All PCR reactions were performed using HiFi HotStart ReadyMix (KAPA Biosystems) according to the manufacturer's protocol and approximately 50 ng extracted DNA per reaction. Thermocycling conditions were set at 95°C for 1 min, 53°C for 1 min, then 72°C for 1 min for 30 cycles, followed by a final extension at 72°C for 5 min. All PCR reactions were performed in 50 μl triplicates and combined after PCR. The amplicon library was prepared using a TruSeq DNA sample preparation kit (Illumina, San Diego, CA, United States). Prior to sequencing, the PCR products were extracted with the MinElute Gel Extraction Kit (QIAGEN) and quantified on a NanoDrop ND-1000 spectrophotometer (Thermo Electron) and a Qubit 2.0 Fluorometer (Invitrogen). The purified amplicons were then pooled in equimolar concentrations and the final concentration of the library was determined using the Qubit 2.0 Fluorometer. Negative DNA extraction samples (lysis buffer and kit reagents only) were amplified and sequenced as contamination controls. Sequencing was performed on a MiSeq instrument (Illumina) using a 300 × 2 V3 kit together with the PhiX Control V3 library (Illumina) (Ling et al., 2019; Wang et al., 2019). MiSeq sequencing and library construction were performed by technical staff at Hangzhou KaiTai Bio-lab.

Bioinformatic Analysis

The ITS sequence dataset generated by the MiSeq run were first merged and demultiplexed into per-sample data using QIIME version 1.9.0 with default parameters (Caporaso et al., 2010). Chimera sequences were detected and removed using USEARCH version 7 software based on the UCHIME algorithm (Edgar et al., 2011). The open-reference operational taxonomic unit (OTU) pick was then performed using USEARCH version 7 referenced against the Greengenes database version 13.8 at 97% sequence similarity (Edgar, 2010; McDonald et al., 2012). OTUs containing a number of sequences <0.005% of the total number of sequences were discarded, as recommended (Navas-Molina et al., 2013). This resulted in an OTU table, which was used for subsequent downstream analysis.

To perform the taxonomic assignment, the most abundant sequence from each OTU was chosen as the representative sequences from that OTU. Taxonomic assignment of individual datasets was performed by classifying the data according to the UNITE database[1] (Abarenkov et al., 2010). Alpha diversity was calculated based on the sequence similarity at the 97% level using QIIME software and Python scripts to calculate a range of estimators, including: index of observed species, abundance-based coverage estimator (ACE), Chao1 estimator, Shannon, Simpson, evenness, and PD whole tree. Sequence coverage was assessed in Mothur software based on calculating rarefaction curves and Good's coverage (Good, 1953; Schloss et al., 2009). Beta diversity was estimated based on the Jaccard, Bray–Curtis, unweighted UniFrac, and weighted UniFrac distances calculated with 10× subsampling in QIIME. These distances were visualized following principal coordinate analysis (PCoA) of the data (Lozupone and Knight, 2005). Hierarchical clustering was performed and a heatmap was generated using a customized script developed in the R statistical package, with Spearman's rank correlation coefficient as the distance measure. The output file was further analyzed using the Statistical Analysis of Metagenomic Profiles (STAMP) software package version 2.1.3 (Parks et al., 2014).

To perform the predictive functional analyses, PiCRUSt software version 1.0.0 was used to identify predicted gene families and associated pathways from the inferred metagenomes of taxa of interest identified during the compositional analyses; this analysis is based on the close link between phylogeny and function (Langille et al., 2013). Predicted functional genes were categorized based on the Clusters of Orthologous Groups (COG) database and on the Kyoto Encyclopedia of Genes and Genome (KEGG) orthology (KO), and then compared across patient groups using STAMP. Pathways and enzymes were assigned using the KEGG database options built into the pipeline. Pathways that were non-prokaryotic, had <2 sequences in each cohort, or had a difference in mean proportions <0.1% were excluded from the analysis. The characterization of microorganismal features differentiating the gastric microbiota was performed using the linear discriminant analysis (LDA) effect size (LEfSe) method[2] for biomarker discovery, which emphasizes both statistical significance and biological relevance (Segata et al., 2011). Based on a normalized relative abundance matrix, the LEfSe method uses the Kruskal–Wallis rank sum test to detect features with significantly different abundances between assigned taxa and then performs LDA to estimate the effect size of each feature. A significant alpha threshold of 0.05 and an effect size threshold of 3 were used to identify all of the biomarkers discussed in this study.

Systemic Inflammatory Cytokines Analysis

Serum samples were obtained from the participants using their fasting blood in the early morning. The following cytokines were quantified using a 27-plex magnetic bead based immunoassay kit (Bio-Rad, Hercules, CA, United States): interleukin-1β (IL-1β), IL-1 receptor antagonist (IL-1ra), IL-2, IL-4, IL-5,

[1] http://unite.ut.ee/repository.php

[2] http://huttenhower.sph.harvard.edu/galaxy/

IL-6, IL-7, IL-8, IL-9, IL-10, IL-12 (p70), IL-13, IL-15, IL-17, eotaxin, fibroblast growth factor-basic (FGF-basic), granulocyte colony-stimulating factor (G-CSF), granulocyte-macrophage colony-stimulating factor (GM-CSF), interferon gamma (IFN-γ), interferon gamma-inducible protein 10 (IP-10), monocyte chemotactic protein-1 (MCP-1), macrophage inflammatory protein-1α (MIP-1α), platelet-derived growth factor (PDGF-bb), MIP-1β, regulated upon activation normal T-cell expressed and secreted (RANTES), tumor necrosis factor-alpha (TNF-α), and vascular endothelial growth factor (VEGF). The Bio-Plex 200 system (Bio-Rad) was used to analyze Bio-Rad 27-plex human group I cytokines, with the Bio-Plex assay performed according to the manufacturer's directions. The results were expressed as picograms per milliliter (pg/mL) using standard curves integrated into the assay and the Bio-Plex Manager v5.0 software (Bio-Rad), yielding reproducible intra-and inter-assay CV values of 5–8%.

Statistical Analysis

White's nonparametric *t*-test, the independent *t*-test, or the Mann-Whitney *U*-test were applied to analyze continuous variables. Pearson's chi-square test or Fisher's exact test were used to analyze categorical variables between groups. Spearman's rank correlation test was used to perform correlation analyses. Statistical analysis was performed using SPSS version 19.0 (SPSS Inc., Chicago, IL, United States) and STAMP version 2.1.3 (Parks et al., 2014). R and GraphPad Prism v6.0 software were used to prepare graphs. All of the tests of significance performed were two sided, with $p < 0.05$ or corrected $p < 0.05$ considered statistically significant.

Accession Number

The sequence data from this study are deposited in the GenBank Sequence Read Archive with the accession number SRP292858.

RESULTS

Subject Characteristics

Eighty-eight stable AD patients and 65 age- and gender-matched cognitively normal, healthy controls were enrolled in the present study (**Table 1**). All participants were older than 65 years of age. There were no significant differences between the healthy controls and the AD patients in terms of gender, body mass index, drinking, or smoking, or in terms of comorbidities with hypertension, hypercholesterolemia, diabetes mellitus, or coronary heart disease (all *p*s > 0.05). However, MMSE, WAIS, and Barthel scores were clearly lower in AD patients than in the healthy controls (all *p*s < 0.05).

TABLE 1 | The fundamental information of subjects.

Parameters	AD patients (*n* = 88)	Healthy control (*n* = 65)
Age (y)	74.28 ± 8.89	73.58 ± 8.15
Gender (male/female)	40/48	32/33
BMI (Mean ± SD)	23.20 ± 3.25	23.68 ± 3.48
Antibiotics use, no.	0	0
Complications, no.		
Hypertension	30	19
Diabetes mellitus	13	8
Hypercholesterolemia	12	8
Coronary heart disease	11	6
Diarrhea	2	3
Constipation	6	4
Cognitive and functional status		
MMSE Score*	4.35 ± 5.89	26.85 ± 3.75
WAIS Score*	36.25 ± 16.84	91.25 ± 11.28
Barthel Score*	22.38 ± 24.20	77.80 ± 9.85

BMI, body mass index; SD, standard deviation; no., numbers; MMSE, Mini-Mental State Examination; WAIS, Wechsler Adult Intelligence Scale.
**p < 0.05.*

Unaltered Overall Structure of the Fungal Microbiota in Stable AD

In the present study, 6,585,557 high-quality reads (2,932,482 reads from the controls and 3,653,075 from the AD patients) were obtained for subsequent analysis of the fungal microbiota, with an average of 43,042 reads per sample. Good's coverage was 99.99% in healthy controls and 99.98% in AD patients, respectively, suggesting that most of the fungal phylotypes (546 OTUs) in the AD-associated fungal microbiota were successfully identified. Interestingly, the calculated fungal alpha-diversity indices, including the Shannon and Simpson indices, show no significant changes of the AD-associated fungal microbiota relative to that of the healthy controls (**Figures 1A,B**); however, there was a trend toward increasing fungal diversity in the stable AD patients. In terms of the richness indices, there were no significant changes in ACE, Chao1, and observed OTUs in stable AD patients compared with healthy controls (**Figures 1C–E**; all *p*s > 0.05). Rarefaction plots reached a plateau for fungal species in both the AD and the control samples. We next assessed and compared the beta diversity of the fungal microbiota in AD patients to that in healthy controls based on the Bray–Curtis, Jaccard, unweighted UniFrac, and weighted UniFrac algorithms. The AD and control groups could not be divided into different clusters (Adonis test, $p > 0.01$; **Figures 1F–I**). In addition, the Venn diagram showed more unique phylotypes in AD patients than those in healthy controls (**Figure 1J**). Taken together, the alpha- and beta-diversity analyses demonstrate that the overall structure of the fungal microbiota in stable AD patients did not change obviously compared with that in the healthy controls.

Taxonomic Alterations of Fecal Fungi in Stable AD

The compositions of the fungal microbiota in the stable AD patients and healthy controls were assessed at different taxonomic levels (**Figure 2**). Overall, four phyla, 20 classes, 52 orders, 97 families, 148 genera, and 247 species were identified by this sequencing analysis. Among the fungal taxa, the phylum Ascomycota dominated the fungal microbiota, while Basidiomycota was observed as the

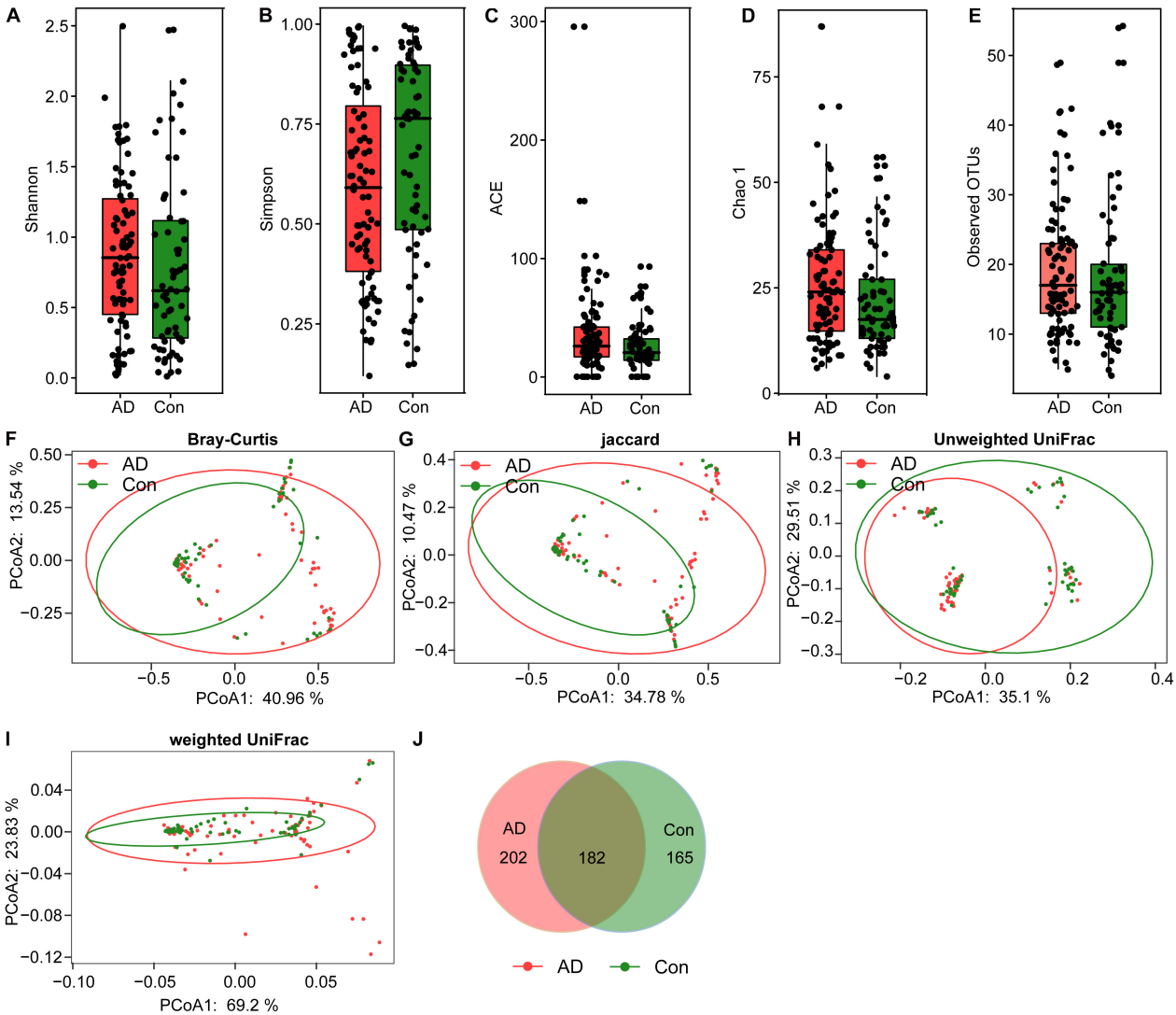

FIGURE 1 | Fungal diversity and richness of the fecal microbiota in Chinese AD patients. The diversity indices of Shannon **(A)** and Simpson **(B)**, and the richness indices of the observed species **(C)**, ACE **(D)**, and Chao1 **(E)** were used to evaluate the overall structure of the fungal microbiota in the stable AD patients and the healthy controls. The data are presented as mean ± standard deviation. Unpaired *t*-tests (two tailed) were used to analyze the variation between the groups. Principal coordinate analysis (PCoA) plots of individual fungal microbiota based on Bray–Curtis **(F)**, Jaccard **(G)**, and unweighted **(H)** and weighted **(I)** UniFrac distances in the AD patients and the healthy controls. Each symbol represents a sample. The Venn diagram illustrates the overlap of OTUs in the fungal microbiota between the two groups **(J)**.

second most abundant phylum in both the AD and control groups. At the family level, Saccharomycetales family Incertae sedis, Trichocomaceae, Meruliaceae, Pleosporaceae, Trichosporonaceae, Schizophyllaceae, and Sclerotiniaceae were found to be dominant in the fungal microbiota, when unclassified fungal taxa were excluded. Interestingly, we found that a greater number of fungal families were observed in the AD patients compared with the healthy controls. At the genus level, classified genera including *Candida*, *Aspergillus*, *Debaryomyces*, *Trichosporon*, *Wickerhamomyces*, *Schizophyllum*, *Phlebia*, and *Asterotremella* were abundant in the fungal microbiota, both in the AD patients and the healthy controls. At the species level, fungal taxa including *Candida albicans*, *Candida tropicalis*, *Candida parapsilosis*, *Schizophyllum commune*, *Phlebia cf. subserialis* MS42b, *Asterotremella* sp., *Candida metapsilosis*, and *Wickerhamomyces anomalus* were observed and classified. *C. albicans*, *C. tropicalis*, and *C. parapsilosis* were the most abundant species in the fungal microbiota, both in the AD patients and the healthy controls. Using the LEfSe method, discriminant analysis showed that many key taxa were clearly different between the AD and control groups (LDA score >2, $p < 0.05$; **Figure 3**). Although the Basidiomycota/Ascomycota ratio is considered to be an indicator of fungal dysbiosis, we found no significant differences in these two abundant phyla between the AD patients and the healthy controls (Coker et al., 2019). The LEfSe analysis revealed that most of the differential

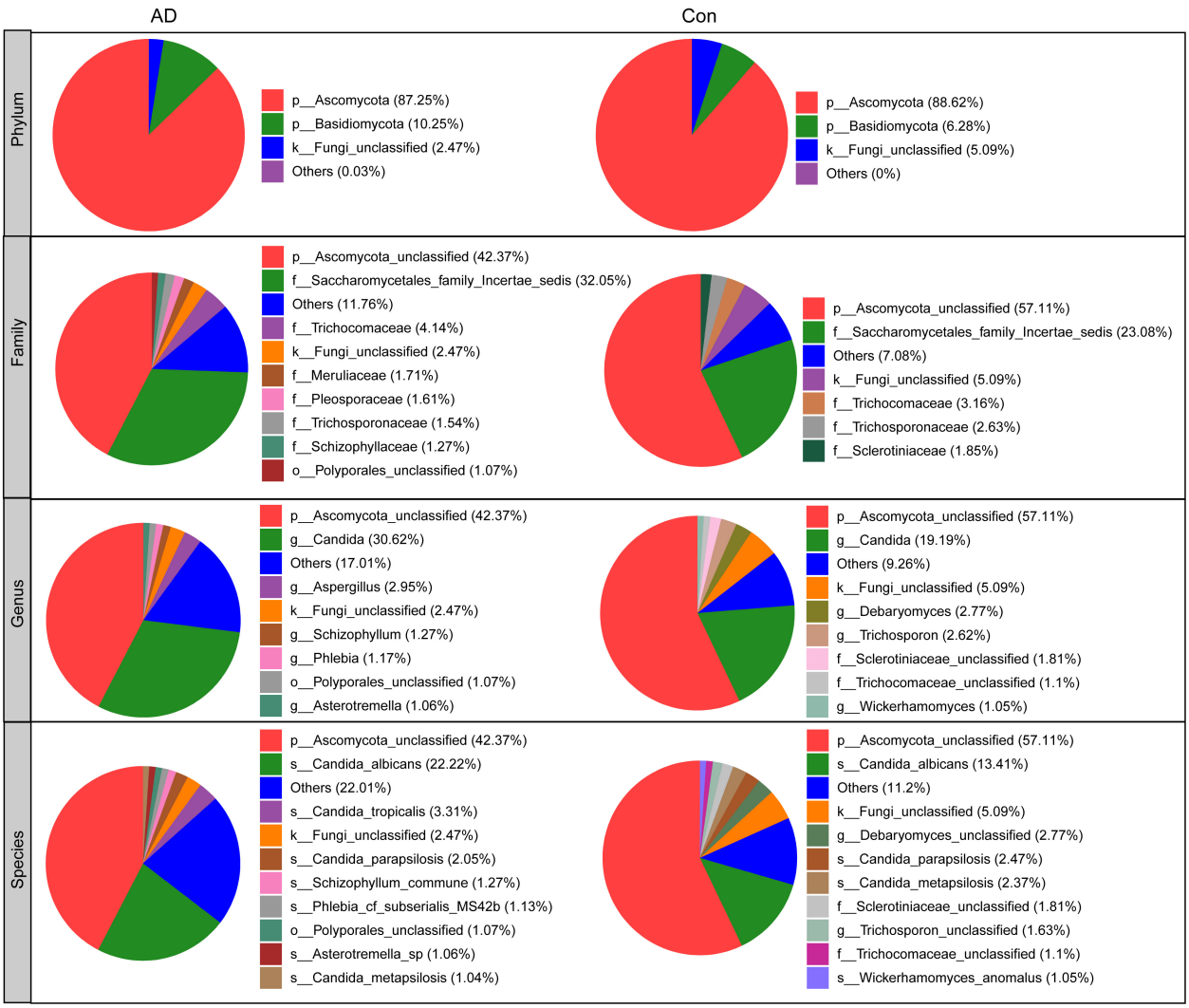

FIGURE 2 | Overall fungal microbiota composition in stable AD patients and healthy controls in phylum, family, genus, and species levels.

fungi could be classified at the species level. *C. parapsilosis*, *Hannaella* sp. CMON52, *C. apicola*, *Cystofilobasidium capitatum*, *C. xylopsoci*, *C. zeylanoides*, *Malassezia globosa*, *Trichosporon veenhuisii*, *Bullera unica*, *Millerozyma farinosa*, and *Rhodotorula mucilaginosa* were enriched in the healthy controls, while *C. tropicalis*, *Trametes versicolor*, *S. commune*, *Davidiella tassiana*, *Exophiala dermatitidis*, and *Erythrobasidium hasegawianum* were prevalent in stable AD patients. The abundances of the most numerous *Candida* species, such as *C. albicans*, did not show obvious changes between the two groups. Despite most of these differential species not being abundant, our results do nevertheless indicate fungal dysbiosis in stable AD patients.

Fungal Functional Alterations in AD

To identify metabolic and functional changes in the fungal microbiota between the AD patients and the controls, we used PiCRUSt to analyze the functional potential of the microbiota based on closed-reference OTU picking. We compared 105 KEGG pathways at level 3 and identified five KEGG categories with clearly differential abundances between the AD patients and the controls. The following KEGG categories decreased prominently in stable AD patients ($p < 0.05$; **Figure 4**): "lipoic acid metabolism," "cell cycle – Caulobacter," "starch and sucrose metabolism," "lysine degradation," and "phosphotransferase system (PTS)." These fungal functional alterations might participate in the pathogenesis and development of AD.

Correlations Between Key Differential Fungi and Host Immunity

We found that the AD-associated clinical indicators we examined, including the MMSE, WAIS, and Barthel scores, were significantly lower in the stable AD patients compared with the healthy controls ($p < 0.01$). Using the Bio-Plex Pro human cytokine group I panel 27-plex analysis, we found

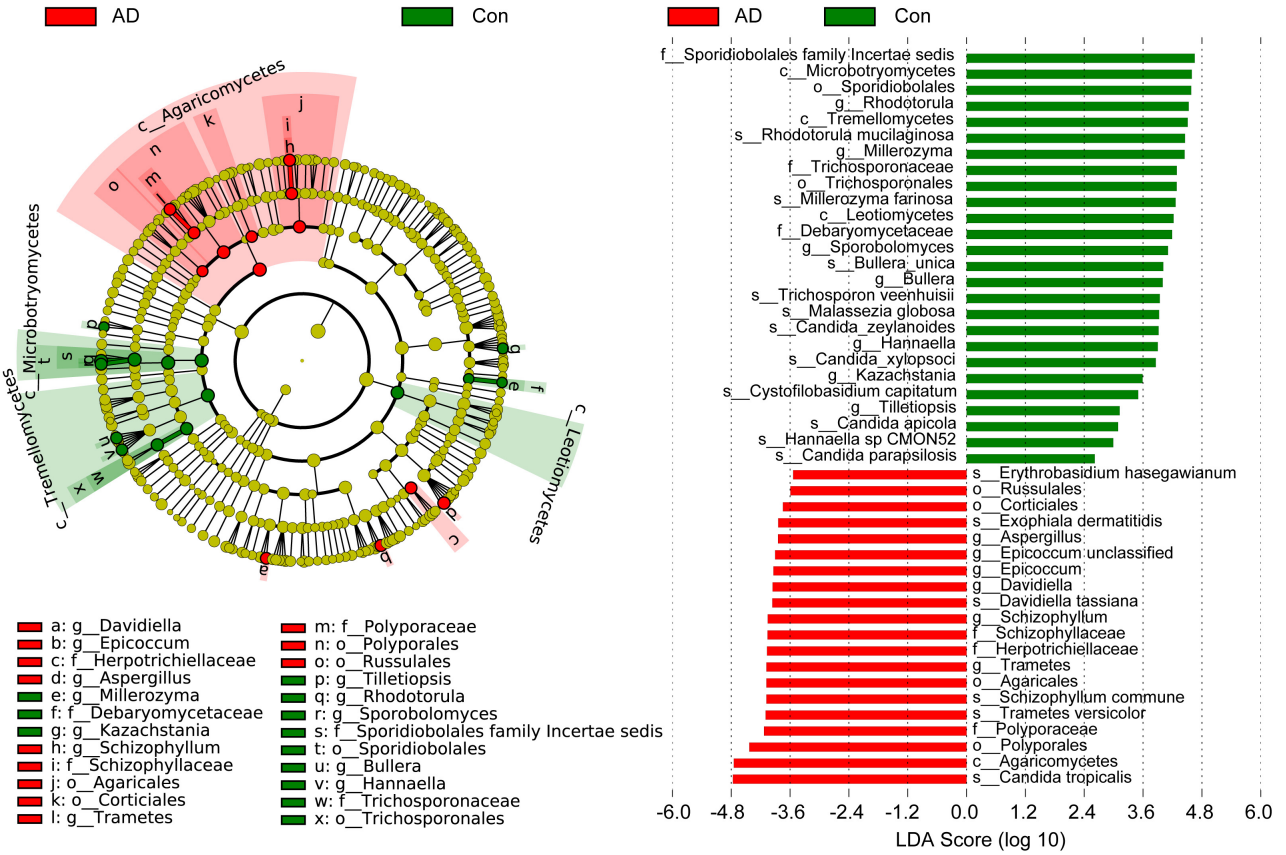

FIGURE 3 | Differential fungal taxa between the stable AD patients and the healthy controls. The LEfSe identified the taxa with the greatest differences in abundance between the AD patients and healthy controls. Only the taxa meeting a significant LDA threshold value of >2 are shown. These differential fungi could be used as potential biomarkers to distinguish AD patients from healthy controls.

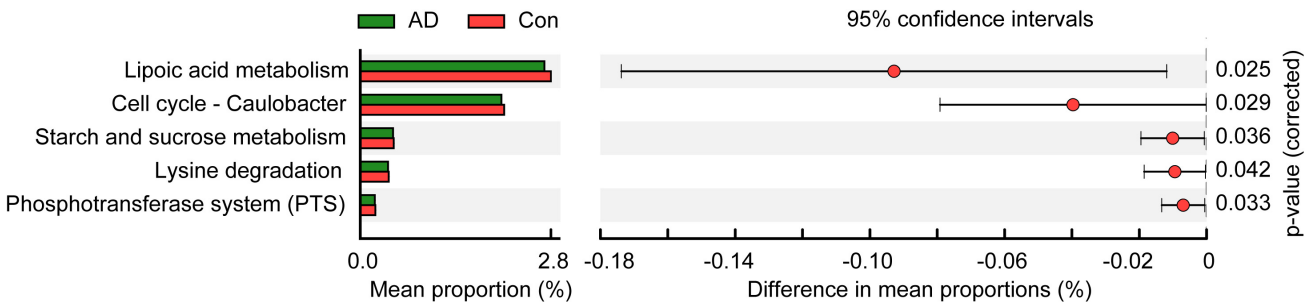

FIGURE 4 | PiCRUSt-based examination of the fungal microbiome of the stable AD patients and the healthy controls. The different fungal functions were evaluated between them based on two-sided Welch's *t*-test. Comparisons between the groups for each KEGG functional category (level 3) are shown by percentage. The Benjamini–Hochberg method was used for multiple testing correction based on the false discovery rate (FDR) through STAMP.

that, in the AD patients relative to the healthy controls, levels of anti-inflammatory cytokines (such as IFN-γ) and several chemokines (such as IL-8, MCP-1, and MIP-1a) were significantly lower ($ps < 0.05$), while levels of pro-inflammatory cytokines (such as TNF-α) were markedly higher ($ps < 0.05$); furthermore, the level of IP-10 was also lower in the AD patients ($ps < 0.05$). Next, we investigated correlations between the key differential fungi and the altered cytokines using Spearman's rank correlation (**Figure 5**). We found that the enriched abundance of *C. tropicalis* in AD correlated negatively with levels of IL-8 and IFN-γ, but correlated positively with levels of IP-10 and TNF-α ($ps < 0.05$). However, the abundance of *C. parapsilosis*, which was prevalent in healthy controls, was not correlated with altered cytokine levels. The abundance of another AD-enriched fungi, *S. commune*, was positively correlated with levels of TNF-α and IP-10 ($ps < 0.05$). The abundance of

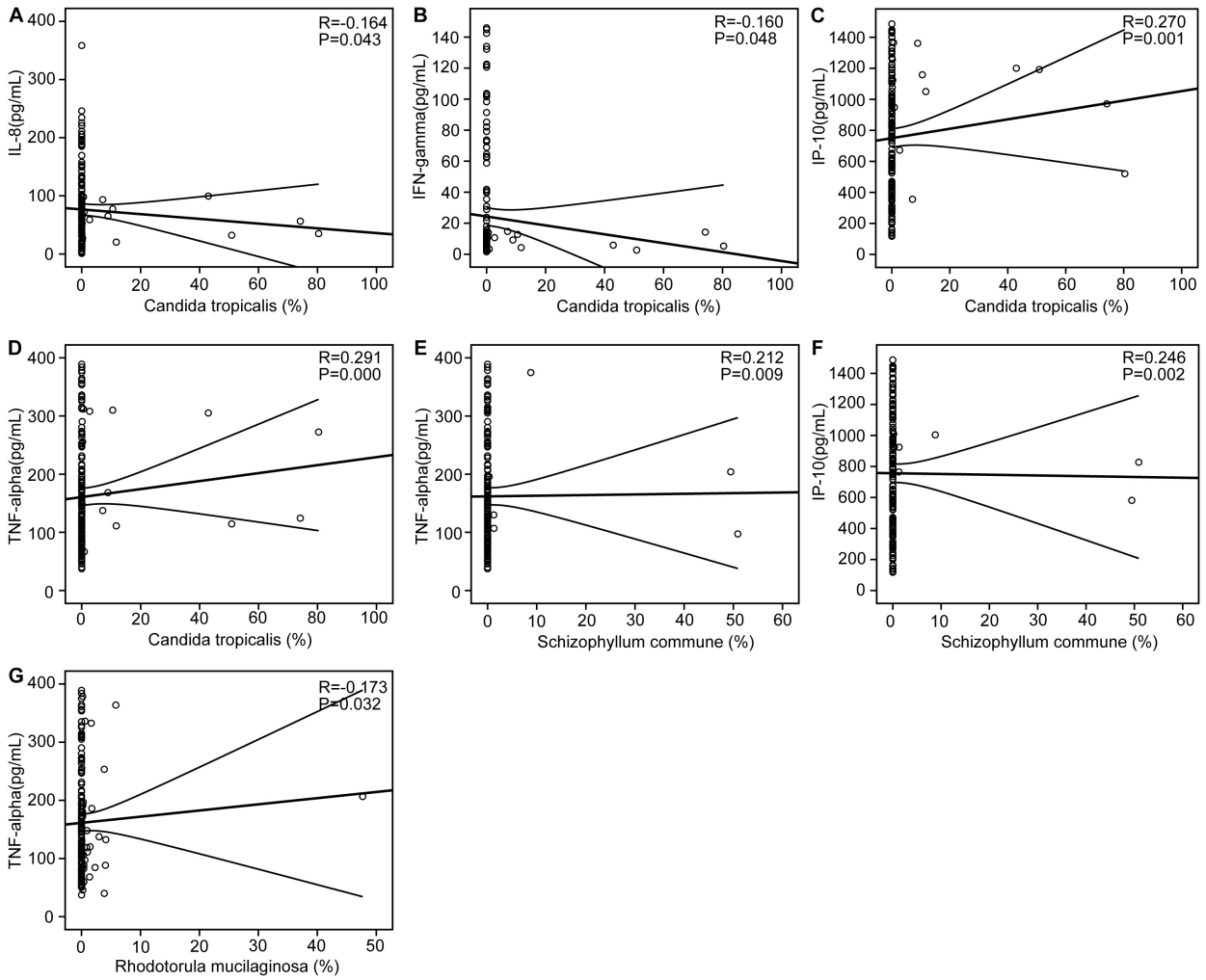

FIGURE 5 | Correlations between pro- and anti-inflammatory cytokines and chemokines with altered concentrations and the relative abundance of the key differential fungi. Correlation between the relative abundance of *Candida tropicalis* and the levels of IL-8 **(A)**, IFN-γ **(B)**, IP-10 **(C)**, and TNF-α **(D)**; the relative abundance of *Schizophyllum commune* and the levels of TNF-α **(E)** and IP-10 **(F)**; the relative abundance of *Rhodotorula mucilaginosa* and the levels of TNF-α **(G)**. Spearman's rank correlation (R) and probability (P) were determined to evaluate the statistical importance.

R. mucilaginosa, a non-abundant fungi that was enriched in healthy controls, was negatively correlated with the level of TNF-α ($p < 0.05$). Thus, these results indicate that the altered key differential fungi regulated the systemic immune response in the AD patients, and may actively contribute to the development and progression of AD.

DISCUSSION

In the present study, we observed fungal microbiota dysbiosis in Chinese patients with stable AD for the first time. Using high-throughput sequencing techniques, we found that alterations to several key differential fungi were associated with AD, and showed clear correlations with the host immune response. These altered fungal taxa may play vital roles in the development and progression of AD.

The human gut microbiota is a complex and diverse ecosystem composed of bacteria, fungi, viruses, and archaea (Hamad et al., 2017). Of course, bacteria represent the majority of the microbial communities that inhabit the human gut, and their roles and mechanisms in human health and disease have been elucidated extensively. Maintaining a healthy balance of gut bacteria can promote good health, and indeed several previous studies have reported that AD pathology is closely correlated with alterations in gut bacterial profiles (Vogt et al., 2017; Zhuang et al., 2018; Li B.Y. et al., 2019; Liu et al., 2019). This suggests that human gut bacteria may play crucial roles in the etiopathology of AD, such that these key differential bacteria could be used as potential targets for non-invasive diagnosis and treatment of AD. Unlike the bacterial community in the human gut, the composition and diversity of the fungal microbiota remains largely unexplored, because of the relatively low abundance of fungi in the human gut, combined

with their neglect in research employing culture-based and molecular analyses (Marchesi, 2010). Nevertheless, intestinal fungi represent an important component of the microbiota in the human gastrointestinal tract that interacts with gut immune cells to maintain a healthy gut (Leonardi et al., 2018; Bacher et al., 2019). The gut fungal microbiota has recently been recognized as a novel and important player in the pathophysiology of intestinal and extraintestinal diseases (Huseyin et al., 2017), and is known to have a profound influence in modulating local as well as peripheral immune responses (Li X.V. et al., 2019). Because of the relatively low abundance of fungi in the human gastrointestinal tract (comprising only 2% of the human gut microbiota) (Anandakumar et al., 2019), little is known about their ability to influence human health and disease. With the advent of deep sequencing technologies, the composition and diversity of the fungal microbiota has been revealed, deepening and clarifying our understanding of the roles and mechanisms of intestinal fungi in host homeostasis (Iliev and Leonardi, 2017; Scheffold et al., 2020; Zhang et al., 2020; Zou et al., 2020). Recent studies have unveiled the potential roles that fungi play in modulating host immune homeostasis and inflammatory disease (Standaert-Vitse et al., 2006; Wheeler et al., 2016; Sokol et al., 2017; Yang et al., 2017; Cirstea et al., 2020; Huang et al., 2020; Jiang et al., 2020). However, the fungal microbiota is still a novel and emerging topic of research that continues to lag behind the level of research and understanding we have of the bacteriome. Prior to this study, there have not been any studies focusing on the roles and mechanisms of gut fungal communities in AD, nor in any other neurodegenerative disorder. Nevertheless, the in-depth analysis of the AD-associated fungal microbiota present here might provide novel insights into the development, progression, and treatment of AD.

Fungal species detected in the human body mainly belong to three different phyla: Ascomycota, Basidiomycota, and Zygomycota (Gouba et al., 2013). Most fungal species can be considered commensal or mutualistic, while several yeast and filamentous fungi have been proved to be pathogenic (Parfrey et al., 2011). In the present study, we obtained more than 40,000 reads per sample, allowing us to characterize fungal diversity and composition in depth. In terms of the overall structure of the AD-associated fungal microbiota, we found no significant differences in alpha- and beta-diversity in the stable AD patients compared with the healthy controls. The finding of a lack of alteration to the fungal diversity differs from the alterations to bacterial diversity observed in AD patients; however, the results of the fungal microbiota analysis presented here are consistent with those observed in Parkinson's disease (Cirstea et al., 2020). Other studies of the fungal microbiota in healthy adults have reported similar findings, including that the fungal microbiota is dominated by yeast and exhibits low fungal diversity and abundance, and high inter-individual variability (Nash et al., 2017; Auchtung et al., 2018). Liu et al. (2019) found that fecal microbial diversity decreased in AD patients compared with healthy controls. Given the significant inter-subject variability in our data, PCoA based on the Bray–Curtis, Jaccard, unweighted UniFrac, and weighted UniFrac algorithms was unable to divide the two groups into different clusters. In contrast, a prior study reported significant compositional differences in the intestinal bacteriome between AD patients and healthy controls based on PCoA using the Bray–Curtis dissimilarity (Liu et al., 2019). Thus, the unaltered diversity of the AD-associated fungal microbiota observed in this study might imply that stable AD does not change the overall structure of the fungal microbiota.

In contrast to bacterial 16S analyses, for which well-established, commonly accepted databases of sequences are available, fungal ITS analysis is relatively undeveloped (Tang et al., 2015), with the UNITE database (see text footnote 1) probably being the most commonly used fungal ITS database. Overall, we were able to classify our fungal ITS reads into different taxonomic levels, but for many of these reads, it was not possible to assign them into specific taxa based on the UNITE database. In the present study, we identified three phyla in the AD-associated fungal microbiota, including Ascomycota, Basidiomycota, and Zygomycota, with most of sequences being assigned to the phylum Ascomycota. Recently, Coker et al. demonstrated that the Ascomycota/Basidiomycota ratio can be considered to be an indicator of fungal dysbiosis (Coker et al., 2019). However, in the present study, we found no significant difference in the Ascomycota/Basidiomycota ratio between the stable AD patients and the healthy controls. This may relate to the stable AD status of the patients, who were not receiving drug treatment. At the genus level, eight genera, namely *Candida*, *Aspergillus*, *Debaryomyces*, *Trichosporon*, *Wickerhamomyces*, *Schizophyllum*, *Phlebia*, and *Asterotremella* were the most abundant in the fecal fungal microbiota and exhibited different levels of prevalence in the AD patients compared with the healthy controls. Specifically, we found that *Aspergillus*, *Schizophyllum*, and *Epicoccum* were enriched in the AD patients, while *Rhodotorula*, *Millerozyma*, *Sporobolomyces*, *Bullera*, *Hannaella*, *Kazachstania*, and *Tilletiopsis* were more prevalent in the healthy controls. These alterations to fungal microbiota composition suggest fungal dysbiosis in the AD-associated fungal microbiota. Furthermore, LEfSe analysis identified several AD-enriched fungal species, including *C. tropicalis*, *Trametes versicolor*, *S. commune*, *Davidiella tassiana*, *Exophiala dermatitidis*, and *Erythrobasidium hasegawianum*, which belong to the genera mentioned above. In contrast, other species, such as *C. parapsilosis*, *Hannaella* sp. CMON52, *C. apicola*, and *R. mucilaginosa*, were prevalent in the healthy controls. Taken together, these species could be used as potential biomarkers for the non-invasive diagnosis of AD. As with bacteria, fungi can be beneficial to host immunity, but they can also exert deleterious effects under pathological conditions associated with disease. Among the altered fungal species identified in the present study, *C. tropicalis*, which is one of the most abundant pathogenic species in the central nervous system (Sanches et al., 2019), was found to be increased significantly in AD patients. Furthermore, we found that the abundance of *C. tropicalis* was negatively correlated with levels of IL-8 and IFN-γ, and positively correlated with those of IP-10 and TNF-α. Our data suggest that *C. tropicalis* might participate in actively regulating the host systemic immune response. Similarly, *S. commune*, a sap-rot Basidiomycota and cosmopolitan species, also exhibited immunomodulatory properties. As with *C. tropicalis*, we found that the enriched

abundance of *S. commune* in AD patients correlated positively with levels of IP-10 and TNF-α. In contrast, the abundance of another species, *R. mucilaginosa*, was reduced significantly in the AD-associated fungal microbiota. Our correlation analysis found that the abundance of *R. mucilaginosa* correlated negatively with the level of TNF-α. In addition, the inferred function of the fungal microbiota also changed significantly in the AD patients. Five KEGG pathways were significantly decreased in AD patients, namely: "lipoic acid metabolism," "cell cycle – Caulobacter," "starch and sucrose metabolism," "lysine degradation," and "phosphotransferase system (PTS)." Previous studies have demonstrated that lipoic acid can function as a novel anti-inflammatory and neuroprotective treatment for AD and related dementias (Holmquist et al., 2007; Maczurek et al., 2008; Sancheti et al., 2014). Sun C. et al. (2020) found that the biological pathway "starch and sucrose metabolism" was associated with serum metabolomic biomarkers that were able to distinguish AD patients from healthy controls. Of course, the relationships between alterations to key functional fungi (especially non-abundant fungi) or inferred functions and AD are still unclear. Collectively, alterations to the composition of the fungal gut microbiota, especially to key functional fungi, and changes in inferred functions actively participate in the development and progression of AD by regulating the host immune response and modulating host metabolic processes.

This study of the fungal microbiota in AD is the first to be conducted, but it did have several limitations. Firstly, the fungal ITS sequencing-based community analysis targeted ITS3/ITS4 with specific PCR primers, which successfully enabled ITS sequencing reads with an average length of nearly 350 bp. However, many ITS sequences could not be correctly annotated and were instead simply annotated as "fungi," which affected the subsequent analyses of these data. Longer ITS sequences, metagenomic sequences, or the use of well-established fungal databases might help to improve taxonomic assignment. Secondly, most of the fungi identified belonged to non-abundant fungal taxa (with low relative abundance) and could not be detected in all samples, exhibiting a low detection rate. The significant inter-subject variations might have influenced the identification of clinically important fungal species. Thirdly, contamination from food could not be completely excluded in the process of collecting feces; thus, several of the fungal species identified might be associated with the food supplement. Fourthly, AD patients with a newly diagnosed onset were not enrolled in our study. Including these patients in the study might have allowed changes in the abundance patterns of the fungal microbiota to be understood more clearly.

In summary, the present study was the first to analyze the fungal microbiota in AD patients. Although fecal fungal diversity did not change significantly between the AD patients and the healthy controls, the composition of the fungal microbiota was significantly altered. Several key fungal species, including *C. tropicalis*, *Trametes versicolor*, *S. commune*, *Davidiella tassiana*, *Exophiala dermatitidis*, *Erythrobasidium hasegawianum*, were enriched in the AD-associated fungal microbiota, while abundances of *C. parapsilosis*, *Hannaella* sp. CMON52, *C. apicola*, and *R. mucilaginosa* clearly decreased. Key functional fungi, such as *C. tropicalis*, *S. commune*, and *R. mucilaginosa*, were shown to actively participate in regulating the host systemic immune response. The large, case–control study presented here provides novel insights in the etiopathogenesis of AD and paves the way for improved diagnosis and treatment of AD in the future.

DATA AVAILABILITY STATEMENT

The original contributions presented in the study are publicly available. This data can be found here: GenBank Sequence Read Archive with the accession number SRP292858.

ETHICS STATEMENT

The studies involving human participants were reviewed and approved by the Ethics Committee of Lishui Second People's Hospital (Zhejiang, China). The patients/participants provided their written informed consent to participate in this study.

AUTHOR CONTRIBUTIONS

ZL, SW, and MZ conceived and designed the experiments. ZL, XY, YC, LS, XL, RJ, and MZ performed the experiments. ZL, XY, LS, and MZ analyzed the data. ZL, XL, and LS wrote and edited the manuscript. All authors read and approved the final manuscript.

FUNDING

This work was funded by the grants of the National Natural Science Foundation of China (81771724, 31700800, and 81790631), National S&T Major Project of China (2018YFC2000500), S&T Major Project of Lishui (2017YSKZ-01 and 2017ZDYF04), Lishui & ZJU Cooperation Project (2018zdhz07), and Foundation of China's State Key Laboratory for Diagnosis and Treatment of Infectious Diseases.

ACKNOWLEDGMENTS

The authors thank all of the participants who recruited patients in this study.

REFERENCES

Abarenkov, K., Henrik Nilsson, R., Larsson, K. H., Alexander, I. J., Eberhardt, U., Erland, S., et al. (2010). The UNITE database for molecular identification of fungi–recent updates and future perspectives. *New Phytol.* 186, 281–285. doi: 10.1111/j.1469-8137.2009.03160.x

Alzheimer's Association (2020). 2020 Alzheimer's disease facts and figures. *Alzheimers Dement.* 16, 391–460. doi: 10.1002/alz.12068

Anandakumar, A., Pellino, G., Tekkis, P., and Kontovounisios, C. (2019). Fungal microbiome in colorectal cancer: a systematic review. *Updates Surg.* 71, 625–630. doi: 10.1007/s13304-019-00683-8

Auchtung, T. A., Fofanova, T. Y., Stewart, C. J., Nash, A. K., Wong, M. C., Gesell, J. R., et al. (2018). Investigating colonization of the healthy adult gastrointestinal tract by fungi. *mSphere* 3:e00092-18. doi: 10.1128/mSphere.00092-18

Bacher, P., Hohnstein, T., Beerbaum, E., Röcker, M., Blango, M. G., Kaufmann, S., et al. (2019). Human Anti-fungal Th17 immunity and pathology rely on cross-reactivity against *Candida albicans*. *Cell* 176, 1340.e15–1355.e15. doi: 10.1016/j.cell.2019.01.041

Brookmeyer, R., Johnson, E., Ziegler-Graham, K., and Arrighi, H. M. (2007). Forecasting the global burden of Alzheimer's disease. *Alzheimers Dement.* 3, 186–191. doi: 10.1016/j.jalz.2007.04.381

Caporaso, J. G., Kuczynski, J., Stombaugh, J., Bittinger, K., Bushman, F. D., Costello, E. K., et al. (2010). QIIME allows analysis of high-throughput community sequencing data. *Nat. Methods* 7, 335–336. doi: 10.1038/nmeth.f.303

Chen, W. T., Lu, A., Craessaerts, K., Pavie, B., Sala Frigerio, C., Corthout, N., et al. (2020). Spatial transcriptomics and in situ sequencing to study Alzheimer's Disease. *Cell* 182, 976.e19–991.e19. doi: 10.1016/j.cell.2020.06.038

Chin, V. K., Yong, V. C., Chong, P. P., Amin Nordin, S., Basir, R., and Abdullah, M. (2020). Mycobiome in the gut: a multiperspective review. *Mediators Inflamm.* 2020:9560684. doi: 10.1155/2020/9560684

Cirstea, M. S., Sundvick, K., Golz, E., Yu, A. C., Boutin, R. C. T., Kliger, D., et al. (2020). The gut mycobiome in Parkinson's disease. *J. Parkinsons Dis.* (in press). doi: 10.3233/jpd-202237

Coker, O. O., Nakatsu, G., Dai, R. Z., Wu, W. K. K., Wong, S. H., Ng, S. C., et al. (2019). Enteric fungal microbiota dysbiosis and ecological alterations in colorectal cancer. *Gut* 68, 654–662. doi: 10.1136/gutjnl-2018-317178

Degnan, P. H., and Ochman, H. (2012). Illumina-based analysis of microbial community diversity. *ISME J.* 6, 183–194. doi: 10.1038/ismej.2011.74

Edgar, R. C. (2010). Search and clustering orders of magnitude faster than BLAST. *Bioinformatics* 26, 2460–2461. doi: 10.1093/bioinformatics/btq461

Edgar, R. C., Haas, B. J., Clemente, J. C., Quince, C., and Knight, R. (2011). UCHIME improves sensitivity and speed of chimera detection. *Bioinformatics* 27, 2194–2200. doi: 10.1093/bioinformatics/btr381

Forbes, J. D., Bernstein, C. N., Tremlett, H., Van Domselaar, G., and Knox, N. C. (2018). A Fungal world: could the gut mycobiome be involved in neurological disease? *Front. Microbiol.* 9:3249. doi: 10.3389/fmicb.2018.03249

Gaugler, J., James, B., Johnson, T., Marin, A., Weuve, J., and Alzheimer's disease (2019). 2019 Alzheimer's disease facts and figures. *Alzheimers Dement.* 15, 321–387. doi: 10.1016/j.jalz.2019.01.010

Good, I. J. (1953). The population frequencies of species and the estimation of population parameters. *Biometrika* 40, 237–264. doi: 10.2307/2333344

Gouba, N., Raoult, D., and Drancourt, M. (2013). Plant and fungal diversity in gut microbiota as revealed by molecular and culture investigations. *PLoS One* 8:e59474. doi: 10.1371/journal.pone.0059474

Hamad, I., Ranque, S., Azhar, E. I., Yasir, M., Jiman-Fatani, A. A., Tissot-Dupont, H., et al. (2017). Culturomics and amplicon-based metagenomic approaches for the study of fungal population in human gut microbiota. *Sci. Rep.* 7:16788. doi: 10.1038/s41598-017-17132-4

Hoarau, G., Mukherjee, P. K., Gower-Rousseau, C., Hager, C., Chandra, J., Retuerto, M. A., et al. (2016). Bacteriome and mycobiome interactions underscore microbial dysbiosis in familial Crohn's Disease. *mBio* 7:e01250-16. doi: 10.1128/mBio.01250-16

Holmquist, L., Stuchbury, G., Berbaum, K., Muscat, S., Young, S., Hager, K., et al. (2007). Lipoic acid as a novel treatment for Alzheimer's disease and related dementias. *Pharmacol. Ther.* 113, 154–164. doi: 10.1016/j.pharmthera.2006.07.001

Honig, L. S., Vellas, B., Woodward, M., Boada, M., Bullock, R., Borrie, M., et al. (2018). Trial of solanezumab for mild dementia due to Alzheimer's Disease. *N. Engl. J. Med.* 378, 321–330. doi: 10.1056/NEJMoa1705971

Huang, C., Yu, Y., Du, W., Liu, Y., Dai, R., Tang, W., et al. (2020). Fungal and bacterial microbiome dysbiosis and imbalance of trans-kingdom network in asthma. *Clin. Transl. Allergy.* 10:42. doi: 10.1186/s13601-020-00345-8

Huseyin, C. E., O'Toole, P. W., Cotter, P. D., and Scanlan, P. D. (2017). Forgotten fungi-the gut mycobiome in human health and disease. *FEMS Microbiol. Rev.* 41, 479–511. doi: 10.1093/femsre/fuw047

Iliev, I. D., and Cadwell, K. (2020). Effects of intestinal fungi and viruses on immune responses and inflammatory bowel diseases. *Gastroenterology* S0016-5085, 35564–35565. doi: 10.1053/j.gastro.2020.06.100

Iliev, I. D., and Leonardi, I. (2017). Fungal dysbiosis: immunity and interactions at mucosal barriers. *Nat. Rev. Immunol.* 17, 635–646. doi: 10.1038/nri.2017.55

Jayasudha, R., Das, T., Kalyana Chakravarthy, S., Sai Prashanthi, G., Bhargava, A., Tyagi, M., et al. (2020). Gut mycobiomes are altered in people with type 2 diabetes mellitus and diabetic retinopathy. *PLoS One* 15:e0243077. doi: 10.1371/journal.pone.0243077

Jiang, L., Stärkel, P., Fan, J. G., Fouts, D. E., Bacher, P., and Schnabl, B. (2020). The gut mycobiome: a novel player in chronic liver diseases. *J. Gastroenterol.* (in press). doi: 10.1007/s00535-020-01740-5

Kinney, J. W., Bemiller, S. M., Murtishaw, A. S., Leisgang, A. M., Salazar, A. M., and Lamb, B. T. (2018). Inflammation as a central mechanism in Alzheimer's disease. *Alzheimers Dement.* 4, 575–590. doi: 10.1016/j.trci.2018.06.014

LaFerla, F. M., Green, K. N., and Oddo, S. (2007). Intracellular amyloid-beta in Alzheimer's disease. *Nat. Rev. Neurosci.* 8, 499–509. doi: 10.1038/nrn2168

Langille, M. G., Zaneveld, J., Caporaso, J. G., McDonald, D., Knights, D., Reyes, J. A., et al. (2013). Predictive functional profiling of microbial communities using 16S rRNA marker gene sequences. *Nat. Biotechnol.* 31, 814–821. doi: 10.1038/nbt.2676

Lemoinne, S., Kemgang, A., Ben Belkacem, K., Straube, M., Jegou, S., Corpechot, C., et al. (2020). Fungi participate in the dysbiosis of gut microbiota in patients with primary sclerosing cholangitis. *Gut* 69, 92–102. doi: 10.1136/gutjnl-2018-317791

Leonardi, I., Li, X., Semon, A., Li, D., Doron, I., Putzel, G., et al. (2018). CX3CR1(+) mononuclear phagocytes control immunity to intestinal fungi. *Science* 359, 232–236. doi: 10.1126/science.aao1503

Li, B. Y., He, Y. X., Ma, J. F., Huang, P., Du, J. J., Cao, L., et al. (2019). Mild cognitive impairment has similar alterations as Alzheimer's disease in gut microbiota. *Alzheimers Dement.* 15, 1357–1366. doi: 10.1016/j.jalz.2019.07.002

Li, X. V., Leonardi, I., and Iliev, I. D. (2019). Gut Mycobiota in Immunity and Inflammatory Disease. *Immunity* 50, 1365–1379. doi: 10.1016/j.immuni.2019.05.023

Ling, Z., Shao, L., Liu, X., Cheng, Y., Yan, C., Mei, Y., et al. (2019). Regulatory T cells and plasmacytoid dendritic cells within the tumor microenvironment in gastric cancer are correlated with gastric microbiota dysbiosis: a preliminary study. *Front. Immunol.* 10:533. doi: 10.3389/fimmu.2019.00533

Liu, P., Wu, L., Peng, G., Han, Y., Tang, R., Ge, J., et al. (2019). Altered microbiomes distinguish Alzheimer's disease from amnestic mild cognitive impairment and health in a Chinese cohort. *Brain Behav. Immun.* 80, 633–643. doi: 10.1016/j.bbi.2019.05.008

Lozupone, C., and Knight, R. (2005). UniFrac: a new phylogenetic method for comparing microbial communities. *Appl. Environ. Microbiol.* 71, 8228–8235. doi: 10.1128/AEM.71.12.8228-8235.2005

Maczurek, A., Hager, K., Kenklies, M., Sharman, M., Martins, R., Engel, J., et al. (2008). Lipoic acid as an anti-inflammatory and neuroprotective treatment for Alzheimer's disease. *Adv. Drug Deliv. Rev.* 60, 1463–1470. doi: 10.1016/j.addr.2008.04.015

Marchesi, J. R. (2010). Prokaryotic and eukaryotic diversity of the human gut. *Adv. Appl. Microbiol.* 72, 43–62. doi: 10.1016/s0065-2164(10)72002-5

McDonald, D., Price, M. N., Goodrich, J., Nawrocki, E. P., DeSantis, T. Z., Probst, A., et al. (2012). An improved Greengenes taxonomy with explicit ranks for ecological and evolutionary analyses of bacteria and archaea. *ISME J.* 6, 610–618. doi: 10.1038/ismej.2011.139

Nash, A. K., Auchtung, T. A., Wong, M. C., Smith, D. P., Gesell, J. R., Ross, M. C., et al. (2017). The gut mycobiome of the human microbiome project healthy cohort. *Microbiome* 5:153. doi: 10.1186/s40168-017-0373-4

Navas-Molina, J. A., Peralta-Sanchez, J. M., Gonzalez, A., McMurdie, P. J., Vazquez-Baeza, Y., Xu, Z. J., et al. (2013). Advancing our understanding of the human microbiome using QIIME. *Method Enzymol.* 531, 371–444. doi: 10.1016/B978-0-12-407863-5.00019-8

Ni, J., Wu, G. D., Albenberg, L., and Tomov, V. T. (2017). Gut microbiota and IBD: causation or correlation? *Nat. Rev. Gastroenterol. Hepatol.* 14, 573–584. doi: 10.1038/nrgastro.2017.88

Parfrey, L. W., Walters, W. A., and Knight, R. (2011). Microbial eukaryotes in the human microbiome: ecology, evolution, and future directions. *Front. Microbiol.* 2:153. doi: 10.3389/fmicb.2011.00153

Parks, D. H., Tyson, G. W., Hugenholtz, P., and Beiko, R. G. (2014). STAMP: statistical analysis of taxonomic and functional profiles. *Bioinformatics* 30, 3123–3124. doi: 10.1093/bioinformatics/btu494

Qiu, X., Zhao, X., Cui, X., Mao, X., Tang, N., Jiao, C., et al. (2020). Characterization of fungal and bacterial dysbiosis in young adult Chinese patients with Crohn's disease. *Therap. Adv. Gastroenterol.* 13:1756284820971202. doi: 10.1177/1756284820971202

Sam, Q. H., Chang, M. W., and Chai, L. Y. (2017). The fungal mycobiome and its interaction with gut bacteria in the host. *Int. J. Mol. Sci.* 18:330. doi: 10.3390/ijms18020330

Sanches, M. D., Mimura, L. A. N., Oliveira, L. R. C., Ishikawa, L. L. W., Garces, H. G., Bagagli, E., et al. (2019). Differential behavior of non-albicans *Candida* species in the central nervous system of immunocompetent and immunosuppressed mice. *Front. Microbiol.* 9:2968. doi: 10.3389/fmicb.2018.02968

Sancheti, H., Kanamori, K., Patil, I., Díaz Brinton, R., Ross, B. D., and Cadenas, E. (2014). Reversal of metabolic deficits by lipoic acid in a triple transgenic mouse model of Alzheimer's disease: a 13C NMR study. *J. Cereb. Blood Flow Metab.* 34, 288–296. doi: 10.1038/jcbfm.2013.196

Scheffold, A., Bacher, P., and LeibundGut-Landmann, S. (2020). T cell immunity to commensal fungi. *Curr. Opin Microbiol.* 58, 116–123. doi: 10.1016/j.mib.2020.09.008

Scheltens, P., Blennow, K., Breteler, M. M., de Strooper, B., Frisoni, G. B., Salloway, S., et al. (2016). Alzheimer's disease. *Lancet* 388, 505–517. doi: 10.1016/s0140-6736(15)01124-1

Schloss, P. D., Westcott, S. L., Ryabin, T., Hall, J. R., Hartmann, M., Hollister, E. B., et al. (2009). Introducing mothur: open-source, platform-independent, community-supported software for describing and comparing microbial communities. *Appl. Environ. Microbiol.* 75, 7537–7541. doi: 10.1128/Aem.01541-09

Segata, N., Izard, J., Waldron, L., Gevers, D., Miropolsky, L., Garrett, W. S., et al. (2011). Metagenomic biomarker discovery and explanation. *Genome Biol.* 12:R60. doi: 10.1186/gb-2011-12-6-r60

Sepulcre, J., Grothe, M. J., d'Oleire Uquillas, F., Ortiz-Terán, L., Diez, I., Yang, H. S., et al. (2018). Neurogenetic contributions to amyloid beta and tau spreading in the human cortex. *Nat. Med.* 24, 1910–1918. doi: 10.1038/s41591-018-0206-4

Sokol, H., Leducq, V., Aschard, H., Pham, H. P., Jegou, S., Landman, C., et al. (2017). Fungal microbiota dysbiosis in IBD. *Gut* 66, 1039–1048. doi: 10.1136/gutjnl-2015-310746

Standaert-Vitse, A., Jouault, T., Vandewalle, P., Mille, C., Seddik, M., Sendid, B., et al. (2006). *Candida albicans* is an immunogen for anti-*Saccharomyces cerevisiae* antibody markers of Crohn's disease. *Gastroenterology* 130, 1764–1775. doi: 10.1053/j.gastro.2006.02.009

Sun, C., Gao, M., Wang, F., Yun, Y., Sun, Q., Guo, R., et al. (2020). Serum metabolomic profiling in patients with Alzheimer disease and amnestic mild cognitive impairment by GC/MS. *Biomed. Chromatogr.* 34:e4875. doi: 10.1002/bmc.4875

Sun, J., Xu, J., Yang, B., Chen, K., Kong, Y., Fang, N., et al. (2020). Effect of clostridium butyricum against microglia-mediated neuroinflammation in Alzheimer's Disease via regulating gut microbiota and metabolites butyrate. *Mol. Nutr. Food Res.* 64:e1900636. doi: 10.1002/mnfr.201900636

Sun, J., Liu, S. Z., Ling, Z. X., Wang, F. Y., Ling, Y., Gong, T. Y., et al. (2019a). Fructooligosaccharides ameliorating cognitive deficits and neurodegeneration in APP/PS1 Transgenic mice through modulating gut microbiota. *J. Agrc. Food Chem.* 67, 3006–3017. doi: 10.1021/acs.jafc.8b07313

Sun, J., Xu, J., Ling, Y., Wang, F., Gong, T., Yang, C., et al. (2019b). Fecal microbiota transplantation alleviated Alzheimer's disease-like pathogenesis in APP/PS1 transgenic mice. *Transl. Psychiatry* 9:189. doi: 10.1038/s41398-019-0525-3

Tang, J., Iliev, I. D., Brown, J., Underhill, D. M., and Funari, V. A. (2015). Mycobiome: approaches to analysis of intestinal fungi. *J. Immunol. Methods* 421, 112–121. doi: 10.1016/j.jim.2015.04.004

van Tilburg Bernardes, E., Gutierrez, M. W., and Arrieta, M. C. (2020). The fungal microbiome and asthma. *Front. Cell Infect. Microbiol.* 10:583418. doi: 10.3389/fcimb.2020.583418

Ventin-Holmberg, R., Eberl, A., Saqib, S., Korpela, K., Virtanen, S., Sipponen, T., et al. (2020). Bacterial and fungal profiles as markers of infliximab drug response in inflammatory bowel disease. *J. Crohns Colitis* jjaa252. (in press). doi: 10.1093/ecco-jcc/jjaa252

Vogt, N. M., Kerby, R. L., Dill-McFarland, K. A., Harding, S. J., Merluzzi, A. P., Johnson, S. C., et al. (2017). Gut microbiome alterations in Alzheimer's disease. *Sci. Rep. U. K.* 7:13537. doi: 10.1038/S41598-017-13601-Y

Wan, Y. W., Al-Ouran, R., Mangleburg, C. G., Perumal, T. M., Lee, T. V., Allison, K., et al. (2020). Meta-analysis of the Alzheimer's disease human brain transcriptome and functional dissection in mouse models. *Cell Rep.* 32:107908. doi: 10.1016/j.celrep.2020.107908

Wang, X., Sun, G., Feng, T., Zhang, J., Huang, X., Wang, T., et al. (2019). Sodium oligomannate therapeutically remodels gut microbiota and suppresses gut bacterial amino acids-shaped neuroinflammation to inhibit Alzheimer's disease progression. *Cell Res.* 29, 787–803. doi: 10.1038/s41422-019-0216-x

Wheeler, M. L., Limon, J. J., Bar, A. S., Leal, C. A., Gargus, M., Tang, J., et al. (2016). Immunological consequences of intestinal fungal dysbiosis. *Cell Host Microbe* 19, 865–873. doi: 10.1016/j.chom.2016.05.003

Yang, A. M., Inamine, T., Hochrath, K., Chen, P., Wang, L., Llorente, C., et al. (2017). Intestinal fungi contribute to development of alcoholic liver disease. *J. Clin. Invest.* 127, 2829–2841. doi: 10.1172/jci90562

Zhang, C. B., Ren, C. H., Wang, Y. L., Wang, Q. Q., Wang, Y. S., and Weng, Q. B. (2020). Uncovering fungal community composition in natural habitat of *Ophiocordyceps sinensis* using high-throughput sequencing and culture-dependent approaches. *BMC Microbiol.* 20:331. doi: 10.1186/s12866-020-01994-2

Zhuang, Z. Q., Shen, L. L., Li, W. W., Fu, X., Zeng, F., Gui, L., et al. (2018). Gut microbiota is altered in patients with Alzheimer's Disease. *J. Alzheimers Dis.* 63, 1337–1346. doi: 10.3233/Jad-180176

Zou, R., Wang, Y., Duan, M., Guo, M., Zhang, Q., and Zheng, H. (2020). Dysbiosis of gut fungal microbiota in children with autism spectrum disorders. *J. Autism. Dev. Disord.* (in press). doi: 10.1007/s10803-020-04543-y

Conflict of Interest: The authors declare that the research was conducted in the absence of any commercial or financial relationships that could be construed as a potential conflict of interest.

frontiers in Cell and Developmental Biology

ORIGINAL RESEARCH
published: 05 February 2021
doi: 10.3389/fcell.2020.624339

Dauricine Attenuates Spatial Memory Impairment and Alzheimer-Like Pathologies by Enhancing Mitochondrial Function in a Mouse Model of Alzheimer's Disease

Chongyang Chen[1†], Pan Liu[1†], Jing Wang[1], Haitao Yu[1], Zaijun Zhang[2], Jianjun Liu[1], Xiao Chen[1], Feiqi Zhu[3] and Xifei Yang[1*]*

[1] Shenzhen Key Laboratory of Modern Toxicology, Shenzhen Medical Key Discipline of Health Toxicology (2020-2024), Shenzhen Center for Disease Control and Prevention, Shenzhen, China, [2] Key Laboratory of Innovative Chemical Drug Research in Cardio-Cerebrovascular Diseases, Institute of New Drug Research and Guangzhou, Jinan University College of Pharmacy, Guangzhou, China, [3] Cognitive Impairment Ward of Neurology Department, The Third Affiliated Hospital of Shenzhen University Medical College, Shenzhen, China

Alzheimer's disease (AD) is characterized by extracellular amyloid plaques composed of β-amyloid (Aβ) and intracellular neurofibrillary tangles containing hyperphosphorylated tau protein. No effective therapy is available for this disease. In this study, we investigated the potential therapeutic effects of dauricine (DAU), a benzyl tetrahydroisoquinoline alkaloid, on AD, and found that DAU administration significantly improved cognitive impairments in 3xTg-AD mice by decreasing Aβ plaques and hyperphosphorylated tau and increasing the hippocampal ATP level. Proteomic and western blot analyses revealed that DAU treatment mainly modified the expression of proteins involved in mitochondrial energy metabolism, such as Aco2, Ndufs1, Cox5a, and SDHB, and that of synapse-related proteins such as Syn1 and Syn2. Pathway analysis revealed that DAU modulated the tricarboxylic acid cycle, synaptic vesicle cycle, glycolysis, and gluconeogenesis in 3xTg-AD mice. Our study suggests that DAU may be a potential drug for the treatment of AD.

Keywords: Alzheimer's disease, dauricine, proteomics, mitochondrial function, synaptic function

OPEN ACCESS

Edited by:
Gong-Ping Liu, Huazhong University of Science and Technology, China

Reviewed by:
Keqiang Ye, Emory University, United States
Xiaochuan Wang, Huazhong University of Science and Technology, China
Fei Liu, New York State Institute for Basic Research in Developmental Disabilities, United States

***Correspondence:**
Xifei Yang
xifeiyang@gmail.com
Feiqi Zhu
zfqzsu2004@aliyun.com

[†]These authors have contributed equally to this work

Specialty section:
This article was submitted to Molecular Medicine, a section of the journal Frontiers in Cell and Developmental Biology

Received: *31 October 2020*
Accepted: *07 December 2020*
Published: *05 February 2021*

Citation:
Chen C, Liu P, Wang J, Yu H, Zhang Z, Liu J, Chen X, Zhu F and Yang X (2021) Dauricine Attenuates Spatial Memory Impairment and Alzheimer-Like Pathologies by Enhancing Mitochondrial Function in a Mouse Model of Alzheimer's Disease. Front. Cell Dev. Biol. 8:624339. doi: 10.3389/fcell.2020.624339

INTRODUCTION

Alzheimer's disease (AD) is an age-dependent neurodegenerative disease. Patients with AD show language obstacle, loss of motor capacity, and inability for self-care as the disease progresses (Burns and Iliffe, 2009). By 2050, the number of people aged 65 and older with AD may rise to 13.8 million (Hebert et al., 2013). Both, the initiation of AD and deterioration in AD, involve protein degradation, inflammation, mitochondrial dysfunction, and synaptic loss (Querfurth and Laferla, 2010; Bonet-Costa et al., 2016). However, single-target drugs designed for these mechanisms have failed in clinical trials (Frautschy and Cole, 2010; Golde et al., 2011). Thus, developing multiple-target drugs may be an alternative strategy, which is more promising for delaying the onset of AD.

Recently, natural compounds with multiple biological activities have aroused widespread interest in the field of AD (Andrade et al., 2019). Dauricine (DAU) is an isoquinoline alkaloid and is extracted from the rootstock of a traditional Chinese medicine, *Menispermum dauricum* DC. In ischemic models, it has been demonstrated that DAU protects neurons and inhibits cell apoptosis by regulating mitochondrial function (Li and Gong, 2007; Wang et al., 2020). In addition, DAU can ameliorate tau hyperphosphorylation (Wang et al., 2005) and promote β-amyloid $(A\beta)_{1-42}$ clearance by releasing bradykinin (Pu et al., 2018). Our group has previously confirmed the neuroprotective effect of DAU on AD model cells (Liu et al., 2018). However, its beneficial effects and the underling mechanisms *in vivo* are unknown and require further investigation in AD animal models.

The present study aimed to investigate whether, and how, DAU could moderate AD pathologies and AD-related learning and memory deficits in an AD mouse model. We found that DAU administration significantly attenuated cognitive impairments in 3xTg-AD mice by decreasing Aβ plaques and hyperphosphorylated tau and increasing the hippocampal ATP level. Mechanically, DAU treatment mainly modified the expression of synapse-related proteins and proteins involved in the mitochondrial energy metabolism. Moreover, pathway analysis showed that DAU modulated glycolysis and gluconeogenesis in 3xTg-AD mice. Our study suggests that DAU may be a potential drug for the treatment of AD.

MATERIALS AND METHODS

Reagents

We purchased DAU (stated purity ≥ 98%) from Shanghai Aladdin Biochemical Technology (CAS: 524-17-4, D115683, Shanghai, China) and have listed the antibodies in **Supplementary Table 1**.

Treatment of Experimental Animals

Triple transgenic AD mice (3xTg-AD; strain: APPSwe, PS1M146V, and TauP301L) and wild-type (WT) mice (strain: B6129SF2/J) were purchased from the Jackson Laboratory (Maine, USA). We intraperitoneally injected 8 month-old female transgenic and wild mice with DAU (1 or 10 mg/kg) and saline of equivalent volume, respectively, for 2 months. Each group comprised 13 mice, and DAU dose was based on a previous study (Jin et al., 2010). The mouse age was based on the pathological stages of 3xTg-AD mice (Oddo et al., 2003). After 2 months of DAU treatment, cognitive abilities of all the animals were assessed. All animals were sacrificed after behavioral tests, for further studies. Animal experiments and manipulation were approved by the Shenzhen Center for Disease Control and Prevention. We made efforts to minimize animal suffering and reduce the number of mice used.

Behavioral Test

Step-Down Passive Avoidance Test

After DAU administration, short-term learning and memory of all mice were evaluated with the step-down passive avoidance test, as previously reported (Kameyama et al., 1986; Zhou et al., 2019). For the training test, each mouse was gently placed on a platform and an electrical shock (36 V) was delivered through grid floor for 5 min. After 24 h, the training and retention tests were performed. Each mouse was placed on the platform and the electrical shock was delivered and all the data were recorded for analysis.

Morris Water Maze Test

After step-down passive avoidance test, hippocampal-dependent spatial learning and memory of all mice were evaluated using the Morris water maze (MWM) test. In brief, mice were trained for 5 consecutive days to find a platform in the water maze. During the training session, each mouse was placed into water, facing the wall, starting from one of the four quadrants, and a computer tracking program was started. The swim time was set to 60 s. The timer was paused once the mouse climbed on the platform. Thereafter, the mouse was removed from the pool. Alternatively, the mouse was placed on the platform for an additional 15 s. The probe trial was performed 6 days after the training session. The platform was removed, and the mouse was allowed to swim freely for 2 min before being removed from the pool. The tracks were recorded by a computer program.

Proteomic Analysis

Protein Preparation and Labeling

After behavioral tests, mice were sacrificed for sample collection. The protocol of proteomic analysis has been reported previously (Huang et al., 2018). Half of the mice hippocampus were lysed in 500 μL DIGE specific lysis buffer for 30 min on ice and centrifuged at 12,000 g for 20 min at 4°C. Thereafter, the supernatant was collected. Each sample supernatant was mixed with lysis buffer to remove salt using a centrifugal filter. After protein quantification, each protein sample was diluted to a final concentration of 5 μg/μL. Thereafter, the sample (5 μL) was labeled with Cy3 or Cy5 in the dark for 30 min. Samples pooled from each group were stained by Cy2, the internal standard. Finally, protein labeling was terminated by adding 10 mM lysine. The labeled protein was mixed into a group and rehydration buffer and 0.002% bromophenol blue were added. Thereafter, they were transferred onto immobilized pH gradient strips.

2-Dimensional Electrophoresis

Briefly, after isoelectric-focusing (IEF), the strips were equilibrated and loaded on the top of 12.5% SDS-PAGE gels. Thereafter, protein separation in the second dimension was performed using an Etan DALTsix electrophoresis system at 15°C. The gels were run at 1 W/gel for 1 h followed by 11 W/gel for 6 h. Finally, gels were scanned using a Typhoon TRIO Variable Mode Imager, with resolution set at 100 μm for image acquisition.

Image Analysis

The DeCyder software package was used for DIGE gel analysis. Briefly, the gel image was imported into the software and processed with the Differential In-gel Analysis. Each protein spot in the Cy3 or Cy5 channel was normalized to the corresponding

spot in the Cy2 channel. The differentially expressed protein spots ($p < 0.05$) were isolated for further study.

In-gel Digestion by Trypsin and Mass Spectrometry

A total of 1-mg protein sample was used for in-gel digestion. In brief, after staining the gels, the differentially expressed spots were manually isolated from the stained gel. A piece from each gel was transferred into a 1.5 mL tube and digested with trypsin at 37°C overnight. The digested peptides were used for mass spectrometry (MS) analysis using an AB SCIEX MALDI-TOF/TOF 5800 mass spectrometer. MASCOT (Matrix Science, UK) was used for database searching against the SwissProt mouse protein database.

Bioinformatics Analysis

The Database for Annotation, Visualization, and Integrated Discovery (DAVID) Bioinformatics Resources 6.8 was used for functional enrichment analysis. Pathway analysis was performed using Wikipathways (https://www.wikipathways.org/) and Kyoto Encyclopedia of Genes and Genomes (KEGG) pathway database (https://www.kegg.jp/kegg/). The protein–protein interaction (PPI) network analysis was visualized using Cytoscape 3.7.1 software.

Western Blot Analysis

The sample was lysed with RIPA lysis buffer. The protein concentration was measured by the BCA method. The sample supernatant was mixed with loading buffer and heated for 10 min at 100°C. Thereafter, samples were separated on an 8–12% SDS–PAGE gel, transferred onto a PVDF membrane, and blocked with 5% skim milk. After blocking, the membranes were incubated with primary antibodies (**Supplementary Table 1**) followed by a secondary antibody. Finally, the membranes were exposed with enhanced chemiluminescence kit and protein quantification was performed using ImageJ software.

Immunohistochemistry Analysis

The mouse brain sections embedded in paraffin were deparaffinized and rehydrated by xylene treatment followed by gradual ethanol treatment (100–70%). Thereafter, the sections were blocked and incubated with a primary antibody, AT8 or 6E10, at 4°C overnight. After incubation with primary antibody, the sections were stained using a DAB kit. The images were observed under a microscope (Olympus BX60, Tokyo, Japan). We used Image-pro plus 6.2 for image quantify analysis.

Detection of the ATP Level

The ATP assay kit (Beyotime, Haimen, China) was used to detect the ATP level in hippocampal tissues. Briefly, samples were extracted using ATP lysis buffer and quantified by the BCA method. The reaction mixture, containing either the sample or standard (100 μL) with ATP detection fluid (100 μL), was incubated at room temperature for 3–5 min. A microplate reader with luminometer function was used to measure the ATP level. The ATP level was calculated as nmol/mg protein.

Statistical Analysis

Data are presented as mean ± standard error of the mean (SEM). Statistical analyses were performed using ANOVA (equal variance) or Welch's ANOVA (unequal variance). SPSS 21.0 software was used for data analysis. A $p < 0.05$ indicated significant difference among the groups.

RESULTS

DAU Treatment Ameliorated Cognitive Impairment in 3xTg-AD Mice

First, we treated 8 month-old 3xTg-AD mice with DAU for 2 months and employed step-down passive avoidance and MWM tests to evaluate the effect of DAU on cognitive function. We found that compared with WT mice, 3xTg-AD mice had a shorter step-down latency and more paw dip counts during the 2 test days, indicating memory deficits in 3xTg-AD mice (**Figures 1A–D**). Interestingly, treatment with 10 mg/kg/d DAU significantly improved cognitive capacity of 3xTg-AD mice, as evidenced by increased step-down latency and less paw dip counts (**Figures 1A–D**). However, treatment with 1 mg/kg/d DAU could only rescue the error numbers and paw dip counts were unchanged (**Figures 1A–D**), indicating partial efficiency at low dosage. Thereafter, we performed MWM test to further evaluate the effect of DAU on spatial memory improvement. No difference was found among the groups during the 5 day training (**Supplementary Figure 1**). However, in the probe trial, DAU treatment at both low and high dosages resulted in robust rescue of memory dysfunction (**Figures 1E–I**). Overall, these data suggested that DAU treatment can improve cognitive capacity of 3xTg-AD mice.

DAU Treatment Reduced Aβ Accumulation and Tau Hyperphosphorylation

Extracellular amyloid plaques of Aβ and intracellular neurofibrillary tangles of hyperphosphorylated tau protein are the two characteristic pathologies in AD brain. Both of them contribute to the cognitive disorder in patients with AD. To explore the effect of DAU on these pathologies, we used 6E10 antibody, which recognizes 1–16 amino acids of Aβ, and AT8 antibody, which recognizes PHF-tau at Ser202/Thr205. Immunohistochemical staining revealed that Aβ accumulation in the hippocampal CA1 and cortical regions was significantly reduced after DAU treatment (10 mg/kg/d) (**Figures 2A,B**). Meanwhile, the positive staining of AT8 significantly reduced in the hippocampal CA1 region (**Figures 2E,F**). Further, Western blot analysis was performed to detect tau phosphorylation at serine 404, 262, and 396, and threonine 231 or unphosphorylated tau (Tau1) (**Figures 2C,D**). In 3xTg-AD mice, compared with vehicle-injected mice, DAU treatment both at 1 and 10 mg/kg/d significantly decreased the level of tau hyperphosphorylation. Interestingly, reversal of tau hyperphosphorylation at pT231 was more efficient with 10 mg/kg/d DAU than 1 mg/kg/d DAU. These data indicated that DAU treatment is beneficial in AD pathologies.

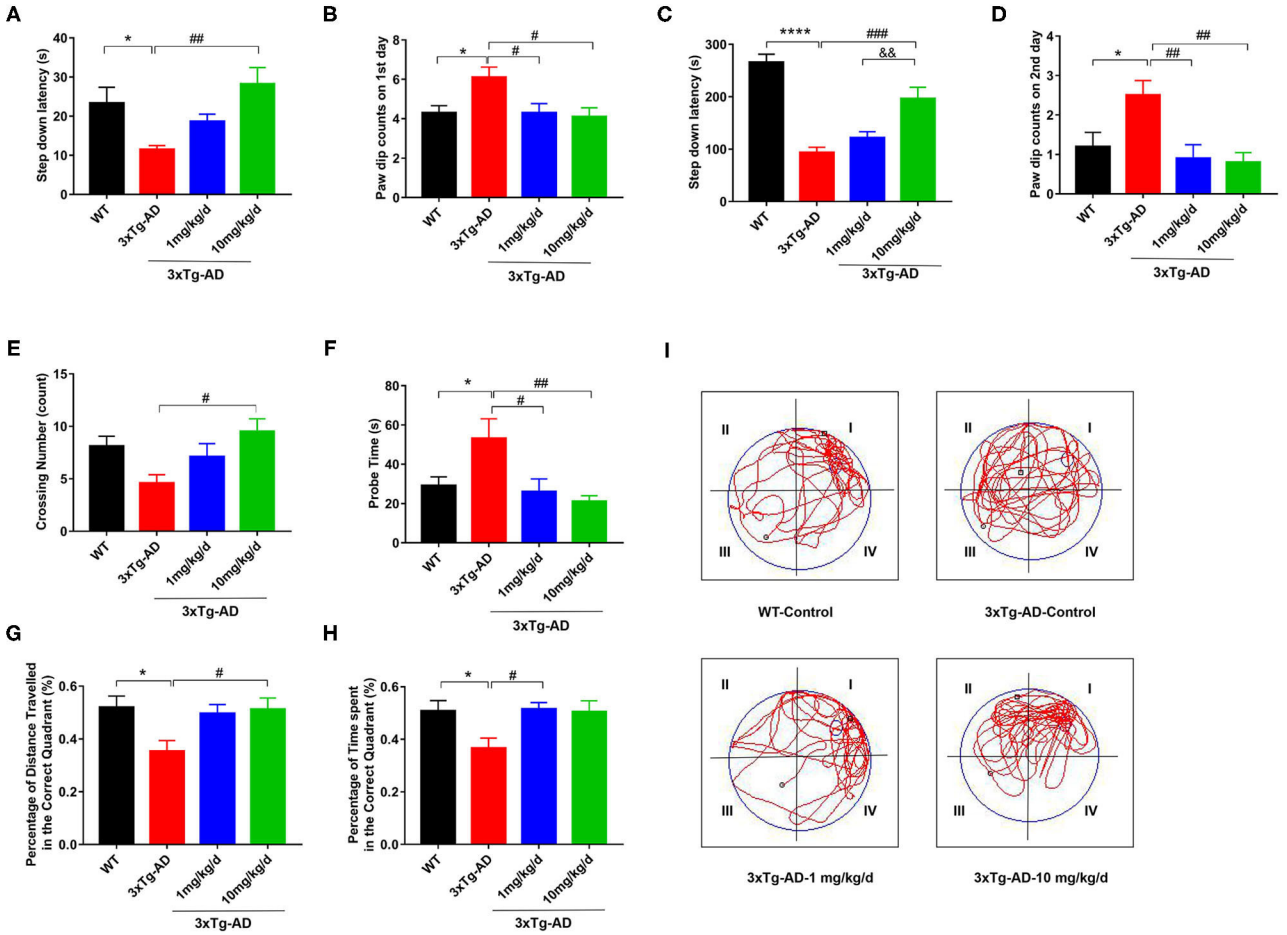

FIGURE 1 | DAU improves the spatial learning and memory abilities of 3xTg-AD mice. **(A,B)** The latency in the retention test and the number of errors on the first day. **(C,D)** The latency in the retention test and the number of errors on the second day. **(E–I)** Morris water maze (MWM) test. **(E)** Crossing number, **(F)** probe time, **(G)** the percentage of distance traveled in the correct quadrant, **(H)** the percentage of time spent in the correct quadrant, and **(I)** the representative swimming path. Data are presented as mean ± SEM. $^{*}p < 0.05$, $^{****}p < 0.0001$ vs. WT saline group. $^{\#}p < 0.05$, $^{\#\#}p < 0.01$, $^{\#\#\#}p < 0.001$ vs. 3xTg-AD saline group. $^{\&\&}p < 0.01$ vs. 3xTg-AD-1 mg/kg/d group. $N = 10$–14 for each group.

Proteomic Analysis Revealed That DAU Treatment Improved Mitochondrial Function

To explore how DAU treatment ameliorated AD pathologies and improved spatial memory, 2D-DIGE separation and MS identification were performed to detect protein changes in the hippocampus of 3xTg-AD mice. We found that 45 proteins were differentially expressed in WT mice compared with 3xTg-AD mice, 51 proteins in 3xTg-AD treated with 1 mg/kg/d DAU compared with 3xTg-AD mice, and 20 proteins in 3xTg-AD mice treated with 10 mg/kg/d DAU compared with 3xTg-AD mice (**Supplementary Table 2**). Heat maps present the change in expression of differentially expressed proteins in different mouse groups (**Supplementary Figure 2**). DAVID was used to determine the biological process and molecular functions of differentially expressed proteins (**Figures 3A–C**). Biological process analysis revealed that differentially expressed proteins were mainly enriched in the tricarboxylic acid (TCA) cycle, ATP metabolic process, glutathione metabolic process, and oxidative stress response process in 3xTg-AD mice, compared with WT mice. Molecular function analysis revealed that these proteins were mainly enriched in nucleotide binding, poly(A) RNA binding, and protein kinase binding (**Figure 3A**). Similarly, differentially expressed proteins were found to be enriched in substantia nigra development, intermediate filament polymerization or depolymerization, neurofilament bundle assembly, regulation of axon diameter, intermediate filament bundle assembly, and axon development by biological process analysis and in ATP binding, protein binding, and poly(A) RNA binding (**Figure 3B**) by molecular function analysis in 3xTg-AD mice treated with 1 mg/kg/d DAU compared with vehicle-treated 3xTg-AD mice. Further, we found that DAU treatment (10 mg/kg/d) resulted in the enrichment of these proteins in the ATP metabolic process, protein folding and transport, ATP biosynthesis, retina homeostasis, and neurotransmitter secretion by biological process analysis, and in nucleotide binding, protein binding, and ATP binding by molecular function

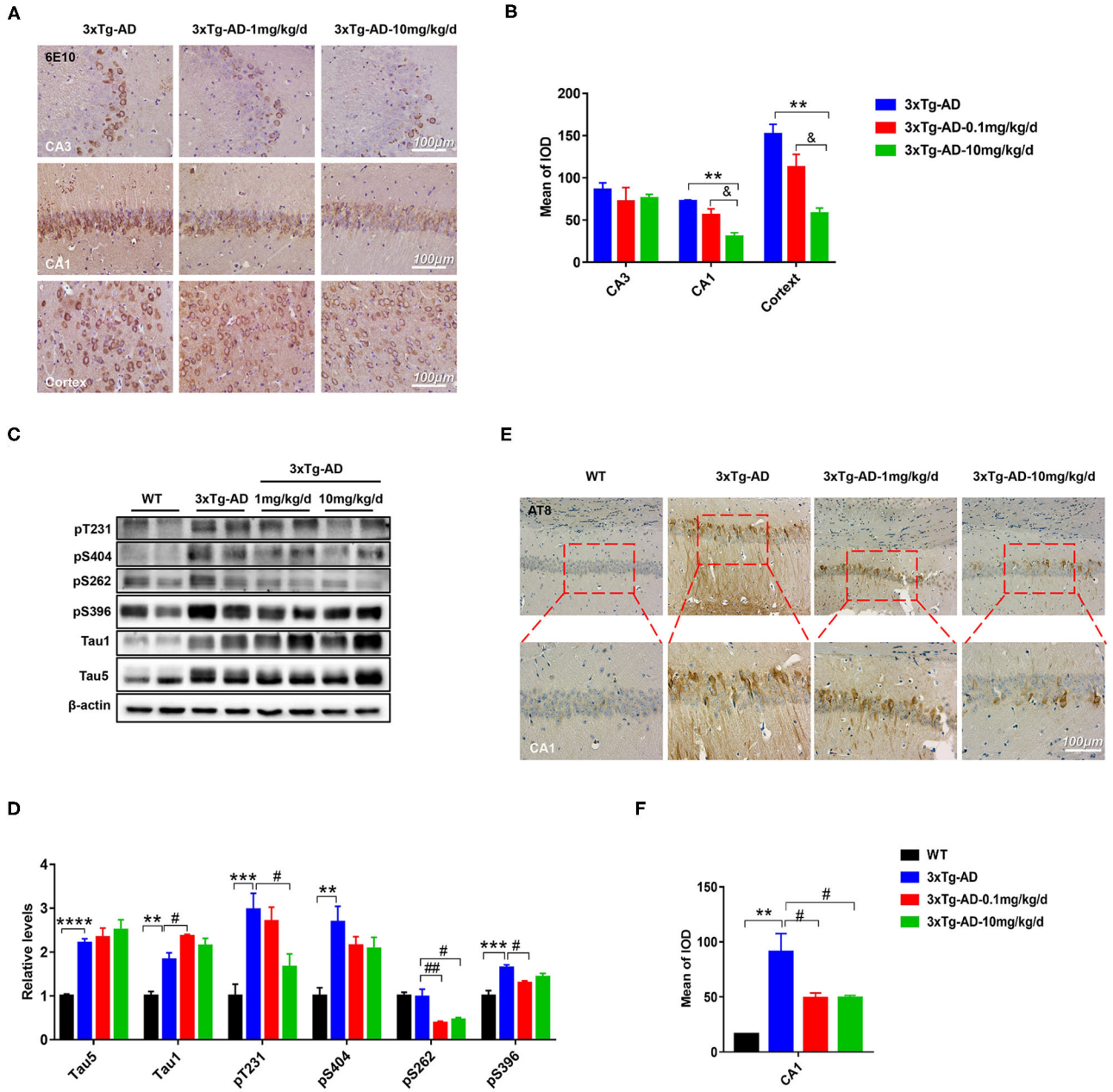

FIGURE 2 | DAU reduced the levels of Aβ and hyperphosphorylated tau in 3xTg-AD mice. **(A,B)** Immunohistochemical staining of the CA1, CA3, and cortex of 3xTg-AD mice with 6E10 and quantitative statistics of positive staining ($n = 3$ per group). **(C,D)** Western blot analysis for the expression level of pT231, p404, p262, p396, Tau1, and Tau5 ($n = 4$ per group). **(E,F)** Immunohistochemical staining of the CA1 region of 3xTg-AD with AT8 and quantitative statistics of positive staining ($n = 3$ per group). Data are presented as mean ± SEM. $^{**}p < 0.01$, $^{***}p < 0.001$, $^{****}p < 0.0001$ vs. WT vehicle group. $^{\#}p < 0.05$, $^{\#\#}p < 0.01$ vs. 3xTg-AD saline group. $^{\&}p < 0.05$ vs. 3xTg-AD-1mg/kg/d group.

analysis (**Figure 3C**). DAVID annotation revealed that the proteins differentially expressed in 3xTg-AD mice, compared with WT mice, were mainly involved in mitochondrial energy metabolism, suggesting a role of mitochondrial dysfunction in AD progression. However, DAU treatment not only rescued abnormal mitochondrial energy metabolism but also improved synaptic function. These results indicated that modifications in mitochondrial function and synaptic function may contribute to the beneficial effects of DAU treatment on AD.

Further, we used String and Wiki pathway databases to analyze PPIs and delineate enriched signaling pathways (**Figures 4**, **5**). The interaction of differential proteins was enriched in synaptic function, pyruvate metabolism, oxidative stress response, and

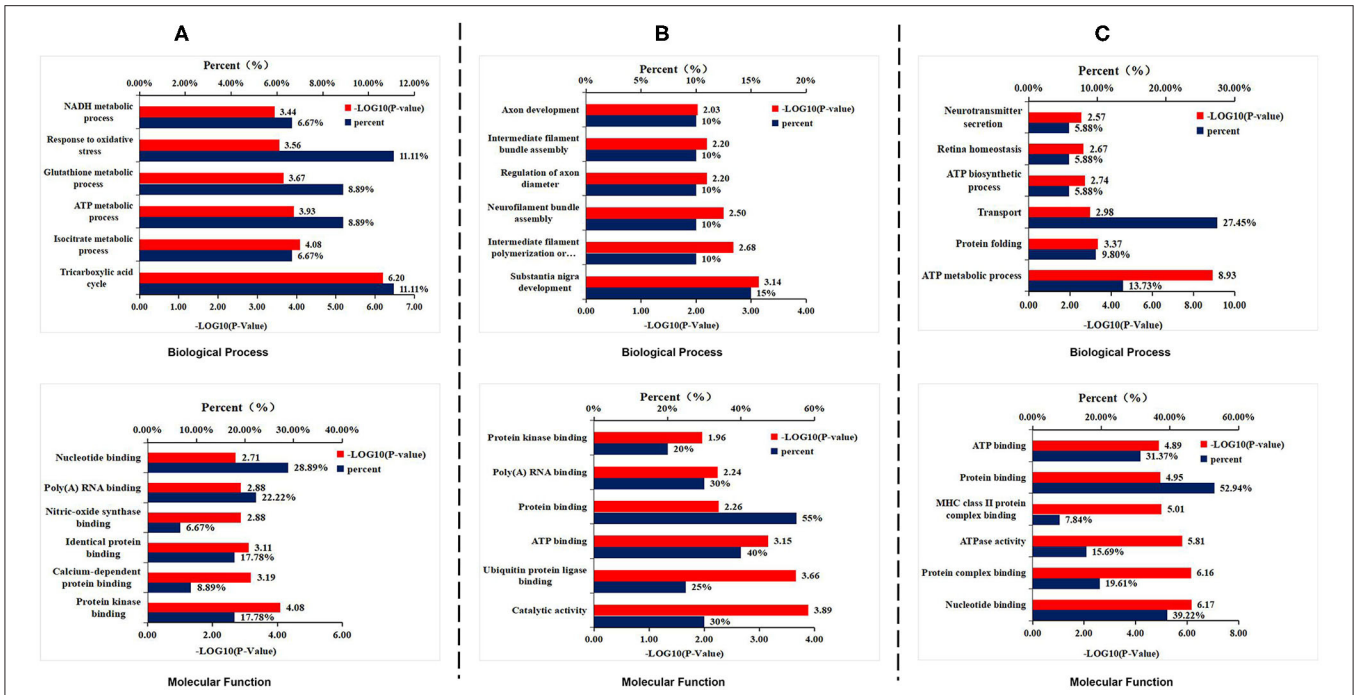

FIGURE 3 | Gene Ontology enrichment analysis for the differentially expressed proteins. **(A)** The biological process and molecular function analyses of the differentially expressed proteins in 3xTg-AD mice. **(B)** 1 mg/kg/d DAU-treated 3xTg-AD mice and **(C)** 10 mg/kg/d DAU-treated 3xTg-AD mice.

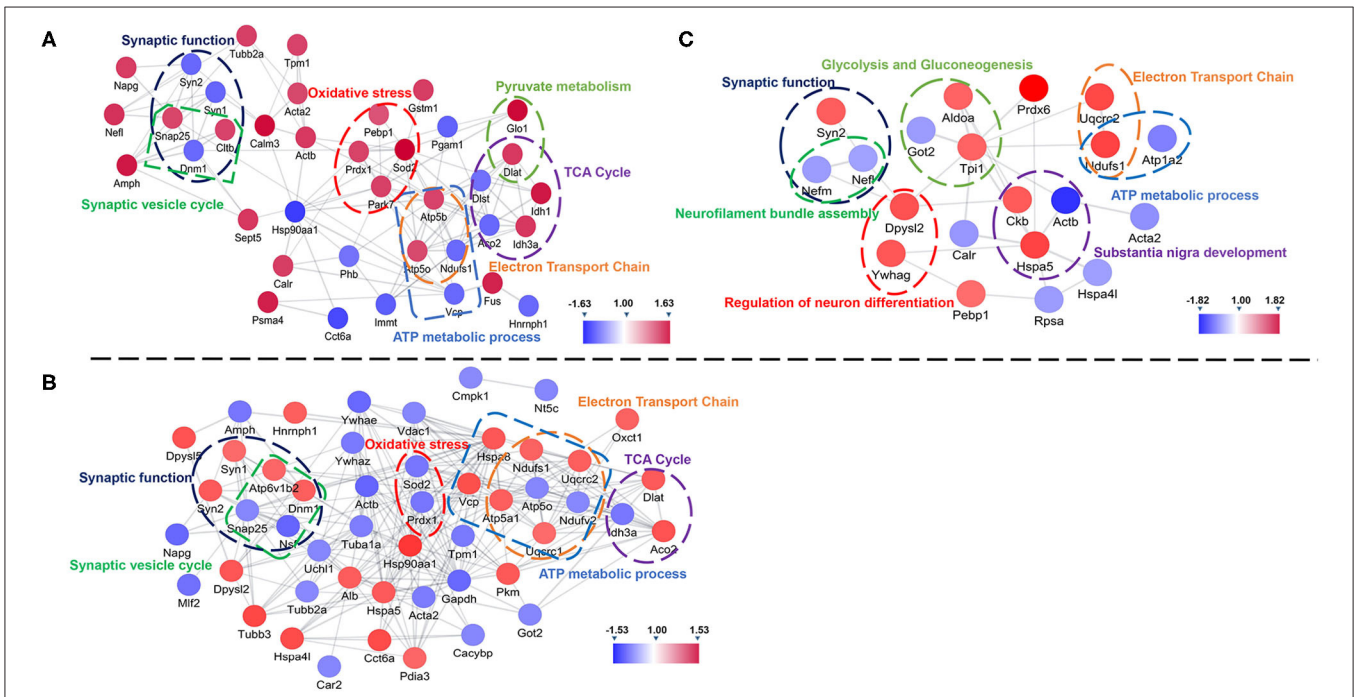

FIGURE 4 | Protein–protein interaction analysis of the differentially expressed proteins using the STRING database. **(A)** The protein–protein interaction (PPI) maps of the differentially expressed proteins in untreated 3xTg-AD mice vs. WT mice. **(B)** The PPI maps of the differentially expressed proteins in 1 mg/kg/d DAU-treated 3xTg-AD mice vs. untreated 3xTg-AD mice. **(C)** The PPI maps of the differentially expressed proteins in 10 mg/kg/d DAU-treated 3xTg-AD mice vs. untreated 3xTg-AD mice. Visualization of PPI maps in Cytoscape 3.7.1 software: green represents downregulation and red represents upregulation.

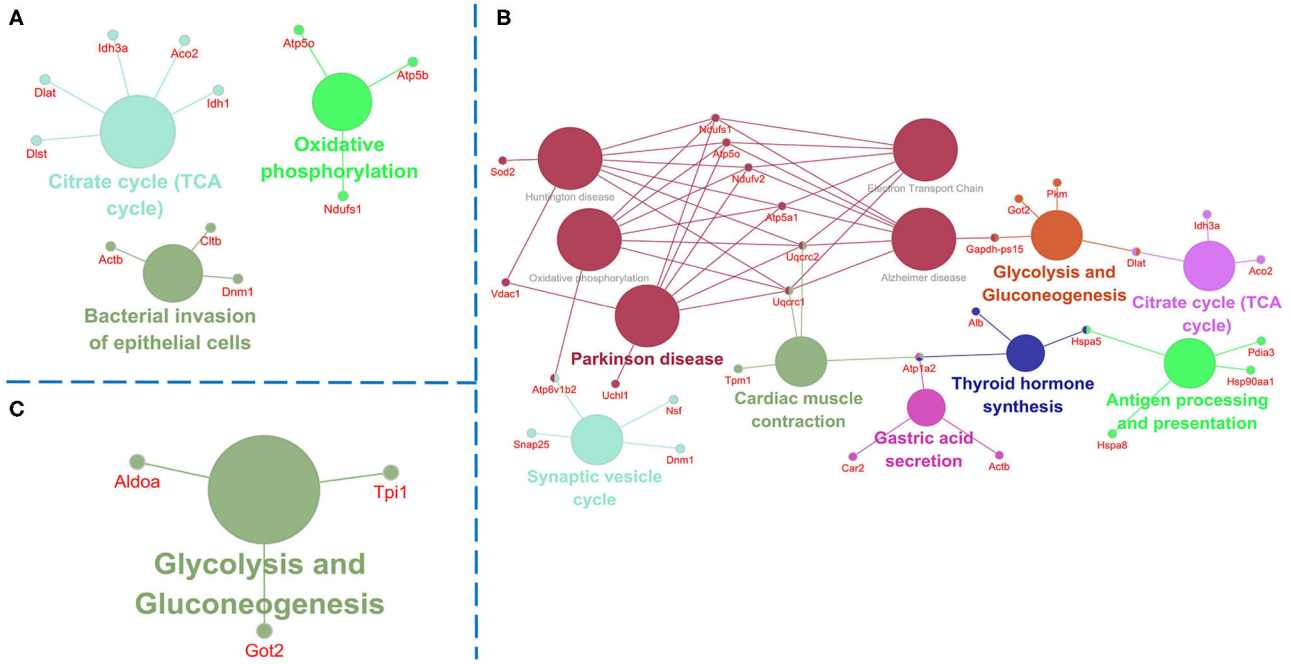

FIGURE 5 | Pathway analysis of the differentially expressed proteins. Pathway analysis using Clue GO software and the *p*-value was set at <0.05. **(A)** Comparison of pathways of the dysregulated proteins between untreated 3xTg-AD mice and WT mice. **(B)** Comparison of pathways of the dysregulated proteins between 1 mg/kg/d DAU-treated 3xTg-AD mice and untreated 3xTg-AD mice. **(C)** Comparison of pathways of the dysregulated proteins between 10 mg/kg/d DAU-treated 3xTg-AD mice and untreated 3xTg-AD mice.

the synaptic vesicle cycle, ATP metabolic process, electron transport chain, and TCA cycle in 3xTg-AD mice compared with WT mice (**Figure 4A**). DAU treatment (1 or 10 mg/kg/d) distinctly changed proteins in the pathway of mitochondrial energy metabolism (electron transport chain, glycolysis, and gluconeogenesis) and synaptic function (synaptic vesicle cycle; **Figures 4B,C**). The PPI analysis revealed that the differentially expressed proteins were mainly enriched in mitochondrial energy metabolism. Additionally, the expression level of the same proteins in other mouse groups, showed in PPI maps, were reversed after DAU treatment. These include synaptic function proteins (Synapsin-1 [Syn1], Synapsin-2 [Syn2]) and mitochondrial energy metabolism proteins (NADH-ubiquinone oxidoreductase 75 kDa subunit [Ndufs1], ATP synthase subunit O [ATP5o], isocitrate dehydrogenase [NAD] subunit alpha [Idh3a], aconitate hydratase [Aco2]).

Pathway analysis showed that differentially expressed proteins were mainly involved in pathways related to mitochondrial energy metabolism (**Figure 5**). Briefly, compared with WT mice, 3xTg-AD mice showed pathways in TCA cycle, oxidative phosphorylation and bacterial invasion of epithelial cells. Treatment with 1 mg/kg/d DAU had an effect on pathways mainly associated with Parkinson disease, glycolysis, gluconeogenesis, the TCA cycle, and the synaptic vesicle cycle. However, treatment with 10 mg/kg/d DAU had an effect only on glycolysis and gluconeogenesis. Thus, we focused on mitochondrial energy metabolism and used Cytoscape software to determine the detailed expression change of proteins in the TCA cycle and electron transport chain in mitochondrial energy metabolism. The TCA cycle and electron transport chain in 3xTg-AD mice vs. WT mice are presented in **Supplementary Figures 3A,B**, and those in 3xTg-AD-1 mg/kg/d mice vs. 3xTg-AD mice are presented in **Supplementary Figures 3C,D**. Pathway analysis revealed that Aco2, Ndufs1, mitochondrial cytochrome b-c1 complex subunit 1 (Uqcrc1), mitochondrial cytochrome b-c1 complex subunit 2 (Uqcrc2), and mitochondrial ATP synthase subunit alpha (ATP5a1) proteins were upregulated after 1 mg/kg/d DAU treatment. Similarly, at 10 mg/kg/d DAU dose, the mitochondrial proteins (Ndufs1 and Uqcrc1) and glycolysis and gluconeogenesis proteins (fructose-bisphosphate aldolase A [Aldoa] and triosephosphate isomerase [Tpi1]) were upregulated after treatment (**Supplementary Table 2**). Moreover, the expression level of Aco2, the key enzyme for the conversion of citrate to isocitrate (ICT; an important biological process in the TCA cycle), was reversed in DAU-treated 3xTg-AD mice compared with vehicle-treated 3xTg-AD mice. These results indicated that DAU treatment may reverse the defects of mitochondrial energy metabolism in 3xTg-AD mice and benefit mitochondrial function. In addition, synaptic proteins (Syn1 and Syn2) were upregulated, whereas oxidative stress protein (mitochondrial superoxide dismutase [Mn-Sod2] and Peroxiredoxin-1[Prdx1]) were downregulated after DAU treatment. The reversed expression of Syn1 and Syn2 in DAU-treated 3xTg-AD mice revealed synaptic protection.

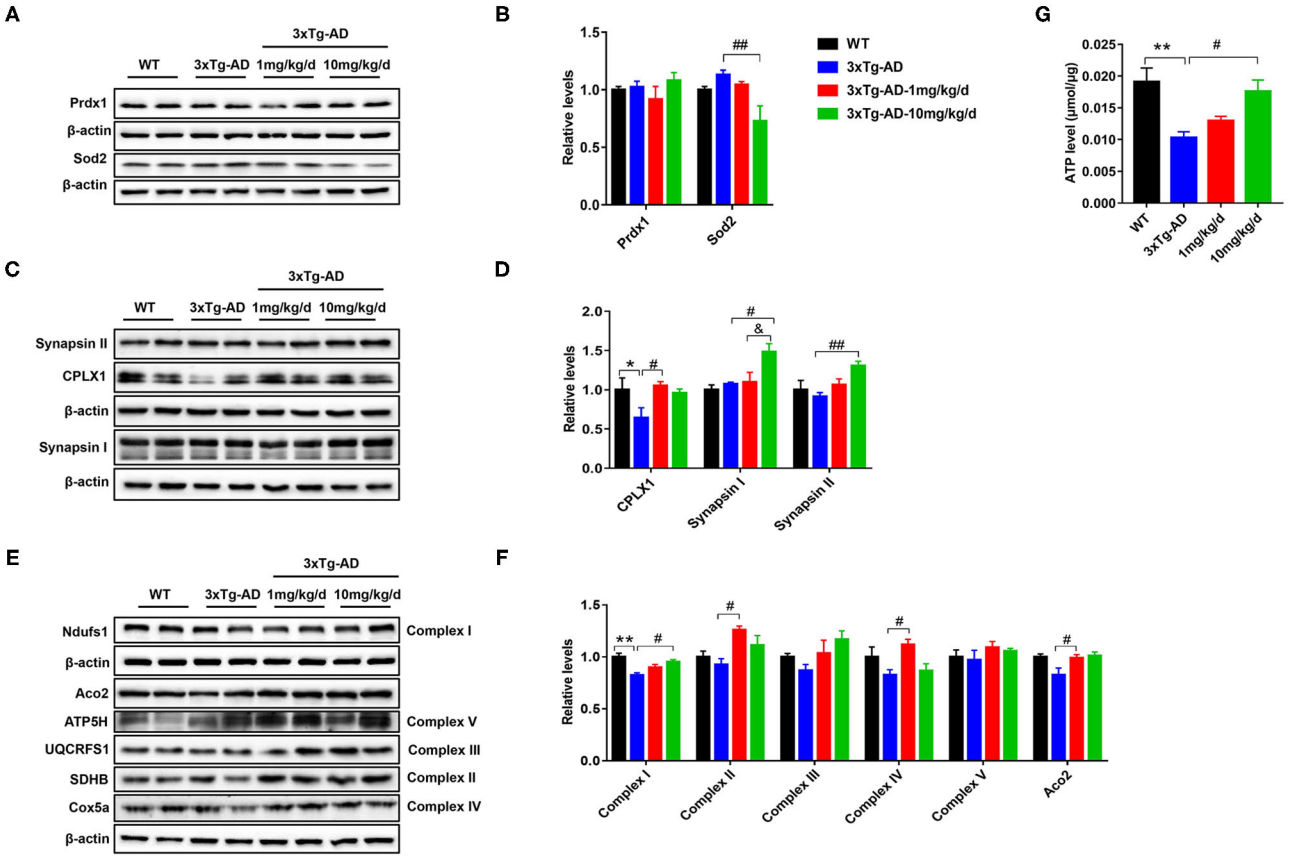

FIGURE 6 | Verification of protein dysregulation and measurement of electron transport chain protein and hippocampal ATP levels. **(A,B)** The changes in the expression levels of oxidative stress proteins—Prdx1 and Sod2. **(C,D)** The expression levels of synaptic function proteins—CPLX1, Synapsin I, and Synapsin II. **(E,F)** The change in the expression levels of Aco2 and election transport chain proteins—Ndufs1, SDHB, UQCRFS1, Cox5a, and ATP5H. **(G)** Hippocampal ATP levels in each group. The data are presented as mean ± SEM. $^{*}p < 0.05$, $^{**}p < 0.01$ vs. WT saline group. $^{\#}p < 0.05$, $^{\#\#}p < 0.01$ vs. 3xTg-AD saline group. $^{\&}p < 0.05$ vs. 3xTg-AD-1 mg/kg/d group. $N = 4$ for each group.

Western Blot Analysis and Functional Detection Proved That DAU Treatment Ameliorated Mitochondrial Function in 3xTg-AD Mice

To further confirm the differentially expressed proteins screened by proteomics, we performed western blot analysis to measure the altered concentrations of Prdx1, Sod2, Syn1, Syn2, Aco2, and Ndufs1 proteins. Compared with untreated 3xTg-AD mice, the expression level of Sod2 was significantly decreased, whereas the expression levels of Syn1, Syn2, and Ndufs1were significantly increased in 10 mg/kg/d DAU-treated 3xTg-AD mice. Moreover, the expression level of Aco2 was significantly increased in 1 mg/kg/d DAU-treated 3xTg-AD mice (**Figures 6A–F**). Further, we measured the expression of electron transport chain proteins (mitochondrial succinate dehydrogenase [ubiquinone] iron-sulfur subunit [SDHB-complex II], mitochondrial cytochrome b-c1 complex subunit Rieske (UQCRFS1-complex III), mitochondrial cytochrome c oxidase subunit 5A [Cox5a-complex IV], mitochondrial ATP synthase subunit d [ATP5H-complex V]), and the ATP level in 3xTg-AD mice to evaluate the beneficial effects of DAU on mitochondria. The expression levels of Aco2, SDHB-complex II, and Cox5a-complex IV proteins were significantly increased in 1 mg/kg/d DAU-treated 3xTg-AD mice, whereas in 10 mg/kg/d DAU-treated 3xTg-AD mice, the expression level of Ndufs1-complex I was significantly increased, UQCRFS1-complex III and SDHB-complex II showed an upregulated trend (**Figures 6E,F**). However, the ATP level was only significantly increased in 10 mg/kg/d DAU-treated 3xTg-AD mice (**Figure 6G**). These data indicated that DAU indeed improved the mitochondrial function in 3xTg-AD mice, especially at 10 mg/kg/d dosage. The upregulation of Syn1 and Syn2 proteins in 3xTg-AD mice after DAU treatment indicated that DAU may simultaneously modulate synaptic function in AD progression.

DISCUSSION

DAU, a bisbenzylisoquinoline alkaloid, is isolated from dauricum DC, and can treat various diseases such as cardiac ischemia,

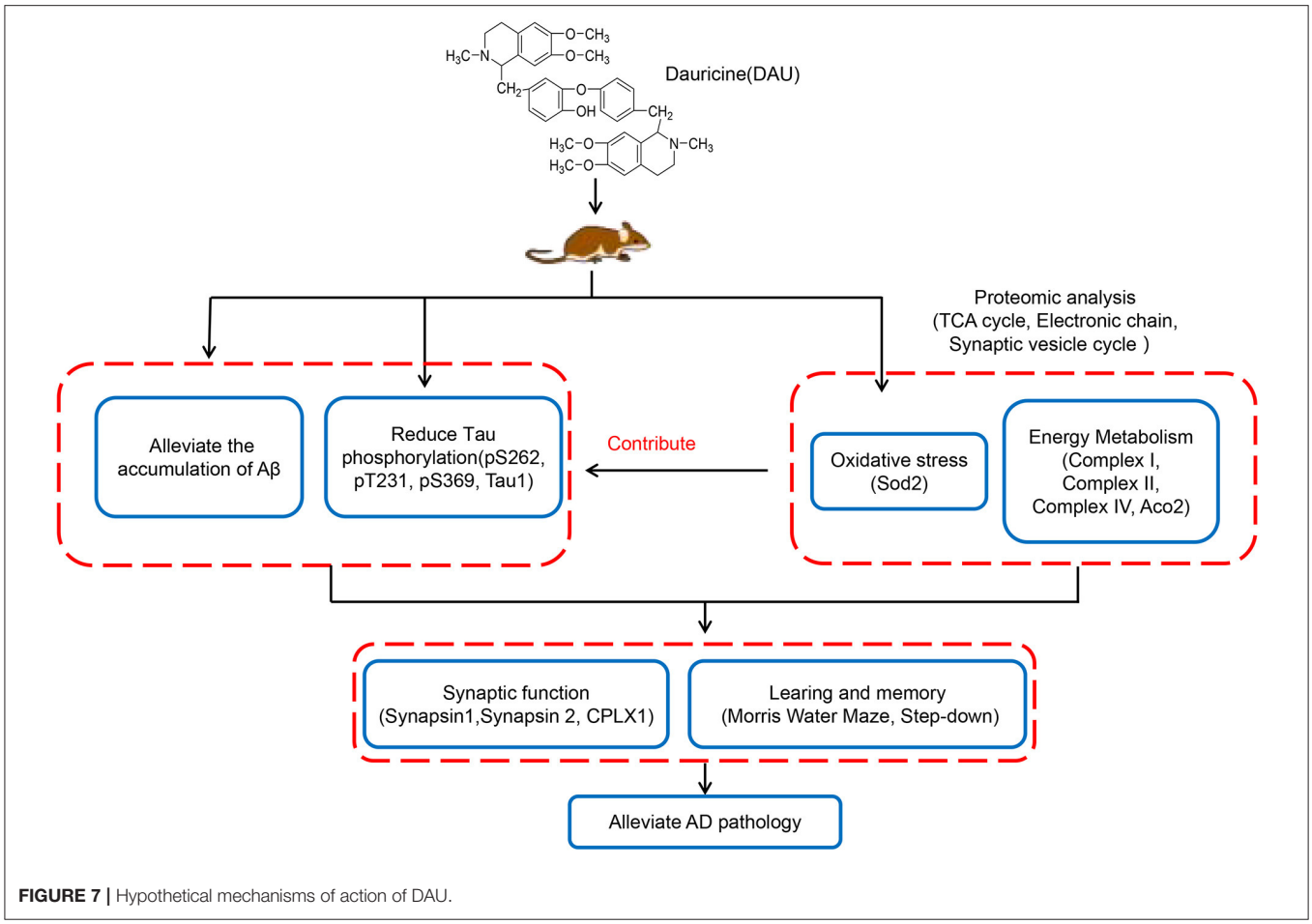

FIGURE 7 | Hypothetical mechanisms of action of DAU.

angina, and inflammation, as well as inhibit angiogenesis in tumors and promote apoptosis in tumor cells (Xia et al., 2002; Tang et al., 2009; Yang et al., 2010). Our previous study showed that DAU treatment attenuated hyperphosphorylation of tau and production of Aβ in N2a/APP cells (Liu et al., 2018). In this study, we further confirmed that DAU can improve cognitive impairment and neurodegeneration in 3xTg-AD mice. Treatment with 10 mg/kg/d DAU can significantly improve the learning and memory ability of AD mice in step-down passive avoidance and MWM tests and decrease Aβ (6E10) and phosphorylated tau (AT8) positive staining. Moreover, Western blot analysis showed that DAU treatment could reduce phosphorylated tau at the dose of 1 mg/kg/d. Pathological changes of Aβ and tau proteins are consistent with the findings of our previous *in vitro* study (Liu et al., 2018). In the *in vitro* study, DAU treatment inhibited APP processing to reduce Aβ production and attenuated tau pathology through PP2A and p35/25, and the main mechanism may have involved antioxidant stress. The homeostatic health of mitochondria contributed to the attenuation of Aβ and tau pathologies (Fang et al., 2019). In this study, it was found that DAU treatment improved mitochondrial function, and that the antioxidant effect may benefit the attenuation of tau phosphorylation and Aβ production.

Proteomics analysis revealed that the biological functions of differentially expressed proteins in three different mouse groups mainly involved mitochondrial energy metabolism. Consistent with the biological function, the differentially express proteins were enriched in the following signaling pathways: the TCA cycle, oxidative phosphorylation, glycolysis, and gluconeogenesis. In terms of mitochondrial energy metabolism, DAU treatment increased the expression of Ndufs1-complex I, SDHB-complex II, and Cox5a-complex IV, and modified the expression of the Ndufs1-complex I and ATP5o- complex V of electron transport chain in 3xTg-AD mice. In DAU-treated 3xTg-AD mice, the expression levels of Aco2 and Idh3a in the TCA cycle were modified. In agreement with these findings, the functional analysis showed an increase in the hippocampal ATP level in 3xTg-AD mice, suggesting that DAU improved mitochondrial energy metabolism. Moreover, DAU treatment increased the expression of Aco2—an enzyme that catalyzes the interconversion of citrate to ICT via cis-aconitate in the second step of the TCA cycle, and is essential for normal cell metabolism (Robbins and Stout, 1989; Gardner et al., 1995). Compared with the WT mice, the expression of Aco2 was decreased and the down-stream protein Idh3a, a catalytic subunit of the enzyme which catalyzes the decarboxylation

of ICT into alpha-ketoglutarate, was increased in 3xTg-AD mice. Therefore, decreased expression of Aco2 and abnormally increased expression of Idh3a suppressed the TCA cycle and thus, the function of electron transport chain and energy metabolism. In contrast, DAU treatment rescued the mitochondrial energy metabolism deficit.

In the TCA cycle, the expression level of Aco2, an upstream independent regulatory enzyme, was different in DAU-treated and vehicle-treated 3xTg-AD mice. Idh3a is only a subunit of Idh3, a catalytic enzyme. Because DAU administration modified the expression of Aco2 in 3xTg-AD, and the TCA cycle being an upstream and important process of energy metabolism, Aco2 may be the key target of DAU treatment for regulating mitochondrial energy metabolism. A previous study revealed that Aco2 expression and activity were decreased in the peripheral blood of patients with AD and MCI (Mangialasche et al., 2015), which is consistent with our observation in this study. Additionally, Aco2 was sensitive to increased oxidative stress, which inactivated Aco2 activity (Tabrizi et al., 1999). DAU treatment decreased the expression of Sod2, resulting in increased ROS levels (De Leo et al., 1998). Sod2, an important enzyme that regulates mitochondrial ROS, and is closely related to mitochondrial function (Brand, 2010; Cox et al., 2018), was decreased in 3xTg-AD mice. DAU treatment modified the expression of Sod2 in 3xTg-AD mice, compared with WT mice. Thus, these data indicated that DAU not only improved mitochondrial function but also exerted antioxidant protective effects.

The energy supply is essential for synaptic activity (Harris et al., 2012). DAU treatment moderated the expression level of proteins involved in the synaptic vesicle cycle in 3xTg-AD mice. DAU administration reversed the expression level of Synaptosomal-associated protein 25 (Snap25)—a protein involved in the molecular regulation of neurotransmitter release (Blasi et al., 1993) and Dynamin-1 (Dnm1), in producing microtubule bundles, and in synaptic vesicle endocytosis (Raimondi et al., 2011). Moreover, Syn1 and Syn2 are involved in the regulation of neurotransmitter secretion (Rosahl et al., 1995), and Syn1 deficiency increases seizure propensity (Li et al., 1995) and alters short-term synaptic plasticity (Rosahl et al., 1993). Our result showed that DUA treatment increased the expression levels of Syn1, Syn2, and CPLX1, which positively regulated synaptic vesicles (Cao et al., 2013). Improved mitochondrial energy metabolism and upregulated synaptic proteins suggested that defects in synaptic function could be prevented by DAU treatment in 3xTg-AD mice.

In summary, this study revealed that DAU can significantly improve learning and memory impairment and AD-like pathologies. The mechanism of action of DAU may be the improvement of mitochondrial function and the modification of some key mitochondrial proteins, synaptic proteins, and antioxidant proteins in AD mice (**Figure 7**). Our data suggest DAU has the potential to be developed for the treatment of AD.

DATA AVAILABILITY STATEMENT

The original contributions presented in the study are included in the article/**Supplementary Materials**, further inquiries can be directed to the corresponding author/s.

ETHICS STATEMENT

The animal study was reviewed and approved by Regulations for Animal Care and Use from the Committee of the Experimental Animal Center at Shenzhen Center for Disease Control and Prevention in Shenzhen, Guangdong Province, China.

AUTHOR CONTRIBUTIONS

CC and PL drafted the manuscript, performed the experiments, and analyzed the data. JW, HY, ZZ, JL, XC, FZ, and XY designed the study and analyzed the data. FZ and XY revised the manuscript. All authors contributed to the article and approved the submitted version.

FUNDING

This work was supported by the National Natural Science Foundation of China (NSFC; 81673134 and 81171191), Guangdong Provincial Key S&T Program (2018B030336001), Guangdong Provincial Natural Science Foundation (2017A030310617), Shenzhen Key Medical Discipline Construction Fund (SZXK069), and Sanming Project of Medicine in Shenzhen (SZSM201611090 and SZSM201801014).

SUPPLEMENTARY MATERIAL

The Supplementary Material for this article can be found online at: https://www.frontiersin.org/articles/10.3389/fcell.2020.624339/full#supplementary-material

Supplementary Figure 1 | The latency of mice in the water maze test after training for 5 consecutive days.

Supplementary Figure 2 | Heat maps of the three mouse groups. **(A–C)** Heat map of the dysregulated proteins in different mouse groups. The rows represent proteins and columns represent groups. Red color indicates high abundance and blue color indicates low abundance.

Supplementary Figure 3 | The TCA cycle and electron transport chain. **(A,B)** Comparison of the differentially expressed proteins associated with the TCA cycle and electron transport chain between untreated 3xTg-AD and WT mice and **(C,D)** between 1 mg/kg/d DAU-treated 3xTg-AD and untreated 3xTg-AD mice. Blue indicates downregulation and red indicates upregulation.

Supplementary Table 1 | Sources and dilution ratios of the antibodies used for immunoblotting.

Supplementary Table 2 | Differentially expressed proteins in DAU-treated vs. untreated 3xTg-AD mice.

REFERENCES

Andrade, S., Ramalho, M. J., Loureiro, J. A., and Pereira, M. D. C. (2019). Natural compounds for Alzheimer's disease therapy: a systematic review of preclinical and clinical studies. *Int. J. Mol. Sci.* 20:2313. doi: 10.3390/ijms20092313

Blasi, J., Chapman, E. R., Link, E., Binz, T., Yamasaki, S., De Camilli, P., et al. (1993). Botulinum neurotoxin A selectively cleaves the synaptic protein SNAP-25. *Nature* 365, 160–163. doi: 10.1038/365160a0

Bonet-Costa, V., Pomatto, L. C., and Davies, K. J. (2016). The proteasome and oxidative stress in Alzheimer's disease. *Antioxid. Redox Signal.* 25, 886–901. doi: 10.1089/ars.2016.6802

Brand, M. D. (2010). The sites and topology of mitochondrial superoxide production. *Exp. Gerontol.* 45, 466–472. doi: 10.1016/j.exger.2010.01.003

Burns, A., and Iliffe, S. (2009). Alzheimer's disease. *BMJ* 338:b158. doi: 10.1136/bmj.b158

Cao, P., Yang, X., and Sudhof, T. C. (2013). Complexin activates exocytosis of distinct secretory vesicles controlled by different synaptotagmins. *J. Neurosci.* 33, 1714–1727. doi: 10.1523/JNEUROSCI.4087-12.2013

Cox, C. S., Mckay, S. E., Holmbeck, M. A., Christian, B. E., Scortea, A. C., Tsay, A. J., et al. (2018). Mitohormesis in mice via sustained basal activation of mitochondrial and antioxidant signaling. *Cell Metab.* 28, 776–786 e775. doi: 10.1016/j.cmet.2018.07.011

De Leo, M. E., Borrello, S., Passantino, M., Palazzotti, B., Mordente, A., Daniele, A., et al. (1998). Oxidative stress and overexpression of manganese superoxide dismutase in patients with Alzheimer's disease. *Neurosci. Lett.* 250, 173–176. doi: 10.1016/S0304-3940(98)00469-8

Fang, E. F., Hou, Y., Palikaras, K., Adriaanse, B. A., Kerr, J. S., Yang, B., et al. (2019). Mitophagy inhibits amyloid-beta and tau pathology and reverses cognitive deficits in models of Alzheimer's disease. *Nat. Neurosci.* 22, 401–412. doi: 10.1038/s41593-018-0332-9

Frautschy, S. A., and Cole, G. M. (2010). Why pleiotropic interventions are needed for Alzheimer's disease. *Mol. Neurobiol.* 41, 392–409. doi: 10.1007/s12035-010-8137-1

Gardner, P. R., Raineri, I., Epstein, L. B., and White, C. W. (1995). Superoxide radical and iron modulate aconitase activity in mammalian cells. *J. Biol. Chem.* 270, 13399–13405. doi: 10.1074/jbc.270.22.13399

Golde, T. E., Schneider, L. S., and Koo, E. H. (2011). Anti-abeta therapeutics in Alzheimer's disease: the need for a paradigm shift. *Neuron* 69, 203–213. doi: 10.1016/j.neuron.2011.01.002

Harris, J. J., Jolivet, R., and Attwell, D. (2012). Synaptic energy use and supply. *Neuron* 75, 762–777. doi: 10.1016/j.neuron.2012.08.019

Hebert, L. E., Weuve, J., Scherr, P. A., and Evans, D. A. (2013). Alzheimer disease in the United States (2010-2050) estimated using the 2010 census. *Neurology* 80, 1778–1783. doi: 10.1212/WNL.0b013e31828726f5

Huang, X., Wang, J., Chen, X., Liu, P., Wang, S., Song, F., et al. (2018). The prenylflavonoid xanthohumol reduces Alzheimer-like changes and modulates multiple pathogenic molecular pathways in the Neuro2a/APPswe cell model of AD. *Front. Pharmacol.* 9:199. doi: 10.3389/fphar.2018.00199

Jin, H., Dai, J., Chen, X., Liu, J., Zhong, D., Gu, Y., et al. (2010). Pulmonary toxicity and metabolic activation of dauricine in CD-1 mice. *J. Pharmacol. Exp. Ther.* 332, 738–746. doi: 10.1124/jpet.109.162297

Kameyama, T., Nabeshima, T., and Kozawa, T. (1986). Step-down-type passive avoidance- and escape-learning method. Suitability for experimental amnesia models. *J. Pharmacol. Methods* 16, 39–52. doi: 10.1016/0160-5402(86)90027-6

Li, L., Chin, L. S., Shupliakov, O., Brodin, L., Sihra, T. S., Hvalby, O., et al. (1995). Impairment of synaptic vesicle clustering and of synaptic transmission, and increased seizure propensity, in synapsin I-deficient mice. *Proc. Natl. Acad. Sci. U.S.A.* 92, 9235–9239. doi: 10.1073/pnas.92.20.9235

Li, Y. H., and Gong, P. L. (2007). Neuroprotective effect of dauricine in cortical neuron culture exposed to hypoxia and hypoglycemia: involvement of correcting perturbed calcium homeostasis. *Can. J. Physiol. Pharmacol.* 85, 621–627. doi: 10.1139/Y07-056

Liu, P., Chen, X., Zhou, H., Wang, L., Zhang, Z., Ren, X., et al. (2018). The isoquinoline alkaloid dauricine targets multiple molecular pathways to ameliorate alzheimer-like pathological changes *in vitro*. *Oxid. Med. Cell. Longev.* 2018:2025914. doi: 10.1155/2018/2025914

Mangialasche, F., Baglioni, M., Cecchetti, R., Kivipelto, M., Ruggiero, C., Piobbico, D., et al. (2015). Lymphocytic mitochondrial aconitase activity is reduced in Alzheimer's disease and mild cognitive impairment. *J. Alzheimers. Dis.* 44, 649–660. doi: 10.3233/JAD-142052

Oddo, S., Caccamo, A., Shepherd, J. D., Murphy, M. P., Golde, T. E., Kayed, R., et al. (2003). Triple-transgenic model of Alzheimer's disease with plaques and tangles: intracellular Abeta and synaptic dysfunction. *Neuron* 39, 409–421. doi: 10.1016/S0896-6273(03)00434-3

Pu, Z., Ma, S., Wang, L., Li, M., Shang, L., Luo, Y., et al. (2018). Amyloid-beta degradation and neuroprotection of dauricine mediated by unfolded protein response in a *Caenorhabditis elegans* model of Alzheimer's disease. *Neuroscience* 392, 25–37. doi: 10.1016/j.neuroscience.2018.09.022

Querfurth, H. W., and Laferla, F. M. (2010). Alzheimer's disease. *N. Engl. J. Med.* 362, 329–344. doi: 10.1056/NEJMra0909142

Raimondi, A., Ferguson, S. M., Lou, X., Armbruster, M., Paradise, S., Giovedi, S., et al. (2011). Overlapping role of dynamin isoforms in synaptic vesicle endocytosis. *Neuron* 70, 1100–1114. doi: 10.1016/j.neuron.2011.04.031

Robbins, A. H., and Stout, C. D. (1989). Structure of activated aconitase: formation of the [4Fe-4S] cluster in the crystal. *Proc. Natl. Acad. Sci. U.S.A.* 86, 3639–3643. doi: 10.1073/pnas.86.10.3639

Rosahl, T. W., Geppert, M., Spillane, D., Herz, J., Hammer, R. E., Malenka, R. C., et al. (1993). Short-term synaptic plasticity is altered in mice lacking synapsin I. *Cell* 75, 661–670. doi: 10.1016/0092-8674(93)90487-B

Rosahl, T. W., Spillane, D., Missler, M., Herz, J., Selig, D. K., Wolff, J. R., et al. (1995). Essential functions of synapsins I and II in synaptic vesicle regulation. *Nature* 375, 488–493. doi: 10.1038/375488a0

Tabrizi, S. J., Cleeter, M. W., Xuereb, J., Taanman, J. W., Cooper, J. M., and Schapira, A. H. (1999). Biochemical abnormalities and excitotoxicity in Huntington's disease brain. *Ann Neurol.* 45, 25–32.

Tang, X. D., Zhou, X., and Zhou, K. Y. (2009). Dauricine inhibits insulin-like growth factor-I-induced hypoxia inducible factor 1alpha protein accumulation and vascular endothelial growth factor expression in human breast cancer cells. *Acta Pharmacol. Sin.* 30, 605–616. doi: 10.1038/aps.2009.8

Wang, L., Pu, Z., Li, M., Wang, K., Deng, L., and Chen, W. (2020). Antioxidative and antiapoptosis: neuroprotective effects of dauricine in Alzheimer's disease models. *Life Sci.* 243:117237. doi: 10.1016/j.lfs.2019.117237

Wang, L., Wang, X. C., Li, H. L., Wang, D. L., Zhou, X. W., and Wang, J. Z. (2005). Dauricine prevents bradykinin–induced alteration of calcium homeostasis and tau hyperphosphorylation in N2a cells. *Sheng Wu Hua Xue Yu Sheng Wu Wu Li Jin Zhan*. 32, 612–617. doi: 10.1562/2005-05-15-RC-528R.1

Xia, J. S., Li, Z., Dong, J. W., Tu, H., and Zeng, F. D. (2002). Dauricine-induced changes in monophasic action potentials and effective refractory period of rabbit left ventricle *in situ*. *Acta Pharmacol. Sin.* 23, 371–375. Available online at: http://www.chinaphar.com/article/view/7530

Yang, Z., Li, C., Wang, X., Zhai, C., Yi, Z., Wang, L., et al. (2010). Dauricine induces apoptosis, inhibits proliferation and invasion through inhibiting NF-kappaB signaling pathway in colon cancer cells. *J. Cell. Physiol.* 225, 266–275. doi: 10.1002/jcp.22261

Zhou, X., Xiao, W., Su, Z., Cheng, J., Zheng, C., Zhang, Z., et al. (2019). Hippocampal proteomic alteration in triple transgenic mouse model of Alzheimer's disease and implication of PINK 1 regulation in donepezil treatment. *J. Proteome Res.* 18, 1542–1552. doi: 10.1021/acs.jproteome.8b00818

Conflict of Interest: The authors declare that the research was conducted in the absence of any commercial or financial relationships that could be construed as a potential conflict of interest.

frontiers in Cell and Developmental Biology

ORIGINAL RESEARCH
published: 18 February 2021
doi: 10.3389/fcell.2020.633725

Targeted Reducing of Tauopathy Alleviates Epileptic Seizures and Spatial Memory Impairment in an Optogenetically Inducible Mouse Model of Epilepsy

*Yang Gao[1], Jie Zheng[1,2], Tao Jiang[1], Guilin Pi[1], Fei Sun[1], Rui Xiong[1], Weijin Wang[1], Dongqin Wu[1], Shihong Li[1], Huiyang Lei[1], Huiling Yu[1], Qiuzhi Zhou[1], Ying Yang[1], Huaqiu Zhang[3] and Jian-Zhi Wang[1,4]**

[1] Department of Pathophysiology, Key Laboratory of Ministry of Education for Neurological Disorders, School of Basic Medicine, Tongji Medical College, Huazhong University of Science and Technology, Wuhan, China, [2] Department of Pharmacology, Key Laboratory of Basic Pharmacology of Ministry of Education and Joint International Research Laboratory of Ethnomedicine of Ministry of Education, Zunyi Medical University, Zunyi, China, [3] Department of Neurosurgery, Key Laboratory of Ministry of Education for Neurological Disorders, Tongji Hospital, Tongji Medical College, Huazhong University of Science and Technology, Wuhan, China, [4] Co-innovation Center of Neuroregeneration, Nantong University, Nantong, China

Intracellular deposition of hyperphosphorylated tau has been reported in the brain of epilepsy patients, but its contribution to epileptic seizures and the association with spatial cognitive functions remain unclear. Here, we found that repeated optogenetic stimulation of the excitatory neurons in ventral hippocampal CA1 subset could induce a controllable epileptic seizure in mice. Simultaneously, the mice showed spatial learning and memory deficits with a prominently elevated total tau and phospho-tau levels in the brain. Importantly, selective facilitating tau degradation by using a novel designed proteolysis-targeting chimera named C4 could effectively ameliorate the epileptic seizures with remarkable restoration of neuronal firing activities and improvement of spatial learning and memory functions. These results confirm that abnormal tau accumulation plays a pivotal role in the epileptic seizures and the epilepsy-associated spatial memory impairments, which provides new molecular target for the therapeutics.

Keywords: epilepsy, cognitive impairment, tau hyperphosphorylation, optogenetics, mouse model

OPEN ACCESS

Edited by:
Peng Lei,
West China Hospital, Sichuan University, China

Reviewed by:
Fei Liu,
New York State Institute for Basic Research in Developmental Disabilities, United States
Xin Wang,
Xiamen University, China
Xiongwei Zhu,
Case Western Reserve University, United States

***Correspondence:**
Jian-Zhi Wang
wangjz@mail.hust.edu.cn

Specialty section:
This article was submitted to Molecular Medicine, a section of the journal Frontiers in Cell and Developmental Biology

Received: *26 November 2020*
Accepted: *29 December 2020*
Published: *18 February 2021*

Citation:
Gao Y, Zheng J, Jiang T, Pi G, Sun F, Xiong R, Wang W, Wu D, Li S, Lei H, Yu H, Zhou Q, Yang Y, Zhang H and Wang J-Z (2021) Targeted Reducing of Tauopathy Alleviates Epileptic Seizures and Spatial Memory Impairment in an Optogenetically Inducible Mouse Model of Epilepsy. Front. Cell Dev. Biol. 8:633725. doi: 10.3389/fcell.2020.633725

INTRODUCTION

Epilepsy is characterized by spontaneously recurring epileptic seizures, with cognitive decline generally occurring as a major comorbidity (So and Penry, 1981; Breuer et al., 2016; Witt and Helmstaedter, 2017). The degree of the epilepsy-induced cognitive impairments varies, depending on the age at seizure onset; location, frequency, and duration of epilepsy; and the history of antiepileptic medication (Avanzini et al., 2013; Witt and Helmstaedter, 2017; Feldman et al., 2018), with the mechanisms not yet fully understood, to date. As a result, there is currently no targeted therapeutic strategy to prevent or halt the development the cognitive decline in epilepsy patients (Paudel et al., 2019).

Hyperphosphorylation and intracellular accumulation of tau protein dysregulate microtubule assembly and aggravate the formation of neurofibrillary tangles, thus remodeling neuronal synapses and exacerbating cognitive decline in a collection of diseases named tauopathies, including Alzheimer disease (AD; Wang et al., 2014; Wang and Mandelkow, 2016; Yang and Wang, 2018). Recent studies also revealed prominent accumulation of hyperphosphorylated tau in the brain of temporal lobe epilepsy patients (Tai et al., 2016; Smith et al., 2019). Given that epilepsy and early stage AD share many neurological characters and psychiatric symptoms (Kanner, 2009; Cheng et al., 2015; Zarea et al., 2016), we wonder whether tau pathology also contributes to the cognitive deficits in epilepsy. Furthermore, although knockdown or knockout of tau proteins have been evidenced to significantly attenuate neuronal network hyperexcitability in the brain of mice with epilepsy (DeVos et al., 2013; Holth et al., 2013), whether and how the abnormal accumulation of hyperphosphorylated tau dysregulates neuronal firing activities thus to affect epileptic seizures in epilepsy still remain to be elucidated.

The current epileptic animal models, produced by systemic or focal injection of convulsant agents such as kainic acid or pilocarpine, always show more extensive neuronal damages than those observed in the clinical patients, and the animal death rate is high (Morimoto et al., 2004). Recently, optogenetics has been used to induce sporadic seizures with high temporal and spatial specificity in animal studies (Osawa et al., 2013; Khoshkhoo et al., 2017; Cela et al., 2019). In the present study, we found that optogenetic stimulation of vCA1 excitatory neurons could induce a controllable epileptic seizure with spatial memory deficit in mice. Simultaneously, tau hyperphosphorylation and accumulation were shown, while targeted reducing phospho-tau accumulation attenuated optogenetics-induced epileptic seizures with improved spatial learning and memory.

RESULTS

Optogenetic Stimulating vCa1 Excitatory Neurons Induces Epileptic Seizures With Impaired Spatial Learning and Memory

To establish a mouse model of temporal lobe epilepsy with high spatiotemporal controllability of seizures, we stereotaxically injected pAAV-CaMKIIα-ChR2(H134R)-mCherry into unilateral mice ventral hippocampal CA1 (vCA1) (**Figures 1A–C**). Mice received optogenetic stimulation once each day for 14 consecutive days (block 1) or 21 days (block 2) to mimic sporadic and repeated seizures in clinic (**Figure 2A**).

Optogenetically hyperactivating vCA1 excitatory neurons with blue light (482 nm, 20 Hz) induced epileptiform discharges in ipsilateral primary motor cortex (M1) (**Figure 1D**). The amplitude and power spectra density (PSD) of M1 local field potential (LFP) were increased prominently during incubation and ictal periods of epilepsy (**Figures 1E–H**). Consistently, behavioral seizures of stages 2–6 by modified Racine scale (MRS; Racine, 1975; Haas et al., 1990) were observed (**Figure 1D**, upper; Video 1). As expected, the epileptic seizures gradually stopped following the cessation of optogenetic stimulation. Further studies revealed that the latency to generalized seizures (MRS stage $\geq$ 4) decreased with repeated induction of epilepsy over time (**Figure 1D**, bottom).

By Morris water maze (MWM) test, we observed that repeated seizures for 14 consecutive days (block 1) increased the latency to find the hidden platform at days 3–4 during the training phase (**Figure 2B**, block 1). Besides, epileptic mice also showed decreased target quadrant crossings at day 6 (**Figure 2C**, block 1). These data indicate that repeated seizures impair both spatial learning and memory of mice. To examine the effect of longer repeat seizures on spatial learning and memory, we stimulated the mice for another 7 consecutive days (block 2). The additional optogenetic stimulation could also induce epileptic seizures with more serious impairments of spatial learning and memory in MWM test (block 2 in **Figures 2B–D**).

The optogenetics-induced seizures did not affect the time and distance of mice traveled in the central area in open-field test (**Figures 2E,F**) nor changed the ratio of open-arm entries in the elevated-plus maze test (**Figures 2G,H**). These results indicated that the repeated induction of seizures using optogenetics did not induce significant anxiety-like behavior, which was generally reported in typical epileptics models (Baxendale et al., 2005; Inostroza et al., 2012; Scott et al., 2017; Yogarajah and Mula, 2019).

Epileptic Seizure Induces Phospho-Tau Accumulation Without Hippocampal Neuron Loss in Mice

We next examined the effect of repeated seizures on tau. The levels of tau phosphorylated at the Ser199/Ser202/Thr205 epitope (recognized by the AT8 antibody) significantly elevated both in the cortex and hippocampus of mice after 21 times of repetitive optogenetic induction of seizures (**Figures 3A–C**). The total tau (recognized by the Tau5 antibody) was also upregulated in the hippocampus of mice with epilepsy (**Figures 3A–D**).

No significant loss of hippocampal neurons was detected after repeated induction of seizures (**Figure 2I**), although the neuron death was commonly seen in the drug-induced epilepsy models (Morimoto et al., 2004). These data also suggest that the seizures-induced learning and memory deficits were not caused by neuron death.

Selectively Facilitating Tau Degradation Using a Proteolysis-Targeting Chimera Effectively Ameliorates Seizures and the Associated Memory Deficits

To directly test the contribution of seizures-induced elevation of phospho-tau and total tau to the seizure inductions and spatial learning and memory impairments, we used a novel small-molecule proteolysis-targeting chimera termed C4 to selectively promote tau degradation (more key information about C4 at https://www.cnipa. gov.cn/with a patent publication number *CN111171113A*).

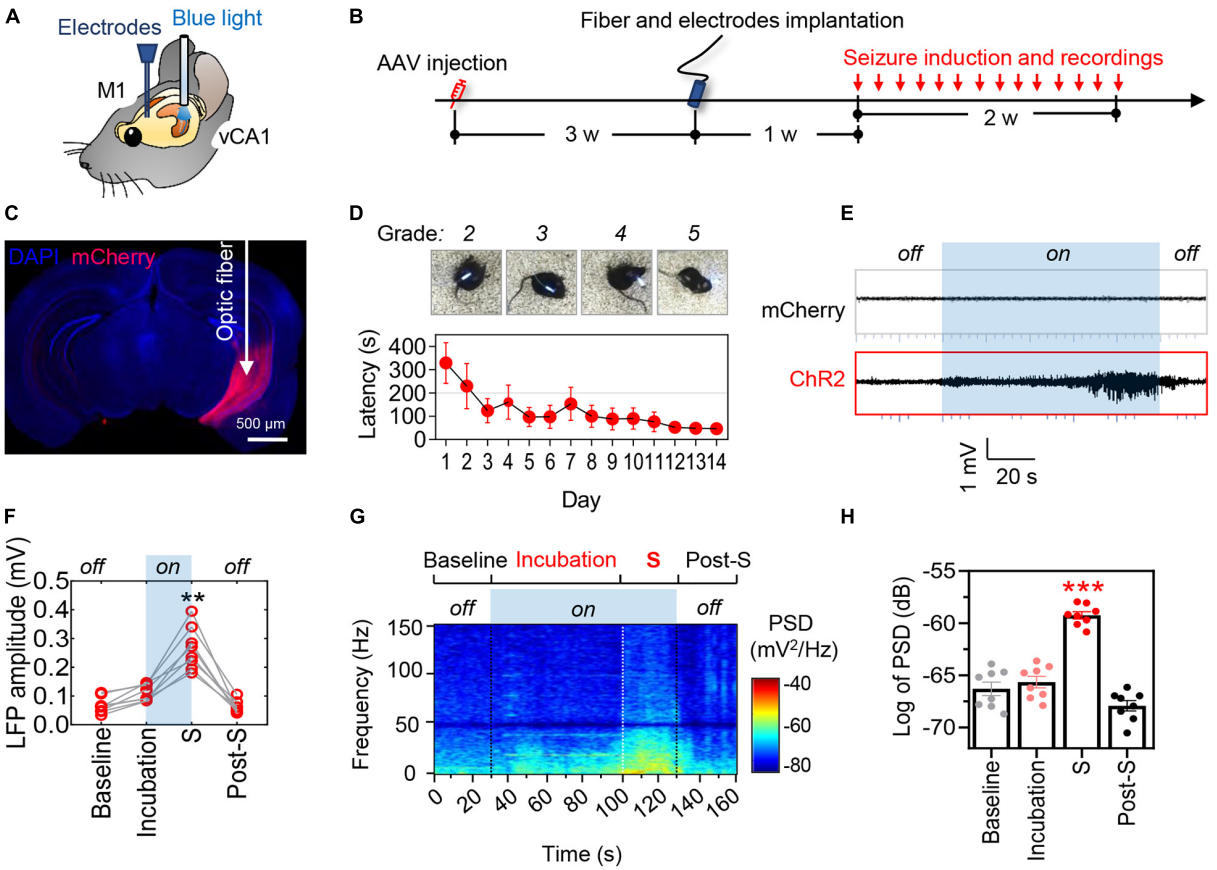

FIGURE 1 | Optogenetic stimulation of ventral hippocampal excitatory neurons induces controllable epileptic seizures. **(A)** Schematic illustrates the locations of optic fiber and recording electrode. **(B)** Experimental procedures of virus injection, optic fiber and electrode implantation, optogenetic seizure induction. **(C)** A representative image showing the AAVs-mediated mCherry expression in the ventral hippocampus. Scale bar, 500 μm. **(D)** The representative images show typical seizure behavior (MRS stages 2–5) and the latency to generalized seizures **(upper)**. Repeated optogenetic stimulation of vCA1 excitatory neurons induced typical seizure behavior, and the latency to generalized seizures was decreasing during repeated induction that showed seizure threshold declined over time (bottom). **(E,F)** Optogenetic hyperactivation of vCA1 excitatory neurons (i.e., blue light on) induced epileptiform neuronal activities in the primary motor cortex (M1). The local field potential (LFP) amplitude in M1 significantly increased during the phase of incubation and generalized seizures (shortened as S). The mice injected with AAV-mCherry were tested as non-seizure controls. Repeat-measures one-way ANOVA followed by Tukey multiple-comparisons tests, $^{**}p < 0.01$, $^{***}p < 0.001$, compared with the baseline, $n = 8$ in each group. **(G,H)** Optogenetic induction of seizures increased the power spectra density (PSD) of LFP in the phase of incubation and generalized seizures. Repeated-measures one-way ANOVA followed by Tukey multiple-comparisons tests. $^{**}p < 0.01$, $^{***}p < 0.001$, compared with the baseline, $n = 8$ in each group. Values are presented as the mean ± SEM.

Mice received repeated opto-stimulation for 14 days and were subcutaneously administered C4 (3 mg/kg, twice a week for 4 weeks) (**Figure 4A**), and then the levels of phospho-tau and total were measured. The results showed that C4 efficiently downregulated both phospho-tau (AT8 epitope) and total tau in the cortex and hippocampus of the epileptic mice (**Figures 4B–D**). Tau reduction by C4 ameliorated the optogenetics-induced seizures as shown by a prolonged latency to generalize seizures, decreased seizure duration, and the severity of seizure compared with vehicle-administered controls (**Figures 5A–G**). Although C4 showed limited effects in alleviating the seizures-induced spatial learning deficits during the training phase in MWM test (**Figure 5H**), C4 significantly improved the spatial memory as indicated by the increased target quadrant crossings (**Figures 5I,J**).

These data together indicate that tau accumulation plays a critical role in repeated seizures and spatial cognitive impairment; targeting tau is promising in alleviating seizures and the associated spatial memory deficits in epilepsy.

DISCUSSION

Optogenetics provides excellent tools to control neuronal activities with high spatiotemporal specificity (Mondoloni et al., 2019), which gains increasing attention in the study of epilepsy (Choy et al., 2017; Tønnesen and Kokaia, 2017). There are several advantages of these optogenetics-based models compared with classical drug-induced status epileptics models. First, optogenetic tools enable cell type- and location-specific induction of seizures. In the present study, we targeted ventral hippocampal excitatory

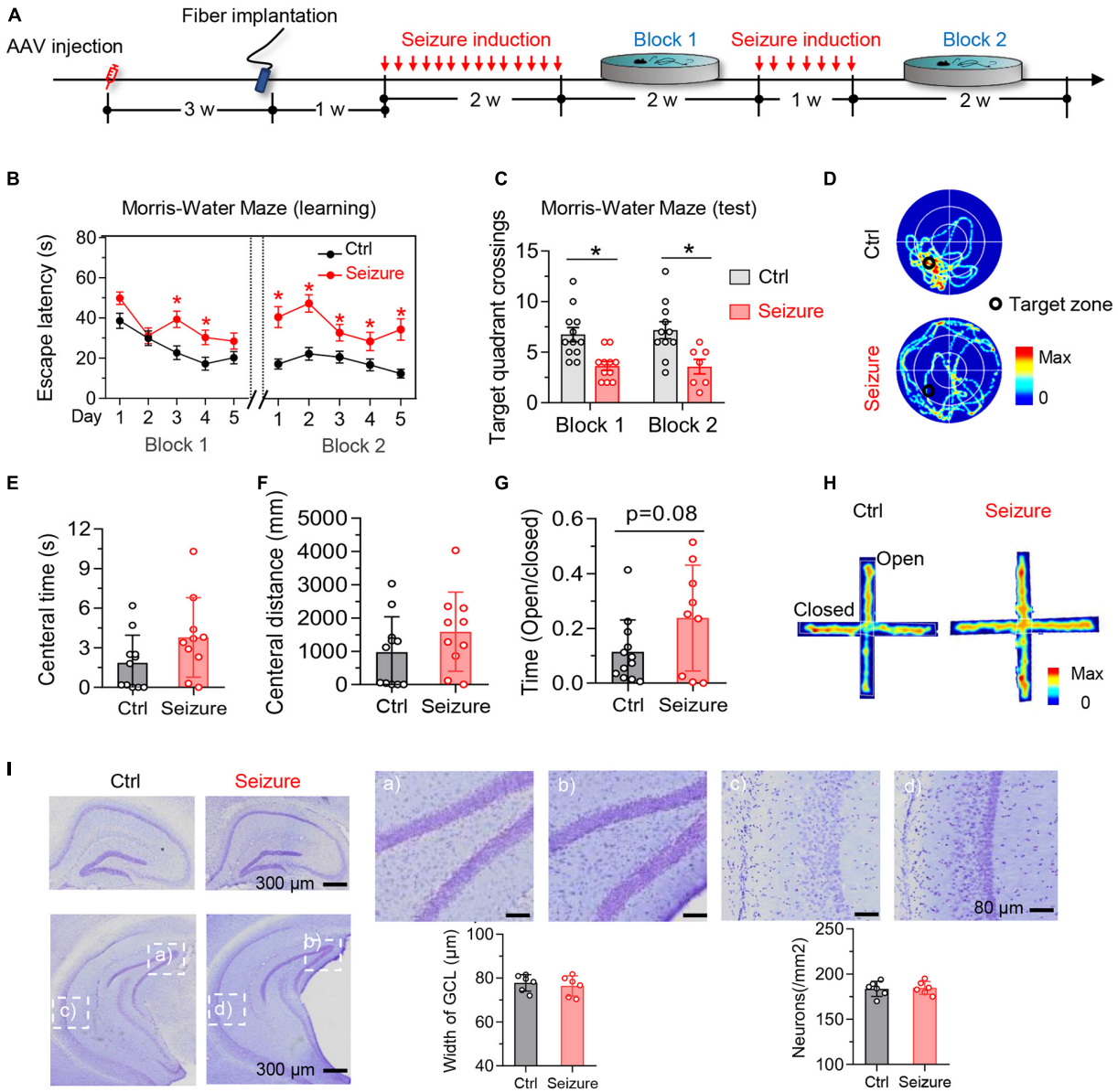

FIGURE 2 | Optogenetic induction of repeated seizures impairs spatial learning and memory without causing anxiety-like behaviors or hippocampal neuron loss in mice. **(A)** Experimental procedures of virus injection, optic fiber implantation, optogenetic seizure induction, and behavioral tests. **(B)** Repeated seizure induction caused spatial learning deficits shown by the increased escape latency during training phase. Repeated-measures ANOVA followed by Tukey multiple-comparisons tests, $^*p < 0.05$. **(C,D)** Repeated seizure induction caused spatial memory deficits shown by the decreased number of target quadrant crossings in water maze test **(B)** and the representative heatmaps **(C)** show traveling time and the trace. Unpaired *t* test, $^*p < 0.05$. **(E,H)** Repeated but controllable seizures did not induce anxiety-like behavior shown by the unchanged central time **(D)** and traveled distance **(E)** in open field test, and the increased open arm stay during elevated plus maze test **(F)**. The representative heatmaps **(G)** show traveling time and the trace. Unpaired *t* test, $^*p < 0.05$. **(I)** Repeated but controllable seizures did not induce neuron loss in the granular cell layer (GCL) of dorsal and ventral hippocampus measured by Nissl staining ($p > 0.05$). Scale bars were as indicated in each panel. $n = 6$ mice in each group. Unpaired *t* tests. Values are presented as the mean ± SEM.

neurons to mimic the etiology of temporal lobe epilepsy. Second, optogenetics brings higher accuracy for quantitatively controlling the onset, frequency, and severity of seizures. Third, by contrast to classical drug-induced status epileptics models, which generally cause approximately 10–44% animals death (Auladell et al., 2017; Welzel et al., 2020), optogenetics-inducible epilepsy model has higher success rate and repeatability and almost no mortality. In the present study, we established a novel mice model of optogenetically inducible sporadic epilepsy with high spatiotemporal specificity and stable repeatability.

Tau is a microtubule-associated protein mainly engaged in the microtubule stabilization and axonal transport under physiological conditions. Hyperphosphorylation of tau hinders its degradation, thus leading to the aggregation of tau and

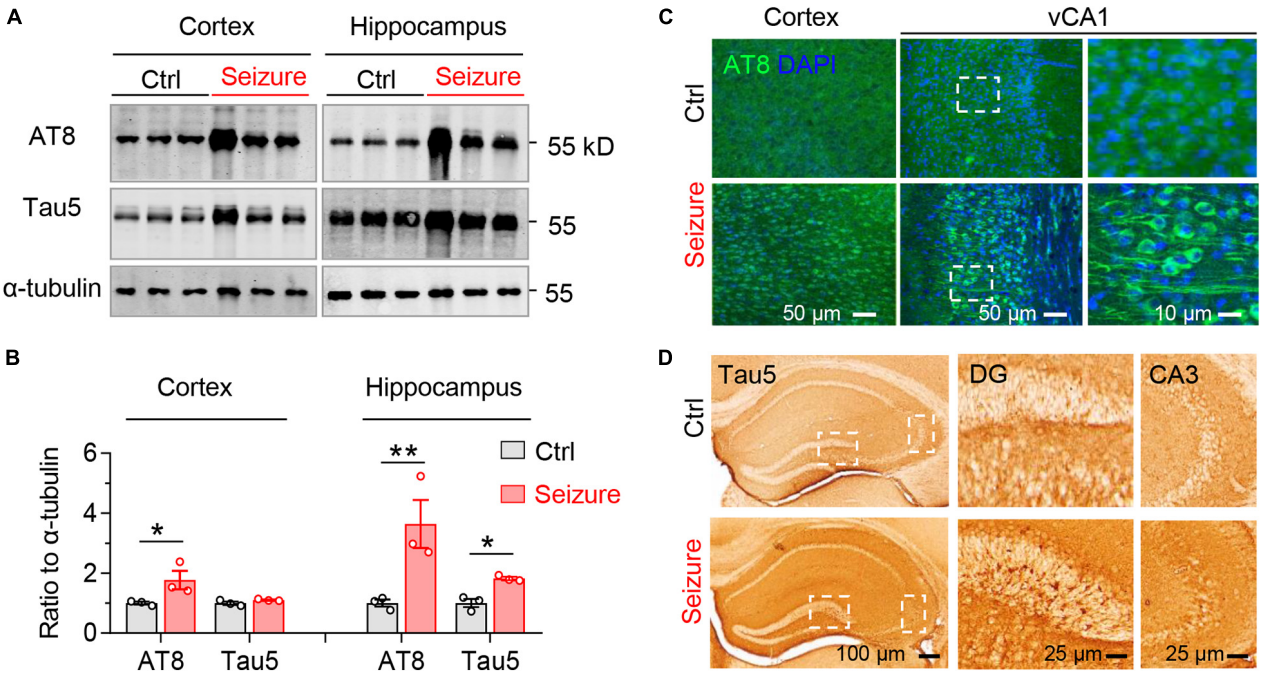

FIGURE 3 | Repeated seizures upregulate phosphorylated and total tau levels in the hippocampus and cortex of mice. Repeated seizures increased phospho-tau (AT8) and total tau (Tau5) levels in hippocampus and cortex measured by Western blotting **(A,B)** and immunostaining **(C,D)**. $n = 3$ mice in each group. Unpaired *t*-tests, $^{*}p < 0.05$, $^{**}p < 0.01$. Scale bars were as indicated in each panel. Values are presented as the mean ± SEM.

forming of neurotoxic paired helices (Sadqi et al., 2002). Abnormal accumulation of hyperphosphorylated tau in the hippocampus or appearance of neuropil threads and NFTs in the resected epileptogenic temporal lobe has been reported in a majority of epilepsy patients (Tai et al., 2016; Smith et al., 2019). Consistently, we found that repeated induction of seizures prominently elevated phosphorylated and total tau levels in the cortex and hippocampus. However, whether and how the tau pathology is involved in epilepsy remain not fully understood. Here, using a specific chimera to facilitate tau degradation in an optogenetically inducible mice model of epilepsy, we found a contribution of intraneuronal phospho-tau accumulation to epileptic seizures and associated spatial memory deficits.

However, molecular mechanisms underlying how epilepsy resulted in phospho-tau accumulation still remain to be elucidated. Given that the tau hyperphosphorylation and accumulation generally resulted from upregulated activity of kinase, such as cyclin-dependent kinase 5 (CDK5) and glycogen synthase kinase-3β (GSK-3β), or downregulated protein phosphatase 2A (PP2A) activity (Iqbal et al., 2009)I, the observed increase of phospho-tau in epilepsy might also be attributed to the dysfunction of these kinase or phosphatases. Indeed, increased activity of glutamatergic neurons has been reported to induce tau hyperphosphorylation through PP2A inhibition by releasing of synaptic Zinc in cultured hippocampal neurons and brain slices of AD mice (Sun et al., 2012). Similarly, CDK5 and GSK-3β were both reported to be overactivated in temporal lobe epilepsy (Liu et al., 2017). Whether these proteins change in the optogenetics-induced epilepsy and their direct links to the abnormal tau accumulation still remain to be elucidated.

Another intriguing question is how the intraneuronal accumulation of phospho-tau dysregulates epileptic seizures. The hyperphosphorylation and abnormal aggregation of tau protein might directly affect neural network activities by causing microtubule depolymerization (Verstraelen et al., 2017) or result in excitation/inhibition imbalance by dysregulating the release of neurotransmitters (Holth et al., 2013; Sánchez et al., 2018). However, it seems currently elusive how tau accumulation determines neuronal network activities. Although mice expressing mutated human tau exhibited suppressed neuronal activity (Busche et al., 2019; Sohn et al., 2019), selective overexpressing human tau in GABAergic interneurons resulted in hyperactivation of neighboring excitatory neurons (Zheng et al., 2020). It deserved further investigation how the hyperphosphorylated tau was distributed in different subsets of neurons in epilepsy.

We have previously evidenced that intracellular accumulation of hyperphosphorylated tau dysregulated neuronal plasticity and interneuronal transmissions in AD (Yin et al., 2016; Ye et al., 2020), the most common form of dementia in the elderly. In fact, neuronal hyperactivation and epileptic seizure were commonly reported in the early stage of AD (Lam et al., 2017; Baker et al., 2019). Thus, the pathological tau-induced neuronal dysfunctions, like those in AD, might also at least partly contribute to the cognitive impairment in epilepsy.

Most importantly, we found that specifically reducing tau with a proteolysis-targeting chimera in the brain significantly

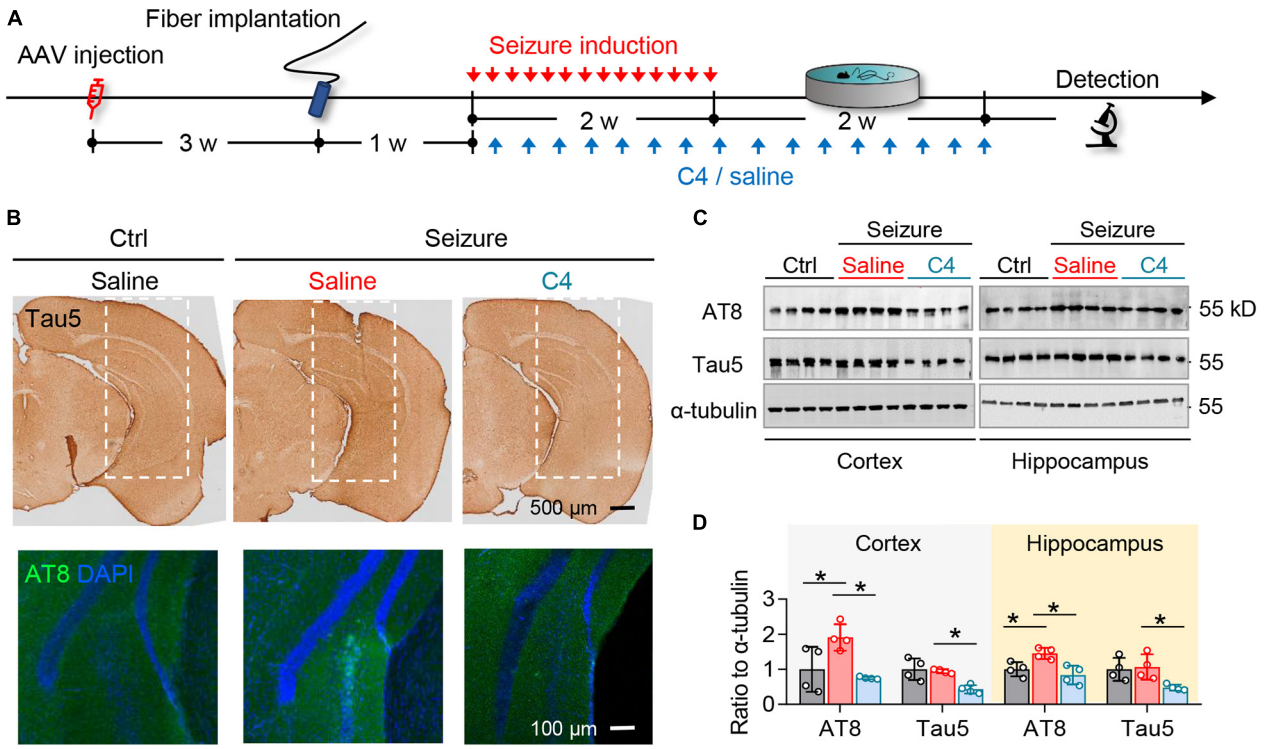

FIGURE 4 | C4 selectively facilitates tau degradation in the optogenetically inducible mouse model of epilepsy. **(A)** Experimental procedure of virus injection, seizure induction, C4 administration, and behavioral tests. **(B–D)** C4 administration diminished the repeated seizure-induced elevation of total tau and phospho-tau levels in hippocampus and cortex measured by immunostaining **(B)** and Western blotting **(C,D)**. $n = 4$ mice in each group. One-way ANOVA followed by Tukey multiple-comparisons tests, $^*p < 0.05$. Scale bars were as indicated in each panel. Values are presented as the mean ± SEM.

inhibited epileptic seizures, as well as alleviated spatial memory impairment in our mice model. Consistently, non-selectively facilitating tau dephosphorylation by enhancing the enzyme activity of PP2A with sodium selenite effectively prolonged the time of epilepsy induction, and reduced the number and degree of seizures (Jones et al., 2012; Liu et al., 2016). Moreover, knocking down or out of the endogenous tau also reduced the frequency and severity of seizures in mice (DeVos et al., 2013; Holth et al., 2013; Gheyara et al., 2014).

Taken together, the present study found that optogenetic overactivation of vCA1 excitatory neurons induced epileptic seizures and cognitive impairments, associating with abnormal accumulation of phospho-tau in hippocampal neurons. Further studies revealed that specific facilitating tau removal partly rescued the epileptic seizures and the associated spatial memory deficits. These findings confirm that abnormal tau accumulation plays a pivotal role in optogenetics-induced epileptic seizures, and targeting tau may be promising in treatment of epilepsy.

MATERIALS AND METHODS

Animals

Adult (8–12 weeks) male C57BL/6 mice weighing 20–30 g were purchased from Beijing Vital River Laboratory Animal Technology Co., Ltd. All mice were housed in groups of four to five per cage and were housed under a 12-h light–dark cycle (lights on at 7:00 PM and off at 7:00 AM) at a stable temperature (23–25°C). Food and water were available *ad libitum*. All animal studies had complied with all relevant ethical regulations for the animal testing and research and were approved by institutional guidelines and the Animal Care and Use Committee of Huazhong University of Science and Technology.

Virus Injection and Optic Fiber Cannula Implantation

Mice were anesthetized with 1% pentobarbital sodium (35 mg/kg) and head-fixed in a stereotactic frame (RWD, Shenzhen, China). Eyes were coated with erythromycin ointment to avoid strong light exposure. The scalp was incised along the skull midline after sterilizing with iodophors. pAAV-CaMKIIα-ChR2(H134R)-mCherry (500 nL, 2–5 × 10^9 pfu/mL; OBio Technology Shanghai, China) was injected into the vCA1 (AP −3.2 mm, ML +3.2 mm, DV −4.5 mm) at a rate of 50 nL/min. The needle syringe was kept for 10 min before withdrawal. The skin was sutured and then sterilized with iodophors. The mice were put on a heat lamp to revive. Three weeks after virus injection, optic fiber cannulas (NA = 0.37, Newdoon, China) were implanted into the vCA1 of mice (AP −3.2 mm, ML +3.2 mm, DV −4.1 mm). Four screws (RWD, Shenzhen, China) were anchored around the fiber cannulas

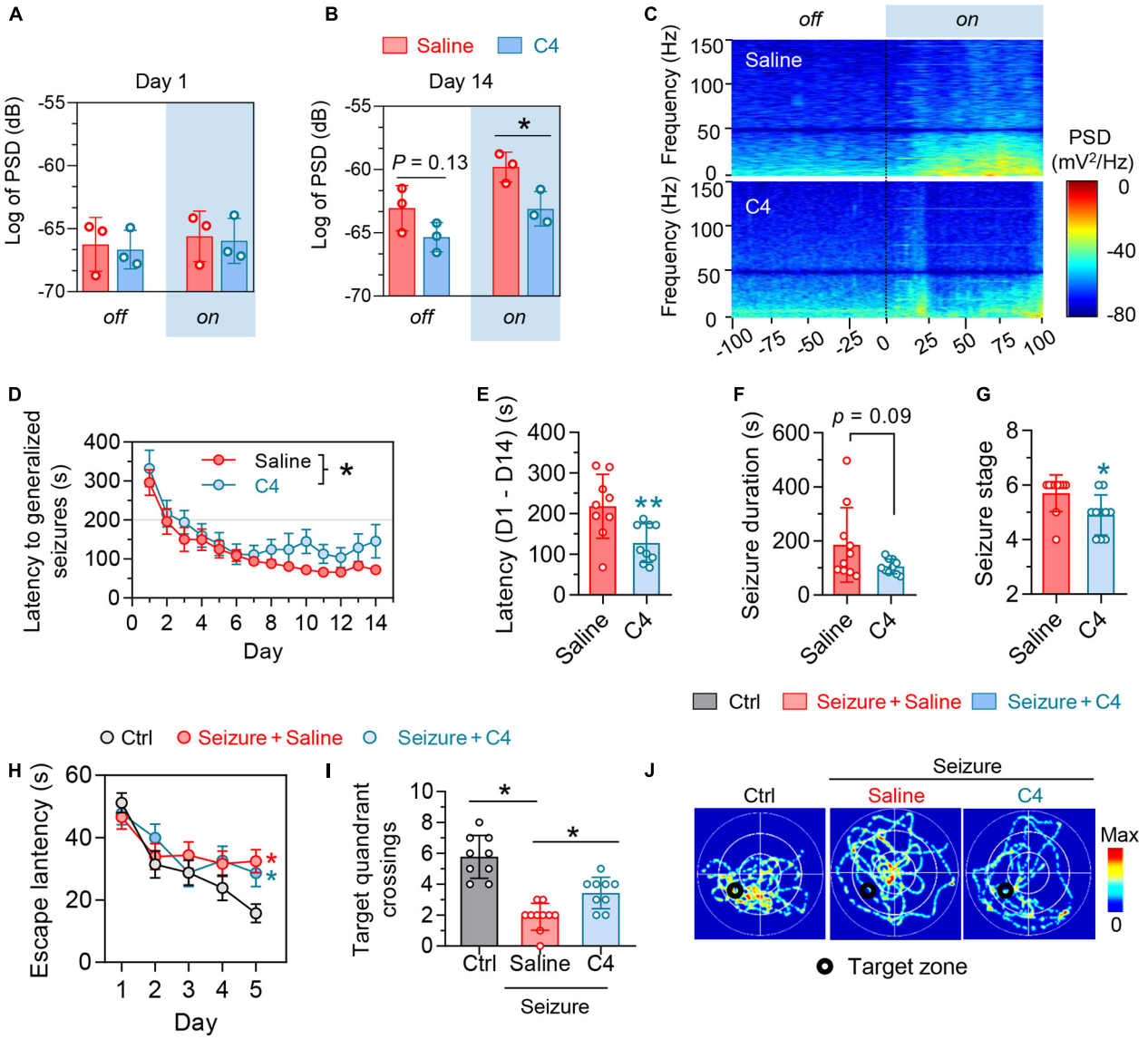

FIGURE 5 | Selectively facilitating tau degradation by C4 alleviates the optogenetics-induced epileptic seizures and the associated spatial memory deficits. **(A–C)** Blue light on did not change basal PSD in primary motor cortex (M1) at day 1, whereas C4 treatment significantly downregulated the PSD in M1 at day 14 during light-on. $n = 3$ mice in each group, unpaired t tests, $^*p < 0.05$. **(D,E)** C4 prolonged the latency of generalized seizures of mice. $n = 7$–9 mice in each group. Repeated-measures ANOVA followed by Tukey multiple-comparisons tests, $^*p < 0.05$. Unpaired t-tests, $^{**}p < 0.01$. **(F,G)** C4 tended to decrease the seizure duration and severity of seizure stages at day 14. Unpaired t tests, $^*p < 0.05$. **(H–J)** C4 showed limited effect on improving the repeated seizures-induced spatial learning impairments in the water maze training phase. $n = 9$–10 mice in each group. Repeated-measures ANOVA followed by Tukey multiple-comparisons tests, $^*p < 0.05$, compared with the non-seizure Ctrl group. **(I,J)** C4 significantly alleviated the seizures-induced spatial memory impairments. One-way ANOVA followed by Tukey multiple-comparisons tests, $^*p < 0.05$. Values are presented as the mean ± SEM.

with dental cement. Mice were put back into the cage for reviving postoperation.

Optogenetic Stimulation and Seizures Induction

Mice were handled for consecutive 3 days before seizure induction and were temporarily anesthetized with isoflurane. The fiber cannulas were connected to a plug line with FC/PC joint at both ends. Seizures were induced 10 s after the mice woke up. Laser output is controlled by a function generator (Tektronix, China, NO. AFG 3022B). After many trials, the stimulation parameters were finally set as 20 Hz, blue light (472 nm), duty cycle 10%, pulse wave. The actual output power of optical fiber outlet was 2.8 mW/mm^2 (when the waveform generator was not connected, the output power of optical fiber outlet was 43.2 mW/mm^2). Mice behaviors were recorded using a digital camera. The severity of mice seizures was evaluated according to MRS (Racine, 1975; Haas et al., 1990): stage 1, facial convulsions,

chewing behavior in the mouth; stage 2, chewing and rhythmic head nodding; stage 3, unilateral forelimb clonus; stage 4, bilateral forelimb clonus with rearing, standing on hind limb; stage 5, rearing and repeated falling; stage 6, wild running, jumping. Stages 1 to 3 were considered as focal seizures, and stages 4–6 considered generalized seizures. The time from stimulation onset to stage 4 was recorded as latency to generalized seizures in this study. There were some differences between Test 1 (**Figures 1**, **2**) and Test 2 (**Figure 4**) in the duration of epileptic induction. The laser was turned off until stage 6 in Test 1, whereas stage 4 in Test 2. After the seizure induction, the mice were anesthetized by isoflurane, and the fiber was removed from their heads.

Local Field Potentials Recording *in vivo*

Three weeks after virus injection into the vCA1, a 16-channel electrode was implanted into the ipsilateral M1 (+1.5 mm AP, +1.5 mm ML, –1.5 mm DV). The ground of the electrode was connected to two screws attached to the skull. Mice skin was sutured and then sterilized with iodophors. Mice were allowed 1 week for recovery postoperation before *in vivo* recording. Each mouse was handled for 5 min and adapted in a box for 10 min before the first time of recording. LFPs in M1 and mouse behaviors were recorded using a Recording System (Plexon, Hong Kong, China). Data were stored for offline analysis with 16-bit format, visualized in Neuro Explore. Amplitude and PSD of LFPs were analyzed in default parameters: shift (0.5 s), number of frequency values (8,192), normalization (log of PSD), show frequency from 0 to 150 HZ. Baseline signals were recorded before the laser was turned on. When the seizure induction began, mice behaviors were observed carefully, and the optogenetic stimulation was stopped at an appropriate time. After the final electrophysiological recording, the mice were killed, and the electrodes locations were confirmed by brain slice section.

Open Field Test

The apparatus was a 60-cm × 60-cm × 50-cm plastic box. The floor was divided into nine equal squares, among which the whole central area takes up 50%. The individual mouse was placed in the center opposite to experimenter. Each mouse was allowed to explore freely for 5 min. Mice behaviors were recorded by a camera. The time and distance that the mice traveled in the central area were analyzed.

Elevated-Plus Maze Test

The elevated plus maze consisted of two enclosed arms (30 cm × 5 cm × 20 cm) and two open arms (30 cm × 5 cm). The apparatus was elevated to 50 cm above the floor. Mice were placed individually in the center of the maze facing the open arm opposite to the experimenter. The time mice spent in the open/closed arms were recorded through tracking the center of the body. The mice explored freely for 5 min.

Morris-Water Maze Test

The spatial learning and memory of mice were assessed by Morris-Water Maze test. For spatial learning, mice were trained in the maze to find a hidden platform for five consecutive days, three trials per day with an interval of 30 min from 2:00 to 5:00 PM each day. In each trial, mice started from one of the four quadrants facing the wall of the pool. Each trial ended when the animal climbed onto the platform. If the mice did not find the platform within 60 s, they were guided to the platform and allowed to stay on the platform for 15 s. The swimming path and time mice used to find the platform (escape latency) during training, as well as time mice pass through the previous platform quadrant in the test phase, were recorded by a video camera fixed to the ceiling, 1.5 m from the water surface.

Western Blotting

Mice brains were removed, and the cortex and hippocampus were dissected on ice. Samples were homogenized with RIPA lysis buffer (Beyotime). Proteins were separated by sodium dodecyl sulfate–polyacrylamide gel electrophoresis, transferred onto nitrocellulose membranes (Merck Millipore) and then blocked with 5% bovine serum albumin (BSA). Blots were probed with polyclonal rabbit anti-Tau5 (1:1,000; cat no. MAB361, Millipore), polyclonal rabbit anti-AT8 (1:1,000; cat no. MN1020, Thermo), and polyclonal rabbit anti-α-tubulin (1:1,000; cat no. T9026, Sigma) and were then incubated with horseradish peroxidase–conjugated secondary antibodies and visualized by an enhanced chemiluminescence substrate system (Santa Cruz, CA, United States). Blots were visualized using an Odyssey Imaging System (LI-COR Biosciences) and quantitatively analyzed by ImageJ.

Immunostaining

Mice were sacrificed 1 day after the last trial of WMW test and then anesthetized and perfused through ventriculus sinister with 0.9% NaCl for 5 min and then phosphate buffer containing 4% paraformaldehyde for 5 min. Brain were cryoprotected in 25% and 30% sucrose solutions in turn for 2 days. The next day, brains were cut into 30-μm sections using a cryostat microtome (CM1900, Leica). For immunohistochemistry, free-floating sections were blocked with 3% H_2O_2 in anhydrous methanol for 30 min, and non-specific sites were blocked with BSA for 30 min at room temperature. Sections were then incubated overnight at 4°C with Tau5 (1:200; cat no. MAB361, Millipore) or AT8 (1:200; cat no. MN1020, Thermo) antibodies. Immunoreactions were developed using a DAB-staining kit (ZSGB-BIO). For immunofluorescence, sections were thoroughly washed with PBS-T [phosphate-buffered saline (PBS) containing 0.1% Triton X-100] and incubated overnight with monoclonal mouse Tau 5 (1:200; cat no. MAB361, Millipore) or AT8 (1:200; cat no. MN1020, Thermo) antibodies. After that, the sections underwent PBS-T washes (three times, 5 min each), followed by 1-h incubation with the secondary antibody at 37°C. Finally, the slice underwent three more washes and counterstained with DAPI. Images were taken by two-photon laser-scanning confocal microscope (LSM710, Zeiss).

Nissl Staining

Mice brain slices were selected and rinsed with PBS for 5 min and then moved to the adhesive slides with a brush and dried naturally. The tar-purple dye drops about 500 μL were spread

evenly over the brain slices. Then, the slices dyed for about 10–15 min, distilled water for 1 min, 75% alcohol, 80% alcohol, 95% alcohol, and anhydrous ethanol for 1 min each, and finally made transparent with xylene for 30–60 min. Slices were sealed with neutral resin and dried naturally.

Statistical Analyses

All data were analyzed and plotted using GraphPad Prism 7 (GraphPad Software, Inc., La Jolla, CA, United States). One-way analysis of variance (ANOVA), Tukey multiple-comparisons *post hoc* tests, and two-tailed unpaired *t* tests were used. $P < 0.05$ was considered significant. Data were shown as mean ± SEM.

DATA AVAILABILITY STATEMENT

The raw data supporting the conclusions of this article will be made available by the authors, without undue reservation.

ETHICS STATEMENT

The animal study was reviewed and approved by institutional guidelines and the Animal Care and Use Committee of Huazhong University of Science and Technology.

AUTHOR CONTRIBUTIONS

YG, JZ, and J-ZW conceived the concept, instructed data analysis, and revised the manuscript. YG and JZ conducted most of the data analysis, prepared the figures, and wrote the manuscript draft. TJ, GP, FS, and RX helped with some experiments. JW reviewed the manuscript with input from all authors. All authors contributed to the article and approved the submitted version.

FUNDING

This work was supported by grants from the National Natural Science Foundation of China (31730035, 91632305, 81721005, and 91949205), the Natural Science Foundation of China-Henan Joint Fund (U1804197), the Program for Science & Technology Innovation Talents in University of Henan Province, and the Guangdong Provincial Key S&T Program (2018B030336001).

ACKNOWLEDGMENTS

We would like to thank Professor Guohe Tan for his good advices on this research.

REFERENCES

Auladell, C., de Lemos, L., Verdaguer, E., Ettcheto, M., Busquets, O., Lazarowski, A., et al. (2017). Role of JNK isoforms in the kainic acid experimental model of epilepsy and neurodegeneration. *Front. Biosci.* 22, 795–814. doi: 10.2741/4517

Avanzini, G., Depaulis, A., Tassinari, A., and de Curtis, M. (2013). Do seizures and epileptic activity worsen epilepsy and deteriorate cognitive function? *Epilepsia* 54(Suppl. 8), 14–21. doi: 10.1111/epi.12418

Baker, J., Libretto, T., Henley, W., and Zeman, A. (2019). The prevalence and clinical features of epileptic seizures in a memory clinic population. *Seizure* 71, 83–92. doi: 10.1016/j.seizure.2019.06.016

Baxendale, S. A., Thompson, P. J., and Duncan, J. S. (2005). Epilepsy & depression: the effects of comorbidity on hippocampal volume–a pilot study. *Seizure* 14, 435–438.

Breuer, L. E., Boon, P., Bergmans, J. W., Mess, W. H., Besseling, R. M., de Louw, A., et al. (2016). Cognitive deterioration in adult epilepsy: does accelerated cognitive ageing exist? *Neurosci. Biobehav. Rev.* 64, 1–11. doi: 10.1016/j.neubiorev.2016.02.004

Busche, M. A., Wegmann, S., Dujardin, S., Commins, C., Schiantarelli, J., Klickstein, N., et al. (2019). Tau impairs neural circuits, dominating amyloid-beta effects, in Alzheimer models in vivo. *Nat. Neurosci.* 22, 57–64. doi: 10.1038/s41593-018-0289-8

Cela, E., McFarlan, A. R., Chung, A. J., Wang, T., Chierzi, S., Murai, K. K., et al. (2019). An optogenetic kindling model of neocortical epilepsy. *Sci. Rep.* 9:5236.

Cheng, C. H., Liu, C. J., Ou, S. M., Yeh, C. M., Chen, T. J., Lin, Y. Y., et al. (2015). Incidence and risk of seizures in Alzheimer's disease: a nationwide population-based cohort study. *Epilepsy Res.* 115, 63–66. doi: 10.1016/j.eplepsyres.2015.05.009

Choy, M., Duffy, B. A., and Lee, J. H. (2017). Optogenetic study of networks in epilepsy. *J. Neurosci. Res.* 95, 2325–2335. doi: 10.1002/jnr.23767

DeVos, S. L., Goncharoff, D. K., Chen, G., Kebodeaux, C. S., Yamada, K., Stewart, F. R., et al. (2013). Antisense reduction of tau in adult mice protects against seizures. *J. Neurosci.* 33, 12887–12897. doi: 10.1523/jneurosci.2107-13.2013

Feldman, L., Lapin, B., Busch, R. M., and Bautista, J. F. (2018). Evaluating subjective cognitive impairment in the adult epilepsy clinic: effects of depression, number of antiepileptic medications, and seizure frequency. *Epilepsy Behav.* 81, 18–24. doi: 10.1016/j.yebeh.2017.10.011

Gheyara, A. L., Ponnusamy, R., Djukic, B., Craft, R. J., Ho, K., Guo, W., et al. (2014). Tau reduction prevents disease in a mouse model of Dravet syndrome. *Ann. Neurol.* 76, 443–456. doi: 10.1002/ana.24230

Haas, K. Z., Sperber, E. F., and Moshé, S. L. (1990). Kindling in developing animals: expression of severe seizures and enhanced development of bilateral foci. *Brain Res. Dev. Brain Res.* 56, 275–280. doi: 10.1016/0165-3806(90)90093-e

Holth, J. K., Bomben, V. C., Reed, J. G., Inoue, T., Younkin, L., Younkin, S. G., et al. (2013). Tau loss attenuates neuronal network hyperexcitability in mouse and *Drosophila* genetic models of epilepsy. *J. Neurosci.* 33, 1651–1659. doi: 10.1523/jneurosci.3191-12.2013

Inostroza, M., Cid, E., Menendez de la Prida, L., and Sandi, C. (2012). Different emotional disturbances in two experimental models of temporal lobe epilepsy in rats. *PLoS One* 7:e38959. doi: 10.1371/journal.pone.0038959

Iqbal, K., Liu, F., Gong, C. X., Alonso, Adel C, and Grundke-Iqbal, I. (2009). Mechanisms of tau-induced neurodegeneration. *Acta Neuropathol.* 118, 53–69. doi: 10.1007/s00401-009-0486-3

Jones, N. C., Nguyen, T., Corcoran, N. M., Velakoulis, D., Chen, T., Grundy, R., et al. (2012). Targeting hyperphosphorylated tau with sodium selenate suppresses seizures in rodent models. *Neurobiol. Dis.* 45, 897–901. doi: 10.1016/j.nbd.2011.12.005

Kanner, A. M. (2009). Psychiatric issues in epilepsy: the complex relation of mood, anxiety disorders, and epilepsy. *Epilepsy Behav.* 15, 83–87. doi: 10.1016/j.yebeh.2009.02.034

Khoshkhoo, S., Vogt, D., and Sohal, V. S. (2017). Dynamic, cell-type-specific roles for GABAergic interneurons in a mouse model of optogenetically inducible seizures. *Neuron* 93, 291–298. doi: 10.1016/j.neuron.2016.11.043

Lam, A. D., Deck, G., Goldman, A., Eskandar, E. N., Noebels, J., and Cole, A. J. (2017). Silent hippocampal seizures and spikes identified by foramen ovale electrodes in Alzheimer's disease. *Nat. Med.* 23, 678–680. doi: 10.1038/nm.4330

Liu, S. J., Zheng, P., Wright, D. K., Dezsi, G., Braine, E., Nguyen, T., et al. (2016). Sodium selenate retards epileptogenesis in acquired epilepsy models reversing changes in protein phosphatase 2A and hyperphosphorylated tau. *Brain* 139(Pt 7), 1919–1938. doi: 10.1093/brain/aww116

Liu, X., Ou, S., Yin, M., Xu, T., Wang, T., Liu, Y., et al. (2017). N-methyl-D-aspartate receptors mediate epilepsy-induced axonal impairment and tau phosphorylation via activating glycogen synthase kinase-3β and cyclin-dependent kinase 5. *Discov. Med.* 23, 221–234.

Mondoloni, S., Durand-de Cuttoli, R., and Mourot, A. (2019). Cell-Specific Neuropharmacology. *Trends Pharmacol. Sci.* 40, 696–710. doi: 10.1016/j.tips.2019.07.007

Morimoto, K., Fahnestock, M., and Racine, R. J. (2004). Kindling and status epilepticus models of epilepsy: rewiring the brain. *Prog. Neurobiol.* 73, 1–60. doi: 10.1016/j.pneurobio.2004.03.009

Osawa, S., Iwasaki, M., Hosaka, R., Matsuzaka, Y., Tomita, H., Ishizuka, T., et al. (2013). Optogenetically induced seizure and the longitudinal hippocampal network dynamics. *PLoS One* 8:e60928. doi: 10.1371/journal.pone.0060928

Paudel, Y. N., Angelopoulou, E., Jones, N. C., O'Brien, T. J., Kwan, P., Piperi, C., et al. (2019). Tau related pathways as a connecting link between epilepsy and Alzheimer's disease. *ACS Chem. Neurosci.* 10, 4199–4212. doi: 10.1021/acschemneuro.9b00460

Racine, R. J. (1975). Modification of seizure activity by electrical stimulation: cortical areas. *Electroencephalogr. Clin. Neurophysiol.* 38, 1–12. doi: 10.1016/0013-4694(75)90204-7

Sadqi, M., Hernández, F., Pan, U., Pérez, M., Schaeberle, M. D., Avila, J., et al. (2002). Alpha-helix structure in Alzheimer's disease aggregates of tau-protein. *Biochemistry* 41, 7150–7155. doi: 10.1021/bi025777e

Sánchez, M. P., García-Cabrero, A. M., Sánchez-Elexpuru, G., Burgos, D. F., and Serratosa, J. M. (2018). Tau-induced pathology in epilepsy and dementia: notions from patients and animal models. *Int. J. Mol. Sci.* 19:1092. doi: 10.3390/ijms19041092

Scott, A. J., Sharpe, L., Hunt, C., and Gandy, M. (2017). Anxiety and depressive disorders in people with epilepsy: a meta-analysis. *Epilepsia* 58, 973–982. doi: 10.1111/epi.13769

Smith, K. M., Blessing, M. M., Parisi, J. E., Britton, J. W., Mandrekar, J., and Cascino, G. D. (2019). Tau deposition in young adults with drug-resistant focal epilepsy. *Epilepsia* 60, 2398–2403. doi: 10.1111/epi.16375

So, E. L., and Penry, J. K. (1981). Epilepsy in adults. *Ann. Neurol.* 9, 3–16.

Sohn, P. D., Huang, C. T., Yan, R., Fan, L., Tracy, T. E., Camargo, C. M., et al. (2019). Pathogenic tau impairs axon initial segment plasticity and excitability homeostasis. *Neuron* 104, 458–470 e5.

Sun, X. Y., Wei, Y. P., Xiong, Y., Wang, X. C., Xie, A. J., Wang, X. L., et al. (2012). Synaptic released zinc promotes tau hyperphosphorylation by inhibition of protein phosphatase 2A (PP2A). *J. Biol. Chem.* 287, 11174–11182. doi: 10.1074/jbc.m111.309070

Tai, X. Y., Koepp, M., Duncan, J. S., Fox, N., Thompson, P., Baxendale, S., et al. (2016). Hyperphosphorylated tau in patients with refractory epilepsy correlates with cognitive decline: a study of temporal lobe resections. *Brain* 139(Pt 9), 2441–2455. doi: 10.1093/brain/aww187

Tønnesen, J., and Kokaia, M. (2017). Epilepsy and optogenetics: can seizures be controlled by light? *Clin. Sci.* 131, 1605–1616. doi: 10.1042/cs20160492

Verstraelen, P., Detrez, J. R., Verschuuren, M., Kuijlaars, J., Nuydens, R., Timmermans, J. P., et al. (2017). Dysregulation of microtubule stability impairs morphofunctional connectivity in primary neuronal networks. *Front. Cell. Neurosci.* 11:173. doi: 10.3389/fncel.2017.00173

Wang, J. Z., Gao, X., and Wang, Z. H. (2014). The physiology and pathology of microtubule-associated protein tau. *Essays Biochem.* 56, 111–123. doi: 10.1042/bse0560111

Wang, Y., and Mandelkow, E. (2016). Tau in physiology and pathology. *Nat. Rev. Neurosci.* 17, 5–21.

Welzel, L., Schidlitzki, A., Twele, F., Anjum, M., and Löscher, W. (2020). A face-to-face comparison of the intra-amygdala and intrahippocampal kainate mouse models of mesial temporal lobe epilepsy and their utility for testing novel therapies. *Epilepsia* 61, 157–170. doi: 10.1111/epi.16406

Witt, J. A., and Helmstaedter, C. (2017). Cognition in epilepsy: current clinical issues of interest. *Curr. Opin. Neurol.* 30, 174–179. doi: 10.1097/wco.0000000000000430

Yang, Y., and Wang, J. Z. (2018). Nature of tau-associated neurodegeneration and the molecular mechanisms. *J. Alzheimers Dis.* 62, 1305–1317. doi: 10.3233/jad-170788

Ye, J., Yin, Y., Yin, Y., Zhang, H., Wan, H., Wang, L., et al. (2020). Tau-induced upregulation of C/EBPβ-TRPC1-SOCE signaling aggravates tauopathies: a vicious cycle in Alzheimer neurodegeneration. *Aging Cell* 19:e13209.

Yin, Y., Gao, D., Wang, Y., Wang, Z. H., Wang, X., Ye, J., et al. (2016). Tau accumulation induces synaptic impairment and memory deficit by calcineurin-mediated inactivation of nuclear CaMKIV/CREB signaling. *Proc. Natl Acad. Sci. U.S.A.* 113, E3773–E3781.

Yogarajah, M., and Mula, M. (2019). Social cognition, psychiatric comorbidities, and quality of life in adults with epilepsy. *Epilepsy Behav.* 100:106321. doi: 10.1016/j.yebeh.2019.05.017

Zarea, A., Charbonnier, C., Rovelet-Lecrux, A., Nicolas, G., Rousseau, S., Borden, A., et al. (2016). Seizures in dominantly inherited Alzheimer disease. *Neurology* 87, 912–919.

Zheng, J., Li, H. L., Tian, N., Liu, F., Wang, L., Yin, Y., et al. (2020). Interneuron accumulation of phosphorylated tau impairs adult hippocampal neurogenesis by suppressing GABAergic transmission. *Cell Stem Cell* 26, 462–466. doi: 10.1016/j.stem.2020.01.021

Conflict of Interest: The authors declare that the research was conducted in the absence of any commercial or financial relationships that could be construed as a potential conflict of interest.

frontiers in Cell and Developmental Biology

ORIGINAL RESEARCH
published: 25 February 2021
doi: 10.3389/fcell.2021.648261

Maternal Lead Exposure Impairs Offspring Learning and Memory via Decreased GLUT4 Membrane Translocation

Zai-Hua Zhao[1†], Ke-Jun Du[1†], Tao Wang[1], Ji-Ye Wang[1], Zi-Peng Cao[1], Xiao-Ming Chen[1], Han Song[1,2], Gang Zheng[1] and Xue-Feng Shen[1*]*

[1] Department of Occupational and Environmental Health and the Ministry of Education Key Lab of Hazard Assessment and Control in Special Operational Environment, School of Public Health, Fourth Military Medical University, Xi'an, China, [2] Department of Health Service, Chinese PLA General Hospital, Beijing, China

OPEN ACCESS

Edited by:
Gong-Ping Liu,
Huazhong University of Science and Technology, China

Reviewed by:
Xihui Liu,
University of Texas Southwestern Medical Center, United States
Aiguo Xuan,
Guangzhou Medical University, China

***Correspondence:**
Xue-Feng Shen
xfshen@fmmu.edu.cn
Gang Zheng
zhenggang@fmmu.edu.cn

[†] These authors have contributed equally to this work

Specialty section:
This article was submitted to Molecular Medicine, a section of the journal Frontiers in Cell and Developmental Biology

Received: 31 December 2020
Accepted: 08 February 2021
Published: 25 February 2021

Citation:
Zhao Z-H, Du K-J, Wang T, Wang J-Y, Cao Z-P, Chen X-M, Song H, Zheng G and Shen X-F (2021) Maternal Lead Exposure Impairs Offspring Learning and Memory via Decreased GLUT4 Membrane Translocation. Front. Cell Dev. Biol. 9:648261. doi: 10.3389/fcell.2021.648261

Lead (Pb) can cause a significant neurotoxicity in both adults and children, leading to the impairment to brain function. Pb exposure plays a key role in the impairment of learning and memory through synaptic neurotoxicity, resulting in the cognitive function. Researches have demonstrated that Pb exposure plays an important role in the etiology and pathogenesis of neurodegenerative diseases, such as Alzheimer's disease. However, the underlying mechanisms remain unclear. In the current study, a gestational Pb exposure (GLE) rat model was established to investigate the underlying mechanisms of Pb-induced cognitive impairment. We demonstrated that low-level gestational Pb exposure impaired spatial learning and memory as well as hippocampal synaptic plasticity at postnatal day 30 (PND 30) when the blood concentration of Pb had already recovered to normal levels. Pb exposure induced a decrease in hippocampal glucose metabolism by reducing glucose transporter 4 (GLUT4) levels in the cell membrane through the phosphatidylinositol 3 kinase-protein kinase B (PI3K-Akt) pathway. *In vivo* and *in vitro* GLUT4 over-expression increased the membrane translocation of GLUT4 and glucose uptake, and reversed the Pb-induced impairment to synaptic plasticity and cognition. These findings indicate that Pb exposure impairs synaptic plasticity by reducing the level of GLUT4 in the cell membrane as well as glucose uptake via the PI3K-Akt signaling pathway, demonstrating a novel mechanism for Pb exposure-induced neurotoxicity.

Keywords: lead, learning and memory, hippocampus synaptic plasticity, glucose transporter 4, PI3K-Akt

HIGHLIGHTS

Maternal (pregnancy/gestational) Pb exposure at a low level induces offspring spatial learning and memory deficits via reducing glucose uptake through the down-regulation of GLUT4 membrane translocation.

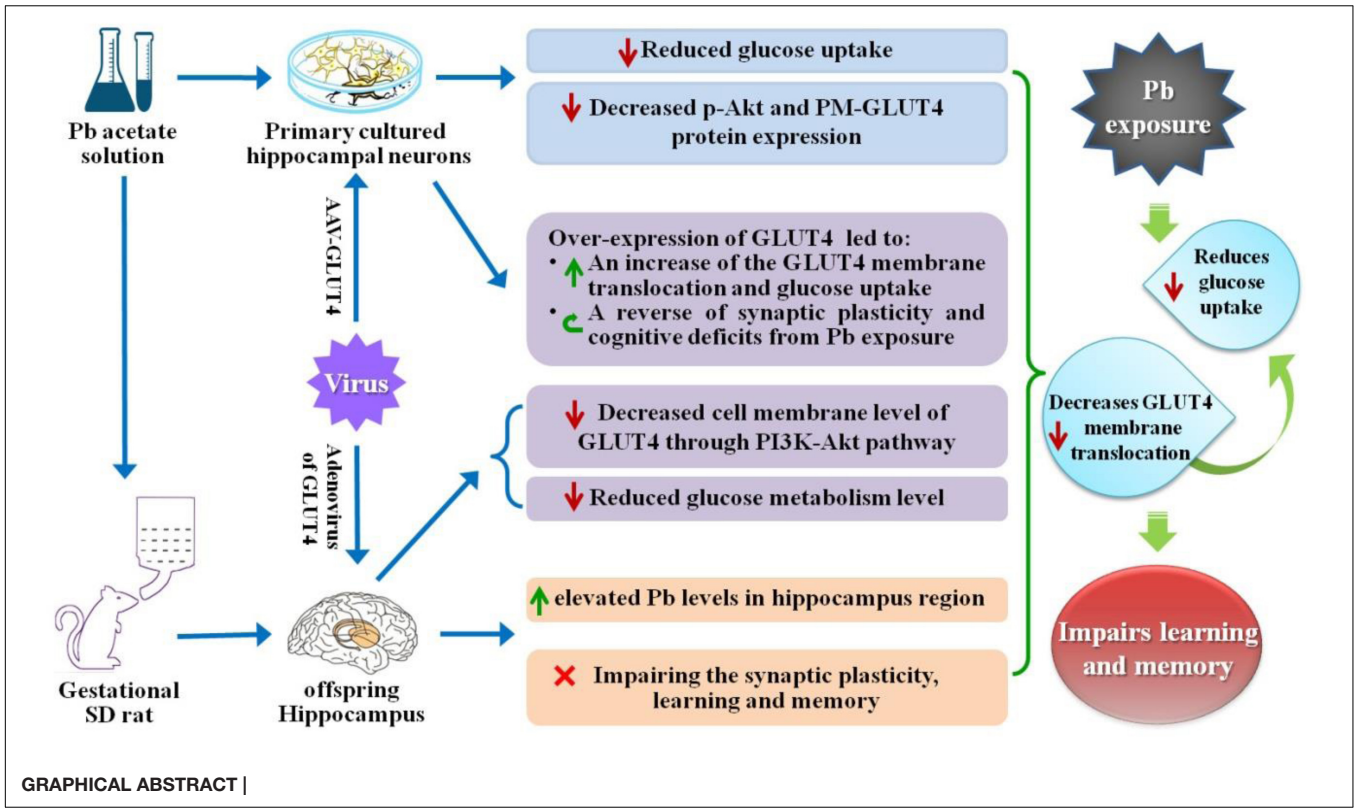

GRAPHICAL ABSTRACT |

INTRODUCTION

The developing brain is particularly vulnerable to lead (Pb) exposure, which causes persistent behavioral and emotional disturbances, such as cognitive dysfunction, including deficits in executive functioning, attention, and memory (Mills et al., 2011). Not only that, but as the course of the disease lengthens, the brain damage induced by Pb exposure can eventually develop into dementia (Genuis and Kelln, 2015). Researches have confirmed that chronic Pb exposure is an important risk factor for Alzheimer's disease related neurodegenerative diseases (Bihaqi and Zawia, 2013). In previous studies, animals exposed to Pb during the perinatal (during gestation through weaning), early postnatal [during postnatal day (PND) 1 through weaning], or late postnatal (during weaning and later) periods were used to evaluate the effects of Pb neurotoxicity on the brain and the underlying mechanisms (Brody et al., 1994). Regardless of the exposure time window, these studies and ours collectively revealed that developmental Pb exposure significantly impairs spatial learning and memory (Hu et al., 2014, 2016; Wang et al., 2016).

As the hippocampus is sensitive to Pb exposure and plays a critical role in spatial learning and memory, which is the basis of cognitive ability (Barha and Galea, 2013), the hippocampus has become a research focus for Pb exposure-induced neurotoxicity (Anderson et al., 2013). Pb exposure during development impairs hippocampus-dependent spatial learning and memory via modifying the levels of *N*-methyl-D-aspartate (NMDA) receptor-dependent brain-derived neurotrophic factors (BDNFs) (Neal et al., 2010), hippocampal long-term potentiation (LTP) (Liu et al., 2012), genomic features (Anderson et al., 2013), and epigenetic regulation by manipulating the expression of DNA methyl-cytosine-binding proteins and methyltransferases (Schneider et al., 2013). Previous animal studies on this topic have enriched our knowledge regarding Pb exposure-induced neurotoxicity. Unfortunately, most of the findings have not been translated to clinical applications. Chelation therapy remains the primary method to treat child Pb poisoning as it helps to lower blood Pb levels while alleviating significant Pb-induced cognitive impairment (Rogan et al., 2001; Bhattacharya et al., 2007). Studies have demonstrated that Pb can accumulate in the blood of pregnant women and subsequently enter the fetus through the placental barrier, eventually leading to fetal mental retardation and long-term adverse effects on offspring learning and memory functions. Moreover, this damage is irreversible, even the damage from low-level Pb exposure to pregnant women (Zartarian et al., 2017; Ettinger and Brown, 2018). Therefore, further clarification of the underlying mechanisms for the impairment of learning and memory induced by environmental Pb exposure is essential.

Glucose is the most important and unique energy substance in the brain and plays a key role in maintaining the structural and functional integrity of neurons in the brain (Im et al., 2019; Yun et al., 2019). It is also reported to be one of the main neuro-modulators that promote brain learning and memory (Smith et al., 2011). Consequently, glucose metabolic disorders always cause cognitive impairments (Kleinridders et al., 2014). Studies have reported that Pb exposure alters the activities of enzymes involved in the glucose metabolic

process, which can lead to abnormal glucose metabolism and eventually results in brain energy metabolic disorders (Yun and Hoyer, 2000; Ahmad et al., 2018). Additionally, recent research has shown that Pb exposure causes glucose tolerance and insulin resistance (Mostafalou et al., 2015). Several hypotheses have been proposed for the mechanism by which glucose metabolic disorders cause cognitive impairments. These include the "hippocampal hypothesis" (McNay et al., 2000), which posits that cognitive activity can deplete extracellular glucose in the hippocampus and that exogenous glucose administration reverses the depletion while enhancing task performance. Additionally, the "insulin hypothesis" (de la Monte et al., 2011) suggests that major abnormalities in brains with fetal alcohol spectrum disorder (FASD) are mediated by impairments in insulin/insulin-like growth factor (IGF) signaling. However, the specific mechanism for the learning and memory deficits induced by glucose metabolic disorders remains unclear and needs to be further explored.

Glucose transporters (GLUTs) include more than ten protein families. Among these transporters, GLUT4 is expressed in the central nervous system (CNS) and contributes to synapse formation in the hippocampus (Reagan, 2002). During learning and memory formation, GLUT4 is translocated into neuronal membranes and provides a glucose supply to neurons to maintain the structural and functional integrity of synapses through a process involving the phosphatidylinositol 3 kinase-protein kinase B (PI3K-Akt) signaling pathway (Piroli et al., 2007; Grillo et al., 2009; Chiu and Cline, 2010). However, it remains unclear whether Pb exposure has an impact on GLUTs and whether this influence leads to spacial memory impairment. In this study, a gestational Pb exposure (GLE) rat model was established and the cognition of the rats was assessed. Through morphological analysis (Golgi-Cox staining) and LTP recording in the hippocampal cornu ammonis 1 (CA1) region of the offspring, we investigated the effect of low-level gestational Pb exposure on hippocampal synaptic plasticity and examined how the offspring's spatial learning and memory functions were affected at PND 30 using Morris water maze (MWM) experiments. Furthermore, the hippocampal glucose metabolism was measured using Positron Emission Tomography-Computed Tomography (PET-CT) scanning and the GLUT4 membrane translocation and expression of hippocampal neurons were measured using immunofluorescence staining and western blot (WB). Finally, we investigated the effects of GLUT4 alterations on hippocampal synaptic plasticity and the offspring's spatial learning and memory functions by over-expressing GLUT4 *in vivo* and *in vitro*. We found that Pb exposure interfered with the expression and translocation of GLUT4 while reducing the glucose supply in hippocampal neurons, leading to spacial memory deficits.

MATERIALS AND METHODS

Study Design

A low-level GLE rat model was established by feeding Pb solutions to female Sprague-Dawley (SD) rats. The experimental gestational rats were randomly assigned to two groups (control and Pb-exposed). Tissue samples were collected from embryonic rats on day 18∼19 (E18∼19) for primary hippocampal neuronal culture and the offspring rats were used in all other experiments in this study. A previous study showed that there are significant differences between female and male infants and children in the GLE model (Gilbert et al., 2005; Fox et al., 2008); thus, only male offspring rats were used in the current study to reduce bias. For morphological analysis (Golgi-Cox staining), basilar dendrites from CA1 pyramidal neurons in plates 58∼63 were selected for analysis. An investigator blinded to the study conditions performed neuron selection and tracing. Pyramidal neurons were identified based on the unique triangular shape of their soma and their apical extensions toward the apical surface. β-actin was employed as the internal reference protein in all WB tests. The animal protocol and experiments were approved by the Laboratory Animal Welfare and Ethics Committee of the Fourth Military Medical University.

Animals and GLE Model

In this study, SD rats were used as experimental animals and were subjected to a 12-h light/dark cycle in a 24°C temperature-controlled room. The animals could obtain food and water at will. Based on the research reports by Gilbert et al. (2005) and Fox et al. (2008) as well as our previous study (Zhao et al., 2018), a dose of 109 ppm was chosen to establish the low-level GLE model. Adult female rats raised alone were randomly divided into two groups: the control group received regular water and the Pb-exposed group was exposed to 109 ppm Pb through drinking solutions containing 0.02% Pb acetate (Fisher Scientific, Pittsburgh, PA, United States). This protocol was initiated 2 weeks before mating and continued throughout the gestation period up to PND 10. The weights of the offspring were recorded on PNDs 0, 10, 21, and 30.

Pb Concentration Analysis

Rats were taken from the control and Pb-exposed groups at PNDs 0, 10, 21, and 30 (n = 6, respectively), anesthetized with an intraperitoneal (i.p.) injection of sodium pentobarbital (60 mg/kg), and sacrificed by decapitation. Venous blood and hippocampal tissues digested by organic tissue solvents were used to determine the Pb concentration. The PerkinElmer 600 atomic absorption spectrometer (AAS) (PerkinElmer, United States) was used to analyze the blood samples and a plasmaQuad3 plasma mass spectrograph (VG Elemental, United Kingdom) was used to analyze the tissue samples.

MWM Tasks

The MWM was used to evaluate the spatial learning and memory of the rats at PND 30 based on the time they took to find an invisible platform. After 5 days of training, the test was performed and the mean time the rats required to reach the platform was recorded. The DigiBehave system (Jiliang Software Company, Shanghai, China) was used to record the routes taken by the rats. The percentage of rats that arrived at the target quadrant within 2 min was calculated. The detailed protocol was described in our previous study (Zhao et al., 2018).

Golgi-Cox Staining and Morphological Analysis

Golgi-Cox Staining

The rats were anesthetized with i.p. injections of 100 mg/kg sodium pentobarbital and cardiac perfusion was performed with 0.9% saline. The rat brains were subsequently extracted for Golgi-Cox staining.

Identification of Target Figures

For each animal, five sections from the hippocampal region were selected. Pyramidal neurons were identified based on the unique triangular shape of their soma and the extensions of their apex toward the apical surface. Basilar dendrites from the hippocampal pyramidal neurons in plates 58–63 in the CA1 region were selected for analysis. Note that neuronal selection and tracing were performed by an experimenter who was blinded to the experimental conditions.

Neuronal Plasticity Analysis

In order to collect information about the changes in the complexity of the dendritic tree, all basal dendritic segments and the cell body of each neuron were reconstructed using a computer-based neuron-tracking system (Bitplane Imaris, Bitplane AG, Zürich, Switzerland). The spines on a terminal dendrite at the tip of the third order from each selected neuron were counted at a magnification of 1000× to measure the spine density (minimal length 20 μm). The spine structure and spine density of each selected dendrite were assessed using the Bitplane Imaris software.

Please refer to our previous study for the specific procedures used in the above experiment (such as detailed steps for Golgi-Cox staining, observation under a microscope, specific inclusion criteria for the Golgi-impregnated neurons in our study, and spine reconstruction and classification) (Zhao et al., 2018).

Hippocampal LTP Recordings

Slice Preparations

The offspring rats were decapitated at PND 30 after anesthesia (n = 6, respectively). The brains were quickly removed and immersed in pre-cooled oxygenated (nearly 0°C, 95% O_2/5% CO_2) artificial cerebrospinal fluid (ACSF) containing (in mM): dextrose 10, KCl 5, NaCl 124, $NaHCO_3$ 26, NaH_2PO_4 1.25, $MgCl_2$ 1.25, and $CaCl_2$ 2.5, pH = 7.30∼7.45. Subsequently, the hippocampus of one hemisphere was extracted and sliced (300 μm) using a sliding microtome (Leica VT1000S, Germany). The hippocampal slices were allowed to recover in ACSF at room temperature (RT) for at least 1 h.

Electrophysiological Recordings

One slice at a time was transferred into the recording chamber (BSC-HT Med. Sys., United States) where the slice was continuously perfused with 28∼30°C ACSF (95% O_2/5% CO_2) at a rate of 1 mL/min. Field excitatory postsynaptic potentials (fEPSPs) were recorded by placing a bipolar stimulating electrode in the Schaffer/commissural fibers while a glass micropipette recording electrode (diameter: 3∼5 μm, resistance: 1∼3 MΩ) was positioned in the dendrites of a CA1 pyramidal cell. The evoking interval for the fEPSPs was 50 s. LTP was induced with a 100 Hz high-frequency stimulation (HFS) for 1 s after recording the baseline responses for 10 min. LTP referred to an increase in the EPSP slope relative to the baseline response (100%) for 40∼45 min after the application of a tetanic stimulus.

Radioligand Preparation and Positron Emission Tomography/Computed Tomography (PET/CT) Imaging

Fluoro-deoxy-glucose (FDG) scanning was performed in the Small Animal Imaging Core at the Department of Nuclear Medicine, Xijing Hospital. The rats received a tail vein injection of ^{18}F-FDG at a dose of 5 μCi/g in saline according to their weights before imaging. After 40 min of uptake while awake, a combination of 5% isoflurane and 95% O_2 was used to anesthetize the rats. The rats were placed in the dedicated PET-CT camera animal enclosure (nanoScan PET/CT, Mediso) in a head-prone position and high-density PET image reconstruction and CT attenuation correction scanning were performed. The body temperature of the rats was maintained at 37°C via a heating pad. All images were measured with a Derenzo phantom and reconstructed with the Tera-Tomo^{TM} 3D PET engine. In order to quantify the FDG, the regional SUV was quantified with PMOD version 3.801 (PMOD Technologies, Zurich, Switzerland) to obtain the FDG uptake, which was expressed as the SUV.

Hippocampal Neuron Culture and Virus Transfection

The hippocampal tissue of embryos from normal pregnant SD rats from embryonic day 18∼19 (E18∼19) without Pb exposure was extracted for hippocampal neuron culture and transfection. The hippocampus tissue from E18∼19 of SD rat was extracted in pre-cooled D-Hank solution. Aspirating tissue pieces with as little solution as possible (about 1 mm^3), and then accutase (Gibco, United States) was added and incubated for enough time at 37°C. After digestion, accutase solution and clasts were removed, Neurobasal (Gibco, United States) media supplemented with B27 and glutamax (GIBCOBRL, United States) was added to suspend the cells. Whereafter, the cells were planted at 2×10^5 cells/mL in 6-well plates precoated by poly-L-lysine. The medium was exchanged every 2 days. In the subsequent experiment, neurons were transfected with the corresponding virus of over-expression GLUT4 at 1 μl (2.5×10^9 ifu/ml) per well for 6-well plates at DIV 6 while cultures were treated with lead acetate (1 μM, Sigma-Aldrich, United States) for 5 days. The details were the same as in our previous study (Zhao et al., 2018).

Cell Membrane Protein Extraction and Western Blot Analysis

The membrane protein of the hippocampus and primary cultured hippocampal neurons were collected. Equal amounts of protein samples (50 μg) were used for WB analysis as described in our previous study (Zhao et al., 2018). The following were the primary antibodies used in the experiment: GLUT4 (ab654), GLUT1 (ab115730), and GLUT3 (ab41525) (dilution ratio 1:200, Abcam), and β-actin (A5441, dilution ratio 1:1000, Sigma). The

peroxidase-conjugated secondary antibodies were F0382 and F9137 (dilution ratio 1:1000, Sigma).

Immunofluorescence Staining

The rats were anesthetized on PDN 30 with 100 mg/kg sodium pentobarbital (i.p.) and cardiac perfusion was performed with 0.9% saline. Some of the brains in each group were extracted for immunofluorescence staining as described in our previous study (Zhao et al., 2018). The primary antibodies and dilution criterions were as follows: ab654, rabbit anti-GLUT4, 1:200; ab177487, mouse anti-NeuN, 1:400; ab7260, and mouse anti-GFAP, 1:800 (Abcam, United States). The secondary antibodies were as follows: A-21145, Alexa Fluor 594, A-11008, and Alexa Fluor 488 (1:1000, Molecular Probes, Invitrogen). All sections were incubated with Hoechst 33342 (Sigma-Aldrich, St. Louis, MO, United States) for 15 min while avoiding light.

Glucose Intake Test

Since day DIV 7 to DIV 12 is the primary time period of dendritic spine growth (Zhao et al., 2018), therefore, to establish Pb-exposure model *in vitro*, 1 μM of Pb acetate (Sigma-Aldrich, United States) was added to the cultured hippocampal neurons for 5 days in this period. On DIV 12, the primary culture medium for the hippocampal neurons was replaced with sugar-free neurobasal medium and the neurons were further cultured for 2 h. Afterward, the neurons were cultured with 100 μM 2-(N-(7-Nitrobenz-2-oxa-1,3-diazol-4-yl) amino)-6-deoxy-glucose (2-NBDG) and 1 μg/ml insulin for 30 min. The cells were subsequently collected for flow cytometry after being resuspended in PBS.

Construction of Neuron-Specific AAV-GLUT4 and Virus Injection

To produce neuron-specific recombination adeno-associated virus (rAAV), the *GLUT4* gene was sub-cloned into plasmids (pAOV-SYN-MCS-EGFP-3FLAG) containing a neuron-specific human synapsin I promoter (hSyn) to generate recombinant plasmids (pAOV-SYN-Slc2a4-P2A-EGFP- 3FLAG) by the company Obio Technology Corp., Ltd (Shanghai, China). AAV-293 cells were then transfected with AAV Rep/Cap expression plasmid, AAV helper plasmid (pAAV Helper), and pAOV-SYN-Slc2a4-P2A-EGFP-3FLAG simultaneously to obtain rAAV (AAV-GLUT4-GFP). Subsequently, viral particles were purified via iodixanol step-gradient ultracentrifugation. The genomic titer ($2.5\sim3.5 \times 10^{12}$ genomic copies per ml) was determined using quantitative polymerase chain reaction (qPCR). Rats were anesthetized with sodium pentobarbital (60 mg/kg, i.p.) before brain stereo localization injection and placed on a brain stereoscopic positioning injector in a prostrate position to maintain the head level. The bregma and lambda point were identified using a locator and confirmed to be at the same level according to the rat brain map. Specific locations in the hippocampus were also determined (bregma backward 3.96 mm, the midline around 3 mm, bregma down 3.2 mm). A skull drill was used to mark the desired locations on the skull by lightly drilling until the skull cracked, after which the drilling was stopped immediately. According to the set parameters, the needle was slowly inserted at the designated positions and a total amount of 1 μl virus was slowly injected in each site at a speed of 0.05 μl/min. The needle was not moved until the injection was completed and the virus had spread, after which the needle was slowly withdrawn. The micro-injector was moved to a marked position on the other side and the virus was injected in the same manner. After the injection in the bilateral hippocampi was completed, the scalp of the rat was sutured.

Spinal Analyses of Cultured Neurons

Each experiment was conducted at least three times in this study. Data used for the calculations were presented as the mean ± SEM from a minimum of three independent biological samples. The final results were analyzed with the student's *T*-test when the number of groups was two, and multiple comparisons were analyzed using one-way analysis of variance (ANOVA) with Dennett's *post hoc* test. All analyses were performed using the Statistical Package for the Social Sciences (SPSS 20.0) software. $p < 0.05$ was considered to indicate a statistical difference.

Statistics

Each experiment was carried out at least three times in this study. Data used for the calculations were presented as the mean ± SEM from a minimum of three independent biological samples. The final results were analyzed with the *T*-test when the number of groups was two, and multiple comparisons were analyzed using one-way ANOVA with Dennett's post-test. All analyses were performed with SPSS 20.0 software. The levels of significance were represented with the following symbols: $^{*}p < 0.05$ and $^{**}p < 0.01$. $P < 0.05$ was considered to indicate a statistical difference.

RESULTS

Low-Level Maternal Pb Exposure Impaired Spatial Learning and Memory in the Offspring

Lead (Pb) exposure was initiated 2 weeks before mating, maintained throughout gestation, and terminated 10 days after the progeny were born (**Figure 1A**). There were no significant differences in the body weights of the offspring at PNDs 0, 10, 21, and 30 between the Pb-exposed and control groups ($p = 0.9736$, $p = 0.7677$, $p = 0.9188$, $p = 0.9172$) (**Figure 1B**). Blood Pb levels were substantially elevated in the Pb-exposed offspring at PNDs 0, 10, and 21 ($p < 0.0001$, $p = 0.0001$, $p = 0.0021$) (**Figure 1C**). Though the blood Pb levels in the offspring were not significantly different between the two groups, hippocampal Pb levels were significantly higher in the Pb-exposed offspring at PND 30 ($p < 0.0001$) (**Figure 1D**). We found that maternal Pb exposure impaired the offspring's learning and memory abilities, evidenced by longer escape latency during the 5 training days ($p = 0.009$, $p = 0.0026$, $p = 0.0019$, $p = 0.003$, $p = 0.0015$) (**Figure 1E**) and a significantly shorter amount of time spent in the target quadrant where the platform was originally located

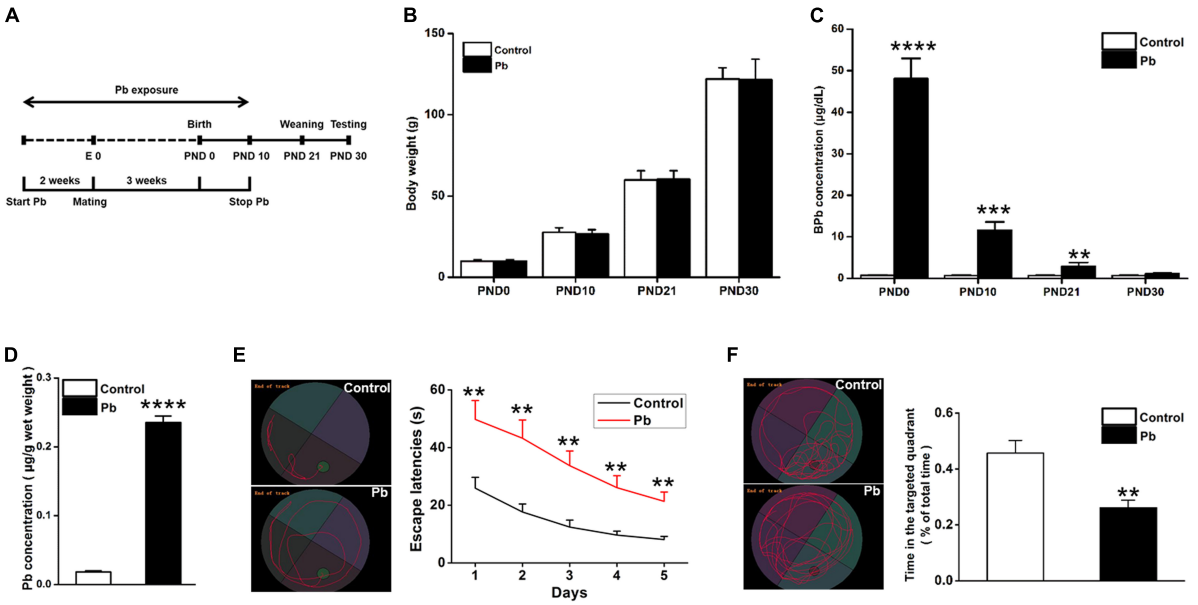

FIGURE 1 | Accumulation of Pb in the hippocampus of PND30 rats and its influence on learning and memory. **(A)** Establishment of Pb exposure model. Female SD rats were given Pb acetate solutions to drink (0 or 0.02%) beginning 2 weeks before mating until PND 10. **(B)** Body weights and **(C)** Blood Pb levels. The concentration of blood Pb in the experimental rats was measured at PND 0, 10, 21, and 30. **(D)** Pb levels in the hippocampus region. **(E,F)** Analysis of MWM results. The MWM tests were only measured at PND30. Data are expressed as mean ± SE, $^{**}p < 0.01$, $^{***}p < 0.001$, $^{****}p < 0.0001$; $n = 6$ per group.

($p = 0.0037$) (**Figure 1F**) on the testing day compared to those in the control group.

Low-Level Maternal Pb Exposure Impaired Hippocampal Dendritic Plasticity

Dendritic plasticity is the basis of learning and memory functions. To investigate the underlying mechanisms for the cognitive deficits induced by maternal Pb exposure, we first determined the dendritic plasticity through Golgi Staining and electrophysiology. We reconstructed and analyzed the dendritic spines of pyramidal neurons in the CA1 region using the Imaris software (**Figures 2A–C**). Pb exposure significantly decreased both the basal ($p = 0.0018$, $p = 0.0017$, $p = 0.0066$) (**Figure 2D**) and apical ($p = 0.0021$, $p = 0.0037$, $p = 0.04$) (**Figure 2E**) dendritic spine density of hippocampal CA1 region neurons compared to those in the control group. We found that maternal Pb exposure significantly reduced the fEPSP slope of LTP in the CA1 region (**Figure 2F**) in the offspring ($p = 0.0096$) (**Figures 2G,H**). Taken together, maternal Pb exposure impaired hippocampal dendritic plasticity.

Maternal Pb Exposure Reduced Glucose Metabolism in the Offspring Hippocampus

Positron Emission Tomography-Computed Tomography PET-CT scanning was used to analyze the effects of maternal Pb exposure on glucose metabolism in the offspring brain (**Figure 3A**). The glucose uptake profiles in the offspring hippocampus, olfactory bulb, and amygdala are shown in **Figure 3B**. The results showed that the levels of glucose metabolism in the hippocampus, amygdala, and olfactory bulb in the Pb-exposed group were significantly reduced compared with those in the control group. The standard uptake value (SUV) for the hippocampus were 3.52 ± 0.12 in the control group and 3.06 ± 0.16 in the Pb-exposed group ($p = 0.0418$). The corresponding values for the olfactory bulb were 3.49 ± 0.14 and 2.93 ± 0.21 ($p = 0.0487$) and the values for the amygdala were 2.84 ± 0.09 and 2.46 ± 0.14 ($p = 0.048$), respectively (**Figure 3C**, $n = 6$).

Maternal Pb Exposure Led to Alterations in Rat Hippocampal Neuron GLUT4 Levels and Membrane Translocation

Glucose plays a vital role in maintaining the integrity of synaptic structures and functions (McNay and Gold, 2002; Im et al., 2019; Yun et al., 2019). The disruption of brain glucose metabolism can impair neuronal synaptic plasticity, which in turn affects brain function. We found that the protein levels of GLUT1 and GLUT3 in the offspring hippocampus were not significantly different between the two groups ($p = 0.5869$, $p = 0.8793$) (**Figures 4A,B**); however, the GLUT4 protein level was significantly lower in the Pb-exposed group ($p = 0.0012$) (**Figure 4B**). The membrane protein levels of GLUT4 in the hippocampal neurons of the Pb-exposed offspring were significantly reduced compared with those in the control group ($p = 0.0014$) (**Figures 4C,D**), and the phosphorylated level of Akt (p-Akt) was lower ($p < 0.0001$) (**Figures 4C,D**). The results showed that exogenous insulin alone was capable of

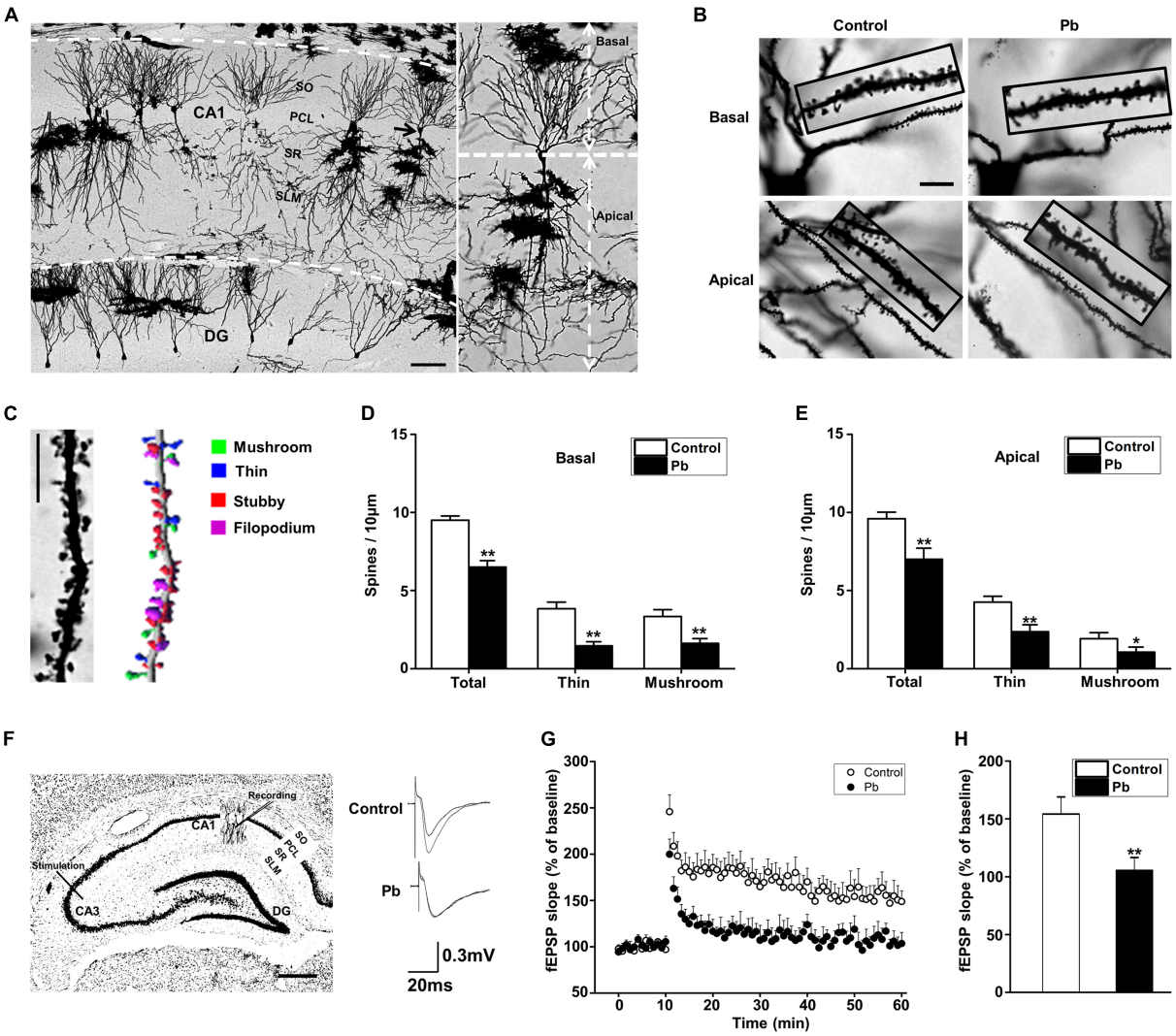

FIGURE 2 | Hippocampal Pb accumulation and impairment of synaptic plasticity in PND30 rats. **(A,B)** Golgi Staining for basal and apical dendritic spines in hippocampal CA1 region. Scale bars = 100 μm in **(A)** and 10 μm in **(B)**. **(C)** Imaris reconstruction of the dendritic spines of pyramidal neurons in CA1 region. Scale bar = 10 μm. **(D,E)** Statistical analysis of the effect of Pb exposure on basal and apical spines. For each group, data are expressed as mean ± SE of spines per 10 μm (16 neurons/8 rats for all groups), $^{*}p < 0.05$, $^{**}p < 0.01$. **(F)** LTP induced by high-frequency tetanic stimulation. Simulations were applied to the CA3 regions of the hippocampus and the signal was collected at the CA1 region. Scale bar = 500 μm. **(G,H)** LTP in hippocampal regions CA3-CA1. Abscissa represented the time of tetanic stimulation. *N* = 16 slices per 8 rats in each group. The patch-clamp recordings showed that the fEPSP slope for rat hippocampal LTP in the Pb-exposed group was significantly reduced compared with that in the control group. Data are expressed as mean ± SE, $^{**}p < 0.01$. SO, stratum oriens; PCL, pyramidal cell layer; SR, stratum radiatum; SL-M, stratum lacunosum-moleculare; DG, dentate gyrus.

inducing a significant increase in Akt phosphorylation and GLUT4 translocation ($p = 0.0016$, $p = 0.0058$) in the normal group (**Figures 4E–G**). However, in the Pb exposure group, insulin treatment neither reversed the phosphorylation level of Akt nor changed the level of GLUT4 membrane translocation ($p = 0.1357$, $p = 0.1456$) (**Figures 4E–G**).

GLUT4 co-localized with NeuN (**Figure 4H**) but not glial fibrillary acidic protein (GFAP) (**Figure 4I**) in the hippocampal CA1 and dentate gyrus (DG) regions, which means that the GLUT4 proteins express in neurons of hippocampus, not astrocytes during brain development in rat offspring. We also found that compared with the control, the immunoreactivity of GLUT4 significantly decreased in the CA1 and DG regions ($p = 0.003$, $p = 0.0098$) (**Figures 4J,K**). These data suggest that gestational Pb exposure causes a decrease in the total and membrane levels of GLUT4 in hippocampal neurons.

Over-Expression of GLUT4 *in vitro* Increased Glucose Uptake and Reversed Synaptic Plasticity in the Pb-Exposed Group

The glucose uptake of neurons was significantly reduced after Pb exposure ($p = 0.0092$) (**Figure 5A**). Compared with the

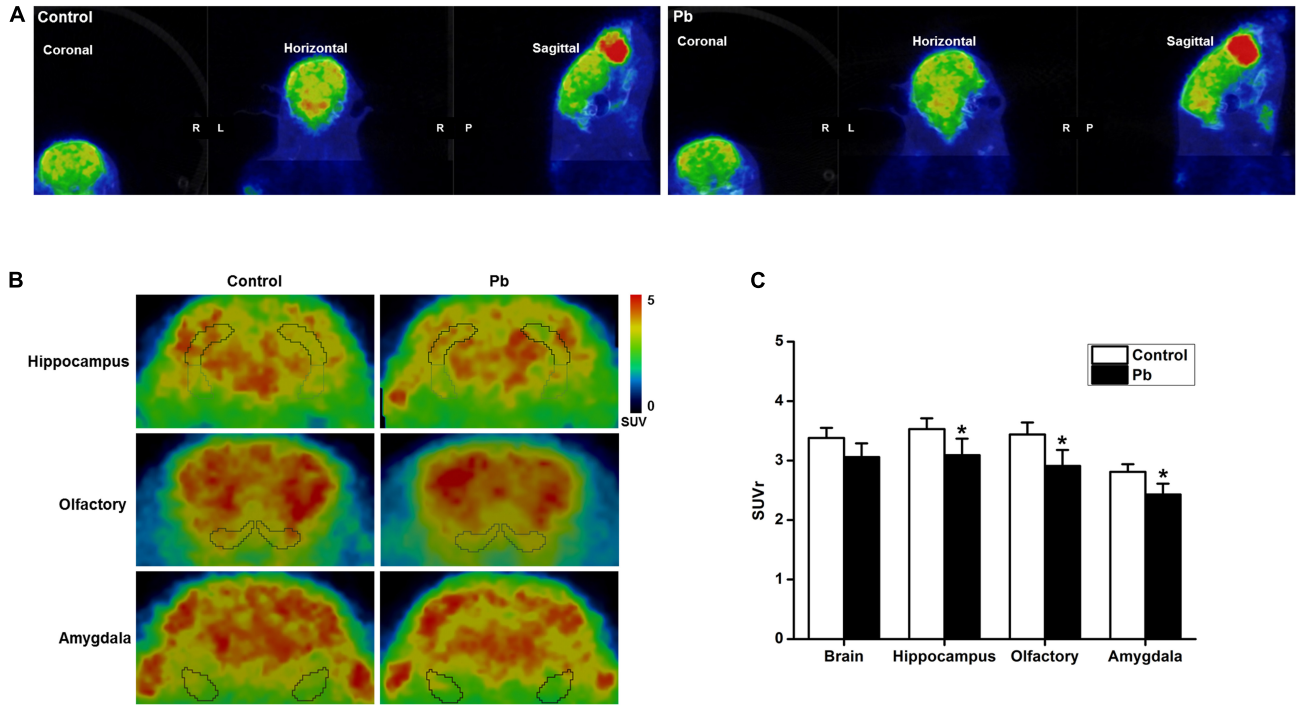

FIGURE 3 | Effect of low-level gestational Pb exposure on glucose uptake in rat brain. **(A)** Representative images of experimental rat brains. **(B)** Representative images of glucose uptake in different brain areas ([18F]-FDG microPET/CT) in the experimental rats at the last scanning point. **(C)** Statistical analysis of PET-CT scanning data. PET-CT results indicated that maternal Pb exposure at a low level significantly reduced the level of glucose metabolism in the rat hippocampus. $^*p < 0.05$, $n = 6$ per group.

control group, the expression levels of total and membrane GLUT4 proteins as well as p-Akt proteins in the Pb-exposed group were significantly decreased ($p = 0.0012$, $p = 0.0011$, $p = 0.0015$) (**Figures 5B,C**). Exogenous insulin was administered to primary hippocampal neurons and the insulin signaling pathway was assessed to determine the effect on the membrane translocation of GLUT4 (**Figure 5D**). The results showed that the p-Akt levels and membrane translocation of GLUT4 were significantly increased after insulin treatment alone ($p = 0.0016$, $p = 0.0022$). However, insulin treatment in the Pb-exposed group did not reverse the reduced levels of p-Akt and plasma membrane (PM)-GLUT4 proteins ($p = 0.1245$, $p = 0.3444$) (**Figures 5E,F**).

After GLUT4 over-expression (**Figures 6A,B**), the transmembrane levels of GLUT4 in the primary hippocampal neurons of the Pb-exposed group were significantly increased ($p = 0.0091$, $p = 0.0099$) (**Figure 6C**), whereas glucose uptake by hippocampal neurons in the Pb-exposed group was significantly decreased ($p = 0.0116$, $p = 0.0499$) (**Figure 6D**). The density of dendritic spines in the hippocampal neurons of the Pb-exposed group was significantly decreased compared to that of the control group and this trend was significantly reversed after the over-expression of GLUT4 ($p = 0.0037$, $p = 0.0071$) (**Figures 6E,F**). In addition, the amplitude of miniature excitatory postsynaptic currents (mEPSCs) from hippocampal neurons in the Pb-exposed group was significantly lower. The over-expression of GLUT4 significantly increased the amplitude of mEPSCs in the Pb-exposed group ($p = 0.001$, $p = 0.0035$) (**Figure 6G**).

Over-Expression of GLUT4 *in vivo* Reversed Cognitive Impairments Induced by Gestational Pb Exposure by Increasing GLUT4 Membrane Translocation and Glucose Uptake

To investigate whether GLUT4 over-expression attenuates the cognitive deficits caused by Pb exposure, GLUT4 transfected with adeno-associated virus (AAV) and tagged with green fluorescent protein (GFP) (AAV-GLUT4-GFP) was injected into the hippocampal CA1 region. The effects of the virus transfection were demonstrated by a strong positive GFP fluorescence (**Figure 7A**) and the WB results (**Figure 7B**). The levels of GLUT4 and PM-GLUT4 proteins in the hippocampus increased after AAV-GLUT4 injection (**Figures 7C,D**). After receiving the same amount of Pb exposure, the levels of GLUT4 and PM-GLUT4 proteins in the AAV-GLUT4-Pb group were lower compared with the levels in the control group (AAV-GLUT4-control) ($p = 0.0082$, $p = 0.0026$), but considerably higher than those in the AAV-Pb group ($p = 0.0004$) (**Figures 7C,D**). Using the MWM test, we found that the over-expression of GLUT4 significantly ameliorated the cognitive deficits induced by Pb exposure, evidenced by a decrease in the escape latency (Day 1: $p = 0.0024$, $p = 0.0281$; Day 2: $p = 0.0024$,

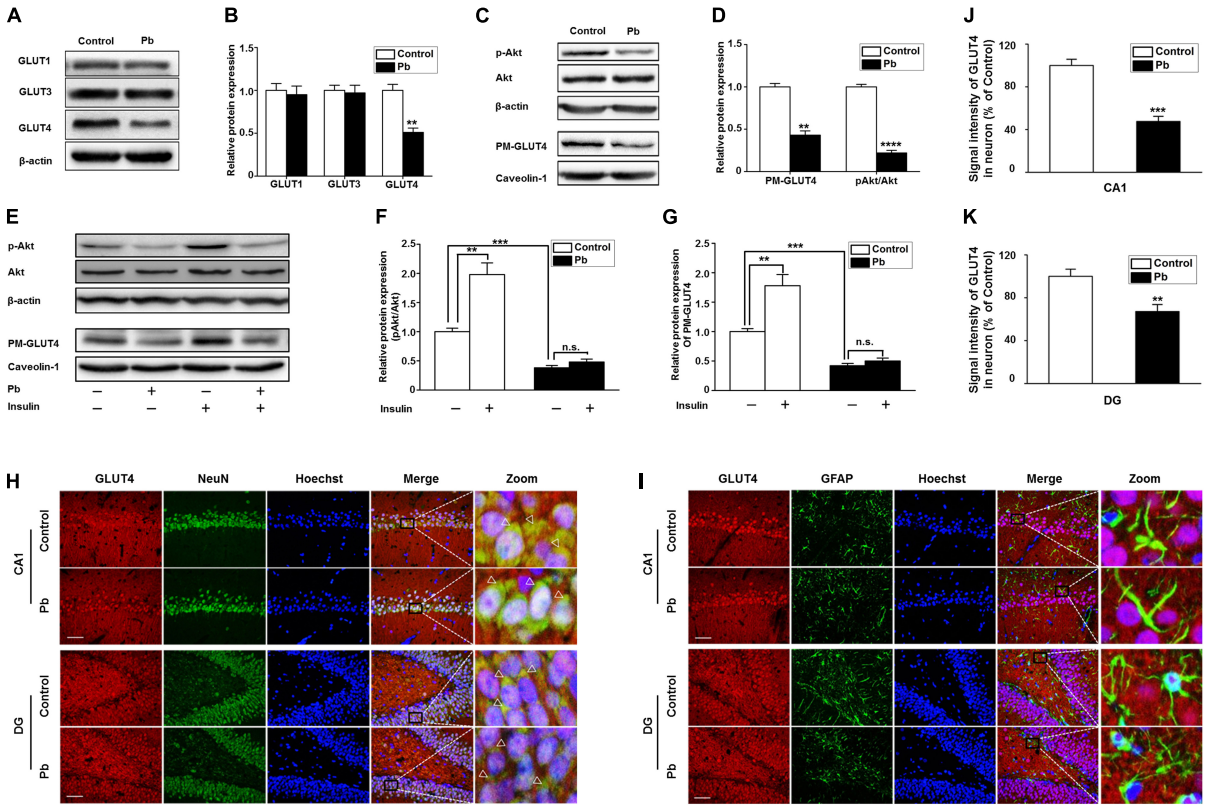

FIGURE 4 | Effects of Pb exposure on GLUT4 expression and membrane translocation in rat hippocampus. **(A–D)** Effects of Pb exposure on the expression of GLUTs, PM-GLUT4, and p-Akt. There were no remarkable changes in GLUT3 and GLUT1 expression in Pb-exposed rat hippocampus, but the GLUT4 expression was significantly reduced. The expression levels of PM-GLUT4 and p-Akt were significantly reduced. Among them, caveolin-1 served as the loading control of PM-GLUT4, and β-actin for other proteins. **(E–G)** Effects of insulin on PM-GLUT4 and p-Akt expression levels. Insulin stimulation significantly increased the expression of p-Akt in rat hippocampus but did not reverse the decrease of p-Akt expression in the Pb-exposed group. $N = 6$ per group, $^{**}p < 0.01$, $^{***}p < 0.001$, $^{****}p < 0.0001$. vs. control. The band intensity was statistically analyzed based on the percentage relative to the control. **(H,I)** Immunofluorescence staining. **(J,K)** Statistical results of signal intensity of GLUT4 expression in neuron in CA1 and DG regions of the hippocampus in rats. The results showed that GLUT4 and NeuN were significantly double-labeled in the CA1 and DG regions of the hippocampus in rats, and double-labeling in the Pb-exposed group was significantly reduced compared to the control group levels. Immunofluorescence staining indicated that GLUT4 and GFAP were not double-labeled in the hippocampal CA1 and DG regions of rats. Scale bars = 50 μm. Data were represented as mean ± SEM and counted based on data from a minimum of three independent experiments, $^{**}p < 0.01$, $^{***}p < 0.001$.

$p = 0.0214$; Day 3: $p = 0.0013$, $p = 0.0105$; Day 4: $p = 0.0011$, $p = 0.0102$; Day 5: $p = 0.0019$, $p = 0.0103$; vs. AAV-Pb) (**Figures 7E,F**) and a longer period of time spent in the target quadrant ($p = 0.005$, $p = 0.0428$) (**Figures 7G,H**). GLUT4 over-expression also significantly reversed the impaired hippocampal glucose metabolism in the Pb-exposed group, as determined using PET-CT ($p = 0.0487$, $p = 0.0188$) (**Figures 7I,J**). AAV-GLUT4 significantly attenuated the inhibitory effect of Pb exposure on hippocampal LTP, indicated by a slope of 108.18 ± 4.96 for fEPSPs in the AAV-Pb group and 146.67 ± 7.83 in the AAV-GLUT4-Pb group ($p = 0.002$) (**Figures 7K,L**). Changes in dendritic plasticity in rat hippocampal neurons after GLUT4 over-expression were observed (**Figure 7M**, $n = 6$). When GLUT4 was overexpressed, the total numbers of basal and apical dendrites in the CA1 region of the Pb-exposed rats were significantly higher ($p = 0.0055$), as were the densities of thin- and mushroom-shaped spines ($p = 0.007$, $p = 0.0027$) (**Figures 7N,O**).

DISCUSSION

Lead (Pb) is a widely distributed environmental heavy metal poison that is a serious health hazard to humans, especially to brain development in children (Olympio et al., 2009; Senut et al., 2012; Hara et al., 2015). However, the mechanism through which Pb damages the developing brain and leads to learning and memory impairments remains unclear (Ettinger and Brown, 2018). According to our experimental results, although the blood Pb level recovered to normal levels in the Pb-exposed offspring at PND 30, the Pb level in the hippocampal tissue from the Pb-exposed group remained substantially higher. Low-level maternal Pb exposure impaired the developing brain, evidenced by increased escape latency and less time spent in the target quadrant. In other words, once the impairment to the developing brain induced by Pb exposure has occurred, it is irreversible and will not be ameliorated even if the blood Pb levels return to normal.

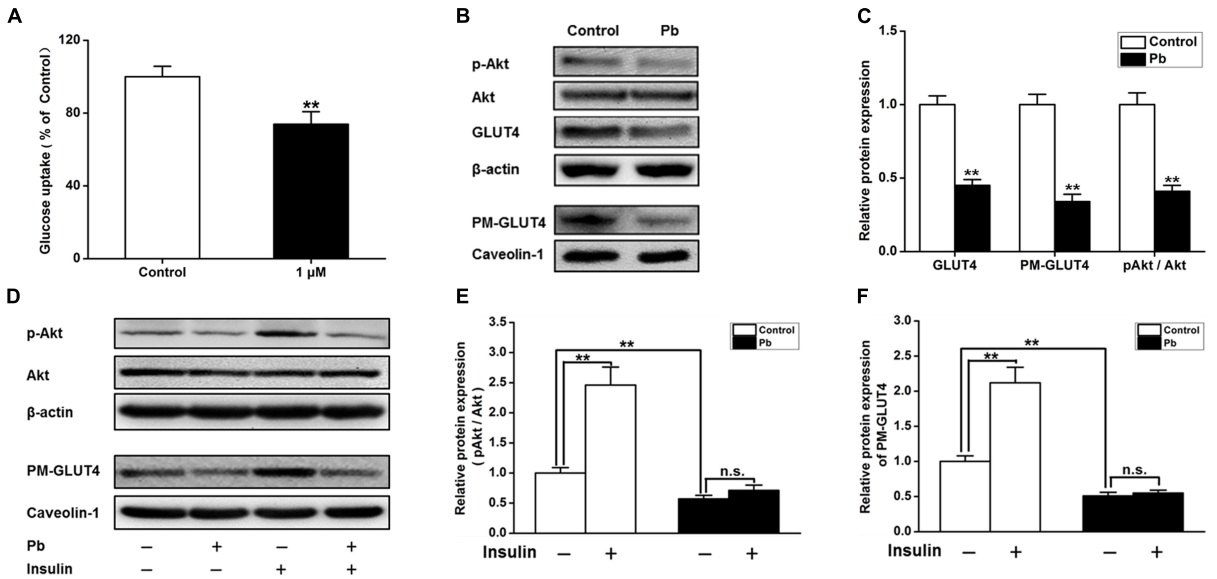

FIGURE 5 | Effects on the glucose uptake and GLUT4, PM-GLUT4, and p-Akt expression in primary hippocampal neurons in the Pb-exposed rats. **(A)** Effect of Pb exposure on the glucose uptake. Using 2-NBDG combined with flow cytometry, glucose uptake in primary cultured rat hippocampal neurons was analyzed. Flow cytometry results showed that glucose uptake was significantly reduced in primary cultured hippocampal neurons after treatment with 1 μmol/L Pb acetate compared with the levels in the control group. **(B,C)** Effect of Pb exposure on expression of glycometabolism-related proteins in the brain. The expression levels of GLUT4, PM-GLUT4, and pAkt proteins in primary cultured hippocampal neurons were dramatically reduced in the Pb-exposed rats. **(D–F)** p-Akt and PM-GLUT4 expression after insulin stimulation in rat primary cultured hippocampal neurons. Insulin stimulation led to the significant increase of p-Akt and PM-GLUT4 protein levels in the control rat hippocampus, but did not reverse the decreased levels in Pb-exposed rats. Among them, caveolin-1 served as the loading control of PM-GLUT4, and β-actin for other proteins. $^{**}p < 0.01$, $n = 6$ per group. Statistical analysis of the band intensity measured as a percentage of the control.

Dendritic plasticity is the basis of learning and memory functions. The density and morphological changes of dendrites have significant effects on excitatory synaptic transmission and are closely related to learning and memory functions (Dumitriu et al., 2010; Haas et al., 2013). Any event that affects the structural foundation (pyramidal cell dendritic spine) of dendrites can eventually lead to impaired LTP as well as cognition. Among these events, hippocampal neuronal (Bott et al., 2013) plasticites are one of the most important factors that can alter the hippocampal LTP. Dendritic spines are classified into the following four categories according to their structural and functional characteristics: mushroom, thin, stubby, and filopodium (Larance et al., 2008). Mushroom and thin dendritic spines are closely associated with learning and memory ability (Fiala et al., 1998; Zhao et al., 2018). In this study, we discovered that the spine densities of the basal and apical dendrites were significantly reduced in the hippocampus of GLE offspring, especially the thin and mushroom spines. Combined with the decreased LTP, maternal Pb exposure impaired the learning and memory abilities of the offspring through synaptic plasticity alterations.

Learning and memory are complex neurophysiological processes that require a large exogenous glucose supply since glucose cannot be synthesized or stored in neurons (Messier, 1997; Hughes and Neeson, 2003; Chen and Zhong, 2013) and must be transported into the neurons by glucose transporters. GLUT4 is expressed in brain regions associated with cognitive behavior, including the hippocampus, amygdala, olfactory bulb, cerebral cortex, and cerebellum (Nagamatsu et al., 1993; Leloup et al., 1996; Ngarmukos et al., 2001). Insulin-mediated GLUT4 membrane translocation is responsible for the hippocampal glucose supply during learning and memory (McNay and Gold, 2002; Grillo et al., 2009; Ren et al., 2019). In this study, Pb exposure had no significant effect on blood glucose levels in rats, but GLUT4 expression was significantly reduced in the hippocampal neuronal membrane proteins after Pb exposure. This suggests that Pb exposure affects the energy supply in the hippocampus-dependent learning and memory process by reducing the membrane translocation of GLUT4. We also found that Pb exposure significantly decreased GLUT4 expression. To further confirm the key role of GLUT4 in learning and memory deficits induced by Pb exposure, we overexpressed GLUT4 using the AAV-GLUT4 virus and evaluated synapse plasticity and spatial memory. GLUT4 over-expression increased the amount of GLUT4 translocated across the membrane as well as glucose uptake in the hippocampus, as determined with PET-CT. These data suggested that GLUT4 is a key molecule that mediates glucose uptake in hippocampal neurons and is also an important toxic target protein for Pb exposure to inhibit neuronal glucose uptake. Over-expression of GLUT4 in the hippocampus also ameliorated learning and memory impairments and the inhibitory effect on hippocampal LTP, as well as the damage to neuronal dendritic spines caused by Pb exposure.

In conclusion, the cognitive defects induced by maternal Pb exposure can persist beyond PND 30 and are not reversed even after the blood Pb concentration returns to normal levels.

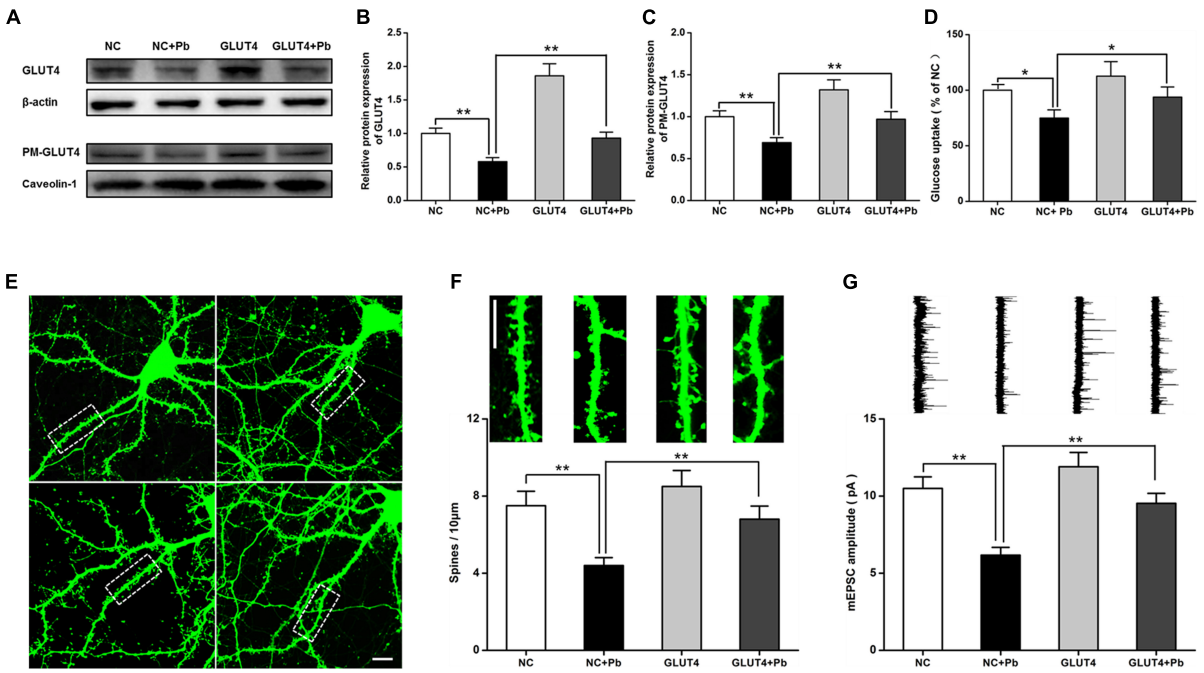

FIGURE 6 | Effects of over-expression of GLUT4 on glucose uptake and synaptic plasticity of primary hippocampal neurons in the Pb-exposed rats. **(A–C)** Expression changes in GLUT4 and PM-GLUT4 in rat hippocampal neurons after AAV-GLUT4 transfection. GLUT4 and PM-GLUT4 expression levels returned to normal in the rat primary cultured hippocampal neurons of the Pb-exposed group after AAV-GLUT4 transfection. Among them, caveolin-1 served as the loading control of PM-GLUT4, and β-actin for GLUT4. **(D)** Effect of GLUT4 over-expression on glucose uptake in rat hippocampal neurons. Over-expression of GLUT4 recovered the glucose uptake levels in the primary hippocampal neurons from the Pb-exposed group. **(E–G)** Effects of GLUT4 over-expression on cell morphology and LTP in Pb-exposed rat hippocampal neurons. After lentivirus infection, the morphology (dendritic spines) of rat primary cultured hippocampal neurons was observed via laser confocal microscopy. Over-expression of GLUT4 reversed the dendritic spine density and LTP lesions in Pb-exposed rats. Scale bar = 10 μm. $^{*}p < 0.05$, $^{**}p < 0.01$, vs. control, $n = 6$ per group.

In other words, this impairment remains in the offspring's brain throughout the developmental stage. Abnormal glucose metabolism plays a role in the spatial learning and memory impairments induced by maternal Pb exposure during the developmental stage; however, the underlying mechanisms were unclear till now. In this study, we found that Pb exposure during pregnancy irreversibly damaged the developing nervous system, especially the hippocampal synaptic plasticity. The exposure caused learning and memory impairments in the offspring by reducing glucose uptake through a decrease in GLUT4 protein expression and membrane translocation in the hippocampus. Pb exposure inhibited the PI3K-Akt signaling pathway, which is critical for the membrane translocation of GLUT4, both *in vivo* and *in vitro*. Over-expression of GLUT4 ameliorated the synaptic plasticity impairments and cognitive deficits induced by gestational Pb exposure via increasing the GLUT4 membrane translocation and glucose uptake *in vivo* and *in vitro*. These findings indicate that Pb exposure causes memory deterioration through PI3K-Akt-induced suppression of GLUT4 membrane translocation, revealing a novel mechanism for Pb exposure-induced synapse and memory impairments. This research may provide a new therapeutic target for brain development impairments in maternal Pb-exposed offspring.

There are some shortcomings in our investigation. For example, a previous study showed that Pb exposure during pregnancy causes more serious damage to boys than girls (Khanna, 2015), but we only focused on the male offspring. Therefore, the mechanism for Pb-related synapse and memory impairments induced by Pb exposure, which causes memory deterioration through PI3K-Akt-induced suppression of GLUT4 membrane translocation, and its underlying molecular mechanism both require further verification in other populations. Moreover, the neuroligin 1 (NLGN1), which is one of the four subtypes of the postsynaptic neuroligins, is one of the most characteristic synaptic cell adhesion molecules. And we had confirmed that low-level gestational Pb exposure also down-regulated NLGN1 expression and dendritic spine density in hippocampal CA1 pyramidal neurons, leading to impairment of learning and memory, and overexpression of NLGN1 rescued the Pb-induced reduction of spine density in hippocampal neurons in our previous study. These results indicate that low-level gestational Pb exposure seems to have the same impact on NLGN1 and GLUT4, and the protein NLGN1 and GLUT4 play similar roles in synaptic plasticity as well as learning and memory function. But whether there would be some connections between these two findings, and whether there are some signaling pathways or regulatory mechanisms, are still unexplained in the present study. However, it will be an important direction for our future research. The findings will contribute to further translation of the theoretical

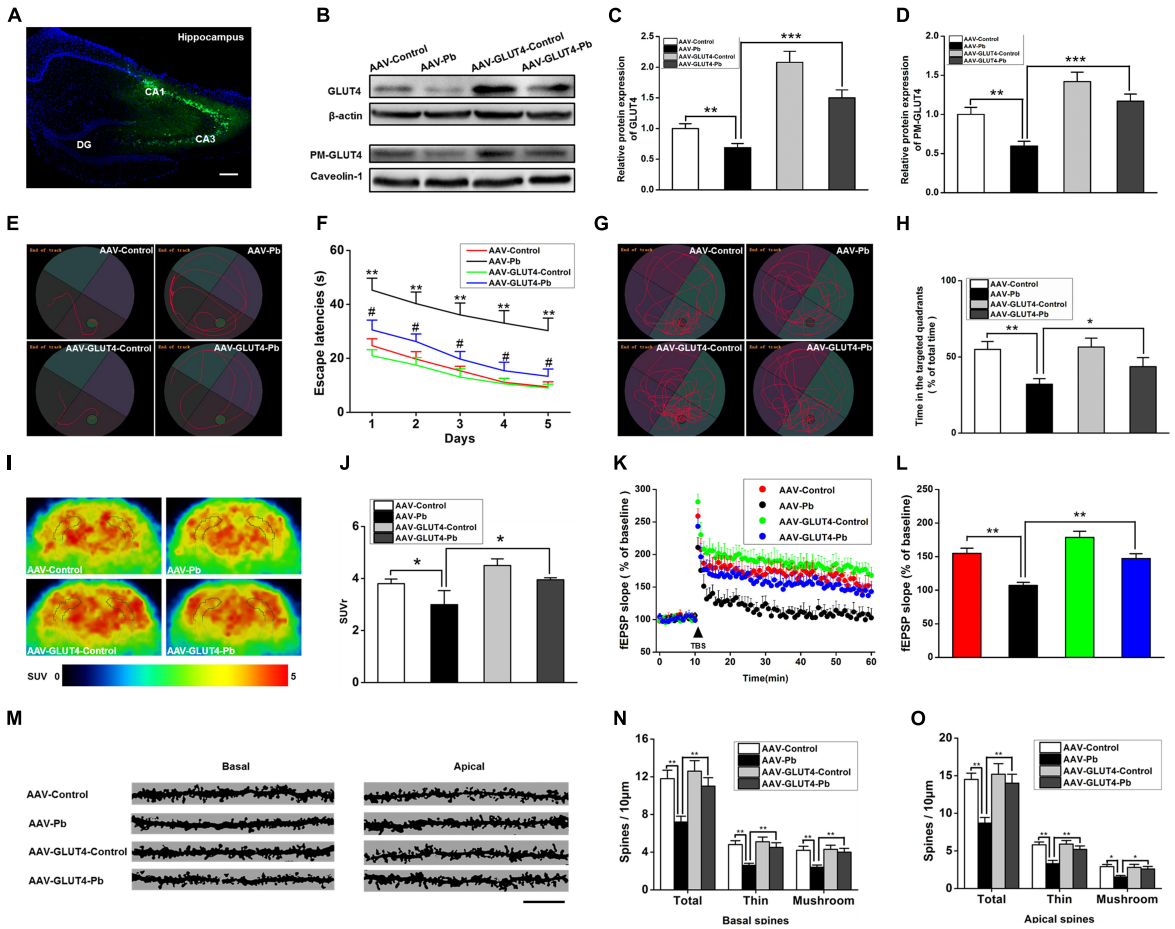

FIGURE 7 | Effects of GLUT4 over-expression in Pb-exposed rat hippocampus on the glucose uptake, synaptic plasticity, as well as learning and memory function. **(A–D)** Over-expression of GLUT4 in rat hippocampus and analysis of its effect on glycometabolism-related proteins. GLUT4 over-expression was induced via stereotactic injection of adenovirus. GLUT4 over-expression reversed the decreased PM-GLUT4 in Pb-exposed rat hippocampus. **(E–H)** Analysis of rat positioning, navigation ability, and space exploration trajectory. Over-expression of GLUT4 in Pb-exposed rat hippocampus reversed the arrival latency and the target quadrant retention time of model rats in MWM tests; $^{*}p < 0.05$, $^{**}p < 0.01$; # $p < 0.05$ vs. AAV-Pb. **(I,J)** PET-CT scanning and analysis of glucose metabolism in rat brain. The glucose metabolism level in Pb-exposed rat hippocampus was reversed after the over-expression of GLUT4. **(K,L)** Effects of Pb exposure on LTP induction in rat hippocampus. After over-expression of GLUT4 in rat hippocampus, the slope of fEPSP in Pb-exposed rat hippocampus was reversed. **(M–O)** Effect of Pb exposure on dendritic spines of hippocampal pyramidal neurons. Over-expression of GLUT4 increased the spinal density of basal and apical dendrites in pyramidal neurons as well as the number of thin and mushroom-shaped dendritic spines in the Pb-exposed rat hippocampus. Scale bar = 10 μm. $^{*}p < 0.05$, $^{**}p < 0.01$, $^{***}p < 0.001$, vs. control, $n = 6$ per group.

research into clinical applications, which is also the focus of our future work.

DATA AVAILABILITY STATEMENT

The original contributions presented in the study are included in the article/supplementary material, further inquiries can be directed to the corresponding authors.

ETHICS STATEMENT

The animal study was reviewed and approved by the Laboratory Animal Welfare and Ethics Committee of the Fourth Military Medical University.

AUTHOR CONTRIBUTIONS

Z-HZ and K-JD wrote the manuscript. TW and J-YW developed the model and performed the molecular biology experiments. Z-PC participated in the *in vivo* experiments. X-MC and HS analyzed the data. GZ and X-FS designed and supervised the experiments. All authors read and approved the final manuscript.

FUNDING

This work was supported by the National Natural Science Foundation of China Grant (Nos 81973073, 81273101, 81803194, 81872577, 81920108030, and 81773378), the National Basic

Research Program of China (973 Program) (No. 2012CB525002), Program for Changjiang Scholars and Innovative Research Team in University (PCSIRT), and Shaanxi Science and Technology Coordinating Innovative Project (2016KTCQ03-01).

REFERENCES

Ahmad, F., Salahuddin, M., Alamoudi, W., and Acharya, S. (2018). Dysfunction of cortical synapse-specific mitochondria in developing rats exposed to lead and its amelioration by ascorbate supplementation. *Neuropsychiatr. Dis. Treat.* 14, 813–824. doi: 10.2147/NDT.S148248

Anderson, D. W., Mettil, W. A., and Schneider, J. S. (2013). Rearing environment, sex and developmental lead exposure modify gene expression in the hippocampus of behaviorally naive animals. *Neurochem. Int.* 62, 510–520. doi: 10.1016/j.neuint.2013.01.003

Barha, C. K., and Galea, L. A. (2013). The hormone therapy, premarin, impairs hippocampus-dependent spatial learning and memory and reduces activation of new granule neurons in response to memory in female rats. *Neurobiol. Aging* 34, 986–1004. doi: 10.1016/j.neurobiolaging.2012.07.009

Bhattacharya, A., Shukla, R., Auyang, E. D., Dietrich, K. N., and Bornschein, R. (2007). Effect of succimer chelation therapy on postural balance and gait outcomes in children with early exposure to environmental lead. *Neurotoxicology* 28, 686–695. doi: 10.1016/j.neuro.2007.03.007

Bihaqi, S. W., and Zawia, N. H. (2013). Enhanced taupathy and AD-like pathology in aged primate brains decades after infantile exposure to lead (Pb). *Neurotoxicology* 39, 95–101. doi: 10.1016/j.neuro.2013.07.010

Bott, J. B., Cosquer, B., Heraud, C., Zerbinatti, C., Kelche, C., Cassel, J. C., et al. (2013). Reduced plasticity and mild cognitive impairment-like deficits after entorhinal lesions in hAPP/APOE4 mice. *Neurobiol. Aging* 34, 2683–2693. doi: 10.1016/j.neurobiolaging.2013.04.018

Brody, D. J., Pirkle, J. L., Kramer, R. A., Flegal, K. M., Matte, T. D., Gunter, E. W., et al. (1994). Blood lead levels in the US population. phase 1 of the Third National Health and Nutrition Examination Survey (NHANES III, 1988 to 1991). *JAMA J. Am. Med. Assoc.* 272, 277–283. doi: 10.1001/jama.1994.03520040039038

Chen, Z., and Zhong, C. (2013). Decoding Alzheimer's disease from perturbed cerebral glucose metabolism: implications for diagnostic and therapeutic strategies. *Prog. Neurobiol.* 108, 21–43. doi: 10.1016/j.pneurobio.2013.06.004

Chiu, S. L., and Cline, H. T. (2010). Insulin receptor signaling in the development of neuronal structure and function. *Neural. Dev.* 5:7. doi: 10.1186/1749-8104-5-7

de la Monte, S. M., Tong, M., Bowling, N., and Moskal, P. (2011). si-RNA inhibition of brain insulin or insulin-like growth factor receptors causes developmental cerebellar abnormalities: relevance to fetal alcohol spectrum disorder. *Brain Stimul.* 4:13. doi: 10.1186/1756-6606-4-13

Dumitriu, D., Hao, J., Hara, Y., Kaufmann, J., Janssen, W. G., Lou, W., et al. (2010). Selective changes in thin spine density and morphology in monkey prefrontal cortex correlate with aging-related cognitive impairment. *J. Neurosci.* 30, 7507–7515. doi: 10.1523/JNEUROSCI.6410-09.2010

Ettinger, A. S., and Brown, M. J. (2018). Re: errata for prevention of childhood lead toxicity. *Pediatrics* 141:e20180064. doi: 10.1542/peds.2018-0064

Fiala, J. C., Feinberg, M., Popov, V., and Harris, K. M. (1998). Synaptogenesis via dendritic filopodia in developing hippocampal area CA1. *J. Neurosci.* 18, 8900–8911. doi: 10.1523/jneurosci.18-21-08900.1998

Fox, D. A., Kala, S. V., Hamilton, W. R., Johnson, J. E., and O'Callaghan, J. P. (2008). Low-level human equivalent gestational lead exposure produces supernormal scotopic electroretinograms, increased retinal neurogenesis, and decreased retinal dopamine utilization in rats. *Environ. Health Perspect.* 116, 618–625. doi: 10.1289/ehp.11268

Genuis, S. J., and Kelln, K. L. (2015). Toxicant exposure and bioaccumulation: a common and potentially reversible cause of cognitive dysfunction and dementia. *Behav. Neurol.* 2015:620143. doi: 10.1155/2015/620143

Gilbert, M. E., Kelly, M. E., Samsam, T. E., and Goodman, J. H. (2005). Chronic developmental lead exposure reduces neurogenesis in adult rat hippocampus but does not impair spatial learning. *Toxicol. Sci.* 86, 365–374. doi: 10.1093/toxsci/kfi156

Grillo, C. A., Piroli, G. G., Hendry, R. M., and Reagan, L. P. (2009). Insulin-stimulated translocation of GLUT4 to the plasma membrane in rat hippocampus is PI3-kinase dependent. *Brain Res.* 1296, 35–45. doi: 10.1016/j.brainres.2009.08.005

Haas, M. A., Bell, D., Slender, A., Lana-Elola, E., Watson-Scales, S., Fisher, E. M., et al. (2013). Alterations to dendritic spine morphology, but not dendrite patterning, of cortical projection neurons in Tc1 and Ts1Rhr mouse models of down syndrome. *PLoS One* 8:e78561. doi: 10.1371/journal.pone.0078561

Hara, A., Thijs, L., Asayama, K., Gu, Y. M., Jacobs, L., Zhang, Z. Y., et al. (2015). Blood pressure in relation to environmental lead exposure in the national health and nutrition examination survey 2003 to 2010. *Hypertension* 65, 62–69. doi: 10.1161/HYPERTENSIONAHA.114.04023

Hu, F., Ge, M. M., and Chen, W. H. (2016). Effects of lead exposure on dendrite and spine development in hippocampal dentate gyrus areas of rats. *Synapse* 70, 87–97. doi: 10.1002/syn.21873

Hu, F., Xu, L., Liu, Z. H., Ge, M. M., Ruan, D. Y., and Wang, H. L. (2014). Developmental lead exposure alters synaptogenesis through inhibiting canonical Wnt pathway in vivo and in vitro. *PLoS One* 9:e101894. doi: 10.1371/journal.pone.0101894

Hughes, R. N., and Neeson, L. T. (2003). Prevention of memory loss for a brightness change in adult and middle-aged rats by postacquisition treatment with glucose. *Pharmacol. Biochem. Behav.* 76, 119–123. doi: 10.1016/s0091-3057(03)00192-8

Im, J. J., Jeong, H., Bikson, M., Woods, A. J., Unal, G., Oh, J. K., et al. (2019). Effects of 6-month at-home transcranial direct current stimulation on cognition and cerebral glucose metabolism in Alzheimer's disease. *Brain Stimul.* 12, 1222–1228. doi: 10.1016/j.brs.2019.06.003

Khanna, M. M. (2015). Boys, not girls, are negatively affected on cognitive tasks by lead exposure: a pilot study. *J. Environ. Health* 77, 72–77.

Kleinridders, A., Ferris, H. A., Cai, W., and Kahn, C. R. (2014). Insulin action in brain regulates systemic metabolism and brain function. *Diabetes* 63, 2232–2243. doi: 10.2337/db14-0568

Larance, M., Ramm, G., and James, D. E. (2008). The GLUT4 code. *Mol. Endocrinol.* 22, 226–233. doi: 10.1210/me.2007-0282

Leloup, C., Arluison, M., Kassis, N., Lepetit, N., Cartier, N., Ferre, P., et al. (1996). Discrete brain areas express the insulin-responsive glucose transporter GLUT4. *Brain Res. Mol. Brain Res.* 38, 45–53. doi: 10.1016/0169-328x(95)00306-d

Liu, M. C., Liu, X. Q., Wang, W., Shen, X. F., Che, H. L., Guo, Y. Y., et al. (2012). Involvement of microglia activation in the lead induced long-term potentiation impairment. *PLoS One* 7:e43924. doi: 10.1371/journal.pone.0043924

McNay, E. C., Fries, T. M., and Gold, P. E. (2000). Decreases in rat extracellular hippocampal glucose concentration associated with cognitive demand during a spatial task. *Proc. Natl. Acad. Sci. U.S.A.* 97, 2881–2885. doi: 10.1073/pnas.050583697

McNay, E. C., and Gold, P. E. (2002). Food for thought: fluctuations in brain extracellular glucose provide insight into the mechanisms of memory modulation. *Behav. Cogn. Neurosci. Rev.* 1, 264–280. doi: 10.1177/1534582302238337

Messier, C. (1997). Object recognition in mice: improvement of memory by glucose. *Neurobiol. Learn. Mem.* 67, 172–175. doi: 10.1006/nlme.1996.3755

Mills, R., Alati, R., O'Callaghan, M., Najman, J. M., Williams, G. M., Bor, W., et al. (2011). Child abuse and neglect and cognitive function at 14 years of age: findings from a birth cohort. *Pediatrics* 127, 4–10. doi: 10.1542/peds.2009-3479

Mostafalou, S., Baeeri, M., Bahadar, H., Soltany-Rezaee-Rad, M., Gholami, M., and Abdollahi, M. (2015). Molecular mechanisms involved in lead induced disruption of hepatic and pancreatic glucose metabolism. *Environ. Toxicol. Pharmacol.* 39, 16–26. doi: 10.1016/j.etap.2014.11.001

Nagamatsu, S., Sawa, H., Kamada, K., Nakamichi, Y., Yoshimoto, K., and Hoshino, T. (1993). Neuron-specific glucose transporter (NSGT): CNS distribution of GLUT3 rat glucose transporter (RGT3) in rat central neurons. *FEBS Lett.* 334, 289–295. doi: 10.1016/0014-5793(93)80697-s

Neal, A. P., Stansfield, K. H., Worley, P. F., Thompson, R. E., and Guilarte, T. R. (2010).). Lead exposure during synaptogenesis alters vesicular proteins and impairs vesicular release: potential role of NMDA receptor-dependent BDNF signaling. *Toxicol. Sci.* 116, 249–263. doi: 10.1093/toxsci/kfq111

Ngarmukos, C., Baur, E. L., and Kumagai, A. K. (2001). Co-localization of GLUT1 and GLUT4 in the blood-brain barrier of the rat ventromedial hypothalamus. *Brain Res.* 900, 1–8. doi: 10.1016/s0006-8993(01)02184-9

Olympio, K. P., Goncalves, C., Gunther, W. M., and Bechara, E. J. (2009). Neurotoxicity and aggressiveness triggered by low-level lead in children: a review. *Rev. Panam. Salud. Publica* 26, 266–275. doi: 10.1590/s1020-49892009000900011

Piroli, G. G., Grillo, C. A., Reznikov, L. R., Adams, S., McEwen, B. S., Charron, M. J., et al. (2007). Corticosterone impairs insulin-stimulated translocation of GLUT4 in the rat hippocampus. *Neuroendocrinology* 85, 71–80. doi: 10.1159/000101694

Reagan, L. P. (2002). Glucose, stress, and hippocampal neuronal vulnerability. *Int. Rev. Neurobiol.* 51, 289–324. doi: 10.1016/s0074-7742(02)51009-6

Ren, H., Vieira-de-Abreu, A., Yan, S., Reilly, A. M., Chan, O., and Accili, D. (2019). Altered central nutrient sensing in male mice lacking insulin receptors in Glut4-expressing neurons. *Endocrinology* 160, 2038–2048. doi: 10.1210/en.2019-00341

Rogan, W. J., Dietrich, K. N., Ware, J. H., Dockery, D. W., Salganik, M., Radcliffe, J., et al. (2001). The effect of chelation therapy with succimer on neuropsychological development in children exposed to lead. *N. Engl. J. Med.* 344, 1421–1426. doi: 10.1056/NEJM200105103441902

Schneider, J. S., Kidd, S. K., and Anderson, D. W. (2013). Influence of developmental lead exposure on expression of DNA methyltransferases and methyl cytosine-binding proteins in hippocampus. *Toxicol. Lett.* 217, 75–81. doi: 10.1016/j.toxlet.2012.12.004

Senut, M. C., Cingolani, P., Sen, A., Kruger, A., Shaik, A., Hirsch, H., et al. (2012). Epigenetics of early-life lead exposure and effects on brain development. *Epigenomics* 4, 665–674. doi: 10.2217/epi.12.58

Smith, M. A., Riby, L. M., Eekelen, J. A., and Foster, J. K. (2011). Glucose enhancement of human memory: a comprehensive research review of the glucose memory facilitation effect. *Neurosci. Biobehav. Rev.* 35, 770–783. doi: 10.1016/j.neubiorev.2010.09.008

Wang, T., Guan, R. L., Liu, M. C., Shen, X. F., Chen, J. Y., Zhao, M. G., et al. (2016). Lead exposure impairs hippocampus related learning and memory by altering synaptic plasticity and morphology during juvenile period. *Mol. Neurobiol.* 53, 3740–3752. doi: 10.1007/s12035-015-9312-1

Yun, S., Wu, Y., Niu, R., Feng, C., and Wang, J. (2019). Effects of lead exposure on brain glucose metabolism and insulin signaling pathway in the hippocampus of rats. *Toxicol.Lett.* 310, 23–30. doi: 10.1016/j.toxlet.2019.04.011

Yun, S. W., and Hoyer, S. (2000). Effects of low-level lead on glycolytic enzymes and pyruvate dehydrogenase of rat brain in vitro: relevance to sporadic Alzheimer's disease? *J. Neural. Transm.* 107, 355–368. doi: 10.1007/s007020050030

Zartarian, V., Xue, J., Tornero-Velez, R., and Brown, J. (2017). Children's lead exposure: a multimedia modeling analysis to guide public health decision-making. *Environ. Health Perspect.* 125:097009. doi: 10.1289/ehp1605

Zhao, Z. H., Zheng, G., Wang, T., Du, K. J., Han, X., Luo, W. J., et al. (2018). Low-level gestational lead exposure alters dendritic spine plasticity in the hippocampus and reduces learning and memory in rats. *Sci. Rep.* 8:3533. doi: 10.1038/s41598-018-21521-8

Conflict of Interest: The authors declare that the research was conducted in the absence of any commercial or financial relationships that could be construed as a potential conflict of interest.

frontiers in Cell and Developmental Biology

ORIGINAL RESEARCH
published: 15 March 2021
doi: 10.3389/fcell.2021.632843

Tetramethylpyrazine Improves Cognitive Impairment and Modifies the Hippocampal Proteome in Two Mouse Models of Alzheimer's Disease

Xianfeng Huang[1†], Jinyao Yang[1,2†], Xi Huang[3], Zaijun Zhang[4], Jianjun Liu[2], Liangyu Zou[3] and Xifei Yang[2*]*

[1] School of Pharmacy and School of Medicine, Changzhou University, Changzhou, China, [2] Key Laboratory of Modern Toxicology of Shenzhen, Shenzhen Medical Key Subject of Modern Toxicology, Shenzhen Center for Disease Control and Prevention, Shenzhen, China, [3] Department of Neurology, Shenzhen People's Hospital (First Affiliated Hospital of Southern University of Science and Technology), Second Clinical College, Jinan University, Shenzhen, China, [4] Institute of New Drug Research and Guangzhou, Key Laboratory of Innovative Chemical Drug Research in Cardio-Cerebrovascular Diseases, Jinan University College of Pharmacy, Guangzhou, China

OPEN ACCESS

Edited by:
Gong-Ping Liu,
Huazhong University of Science and Technology, China

Reviewed by:
Xihui Liu,
University of Texas Southwestern Medical Center, United States
Halesha Dhurvigere Basavarajappa,
Beckman Research Institute, City of Hope, United States
Qing Tian,
Huazhong University of Science and Technology, China

***Correspondence:**
Liangyu Zou
zouliangyu@yahoo.com
Xifei Yang
xifeiyang@gmail.com

[†] These authors have contributed equally to this work

Specialty section:
This article was submitted to Molecular Medicine, a section of the journal Frontiers in Cell and Developmental Biology

Received: 24 November 2020
Accepted: 15 February 2021
Published: 15 March 2021

Citation:
Huang X, Yang J, Huang X, Zhang Z, Liu J, Zou L and Yang X (2021) Tetramethylpyrazine Improves Cognitive Impairment and Modifies the Hippocampal Proteome in Two Mouse Models of Alzheimer's Disease. Front. Cell Dev. Biol. 9:632843. doi: 10.3389/fcell.2021.632843

Alzheimer's disease (AD), one of the most common neurodegenerative diseases, has no effective treatment. We studied the potential effects of tetramethylpyrazine (TMP), an alkaloid in the rhizome of *Ligusticum chuanxiong* Hort. used in Traditional Chinese Medicine (*chuānxiong*) to treat ischemic stroke, on AD progression in two AD mouse models. Eight-month-old 3xTg-AD mice received TMP treatment (10 mg/kg/d) for 1 month, and 4-month-old APP/PS1-AD mice received TMP treatment (10 mg/kg/d) for 2 months. Behavioral tests, including step-down passive avoidance (SDA), new object recognition (NOR), Morris water maze (MWM), and Contextual fear conditioning test showed that TMP significantly improved the learning and memory of the two AD-transgenic mice. In addition, TMP reduced beta-amyloid (Aß) levels and tau phosphorylation (p-tau). Venny map pointed out that 116 proteins were commonly changed in 3xTg mice vs. wild type (WT) mice and TMP-treated mice vs. -untreated mice. The same 130 proteins were commonly changed in APP/PS1 mice vs. WT mice and TMP-treated mice vs. -untreated mice. The functions of the common proteins modified by TMP in the two models were mainly involved in mitochondrial, synaptic, cytoskeleton, ATP binding, and GTP binding. Mitochondrial omics analysis revealed 21 and 20 differentially expressed mitochondrial proteins modified by TMP in 3xTg-AD mice and APP/PS1 mice, respectively. These differential proteins were located in the mitochondrial inner membrane, mitochondrial outer membrane, mitochondrial gap, and mitochondrial matrix, and the function of some proteins is closely related to oxidative phosphorylation (OXPHOS). Western-blot analysis confirmed that TMP changed the expression of OXPHOS complex proteins (sdhb, ndufa10, uqcrfs1, cox5b, atp5a) in the hippocampus of the two AD mice. Taken together, we demonstrated that TMP treatment changed the hippocampal proteome, reduced AD pathology, and reduced cognitive

impairment in the two AD models. The changes might be associated with modification of the mitochondrial protein profile by TMP. The results of the study suggest that TMP can improve the symptoms of AD.

Keywords: tetramethylpyrazine, Alzheimer's disease, proteomics, mitochondria, OxPhoS

INTRODUCTION

Alzheimer's disease (AD), a common form of neurodegenerative dementia, has a huge impact on the health system (Hyman et al., 2012; Oboudiyat et al., 2013). The amount of patients with AD is increasing dramatically in aging populations worldwide, such that identification of effective therapeutics is a top priority for society (Foloppe et al., 2018).

Alzheimer's disease (AD) is featured by prominent neuropathological changes, including β-amyloid (Aβ) plaques and neurofibrillary tangles (NFT) formed from hyperphosphorylated tau (p-tau). The pathogenesis of AD has suggested various hypthotheses including roles for inflammation, cholinergic function, Aβ deposition, tau hyperphosphorylation, and mitochondrial dysfunction (Scholtzova et al., 2008). As for AD treatment, prior to 2019, the US Food and Drug Administration approved only six drugs market use (Briggs et al., 2016). Other more effective medicines are urgently needed to address the growing AD patient load.

We studied the potential effects of tetramethylpyrazine (TMP), an alkaloid in the rhizome of *Ligusticum chuanxiong* Hort, used in Traditional Chinese Medicine (chuānxiong) to treat ischemic stroke, on AD progression in two AD mouse models.

Tetramethylpyrazine (TMP), a type of calcium antagonist, is an alkaloid extracted from the rhizome of *Ligusticum chuanxiong* Hort, which has been widely used in Chinese Traditional Medicine. According to reports in the literature, TMP has shown a strong neuroprotective effect in brain ischemia models (Chang et al., 2007). In the rat model of Parkinson's disease (PD) induced by systemic treatment with methylphenyltetrahydrodpyridine, TMP has a neuroprotective effect on dopaminergic neurons (Lu et al., 2014), and TMP reduces the severity of rotenone-induced PD-like disease in rats (Michel et al., 2017). Additionally, TMP reversed streptozotocin-induced memory impairment by inhibiting glycogen synthase kinase-3β (GSK-3β) (Lu et al., 2017). Taken in concert, these data suggest that TMP may have a potential therapeutic effect via neuroprotection. We therefore studied the potential neuroprotective effect of TMP on AD and its molecular mechanism through the use of two validated AD mouse models.

MATERIALS AND METHODS

Animals and Treatment Protocol

Animals used included: (a) triple transgenic AD mice (3xTg-AD) (B6; 129-Psen1^{tm1Mpm} Tg [APPSwe, tauP301L] 1Lfa/Mmjax) and wild-type (WT) mice (B6129SF2/J) and (b) APPswe/PSEN 1dE9 (APP/PS1) mice and matched wild-type (WT) animals (APP/PS1-negative mice). Mice were obtained from the Jackson Laboratory in the United States, delivered by air to Shenzhen, and bred locally at the Shenzhen Center for Disease Control. Animal housing, breeding, and experimental studies used standards employed for breeding laboratory animals.

Eight-month-old 3xTg-AD mice were treated by gavage with 10 mg/kg/d TMP (10 mg/kg/d) in saline for 1 month. Eight-month-old WT mice and untreated 3xTg-AD mice were given normal saline by the same route. Additionally, 4-month-old APP/PS1-positive mice were treated by gavage with 10 mg/kg/d TMP (TMP+10 mg/kg/d) in saline for 2 months, and 4-month-old negative mice and untreated positive mice were given normal saline (**Figure 1**). The experiments were performed in accordance with the National Institutes of Health Guide for the Care and Use of Laboratory Animals (NIH Publication No. 8023, Revised 1978) and approved by the Ethics Committee of Shenzhen Center for Disease Control and Prevention. Every effort was made to reduce the suffering of the animals and the number of mice.

Behavioral Tests

Cognition Test

We performed a new object recognition (NOR) test using a previously published method (Wang et al., 2019). On the first day, mice were conditioned to move freely in an empty plastic box for 5 min. After 24 h of training, the mice were placed back in the same box with two objects of the same size and shape and allowed to explore freely for 5 min. After 1 h, one of the objects was replaced with a new object of the same size but different shape, and the mice were allowed to explore freely for another 5 min. Simultaneous video and tracking documented the detection time of each object. Detection was defined as the mouse facing the object, sniffing or touching with the nose, and the distance was recorded from the nose to the object $\leq$2 cm. The calculation method was: (time to explore new objects)/(time to explore new objects + time to explore old objects) * 100%.

Step-Down Passive Avoidance Test

We used step-down passive avoidance (SDA) test to assess aversive learning and memory in the models (Zhou et al., 2019a). The device consisted of five glass rooms with length, width and height of 15 × 15 × 46 cm^3. The floors were spaced 1 cm apart and a platform with a diameter of 4.5 cm was placed in the middle. On day one, the mouse was placed into the electrical stimulation box and electrical stimulation administered to the animal. The response time for the animal to jump onto platform and number of platforms used was recorded (error number). After 24 h, the mouse was directly placed on the platform and the time (latency) and error times of the mouse jumping off the platform for the first time were recorded.

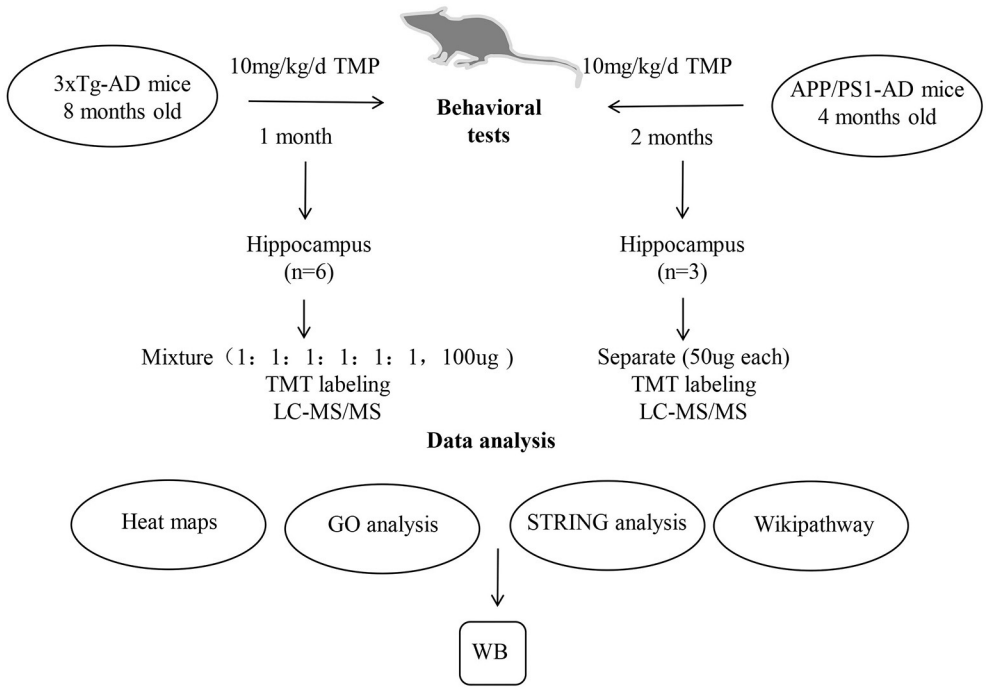

FIGURE 1 | A schematic diagram of the experimental design. 3xTg-AD and APP/PS1-AD female mice were treated by gavage with TMP (10 mg/kg/d) in saline or an equal volume of saline. After the behavioral assessment, the brain removed and the hippocampus isolated for proteomic analysis. Protein samples from the brains of 6 mice per group (WT mice, 3xTg mice, and TMP-treated mice) were collected. Protein samples from the brains of 3 mice of each group (WT mice, APP/PS1 mice, and TMP-treated mice) were collected. The peptides were further graded with 6-plex TMT and HPRP and then analyzed by LC-MS/MS. Bioinformatics analysis (heat map, GO, String, and Wikipathway) was performed with David 6.8 and Cytoscape software. WB, Western blots.

Morris Water Maze Test

We used the Morris water maze (MWM) test according to a previously published method to evaluate the spatial learning and memory abilities of mice (Zhou et al., 2019b). The water maze consists of a circular pool and a white escape platform; the pool is filled with opaque water and has a white escape platform with a diameter of 10 cm under the water surface. If the platform was found by the animal within 1 min of water immersion, the time to platform was recorded; if the platform was not found within 1 min, the animal was helped to find the platform and allowed to stay there for 15 s. The training lasted for 5 days, starting from the four starting positions, and performed four times a day, with an interval of 15 s. Animal performance was tested on the seventh day after training. The times of crossing the platform area, time on the platform, activity track, activity time, and distance of target quadrant were all recorded.

Contextual Fear Conditioning Test

Previously reported methods were used to conduct the conditional fear experiment (Bolton et al., 2012; Zhou et al., 2012). In short, the fear regulator consists of a conditioning chamber. The sound chamber is closed by silencers and the noise is shielded by exhaust fans. The infrared digital camera is placed at the top of the enclosure, about 50 cm from the chamber. On the first day of training, the mice explored freely for 2 min without any stimulation. The loudspeaker (4 Hz, 80 dB) was started and stopped after 30 s. Electrical stimulation (0.5 mA) was started 2.5 s later and ended after 1 s. The mice were exposed to no stimulation for 2 min and then the entire procedure was repeated three times. The chamber was cleaned with 70% alcohol 24 h after training. The mice were exposed to the changed environment for 11 min. The training included 2 min of free exploration, 60 s of speaker (4 Hz, 80 dB), and three repetitions. Fourty-eight hours after the training in the original training room. The mice were left in the same room and allow to explore for 6 min without any electrical or sound stimulation.

Protein Extraction and Digestion

Hippocampal protein samples were prepared (Xu et al., 2018). Hippocampal tissue of mice was dispersed in 8 M urea phosphate buffer solution by ultrasound and then centrifuged. The hippocampus of 3xTg mice (6 mice in each group) was mixed into 100 μg protein according to (1:1:1:1:1:1). The hippocampal proteins of APP/PS1 mice (three in each group) were similarly taken in 100 μg protein. Protein samples were incubated with 10 mM 1,4-Dithiothreitol (DTT) at 55°C for 30 min and then with 25 mM diamine iodoacetate (IAA) for 1 h at room temperature. Samples were then digested with trypsin at 37°C, adjusted to pH 1–2 by adding 1% trifluoroarboxylic acid (TFA), and centrifuged at 12,000 g for 20 min to collect the supernatant. Inverse phase column chromatography (HLB, Waters OASIS, USA) was used for desalting. After desalination, samples were

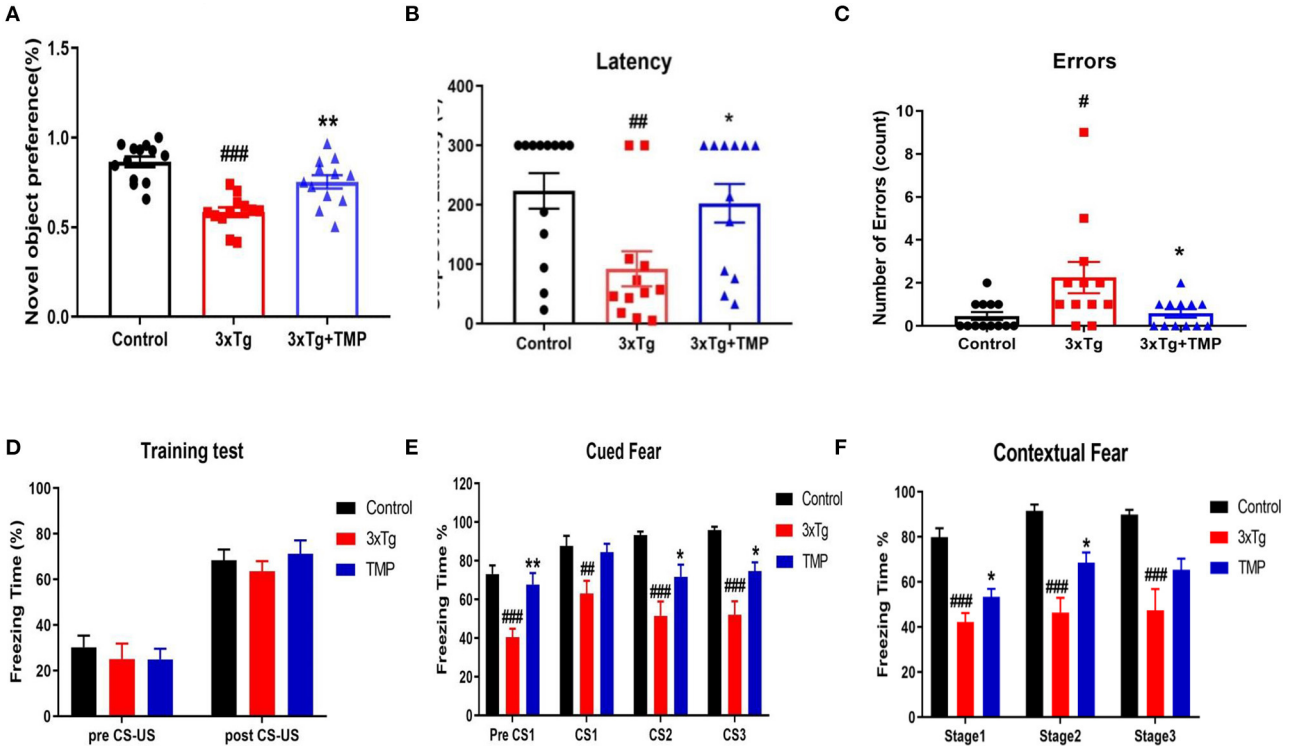

FIGURE 2 | TMP improved cognitive function of 3xTg-AD mice. Differences in **(A)** the exploration time of a novel object in the novel object recognition test and **(B,C)** the latency and number of errors in the step-down passive avoidance test **(B,C)**. Mean proportion time freezing on the training day **(D)**. Mean proportion time freezing 24 h after training in the altered context **(E)**. Mean proportion time freezing 48 h after training **(F)**. $N = 12$–13 per group. Data are presented as mean ± SEM, $^{**}p < 0.01$, $^{*}p < 0.05$ vs. 3xTg-AD mice. $^{\#\#\#}p < 0.001$, $^{\#\#}p < 0.01$, $^{\#}p < 0.05$ vs. WT mice.

dried and dissolved in a buffer of triethylamine bicarbonate (TEAB, 200 mM, pH 8.5).

Tandem Mass Tag (TMT) Labeling

The samples were labeled with TMT reagent at room temperature, 5 μl 5% hydroxylamine added, and the reaction terminated after incubation. The samples were labeled with different TMT Tags: TMT-126 for samples from WT mice; TMT-127, 3xTg mice; TMT-128, TMP-treated mice, TMT-129, APP/PS1 wild mice; TMT-130, APP/PS1-positive mice, TMT-131, TMP-treated mice. The total peptides labeled in each group were mixed, desalted, dried, and fractionated.

LC-MS/MS Analysis and Database Searching

The labeled peptides were then loaded onto an Xbridge BEH300 C18 column (Waters, USA) and the peptide samples were separated into 15 fractions using an UltiMate 3000 UHPLC (Thermo Fisher Scientific, USA) (He et al., 2019). Then, fractions were dried and used for LC-MS/MS analyses. LC-MS/MS analyses were used previously method (Chen et al., 2019). An analytical capillary column was used to separate peptides and filled with C18 silicone resin (Varian, Lexington, Massachusetts, USA). Data were interpreted using the UniProt muscle database (released in October 2018), and the original mass spectra were searched using Proteome Finder 2.1 software.

Mass spectrometry proteomics data were deposited in the ProteomeXchange Consortium via the PRIDE partner repository with the dataset identifier PXD022862 and PXD022840.

Bioinformatics Analysis

We used Venny 2.1 to analyze differentially expressed proteins. Functional enrichment analysis of biological processes (BP) and molecular function (MF) was performed using DAVID Bioinformatics Resources 6.8. STRING database version 10.5 was used to analyze protein–protein interaction networks.

Western-Blot Analysis

Hippocampal tissues were sonicated with RIPA lysate (Thermo Science, New Jersey, USA) containing 1X protease and phosphatase inhibitors. The protein concentration was quantified using the Thermo Fisher Scientific BCA protein analysis kit and then mixed with the loading buffer, heated at 95°C for 8 min; the protein was isolated by 10% SDS-PAGE and transferred to PVDF membrane, and then the 5% skimmed milk was dissolved in TBST buffer and blocked for 2 h. The blocked membrane was incubated overnight with the primary antibody in an ice box, including β-actin (1:3,000), α-tubulin (1:3,000), NDUFA10 (1:1,000), SDHB (1:1,000), UQCRFS1 (1:1,500),

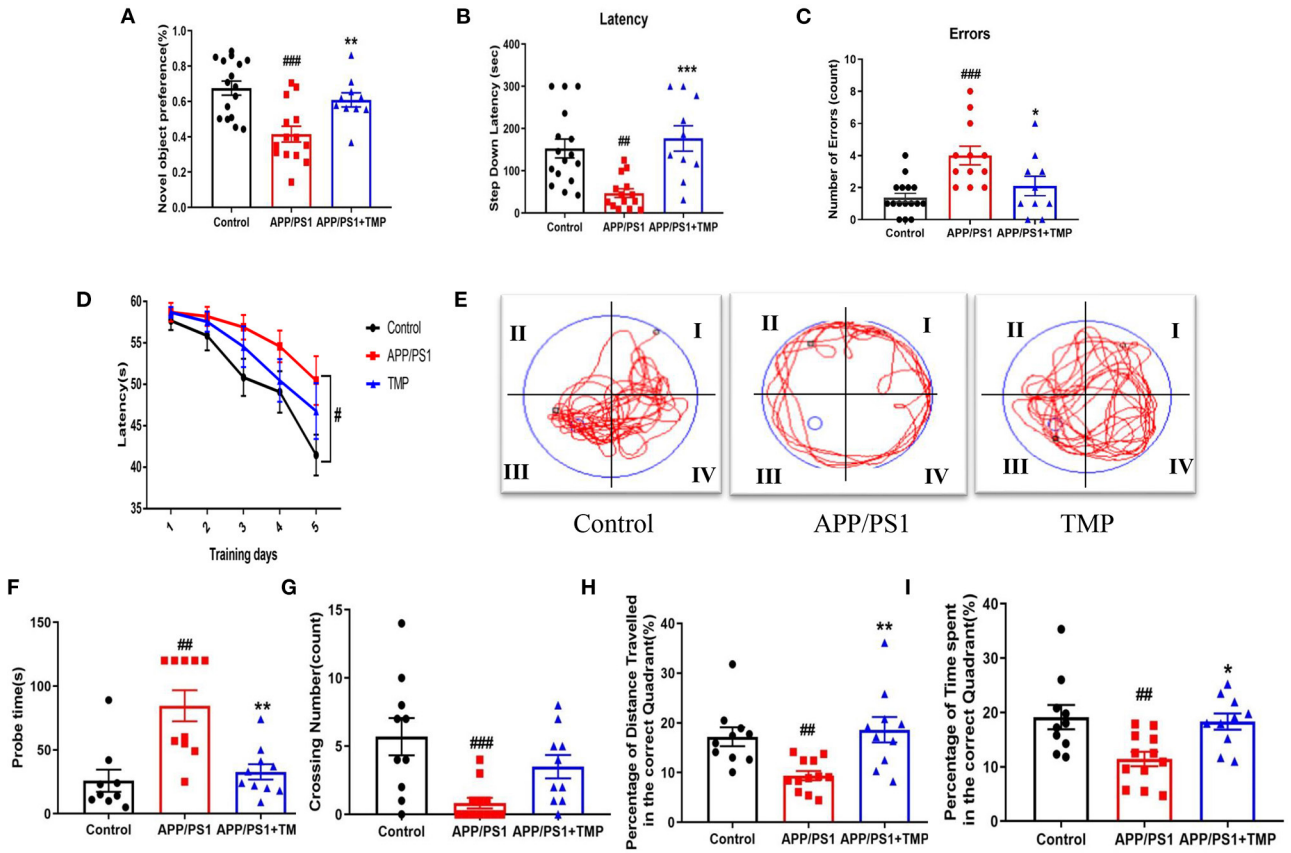

FIGURE 3 | TMP improved cognitive function in APP/PS1-AD mice. Group differences in: **(A)** the exploration time percentage of novel objects in the novel object recognition test; **(B,C)** the latency waiting time and the number of errors in the downgrade passive avoidance test, and **(D)** the escape latency in the Morris water maze training test. Group differences in representative trajectories of motion patterns **(E)**, detection time **(F)**, the number of crossover movements **(G)**, the percentage of time spent in the platform quadrant **(H),** and the percentage of distance moved in the platform quadrant **(I)** in probe trials of the Morris water maze test (n = 10–16 per group). The data are expressed as mean ± SEM. $^{***}p < 0.001$, $^{**}p < 0.01$, $^{*}p < 0.05$ vs. APP/PS1 mice; $^{\#\#\#}p < 0.001$, $^{\#\#}p < 0.01$ vs. Control mice.

COX5B (1:1,000), ATP5A (1:1,000), APP (1:1,000), BACE1 (1:1,000), PS1 (1:1,000), ADAM10 (1:1,000), IDE (1:1,000), PS396 (1:1,000), PS202 (1:1,000) in TBST. The membrane was washed three times in TBST and then incubated with the secondary antibody, diluted (1:3,000) in TBST for 50 min, and finally the ECL kit (Thermo Science, New Jersey, USA) was used to run the Western blot. The membrane was exposed, and ImageJ software used for quantitative analysis.

Dot Blot Analysis

Mouse cortical tissue was sonicated with RIPA lysate. Total protein concentration used BCA protein assay kit and the total protein was diluted to the same concentration and applied to the NC film. The NC film was placed at room temperature for 3 h, transferred to 5% skimmed milk dissolved in TBST buffer and blocked for 2 h. The blocked membrane was incubated overnight with the 6E10 (1:1,000) antibody in an ice box. The membranes were washed three times in TBST and incubated with the secondary antibody diluted 1:3,000 in TBST for 50 min. The membrane was exposed, and ImageJ software used for quantitative analysis.

ATP Levels

Cortical tissues of APP/PS1 mice were used to detect ATP levels in the brains of APP/PS1 mice. Briefly, to extract and determine protein concentration, samples (40 μl) were mixed with ATP assay solution (100 μl) and incubated for 3 min at room temperature. ATP levels were read using a microtiter plate with photometric capabilities.

MDA Levels

Cortical tissues of APP/PS1 mice were used to detect MDA levels in the brains of APP/PS1 mice. Briefly, freshly extracted samples were subjected to protein concentration determination, and then the samples (100 μl) were incubated with MDA working solution (200 μl) at 100°C for 15 min and centrifuged at 1,000 g for 10 min. At the end, add 200 μl of supernatant to a 96-well plate and measure the absorbance at 532 nm. Lipid peroxidation levels were calculated as nmol/mg protein.

Statistical Analysis

All the data were statistically processed using GraphPad Prism 8.0 software and the data expressed as the mean ± SEM. The

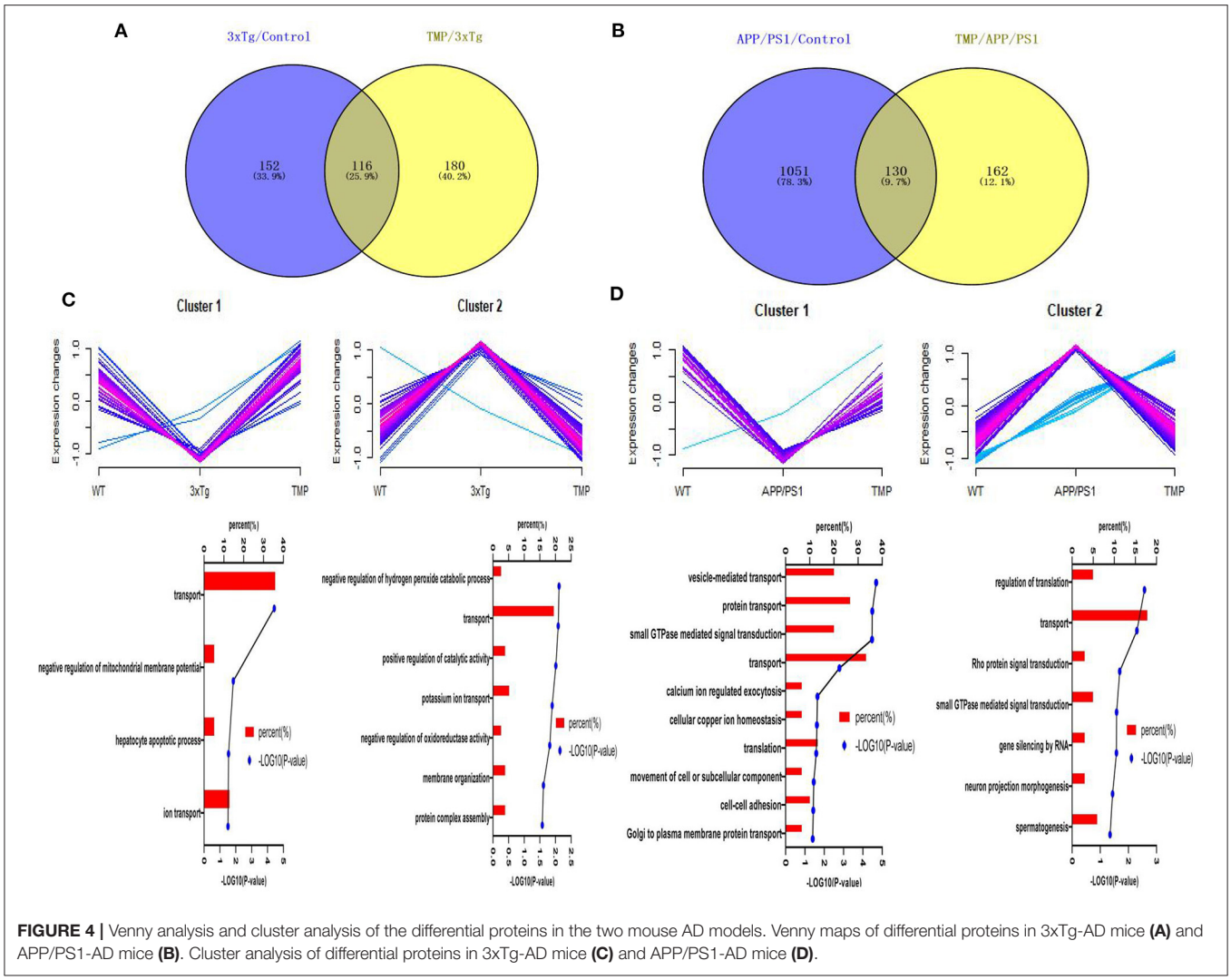

FIGURE 4 | Venny analysis and cluster analysis of the differential proteins in the two mouse AD models. Venny maps of differential proteins in 3xTg-AD mice **(A)** and APP/PS1-AD mice **(B)**. Cluster analysis of differential proteins in 3xTg-AD mice **(C)** and APP/PS1-AD mice **(D)**.

data were tested by One-way ANOVA. $p < 0.05$ was set as statistically significant.

RESULTS

TMP Improves Cognitive Function in 3xTg-AD Mice

The NOR test showed that the exploration time of new objects by 3xTg mice was shorter than for WT mice. The exploration time of new objects increased after TMP treatment (**Figure 2A**). Compared with WT mice, the step-down latency decreased, and the number of errors increased in 3xTg mice, TMP treatment significantly increased the step-down latency and reduced the number of errors (**Figures 2B,C**). Result of the contextual fear conditioning test showed no difference in the proportion of freezing time in the first day of training among all groups (**Figure 2D**). After 24 h training, in the clue fear test, 3xTg-AD mice showed significantly shorter freezing time relative to controls, and the freezing time was recovered after TMP treatment (**Figure 2E**). After 48 h training, in the contextual fear test, 3xTg-AD mice showed significant shorter freezing time than controls, and the freezing time was recovered after TMP treatment (**Figure 2F**). These data suggested that TMP reduced the spatial memory impairment of 3xTg-AD mice.

TMP Improves Cognitive Function in APP/PS1-AD Mice

The NOR test showed that the exploration time of new objects by APP/PS1 mice was shorter than that for the WT mice, and the exploration time for new objects was increased after TMP treatment (**Figure 3A**). The SDA test showed that, in APP/PS1 mice, the step-down latency was shorter than that of the WT mice. TMP treatment mice increased the step-down latency (**Figure 3B**). The error number in APP/PS1 mice was higher than that of the WT mice, and TMP reduced the error number (**Figure 3C**). The MWM test showed that during the continuous 5 days of training, the escape latency of the APP/PS1 mice was prolonged relative to that for the

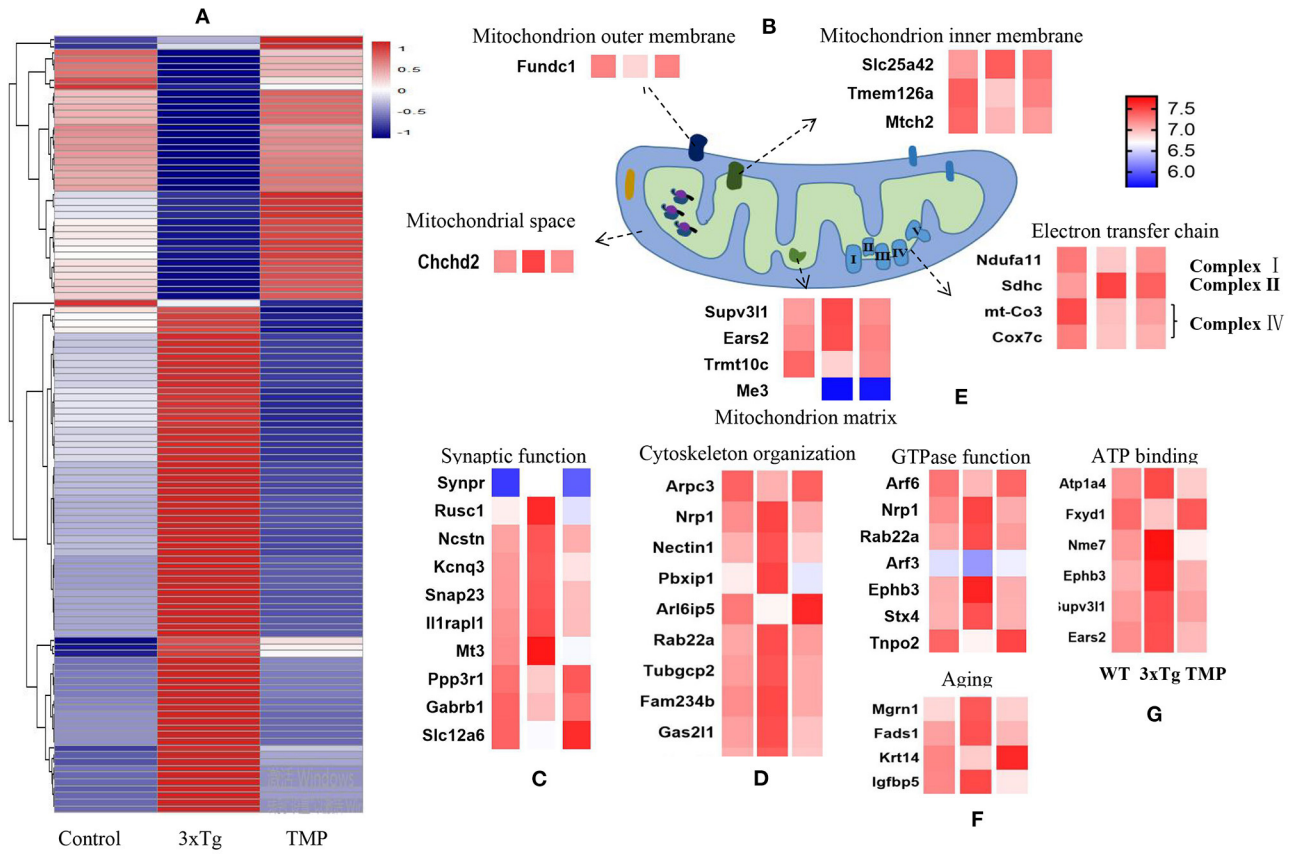

FIGURE 5 | Heat map of differentially expressed proteins and mitochondrial protein projection. Classification maps of 116 differentially expressed proteins in 3xTg-AD mice **(A)**. Mitochondrial function, synaptic function **(C)**, cytoskeleton **(D)**, GTPase binding **(E)**, aging **(F)**, and ATP binding **(G)**. Mitochondrial proteins were specifically located in the mitochondrial inner membrane, mitochondrial outer membrane, mitochondrial matrix, mitochondrial gap, and electron transport chain **(B)**. Abundance value was calculated as log2 (abundance value).

WT mice, and the escape latency was significantly decreased after TMP treatment (**Figure 3D**). The navigation path showed that the performance of the APP/PS1 mice was worse than that of the WT mice, and TMP treatment improved APP/PS1 performance (**Figure 3E**). In the probe test, compared with the WT mice, the probe time of APP/PS1 mice was longer and the time after TMP treatment was shortened (**Figure 3F**). Compared with the WT mice, the number of crossing in APP/PS1 mice was significantly fewer, and the number of crossing increased after TMP administration (**Figure 3G**). Compared to WT mice, APP/PS1 mice had reduced percentage of time in the target quadrant and percentage of distance traveled in the target quadrant, and both were increased after TMP treatment (**Figures 3H,I**). These data suggested that TMP improved the spatial memory impairment of APP/PS1 mice.

Hierarchical Heat Map and Clustering Analysis

Hippocampal proteomics of 3xTg-AD mice identified a total of 5,390 proteins by one or more unique peptides. Venny analysis showed that, compared with the WT mice, 3xTg mice had 268 differentially expressed proteins, while TMP-treated 3xTg mice had 296 differentially expressed proteins compared with untreated 3xTg mice, of which 116 proteins were commonly changed (standard ratio $\geq$1.2 or $\leq$0.83) (**Figure 4A**). These 116 proteins were involved in mitochondrial function, ATP binding, synaptic function, cytoskeleton, GTP binding, and other functions (**Figure 5**). Hippocampal proteomics of APP/PS1 mice identified a total of 4,858 proteins by one or more unique peptides. Compared with the WT mice, there were 1,181 differentially expressed hippocampal proteins in APP/PS1 mice, while there were 282 proteins in the hippocampus of APP/PS1 mice treated with TMP vs. untreated APP/PS1 mice, of which 130 proteins were commonly changed (adjusted $P < 0.05$ and ratio $\geq$1.2 or $\leq$0.83) (**Figure 4B**). These 130 proteins were related to mitochondrial function, ATP binding, synaptic function, GTPase function, cytoskeleton, and so on (**Figure 6**). According to t cluster analyses for the two models, expression levels of most of the proteins in the TMP-treatment group returned to the level of the WT group (**Figures 4C,D**).

We further analyzed the BP of proteins classified by different cluster patterns. In 3xTg mice, Cluster 1 showed the proteins

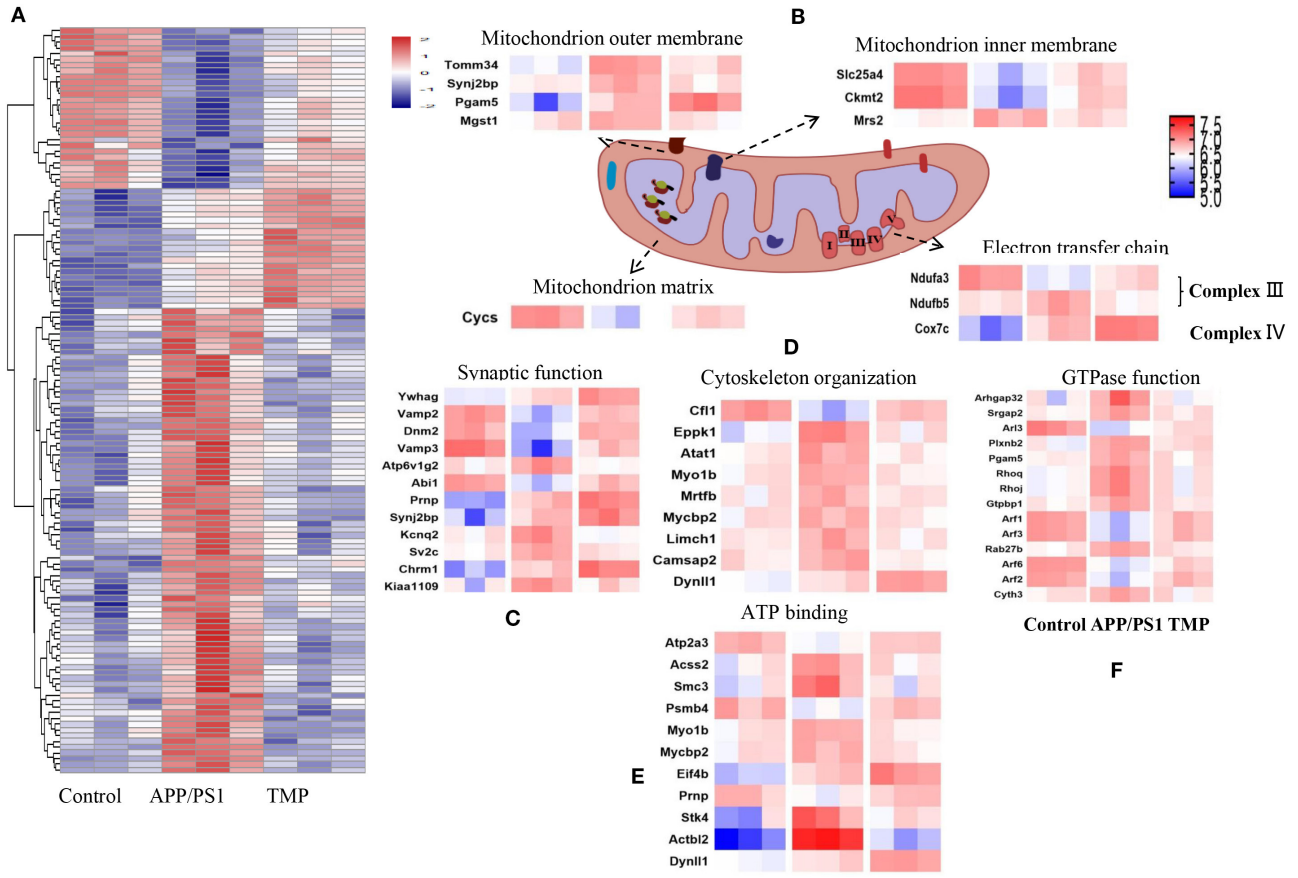

FIGURE 6 | Differential protein heat map and mitochondrial protein profile. Classification maps of 130 differentially expressed proteins in APP/PS1-AD mice **(A)**. Mitochondrial function, synaptic function **(C)**, cytoskeleton organization **(D)**, ATP binding **(E)**, and GTP binding **(F)**. Mitochondrial proteins were specifically located in the mitochondrial inner membrane, mitochondrial outer membrane, mitochondrial matrix, mitochondrial gap and electron transport chain **(B)**. Abundance value was calculated as log2 (abundance value).

with an increasing trend of TMP administration, and the BP of these proteins included transport, negative regulation of mitochondrial membrane potential, hepatocyte apoptotic process, and ion transport. Cluster 2 mainly showed the proteins with a decreasing trend of TMP administration, the BP of these proteins included the negative regulation of hydrogen peroxide catabolic process, transport, positive regulation of catalytic activity of potassium ion transport, negative regulation of oxidoreductase activity, be organization, and protein complex assembly. In APP/PS1 mice, Cluster 1 showed the proteins with increasing TMP administration trend, and the BP of these proteins including vesicle-mediated transport, protein transport, small GTPase-mediated signal transduction, transport, calcium ion-regulated exocytosis, interfaces of cell and cell adhesion in cellular copper ion homeostasis, translation, movement of cell or subcellular component, and Golgi to plasma membrane protein transport. Cluster 2 mainly showed proteins with declining tendency of TMP administration; the BP of these proteins included regulation of translation, transport, Rho protein signal transduction, small GTPase-mediated signal transduction, gene silencing by RNA, neuron projection morphogenesis, and spermatogenesis.

We carried out sub-cellular localization analysis on the common changes of mitochondrial proteins. The mitochondrial proteins were projected to the inner mitochondrial membrane, outer mitochondrial membrane, mitochondrial matrix, mitochondrial space, and electron transport chain (**Figures 5B**, **6B**). Compared with AD mice, TMP treatment changed the expression of most mitochondrial proteins.

Enrichment Analysis of Differentially Expressed Proteins

To better understand the biological function of differentially expressed proteins, in terms of BP and MFs, we identified the top 10 enriched groups. Gene ontology (GO) analysis of differential expressed proteins in 3xTg mice and WT mice, revealed BP involving transport, vesicle-mediated transport, astrocyte development, ion transport, aging, protein complex assembly, substantia nigra development, fibrinolysis, cellular response to organic cyclic compound, and protein transport

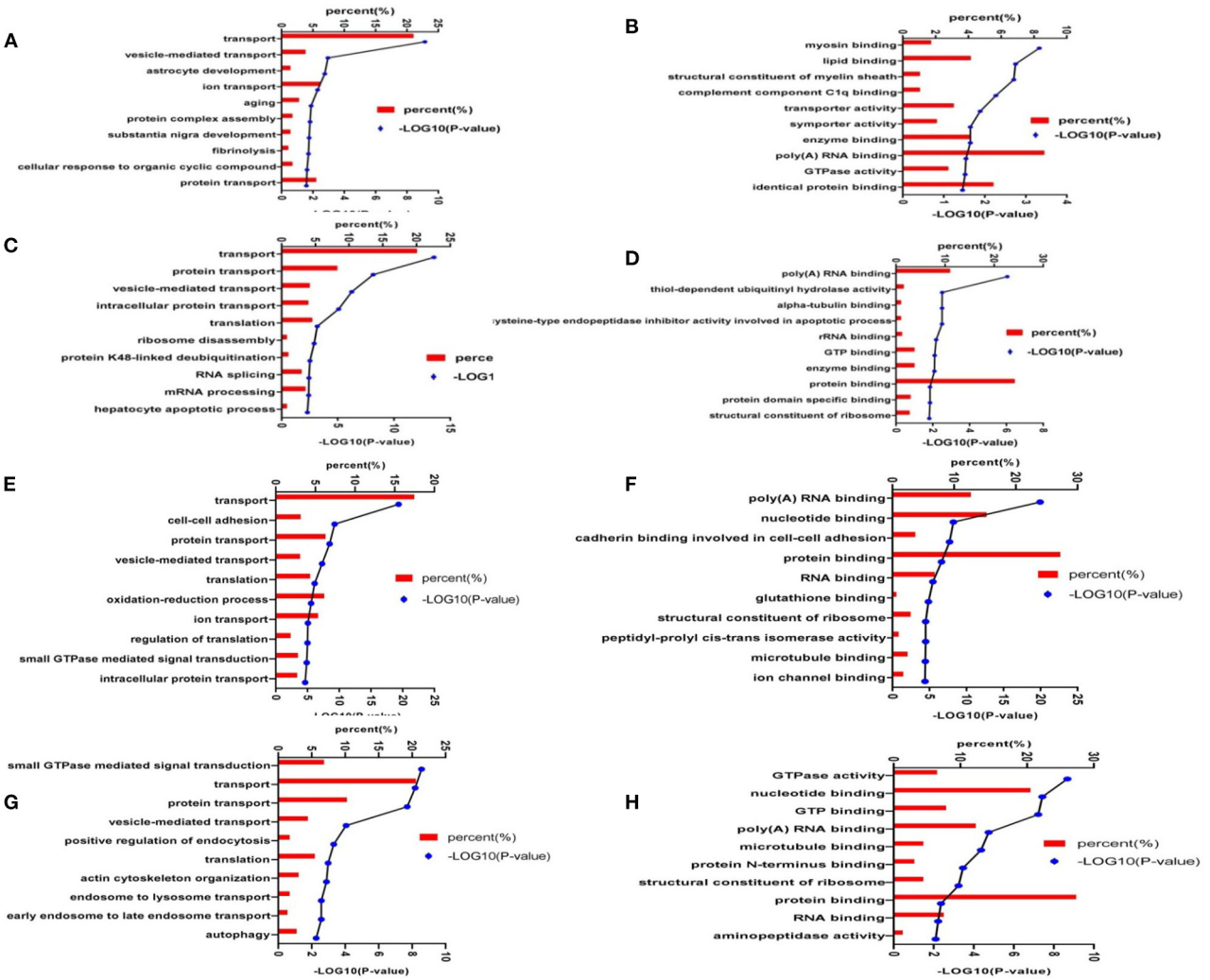

FIGURE 7 | Enrichment analysis of the differentially expressed hippocampal proteins. The proteins were functionally annotated according to their biological processes, molecular functional terms, and listed by -log10(*p*-value). Biological processes of 3xTg mice vs. WT mice **(A)**; molecular functions of 3xTg mice vs. WT mice **(B)**; biological processes of TMP-treated mice vs. -untreated mice **(C)**; molecular functions of TMP-treated mice vs. -untreated mice **(D)**; biological processes of APP/PS1 mice vs. WT mice **(E)**; molecular functional of APP/PS1 mice vs. WT mice **(F)**; biological processes of TMP-treated mice vs. -untreated mice **(G)**, and molecular function of TMP-treated mice vs. -untreated mice **(H)**.

(**Figure 7A**). Molecular functions included: protein binding, poly (A) RNA binding, myosin binding, lipid binding, structural constituent of myelin sheath, transporter activity, symporter activity, enzyme binding, GTPase activity, and identical protein binding (**Figure 7B**). For GO analysis of differential proteins in TMP-treated mice and 3xTg mice, the BP included: transporter, protein transport, vesicle-mediated transport, intracellular protein transport, translation, ribosome disassembly, protein K48-linked de-ubiquination, RNA splicing, mRNA processing, and hepatocyte apoptotic process (**Figure 7C**). Molecular functions included poly (A) RNA binding, thiol-dependent ubiquitin hydrolase activity, alpha-tubulin binding, rRNA binding, GTP binding, enzyme binding, protein binding, protein domain specific binding, structural constituent of ribosome (**Figure 7D**). For GO analysis of differential proteins in APP/PS1 mice and WT mice, the BP involved transport, cell–cell adhesion, vesicle-mediated transport, translation, oxidation-reduction process, ion transport, regulation of translation, intracellular protein transport, protein transport (**Figure 7E**). Molecular functions involved poly (A) RNA binding, nucleotide binding, protein binding, RNA binding, glutathione binding, microtubule binding, ion channel binding (**Figure 7F**). For GO analysis of differential proteins in TMP-treated mice and APP/PS1 mice, the BP involved transport, protein transport, small GTPase mediated signal transduction, translation, autophagy (**Figure 7G**). Molecular functions included GTPase activity, nucleotide

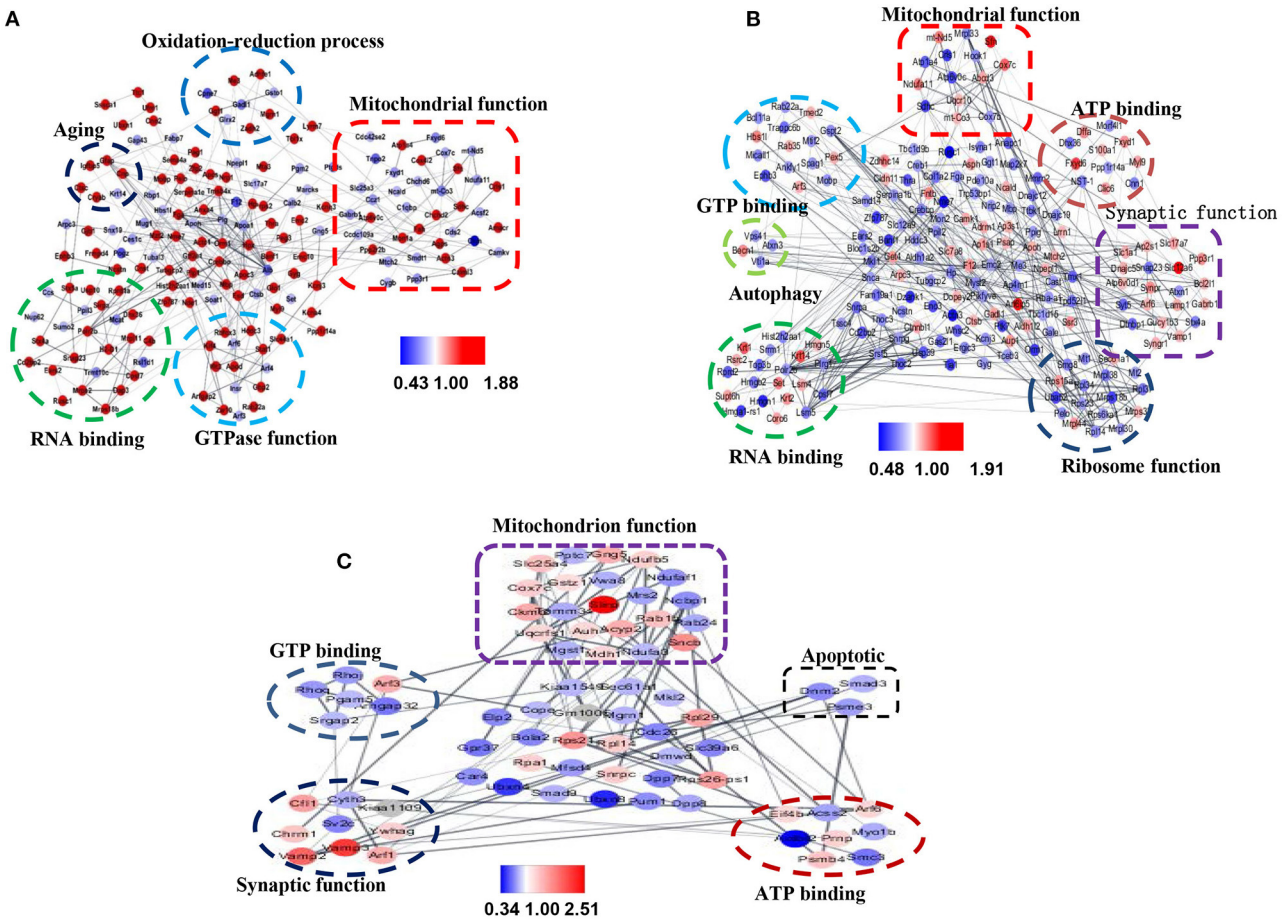

FIGURE 8 | Protein–protein interaction (PPI) maps of significantly changed hippocampal proteins mapped by Cystoscape 3.7.1. PPI network of differentially expressed proteins in 3xTg mice vs. WT mice **(A)**. PPI network of differentially expressed proteins in TMP-treated mice vs. -untreated 3xTg mice **(B)**. PPI network of differentially expressed proteins in TMP-treated APP/PS1 mice vs. APP/PS1 mice **(C)**. Gray lines represent interactions between two proteins. Red nodes represent increased proteins, and blue nodes represent decreased proteins.

binding, GTP binding, poly (A) RNA binding, microtubule binding, protein binding, RNA binding, aminopeptidase activity (**Figure 7H**).

STRING Analysis

To evaluate the relationship between differentially expressed proteins (ratio $\geq$1.2 or $\leq$0.83), we used Cytoscape software to perform STRING analysis and to visualize protein–protein interaction networks. Most of the proteins were interlinked, many of which were involved in AD. The interactions of differentially expressed proteins between 3xTg and WT mice mainly included mitochondrial function, synaptic function, GTP binding, and aging (**Figure 8A**). The interaction of the differential proteins between TMP treatment 3xTg mice and 3xTg mice mainly included mitochondrial function, synaptic function, GTP binding, and autophagy (**Figure 8B**). The interaction of the differential proteins between TMP treatment and APP/PS1 mice mainly included mitochondrial function, synaptic function, GTP binding (**Figure 8C**).

Comparison of Differential Expressed Proteins in Two AD Models After Administration

We found that 20 proteins commonly changed after TMP administration in the two AD mouse models (**Figure 9A**). Among them, H1-4, Rpl14, Sncb, Krt1, Hbs1l, Sec61a1, Pex5, Cacng3 showed different trends, while the others all had the same increasing or decreasing trend (**Figure 9B**). The STING diagram showed the PPI network of 20 proteins, of which only 4 proteins interacted with each other (**Figure 9C**). The BP included protein transport, protein localization establishment, and protein localization (**Figure 9D**).

TMP Affected the Activity of Electron Transport Chain Proteins

Western-blot analysis was performed on the electron transport chain-related proteins, Complex I (NDUFA10), Complex II (SDHB), Complex III (UQCRFS1), Complex IV (COX5B), and Complex V (ATP5A). The level of SDHB in 3xTg-AD mice was

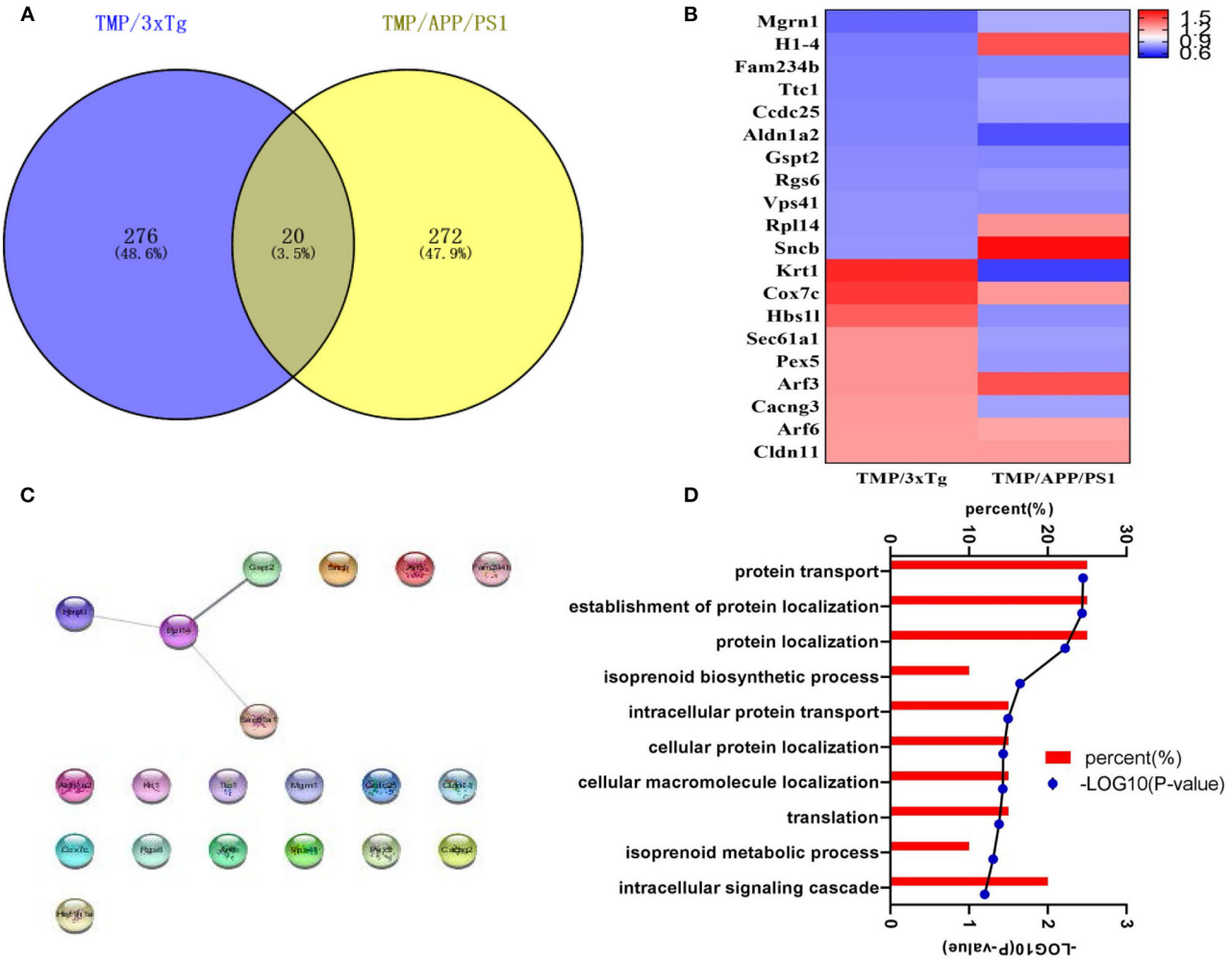

FIGURE 9 | The analysis of differential proteins in 3xTg-AD and APP/PS1-AD with or without TMP treatment. **(A)** Venny analysis. **(B)** Heat map; the abundance value was calculated as log2 (abundance, value). **(C)** Biological processes. **(D)** The STING diagram showed the PPI network of 24 proteins. Among the 20 altered proteins, only four were found to interact.

significantly modified to the level of WT mice (**Figure 10A**). In APP/PS1-AD mice, SDHB and UQCRFS1 levels were modified to the level of WT mice (**Figure 10B**). Compared with WT mice, ATP levels were significantly lower and MDA levels were significantly higher in APP/PS1 mice, and ATP levels were significantly higher and MDA did not change significantly after TMP treatment (**Figures 10C,D**).

TMP Inhibited APP Processing and Aβ Accumulation

Western-blot analysis showed, that compared with the WT mice, the levels of APP, BACE1, and PS1 in 3xTg mice were significantly increased and the expression of APP, BACE1, and PS1 was significantly decreased after TMP treatment (**Figure 11A**). Compared with the WT mice, the levels of APP and BACE1 in APP/PS1 mice were significantly increased, while ADAM10 and IDE tended to be decreased, after TMP treatment; the expression of APP, BACE1, and PS1 was significantly reduced, but there was no significant difference in the expression of ADAM10 or IDE (**Figure 11B**). Dot blot analysis showed that in the cortical tissue of the two models, compared with the WT mice, the level of 6E10 in 3xTg and APP/PS1 mice was significantly increased, while it was significantly decreased after TMP treatment (**Figures 11C,D**). These results indicated that TMP inhibited APP processing and thus reduced the accumulation of Aβ.

TMP Reduced p-tau Levels in the Brains of AD Mice

Western-blot analysis showed that the levels of tau-5 and pS396 in 3xTg mice treated with TMP were significantly decreased compared with the untreated 3xTg mice (**Figure 11E**). Similarly, the levels of tau-5, pS202, and pS396 in APP/PS1 mice treated with TMP were significantly decreased (**Figure 11F**). These results indicated that TMP could reduce level of p-tau.

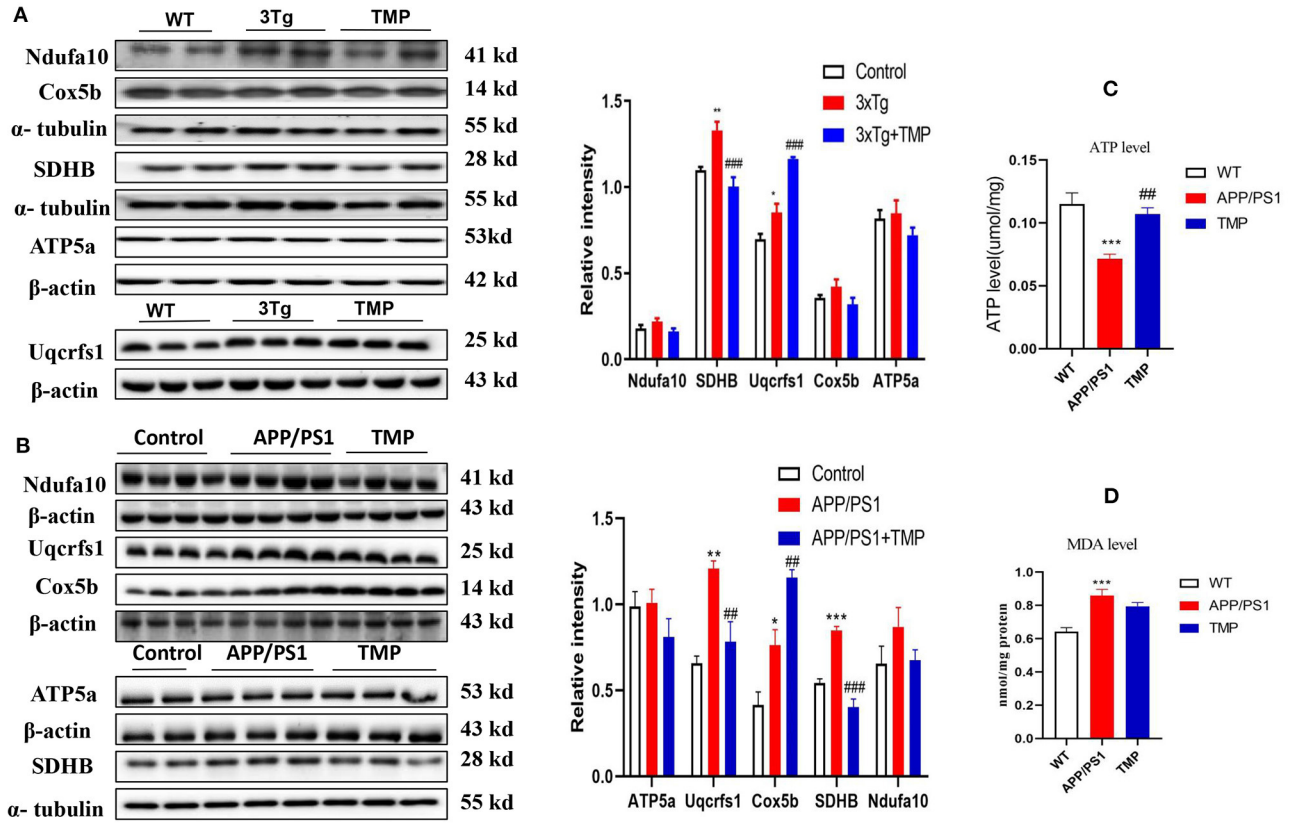

FIGURE 10 | Relative levels of mitochondrial electron transport chain-related brain cortical proteins in 3xTg mice and APP/PS1 mice. For 3xTg-AD mice, the electron transport chain proteins Uqcrfs1, ATP5a, SDHB and Cox5b were measured by Western blot and quantitative analysis **(A)**. For APP/PS1 mice, the electron transport chain proteins Uqcrfs1, ATP5a, SDHB, and Cox5a were measured by Western blot analysis **(B)**. $N = 4$. ATP levels **(C)**, MDA levels **(D)** in cortical tissue of APP/PS1 mice. $N = 4$–5. $^{\#\#\#}p < 0.001$, $^{\#\#}p < 0.01$, vs. 3xTg mice, $^{***}p < 0.001$, $^{**}p < 0.01$, $^{*}p < 0.05$ vs. WT mice; $^{\#\#\#}p < 0.001$, $^{\#\#}p < 0.01$ vs. APP/PS1 mice, $^{***}p < 0.001$, $^{**}p < 0.01$, $^{*}p < 0.05$ vs. WT mice.

DISCUSSION

The 3xTg and APP/PS1 mouse models have been widely used for AD-related studies (Esquerda-Canals et al., 2017). Among them, 3xTg-AD mice had obvious Aβ deposition in the hippocampus of 3–6 month-old animals, and hyperphosphorylated tau (p-tau) was present by 6–12 months of age (Oddo et al., 2003). APP/PS1-AD mice may exhibit abnormal behavior and Aβ deposition starting from 4 to 6 months of age (Izco et al., 2014). We investigated the therapeutic effect of TMP on cognitive function in the two AD models (3xTg-AD and APP/PS1-AD) and used proteomics methods to explore its potential biological mechanisms of action. Behavioral tests showed that TMP significantly reduced memory impairment of the two AD mouse models. These results are consistent with previous reported studies that TMP can protect against isoflurane-induced cognitive dysfunction in rats (Cui et al., 2020) and restore spatial learning and memory impairment in rats injected with streptozotocin (Lu et al., 2017).

A prominent pathological feature of AD brains is the accumulation of Aβ and NFTs composed of hyperphosphoryled tau (Grontvedt et al., 2018) and a growing body of evidence suggests that that Aβ and tau have synergistic effects in advancing AD-type neurodegeneration (Busche and Hyman, 2020). We found that TMP treatment significantly reduced the levels of Aβ accumulation and tau hyper phosphorylation in the two AD models relative to controls. Beta-secretase 1 (BACE1) plays an important role in APP processing and is closely related to tau protein (Zhang et al., 2018). Our results show that TMP creduces the accumulation of Aβ by inhibiting the activity of BACE1, which could affect levels of p-tau.

We used Venny analysis, GO analysis and protein–protein interaction (PPI) network diagram to analyze the proteomic data and to further explore the molecular mechanisms underlying the apparent murine therapeutic effect of TMP. Venny analysis showed that 116 differentially expressed proteins were commonly changed in 3xTg mice vs. WT mice and TMP-treated mice vs. untreated mice. GO analysis showed that the 116 differential expressed proteins were mainly enriched in processes such as transportation and ion migration, and to participate in MFs such as metal ion binding and ion channel activity. The same 130 differentially expressed proteins were commonly changed in APP/PS1 mice vs. WT mice and TMP-treated mice vs. untreated mice. GO analysis showed that the 130 differential

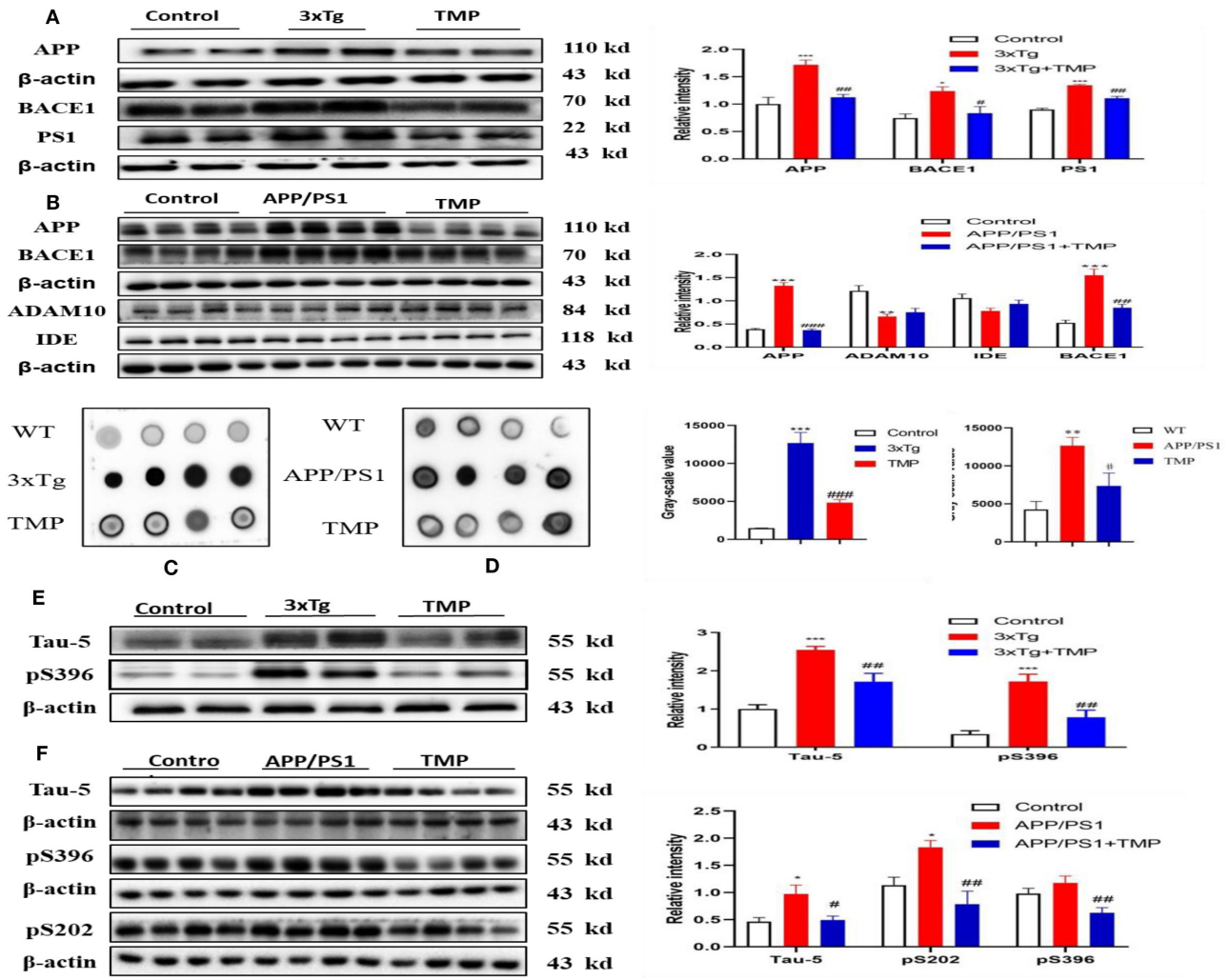

FIGURE 11 | TMP reduced APP levels and p-tau levels in the hippocampus. The proteins related to APP processing by Western blot analysis of 3xTg-AD mice **(A)** and APP/PS1 mice **(B)**. Dot blot analysis was performed to detect Aβ accumulation **(C,D)**. Tau phosphorylation was detected by Western blot analysis **(E,F)**. PS1 and TAU-5 ($N = 3$), others $N = 4$. $^{###}p < 0.001$, $^{##}p < 0.01$, $^{#}p < 0.05$ vs. 3xTg mice, $^{***}p < 0.001$, $^{**}p < 0.01$, $^{*}p < 0.05$ vs. WT mice; $^{###}p < 0.001$, $^{##}p < 0.01$ vs. APP/PS1 mice; $^{***}p < 0.001$, $^{**}p < 0.01$, $^{*}p < 0.05$ vs. WT mice.

expressed proteins were mainly enriched in processes such as protein transport and protein localization establishment, and to participate in MFs such as protein binding and nucleotide binding. Through proteomics analysis, some proteins functionally related to AD were found in these two mouse models, such as proteins related to mitochondria, GTP binding, synapse, and cytoskeleton. Among them, mitochondria play a significant role in energy production, synaptic transmission, and cognitive function (Picard and McEwen, 2014). Increased reactive oxygen species may impair mitochondrial function may promote neurodegenerative disease (Hroudova et al., 2014). Mitochondrial dysfunction occurred in both the 3xTg and APP/PS1 mice (Coskun et al., 2012).

The differentially expressed proteins located in the mitochondria and mapped the mitochondrial protein profile. Most of the mitochondrial proteins were modified by TMP treatment. For example, FUNDC1 controlled the dynamics and quality of mitochondria by regulating the fission or fusion of mitochondria (Chen M. et al., 2016), while the electron carrier protein CYCS transferred electrons to the cytochrome oxidase complex (Baechler et al., 2019). Western-blot analysis showed that TMP modified the level of mitochondrial Complex II protein SDHB in 3xTg mice and modified the level of mitochondrial Complex II protein SDHB and III protein UQCRFS1 in APP/PS1 mice. APP and Aβ can accumulate on the mitochondrial membrane and interact with mitochondrial components to cause damage to mitochondrial function and structure (Pagani and Eckert, 2011). Mitochondria are central to cellular energy metabolism and the site of most ATP production (Brookes et al., 2004). Mitochondrial dysfunction reduced ATP production in murine AD pathogenesis (Cai and Tammineni, 2017). The increased ATP production after

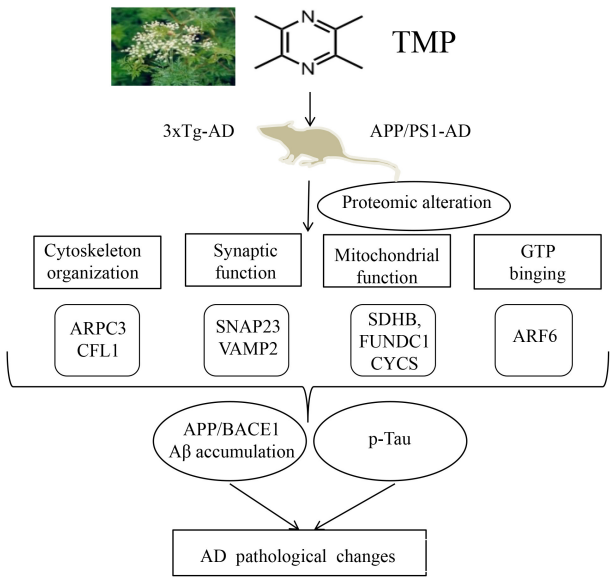

FIGURE 12 | Supposed mode of TMP action. TMP treatment inhibited AD-related changes, including Aβ accumulation and tau phosphorylation, which may be attributed to the modification of mitochondrial function, synaptic function, cytoskeleton, and GTP binding.

TMP treatment suggested that mitochondrial function was restored in APP/PS1 mice. Aβ, phosphorylated tau protein and the VDAC of the mitochondrial channel interact to cause mitochondrial dysfunction, and synergistic effects of Aβ and tau proteins may cause mitochondrial dysfunction (Manczak and Reddy, 2013). MAPT protein was identified in 3xTg by MS, which was responsible for promoting microtubule assembly and stabilization. WB validation was consistent with proteomic results, with increased tau expression in 3xTg mice compared to WT mice, with decreased expression after TMP administration. APP protein was identified in APP/PS1 mice by MS. APP protein was processed to produce Aβ, which aggregates to form age spots. The WB validation results were consistent with the proteomic results. APP expression was increased in APP/PS1 mice compared to the WT mice and decreased after TMP administration. Aβ and p-tau proteins can directly contribute to mitochondrial dysfunction, and dysfunctional mitochondria in turn accelerate the process of AD (Manczak and Reddy, 2012). It has been reported in the literature that Icariin protects mitochondria and inhibits Aβ production and p-tau protein to improve learning and memory in AD rats (Chen Y. et al., 2016). In our proteomic analysis, mitochondrial proteins were significantly changed after TMP treatment, with improved electron transport chain function and increased ATP levels in the brains of APP/PS1 mice, suggesting that mitochondrial function plays an important role in TMP treatment. The reduction of Aβ and p-tau in the brains of test animals reduced mitochondrial dysfunction, and this was associated with an attenuation of the hallmarks of AD. These data indicated that TMP may protect mitochondrial function in AD mice; this is consistent with reports that systemic TMP treatment restores mitochondrial function and reduces brain damage caused by oxidative stress and cobalt chloride (CoCl2) (Guan et al., 2015). Additionally, TMP can reduce oxidative damage, restore mitochondrial dysfunction and protect HUVEC cells from Hcy-induced apoptosis (Fan et al., 2019).

Synaptic dysfunction also is important to the pathogenesis of AD. Soluble Aβ oligomers reportedly can impair synaptic function (Takahashi et al., 2013), as can tau protein oligomers (Lasagna-Reeves et al., 2011), and Aβ and tau proteins play a synergistic role in synaptic dysfunction (Ittner et al., 2010; Larson et al., 2012). Proteomics showed that TMP modified the expression of some synapse-related proteins. For example, SNAP23 played a major role in transport vesicle docking and fusion, and VAMP2 played a major role in synaptic transmission and neurotransmitter release (Martin et al., 1998; Deak et al., 2004). Consistent with our results in the two mouse models of AD, VAMP2 was down-regulated in AD patients (Pham et al., 2010), but significantly increased after TMP treatment, suggesting that TMP treatment improves synaptic dysfunction.

We noticed that TMP treatment increased some cytoskeleton proteins expression, such as Actin-related protein 2/3 complex subunit 3(Arpc3), Cofilin-1(Cof1), and Arpc3, which is mainly responsible for starting the branches of actin filaments. Mir-29a/B can affect the ARp2/3 complex through the Arpc3 subunit, thus maintaining the flexibility of the neuronal network (Lippi et al., 2011). Cof1 mainly regulates actin cytoskeleton dynamics and plays an important role in neural cell (Gurniak et al., 2005). Our results indicated that TMP may exert a neuroprotective effect by modifying the expression of cytoskeleton proteins.

We found that TMP treatment increased brain ADP-ribosylation factor 6 (ARF6) the two AD model mice. ARF6 is a GTP binding protein, mainly involved in vesicle transport, cytoskeleton, and some other functions (Donaldson, 2003; D'Souza-Schorey and Chavrier, 2006). Activation of ARF6 contributes to the generation of synaptic vesicles in the PC12 nerve (Powelka and Buckley, 2001) and can also recruit AP2/Clathrin-dependent synaptic vesicle membranes to the presynaptic membrane to be endocytosed, thereby accelerating the recovery of neurotransmitters (Krauss et al., 2003). Our results suggest that ARF6 may also be also involved in the neuroprotection of TMP.

CONCLUSION

In summary, our study of 3xTg-AD and APP/PS1-AD female mice showed that systemic TMP treatment improved memory deficits, reduced Aβ deposition and tau phosphorylation levels, and modified the mitochondrial protein profile, including some oxidative phosphorylation (OXPHOS) proteins. Proteomics suggested that the action of TMP may be closely related to mitochondria, synapses, GTP binding, and cytoskeleton proteins. Although the precise molecular mechanisms remain to be elucidated, our data suggest that TMP has potential for positive therapeutic modification of AD (**Figure 12**).

DATA AVAILABILITY STATEMENT

The datasets generated for this study can be found in online repositories. The names of the repository/repositories and accession number(s) can be found below: ProteomeXchange Consortium; PXD022862 and PXD022840.

ETHICS STATEMENT

The animal study was reviewed and approved by All experiments were approved by the Ethics Committee of Shenzhen Center for Disease Control and Prevention.

AUTHOR CONTRIBUTIONS

LZ and XY conceived the project, designed the experiments, and wrote the manuscript. XfH and JY designed and performed most of the experiments. XiH performed the informatics analysis and the proteomics analysis. ZZ and JL designed the experiments, analyzed the data, and revised the manuscript. All authors contributed to the article and approved the submitted version.

FUNDING

This work was supported in parts by Natural Science Foundation of China (81673134), Guangdong Provincial Key S&T Program (2018B030336001), and Sanming Project of Medicine in Shenzhen (SZSM201611090).

SUPPLEMENTARY MATERIAL

The Supplementary Material for this article can be found online at: https://www.frontiersin.org/articles/10.3389/fcell.2021.632843/full#supplementary-material

REFERENCES

Baechler, B. L., Bloemberg, D., and Quadrilatero, J. (2019). Mitophagy regulates mitochondrial network signaling, oxidative stress, and apoptosis during myoblast differentiation. *Autophagy* 15, 1606–1619. doi: 10.1080/15548627.2019.1591672

Bolton, M. M., Heaney, C. F., Sabbagh, J. J., Murtishaw, A. S., Magcalas, C. M., and Kinney, J. W. (2012). Deficits in emotional learning and memory in an animal model of schizophrenia. *Behav. Brain Res.* 233, 35–44. doi: 10.1016/j.bbr.2012.04.049

Briggs, R., Kennelly, S. P., and O'Neill, D. (2016). Drug treatments in Alzheimer's disease. *Clin. Med. Lond.* 16, 247–253. doi: 10.7861/clinmedicine.16-3-247

Brookes, P. S., Yoon, Y., Robotham, J. L., Anders, M. W., and Sheu, S. S. (2004). Calcium ATP and ROS: a mitochondrial love-hate triangle. *Am. J. Physiol. Cell Physiol.* 287, C817–C833. doi: 10.1152/ajpcell.00139.2004

Busche, M. A., and Hyman, B. T. (2020). Synergy between amyloid-β and tau in Alzheimer's disease. *Nat. Neurosci.* 23, 1183–1193. doi: 10.1038/s41593-020-0687-6

Cai, Q., and Tammineni, P. (2017). Mitochondrial aspects of synaptic dysfunction in Alzheimer's disease. *J. Alzheimers. Dis.* 57, 1087–1103. doi: 10.3233/JAD-160726

Chang, Y., Hsiao, G., Chen, S. H., Chen, Y. C., Lin, J. H., Lin, K. H., et al. (2007). Tetramethylpyrazine suppresses HIF-1α, TNF-α, and activated caspase-3 expression in middle cerebral artery occlusion-induced brain ischemia in rats. *Acta Pharmacol. Sin.* 28, 327–333. doi: 10.1111/j.1745-7254.2007.00514.x

Chen, C., Jiang, X., Li, Y., Yu, H., Li, S., Zhang, Z., et al. (2019). Low-dose oral copper treatment changes the hippocampal phosphoproteomic profile and perturbs mitochondrial function in a mouse model of Alzheimer's disease. *Free Radic. Biol. Med.* 135, 144–156. doi: 10.1016/j.freeradbiomed.2019.03.002

Chen, M., Chen, Z., Wang, Y., Tan, Z., Zhu, C., Li, Y., et al. (2016). Mitophagy receptor FUNDC1 regulates mitochondrial dynamics and mitophagy. *Autophagy* 12, 689–702. doi: 10.1080/15548627.2016.1151580

Chen, Y., Han, S., Huang, X., Ni, J., and He, X. (2016). The protective effect of icariin on mitochondrial transport and distribution in primary hippocampal neurons from 3x Tg-AD mice. *Int. J. Mol. Sci.* 17:163. doi: 10.3390/ijms17020163

Coskun, P., Wyrembak, J., Schriner, S. E., Chen, H. W., Marciniack, C., Laferla, F., et al. (2012). A mitochondrial etiology of Alzheimer and Parkinson disease. *Biochim. Biophys. Acta* 1820, 553–564. doi: 10.1016/j.bbagen.2011.08.008

Cui, H., Xu, Z., and Qu, C. (2020). Tetramethylpyrazine ameliorates isoflurane-induced cognitive dysfunction by inhibiting neuroinflammation via miR-150 in rats. *Exp. Ther. Med.* 20, 3878–3887. doi: 10.3892/etm.2020.9110

Deak, F., Schoch, S., Liu, X., Sudhof, T. C., and Kavalali, E. T. (2004). Synaptobrevin is essential for fast synaptic-vesicle endocytosis. *Nat. Cell Biol.* 6, 1102–1108. doi: 10.1038/ncb1185

Donaldson, J. G. (2003). Multiple roles for Arf6: sorting, structuring, and signaling at the plasma membrane. *J. Biol. Chem.* 278, 41573–41576. doi: 10.1074/jbc.R300026200

D'Souza-Schorey, C., and Chavrier, P. (2006). ARF proteins: roles in membrane traffic and beyond. *Nat. Rev. Mol. Cell Biol.* 7, 347–358. doi: 10.1038/nrm1910

Esquerda-Canals, G., Montoliu-Gaya, L., Guell-Bosch, J., and Villegas, S. (2017). Mouse models of Alzheimer's disease. *J. Alzheimers. Dis.* 57, 1171–1183. doi: 10.3233/JAD-170045

Fan, X., Wang, E., He, J., Zhang, L., Zeng, X., Gui, Y., et al. (2019). Ligustrazine protects homocysteine-induced apoptosis in human umbilical vein endothelial cells by modulating mitochondrial dysfunction. *J. Cardiovasc. Transl. Res.* 12, 591–599. doi: 10.1007/s12265-019-09900-6

Foloppe, D. A., Richard, P., Yamaguchi, T., Etcharry-Bouyx, F., and Allain, P. (2018). The potential of virtual reality-based training to enhance the functional autonomy of Alzheimer's disease patients in cooking activities: a single case study. *Neuropsychol. Rehabil.* 28, 709–733. doi: 10.1080/09602011.2015.1094394

Grontvedt, G. R., Schroder, T. N., Sando, S. B., White, L., Brathen, G., and Doeller, C. F. (2018). Alzheimer's disease. *Curr. Biol.* 28, R645–R649. doi: 10.1016/j.cub.2018.04.080

Guan, D., Su, Y., Li, Y., Wu, C., Meng, Y., Peng, X., et al. (2015). Tetramethylpyrazine inhibits CoCl2-induced neurotoxicity through enhancement of Nrf2/GCLc/GSH and suppression of HIF1α/NOX2/ROS pathways. *J. Neurochem.* 134, 551–565. doi: 10.1111/jnc.13161

Gurniak, C. B., Perlas, E., and Witke, W. (2005). The actin depolymerizing factor n-cofilin is essential for neural tube morphogenesis and neural crest cell migration. *Dev. Biol.* 278, 231–241. doi: 10.1016/j.ydbio.2004.11.010

He, K., Nie, L., Zhou, Q., Rahman, S. U., Liu, J., Yang, X., et al. (2019). Proteomic profiles of the early mitochondrial changes in APP/PS1 and ApoE4 transgenic mice models of Alzheimer's disease. *J. Proteome Res.* 18, 2632–2642. doi: 10.1021/acs.jproteome.9b00136

Hroudova, J., Singh, N., and Fisar, Z. (2014). Mitochondrial dysfunctions in neurodegenerative diseases: relevance to Alzheimer's disease. *Biomed. Res. Int.* 2014:175062. doi: 10.1155/2014/175062

Hyman, B. T., Phelps, C. H., Beach, T. G., Bigio, E. H., Cairns, N. J., Carrillo, M. C., et al. (2012). National Institute on Aging-Alzheimer's Association guidelines for

the neuropathologic assessment of Alzheimer's disease. *Alzheimers. Dement.* 8, 1–13. doi: 10.1016/j.jalz.2011.10.007

Ittner, L. M., Ke, Y. D., Delerue, F., Bi, M., Gladbach, A., van Eersel, J., et al. (2010). Dendritic function of tau mediates amyloid-β toxicity in Alzheimer's disease mouse models. *Cell* 142, 387–397. doi: 10.1016/j.cell.2010.06.036

Izco, M., Martinez, P., Corrales, A., Fandos, N., Garcia, S., Insua, D., et al. (2014). Changes in the brain and plasma Aβ peptide levels with age and its relationship with cognitive impairment in the APPswe/PS1dE9 mouse model of Alzheimer's disease. *Neuroscience* 263, 269–279. doi: 10.1016/j.neuroscience.2014.01.003

Krauss, M., Kinuta, M., Wenk, M. R., De Camilli, P., Takei, K., and Haucke, V. (2003). ARF6 stimulates clathrin/AP-2 recruitment to synaptic membranes by activating phosphatidylinositol phosphate kinase type Iγ. *J. Cell Biol.* 162, 113–124. doi: 10.1083/jcb.200301006

Larson, M., Sherman, M. A., Amar, F., Nuvolone, M., Schneider, J. A., Bennett, D. A., et al. (2012). The complex $PrP^{(c)}$-Fyn couples human oligomeric Aβ with pathological tau changes in Alzheimer's disease. *J. Neurosci.* 32, 16857–16871. doi: 10.1523/JNEUROSCI.1858-12.2012

Lasagna-Reeves, C. A., Castillo-Carranza, D. L., Sengupta, U., Clos, A. L., Jackson, G. R., and Kayed, R. (2011). Tau oligomers impair memory and induce synaptic and mitochondrial dysfunction in wild-type mice. *Mol. Neurodegener.* 6:39. doi: 10.1186/1750-1326-6-39

Lippi, G., Steinert, J. R., Marczylo, E. L., D'Oro, S., Fiore, R., Forsythe, I. D., et al. (2011). Targeting of the Arpc3 actin nucleation factor by miR-29a/b regulates dendritic spine morphology. *J. Cell Biol.* 194, 889–904. doi: 10.1083/jcb.201103006

Lu, C., Zhang, J., Shi, X., Miao, S., Bi, L., Zhang, S., et al. (2014). Neuroprotective effects of tetramethylpyrazine against dopaminergic neuron injury in a rat model of Parkinson's disease induced by MPTP. *Int. J. Biol. Sci.* 10, 350–357. doi: 10.7150/ijbs.8366

Lu, F., Li, X., Li, W., Wei, K., Yao, Y., Zhang, Q., et al. (2017). Tetramethylpyrazine reverses intracerebroventricular streptozotocin-induced memory deficits by inhibiting GSK-3β. *Acta Biochim. Biophys. Sin. Shanghai* 49, 722–728. doi: 10.1093/abbs/gmx059

Manczak, M., and Reddy, P. H. (2012). Abnormal interaction between the mitochondrial fission protein Drp1 and hyperphosphorylated tau in Alzheimer's disease neurons: implications for mitochondrial dysfunction and neuronal damage. *Hum. Mol. Genet.* 21, 2538–2547. doi: 10.1093/hmg/dds072

Manczak, M., and Reddy, P. H. (2013). Abnormal interaction of oligomeric amyloid-β with phosphorylated tau: implications to synaptic dysfunction and neuronal damage. *J. Alzheimers. Dis.* 36, 285–295. doi: 10.3233/JAD-130275

Martin, L. B., Shewan, A., Millar, C. A., Gould, G. W., and James, D. E. (1998). Vesicle-associated membrane protein 2 plays a specific role in the insulin-dependent trafficking of the facilitative glucose transporter GLUT4 in 3T3-L1 adipocytes. *J. Biol. Chem.* 273, 1444–1452. doi: 10.1074/jbc.273.3.1444

Michel, H. E., Tadros, M. G., Esmat, A., Khalifa, A. E., and Abdel-Tawab, A. M. (2017). Tetramethylpyrazine ameliorates rotenone-induced Parkinson's disease in rats: involvement of its anti-inflammatory and anti-apoptotic actions. *Mol. Neurobiol.* 54, 4866–4878. doi: 10.1007/s12035-016-0028-7

Oboudiyat, C., Glazer, H., Seifan, A., Greer, C., and Isaacson, R. S. (2013). Alzheimer's disease. *Semin. Neurol.* 33, 313–329. doi: 10.1055/s-0033-1359319

Oddo, S., Caccamo, A., Kitazawa, M., Tseng, B. P., and LaFerla, F. M. (2003). Amyloid deposition precedes tangle formation in a triple transgenic model of Alzheimer's disease. *Neurobiol. Aging* 24, 1063–1070. doi: 10.1016/j.neurobiolaging.2003.08.012

Pagani, L., and Eckert, A. (2011). Amyloid-Beta interaction with mitochondria. *Int. J. Alzheimers. Dis.* 2011:925050. doi: 10.4061/2011/925050

Pham, E., Crews, L., Ubhi, K., Hansen, L., Adame, A., Cartier, A., et al. (2010). Progressive accumulation of amyloid-β oligomers in Alzheimer's disease and in amyloid precursor protein transgenic mice is accompanied by selective alterations in synaptic scaffold proteins. *FEBS J.* 277, 3051–3067. doi: 10.1111/j.1742-4658.2010.07719.x

Picard, M., and McEwen, B. S. (2014). Mitochondria impact brain function and cognition. *Proc. Natl. Acad. Sci. U.S.A.* 111, 7–8. doi: 10.1073/pnas.1321881111

Powelka, A. M., and Buckley, K. M. (2001). Expression of ARF6 mutants in neuroendocrine cells suggests a role for ARF6 in synaptic vesicle biogenesis. *FEBS Lett.* 501, 47–50. doi: 10.1016/S0014-5793(01)02624-2

Scholtzova, H., Wadghiri, Y. Z., Douadi, M., Sigurdsson, E. M., Li, Y. S., Quartermain, D., et al. (2008). Memantine leads to behavioral improvement and amyloid reduction in Alzheimer's-disease-model transgenic mice shown as by micromagnetic resonance imaging. *J. Neurosci. Res.* 86, 2784–2791. doi: 10.1002/jnr.21713

Takahashi, R. H., Capetillo-Zarate, E., Lin, M. T., Milner, T. A., and Gouras, G. K. (2013). Accumulation of intraneuronal β-amyloid 42 peptides is associated with early changes in microtubule-associated protein 2 in neurites and synapses. *PLoS ONE* 8:e51965. doi: 10.1371/journal.pone.0051965

Wang, X., Zhang, J., Zhou, L., Xu, B., Ren, X., He, K., et al. (2019). Long-term iron exposure causes widespread molecular alterations associated with memory impairment in mice. *Food Chem. Toxicol.* 130, 242–252. doi: 10.1016/j.fct.2019.05.038

Xu, B., Zhang, Y., Zhan, S., Wang, X., Zhang, H., Meng, X., et al. (2018). Proteomic profiling of brain and testis reveals the diverse changes in ribosomal proteins in fmr1 knockout mice. *Neuroscience* 371, 469–483. doi: 10.1016/j.neuroscience.2017.12.023

Zhang, Z., Li, X. G., Wang, Z. H., Song, M., Yu, S. P., Kang, S. S., et al. (2018). δ-Secretase-cleaved tau stimulates Aβ production via upregulating STAT1-BACE1 signaling in Alzheimer's disease. *Mol. Psychiatry* 26, 586–603. doi: 10.1038/s41380-018-0286-z

Zhou, I. Y., Ding, A. Y., Li, Q., McAlonan, G. M., and Wu, E. X. (2012). Magnetic resonance spectroscopy reveals N-acetylaspartate reduction in hippocampus and cingulate cortex after fear conditioning. *Psychiatry Res.* 204, 178–183. doi: 10.1016/j.pscychresns.2012.09.010

Zhou, X., Wang, L., Xiao, W., Su, Z., Zheng, C., Zhang, Z., et al. (2019a). Memantine improves cognitive function and alters hippocampal and cortical proteome in triple transgenic mouse model of Alzheimer's disease. *Exp. Neurobiol.* 28, 390–403. doi: 10.5607/en.2019.28.3.390

Zhou, X., Xiao, W., Su, Z., Cheng, J., Zheng, C., Zhang, Z., et al. (2019b). Hippocampal proteomic alteration in triple transgenic mouse model of Alzheimer's disease and implication of PINK 1 regulation in donepezil treatment. *J. Proteome Res.* 18, 1542–1552. doi: 10.1021/acs.jproteome.8b00818

Conflict of Interest: The authors declare that the research was conducted in the absence of any commercial or financial relationships that could be construed as a potential conflict of interest.

frontiers in Cell and Developmental Biology

REVIEW
published: 14 June 2021
doi: 10.3389/fcell.2021.680118

The Implication of STEP in Synaptic Plasticity and Cognitive Impairments in Alzheimer's Disease and Other Neurological Disorders

Yacoubou Abdoul Razak Mahaman[1,2], Fang Huang[2], Kidane Siele Embaye[2], Xiaochuan Wang[2,3] and Feiqi Zhu[1]**

[1] Cognitive Impairment Ward of Neurology Department, The Third Affiliated Hospital, Shenzhen University, Shenzhen, China, [2] Department of Pathophysiology, School of Basic Medicine, Key Laboratory of Education Ministry of China for Neurological Disorders, Tongji Medical College, Huazhong University of Science and Technology, Wuhan, China, [3] Co-Innovation Center of Neuroregeneration, Nantong University, Nantong, China

STriatal-Enriched protein tyrosine Phosphatase (STEP) is a tyrosine phosphatase that has been implicated in Alzheimer's disease (AD), the most common form of dementia, and many other neurological diseases. The protein level and activity of STEP have been found to be elevated in most of these disorders, and specifically in AD as a result of dysregulation of different pathways including PP2B/DARPP32/PP1, PKA as well as impairments of both proteasomal and lysosomal systems. The upregulation in STEP leads to increased binding to, and dephosphorylation of, its substrates which are mainly found to be synaptic plasticity and thus learning and memory related proteins. These proteins include kinases like Fyn, Pyk2, ERK1/2 and both NMDA and AMPA receptor subunits GluN2B and GluA2. The dephosphorylation of these molecules results in inactivation of these kinases and internalization of NMDA and AMPA receptor complexes leading to synapse loss and cognitive impairments. In this study, we aim to review STEP regulation and its implications in AD as well as other neurological disorders and then summarize data on targeting STEP as therapeutic strategy in these diseases.

Keywords: STEP, GluN2B, GluA2, Fyn, ERK1/2, synapses loss, cognitive impairment

OPEN ACCESS

Edited by:
Shupeng Li,
Peking University, China

Reviewed by:
Mark L. Dell'Acqua,
University of Colorado, United States
Xavier Xifró,
University of Girona, Spain

****Correspondence:***
Feiqi Zhu
zfqzsu2004@aliyun.com
Xiaochuan Wang
wxch@mails.tjmu.edu.cn

Specialty section:
This article was submitted to Molecular Medicine, a section of the journal Frontiers in Cell and Developmental Biology

Received: *13 March 2021*
Accepted: *06 May 2021*
Published: *14 June 2021*

Citation:
Mahaman YAR, Huang F, Embaye KS, Wang X and Zhu F (2021) The Implication of STEP in Synaptic Plasticity and Cognitive Impairments in Alzheimer's Disease and Other Neurological Disorders. Front. Cell Dev. Biol. 9:680118. doi: 10.3389/fcell.2021.680118

INTRODUCTION

Alzheimer's disease (AD) is the most common form of dementia and is characterized by a gradual loss of short-term memory and a progressive decline of cognitive functions. It has been a major public health problem in modern society which will undoubtedly increase dramatically in the coming years, unless drugs that can prevent or cure the disease become available. According to the World Alzheimer Report, over 50 million people worldwide are currently living with dementia, and this number is estimated to reach 152 million by 2050 (Alzheimer's Disease International, 2019). The two main histopathological hallmarks of AD are extracellular deposit of amyloid beta (Aβ) forming senile plaques, and intracellular hyperphosphorylated tau forming neurofibrillary tangles (Bennett et al., 2004). In addition to these, age-dependent synapse loss and the accompanying memory impairment are the next most common characteristics of AD patients as well as many AD models (Terry et al., 1991; Knobloch and Mansuy, 2008). Due to failure of many tau and Aβ based

therapeutic strategies (Extance, 2010; Rinne et al., 2010), more drug development researches are now being shifted toward multitarget-directed ligands approaches like disease-modifying therapies (DMTs) which temporarily slow the worsening of dementia symptoms of those patients with AD and other dementias (Paoletti et al., 2013; Henley and Wilkinson, 2016). The 2020 Alzheimer's disease drug development pipeline revealed that synaptic plasticity/neuroprotection agents in Phase 3 and Phase 2 clinical trials have reached up to 23.5% and 27.3% of DMT, respectively (Cummings et al., 2020), indicating that preventing and/or correcting alterations in synaptic functions in AD and other dementia patients might be a promising strategy in the management of these diseases.

Synapse has been regarded as a key target for different molecular assaults, like Aβ, that lead to the development and progression of AD, and synaptic dysfunction also correlates with the degree of cognitive decline in AD patients and transgenic AD mice (Terry et al., 1991). Glutamate receptors, including NMDA and AMPA receptors, play crucial roles in the mammalian central nervous system (CNS), where they involve in excitatory neuronal transmission and many other forms of synaptic plasticity (Paoletti et al., 2013; Henley and Wilkinson, 2016). Subunits that constitute NMDA receptors (NMDARs) include GluN1, GluN2A-D, GluN3A/B, while those that make up the AMPA receptors (AMPARs) are GluA1-4 (Henley and Wilkinson, 2016; Iacobucci and Popescu, 2017). NMDARs play central roles in brain development, synaptic plasticity, and learning and memory (Bliss and Collingridge, 1993; Aamodt and Constantine-Paton, 1999). Stimulating synaptic NMDARs activates pro-survival PI3K/AKt/CREB signaling pathways (Hardingham et al., 2002; Ivanov et al., 2006; Hardingham, 2009), which are involved in learning and memory formation. Interestingly, a reduced concentration of the GluN2B subunit of NMDAR and the postsynaptic density protein 95 (PSD-95), impaired long-term potentiation (LTP) and decreased NMDA and AMPA receptors' currents in hippocampal CA1 region have also been reported in transgenic AD mice (Dewachter et al., 2009). It has been previously found that STriatal-Enriched protein tyrosine Phosphatase (STEP) is increased in AD, and opposes the development and strengthening of synapses via dephosphorylating and inactivating synaptic proteins including kinases such as Fyn, Pyk2, and ERK1/2 (Venkitaramani et al., 2009; Xu et al., 2012; Li et al., 2014). Besides, it can also lead to the dephosphorylation and internalization of synaptic receptor complexes like GluN2B/GluN1 and GluA2/GluA1 subunits of NMDA and AMPA receptors, respectively (Snyder et al., 2005; Zhang et al., 2008; Poddar et al., 2010; Wu et al., 2011).

STriatal-Enriched protein tyrosine Phosphatase is an intracellular phosphatase, enriched in the CNS except in the cerebellum, that is encoded by the PTPN5 gene, and is a member of a family of over a hundred protein tyrosine phosphatases (PTPs) (Lombroso et al., 1991, 1993), and it is one of the targets via which Aβ exerts its deleterious effects in AD. Elevated level of Aβ in AD is believed to be, at least in part, responsible for the activation of STEP via binding to and activation of the α7 nicotinic acetylcholine receptors (α7nAChRs) (Dineley et al., 2001; Stevens et al., 2003; Lacor et al., 2004). The activation of these receptors leads to increased calcium influx resulting in the activation of calcineurin, also known as protein phosphatase 2B (PP2B) (Stevens et al., 2003), and subsequent dephosphorylation and inactivation of DARPP-32, the inhibitor of protein phosphatase 1 (PP1). This process activates PP1, which then dephosphorylates STEP at the regulatory serine residue within the kinase-interacting motif (KIM) domain (Snyder et al., 2005), thereby activating STEP. Also, prolonged stimulation of NMDA receptors was found to dephosphorylate and activate STEP via the activation of the PP2B/PP1 pathway (Paul et al., 2003; Valjent et al., 2005). Dysregulations of STEP levels and activity have also been implicated in many neuropsychiatric disorders with cognitive dysfunctions including Parkinson's disease (PD), Schizophrenia (SZ), Fragile-X syndrome (FXS), Huntington's disease (HD) and others (Kurup et al., 2010, 2015; Zhang et al., 2010; Gladding et al., 2012; Chatterjee et al., 2018; Xu et al., 2018). The net result of this dysregulated function is alterations and mainly inactivation of many synaptic proteins including kinases and receptor complexes leading to learning and memory impairment, and cognitive deficits. In this study, we mainly summarized STEP isoforms, their activation and regulation via different posttranslational modifications, reviewed data on the implication of STEP in AD and other neuropsychiatric disorders, and finally highlighted the therapeutic strategies targeting STEP.

STEP ISOFORMS EXPRESSION, POSTTRANSLATIONAL MODIFICATIONS AND FUNCTION

The family of STEP protein contains five isoforms that are presently known. Of these, four (STEP61, STEP46, STEP38, and STEP20) are the result of alternative splicing from the STEP gene (*PTPN5*), while the other one (STEP33) is the cleavage product of the protease calpain (**Figure 1**; Lombroso et al., 2016). Like other PTPs, the normal fully functional STEP contains a C-terminus catalytic signature consensus sequence [I/V]HCxAGxxR[S/T]G, and upstream KIM and kinase-specificity sequence (KIS) domains that allow the binding and specificity of STEP to its substrates, respectively (Bult et al., 1996; Pulido et al., 1998; Muñoz et al., 2003; Francis et al., 2014; Xu et al., 2015). The KIM domain is critical for binding, while KIS domain affects the binding, as evidenced by the fact that deleting both KIM and KIS domains decreased GluA2 binding to 7%, whereas deleting only the KIS domain decreased it to 45% (Won et al., 2019). In another study evaluating the effect of STEP on ERK1/2 phosphorylation, it was found that deletion of both KIM and KIS, KIM or KIS alone, or the C-terminal KIS resulted in a decreased k_{cat}/K_m ratio by 50-60-fold, whereas deletion of the N-terminal KIS decreased the ratio by only 20-fold (Li et al., 2014). Moreover, mutations involving the conserved arginine residues or the hydrophobic motif around the KIM domain were found to decrease the k_{cat}/K_m by 4-6-fold and 2.5-7-fold, respectively (Li et al., 2014). Also, deletion of the KIM domain decreased the ability of STEP interaction with both Fyn and Pyk2 (Nguyen et al., 2002; Xu et al., 2012). These further indicate that both KIM and KIS are required for efficient ERK,

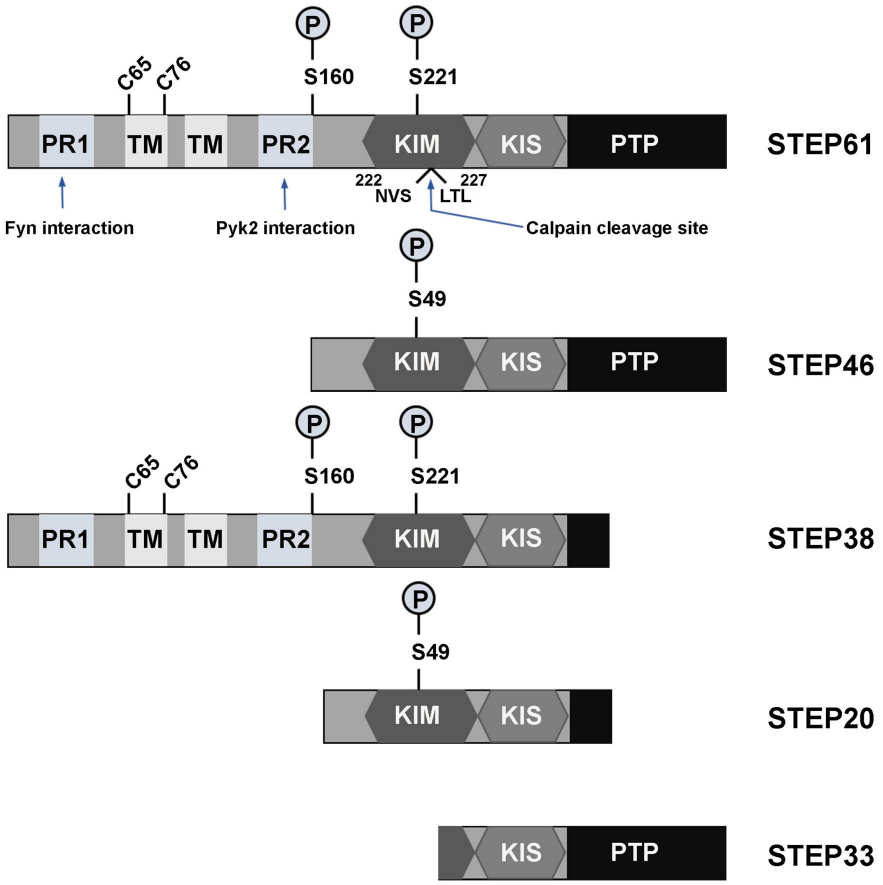

FIGURE 1 | Isoforms and domains structure of STEP. The alternative splicing of *PTPN5* gene results in the production of four STEP isoforms (STEP61, STEP46, STEP38, and STEP20), while the fifth STEP isoform, STEP33, is the result of calpain cleavage of STEP61 at Ser224/Leu225 site. STEP61 and STEP46 are the fully active and major STEP proteins in the CNS. These two isoforms contain the KIM, KIS and PTP domains, which are respectively required for substrate interaction, specificity and phosphatase activity. STEP61 has two additional TM domains that serve for targeting it to the ER and PSD, as well as two PR (PR1 and PR2) regions that specifically provide binding with Fyn and Pyk2, respectively. The activity of STEP is inhibited via PKA phosphorylation at Ser221 and Ser49 within the KIM domain for STEP61 and STEP46, respectively. PKA can also phosphorylate STEP at Ser160 around the PR2 region, but its function is still unknown. The function of STEP can also be decreased by dimerization of STEP molecules via the C65 and C76 present within the TM domain. Together with STEP33 (the isoform that has disrupted binding domain), STEP38 and STEP20 are inactive variants since they have no PTP domain and thus lack phosphatase activity. Therefore, it is speculated that they may serve as negative regulators of STEP substrates by competitive binding. Adapted from Lombroso et al. (2016).

Fyn and Pyk2 dephosphorylation by STEP. The two fully active and most abundant forms of STEP are STEP61 and STEP46 which, are differentially expressed in the brain in terms of space and time (Boulanger et al., 1995; Sharma et al., 1995; Bult et al., 1997; Xu et al., 2015). STEP46 is a cytosolic protein, whereas STEP61 contains a unique 172-amino-acid domain at its N-terminus that targets it to the endoplasmic reticulum (ER) and both synaptic and extra-synaptic membranes (Boulanger et al., 1995; Oyama et al., 1995; Bult et al., 1996). STEP61 has two polyproline-rich regions that are necessary for Fyn (Nguyen et al., 2002) and Pyk2 (Xu et al., 2012) interactions (**Figure 1**). Both STEP46 and STEP61 isoforms are present in glial cells and neurons including excitatory and inhibitory neurons (Hasegawa et al., 2000; Lorber et al., 2004; Goebel-Goody et al., 2009), and are expressed in various regions of the brain including, but not limited to, the striatum, hippocampus and cortex (Boulanger et al., 1995; Lorber et al., 2004). While STEP46 is not expressed until day 6 postnatally, STEP61 is readily expressed in abundance at birth and throughout adulthood (Raghunathan et al., 1996; Okamura et al., 1997). The other two isoforms that result from alternative splicing (STEP38 and STEP20) do not have the PTP signature consensus sequence (**Figure 1**) and, therefore, are catalytically inactive (Sharma et al., 1995). But they both do contain KIM domain, indicating their ability to bind to target substrates and thus might protect from active STEP dephosphorylation. Several mechanisms including posttranslational modifications and others regulate the ability of STEP to bind and dephosphorylate its substrates. These processes include phosphorylation, ubiquitination, dimerization, proteolytic cleavage, and local translation.

The phosphorylation of STEP within the KIM domain decreases its ability to bind and dephosphorylate its substrates. This process is mainly regulated by two key enzymes including the cAMP dependent protein kinase A (PKA) and PP1 that

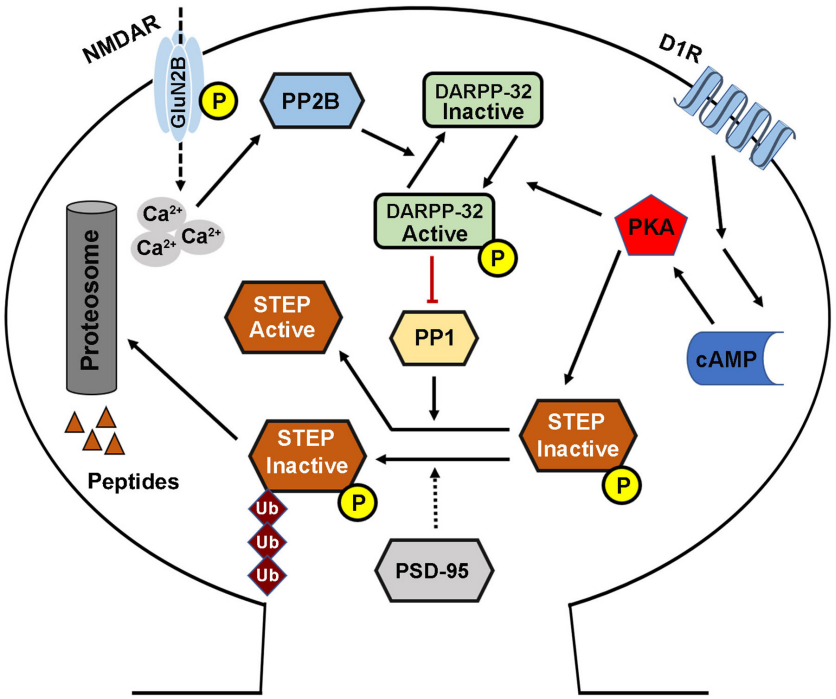

FIGURE 2 | STriatal-enriched protein tyrosine phosphatase activity regulation. The phosphorylation (deactivation) of STEP is mediated by the D1R stimulation of cAMP synthesis that activates PKA. The activated PKA directly phosphorylates STEP in the KIM domain, and this inhibits the binding of STEP to its substrates. PKA can also indirectly mediate the phosphorylation of STEP via the phosphorylation and activation of DARPP-32, an inhibitor of PP1. This leads to the inhibition of PP1 activity, the STEP phosphatase, thereby increasing the phosphorylation of STEP. Phosphorylation of STEP downregulates its ability to bind and dephosphorylate its substrates. On the other hand, the dephosphorylation (activation) of STEP is mediated via NMDAR, and in other condition via α7nAChR, activation that induce intracellular calcium influx and activation of PP2B. The activated PP2B dephosphorylates and inactivates DARPP-32, thereby removing its inhibitory effect, leading to the activation of PP1 and thus increasing STEP dephosphorylation and activation. STEP level and thus activity could also be regulated via ubiquitination and proteasomal degradation which are mediated by synaptic activation of NMDARs, and could be enhanced by PSD-95.

are involved in its phosphorylation and dephosphorylation, respectively (Paul et al., 2000; Valjent et al., 2005). Directly, PKA phosphorylates STEP61 and STEP46 at regulatory Ser221 and Ser49 within their KIM domains, respectively (Paul et al., 2000), and thus sterically hindering STEP from binding to its substrates. Indirectly, PKA phosphorylates DARPP-32, a potent inhibitor of PP1, thereby maintaining STEP at its phosphorylated inactive state (Valjent et al., 2005). PKA can also phosphorylate STEP61 at Ser160 but its function is still unknown (Paul et al., 2000). The phosphorylation state of STEP could also be indirectly regulated by PP2B, which in the presence of increased intracellular calcium dephosphorylates and inactivates DARPP-32 thereby removing the inhibitory effect on PP1 which then dephosphorylates and activates STEP (**Figure 2**; Paul et al., 2003; Snyder et al., 2005; Valjent et al., 2005).

Moreover, the cellular level of STEP could be regulated by ubiquitin proteasome system (UPS) (**Figure 2**). This is evidenced by the finding that upon synaptic NMDAR activation, STEP is rapidly ubiquitinated and degraded (Xu et al., 2009), probably to decrease the dephosphorylation of STEP substrates and promote synaptic plasticity. In line with this hypothesis, it was found that following synaptic NMDAR activation, the phosphorylation of ERK1/2, a positive synaptic plasticity related protein, positively correlated with ubiquitination and degradation of STEP, leading to upregulation of dendritic spines' size and density, and therefore, memory formation. However, the molecular mechanisms underlying ubiquitination of STEP are still unknown, but were speculated to be related to PEST sequences which were found at the amino terminal of STEP61 (Bult et al., 1996), as these sequences are often found in UPS degraded proteins (Spencer et al., 2004).

The activity of STEP could also be affected by two molecules of this protein itself coming together to form dimers. Under basal physiological conditions this dimerization process fundamentally occurs with STEP61, but not STEP46, via the formation of intermolecular disulfide bonds between the two cysteine residues (Cys65 and Cys76), that are present within the hydrophobic region of the amino terminus of STEP61 (**Figure 1**; Deb et al., 2011). However, oxidative stress can induce oligomerization of both STEP61 and STEP46 leading to a decrease in their phosphatase activity (Deb et al., 2011), possibly via involving additional sites other than Cys65 and Cys76. Interestingly, calpain can proteolytically cleave STEP61 between the Ser224 and Leu225 residues within the KIM domain (**Figure 1**), producing STEP33 that cannot associate with its substrates. It was found that STEP33 is produced after extra-synaptic NMDAR stimulation, and since STEP33 is inactive, this results in increased activation (phosphorylation) of the STEP61

substrate, p38, and initiation of cell death signaling pathways (Xu et al., 2009).

Local translation is another way to rapidly regulate STEP level in neuronal cells. Synaptic plasticity sometimes requires rapid translation of messages at distinct synapses via local translation. More importantly, this process is required in LTP as well as long-term depression (LTD) (Huber et al., 2000; Sutton and Schuman, 2006; Bramham and Wells, 2007; Costa-Mattioli et al., 2009). These plastic changes are possible due to the presence of mRNAs in a suppressed form along dendrites, until an appropriate synaptic stimulus ignites their translation (Bramham and Wells, 2007; Glock et al., 2017; Fonkeu et al., 2019). Interestingly, STEP was found to be locally translated as elaborated by the findings that STEP mRNA and protein were present in puncta along dendrites and near postsynaptic densities (PSDs), and its translation was upregulated within synaptosomes following (R, S)-3,5-dihydroxyphenylglycine (DHPG) activation of mGlu5 (Zhang et al., 2008). The dendritic local translation of STEP is believed to be regulated by the cytoplasmic polyadenylation element binding protein (Piqué et al., 2008) and fragile X mental retardation protein (FMRP) (Darnell et al., 2011; Goebel-Goody et al., 2012a; Chatterjee et al., 2018), that associate with, and repress STEP mRNA in dendrites until the arrival of appropriate stimuli, such as mGlu5 agonist activation. Moreover, there is evidence suggesting that STEP mRNAs, together with several other mRNAs, that are locally translated in response to synaptic activity, are shuttled by major vault protein to dendritic location (Paspalas et al., 2009).

STEP ACTIVATION AND REGULATION

The activity of the tyrosine phosphatase STEP is regulated by kinases and phosphatases as well as processes like dimerization. As mentioned above, the two main enzymes that regulate STEP activity are PKA and PP1. In normal conditions, STEP exists in a phosphorylated inactive state. This phosphorylation status is mainly due to the activation of PKA which can either directly or indirectly (**Figure 2**) maintain the phosphorylation of STEP and hence control its activity. Moreover, it has been demonstrated by previous studies that dopamine signaling can regulate STEP activity. In this model, the stimulation of dopamine D1 or blockage of D2 receptors was found to activate PKA which then phosphorylates and inactivates STEP, whereas the stimulation of D2 receptors had the opposite effects (Paul et al., 2000; Fitzpatrick and Lombroso, 2011). This is in support to the hypothesis that STEP is an intermediate bridge between the dopamine signaling and the glutamate signaling pathways, whereby dopamine regulates STEP activity and thus, tyrosine phosphorylation and surface expression of both NMDA and AMPA receptor complexes (Pelkey et al., 2002; Snyder et al., 2005; Zhang et al., 2008; Venkitaramani et al., 2011). In addition, the UPS regulates STEP level and thus its activity (**Figure 2**), via ubiquitination following synaptic NMDAR activation (Xu et al., 2009). Moreover, PSD-95 increases proteasomal degradation of STEP, and at the same time stabilizes NMDA receptors at the PSD favoring synaptic strengthening (Won et al., 2016). Interestingly, the expression of STEP in the PSD was increased in both PSD-95 knockdown neuronal cultures and PSD-95 KO mice (Won et al., 2016), indicating that PSD-95 is an important regulator of STEP.

On the other hand, stimulation of NMDARs was found to lead to a rapid but transient phosphorylation of ERK1/2, which has limited duration due to dephosphorylation and activation of STEP via the activation of the PP2B/DARPP-32/PP1 pathway (Paul et al., 2003; Valjent et al., 2005). The activated STEP can readily bind to its target proteins and lead to their dephosphorylation. It has been previously reported that there is a two- to three-fold increase in the level of STEP at the extra-synaptic sites as compared to synaptic sites (Goebel-Goody et al., 2009). This is supported by the findings that only extra-synaptic NMDAR expression and currents were increased upon STEP knockdown (Won et al., 2016, 2019). In a situation where glutamate levels increase at the synapse, there is subsequent activation of extra-synaptic NMDA receptors resulting in more calcium influx and activation of calpain which cleaves STEP61 into STEP33 that can no longer bind to and/or dephosphorylate its substrates (Xu et al., 2009; Lombroso et al., 2016). This decrease in the STEP activation promotes the activation of cell death signaling pathways via p38 (Xu et al., 2009). It is worth to note that recently conducted *in vitro* studies showed that STEP can be activated by a small molecule termed BI-0314 which binds to its phosphatase domain (Tautermann et al., 2019), however, further studies are needed before *in vivo* testing of this molecule.

STEP SUBSTRATES

STriatal-Enriched protein tyrosine Phosphatase acts via dephosphorylating its substrates, and the discovery of these substrates has elucidated the role played by STEP in neuronal signaling. Several proteins have been recognized as substrates of STEP, and many of them are related to learning and memory processes. These include subunits of both AMPA and NMDA receptors, kinases like ERK1/2, p38, Fyn, Pyk2 and other proteins such as PTPα and SPIN90 (**Table 1**).

The phosphorylation of GluN2B subunit of NMDARs is regulated by STEP via two different pathways, including direct dephosphorylation of Tyr1472 and the inactivation of Fyn, that phosphorylates GluN2B at the above-mentioned site (Nakazawa et al., 2001; Nguyen et al., 2002). Upon dephosphorylation by STEP, GluN2B binds to clathrin adaptor proteins which promote the internalization of GluN1/GluN2B receptor complex (Roche et al., 2001; Lavezzari et al., 2003). In concordance with this, it was observed that STEP KO mice showed an increased surface expression of GluN1/GluN2B receptor complex (Zhang et al., 2010; Venkitaramani et al., 2011). Moreover, it was found that increased amounts of STEP decreased NMDA receptors' excitatory postsynaptic currents (EPSCs) and abolished LTP, while inhibition of STEP by anti-STEP antibody led to an enhanced EPSCs (Pelkey et al., 2002), and both genetic deletion (Olausson et al., 2012) and pharmacological inhibition (Saavedra et al., 2019) of STEP promoted LTP. Also, STEP ubiquitination and degradation following NMDAR stimulation ultimately permits the induction of LTP (Xu et al., 2009).

TABLE 1 | STriatal-enriched protein tyrosine phosphatase substrates dephosphorylation and the consequent effects.

STEP substrates	Phosphorylation mechanism	Site	Consequences of STEP action	References
GluN2B	Directly and indirectly via Fyn dephosphorylation	Tyr1472	Internalization of GluN1/GluN2B receptor complex and impaired synaptic plasticity	Nakazawa et al., 2001; Roche et al., 2001; Nguyen et al., 2002; Lavezzari et al., 2003
GluA2	Direct dephosphorylation	Tyr876	Internalization of GluA1/GluA2 receptor complex and impaired synaptic plasticity	Zhang et al., 2008; Won et al., 2016, 2019
ERK1/2	Direct dephosphorylation	Tyr204/187	Decreased ERK1/2 substrates (CREB, Elk1) phosphorylation, synaptic plasticity deficits	Paul et al., 2003; Valjent et al., 2005; Paul and Connor, 2010; Li et al., 2014
p38	Direct dephosphorylation	Tyr182	Inhibition of cell death pathways, enhanced cell survival	Xu et al., 2009; Poddar et al., 2010
Fyn	Directly and indirectly via Pyk2 dephosphorylation	Tyr420	Inhibition of Fyn substrates (GluN2B) phosphorylation	Nguyen et al., 2002; Venkitaramani et al., 2011
Pyk2	Direct dephosphorylation	Tyr402	Inhibition of Pyk2 substrates (Fyn) phosphorylation	Xu et al., 2012
PTPα	Direct dephosphorylation	Tyr789	Inhibition of Fyn dephosphorylation at inhibitory Try531 residue (Fyn inhibition)	Engen et al., 2008; Ingley, 2008; Xu et al., 2015
SPIN90	Direct dephosphorylation	Y85, Y161or Y227*	Activation of cofilin which depolymerizes actin leading to spine collapse, memory impairment	Cho et al., 2013a,b

**It is not confirmed which of these sites is/are STEP dephosphorylation residue (s).*

The other memory related receptor that is also regulated by STEP is AMPA receptor. It has been shown that trafficking of AMPA receptor occurred in LTD via its endocytosis from synaptic surface (Snyder et al., 2001; Hsieh et al., 2006). STEP was reported to regulate the Tyr dephosphorylation of the GluA2 subunit of AMPARs favoring the internalization of GluA1/GluA2 complex (Zhang et al., 2008; Won et al., 2019). Also, the surface expression of GluA1/GluA2-containing AMPA receptors was reported to be elevated in STEP KO mice (Zhang et al., 2008; Venkitaramani et al., 2011; Won et al., 2019). It was previously not clear whether STEP directly or indirectly induces the dephosphorylation and endocytosis of AMPARs complex since the Tyr876 of GluA2 can also be phosphorylated by SFKs (Hayashi and Huganir, 2004), which might also be dephosphorylated and inactivated by STEP. Additionally, GluA2 can directly interact with BRAG2 and activate Arf6, which then recruits adaptor protein-2 and clathrin to synaptic membranes (Krauss et al., 2003), to promote GluA2 endocytosis (Scholz et al., 2010). However, a recent study highlighted the mechanism of STEP regulation of AMPARs, whereby STEP binds to the C termini of GluA2 and GluA3, but not GluA1, to promote their tyrosine dephosphorylation (Won et al., 2019). Interestingly, in STEP overexpressing neuronal cultures, treatment with chloroquine (a lysosomal degradation blocker), but not MG-132 (a proteasomal degradation blocker), rescued GluA2/3 proteins and GluA2-PSD95 colocalization to control level (Won et al., 2019), indicating that STEP regulation of synaptic AMPARs is mediated by lysosomal degradation.

Together, these findings indicate that fine-tuning of STEP activity is important for the regulation of proper levels of these glutamate receptors at synapses, since prolonged neuronal activity results in the upregulation of STEP that leads to the removal of NMDA and AMPA receptors from synaptic membranes, while prolonged neuronal inhibition has the opposite effect. Moreover, knocking down STEP in hippocampal slices increases AMPAR-mediated, but not NMDAR-mediated synaptic currents, while its overexpression reduced both synaptic expression and currents of AMPARs as well as NMDARs (Won et al., 2016, 2019). These facts together indicate that STEP preferentially regulates synaptic AMPA receptors, while on the other hand it regulates extra-synaptic NMDA receptors, suggesting a modulatory role of STEP in defining activity-dependent glutamate receptor localization. Thus, STEP is involved in the regulation of homeostatic synaptic plasticity (Jang et al., 2015) by regulating the surface expression of both NMDARs and AMPARs (**Figure 3**).

Other molecules that are involved in synaptic plasticity and memory, and have also been confirmed substrates of STEP are the two members of the MAPK family ERK1/2 and p38 (Muñoz et al., 2003; Paul et al., 2003; Kim et al., 2008; Paul and Connor, 2010). ERK1/2 is centrally implicated in synaptic plasticity and memory formation via several mechanisms including dendritic spines stabilization, local dendritic protein synthesis, nuclear transcription, and transmission of action potentials (Davis et al., 2000; Sweatt, 2004; Venkitaramani et al., 2009, 2011). The activity of ERK1/2 is dependent on its phosphorylation at the regulatory residues Thr202/185 and Tyr204/187 by MAPK kinases (MAPKK) such as MEK1/2 (Robinson and Cobb, 1997). To inactivate ERK1/2, the Tyr sites are dephosphorylated by STEP (Paul et al., 2003; Valjent et al., 2005; Paul and Connor, 2010; Li et al., 2014), and both KIM and KIS domains of STEP are required for ERK interaction (Li et al., 2014). Moreover, it was reported that ERK1/2 is necessary for the development of synaptic strengthening as well as the consolidation of fear memories in the amygdala, and STEP colocalizes with ERK1/2 in this brain area (Paul et al., 2007). Moreover, STEP KO mice showed a significant increase in the level of phospho-ERK1/2 and its downstream targets, CREB and Elk1, and improved hippocampal learning and memory (Venkitaramani et al., 2009, 2011). Also, UPS degradation of STEP led to the activation of ERK1/2, synaptic strengthening and neuronal survival pathways (Xu et al., 2009).

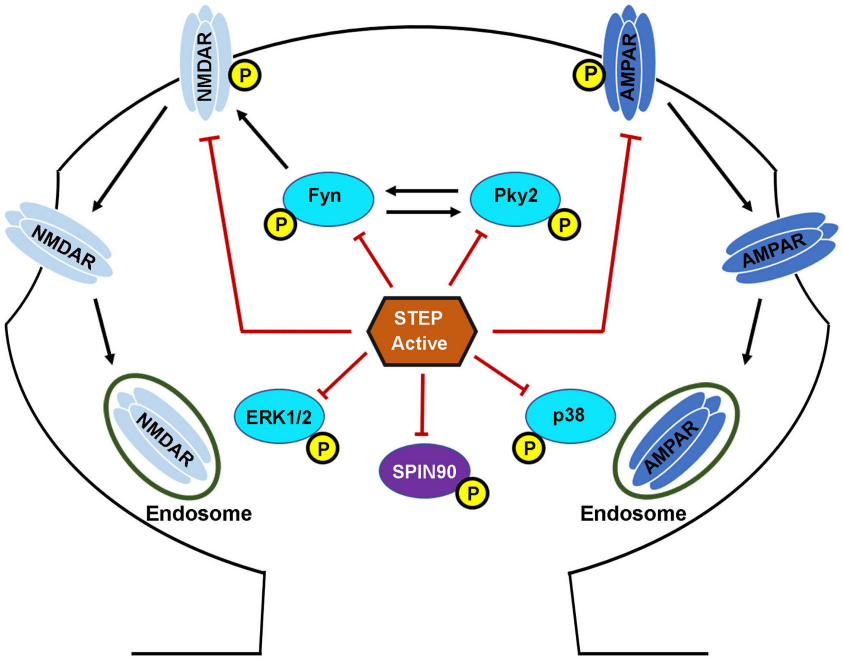

FIGURE 3 | STriatal-enriched protein tyrosine phosphatase substrates. Following the NMDAR or α7nAChR stimulation mediated activation, STEP can then bind and dephosphorylate regulatory tyrosines within its substrates. The dephosphorylation of STEP substrates including GluN2B, GluA2\GluA3, Fyn, Pyk2, ERK1/2, p38 and SPIN90 leads to their inactivation. The dephosphorylation of GluN2B and GluA2\GluA3 subunits of NMDARs and AMPARs, respectively, results in internalization from the PSD. The dephosphorylation of Fyn, Pyk2, ERK1/2, and p38 leads to inhibition of their kinase activity and impairment of the downstream effects. The dephosphorylation of SPIN90 leads to its translocation to the dendritic shaft causing the release of its binding partner cofilin. STEP dephosphorylates GluN2B subunit of NMDARs by two mechanisms. First, STEP can directly dephosphorylate GluN2B at Tyr1472. Secondly, STEP can indirectly mediate the dephosphorylation of GluN2B via the inactivation of Fyn, the kinase that phosphorylates GluN2B at the same Tyr1472. The net result is endocytosis of GluN2B-containing NMDARs. STEP can also mediate the endocytosis of AMPARs via direct dephosphorylation of GluA2 and GluA3 subunits of these receptors.

The p38 is another family member of MAPK and also a substrate of STEP (Poddar et al., 2010). However, in contrast to ERK1/2, p38 is implicated in cell death pathways and extra-synaptic NMDAR-mediated excitotoxicity (Ivanov et al., 2006; Semenova et al., 2007). As a phosphatase, STEP can dephosphorylate and inactivate p38 at the Tyr182 residue in the activation loop of p38 (Xu et al., 2009; Poddar et al., 2010). In this circumstance, STEP might play a protective role. However, the activation of extra-synaptic NMDA receptors leads to increased calcium and calpain activation, which in turn, cleaves STEP into an inactive STEP33 variant that is unable to bind to its substrates. This leads to increased phosphorylation and activation of p38 and thus activation of cell death signaling pathway (Xu et al., 2009). It should be noted that, synaptic NMDA receptor stimulation increases STEP activity which shortens the duration of p38 MAPK activation and favors neuronal survival, but extra-synaptic NMDARs stimulation causes significant degradation of active STEP via calpain-mediated proteolysis, leading to p38 MAPK activation (Poddar et al., 2010). This indicates that STEP serves as a modulator of NMDA receptor-mediated cell death by regulating p38 MAPK. On the other hand, both ERK1/2 and p38, can in turn, regulate STEP expression levels by modulating two phosphorylation sites (Ser59 and Thr72) within the KIS domain of STEP, dephosphorylation of which sites can trigger ubiquitination and thus degradation of STEP (Mukherjee et al., 2011).

Other substrates of STEP include Pyk2 and Fyn kinases. The two polyproline-rich (PR1 & PR2) regions of STEP (**Figure 1**) are implicated in substrate binding as well as specificity for Fyn (Nguyen et al., 2002) and Pyk2 (Xu et al., 2012), respectively. Upon binding, STEP can dephosphorylate the regulatory tyrosines in the activation loops of these kinases and inactivate them (Nguyen et al., 2002; Xu et al., 2012). Another identified substrate of STEP is PTPα, which is an activator of Fyn (Xu et al., 2015). STEP was reported to dephosphorylate PTPα at a Tyr789 site which, when phosphorylated, normally results in the translocation of PTPα to the lipid rafts to activate Fyn. PTPα dephosphorylates Fyn at an inhibitory Tyr531 residue in contrast to STEP which acts on the activation loop of Fyn at Tyr420 (Engen et al., 2008; Ingley, 2008). Thus, STEP can directly inactivate Fyn via Tyr420 dephosphorylation, or indirectly by dephosphorylating and blocking PTPα translocation to the membrane, thus maintaining the inhibitory Tyr531phosphorylation of Fyn.

SPIN90 is another substrate of STEP which in its phosphorylated form binds to and reduces the actin-depolymerizing activity of cofilin (Cho et al., 2013a). However, when SPIN90 is dephosphorylated by STEP (**Figures 3**, **4**), it leads to cofilin activation and actin depolymerization, therefore,

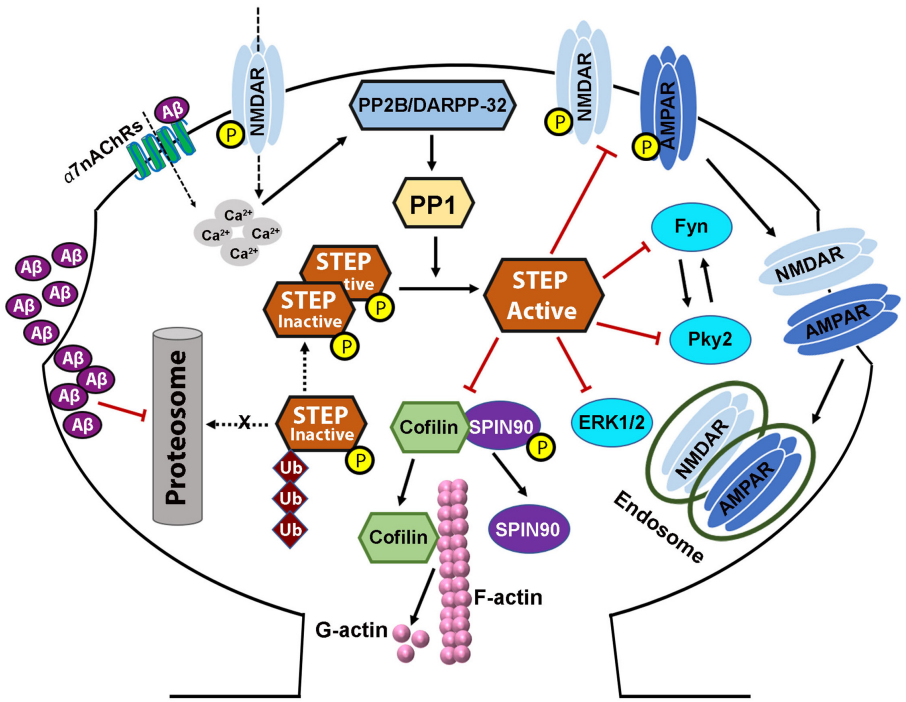

FIGURE 4 | STriatal-enriched protein tyrosine phosphatase dysregulation in Alzheimer's disease. Both protein level and activity of STEP are implicated in Alzheimer's disease, and are thought to be the result of increased Aβ. Increased soluble Aβ levels precede the appearance of cognitive impairments. Aβ activation of α7nAChRs, together with glutamatergic NMDAR stimulation, increased calcium influx which then activates PP2B/DARPP-32/PP1 pathway leading to the dephosphorylation and activation of STEP. On the other hand, Aβ can also inhibit the proteasomal degradation of STEP leading to accumulation of STEP. These together lead to increased level of active STEP which aberrantly dephosphorylates its substrates. Dephosphorylation of SPIN90 by STEP also leads to the dissociation of SPIN90 from cofilin, leading to the activation of cofilin which then depolymerizes F-actin to G-actin. These events, together with the inactivation of other STEP substrates, and AMPA and NMDA receptors' internalization, lead to dendritic spine and synapse loss resulting in the learning and memory and cognitive impairments seen in AD. Aβ-induced alterations in PKA/Akt/CREB pathway result in deficient BDNF/TrkB signaling, which in turn, contributes to the synapses loss and synaptic plasticity and cognitive deficits, via impairing the degradation of STEP.

contributing to spine collapse (Cho et al., 2013b). Interestingly, it was found that loss of synaptic clustering with either Shank or PSD-95 following SPIN90 dephosphorylation by STEP affects both the size and density of dendritic spines (Cho et al., 2013a). The results from these studies indicate that SPIN90 dephosphorylation could be another way that STEP mediates Aβ-induced synaptic plasticity and memory impairments.

Recently, a study by Won et al. (2019) has identified 315 STEP interactors candidate proteins in WT mouse brain samples, including cytoskeletal-associated proteins and motor proteins like α-actinin, DBN1, myosin-10, MAP2, Arp2/3 complex; vesicle trafficking proteins like AP-2, Rab3a, SNX1, SNX4, NBEA; kinases and phosphatases like Fyn, PKA, PP2A, PP1; ion channels, receptors, and transporters like GluN2B, GluN1, GluA2, mGlu5; ATP synthase and ATPases like Na^+/K^+-transporting ATPase α-subunit; scaffolding proteins such as PSD-95, SynGAP, Kalirin, Shank; cell adhesion proteins like δ-catenin, NLGN-1; G protein-coupled receptor signaling proteins like Gα(o), Gα(q), Gβ-5; and ubiquitin enzyme proteins like Nedd4, RNF14, KCMF1. Among these, some proteins such as GluN2B and Fyn are already established STEP substrates, GluA2 recently confirmed, while many others will probably be confirmed in future studies.

STEP AND DENDRITIC SPINES

Loss of dendritic spines and decline of cognitive function are hallmarks of patients with AD and the loss of synapses correlated with cognitive deficits. Notably, in early stage of AD, studies revealed the existence of reduced dendritic spine density in the frontal cortex and hippocampal CA1 region of AD patients (DeKosky and Scheff, 1990; Scheff et al., 2006). Moreover, a decrease in the mushroom (memory) type spine density was reported in *in vivo* and *in vitro* Aβ toxicity (Popugaeva et al., 2015; Qu et al., 2017), cultures of hippocampal slice from AD transgenic mice (Tackenberg and Brandt, 2009; Penazzi et al., 2016), as well as in AD mouse models (Saito et al., 2014; Sun et al., 2014). Consistently, another study reported a shift from mushroom to stubby spines in cortical biopsies from AD patients (Androuin et al., 2018), indicating loss of memory-related spines. This loss of spines might be caused by Aβ peptide long before the appearance of clinical manifestations of the disease, that is, during the prodromal phase of AD, and was found to occur even before the disintegration of neuronal networks and consequent cognitive decline (Palop and Mucke, 2010; Kashyap et al., 2019). Several studies have revealed that transgenic AD mouse models as well as neurons exposed to Aβ show loss of spines (Lacor et al., 2004;

Calabrese et al., 2007; Shankar et al., 2007; Wei et al., 2010; Spires-Jones and Hyman, 2014). Interestingly, it was recently shown that dendritic spine plasticity can provide cognitive resilience against dementia among AD patients (Boros et al., 2017).

It has been previously found that STEP is increased in AD and it was reported to oppose the development and strengthening of synapses via dephosphorylating and inactivating synaptic proteins including kinases like Fyn, Pyk2, and ERK1/2 (Venkitaramani et al., 2009; Xu et al., 2012; Li et al., 2014), as well as leading to the internalization of synaptic receptor complexes like GluN1/GluN2B and GluA1/GluA2 subunits of NMDA and AMPA receptors, respectively (Snyder et al., 2005; Zhang et al., 2008; Poddar et al., 2010; Wu et al., 2011; Won et al., 2019). Moreover, it was found that pharmacological inhibition as well as genetic depletion of STEP were able to ameliorate cognitive function and hippocampal memory in the 3×Tg-AD mouse model. In line with this, it was reported that STEP inhibition not only improved cognitive functions, but also increased synaptic connectivity in both cell cultures and 3×Tg-AD mouse model (Chatterjee et al., 2021), further highlighting the potential of STEP inhibitors as therapeutic agents. It has been reported that abundant ER are present in hippocampal dendritic spines and play an important role in synaptic plasticity (Holbro et al., 2009). Moreover, the ER in the spines exhibit highly dynamic changes that are largely dependent on NMDARs activity (Ng et al., 2014). Previous studies have also pointed out the involvement of STEP in the dynamics of dendritic spines, whereby dephosphorylation of SPIN90 by STEP led to cofilin activation and actin depolymerization to induce spine collapse, while elimination of STEP induced upregulation of dendritic ER-positive spines as well as dendritic spines' ER growth (Cho et al., 2013b; Ng et al., 2014). Therefore, the upregulated ER changes observed upon STEP elimination might be, at least in part, due to the abrogation of the negative regulation of STEP on NMDAR.

Evidence from studies has indicated that LTD can induce removal of postsynaptic AMPA receptors and loss of spines (Snyder et al., 2001). Increased Aβ levels was shown to reduce pyramidal neuron spine density via LTD driven endocytosis of synaptic AMPA receptors, and removal of synaptic AMPA receptors was necessary and sufficient to produce dendritic spine loss and synaptic NMDA responses (Hsieh et al., 2006). Interestingly, it was recently reported that STEP can bind to and results in the dephosphorylation and decreased synaptic expression of GluA2 (Won et al., 2019), suggesting that STEP might mediate the Aβ-induced AMPA receptor internalization and synaptic impairment. Also, a 120 min Aβ treatment of cortical neurons resulted in increased STEP levels in these neurons with concomitant tyrosine dephosphorylation of STEP substrates, and a reduction in the protein levels of GluN2B receptors on membrane fractions (Kurup et al., 2010), while application of 1 μM of the STEP inhibitor TC-2153 was found to inhibit STEP activity in cortical cultures and restore the Tyr1472 phosphorylation of GluN2B receptor subunits (Xu et al., 2014).

Since studies have shown that Aβ leads to loss of spine in exposed neurons and that Aβ also increases STEP protein level and activity, it is interesting to investigate whether or not STEP is implicated in spine loss. Recently, a study reported that treatment of 18-day-old cortical neurons with conditioned media from mutant CHO cells containing Aβ showed significant decrease in dendritic complexity (dendritic junctions or nodes and Ends), as analyzed by Sholl analysis, compared to control neurons (Chatterjee et al., 2021). Interestingly, a 48 h pretreatment with the STEP inhibitor TC-2153 prior to Aβ treatment in cortical neurons significantly minimized the loss of dendritic complexity (Chatterjee et al., 2021). Moreover, in two studies using presynaptic and postsynaptic markers colocalization puncta to indicate the presence of synapse, it was also reported that Aβ-treated neurons showed significantly fewer colocalized synaptic puncta than control neurons (Kono et al., 2019), and that pretreatment with TC-2153 significantly increased the colocalized synaptic puncta in Aβ-treated neurons, and rescued the loss of dendritic spine density in 3×Tg-AD mice (Chatterjee et al., 2021).

Aβ and STEP also influence dendritic spines via their effect on actin. It was recently reported that upon Aβ exposure, fibrillar actin (F-actin), a major cytoskeletal protein that determines the shape of spines, depolymerizes to globular actin (G-actin) and, therefore, contributes to the decrease and collapse of spines (Kommaddi et al., 2018). Interestingly, the phosphorylation of the STEP substrate, SPIN90, leads to its binding with cofilin thereby reducing the actin-depolymerizing activity of cofilin (Cho et al., 2013a). However, when SPIN90 is dephosphorylated by STEP, it dissociates from cofilin leading to cofilin activation and thus, actin depolymerization, therefore, contributing to spine collapse (**Figures 3**, **4**; Cho et al., 2013b). Furthermore, it was also reported that phosphorylated SPIN90 interacts with scaffolding proteins PSD-95 and Shank in the post-synaptic compartment. There are also substantial evidences showing the role of PSD-95 in increasing spine density as well as the number of synapses (El-Husseini et al., 2000), and of Shank in promoting spine maturation and enlargement (Sala et al., 2001). Consistent with these findings, a study reported a loss of synaptic clustering with both Shank and PSD-95 following SPIN90 dephosphorylation by STEP, that led to downregulation of dendritic spines in terms of size and density (Cho et al., 2013a). It should also be noted that inhibition of STEP with TC-2153 was able to improve dendritic spine abnormalities in *Fmr1* KO cultures and spine density in *Fmr1* KO mice model of FXS (Chatterjee et al., 2018).

Together, the data reviewed here strongly suggest that STEP is centrally involved in the loss of dendritic complexity and decrease spine density observed in AD patients as well as AD animal models and even in other neurological disorders.

STEP IN SYNAPTIC PLASTICITY AND COGNITIVE IMPAIRMENT

Cognitive and behavioral impairments are some of the primary and main clinical manifestations of neurodegenerative disorders like AD. Synaptic dysfunctions seen as synapse loss seem to significantly correlate with the functional and cognitive deficits observed in different stages of AD (Terry et al., 1991). Numerous studies have highlighted the role of STEP in the alterations of cognitive function in AD. For example, the Tg-2576 AD

model mouse line carries mutations in APP that are found in early onset familial AD (Mirra et al., 1991; Terry et al., 1991; Khachaturian, 2006). These mice show normal cognitive functions at 3 months of age, however, at 10 months of age they exhibit significant cognitive impairments (Hsiao et al., 1996). Interestingly, the levels of STEP were found to be normal in these mice at 3 months but significantly elevated at 10 moths (Kurup et al., 2010), suggesting an implication of STEP in the observed alterations in these animals. Similarly, in 3×Tg-AD mouse model that has the same mutation with the Tg-2576 in addition to the presenilin and tau mutations, it was also found that the levels of STEP were normal at early stage of life, but increased at late stage and this change went together with the appearance of behavioral alterations. This has been corroborated by reports which showed that in 3×Tg-AD mice, STEP activity is significantly elevated after 6 months of age, which coincides with the start of memory deficits (Zhang et al., 2010). Moreover, crossing STEP KO mice with 3×Tg-AD mice prevents these cognitive alterations (Kurup et al., 2010; Zhang et al., 2010). These STEP KO mice have enhanced learning abilities including hippocampal-dependent learning (Venkitaramani et al., 2011) as well as amygdala-dependent learning (Olausson et al., 2012), indicating that elevated levels of STEP might disrupt synaptic plasticity and thus learning and memory formation. Interestingly, the STEP inhibitor, TC-2153, was reported to significantly rescue cognitive impairments (Xu et al., 2014) and the loss of dendritic spine density in 3×Tg-AD (Chatterjee et al., 2021), suggesting that inhibition of STEP might at least decrease the progression of neuronal deterioration in these AD mice models.

From the data reviewed above, it is clear that the loss of STEP leads to increased phosphorylation of its substrates including NMDA and AMPA receptors as well as ERK1/2, Fyn and Pyk2. Thus, it is logical to stipulate that loss of STEP could favor learning and memory. In line with this idea, a study reported that in a water maze reversal training task, STEP KO mice showed significantly better performance than WT (Venkitaramani et al., 2011), suggesting a higher degree of cognitive flexibility in STEP KO mice. The same study also revealed that in the water-escape motivated radial arm maze, STEP KO mice also outperformed WT mice. This test simultaneously evaluates spatial working and reference memories, and during the first 2 days of training in this test, STEP KO mice committed fewer reference and working memory errors compared with WT mice (Venkitaramani et al., 2011). Moreover, fear conditioning that tests amygdala-dependent memory showed that STEP KO mice exhibited a greater degree of fear memory (Olausson et al., 2012). However, no significant differences were found between these two groups when evaluating anxiety, motor coordination, and motor learning (Venkitaramani et al., 2011). This is in line with other studies showing that animals with increased expression or activation of STEP substrates like GluN2B, GluA1 and ERK1/2 had enhanced memory in MWM, fear conditioning and novel object recognition tasks (Tang et al., 1999; Wang et al., 2004; Okun et al., 2010). Pyk2 lies upstream of Fyn and when Pyk2 is activated following its phosphorylation at Tyr402, it phosphorylates and activates Fyn, which can then phosphorylate GluN2B at Tyr1472. Consequently, activation of Pyk2 leads to a greater phosphorylation and increased surface expression of GluN2B (Le et al., 2006), as well as enhanced phosphorylation of ERK1/2 (Nicodemo et al., 2010). Interestingly, the inhibition of Pyk2 results in blockage of LTP induction (Huang et al., 2001). As discussed earlier, Pyk2 is a substrate of STEP, and thus Pyk2 dephosphorylation by STEP would oppose these processes and impairs synaptic plasticity. In support of this, upregulated phosphorylation of Pyk2 was reported in STEP KO mice (Venkitaramani et al., 2011).

Numerous studies have suggested that BDNF and its receptor TrkB signaling alterations were also implicated in synaptic plasticity and memory impairments, and evidence suggested that this might be related to STEP dysregulation. For example, it was reported that the decreased BDNF level in AD was associated with reduced cortical cholinergic synapses, emphasizing the fact that dysregulation of BDNF might affect cholinergic synapses and thus synaptic plasticity (Amidfar et al., 2020). Recently, it was shown that upregulation of BDNF/TrkB mRNAs expression in the hippocampus is associated with improvement of memory (Amidfar et al., 2018). Moreover, alterations in BDNF expression and BDNF/TrkB signaling pathway might induce synapse loss and the consequent cognitive dysfunction (Song et al., 2015), while early downregulation of BDNF in AD was associated with the severity of cognitive impairments (Peng et al., 2005; Garzon and Fahnestock, 2007). In addition, BDNF/TrkB deprivation was recently found to activate JAK2/STAT3 pathway, leading to the upregulation of C/EBPβ, which in turn, increased the expression of asparaginyl endopeptidase (AEP), resulting in the cleavage of both APP and Tau, thus aggravating neuronal loss. Interestingly, inhibition of this cascade was able to rescue synaptic plasticity and cognitive impairments (Wang et al., 2019). CREB was shown to induce transcription and translation of BDNF (which binds to TrKB) leading to the phosphorylation of AMPA and NMDA receptors, while Aβ-induced inactivation of PKA/Akt inactivates CREB, and induces deficient BDNF/TrKB signaling leading to hippocampal synapse loss, synaptic plasticity and memory impairments in AD (Amidfar et al., 2020). Interestingly, it was found that BDNF/TrkB signaling can induce a decrease in the protein level of STEP in primary cortical neurons, via rapid ubiquitination and degradation of STEP, while downregulation of BDNF in cell and animal models increased the level of STEP (Saavedra et al., 2016; Xu et al., 2016). Moreover, the use of TrkB antagonist led to STEP accumulation and impaired long-term memory formation (Saavedra et al., 2019). The levels of Tyr phosphorylation of GluN2B and pERK1/2 were also increased in neuronal cultures following BDNF treatment or TrkB activation (Saavedra et al., 2016; Xu et al., 2016). Together, these studies indicate that the increased STEP in AD patients and animal models might possibly reflect the alterations in BDNF/TrkB signaling. In support of this hypothesis, it was reported that the TrkB signaling activator 7,8-DHF as well as the STEP inhibitor TC-2153 both ameliorated motor hyperactivity and Tyr phosphorylation of STEP substrates in $BDNF^{\pm}$ mice (Xu et al., 2016).

Moreover, in other neurological disorder models, either pharmacological or genetic inhibition of STEP was able to ameliorate behavioral alterations. For example, it was found that

inhibition of STEP improved locomotion, hyperactivity, memory, novel object recognition, anxiety and sociability observed in different models of SZ as well as in a model of FXS (Chatterjee et al., 2018; Xu et al., 2018). Furthermore, genetic deletion of STEP could delay the onset of motor dysfunction and prevent the appearance of cognitive deficits in R6/1 mice of HD, and this effect was associated with an increase in pERK1/2 levels and a reduction in the size of mHTT aggregates, in both the striatum and CA1 hippocampal region. Moreover, pharmacological inhibition of STEP with TC-2153 improved cognitive function in these mice (García-Forn et al., 2018).

STEP ALTERATIONS IN AD AND OTHER NEUROLOGICAL DISEASES

STriatal-Enriched protein tyrosine Phosphatase is highly expressed in different brain regions except in the cerebellum, thus, it is not surprising that many studies have evaluated and confirmed the implications of STEP in several neurodegenerative disorders (**Table 2**), including AD (Kurup et al., 2010; Zhang et al., 2010), Parkinson's disease (Kurup et al., 2015), Huntington's disease (Gladding et al., 2012), schizophrenia (Xu et al., 2018), fragile X syndrome (Chatterjee et al., 2018), age-related memory decline (Castonguay et al., 2018), depressive disorders (Elizabeth and Alexander, 2017) and in mouse model of Sepsis-Associated Encephalopathy (Zong et al., 2019).

Alzheimer's Disease

There is accumulating evidence that STEP activity, Aβ levels, and synapse regulation are closely related. The level of STEP has been reported to be elevated in AD, the most common neurodegenerative disorder, including in the brain of post-mortem AD patients and in several AD mice models like the Tg2576 (Kurup et al., 2010), J20 (Chin et al., 2005), APP/PS1 (Zhang et al., 2013), and 3×Tg-AD mice (Zhang et al., 2010).

TABLE 2 | STEP alteration mechanisms in neurological disorders and the therapeutic strategies.

Disease	Model (s)	Changes in STEP	Mechanism of STEP alterations	Intervention strategies and outcome	References
Alzheimer's disease	Humans, Mice & Cells	↑	Aβ-induced dysregulation of UPS, activation of α7nAChRs and dysregulation of BDNF/TrkB signaling	Pharmacologic (TC-2153) or genetic inhibition (KO, KD) of STEP improved phosphorylation of GluN2B, GluA2, ERK1/2, Fyn, Pyk2, synaptic connectivity, BDNF and cognitive functions	Dineley et al., 2001; Stevens et al., 2003; Lacor et al., 2004; Chin et al., 2005; Almeida et al., 2006; Venkitaramani et al., 2007, 2011; Tseng et al., 2008; Kurup et al., 2010; Zhang et al., 2010, 2013; Olausson et al., 2012; Xu et al., 2014, 2016; Saavedra et al., 2016
Parkinson's disease	Humans, Rats, Mice & Cells	↑	Disrupted UPS associated with mutation/decreased activity of parkin, a product of PARK2 gene and downregulation of BDNF/TrkB signaling	Activation of BDNF signling decreases STEP level and activity which results in upregulation of pERK, pCREB and BDNF	Kitada et al., 2009; Chagniel et al., 2014; Kurup et al., 2015; Saavedra et al., 2016; Xu et al., 2016
Huntington's disease	Mice	↑↓	Downregulation: enhanced PKA and reduced PP2B activities; Upregulation: decrease DARPP-32 levels	Genetic deletion of STEP delayed onset of motor and cognitive symptoms. TC-2153 improved cognition, TAT-STEP increased VGLUT1-GluN2B colocalization, Y1472GluN2B and BDNF expression	Desplats et al., 2006; Hodges et al., 2006; Saavedra et al., 2011; Gladding et al., 2012; García-Forn et al., 2018
Schizophrenia	Humans, Mice & Cells	↑	NRG1 mutation and NRG1/ErbB4 signaling abnormality	Neuroleptic drugs or genetic inhibition of STEP improved synaptic proteins (NRG1, GluN2B, Pyk2 and ERK1/2) and behavioral deficits	Stefansson et al., 2004; Barros et al., 2009; Belforte et al., 2010; Carty et al., 2012; Goebel-Goody et al., 2012a; Loh et al., 2013; Xu et al., 2018
Fragile X syndrome	Mice & Cells	↑	Defect in the *Fmr1* gene causes deficiency of FMRP, the protein product of *Fmr1*, which normally binds to and suppresses mRNAs translation including that of STEP; mGlu signaling alteration	TC-2153 or genetic deletion of Fmr1 or STEP/Fmr1 double KO improved exaggerated LTD, audiogenic seizure incidences, c-Fos-positive neurons hyperactivity, anxiety and synaptic aberrations	Huber et al., 2002; Hou et al., 2006; Gross et al., 2010; Darnell et al., 2011; Goebel-Goody et al., 2012b; Chatterjee et al., 2018
Age-related memory decline	Humans, Monkeys, Mice & Cells	↑	Abnormalities in the UPS as well as alteration in the NMDAR and ERK signaling pathways	Up- or down-regulation, led to worsening or alleviation of age-related memory deficits, respectively; TC-2153 improved synaptic proteins and alleviated cognitive impairments	Castonguay et al., 2018
Depressive disorders	Humans & Mouse	↑*	Downregulation of BDNF signaling pathway	TC-2153 mitigates depressive-like symptoms in mice via decreasing 5-HT_{2A} receptor and increasing BDNF	Kulikov et al., 2012; Elizabeth and Alexander, 2017; Kulikova et al., 2018

**There is a controversy regarding the level of STEP in depressive disorders with elevation of this enzyme seen in mice but no changes were observed in postmortem human study. Therefore, further researches are needed to draw a conclusion.*

The increment in STEP is believed to be the consequence of increased levels of Aβ in AD, which leads to the dysregulation of the UPS and activation of α7nAChRs, both of which eventually lead to an increase in the expression levels and activity of STEP (Kurup et al., 2010; Zhang et al., 2013). Aβ can bind to and activate α7nAChRs (Dineley et al., 2001; Stevens et al., 2003; Lacor et al., 2004), triggering calcium influx that activates PP2B, that in turn, inactivates DARPP-32, leading to the activation of PP1, which then dephosphorylates and activates STEP (**Figure 4**; Snyder et al., 2005). Consequently, the activated STEP can readily bind to and dephosphorylate its target proteins. It has been shown that transgenic AD mouse models as well as neurons exposed to Aβ show loss of spines (Lacor et al., 2004; Calabrese et al., 2007; Shankar et al., 2007; Wei et al., 2010; Spires-Jones and Hyman, 2014). Consistently, neurons treated with Aβ or those that overexpress APP exhibit decreased glutamatergic transmission (Ting et al., 2007). Moreover, exogenous Aβ treatment was shown to induce endocytosis of NMDA receptors through a STEP-dependent pathway (Kurup et al., 2010). Additionally, NMDA receptors are involved in the regulation of dendritic spine density and morphology (Ultanir et al., 2007), suggesting that STEP-mediated downregulation of NMDA receptors may contribute to the loss of synaptic density in AD. It was also believed that Aβ oligomers might also cause synaptic dysfunction by inducing PP2B-dependent internalization of AMPA receptor (Hsieh et al., 2006). Moreover, it was recently reported that STEP binding results in the dephosphorylation and decreased synaptic expression of GluA2, while synaptic expression of GluA2 is increased in the brain of STEP-KO mice (Won et al., 2019). This could therefore be at least one of the ways Aβ mediates AMPA receptor internalization and synaptic impairment. It was also observed that both neuronal cultures treated with Aβ and AD mouse models have an accumulation of active STEP (Chin et al., 2005; Kurup et al., 2010; Zhang et al., 2010, 2013) associated with the Aβ-mediated impairment of the UPS (Almeida et al., 2006; Tseng et al., 2008), since neither transcription nor translation of STEP was altered. Moreover, studies have reported an increase in STEP level as a result of Aβ-mediated disruption of the UPS pathway (Venkitaramani et al., 2007; Kurup et al., 2010). Thus, in AD, a decrease in its degradation together with an increase in its dephosphorylation would be in part responsible for the significant increase in the level of active STEP. The net outcome of increased active STEP in the brain is the dephosphorylation of GluN2B Tyr1472 and internalization of GluN1/GluN2B receptor complex (Snyder et al., 2005; Kurup et al., 2010; Zhang et al., 2010), dephosphorylation of the GluA2 subunit of AMPA receptor and internalization of GluA1/GluA2 complex (Zhang et al., 2008; Won et al., 2019), dephosphorylation and inactivation of Fyn, Pyk2 (Nguyen et al., 2002; Xu et al., 2012), ERK1/2 (Paul et al., 2003; Valjent et al., 2005; Paul and Connor, 2010), SPIN90 (Cho et al., 2013b; **Figure 4**). Taken together, these indicate that STEP mediates the Aβ induced synaptic plasticity and cognitive impairments seen in AD animal models as well as AD patients via inactivation of synapse related proteins and endocytosis of both NMDA and AMPA receptors.

As summarized above, substantial evidence has highlighted the implication of BDNF in AD (Peng et al., 2005; Garzon and Fahnestock, 2007; Song et al., 2015; Amidfar et al., 2018; Wang et al., 2019). Both protein levels and mRNA expression of BDNF were reported to be reduced in postmortem brain samples of AD patients (Tanila, 2017) and in animal models of AD resulting in decreased cholinergic synapses (Iulita et al., 2017; Amidfar et al., 2020). It is known that CREB could induce the transcription and translation of BDNF leading to the phosphorylation of AMPA and NMDA receptors, while Aβ can inactivate the PKA and dephosphorylate Akt which would inactivate CREB and induce deficit in BDNF pathway leading to hippocampal synaptic loss, synaptic plasticity impairment and memory deficit in AD (Amidfar et al., 2020). Activation of BDNF/TrkB signaling can induce a decrease in the protein level of STEP and increased phosphorylation of its substrates, while downregulation of BDNF had the opposite effect (Saavedra et al., 2016; Xu et al., 2016). The level of STEP was reported to be increased while that of BDNF to be decreased in AD patients and animal models. This is an indication that the decreased BDNF and/or BDNF/TrkB signaling in AD could possibly be, at least in part, responsible for the increase in the STEP level, suggesting that, in AD, Aβ induces alterations in BDNF/TrkB signaling to alter synaptic morphology possibly via increasing activation and protein level of STEP.

Another way that STEP mediates the Aβ-induced cognitive impairment is via the STEP dephosphorylation of SPIN90 that induce F- to G-actin depolymerization of cofilin (Cho et al., 2013a,b; Kommaddi et al., 2018). Moreover, STEP also disrupts the interaction of PSD-95 and Shank that is important in the maintenance of dendritic spine integrity (El-Husseini et al., 2000; Sala et al., 2001). These together, lead to decreased size and density of dendritic spines and eventually spine collapse. This evidence highlights an additional pathway via which Aβ/STEP triggers AD pathology via reduced dendritic spine density and synapse loss which appears as the learning and memory and cognitive impairments seen in AD patients and AD animal models.

Parkinson's Disease

Studies have also reported an upregulation of STEP in PD brain as well as in MPTP-induced PD model (Kurup et al., 2015), the next most common neurodegenerative disorder after AD, which is characterized by loss of dopaminergic neurons in the substantia nigra and dopamine depletion in the striatum (Saiki et al., 2012). The increase in STEP is correlated with a decrease in the phosphorylation of ERK1/2 and CREB, an effect that might contribute to the synaptic and cognitive impairments seen in PD (Kurup et al., 2015). There is substantial evidence indicating that a decrease in the expression of parkin, a product of *PARK2* gene, is involved in the genetic forms of PD. This is supported by the fact that mutations of the *PARK2* gene result in an autosomal recessive juvenile parkinsonism with early onset of PD symptoms (Shimura et al., 2000; Tanaka et al., 2004), and alterations in the activity of parkin were involved in both familial and sporadic PD (Sriram et al., 2005; Dawson and Dawson, 2010, 2014). Moreover, the dopaminergic neurotoxins MPP^+ and MPTP induced alterations in the levels or activity of parkin with consequent accumulation in pathogenic parkin

substrates such as AIMP2 and PARIS (Ko et al., 2010; Imam et al., 2011; Dawson and Dawson, 2014). Interestingly, the level of STEP is increased in both human PD samples and PD models (Kurup et al., 2015). STEP is normally degraded via the ubiquitin proteasome system, and it was found that parkin is an E3 ligase that ubiquitinates STEP *in vivo* and *in vitro*, suggesting that the decrease in parkin activity might be responsible for the observed increase in STEP protein in PD (Kurup et al., 2015). In support of this, it was found that shRNA-downregulated and parkin KO rats showed an increase in the level of STEP, and that STEP upregulation was associated with down-regulation of synaptic proteins in the striatum (Kurup et al., 2015). Interestingly, the striatum of *PARK2* KO mice showed a decrease in evoked dopamine release and resulted in impaired LTP and LTD in striatal medium spiny neurons (Kitada et al., 2009). As reviewed above, increased STEP can impair LTP and LTD via inactivation of its substrates including GluN2B, GluA2, ERK1/2, Fyn and others. Thus, these indicate that the reduction in dopamine release in *PARK2* KO mice might decrease the PKA-induced STEP phosphorylation (inactivation), resulting in increased STEP activity and consequent cognitive deficits seen in PD. Consistent with this, it was found that PKA-mediated phosphorylation of STEP correlated with enhanced motor learning, and attenuating striatal STEP activity via PKA phosphorylation was believed to be associated with a striatal molecular pathway involved in the consolidation of complex motor skills during motor learning (Chagniel et al., 2014).

Moreover, it was also found that BDNF signaling could lead to a rapid ubiquitination and degradation of STEP via binding to its receptor TrkB, which results in the activation of the phospholipase Cγ and protein kinase C (PKC) pathways (Saavedra et al., 2016; Xu et al., 2016). Decreased neurotrophic factor signaling has been proposed to be implicated in the pathophysiology of PD (Baquet et al., 2005; Rangasamy et al., 2010; He et al., 2013), and STEP levels are increased in human PD samples and MPTP-lesioned mice (Kurup et al., 2015). These are indications that the increase in STEP expression levels in PD could be the result of decreased neurotrophic factor signaling which may probably contribute to PD pathophysiology. In line with this, previous studies reported that inhibiting PTPs protected dopaminergic neurons from PD toxins by activating ERK1/2 via increasing BDNF signaling (Lu et al., 2002), and that phosphorylation of ERK1/2 and CREB was decreased in sporadic PD samples (Kurup et al., 2015). In summary, BDNF leads to a downregulation of the protein level of STEP, whereas increased STEP levels result in decreased pERK1/2/pCREB-mediated expression of BDNF, suggesting a feedback regulation.

Huntington's Disease

STriatal-Enriched protein tyrosine Phosphatase alterations have also been documented in Huntington's Disease (HD), a genetic disorder characterized by progressive neurodegeneration, poor muscle coordination, mood disorders, and dementia (Ross and Tabrizi, 2011). There are controversies in the dysregulation of STEP in HD as both downregulation and upregulation have been observed. For instance, a study by Saavedra et al., reported a decreased STEP activity. In their study, these authors showed that with age a decrease in protein level of STEP was observed in the striatum and cortex of R6/1 HD mouse model, while increased STEP phosphorylation was seen in striatum, cortex and hippocampus (Saavedra et al., 2011). These changes together resulted in decreased STEP activity which correlated with enhanced PKA and reduced PP2B activities as well as an increased phosphorylation of two STEP substrates ERK1/2 and p38. Downregulation of STEP activity was also reported in other HD mouse models including R6/2, Tet/HD^{94}, and Hdh$^{Q7/Q111}$ (Saavedra et al., 2011). Interestingly, it was reported that R6/1 mice showed resistance to quinpirole, an NMDA receptor agonist, induced excitotoxicity (Hansson et al., 2001), while co-administration of quinpirole with WT TAT-STEP exacerbated excitotoxicity in both WT and R6/1 mice (Saavedra et al., 2011). These findings suggest that STEP increases the vulnerability of striatal neurons to excitotoxity and that the decreased STEP in HD mouse models may confer to these mice their resistance to excitotoxicity. In support of this, a decrease in the mRNA levels of STEP was previously reported in the caudate nucleus and cortex of HD patients (Hodges et al., 2006) as well as in the striatum of R6/1 mice (Desplats et al., 2006).

On the other hand, a recent study revealed that genetic deletion of STEP delayed both the onset of motor dysfunction and the decrease of striatal DARPP-32 levels, and prevented the appearance of cognitive deficits in R6/1 mice (García-Forn et al., 2018). Importantly, this was associated with an increase in pERK1/2 levels and a reduction in the size of mHTT aggregates, in both the striatum and CA1 hippocampal region. Moreover, pharmacological inhibition of STEP with TC-2153 improved cognitive function in these mice (García-Forn et al., 2018). In addition, another study also reported a significantly increased synaptic STEP activity in the striatum of YAC128, a mouse model of HD, compared to WT mice, and this correlated with decreased GluN2B Y1472 phosphorylation (Gladding et al., 2012). Moreover, calpain activation leads to GluN2B cleavage at both synaptic and extra-synaptic sites, thereby further decreasing surface expression of GluN2B. These authors also showed that in striatal neuron cultures C-S mutant TAT-STEP (non-active STEP) significantly increased VGLUT1-GluN2B colocalization, as well as increasing Try1472 phosphorylation and synaptic GluN2B expression, while *in vivo* STEP inhibition also increased synaptic GluN2B expression in the YAC128 striatum (Gladding et al., 2012). Of interest is the fact that combined inhibition of STEP and calpain reduced extra-synaptic, but increases synaptic expression of GluN2B in the YAC128 striatum (Gladding et al., 2012). These results together suggest that upregulated activity of both STEP and calpain could be responsible for the mis-localization of NMDAR from synaptic to extra-synaptic site in YAC128 mouse model of HD.

The discrepancies reported in the dysregulation of the level of STEP in these HD animal models could be attributed to the differential mechanisms involved. Whereas Saavedra et al., focused on the dopaminergic activation of PKA, García-Forn et al., highlighted the role of DARPP-32 pathway. However, further investigations are needed to clarify the existing differences. Another potential reason could be the HD animal model used.

Fragile-X Syndrome

Fragile-X syndrome (FXS) is another neurological disorder, the leading cause of inherited intellectual disability, with core symptoms including cognitive deficits, anxiety and seizures. This condition is mainly due to a genetic alteration that suppresses the transcription of *Fmr1* gene. Interestingly, this gene was shown to be related to learning and memory functions as suggested by the fact that *Fmr1* KO mice have decreased surface expression of NMDA and AMPA receptors (Suvrathan et al., 2010; Eadie et al., 2012). FMRP, the product of *Fmr1* expression, normally binds to and suppresses dendritic translation of a myriad of mRNAs following mGlu5 stimulation (Antar and Bassell, 2003; Bear et al., 2004). Therefore, due to the absence of FMRP in FXS, the translation of many of these mRNAs is upregulated including STEP mRNA (Huber et al., 2002; Hou et al., 2006; Gross et al., 2010; Darnell et al., 2011; Chatterjee et al., 2018). It was found that STEP mRNA can associate with FMRP (Darnell et al., 2011; Goebel-Goody et al., 2012a), and upregulation of STEP translation was demonstrated in *Fmr1* KO (Goebel-Goody et al., 2012b; Chatterjee et al., 2018). Moreover, the mGlu5 agonist, DHPG, leads to a rapid and dose-dependent increase in STEP translation (Zhang et al., 2008), while STEP inhibition was found to be beneficial in maintaining synaptic homeostasis in the hippocampal neurons in mouse models of FXS (Chatterjee et al., 2018). Interestingly, a decrease in both audiogenic seizures and seizure-induced c-Fos-positive neurons in the periaqueductal gray matter were observed in STEP/*Fmr1* double KO mice compared to *Fmr1* KO (Goebel-Goody et al., 2012b). In addition, the STEP inhibitor TC-2153 was found to reverse audiogenic seizure incidences, hyperactivity, mGlu5-mediated exaggerated LTD, ameliorated behavioral alterations like anxiety, and sociability in *Fmr1* KO mice, as well as improved synaptic aberrations both *in vivo* and in *Fmr1* KO neuronal cultures (Chatterjee et al., 2018). These results imply that the translation of STEP is increased in FXS model as a result of *Fmr1* gene downregulation, and decreased STEP expression is associated with improvement of the cognitive impairments.

Schizophrenia

Alterations in STEP are also observed in schizophrenia (SZ), a neurological disease with complex etiology, where neuronal dysfunction, genetics, and environment come together (Tsuang et al., 2001; van de Leemput et al., 2016). Cognitive deficits are some of the symptoms of patients with SZ, and one proposed mechanism involved in the behavioral alterations in SZ is decreased NMDAR function and/or decreased surface expression of NMDARs (Xu et al., 2018). Several studies have provided results that are consistent with this hypothesis. For instance, a study reported abnormalities in glutamate receptor density in postmortem SZ brains in the prefrontal cortex, temporal lobe, and thalamus (Goebel-Goody et al., 2012a). In addition, a decrease in the mRNA level of GluN1 was reported in postmortem SZ brain, and it was correlated with antemortem severity of cognitive impairment (Humphries et al., 1996; Catts et al., 2016), while d-serine and glycine (facilitators of NMDRs activation) administration improved symptoms in medicated SZ patients (Kantrowitz et al., 2010; Balu and Coyle, 2015). Moreover, SZ-like behaviors were reported in mice with reduced expression of NMDAR (Belforte et al., 2010), and in persons taking non-competitive NMDAR antagonists like phencyclidine (PCP) or ketamine (Goebel-Goody et al., 2012a). In line with this, it was found that NRG1, a growth factor that promotes phosphorylation and surface retention of NMDARs was mutated in patients with SZ (Stefansson et al., 2004; Loh et al., 2013). Upon binding to its receptor (ErbB4), NRG1 normally activates Fyn leading to Tyr1472 phosphorylation and surface expression of GluN2B (Bjarnadottir et al., 2007). This finding is supported by a study where NRG1/ErbB4 signaling was revealed to promote synaptic incorporation of NMDARs via NRG1/ErbB4-stimulated binding of PSD-95 to Erbin (Barros et al., 2009). Moreover, Tyr1472 phosphorylation of GluN2B was found to be decreased in NRG1 heterozygous mice (Bjarnadottir et al., 2007; Xu et al., 2018). Also, the locomotor and cognitive deficits induced by the NMDA receptor antagonist MK801 and PCP were attenuated in STEP KO mice (Carty et al., 2012). All these suggest that increase in STEP might be responsible for the SZ symptoms via decreasing surface NMDA receptors. However, an opposite result was reported by Pitcher et al., where stimulation of NRG1 was reported to attenuate NMDAR activity via suppressing Src-mediated phosphorylation of GluN2B and potentiation of NMDARs (Pitcher et al., 2011). This evidence, therefore, suggests that NRG1 hyperactivation in SZ leads to NMDAR hypofunction (Hahn et al., 2006). The above-mentioned discrepancy could be attributed to differential effect of the two different kinases Fyn and Src evaluated in these two studies, even though these are both SFKs, and thus further investigation is needed to explore the pathways involved. It is clear that NMDA receptors' hypofunction is implicated in SZ, and STEP can decrease both surface expression and activity of these receptors. Thus, STEP might also be involved in SZ. Interestingly, it was recently found that the protein levels of STEP are significantly upregulated in heterozygous NRG1 and CNS-specific ErbB2/4 KO mouse models of SZ, hiPSC neurons from forebrain of SZ patients (Xu et al., 2018), and in the cortex of postmortem SZ patients (Carty et al., 2012). Also, genetically eliminating STEP in mice decreased their susceptibility to PCP-induced locomotor activity and cognitive deficits when compared with WT mice (Carty et al., 2012; Xu et al., 2018). Moreover, treatment of WT mice with neuroleptics (haloperidol, clozapine, and risperidone), used to treat SZ, increased the PKA-mediated Ser221 phosphorylation of STEP via DARPP-32/PP1 pathway, along with increased phosphorylation of GluN2B, Pyk2, and ERK1/2, and surface expression of GluN2B (Carty et al., 2012). Additionally, both pharmacological and genetic inhibition of STEP increased the phosphorylation of NRG1, GluN2B and ERK1/2 (Xu et al., 2018). Together, the data summarized here clearly indicate the implication of STEP in the etiopathogenesis of SZ.

STEP AS THERAPEUTIC TARGET

Several studies have documented the involvement of STEP in several neuropsychiatric disorders, including Alzheimer's disease

(Kurup et al., 2010; Zhang et al., 2010), Parkinson's disease (Kurup et al., 2015), Huntington's disease (Gladding et al., 2012), Schizophrenia (Xu et al., 2018), Fragile X syndrome (Chatterjee et al., 2018), age-related memory decline (Castonguay et al., 2018) and depressive disorders (Elizabeth and Alexander, 2017; **Table 2**). Most of these disorders have reported an increase in the STEP protein level and/or activity, thus making STEP an important therapeutic target leading to the search and development of STEP inhibitors. The level of STEP has been reported to be elevated in AD, including in post-mortem AD patients and several AD mice models (Chin et al., 2005; Kurup et al., 2010; Zhang et al., 2010, 2013). This increase in STEP is believed to be the consequence of the accumulation of Aβ that leads to the dysregulation of the UPS and activation of α7nAChRs, both of which eventually lead to increased levels of activated STEP (Kurup et al., 2010; Zhang et al., 2013). Interestingly, it was found that pharmacological (TC-2153) as well as genetic inhibition of STEP were able to ameliorate cognitive function and hippocampal memory in the 3×Tg-AD mouse model (Zhang et al., 2010; Xu et al., 2014). Moreover, it was reported that STEP inhibition not only improved cognitive functions, but also increased synaptic connectivity in both cell cultures and 3×Tg-AD mouse model (Chatterjee et al., 2021). Similar results were also reported in SZ models, where inhibition of STEP was sufficient to improve both biochemical and behavioral deficits in these SZ mice models (Xu et al., 2018). Also, in mice model of FXS, pharmacological inhibition of STEP with TC-2153 was able to reverse mGlu5-mediated exaggerated LTD, audiogenic seizure incidences, hyperactivity, ameliorated behavioral alterations like anxiety and sociability in *Fmr1* KO mice, as well as improved synaptic aberrations both *in vivo* and in *Fmr1* KO neuronal cultures (Chatterjee et al., 2018). TC-2153 was also reported to have antidepressant-like effect via decreasing both activity and protein level of the serotoninergic 5-HT_{2A} receptor in the hippocampus and frontal cortex, but not in the striatum (Kulikova et al., 2018), and increasing BNDF in brains of mice genetically predisposed to depressive-like behavior (Kulikov et al., 2012). As reported earlier, BDNF was found to induce rapid STEP ubiquitination pathways (Saavedra et al., 2016; Xu et al., 2016). Therefore, the inhibition of STEP might be responsible for the increase in BDNF, which can further induce rapid degradation of STEP resulting in decreased STEP activity, and might consequently increase the phosphorylation of STEP substrates. In line with this, it was revealed that treatment of cortical neurons with TC-2153 as well as TC-2153 injection of mice induced a significant improvement in the Tyr phosphorylation of STEP substrates GluN2B, Pyk2, and ERK1/2, and behavioral deficits (Xu et al., 2014). In addition, crossing STEP KO mice with 3×Tg-AD mice improved cognitive alterations (Kurup et al., 2010; Zhang et al., 2010), and the STEP KO mice have facilitated learning abilities in hippocampal-dependent (Venkitaramani et al., 2011) as well as amygdala-dependent learning (Olausson et al., 2012). Overall, these findings indicate that STEP regulates learning and memory signaling pathways, and that elevated levels of STEP might disrupt synaptic plasticity and thus learning and memory formation.

TC-2153 is the currently most experimentally used STEP inhibitor. Interestingly, phosphatase assay following TC-2153 treatment showed selectivity toward STEP inhibition among an array of PTPs, including He-PTP and PTP-SL (Xu et al., 2014). Moreover, following injection with TC-2153, WT and STEP KO mice showed a significant increase in Tyr phosphorylation of ERK1/2 and Pyk2, only in the frontal cortex and hippocampus, but not in tissues outside of the brain or in the cerebellum which lack STEP (Xu et al., 2014). These together, indicate the selectivity of TC-2153 toward STEP, as compared to other phosphatases. The inhibitory effect of TC-2153 on STEP was speculated to probably be through the formation of a covalent bond within the catalytic domain of STEP involving a cysteine residue (Boivin et al., 2010). In line with this, mutation of the active cysteine to sulfur (C-S TAT-STEP) was found to produce an inactive form of STEP (Gladding et al., 2012).

Other STEP inhibitors are also under investigation and development. For instance, a substrate-based method called substrate activity screening (SAS) was also used to develop a low molecular weight STEP inhibitor 12t, which resulted in significant levels of STEP inhibition in rat cortical neurons (Baguley et al., 2013). The X-ray crystal structures of some of these STEP inhibitors were disclosed and these inhibitors showed a 15-60-fold selectivity toward STEP across a series of phosphatases (Witten et al., 2017). Using machine learning based computational models, another study also predicted two major compounds as candidate STEP inhibitors that could be potentially used for AD treatment (Jamal et al., 2015). Recently, a group of researchers combined molecular dynamics simulations and fragment-centric topographical mapping to identify transiently open cryptic pockets based on which they identified 12 new STEP inhibitors. Furthermore, they showed that the two most potent compounds ST2-5 and ST3-5 (analogs of ST2 and ST3) could reversibly bind and competitively inhibit STEP with selectivity for STEP against a panel of protein phosphatases. Moreover, these potent inhibitors were found to modulate the Tyr phosphorylation of both ERK1/2 and Pyk2, have relatively no toxicity in PC12 cell cultures, and also favor cell differentiation and migration functions (Hou et al., 2020). However, most of these STEP inhibitors are at their embryonic developmental level and further rigorous studies are needed to evaluate their therapeutic efficacy, selectivity, specificity and safety. It is unfortunate to note that some still lack enough drug availabilities for further development.

Although nearly all discussed diseases reported increase in STEP activity leading to STEP inhibitor development, a decreased activity of STEP has also been reported and STEP activator could also be beneficial. Recently, the discovery of the first small molecule allosteric activator of STEP (BI-0314) that binds to the phosphatase domain has been reported (Tautermann et al., 2019). BI-0314 is a hSTEP specific positive allosteric modulator which, due to the low conservation of the residues in the allosteric site, has been shown to be inactive when tested on two other related tyrosine phosphatases (Tautermann et al., 2019). However, further studies are warranted before *in vivo* testing of this molecule is carried out.

SUMMARY AND CONCLUDING REMARKS

From the data reviewed in this study, it is evident that increased STEP as a result of alteration of UPS, increased translation, as well as decreased phosphorylation (PKA and PP1) has been implicated in many neuropsychiatric diseases. This increase in STEP generally leads to a decreased phosphorylation of the STEP substrates which are basically found to be synapse related proteins. They include, but are not limited to, GluN2B, GluA2, GluA3, ERK1/2, p38, Fyn, Pyk2 and SPIN90. These alterations lead to internalization of NMDA and AMPA receptors, collapse and loss of dendritic spines together culminating into synaptic plasticity and learning and memory impairments, which are expressed in human patients and animal models of these diseases as cognitive deficits. In light of these observations, numerous studies have provided evidence of cognitive improvements following STEP inhibition. These improvements might be the reflection of improvements of healthy synaptic markers and morphology, reinforcing the role of STEP in AD and other neuropsychiatric pathologies. The observations that STEP is implicated in many neurological disorders, and the fact that modulating STEP level and activity have some beneficial effects in these disorders, make STEP a potential therapeutic target and led to the development of STEP inhibitors. These inhibitors are at their early developmental stage and, therefore, there is a long way to go before their clinical application. Although STEP inhibition has been reported, to be beneficial in improving both biochemical and behavioral parameters, it should be noted that, a study had reported that both genetic deletion and pharmacological inhibition of STEP were associated with thermal hyperalgesia and mechanical allodynia, accompanying the increased GluN2B Tyr1472 and ERK1/2 Thr202/Tyr204 phosphorylation in the lumbar spinal cord (Azkona et al., 2016). Moreover, a protective role of increased STEP activity has been reported, whereby a transient NMDA receptors stimulation increases STEP activity and appears to limit the duration of activation of the excitotoxicity and death related p38 MAPK and thus improving neuronal survival (Poddar et al., 2010). These findings suggest that the side effects of STEP inhibitors and the degree to which STEP should be inhibited have to be meticulously considered.

It has been over three decades since STEP was discovered to be involved in neurological diseases, however, there is still a lot to explore in the molecular mechanisms of STEP. For example, it will be interesting to investigate the molecular mechanisms responsible for initiating STEP ubiquitination which will further lead to a strategy in reducing STEP function. Moreover, discovering more STEP substrates and upstream modulators will also pave more opportunities in STEP therapeutics. Also, it was recently found that the activity of STEP is modulated by adenosine A_{2A} receptor ($A_{2A}R$) in neuronal cells. $A_{2A}R$ is a G protein-coupled receptor which is widely expressed in the brain where it regulates important functions, such as motor behavior and cognition (Chen et al., 2014; Pinna et al., 2018), and plays a key role in cell survival and neurodegeneration (Cunha, 2016). Interestingly, $A_{2A}R$ stimulation was found to result in PKA activation (Fresco et al., 2004; Borea et al., 2018), and was involved in cocaine-induced stimulation of STEP (Chiodi et al., 2014). Moreover, $A_{2A}R$ is considered as a promising target in the treatment of neuropsychiatric disorders, and so is STEP (Zhang et al., 2010; Xu et al., 2014, 2018; García-Forn et al., 2018). Recently, it was found that STEP activity was increased in $NSEA_{2A}$ (a transgenic rats overexpressing $A2_{ARs}$ in the CNS) compared to WT rats (Mallozzi et al., 2020). STEP was also reported to mediate the cocaine-induced synaptic transmission depression probably via reducing AMPA- and NMDA-mediated excitatory post-synaptic currents (Chiodi et al., 2014).

AUTHOR CONTRIBUTIONS

YM and XW wrote the manuscript. FH, KE, and FZ assisted with data analysis and interpretation and critically read the manuscript. All authors contributed to the article and approved the submitted version.

FUNDING

This review article was supported by grant from the Ministry of Science and Technology of China (2016YFC1305800), Sanming Project of Medicine in Shenzhen (SZSM201801014), grants from the National Natural Science Foundation of China (92049107, 31771114, and 31929002), grant from the Innovative Research Groups of the National Natural Science Foundation of China (81721005), and the Academic Frontier Youth Team Project to Xiaochuan Wang from the Huazhong University of Science and Technology.

REFERENCES

Aamodt, S. M., and Constantine-Paton, M. (1999). The role of neural activity in synaptic development and its implications for adult brain function. *Adv. Neurol.* 79, 133–144.

Almeida, C. G., Takahashi, R. H., and Gouras, G. K. (2006). Beta-amyloid accumulation impairs multivesicular body sorting by inhibiting the ubiquitin-proteasome system. *J. Neurosci.* 26, 4277–4288.

Alzheimer's Disease International (2019). *World Alzheimer Report 2019: Attitudes to dementia*. Avaliable online at: https://www.alzint.org/resource/world-alzheimer-report-2019/. doi: 10.1523/jneurosci.5078-05.2006 (accessed July 6, 2019).

Amidfar, M., de Oliveira, J., Kucharska, E., Budni, J., and Kim, Y. K. (2020). The role of CREB and BDNF in neurobiology and treatment of Alzheimer's disease. *Life Sci.* 257:118020. doi: 10.1016/j.lfs.2020.118020

Amidfar, M., Kim, Y. K., and Wiborg, O. (2018). Effectiveness of memantine on depression-like behavior, memory deficits and brain mRNA levels of BDNF and TrkB in rats subjected to repeated unpredictable stress. *Pharmacol. Rep.* 70, 600–606. doi: 10.1016/j.pharep.2017.12.007

Androuin, A., Potier, B., Nägerl, U. V., Cattaert, D., Danglot, L., Thierry, M., et al. (2018). Evidence for altered dendritic spine compartmentalization in Alzheimer's disease and functional effects in a mouse model. *Acta Neuropathol.* 135, 839–854. doi: 10.1007/s00401-018-1847-6

Antar, L. N., and Bassell, G. J. (2003). Sunrise at the synapse: the FMRP mRNP shaping the synaptic interface. *Neuron* 37, 555–558. doi: 10.1016/s0896-6273(03)00090-4

Azkona, G., Saavedra, A., Aira, Z., Aluja, D., Xifró, X., Baguley, T., et al. (2016). Striatal-enriched protein tyrosine phosphatase modulates nociception: evidence from genetic deletion and pharmacological inhibition. *Pain* 157, 377–386. doi: 10.1097/j.pain.0000000000000329

Baguley, T. D., Xu, H. C., Chatterjee, M., Nairn, A. C., Lombroso, P. J., and Ellman, J. A. (2013). Substrate-based fragment identification for the development of selective, nonpeptidic inhibitors of striatal-enriched protein tyrosine phosphatase. *J. Med. Chem.* 56, 7636–7650. doi: 10.1021/jm401037h

Balu, D. T., and Coyle, J. T. (2015). The NMDA receptor 'glycine modulatory site' in schizophrenia: D-serine, glycine, and beyond. *Curr. Opin. Pharmacol.* 20, 109–115. doi: 10.1016/j.coph.2014.12.004

Baquet, Z. C., Bickford, P. C., and Jones, K. R. (2005). Brain-derived neurotrophic factor is required for the establishment of the proper number of dopaminergic neurons in the substantia nigra pars compacta. *J. Neurosci.* 25, 6251–6259. doi: 10.1523/jneurosci.4601-04.2005

Barros, C. S., Calabrese, B., Chamero, P., Roberts, A. J., Korzus, E., Lloyd, K., et al. (2009). Impaired maturation of dendritic spines without disorganization of cortical cell layers in mice lacking NRG1/ErbB signaling in the central nervous system. *Proc. Natl. Acad. Sci. U.S.A.* 106, 4507–4512. doi: 10.1073/pnas.0900355106

Bear, M. F., Huber, K. M., and Warren, S. T. (2004). The mGluR theory of fragile X mental retardation. *Trends Neurosci.* 27, 370–377. doi: 10.1016/j.tins.2004.04.009

Belforte, J. E., Zsiros, V., Sklar, E. R., Jiang, Z., Yu, G., Li, Y., et al. (2010). ., Postnatal NMDA receptor ablation in corticolimbic interneurons confers schizophrenia-like phenotypes. *Nat. Neurosci.* 13, 76–83. doi: 10.1038/nn.2447

Bennett, D. A., Schneider, J. A., Wilson, R. S., Bienias, J. L., and Arnold, S. E. (2004). Neurofibrillary tangles mediate the association of amyloid load with clinical Alzheimer disease and level of cognitive function. *Arch. Neurol.* 61, 378–384. doi: 10.1001/archneur.61.3.378

Bjarnadottir, M., Misner, D. L., Haverfield-Gross, S., Bruun, S., Helgason, V. G., Stefansson, H., et al. (2007). Neuregulin1 (NRG1) signaling through Fyn modulates NMDA receptor phosphorylation: differential synaptic function in NRG1+/- knock-outs compared with wild-type mice. *J. Neurosci.* 27, 4519–4529. doi: 10.1523/jneurosci.4314-06.2007

Bliss, T. V., and Collingridge, G. L. (1993). A synaptic model of memory: long-term potentiation in the hippocampus. *Nature* 361, 31–39. doi: 10.1038/361031a0

Boivin, B., Yang, M., and Tonks, N. K. (2010). Targeting the reversibly oxidized protein tyrosine phosphatase superfamily. *Sci. Signal.* 3:l2.

Borea, P. A., Gessi, S., Merighi, S., Vincenzi, F., and Varani, K. (2018). Pharmacology of adenosine receptors: the state of the art. *Physiol. Rev.* 98, 1591–1625. doi: 10.1152/physrev.00049.2017

Boros, B. D., Greathouse, K. M., Gentry, E. G., Curtis, K. A., Birchall, E. L., Gearing, M., et al. (2017). Dendritic spines provide cognitive resilience against Alzheimer's disease. *Ann. Neurol.* 82, 602–614. doi: 10.1002/ana.25049

Boulanger, L. M., Lombroso, P. J., Raghunathan, A., During, M. J., Wahle, P., and Naegele, J. R. (1995). Cellular and molecular characterization of a brain-enriched protein tyrosine phosphatase. *J. Neurosci.* 15, 1532–1544. doi: 10.1523/jneurosci.15-02-01532.1995

Bramham, C. R., and Wells, D. G. (2007). Dendritic mRNA: transport, translation and function. *Nat. Rev. Neurosci.* 8, 776–789. doi: 10.1038/nrn2150

Bult, A., Zhao, F., Dirkx, R. Jr., Raghunathan, A., Solimena, M., and Lombroso, P. J. (1997). STEP: a family of brain-enriched PTPs. Alternative splicing produces transmembrane, cytosolic and truncated isoforms. *Eur. J. Cell Biol.* 72, 337–344.

Bult, A., Zhao, F., Dirkx, R. Jr., Sharma, E., Lukacsi, E., Solimena, M., et al. (1996). STEP61: a member of a family of brain-enriched PTPs is localized to the endoplasmic reticulum. *J. Neurosci.* 16, 7821–7831. doi: 10.1523/jneurosci.16-24-07821.1996

Calabrese, B., Shaked, G. M., Tabarean, I. V., Braga, J., Koo, E. H., and Halpain, S. (2007). Rapid, concurrent alterations in pre- and postsynaptic structure induced by naturally-secreted amyloid-beta protein. *Mol. Cell Neurosci.* 35, 183–193. doi: 10.1016/j.mcn.2007.02.006

Carty, N. C., Xu, J., Kurup, P., Brouillette, J., Goebel-Goody, S. M., Austin, D. R., et al. (2012). The tyrosine phosphatase STEP: implications in schizophrenia and the molecular mechanism underlying antipsychotic medications. *Transl. Psychiatry* 2:e137. doi: 10.1038/tp.2012.63

Castonguay, D., Dufort-Gervais, J., Ménard, C., Chatterjee, M., Quirion, R., Bontempi, B., et al. (2018). The tyrosine phosphatase STEP is involved in age-related memory decline. *Curr. Biol.* 28, 1079.e4–1089.e4.

Catts, V. S., Lai, Y. L., Weickert, C. S., Weickert, T. W., and Catts, S. V. (2016). A quantitative review of the postmortem evidence for decreased cortical N-methyl-D-aspartate receptor expression levels in schizophrenia: how can we link molecular abnormalities to mismatch negativity deficits? *Biol. Psychol.* 116, 57–67. doi: 10.1016/j.biopsycho.2015.10.013

Chagniel, L., Bergeron, Y., Bureau, G., Massicotte, G., and Cyr, M. (2014). Regulation of tyrosine phosphatase STEP61 by protein kinase A during motor skill learning in mice. *PLoS One* 9:e86988. doi: 10.1371/journal.pone.0086988

Chatterjee, M., Kurup, P. K., Lundbye, C. J., Hugger Toft, A. K., Kwon, J., Benedict, J., et al. (2018). STEP inhibition reverses behavioral, electrophysiologic, and synaptic abnormalities in Fmr1 KO mice. *Neuropharmacology* 128, 43–53. doi: 10.1016/j.neuropharm.2017.09.026

Chatterjee, M., Kwon, J., Benedict, J., Kamceva, M., Kurup, P., and Lombroso, P. J. (2021). STEP inhibition prevents Aβ-mediated damage in dendritic complexity and spine density in Alzheimer's disease. *Exp. Brain Res.* 239, 881–890. doi: 10.1007/s00221-020-06028-x

Chen, J. F., Lee, C. F., and Chern, Y. (2014). Adenosine receptor neurobiology: overview. *Int. Rev. Neurobiol.* 119, 1–49. doi: 10.1016/b978-0-12-801022-8.00001-5

Chin, J., Palop, J. J., Puoliväli, J., Massaro, C., Bien-Ly, N., Gerstein, H., et al. (2005). Fyn kinase induces synaptic and cognitive impairments in a transgenic mouse model of Alzheimer's disease. *J. Neurosci.* 25, 9694–9703. doi: 10.1523/jneurosci.2980-05.2005

Chiodi, V., Mallozzi, C., Ferrante, A., Chen, J. F., Lombroso, P. J., Di Stasi, A. M., et al. (2014). Cocaine-induced changes of synaptic transmission in the striatum are modulated by adenosine A2A receptors and involve the tyrosine phosphatase STEP. *Neuropsychopharmacology* 39, 569–578. doi: 10.1038/npp.2013.229

Cho, I. H., Kim, D. H., Lee, M. J., Bae, J., Lee, K. H., and Song, W. K. (2013a). SPIN90 phosphorylation modulates spine structure and synaptic function. *PLoS One* 8:e54276. doi: 10.1371/journal.pone.0054276

Cho, I. H., Lee, M. J., Kim, D. H., Kim, B., Bae, J., Choi, K. Y., et al. (2013b). SPIN90 dephosphorylation is required for cofilin-mediated actin depolymerization in NMDA-stimulated hippocampal neurons. *Cell Mol. Life Sci.* 70, 4369–4383. doi: 10.1007/s00018-013-1391-4

Costa-Mattioli, M., Sossin, W. S., Klann, E., and Sonenberg, N. (2009). Translational control of long-lasting synaptic plasticity and memory. *Neuron* 61, 10–26. doi: 10.1016/j.neuron.2008.10.055

Cummings, J., Lee, G., Ritter, A., Sabbagh, M., and Zhong, K. (2020). Alzheimer's disease drug development pipeline: 2020. *Alzheimers Dement.* 6:e12050.

Cunha, R. A. (2016). How does adenosine control neuronal dysfunction and neurodegeneration? *J. Neurochem.* 139, 1019–1055. doi: 10.1111/jnc.13724

Darnell, J. C., Van Driesche, S. J., Zhang, C., Hung, K. Y., Mele, A., Fraser, C. E., et al. (2011). FMRP stalls ribosomal translocation on mRNAs linked to synaptic function and autism. *Cell* 146, 247–261. doi: 10.1016/j.cell.2011.06.013

Davis, S., Vanhoutte, P., Pages, C., Caboche, J., and Laroche, S. (2000). The MAPK/ERK cascade targets both Elk-1 and cAMP response element-binding protein to control long-term potentiation-dependent gene expression in the dentate gyrus in vivo. *J. Neurosci.* 20, 4563–4572. doi: 10.1523/jneurosci.20-12-04563.2000

Dawson, T. M., and Dawson, V. L. (2010). The role of parkin in familial and sporadic Parkinson's disease. *Mov. Disord.* 25(Suppl. 1), S32–S39.

Dawson, T. M., and Dawson, V. L. (2014). Parkin plays a role in sporadic Parkinson's disease. *Neurodegener. Dis.* 13, 69–71. doi: 10.1159/000354307

Deb, I., Poddar, R., and Paul, S. (2011). Oxidative stress-induced oligomerization inhibits the activity of the non-receptor tyrosine phosphatase STEP61. *J. Neurochem.* 116, 1097–1111. doi: 10.1111/j.1471-4159.2010.07165.x

DeKosky, S. T., and Scheff, S. W. (1990). Synapse loss in frontal cortex biopsies in Alzheimer's disease: correlation with cognitive severity. *Ann. Neurol.* 27, 457–464. doi: 10.1002/ana.410270502

Desplats, P. A., Kass, K. E., Gilmartin, T., Stanwood, G. D., Woodward, E. L., Head, S. R., et al. (2006). Selective deficits in the expression of striatal-enriched

mRNAs in Huntington's disease. *J. Neurochem.* 96, 743–757. doi: 10.1111/j.1471-4159.2005.03588.x

Dewachter, I., Filipkowski, R. K., Priller, C., Ris, L., Neyton, J., Croes, S., et al. (2009). Deregulation of NMDA-receptor function and down-stream signaling in APP[V717I] transgenic mice. *Neurobiol. Aging* 30, 241–256. doi: 10.1016/j.neurobiolaging.2007.06.011

Dineley, K. T., Westerman, M., Bui, D., Bell, K., Ashe, K. H., and Sweatt, J. D. (2001). Beta-amyloid activates the mitogen-activated protein kinase cascade via hippocampal alpha7 nicotinic acetylcholine receptors: in vitro and in vivo mechanisms related to Alzheimer's disease. *J. Neurosci.* 21, 4125–4133. doi: 10.1523/jneurosci.21-12-04125.2001

Eadie, B. D., Cushman, J., Kannangara, T. S., Fanselow, M. S., and Christie, B. R. (2012). NMDA receptor hypofunction in the dentate gyrus and impaired context discrimination in adult Fmr1 knockout mice. *Hippocampus* 22, 241–254. doi: 10.1002/hipo.20890

El-Husseini, A. E., Schnell, E., Chetkovich, D. M., Nicoll, R. A., and Bredt, D. S. (2000). PSD-95 involvement in maturation of excitatory synapses. *Science* 290, 1364–1368.

Elizabeth, K., and Alexander, K. (2017). Striatal-enriched tyrosine protein phosphatase (STEP) in the mechanisms of depressive disorders. *Curr. Protein Peptide Sci.* 18, 1152–1162.

Engen, J. R., Wales, T. E., Hochrein, J. M., Meyn, M. A. III, Banu Ozkan, S., Bahar, I., et al. (2008). Structure and dynamic regulation of Src-family kinases. *Cell Mol. Life Sci.* 65, 3058–3073.

Extance, A. (2010). Alzheimer's failure raises questions about disease-modifying strategies. *Nat. Rev. Drug Discov.* 9, 749–751. doi: 10.1038/nrd3288

Fitzpatrick, C. J., and Lombroso, P. J. (2011). The role of striatal-enriched protein tyrosine phosphatase (STEP) in cognition. *Front. Neuroanat.* 5:47. doi: 10.3389/fnana.2011.00047

Fonkeu, Y., Kraynyukova, N., Hafner, A. S., Kochen, L., Sartori, F., Schuman, E. M., et al. (2019). How mRNA localization and protein synthesis sites influence dendritic protein distribution and dynamics. *Neuron* 103, 1109.e7–1122.e7.

Francis, D. M., Koveal, D., Tortajada, A., Page, R., and Peti, W. (2014). Interaction of kinase-interaction-motif protein tyrosine phosphatases with the mitogen-activated protein kinase ERK2. *PLoS One* 9:e91934. doi: 10.1371/journal.pone.0091934

Fresco, P., Diniz, C., and Gonçalves, J. (2004). Facilitation of noradrenaline release by activation of adenosine A(2A) receptors triggers both phospholipase C and adenylate cyclase pathways in rat tail artery. *Cardiovasc. Res.* 63, 739–746. doi: 10.1016/j.cardiores.2004.05.015

García-Forn, M., Martínez-Torres, S., García-Díaz Barriga, G., Alberch, J., Milà, M., Azkona, G., et al. (2018). Pharmacogenetic modulation of STEP improves motor and cognitive function in a mouse model of Huntington's disease. *Neurobiol. Dis.* 120, 88–97. doi: 10.1016/j.nbd.2018.08.024

Garzon, D. J., and Fahnestock, M. (2007). Oligomeric amyloid decreases basal levels of brain-derived neurotrophic factor (BDNF) mRNA via specific downregulation of BDNF transcripts IV and V in differentiated human neuroblastoma cells. *J. Neurosci.* 27, 2628–2635. doi: 10.1523/jneurosci.5053-06.2007

Gladding, C. M., Sepers, M. D., Xu, J., Zhang, L. Y., Milnerwood, A. J., Lombroso, P. J., et al. (2012). Calpain and STriatal-Enriched protein tyrosine phosphatase (STEP) activation contribute to extrasynaptic NMDA receptor localization in a Huntington's disease mouse model. *Hum. Mol. Genet.* 21, 3739–3752. doi: 10.1093/hmg/dds154

Glock, C., Heumüller, M., and Schuman, E. M. (2017). mRNA transport & local translation in neurons. *Curr. Opin. Neurobiol.* 45, 169–177.

Goebel-Goody, S. M., Baum, M., Paspalas, C. D., Fernandez, S. M., Carty, N. C., Kurup, P., et al. (2012a). Therapeutic implications for striatal-enriched protein tyrosine phosphatase (STEP) in neuropsychiatric disorders. *Pharmacol. Rev.* 64, 65–87. doi: 10.1124/pr.110.003053

Goebel-Goody, S. M., Wilson-Wallis, E. D., Royston, S., Tagliatela, S. M., Naegele, J. R., and Lombroso, P. J. (2012b). Genetic manipulation of STEP reverses behavioral abnormalities in a fragile X syndrome mouse model. *Genes Brain Behav.* 11, 586–600. doi: 10.1111/j.1601-183x.2012.00781.x

Goebel-Goody, S. M., Davies, K. D., Alvestad Linger, R. M., Freund, R. K., and Browning, D. (2009). Phospho-regulation of synaptic and extrasynaptic N-methyl-d-aspartate receptors in adult hippocampal slices. *Neuroscience* 158, 1446–1459. doi: 10.1016/j.neuroscience.2008.11.006

Gross, C., Nakamoto, M., Yao, X., Chan, C.-B., Yim, S. Y., Ye, K., et al. (2010). Excess phosphoinositide 3-Kinase subunit synthesis and activity as a novel therapeutic target in fragile X syndrome. *J. Neurosci.* 30, 10624–10638. doi: 10.1523/jneurosci.0402-10.2010

Hahn, C. G., Wang, H. Y., Cho, D. S., Talbot, K., Gur, R. E., Berrettini, W. H., et al. (2006). Altered neuregulin 1-erbB4 signaling contributes to NMDA receptor hypofunction in schizophrenia. *Nat. Med.* 12, 824–828. doi: 10.1038/nm1418

Hansson, O., Guatteo, E., Mercuri, N. B., Bernardi, G., Li, X. J., Castilho, R. F., et al. (2001). Resistance to NMDA toxicity correlates with appearance of nuclear inclusions, behavioural deficits and changes in calcium homeostasis in mice transgenic for exon 1 of the huntington gene. *Eur. J. Neurosci.* 14, 1492–1504. doi: 10.1046/j.0953-816x.2001.01767.x

Hardingham, G. E. (2009). Coupling of the NMDA receptor to neuroprotective and neurodestructive events. *Biochem. Soc. Trans.* 37(Pt 6), 1147–1160. doi: 10.1042/bst0371147

Hardingham, G. E., Fukunaga, Y., and Bading, H. (2002). Extrasynaptic NMDARs oppose synaptic NMDARs by triggering CREB shut-off and cell death pathways. *Nat. Neurosci.* 5, 405–414. doi: 10.1038/nn835

Hasegawa, S., Morioka, M., Goto, S., Korematsu, K., Okamura, A., Yano, S., et al. (2000). Expression of neuron specific phosphatase, striatal enriched phosphatase (STEP) in reactive astrocytes after transient forebrain ischemia. *Glia* 29, 316–329. doi: 10.1002/(sici)1098-1136(20000215)29:4<316::aid-glia3>3.0.co;2-o

Hayashi, T., and Huganir, R. L. (2004). Tyrosine phosphorylation and regulation of the AMPA receptor by SRC family tyrosine kinases. *J. Neurosci.* 24, 6152–6160. doi: 10.1523/jneurosci.0799-04.2004

He, Y. Y., Zhang, X. Y., Yung, W. H., Zhu, J. N., and Wang, J. J. (2013). Role of BDNF in central motor structures and motor diseases. *Mol .Neurobiol.* 48, 783–793. doi: 10.1007/s12035-013-8466-y

Henley, J. M., and Wilkinson, K. A. (2016). Synaptic AMPA receptor composition in development, plasticity and disease. *Nat. Rev. Neurosci.* 17, 337–350. doi: 10.1038/nrn.2016.37

Hodges, A., Strand, A. D., Aragaki, A. K., Kuhn, A., Sengstag, T., Hughes, G., et al. (2006). Regional and cellular gene expression changes in human Huntington's disease brain. *Hum. Mol. Genet.* 15, 965–977. doi: 10.1093/hmg/ddl013

Holbro, N., Grunditz, A., and Oertner, T. G. (2009). Differential distribution of endoplasmic reticulum controls metabotropic signaling and plasticity at hippocampal synapses. *Proc. Natl. Acad. Sci. U.S.A.* 106, 15055–15060. doi: 10.1073/pnas.0905110106

Hou, L., Antion, M. D., Hu, D., Spencer, C. M., Paylor, R., and Klann, E. (2006). Dynamic translational and proteasomal regulation of fragile X mental retardation protein controls mGluR-dependent long-term depression. *Neuron* 51, 441–454. doi: 10.1016/j.neuron.2006.07.005

Hou, X., Sun, J. P., Ge, L., Liang, X., Li, K., Zhang, Y., et al. (2020). Inhibition of striatal-enriched protein tyrosine phosphatase by targeting computationally revealed cryptic pockets. *Eur. J. Med. Chem.* 190:112131. doi: 10.1016/j.ejmech.2020.112131

Hsiao, K., Chapman, P., Nilsen, S., Eckman, C., Harigaya, Y., Younkin, S., et al. (1996). Correlative memory deficits, Abeta elevation, and amyloid plaques in transgenic mice. *Science* 274, 99–102. doi: 10.1126/science.274.5284.99

Hsieh, H., Boehm, J., Sato, C., Iwatsubo, T., Tomita, T., Sisodia, S., et al. (2006). AMPAR removal underlies Abeta-induced synaptic depression and dendritic spine loss. *Neuron* 52, 831–843. doi: 10.1016/j.neuron.2006.10.035

Huang, Y., Lu, W., Ali, D. W., Pelkey, K. A., Pitcher, G. M., Lu, Y. M., et al. (2001). CAKbeta/Pyk2 kinase is a signaling link for induction of long-term potentiation in CA1 hippocampus. *Neuron* 29, 485–496. doi: 10.1016/s0896-6273(01)00220-3

Huber, K. M., Gallagher, S. M., Warren, S. T., and Bear, M. F. (2002). Altered synaptic plasticity in a mouse model of fragile X mental retardation. *Proc. Natl. Acad. Sci. U.S.A.* 99, 7746–7750. doi: 10.1073/pnas.122205699

Huber, K. M., Kayser, M. S., and Bear, M. F. (2000). Role for rapid dendritic protein synthesis in hippocampal mGluR-dependent long-term depression. *Science* 288, 1254–1257. doi: 10.1126/science.288.5469.1254

Humphries, C., Mortimer, A., Hirsch, S., and de Belleroche, J. (1996). NMDA receptor mRNA correlation with antemortem cognitive impairment in schizophrenia. *Neuroreport* 7, 2051–2055. doi: 10.1097/00001756-199608120-00040

Iacobucci, G. J., and Popescu, G. K. (2017). NMDA receptors: linking physiological output to biophysical operation. *Nat. Rev. Neurosci.* 18, 236–249. doi: 10.1038/nrn.2017.24

Imam, S. Z., Zhou, Q., Yamamoto, A., Valente, A. J., Ali, S. F., Bains, M., et al. (2011). Novel regulation of parkin function through c-Abl-mediated tyrosine phosphorylation: implications for Parkinson's disease. *J. Neurosci.* 31, 157–163. doi: 10.1523/jneurosci.1833-10.2011

Ingley, E. (2008). Src family kinases: regulation of their activities, levels and identification of new pathways. *Biochim. Biophys. Acta* 1784, 56–65. doi: 10.1016/j.bbapap.2007.08.012

Iulita, M. F., Bistué Millón, M. B., Pentz, R., Aguilar, L. F., Do Carmo, S., Allard, S., et al. (2017). Differential deregulation of NGF and BDNF neurotrophins in a transgenic rat model of Alzheimer's disease. *Neurobiol. Dis.* 108, 307–323. doi: 10.1016/j.nbd.2017.08.019

Ivanov, A., Pellegrino, C., Rama, S., Dumalska, I., Salyha, Y., Ben-Ari, Y., et al. (2006). Opposing role of synaptic and extrasynaptic NMDA receptors in regulation of the extracellular signal-regulated kinases (ERK) activity in cultured rat hippocampal neurons. *J. Physiol.* 572(Pt 3), 789–798. doi: 10.1113/jphysiol.2006.105510

Jamal, S., Goyal, S., Shanker, A., and Grover, A. (2015). Checking the STEP-associated trafficking and internalization of glutamate receptors for reduced cognitive deficits: a machine learning approach-based cheminformatics study and its application for drug repurposing. *PLoS One* 10:e0129370. doi: 10.1371/journal.pone.0129370

Jang, S. S., Royston, S. E., Xu, J., Cavaretta, J. P., Vest, M. O., Lee, K. Y., et al. (2015). Regulation of STEP61 and tyrosine-phosphorylation of NMDA and AMPA receptors during homeostatic synaptic plasticity. *Mol. Brain* 8:55.

Kantrowitz, J. T., Malhotra, A. K., Cornblatt, B., Silipo, G., Balla, A., Suckow, R. F., et al. (2010). High dose D-serine in the treatment of schizophrenia. *Schizophr. Res.* 121, 125–130. doi: 10.1016/j.schres.2010.05.012

Kashyap, G., Bapat, D., Das, D., Gowaikar, R., Amritkar, R. E., Rangarajan, G., et al. (2019). Synapse loss and progress of Alzheimer's disease -A network model. *Sci. Rep.* 9:6555.

Khachaturian, Z. S. (2006). Diagnosis of Alzheimer's disease: two-decades of progress. *J. Alzheimers Dis.* 9(3 Suppl.), 409–415. doi: 10.3233/jad-2006-9s346

Kim, S. Y., Lee, H. J., Kim, Y. N., Yoon, S., Lee, J. E., Sun, W., et al. (2008). Striatal-enriched protein tyrosine phosphatase regulates dopaminergic neuronal development via extracellular signal-regulated kinase signaling. *Exp. Neurol.* 214, 69–77. doi: 10.1016/j.expneurol.2008.07.014

Kitada, T., Pisani, A., Karouani, M., Haburcak, M., Martella, G., Tscherter, A., et al. (2009). Impaired dopamine release and synaptic plasticity in the striatum of parkin-/- mice. *J. Neurochem.* 110, 613–621. doi: 10.1111/j.1471-4159.2009.06152.x

Knobloch, M., and Mansuy, I. M. (2008). Dendritic spine loss and synaptic alterations in Alzheimer's disease. *Mol. Neurobiol.* 37, 73–82. doi: 10.1007/s12035-008-8018-z

Ko, H. S., Lee, Y., Shin, J. H., Karuppagounder, S. S., Gadad, B. S., Koleske, A. J., et al. (2010). Phosphorylation by the c-Abl protein tyrosine kinase inhibits parkin's ubiquitination and protective function. *Proc. Natl. Acad. Sci. U.S.A.* 107, 16691–16696. doi: 10.1073/pnas.1006083107

Kommaddi, R. P., Das, D., Karunakaran, S., Nanguneri, S., Bapat, D., Ray, A., et al. (2018). Aβ mediates F-actin disassembly in dendritic spines leading to cognitive deficits in Alzheimer's disease. *J. Neurosci.* 38, 1085–1099. doi: 10.1523/jneurosci.2127-17.2017

Kono, R., Kim, G. L., Nagata, H., Ikegaya, Y., and Koyama, R. (2019). Induced neuronal activity does not attenuate amyloid beta-induced synaptic loss in vitro. *Neuropsychopharmacol. Rep.* 39, 306–311. doi: 10.1002/npr2.12074

Krauss, M., Kinuta, M., Wenk, M. R., Camilli, P. De, Takei, K., and Haucke, V. (2003). ARF6 stimulates clathrin/AP-2 recruitment to synaptic membranes by activating phosphatidylinositol phosphate kinase type Igamma. *J. Cell Biol.* 162, 113–124. doi: 10.1083/jcb.200301006

Kulikov, A. V., Tikhonova, M. A., Kulikova, E. A., Volcho, K. P., Khomenko, T. M., Salakhutdinov, N. F., et al. (2012). A new synthetic varacin analogue, 8-(trifluoromethyl)-1,2,3,4,5-benzopentathiepin-6-amine hydrochloride (TC-2153), decreased hereditary catalepsy and increased the BDNF gene expression in the hippocampus in mice. *Psychopharmacology* 221, 469–478. doi: 10.1007/s00213-011-2594-8

Kulikova, E. A., Khotskin, N. V., Illarionova, N. B., Sorokin, I. E., Bazhenova, E. Y., Kondaurova, E. M., et al. (2018). Inhibitor of striatal-enriched protein tyrosine phosphatase, 8-(Trifluoromethyl)-1,2,3,4,5-Benzopentathiepin-6-Amine hydrochloride (TC-2153), produces antidepressant-like effect and decreases functional activity and protein level of 5-HT(2A) receptor in the brain. *Neuroscience* 394, 220–231. doi: 10.1016/j.neuroscience.2018.10.031

Kurup, P., Zhang, Y., Xu, J., Venkitaramani, D. V., Haroutunian, V., Greengard, P., et al. (2010). Abeta-mediated NMDA receptor endocytosis in Alzheimer's disease involves ubiquitination of the tyrosine phosphatase STEP61. *J. Neurosci.* 30, 5948–5957. doi: 10.1523/jneurosci.0157-10.2010

Kurup, P. K., Xu, J., Videira, R. A., Ononenyi, C., Baltazar, G., and Lombroso, P. J. (2015). STEP61 is a substrate of the E3 ligase parkin and is upregulated in Parkinson's disease. *Proc. Natl. Acad. Sci. U.S.A.* 112, 1202–1207. doi: 10.1073/pnas.1417423112

Lacor, P. N., Buniel, M. C., Chang, L., Fernandez, S. J., Gong, Y., Viola, K. L., et al. (2004). Synaptic targeting by Alzheimer's-related amyloid beta oligomers. *J. Neurosci.* 24, 10191–10200. doi: 10.1523/jneurosci.3432-04.2004

Lavezzari, G., McCallum, J., Lee, R., and Roche, K. W. (2003). Differential binding of the AP-2 adaptor complex and PSD-95 to the C-terminus of the NMDA receptor subunit NR2B regulates surface expression. *Neuropharmacology* 45, 729–737. doi: 10.1016/s0028-3908(03)00308-3

Le, H. T., Maksumova, L., Wang, J., and Pallen, C. J. (2006). Reduced NMDA receptor tyrosine phosphorylation in PTPalpha-deficient mouse synaptosomes is accompanied by inhibition of four src family kinases and Pyk2: an upstream role for PTPalpha in NMDA receptor regulation. *J. Neurochem.* 98, 1798–1809. doi: 10.1111/j.1471-4159.2006.04075.x

Li, R., Xie, D. D., Dong, J. H., Li, H., Li, K. S., Su, J., et al. (2014). Molecular mechanism of ERK dephosphorylation by striatal-enriched protein tyrosine phosphatase. *J. Neurochem.* 128, 315–329.

Loh, H. C., Tang, P. Y., Tee, S. F., Chow, T. J., Choong, C. Y., Lim, S. Y., et al. (2013). Neuregulin-1 (NRG-1) and its susceptibility to schizophrenia: a case-control study and meta-analysis. *Psychiatry Res.* 208, 186–188. doi: 10.1016/j.psychres.2013.01.022

Lombroso, P. J., Murdoch, G., and Lerner, M. (1991). Molecular characterization of a protein-tyrosine-phosphatase enriched in striatum. *Proc. Natl. Acad. Sci. U.S.A.* 88, 7242–7246.

Lombroso, P. J., Naegele, J. R., Sharma, E., and Lerner, M. (1993). A protein tyrosine phosphatase expressed within dopaminoceptive neurons of the basal ganglia and related structures. *J. Neurosci.* 13, 3064–3074. doi: 10.1523/jneurosci.13-07-03064.1993

Lombroso, P. J., Ogren, M., Kurup, P., and Nairn, A. C. (2016). Molecular underpinnings of neurodegenerative disorders: striatal-enriched protein tyrosine phosphatase signaling and synaptic plasticity. *F1000Res.* 5:F1000FacultyRev-2932.

Lorber, B., Berry, M., Hendriks, W., den Hertog, J., Pulido, R., and Logan, A. (2004). Stimulated regeneration of the crushed adult rat optic nerve correlates with attenuated expression of the protein tyrosine phosphatases RPTPalpha, STEP, and LAR. *Mol. Cell Neurosci.* 27, 404–416. doi: 10.1016/j.mcn.2004.06.012

Lu, X., Maysinger, D., and Hagg, T. (2002). Tyrosine phosphatase inhibition enhances neurotrophin potency and rescues nigrostriatal neurons in adult rats. *Exp. Neurol.* 178, 259–267. doi: 10.1006/exnr.2002.8042

Mallozzi, C., Pepponi, R., Visentin, S., Chiodi, V., Lombroso, P. J., Bader, M., et al. (2020). The activity of the Striatal-enriched protein tyrosine phosphatase in neuronal cells is modulated by adenosine A(2A) receptor. *J. Neurochem.* 152, 284–298. doi: 10.1111/jnc.14866

Mirra, S. S., Heyman, A., McKeel, D., Sumi, S. M., Crain, B. J., Brownlee, L. M., et al. (1991). The Consortium to Establish a Registry for Alzheimer's Disease (CERAD). Part II. Standardization of the neuropathologic assessment of Alzheimer's disease. *Neurology* 41, 479–486. doi: 10.1212/wnl.41.4.479

Mukherjee, S., Poddar, R., Deb, I., and Paul, S. (2011). , Dephosphorylation of specific sites in the kinase-specificity sequence domain leads to ubiquitin-mediated degradation of the tyrosine phosphatase STEP. *Biochem. J.* 440, 115–125. doi: 10.1042/bj20110240

Muñoz, J. J., Tárrega, C., Blanco-Aparicio, C., and Pulido, R. (2003). Differential interaction of the tyrosine phosphatases PTP-SL, STEP and HePTP with the mitogen-activated protein kinases ERK1/2 and p38alpha is determined by a kinase specificity sequence and influenced by reducing agents. *Biochem. J.* 372(Pt 1), 193–201. doi: 10.1042/bj20021941

Nakazawa, T., Komai, S., Tezuka, T., Hisatsune, C., Umemori, H., Semba, K., et al. (2001). Characterization of Fyn-mediated tyrosine phosphorylation sites on GluR epsilon 2 (NR2B) subunit of the N-methyl-D-aspartate receptor. *J. Biol. Chem.* 276, 693–699. doi: 10.1074/jbc.m008085200

Ng, A. N., Doherty, A. J., Lombroso, P. J., Emptage, N. J., and Collingridge, G. L. (2014). Rapid regulation of endoplasmic reticulum dynamics in dendritic spines by NMDA receptor activation. *Mol. Brain* 7:60.

Nguyen, T. H., Liu, J., and Lombroso, P. J. (2002). Striatal enriched phosphatase 61 dephosphorylates Fyn at phosphotyrosine 420. *J. Biol. Chem.* 277, 24274–24279. doi: 10.1074/jbc.m111683200

Nicodemo, A. A., Pampillo, M., Ferreira, L. T., Dale, L. B., Cregan, T., Ribeiro, F. M., et al. (2010). Pyk2 uncouples metabotropic glutamate receptor G protein signaling but facilitates ERK1/2 activation. *Mol. Brain* 3:4. doi: 10.1186/1756-6606-3-4

Okamura, A., Goto, S., Nishi, T., Yamada, K., Yoshikawa, M., and Ushio, Y. (1997). Postnatal ontogeny of striatal-enriched protein tyrosine phosphatase (STEP) in rat striatum. *Exp. Neurol.* 145, 228–234. doi: 10.1006/exnr.1997.6435

Okun, E., Griffioen, K., Barak, B., Roberts, N. J., Castro, K., Pita, M. A., et al. (2010). Toll-like receptor 3 inhibits memory retention and constrains adult hippocampal neurogenesis. *Proc. Natl. Acad. Sci. U.S.A.* 107, 15625–15630. doi: 10.1073/pnas.1005807107

Olausson, P., Venkitaramani, D. V., Moran, T. D., Salter, M. W., Taylor, J. R., and Lombroso, P. J. (2012). The tyrosine phosphatase STEP constrains amygdala-dependent memory formation and neuroplasticity. *Neuroscience* 225, 1–8. doi: 10.1016/j.neuroscience.2012.07.069

Oyama, T., Goto, S., Nishi, T., Sato, K., Yamada, K., Yoshikawa, M., et al. (1995). Immunocytochemical localization of the striatal enriched protein tyrosine phosphatase in the rat striatum: a light and electron microscopic study with a complementary DNA-generated polyclonal antibody. *Neuroscience* 69, 869–880. doi: 10.1016/0306-4522(95)00278-q

Palop, J. J., and Mucke, L. (2010). Amyloid-beta-induced neuronal dysfunction in Alzheimer's disease: from synapses toward neural networks. *Nat. Neurosci.* 13, 812–818. doi: 10.1038/nn.2583

Paoletti, P., Bellone, C., and Zhou, Q. (2013). NMDA receptor subunit diversity: impact on receptor properties, synaptic plasticity and disease. *Nat. Rev. Neurosci.* 14, 383–400. doi: 10.1038/nrn3504

Paspalas, C. D., Perley, C. C., Venkitaramani, D. V., Goebel-Goody, S. M., Zhang, Y., Kurup, P., et al. (2009). Major vault protein is expressed along the nucleus-neurite axis and associates with mRNAs in cortical neurons. *Cereb. Cortex* 19, 1666–1677. doi: 10.1093/cercor/bhn203

Paul, S., and Connor, J. A. (2010). NR2B-NMDA receptor-mediated increases in intracellular Ca2+ concentration regulate the tyrosine phosphatase, STEP, and ERK MAP kinase signaling. *J. Neurochem.* 114, 1107–1118.

Paul, S., Nairn, A. C., Wang, P., and Lombroso, P. J. (2003). NMDA-mediated activation of the tyrosine phosphatase STEP regulates the duration of ERK signaling. *Nat. Neurosci.* 6, 34–42. doi: 10.1038/nn989

Paul, S., Olausson, P., Venkitaramani, D. V., Ruchkina, I., Moran, T. D., Tronson, N., et al. (2007). The striatal-enriched protein tyrosine phosphatase gates long-term potentiation and fear memory in the lateral amygdala. *Biol. Psychiatry* 61, 1049–1061. doi: 10.1016/j.biopsych.2006.08.005

Paul, S., Snyder, G. L., Yokakura, H., Picciotto, M. R., Nairn, A. C., and Lombroso, P. J. (2000). The Dopamine/D1 receptor mediates the phosphorylation and inactivation of the protein tyrosine phosphatase STEP via a PKA-dependent pathway. *J. Neurosci.* 20, 5630–5638. doi: 10.1523/jneurosci.20-15-05630.2000

Pelkey, K. A., Askalan, R., Paul, S., Kalia, L. V., Nguyen, T. H., Pitcher, G. M., et al. (2002). Tyrosine phosphatase STEP is a tonic brake on induction of long-term potentiation. *Neuron* 34, 127–138. doi: 10.1016/s0896-6273(02)00633-5

Penazzi, L., Tackenberg, C., Ghori, A., Golovyashkina, N., Niewidok, B., Selle, K., et al. (2016). Aβ-mediated spine changes in the hippocampus are microtubule-dependent and can be reversed by a subnanomolar concentration of the microtubule-stabilizing agent epothilone D. *Neuropharmacology* 105, 84–95. doi: 10.1016/j.neuropharm.2016.01.002

Peng, S., Wuu, J., Mufson, E. J., and Fahnestock, M. (2005). Precursor form of brain-derived neurotrophic factor and mature brain-derived neurotrophic factor are decreased in the pre-clinical stages of Alzheimer's disease. *J. Neurochem.* 93, 1412–1421. doi: 10.1111/j.1471-4159.2005.03135.x

Pinna, A., Serra, M., Morelli, M., and Simola, N. (2018). Role of adenosine A(2A) receptors in motor control: relevance to Parkinson's disease and dyskinesia. *J. Neural Transm.* 125, 1273–1286. doi: 10.1007/s00702-018-1848-6

Piqué, M., López, J. M., Foissac, S., Guigó, R., and Méndez, R. (2008). A combinatorial code for CPE-mediated translational control. *Cell* 132, 434–448. doi: 10.1016/j.cell.2007.12.038

Pitcher, G. M., Kalia, L. V., Ng, D., Goodfellow, N. M., Yee, K. T., Lambe, E. K., et al. (2011). Schizophrenia susceptibility pathway neuregulin 1-ErbB4 suppresses Src upregulation of NMDA receptors. *Nat. Med.* 17, 470–478. doi: 10.1038/nm.2315

Poddar, R., Deb, I., Mukherjee, S., and Paul, S. (2010). NR2B-NMDA receptor mediated modulation of the tyrosine phosphatase STEP regulates glutamate induced neuronal cell death. *J. Neurochem.* 115, 1350–1362. doi: 10.1111/j.1471-4159.2010.07035.x

Popugaeva, E., Pchitskaya, E., Speshilova, A., Alexandrov, S., Zhang, H., and Vlasova, O. (2015). STIM2 protects hippocampal mushroom spines from amyloid synaptotoxicity. *Mol. Neurodegener.* 10:37.

Pulido, R., Zúñiga, A., and Ullrich, A. (1998). PTP-SL and STEP protein tyrosine phosphatases regulate the activation of the extracellular signal-regulated kinases ERK1 and ERK2 by association through a kinase interaction motif. *Embo J.* 17, 7337–7350. doi: 10.1093/emboj/17.24.7337

Qu, X., Yuan, F. N., Corona, C., Pasini, S., Pero, M. E., Gundersen, G. G., et al. (2017). Stabilization of dynamic microtubules by mDia1 drives Tau-dependent Aβ(1-42) synaptotoxicity. *J. Cell Biol.* 216, 3161–3178. doi: 10.1083/jcb.201701045

Raghunathan, A., Matthews, G. A., Lombroso, P. J., and Naegele, J. R. (1996). Transient compartmental expression of a family of protein tyrosine phosphatases in the developing striatum. *Brain Res. Dev. Brain Res.* 91, 190–199. doi: 10.1016/0165-3806(95)00176-x

Rangasamy, S. B., Soderstrom, K., Bakay, R. A., and Kordower, J. H. (2010). Neurotrophic factor therapy for Parkinson's disease. *Prog. Brain Res.* 184, 237–264.

Rinne, J. O., Brooks, D. J., Rossor, M. N., Fox, N. C., Bullock, R., Klunk, W. E., et al. (2010). 11C-PiB PET assessment of change in fibrillar amyloid-beta load in patients with Alzheimer's disease treated with bapineuzumab: a phase 2, double-blind, placebo-controlled, ascending-dose study. *Lancet Neurol.* 9, 363–372. doi: 10.1016/s1474-4422(10)70043-0

Robinson, M. J., and Cobb, M. H. (1997). Mitogen-activated protein kinase pathways. *Curr. Opin. Cell Biol.* 9, 180–186.

Roche, K. W., Standley, S., McCallum, J., Dune Ly, C., Ehlers, M. D., and Wenthold, R. J. (2001). Molecular determinants of NMDA receptor internalization. *Nat. Neurosci.* 4, 794–802. doi: 10.1038/90498

Ross, C. A., and Tabrizi, S. J. (2011). Huntington's disease: from molecular pathogenesis to clinical treatment. *Lancet Neurol.* 10, 83–98. doi: 10.1016/s1474-4422(10)70245-3

Saavedra, A., Ballesteros, J. J., Tyebji, S., Martínez-Torres, S., Blázquez, G., López-Hidalgo, R., et al. (2019). Proteolytic degradation of hippocampal STEP61 in LTP and learning. *Mol. Neurobiol.* 56, 1475–1487. doi: 10.1007/s12035-018-1170-1

Saavedra, A., Giralt, A., Rué, L., Xifró, X., Xu, J., Ortega, Z., et al. (2011). Striatal-enriched protein tyrosine phosphatase expression and activity in Huntington's disease: a STEP in the resistance to excitotoxicity. *J. Neurosci.* 31, 8150–8162. doi: 10.1523/jneurosci.3446-10.2011

Saavedra, A., Puigdellívol, M., Tyebji, S., Kurup, P., Xu, J., Ginés, S., et al. (2016). BDNF induces striatal-enriched protein tyrosine phosphatase 61 Degradation through the proteasome. *Mol. Neurobiol.* 53, 4261–4273. doi: 10.1007/s12035-015-9335-7

Saiki, S., Sato, S., and Hattori, N. (2012). Molecular pathogenesis of Parkinson's disease: update. *J. Neurol. Neurosurg. Psychiatry* 83, 430–436.

Saito, T., Matsuba, Y., Mihira, N., Takano, J., Nilsson, P., Itohara, S., et al. (2014). Single App knock-in mouse models of Alzheimer's disease. *Nat. Neurosci.* 17, 661–663. doi: 10.1038/nn.3697

Sala, C., Piëch, V., Wilson, N. R., Passafaro, M., Liu, G., and Sheng, M. (2001). Regulation of dendritic spine morphology and synaptic function by Shank and Homer. *Neuron* 31, 115–130. doi: 10.1016/s0896-6273(01)00339-7

Scheff, S. W., Price, D. A., Schmitt, F. A., and Mufson, E. J. (2006). Hippocampal synaptic loss in early Alzheimer's disease and mild cognitive impairment. *Neurobiol. Aging* 27, 1372–1384. doi: 10.1016/j.neurobiolaging.2005.09.012

Scholz, R., Berberich, S., Rathgeber, L., Kolleker, A., Köhr, G., and Kornau, H. C. (2010). AMPA receptor signaling through BRAG2 and Arf6 critical for long-term synaptic depression. *Neuron* 66, 768–780. doi: 10.1016/j.neuron.2010.05.003

Semenova, M. M., Mäki-Hokkonen, A. M., Cao, J., Komarovski, V., Forsberg, K. M., Koistinaho, M., et al. (2007). Rho mediates calcium-dependent activation of p38alpha and subsequent excitotoxic cell death. *Nat. Neurosci.* 10, 436–443. doi: 10.1038/nn1869

Shankar, G. M., Bloodgood, B. L., Townsend, M., Walsh, D. M., Selkoe, D. J., and Sabatini, B. L. (2007). Natural oligomers of the Alzheimer amyloid-beta protein induce reversible synapse loss by modulating an NMDA-type glutamate receptor-dependent signaling pathway. *J. Neurosci.* 27, 2866–2875. doi: 10.1523/jneurosci.4970-06.2007

Sharma, E., Zhao, F., Bult, A., and Lombroso, P. J. (1995). Identification of two alternatively spliced transcripts of STEP: a subfamily of brain-enriched protein tyrosine phosphatases. *Brain Res. Mol. Brain Res.* 32, 87–93. doi: 10.1016/0169-328x(95)00066-2

Shimura, H., Hattori, N., Kubo, S., Mizuno, Y., Asakawa, S., Minoshima, S., et al. (2000). Familial Parkinson disease gene product, parkin, is a ubiquitin-protein ligase. *Nat. Genet.* 25, 302–305. doi: 10.1038/77060

Snyder, E. M., Nong, Y., Almeida, C. G., Paul, S., Moran, T., Choi, E. Y., et al. (2005). Regulation of NMDA receptor trafficking by amyloid-beta. *Nat. Neurosci.* 8, 1051–1058.

Snyder, E. M., Philpot, B. D., Huber, K. M., Dong, X., Fallon, J. R., and Bear, M. F. (2001). Internalization of ionotropic glutamate receptors in response to mGluR activation. *Nat. Neurosci.* 4, 1079–1085. doi: 10.1038/nn746

Song, J. H., Yu, J. T., and Tan, L. (2015). Brain-derived neurotrophic factor in Alzheimer's Disease: risk, mechanisms, and therapy. *Mol. Neurobiol.* 52, 1477–1493. doi: 10.1007/s12035-014-8958-4

Spencer, M. L., Theodosiou, M., and Noonan, D. J. (2004). NPDC-1, a novel regulator of neuronal proliferation, is degraded by the ubiquitin/proteasome system through a PEST degradation motif. *J. Biol. Chem.* 279, 37069–37078. doi: 10.1074/jbc.m402507200

Spires-Jones, T. L., and Hyman, B. T. (2014). The intersection of amyloid beta and tau at synapses in Alzheimer's disease. *Neuron* 82, 756–771. doi: 10.1016/j.neuron.2014.05.004

Sriram, S. R., Li, X., Ko, H. S., Chung, K. K., Wong, E., Lim, K. L., et al. (2005). Familial-associated mutations differentially disrupt the solubility, localization, binding and ubiquitination properties of parkin. *Hum. Mol. Genet.* 14, 2571–2586. doi: 10.1093/hmg/ddi292

Stefansson, H., Steinthorsdottir, V., Thorgeirsson, T. E., Gulcher, J. R., and Stefansson, K. (2004). Neuregulin 1 and schizophrenia. *Ann. Med.* 36, 62–71.

Stevens, T. R., Krueger, S. R., Fitzsimonds, R. M., and Picciotto, M. R. (2003). Neuroprotection by nicotine in mouse primary cortical cultures involves activation of calcineurin and L-type calcium channel inactivation. *J. Neurosci.* 23, 10093–10099. doi: 10.1523/jneurosci.23-31-10093.2003

Sun, S., Zhang, H., Liu, J., Popugaeva, E., Xu, N. J., Feske, S., et al. (2014). Reduced synaptic STIM2 expression and impaired store-operated calcium entry cause destabilization of mature spines in mutant presenilin mice. *Neuron* 82, 79–93. doi: 10.1016/j.neuron.2014.02.019

Sutton, M. A., and Schuman, E. M. (2006). Dendritic protein synthesis, synaptic plasticity, and memory. *Cell* 127, 49–58. doi: 10.1016/j.cell.2006.09.014

Suvrathan, A., Hoeffer, C. A., Wong, H., Klann, E., and Chattarji, S. (2010). Characterization and reversal of synaptic defects in the amygdala in a mouse model of fragile X syndrome. *Proc. Natl. Acad. Sci. U.S.A.* 107, 11591–11596. doi: 10.1073/pnas.1002262107

Sweatt, J. D. (2004). Mitogen-activated protein kinases in synaptic plasticity and memory. *Curr. Opin. Neurobiol.* 14, 311–317. doi: 10.1016/j.conb.2004.04.001

Tackenberg, C., and Brandt, R. (2009). Divergent pathways mediate spine alterations and cell death induced by amyloid-beta, wild-type tau, and R406W tau. *J. Neurosci.* 29, 14439–14450. doi: 10.1523/jneurosci.3590-09.2009

Tanaka, K., Suzuki, T., Hattori, N., and Mizuno, Y. (2004). Ubiquitin, proteasome and parkin. *Biochim. Biophys. Acta* 1695, 235–247.

Tang, Y. P., Shimizu, E., Dube, G. R., Rampon, C., Kerchner, G. A., Zhuo, M., et al. (1999). Genetic enhancement of learning and memory in mice. *Nature* 401, 63–69. doi: 10.1038/43432

Tanila, H. (2017). The role of BDNF in Alzheimer.s disease. *Neurobiol. Dis.* 97(Pt B), 114–118.

Tautermann, C. S., Binder, F., Büttner, F. H., Eickmeier, C., Fiegen, D., Gross, U., et al. (2019). Allosteric activation of striatal-enriched protein tyrosine phosphatase (STEP, PTPN5) by a fragment-like molecule. *J. Med. Chem.* 62, 306–316. doi: 10.1021/acs.jmedchem.8b00857

Terry, R. D., Masliah, E., Salmon, D. P., Butters, N., DeTeresa, R., Hill, R., et al. (1991). Physical basis of cognitive alterations in Alzheimer's disease: synapse loss is the major correlate of cognitive impairment. *Ann. Neurol.* 30, 572–580. doi: 10.1002/ana.410300410

Ting, J. T., Kelley, B. G., Lambert, T. J., Cook, D. G., and Sullivan, J. M. (2007). Amyloid precursor protein overexpression depresses excitatory transmission through both presynaptic and postsynaptic mechanisms. *Proc. Natl. Acad. Sci. U.S.A.* 104, 353–358. doi: 10.1073/pnas.0608807104

Tseng, B. P., Green, K. N., Chan, J. L., Blurton-Jones, M., and LaFerla, F. M. (2008). Abeta inhibits the proteasome and enhances amyloid and tau accumulation. *Neurobiol. Aging* 29, 1607–1618. doi: 10.1016/j.neurobiolaging.2007.04.014

Tsuang, M. T., Stone, W. S., and Faraone, S. V. (2001). Genes, environment and schizophrenia. *Br. J. Psychiatry Suppl.* 40, s18–s24.

Ultanir, S. K., Kim, J. E., Hall, B. J., Deerinck, T., Ellisman, M., and Ghosh, A. (2007). Regulation of spine morphology and spine density by NMDA receptor signaling in vivo. *Proc. Natl. Acad. Sci. U.S.A.* 104, 19553–19558. doi: 10.1073/pnas.0704031104

Valjent, E., Pascoli, V., Svenningsson, P., Paul, S., Enslen, H., Corvol, J. C., et al. (2005). Regulation of a protein phosphatase cascade allows convergent dopamine and glutamate signals to activate ERK in the striatum. *Proc. Natl. Acad. Sci. U.S.A.* 102, 491–496. doi: 10.1073/pnas.0408305102

van de Leemput, J., Hess, J. L., Glatt, S. J., and Tsuang, M. T. (2016). Genetics of schizophrenia: historical insights and prevailing evidence. *Adv. Genet.* 96, 99–141.

Venkitaramani, D. V., Chin, J., Netzer, W. J., Gouras, G. K., Lesne, S., Malinow, R., et al. (2007). Beta-amyloid modulation of synaptic transmission and plasticity. *J. Neurosci.* 27, 11832–11837.

Venkitaramani, D. V., Moura, P. J., Picciotto, M. R., and Lombroso, P. J. (2011). Striatal-enriched protein tyrosine phosphatase (STEP) knockout mice have enhanced hippocampal memory. *Eur. J. Neurosci.* 33, 2288–2298. doi: 10.1111/j.1460-9568.2011.07687.x

Venkitaramani, D. V., Paul, S., Zhang, Y., Kurup, P., Ding, L., Tressler, L., et al. (2009). Knockout of striatal enriched protein tyrosine phosphatase in mice results in increased ERK1/2 phosphorylation. *Synapse* 63, 69–81. doi: 10.1002/syn.20608

Wang, H., Ferguson, G. D., Pineda, V. V., Cundiff, P. E., and Storm, D. R. (2004). Overexpression of type-1 adenylyl cyclase in mouse forebrain enhances recognition memory and LTP. *Nat. Neurosci.* 7, 635–642. doi: 10.1038/nn1248

Wang, Z. H., Xiang, J., Liu, X., Yu, S. P., Manfredsson, F. P., Sandoval, I. M., et al. (2019). Deficiency in BDNF/TrkB neurotrophic activity stimulates δ-Secretase by upregulating C/EBPβ in Alzheimer's Disease. *Cell Rep.* 28, 655.e5–669.e5.

Wei, W., Nguyen, L. N., Kessels, H. W., Hagiwara, H., Sisodia, S., and Malinow, R. (2010). Amyloid beta from axons and dendrites reduces local spine number and plasticity. *Nat. Neurosci.* 13, 190–196. doi: 10.1038/nn.2476

Witten, M. R., Wissler, L., Snow, M., Geschwindner, S., Read, J. A., Brandon, N. J., et al. (2017). X-ray characterization and structure-based optimization of striatal-enriched protein tyrosine phosphatase inhibitors. *J. Med. Chem.* 60, 9299–9319. doi: 10.1021/acs.jmedchem.7b01292

Won, S., Incontro, S., Li, Y., Nicoll, R. A., and Roche, K. W. (2019). The STEP(61) interactome reveals subunit-specific AMPA receptor binding and synaptic regulation. *Proc. Natl. Acad. Sci. U.S.A.* 116, 8028–8037. doi: 10.1073/pnas.1900878116

Won, S., Incontro, S., Nicoll, R. A., and Roche, K. W. (2016). PSD-95 stabilizes NMDA receptors by inducing the degradation of STEP61. *Proc. Natl. Acad. Sci. U.S.A.* 113, E4736–E4744.

Wu, P. H., Coultrap, S. J., Browning, M. D., and Proctor, W. R. (2011). Functional adaptation of the N-methyl-D-aspartate receptor to inhibition by ethanol is modulated by striatal-enriched protein tyrosine phosphatase and p38 mitogen-activated protein kinase. *Mol. Pharmacol.* 80, 529–537. doi: 10.1124/mol.110.068643

Xu, J., Chatterjee, M., Baguley, T. D., Brouillette, J., Kurup, P., Ghosh, D., et al. (2014). Inhibitor of the tyrosine phosphatase STEP reverses cognitive deficits in a mouse model of Alzheimer's disease. *PLoS Biol.* 12:e1001923. doi: 10.1371/journal.pbio.1001923

Xu, J., Hartley, B. J., Kurup, P., Phillips, A., Topol, A., Xu, M., et al. (2018). Inhibition of STEP(61) ameliorates deficits in mouse and hiPSC-based schizophrenia models. *Mol. Psychiatry* 23, 271–281. doi: 10.1038/mp.2016.163

Xu, J., Kurup, P., Azkona, G., Baguley, T. D., Saavedra, A., Nairn, A. C., et al. (2016). Down-regulation of BDNF in cell and animal models increases striatal-enriched protein tyrosine phosphatase 61 (STEP61) levels. *J. Neurochem.* 136, 285–294. doi: 10.1111/jnc.13295

Xu, J., Kurup, P., Bartos, J. A., Patriarchi, T., Hell, J. W., and Lombroso, P. J. (2012). Striatal-enriched protein-tyrosine phosphatase (STEP) regulates Pyk2 kinase activity. *J. Biol. Chem.* 287, 20942–20956. doi: 10.1074/jbc.m112.368654

Xu, J., Kurup, P., Foscue, E., and Lombroso, P. J. (2015). Striatal-enriched protein tyrosine phosphatase regulates the PTPα/Fyn signaling pathway. *J. Neurochem.* 134, 629–641. doi: 10.1111/jnc.13160

Xu, J., Kurup, P., Zhang, Y., Goebel-Goody, S. M., Wu, P. H., Hawasli, A. H., et al. (2009). Extrasynaptic NMDA receptors couple preferentially to excitotoxicity via calpain-mediated cleavage of STEP. *J. Neurosci.* 29, 9330–9343. doi: 10.1523/jneurosci.2212-09.2009

Zhang, L., Xie, J. W., Yang, J., and Cao, Y. P. (2013). Tyrosine phosphatase STEP61 negatively regulates amyloid β-mediated ERK/CREB signaling pathways via α7 nicotinic acetylcholine receptors. *J. Neurosci. Res.* 91, 1581–1590. doi: 10.1002/jnr.23263

Zhang, Y., Kurup, P., Xu, J., Carty, N., Fernandez, S. M., Nygaard, H. B., et al. (2010). Genetic reduction of striatal-enriched tyrosine phosphatase (STEP) reverses cognitive and cellular deficits in an Alzheimer's disease mouse model. *Proc. Natl. Acad. Sci. U.S.A.* 107, 19014–19019. doi: 10.1073/pnas.1013543107

Zhang, Y., Venkitaramani, D. V., Gladding, C. M., Zhang, Y., Kurup, P., Molnar, E., et al. (2008). The tyrosine phosphatase STEP mediates AMPA receptor endocytosis after metabotropic glutamate receptor stimulation. *J. Neurosci.* 28, 10561–10566. doi: 10.1523/jneurosci.2666-08.2008

Zong, M. M., Yuan, H. M., He, X., Zhou, Z. Q., Qiu, X. D., Yang, J. J., et al. (2019). Disruption of striatal-enriched protein tyrosine phosphatase signaling might contribute to memory impairment in a mouse model of sepsis-associated encephalopathy. *Neurochem. Res.* 44, 2832–2842. doi: 10.1007/s11064-019-02905-2

Conflict of Interest: The authors declare that the research was conducted in the absence of any commercial or financial relationships that could be construed as a potential conflict of interest.

frontiers in Cell and Developmental Biology

REVIEW
published: 28 July 2021
doi: 10.3389/fcell.2021.707268

Possible Mechanisms of Tau Spread and Toxicity in Alzheimer's Disease

Huiqin Zhang, Yu Cao, Lina Ma, Yun Wei and Hao Li**

Institute of Geriatrics, Xiyuan Hospital, China Academy of Chinese Medical Sciences, Beijing, China

Tau is a protein that associates with microtubules (MTs) and promotes their assembly and stability. The protein loses its ability to bind MTs in tauopathies, and detached tau can misfold and induce the pathological changes that characterize Alzheimer's disease (AD). A growing body of evidence indicates that tauopathies can spread between cells or connected regions. Pathological tau transmission in the brain of patients with AD and other tauopathies is due to the spread of various tau species along neuroanatomically connected regions in a "prion-like" manner. This complex process involves multiple steps of secretion, cellular uptake, transcellular transfer, and/or seeding, but the precise mechanisms of tau pathology propagation remain unclear. This review summarizes the current evidence on the nature of propagative tau species and the possible steps involved in the process of tau pathology spread, including detachment from MTs, degradations, and secretion, and discusses the different mechanisms underlying the spread of tau pathology.

Keywords: tau, tauopathy, spread, toxicity, mechanism, Alzheimer's disease

OPEN ACCESS

Edited by:
Zhifang Dong,
Chongqing Medical University, China

Reviewed by:
Vladimir I. Titorenko,
Concordia University, Canada
Chandrasekar Raman,
Joslin Diabetes Center and Harvard Medical School, United States

****Correspondence:***
Yun Wei
weiyun_0913@163.com
Hao Li
xyhplihao1965@126.com

Specialty section:
This article was submitted to Molecular and Cellular Pathology, a section of the journal Frontiers in Cell and Developmental Biology

Received: *09 May 2021*
Accepted: *09 July 2021*
Published: *28 July 2021*

Citation:
Zhang H, Cao Y, Ma L, Wei Y and Li H (2021) Possible Mechanisms of Tau Spread and Toxicity in Alzheimer's Disease. Front. Cell Dev. Biol. 9:707268. doi: 10.3389/fcell.2021.707268

INTRODUCTION

The microtubule (MT)-binding protein tau is mainly expressed in the cytoplasm of neurons (Pérez et al., 2016) and plays key roles in regulating MT dynamics, axonal transport, and neurite outgrowth (Johnson and Stoothoff, 2004). Tau protein changes affect its MT-binding ability and consequently alter its normal physiological functions. For example, the phosphorylation of tau protein in and around its microtubule-binding domain (MBD) may neutralize its positive charges (Jho et al., 2010), alter MBD conformation, and lead to its detachment from MTs (Fischer et al., 2009). Once detached, tau accumulates in neurites and neuronal cell bodies, where it forms insoluble intracellular aggregates or inclusion bodies such as neurofibrillary tangles (NFTs), which are one of the major pathological features of Alzheimer's disease (AD) (Lee et al., 2001; von Bergen et al., 2005; Zhang et al., 2009). Following detachment from MTs, tau can undergo structural transition, misfolding, and degradation (Frost et al., 2009). Tau can also be secreted into the extracellular space (Riemenschneider et al., 2003; Barthélemy et al., 2016) either in its naked form (Chai et al., 2012) or packaged in exosomes or other membranes (Saman et al., 2012; Simón et al., 2012; Polanco et al., 2016) following neuronal activity in mature neurons (Pooler et al., 2013; Dujardin et al., 2014b), neuron death (Gómez-Ramos et al., 2006), and/or when accumulated tau reaches a certain

level in non-neuronal cells. In agreement with these findings, exogenous misfolded tau protein can be internalized by cells (Guo and Lee, 2011; Wu et al., 2013), a process that is mediated by heparin sulphate proteoglycans (HSPGs) and cell membrane receptors such as muscarinic (M1, M3) and a-amino-3-hydroxy-5-methyl-4-isoxazolepropionic acid (AMPA) receptors, as well as via endocytosis (Gómez-Ramos et al., 2008; Holmes et al., 2013; Tian H. et al., 2013). Once internalized, pathogenic misfolded tau proteins act as "seeds" that recruits soluble endogenous tau into larger aberrant conformations (Jucker and Walker, 2013) that slowly propagate across interconnected brain regions, as shown in various animal models (Clavaguera et al., 2009, 2013; Lasagna-Reeves et al., 2012). Fibrillar tau species can also transfer between cells and then recruit endogenous tau proteins onto their ends (Kfoury et al., 2012), a mechanism that may be responsible for the intracerebral spread of tau pathology (de Calignon et al., 2012; Iba et al., 2013).

Tau pathology spreading between neuronal cells and adjacent brain regions is a complex process involving many physiological and pathological aspects of tau protein, including its degradation, secretion, transmission, and toxicity. However, the exact mechanism underlying the spread of tau pathology after its release from cells remains unclear, and understanding these processes is the focus of an increasing number of studies (Le et al., 2012; Mohamed et al., 2013). There is some evidence that progressive accumulation of tau pathology in affected brain regions during AD development is due to the spread of aggregated tau along anatomically connected pathways (Hanger et al., 2014; Clavaguera et al., 2015; Lewis and Dickson, 2016). Accumulation of aggregates leads to neuronal loss and trans-synaptic spread of tau aggregates to more distal regions of the brain (Liu et al., 2012; Croft et al., 2017). The spread of extracellular species is the main pathway propagating neurofibrillary lesions and tau toxicity throughout different brain regions in neurodegenerative diseases (Iba et al., 2013; Pérez et al., 2018). A better understanding of the precise molecular mechanisms underlying tau propagation will contribute to the development of new therapeutic approaches for halting this process and provide new perspectives for the early diagnosis and prevention of tau pathologies (Fuster-Matanzo et al., 2018; Pérez et al., 2018). This review covers the most recent advances in our understanding of tau-spreading mechanisms, as well as the underlying implications of tauopathy-associated toxicity in AD. We further outline the possible mechanisms involved in pathology propagation including tau protein detachment from MTs; tau cleavage; tau degradation; and the release, uptake, and movement of pathogenic tau among synaptically connected neurons (Usenovic et al., 2015).

PHYSIOLOGICAL CHARACTERISTICS AND DISSOCIATION OF TAU PROTEIN FROM MTs

Tau protein can be divided into four functional domains: an N-terminal projection region, a proline-rich domain, an MBD, and a C-terminal region (Goedert and Spillantini, 2011). Tau can bind to the outside—and possibly also the inside—of MTs with the N- and C-terminal regions projecting out (Kar et al., 2003; Santarella et al., 2004). The N-terminal region can associate with the cell membrane and may be as a part of a membrane-associated complex; it also regulates the spacing between MTs (Maas et al., 2000; Al-Bassam et al., 2002). The proline-rich domain includes multiple phosphorylation sites (Augustinack et al., 2002) and can bind to Src homology 3 (SH3) domains of other proteins (Reynolds et al., 2008) such as the tyrosine kinase Fyn (Lee et al., 1998; **Figure 1**). Tau protein not only plays a crucial role in regulating MT dynamics but also promotes MT assembly and stabilization, processes that are required for morphogenesis and axonal transport in the nervous system (Johnson and Hartigan, 1999). However, the ability of tau to stabilize MTs is due in large part to its MBD (Gustke et al., 1994). Tau is thought to directly bind MTs through positively charged tandem repeat sequences within its MBD that are attracted to tubulin's negatively charged residues (Kar et al., 2003; Jho et al., 2010).

The human tau gene, microtubule-associated protein tau (MAPT), is located on chromosome 17q21 and comprises 16 exons. Alternative splicing of exons 2, 3, and 10 generates six isoforms of the tau protein (Goedert et al., 1989). They are equally expressed in central nervous system neurons of a healthy adult brain (Goedert et al., 1989; Garcia and Cleveland, 2001), and can be grouped into tau-3R class members, which contain three MT-binding repeats (MTBRs), and tau-4R class members contain four MTBRs (**Figure 1**). Because of the extra repeat, 4R isoforms have a higher affinity for MTs and can therefore bind and stabilize MTs more efficiently (Goedert and Spillantini, 2011; Morris et al., 2011; Chen and Jiang, 2019).

Tau protein functions are regulated by complex post-translational modifications including phosphorylation, glycation, isomerization, sumoylation, nitration, acetylation, and truncation (Morris et al., 2011). Moreover, tau contains numerous serine and threonine residues, so almost 20% of the protein has the potential to be phosphorylated (Wang and Mandelkow, 2016). The phosphorylation state of tau and its MT-binding affinity are controlled by a balance between kinase and phosphatase activity (Brandt et al., 1995; Shackelford and Yeh, 1998). Tau phosphorylation is mediated by MT affinity-regulating kinases (also known as PAR1 kinases), cyclic AMP-dependent protein kinase A, calcium (Ca^{2+}), or calmodulin-dependent protein kinase II (CaMKII), and tyrosine kinases like Src family members (Hanger et al., 2009). The activation of tau phosphorylation-associated kinases (e.g., CDK-5 and GSK-3β) can induce tau hyperphosphorylation, which drives dissociation of tau protein from MTs (Hanger et al., 2009). Dissociated tau can misfold and become toxic seeds that are secreted from the cell. In contrast, fully dephosphorylated tau binds to MTs with high affinity (Shackelford and Yeh, 1998). Tau dephosphorylation is mediated by protein phosphatases 1, 2A, 2B, 2C, and 5 (Hanger et al., 2009; Pérez et al., 2018). In addition, detached tau can accumulate in neurites and neuronal cell bodies, first forming insoluble filaments and eventually NFTs (Lee et al., 2001; von Bergen et al., 2005; **Figure 2**). Abnormal tau phosphorylation decreases MT binding and likely increases tau-tau interactions (Morris et al., 2011). Physiologically,

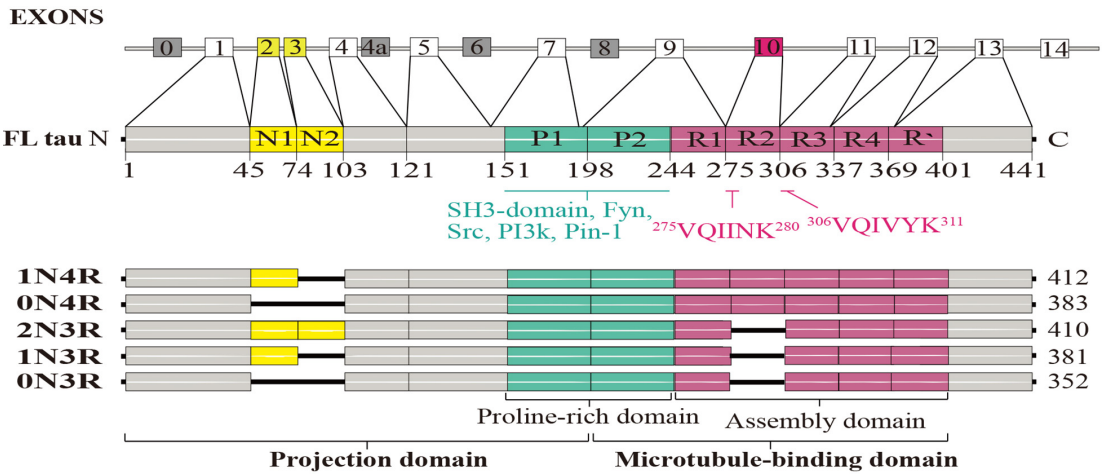

FIGURE 1 | Structural features of the tau protein. The human tau gene, microtubule-associated protein tau (MAPT), contains 16 exons; alternative splicing of exons 2, 3, and 10 generates six tau protein isoforms: oN3R, 1N4R, 2N3R, 0N4R, 1N4R, and 2N4R. Full-length human tau protein (2N4R) contains 441 amino acids and four functional domains: an N-terminal projection region, a proline-rich domain, a microtubule-binding domain (MBD), and a C-terminal region. The N-terminal inserts are N1 and N2. The proline-rich domains P1 and P2 contain many phosphorylation sites and can bind to SH3 domains of other proteins, such as the tyrosine kinase Fyn. R1-R4 make up the repeat domain, which, together with the R'-flanking region, constitute the MT-binding domain. Two sequences are necessary for tau aggregation: ^{275}VQIINK^{280} and ^{306}VQIVYK^{311}.

tau is continuously phosphorylated and dephosphorylated to ensure its proper function; however, when the balance shifts toward phosphorylation, tau affinity for MTs decreases (Alonso et al., 1997), resulting in higher cytosolic tau levels, which facilitates tau aggregation (Wegmann et al., 2018). Additionally, aberrantly phosphorylated tau protein appears to sequester other microtubule-associated proteins (MAPs), further destabilizing MTs (Alonso et al., 1997). Similarly, aberrant tau phosphorylation and self-aggregation lead to the formation of oligomers and higher-order aggregates that can lead to tau detachment from MTs and disturb the binding of other MAPs to MTs (von Bergen et al., 2000).

TAU PROTEIN CLEAVAGE AND DEGRADATION

Tau cleavage and degradation are closely related to its pathological transmission and aggregation. The cleavage of tau generates seeds that promote tau aggregation (Wang et al., 2014), alter tau clearance, and can impair cognition and motor ability (Bondulich et al., 2016). Tau cleavage occurs at its N- and C-terminals (García-Sierra et al., 2008) and depends on associated proteases, mainly caspase-3, calpain, and cathepsin L (Wang et al., 2009; de Calignon et al., 2010; **Table 1**). Tau truncation can be initiated by caspase-3, which cleaves tau at residue D421, its predominant target (Chung et al., 2001). Caspase-3 can be activated by amyloid-beta (Aβ) and caspase-2 (Gamblin et al., 2003), following which caspase-3 can cleave tau at D25-Q26 (Corsetti et al., 2008) and D421-S422 (Gamblin et al., 2003). Cleavage at D421-S422 produces the N-terminal fragment (NTF) tau_{1-421} (Tau-C) (Nicholls et al., 2017). Caspase-2 is a protease that initiates activation of other caspases; it cleaves tau at D314-L315 to produce a soluble, toxic NTF (tau_{1-314}; Δtau_{314}; Zhao et al., 2016). Tau_{1-314} levels were elevated in the brains of mice with mild cognitive impairment (MCI) and in the brains of AD patients compared with healthy controls (Zhao et al., 2016). Moreover, memory deficits were ameliorated following the application of anticaspase-2 morpholino oligonucleotides (Zhao et al., 2016). However, *in vitro* experiments using recombinant tau preparations suggested that caspase-2 preferentially cleaves tau at D421-S422 (Zhao et al., 2016). Another effector caspase, caspase-6, and puromycin-sensitive aminopeptidase (PSA) were reported to cleave recombinant human tau_{441} at D13-H14 (Sengupta et al., 2006), which was sufficient to cause axonal degeneration (Sokolowski et al., 2014). Caspase-6 cleavage at D402-T403 produces the NTF tau_{1-402}, a cerebrospinal fluid (CSF) biomarker for AD (Ramcharitar et al., 2013). In addition, calpain-1 and -2 can both cleave tau (Chesser et al., 2013) and play opposing roles in regulating synaptic plasticity and promoting neurodegeneration (Baudry and Bi, 2016). The 17-kDa tau_{45-230} fragment is generated through cleavage by calpain-1 at K44-E45 (Yang and Ksiezak-Reding, 1995) or via calpain-1 (Park and Ferreira, 2005) or -2 (Garg et al., 2011) action at R230-T231. Tau is also cleaved by calpain-1 at R242-L243 to produce the 24-kDa C-terminal fragment (CTF) $tau_{243-441}$ (Matsumoto et al., 2015). The levels of the $tau_{243-441}$ fragment increase with aging in a tauopathy mouse model (Tg601 mice expressing wild-type human tau), and CTFs with sizes ranging from 20 to 28 kDa are present in brain samples from patients with AD and familial frontotemporal dementia (Matsumoto et al., 2015). $Tau_{243-441}$ can proficiently propagate to other tau-expressing cells, leading to further seeding and tau_{441} phosphorylation (Matsumoto et al., 2015). Interestingly, tau_{441} build up can activate calpain-2, which leads to the degradation of nicotinic acetylcholine receptor subunit 4 (Yin et al., 2016), a crucial

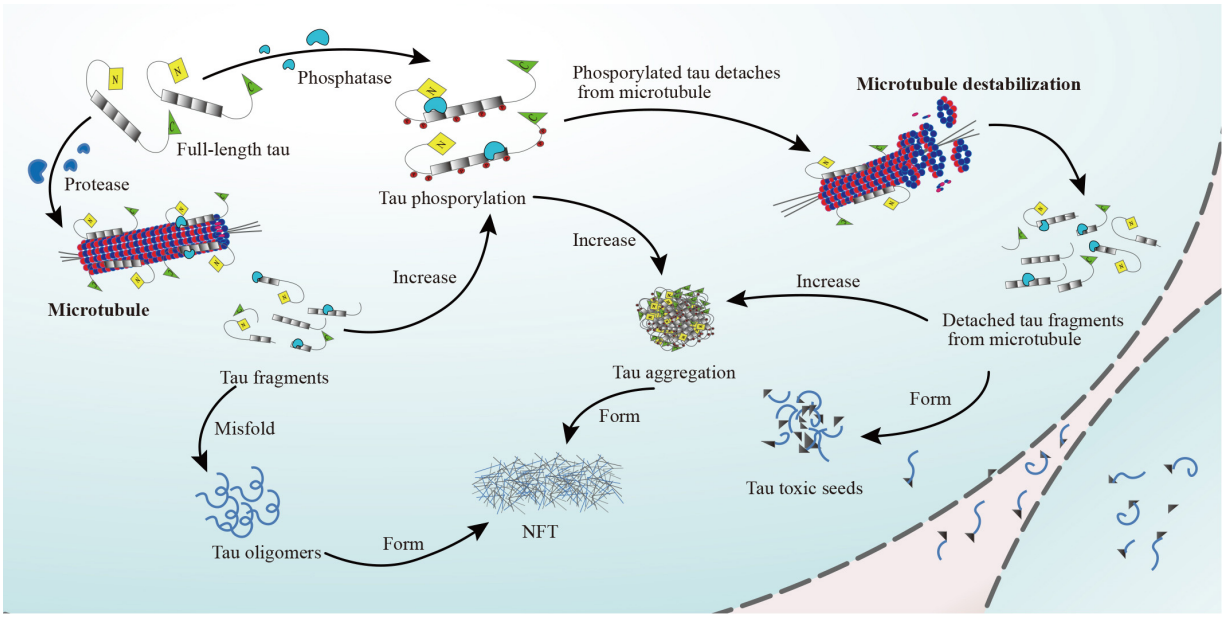

FIGURE 2 | Detachment of tau protein from MTs. The full-length tau protein binds to MTs, stabilizing them under the regulation of phosphatases (e.g., PP1, PP2A, PP2B, PP2C, and PP5). When tau protein phosphorylates, tau protein will detach from MTs. The microtubules will destabilize and dissociate. Detached tau fragments form tau aggregation, which ultimately leads to the formation of NFTs. At the same time, phosphorylated tau protein and detached tau fragments misfold and form tau oligomers, which are the precursors of NFTs, or toxic tau seeds.

component of cholinergic signaling. Calpain-2 activation by tau_{441} creates a positive feedback loop that enhances neurotoxic tau fragment generation. Cathepsins B, D, and L can also proteolytically cleave tau. One study reported that cathepsin B was associated with intracellular NFTs, and its expression was elevated around Aβ plaques (Ii et al., 1993). Cathepsin D can cleave recombinant tau at F8-E9, M419-V420, and L436-A437; there is another potential cleavage site at either T427-L428 or L428-A429 and additional cleavage sites in D34-G161, P200-K257, and K267-D358 (Kenessey et al., 1997). In Neuro-2A murine cells, cathepsin L can cleave $tau_{244-372}$ (lacking K280; $tau_{RD}\Delta K$), which is a mutated version of the aggregation-prone MBD tau fragment (García-Sierra et al., 2008). $Tau_{RD}\Delta K$ cleavage by cathepsin L depends on an initial cleavage at K257-S258 by an unknown cytosolic protease that generates $tau_{258-372}$; this fragment is further cleaved by cathepsin L at V363-P364 to produce $tau_{258-363}$ that is subsequently cleaved at I360-T361 to produce $tau_{258-360}$ (García-Sierra et al., 2008). $Tau_{258-360}$ and $tau_{258-363}$ induce aggregation of intact $tau_{RD}\Delta K$ and full-length tau, which is coincident with lysosomal leakage (García-Sierra et al., 2008). Asparagine endopeptidase-mediated tau cleavage occurs at both N255-V256 and N368-K369 and produces five tau fragments. Among them, tau_{1-368} and $tau_{256-368}$ were the only critical drivers of enhanced apoptosis in rat primary neurons, while only tau_{1-368} has been found in the brains of patients with AD (Zhang et al., 2014; Quinn et al., 2018).

Intracellular tau degradation mainly involves two major proteolytic systems: ubiquitin-proteasome and autophagy-lysosomal (Chesser et al., 2013; Lee et al., 2013; Guo et al., 2017). Full-length tau is cleared via the former system (Liu et al., 2009; Dolan and Johnson, 2010), whereas its mutated and truncated forms appear to be degraded through the latter pathway (García-Sierra et al., 2008; Fernández-Montoya and Pérez, 2015). Moreover, tau phosphorylation can exacerbate its proteolytic degradation (Kenessey et al., 1997), while hyperphosphorylation is associated with impaired tau degradation via the ubiquitin-proteasome system (Dickey et al., 2007) and tau secretion. Tau can undergo natural self-degradation at cysteine residues by acetyl-coenzyme A-induced autoacetylation (Cohen et al., 2016) following its dissociation from MTs (Cohen et al., 2013, 2016). Tau accumulation can also result from increased expression or decreased degradation of the protein (Barton et al., 1990; Zhang et al., 2014), and degradation is impaired by a modified form of tau (Zhang et al., 2014). Thus, tau acetylation may both inhibit and facilitate its degradation and also suppress its phosphorylation and aggregation (Min et al., 2010; Cook et al., 2014). Acetylated tau has been found in brains from patients with AD and other tauopathies. For example, Lys174 acetylation was recently described in AD brains and may be a critical determinant for tau-induced toxicity by delaying tau turnover (Min et al., 2015). This result indicates that targeting tau acetylation could be a novel therapeutic option for AD and other human tauopathies.

SECRETION AND RELEASE OF TAU FRAGMENTS

Although tau is intracellular, recent studies have indicated that it is also present in the extracellular space both *in vitro*

TABLE 1 | Tau protein cleavage at different sites by known proteases.

Protease	Cleavage site	Cleavage domain	Tau fragment	Effect on AD	References
Caspase-2	D314-L315	MBD	Tau_{1-314} (Δtau_{314})	Caspase-2 preferentially cleaves recombinant tau at D421-S422 compared to D314-L315. Detached from MTs, tau invades healthy dendritic spines. This impaired synaptic transmission and drove hippocampal neuronal loss, but spatial memory deficits and toxicity were only observed when tau_{1-314} promoted mislocalization of full-length tau to dendritic spines.	Zhao et al., 2016
			$Tau_{315-441}$	Unclear	Zhao et al., 2016
Caspase-3	D421-S422	C-terminus	Tau_{1-421} (Tau-C)	Linked to other tauopathies	Gamblin et al., 2003; Corsetti et al., 2008; Zhao et al., 2015
	D25-Q26	N-terminus	Tau_{1-25}	No toxicity to neurons	Corsetti et al., 2008
Caspase-3 Calpain-1	D25-Q26 K44-E45	N-terminus	Tau_{26-44}	Caused NMDAR-mediated cell death in rat CGCs	Gamblin et al., 2003; Park and Ferreira, 2005; Corsetti et al., 2008; Garg et al., 2011; Zhao et al., 2015
Caspase-3 Calpain-1 Calpain-2	D25-Q26	N-terminus	Tau_{26-230} (20–22kDa fragment)	Enriched in synaptic mitochondria; binds to Aβ peptides and exacerbates mitochondrial dysfunction. Induced NMDAR-mediated death of rat CGCs.	Gamblin et al., 2003; Park and Ferreira, 2005; Corsetti et al., 2008; Garg et al., 2011; Zhao et al., 2015
	R230-T231	MBD			
Caspase-6	D13-H14	N-terminus	Tau_{1-13}	Caused axonal degeneration	Sengupta et al., 2006; Sokolowski et al., 2014
			Tau_{14-441}	Possible role in tangle maturation	Sengupta et al., 2006; Sokolowski et al., 2014
	D402-T403	C-terminus	Tau_{1-402} (TauΔCasp6)	Serves as a CSF biomarker of neurodegeneration in AD	Ramcharitar et al., 2013
			$Tau_{403-441}$	Unclear	Ramcharitar et al., 2013
Caspase-1, -3, -6, -7, -8	D421-S422	C-terminus	$Tau_{422-441}$	Unclear	Quinn et al., 2018
	D421-S422	C-terminus	$Tau_{151-421}$ (Δtau)	Led to tau aggregation and disrupted axonal transport, mitochondrial function, Golgi apparatus, and synaptic protein levels	
	K150-I151	N-terminus			
PSA	D13-H14	N-terminus	Tau_{1-13}	Caused axonal degeneration	Sengupta et al., 2006; Sokolowski et al., 2014
Calpain-1	K44-E45	N-terminus	Tau_{1-44}	Caused NMDAR-mediated cell death in rat CGCs	Park and Ferreira, 2005; Garg et al., 2011
			Tau_{45-441}	Unclear	Yang and Ksiezak-Reding, 1995
	R242-L243	MBD	$Tau_{243-441}$ (24kDa CTF)	Accelerated the propagation to other tau-expressing cells, causing further seeding of aggregates and tau_{441} phosphorylation; reduced capacity for promoting MT assembly compared with tau_{441}	Matsumoto et al., 2015
			Tau_{1-242}	Unclear	Matsumoto et al., 2015
Calpain-1 and thrombin, Calpain-1 and -2	K44-E45	N-terminus	Tau_{45-230} (17kDa fragment)	Caused synapse loss and behavioral abnormalities; impaired organelle transport	Yang and Ksiezak-Reding, 1995; Park and Ferreira, 2005; Garg et al., 2011; Quinn et al., 2018
	R230-T231	MBD			
Calpain-2 and thrombin, Calpain-1 and -2	A2-E3	N-terminus	Tau_{3-230}	Unclear	Quinn et al., 2018
	R230-T231	MBD			
	R230-T231	MBD	$Tau_{125-230}$	Not toxic	
	Q124-A125	Projection domain			

(Continued)

TABLE 1 | Continued

Protease	Cleavage site	Cleavage domain	Tau fragment	Effect on AD	References
Calpain-2	A2-E3	N-terminus	Tau_{3-124}	Unclear	Quinn et al., 2018
	Q124-A125	Projection domain			
Cathepsin L	K257-S258	MBD	$Tau_{258-372}$	Unclear	García-Sierra et al., 2008
	V363-P364	MBD	$Tau_{258-363}$	Induced the aggregation of full-length tau and intact $tau_{RD}\Delta K$ coincident with lysosomal leakage	
	I360-T361	MBD	$Tau_{258-360}$		
AEP	N255-V256	MBD	Tau_{1-255}	Unable to promote MT polymerization or aggregation into PHFs, but tau_{1-255} had strong AT8 immunoreactivity (at phosphorylation sites S202 and T205)	Zhang et al., 2014; Quinn et al., 2018
	N255-V256	MBD	$Tau_{256-441}$	Significantly reduced MT polymerization and showed increased propensity to aggregate into PHFs compared with tau_{441}	
	N255-V256	MBD	Tau_{1-368}, $Tau_{256-368}$	Enhanced apoptosis; increased ability to aggregate into PHFs	
	N368-K369	MBD			
	N368-K369	MBD	$Tau_{369-441}$	Unable to cause MT polymerization and aggregation into PHFs	
Thrombin	R155-G156	Proline-rich domain	$Tau_{156-441}$	Unclear	Quinn et al., 2018
	R155-G156	Proline-rich domain	$Tau_{156-209}$	Unclear	
	R209-S210	MBD			
	R209-S210	MBD	$Tau_{210-441}$	Unclear	
	R209-S210	MBD	$Tau_{210-230}$	Unclear	
	R230-T231	MBD			
	R230-T231	MBD	$Tau_{231-441}$	Unclear	
Chymotrypsin	Y197-S198	Projection domain	Tau_{1-197}	Unclear	Quinn et al., 2018
	Y197-S198	MBD	$Tau_{198-441}$	Unclear	
ADAM10	A152-T153	Proline-rich domain	Tau_{1-152}	Unclear	Quinn et al., 2018
			$Tau_{153-441}$ (Tau-A)	Unclear	

Aβ, amyloid-beta; AD, Alzheimer's disease; ADAM10, a disintegrin and metalloprotease 10; AEP, asparagine endopeptidase; AMPA, a-amino-3-hydroxy-5-methyl-4-isoxazolepropionic acid; CGC, cerebellar granule cell; CSF, cerebrospinal fluid; CTF, C-terminal fragment; MBD, microtubule-binding domain; MT, microtubule; NFT, neurofibrillary tangle; NMDAR, N-methyl-D-aspartate receptor; NTF, N-terminal fragment; PHF, paired-helical filament; PSA, puromycin-sensitive aminopeptidase; PSP, progressive supranuclear palsy.

and *in vivo* (Kim et al., 2010a,b; Chai et al., 2012). Tau has been detected in both the CSF and interstitial fluid of tau transgenic mouse brains (Yamada et al., 2011; Barten et al., 2012). *In vitro* studies have shown that human tau is secreted by both neuronal and non-neuronal cell lines when the protein is overexpressed (Chai et al., 2012; Saman et al., 2012; Simón et al., 2012; Pérez et al., 2016). Extracellular tau may elicit toxicity (Gómez-Ramos et al., 2006; Díaz-Hernández et al., 2010) by binding to cellular receptors such as muscarinic receptors (Gómez-Ramos et al., 2008), but the mechanisms by which tau exits into the extracellular space remain unclear (Nickel and Rabouille, 2009). Another study showed that tau can be released into the extracellular space following neuronal death (Simón et al., 2012) and can subsequently be identified in the CSF (Iqbal et al., 2005). Secreted extracellular tau can be toxic to surrounding cells through interactions with specific cell receptors (Gómez-Ramos et al., 2008; Díaz-Hernández et al., 2010; **Figure 3**). This toxic effect may result in cell death and the subsequent detection of tau in the CSF of patients with disorders such as AD (Iqbal et al., 2005; Yamada et al., 2011). Additionally, in affected regions such as the hippocampus, there is an inverse relationship between the numbers of surviving cells and extracellular tangles (Cras et al., 1995; Fukutani et al., 1995). This suggests that degenerating neurons containing fibrillar lesions might release NFT contents into the extracellular environment (Goedert, 1999). Meanwhile, several *in vitro* and *in vivo* studies reported that stimulation of neuronal activity can regulate the physiological secretion of endogenous tau by cortical neurons and enhance the release of pathological tau, a process that is Ca^{2+}-dependent and modulated by phosphorylation (Sokolow et al., 2015; Fá et al., 2016; Wang et al., 2017). AMPA receptor stimulation promotes

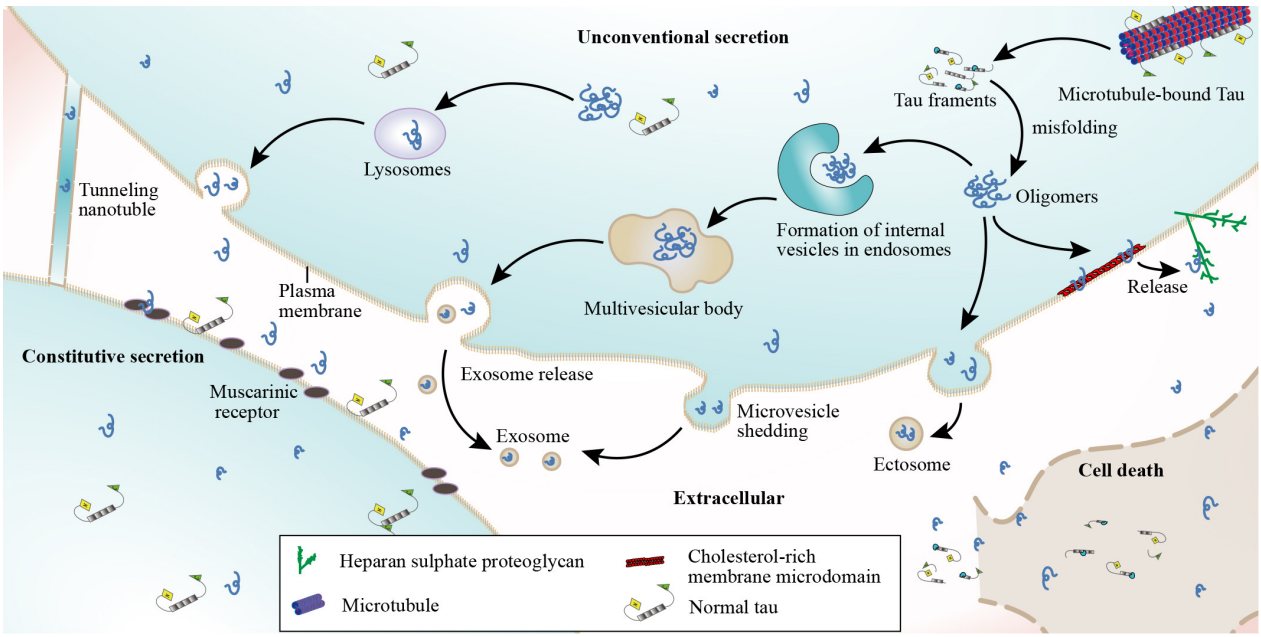

FIGURE 3 | Tau protein secretion and release. The possible mechanisms underlying the presence of tau in the extracellular space include cell death, neuroactive stimulation, constitutive secretion, and unconventional secretion. A small amount of tau can be released into the extracellular space in free form or by penetrating adjacent membranes, which can be achieved by stimulating neuroactivity or constitutive secretion. However, the methods involved in unconventional tau protein secretion include (1) non-vesicular direct translocation across the plasma membrane from the cytoplasm and extracellular trapping via HSPGs, (2) release via secretory lysosomes that fuse with the plasma membrane and release their contents into the extracellular space, (3) microvesicle shedding from the plasma membrane, and (4) vesicle-mediated exosome release. Tau can also be secreted by both neuronal and non-neuronal cells when tau protein is exogenously expressed, while extracellular tau can bind muscarinic (M1, M3) receptors. Tau may also be released through nanotubes that connect the cytoplasmic compartments of adjoining cells.

tau release through a Ca^{2+}-dependent mechanism and the exocytosis of presynaptic vesicles. AMPA receptor stimulation generates action potentials that increase presynaptic Ca^{2+} concentrations, evoking vesicle release (Schmitz et al., 2009), and this plays a role in Ca^{2+}-mediated regulation of neuronal tau release (Pooler et al., 2013). The relationship between neuronal activity and tau release appears to be bidirectional; both extracellular tau and Aβ perpetuate further neuronal tau release through feedback mechanisms (Bright et al., 2015). These results indicate that tau release partially occurs in a neuronal excitability-dependent manner in response to regional changes in the AD brain.

Tau can also be detected in the extracellular space before neurodegeneration, indicating that it can be released through mechanisms other than cell death (Yamada et al., 2011; Barten et al., 2012). Preliminary results demonstrated that tau can be released into the extracellular space via membrane vesicles in the absence of cell death (Simón et al., 2012). Tau secretion likely transpires via the unconventional vesicular- or non-vesicular-mediated secretory pathway since tau lacks an apparent endoplasmic reticulum-targeting sequence, which is necessary in the conventional secretory pathway (Yamada, 2017). Vesicle-mediated secretion might serve as a mechanism to regulate (proteostasis) cellular tau concentrations, maintaining them below a certain threshold level (Simón et al., 2012). Tau can also be transported through membrane vesicles after lysosomal degradation (García-Sierra et al., 2008). Four different mechanisms have been proposed for the unconventional secretion of soluble, cytoplasmic tau: (1) non-vesicular direct translocation from the cytoplasm across the plasma membrane, (2) release via secretory lysosomes that fuse with plasma membranes and release their contents into the extracellular space, (3) microvesicle shedding from the plasma membrane, and (4) vesicle-mediated exosome release (Nickel and Rabouille, 2009; Saman et al., 2012). In the last two scenarios, tau is surrounded by a membrane when it is released into the extracellular space (Nickel and Rabouille, 2009; Chai et al., 2012); **Figure 3**). It has also been proposed that tau may be released from cells through an exosome-independent pathway that requires heat shock cognate 70, its co-chaperone DnaJ (Hsp40), and synaptosomal-associated protein 23 (Fontaine et al., 2016). Additionally, tau secretion reportedly occurs through membrane vesicles when tau is overexpressed (Simón et al., 2012). Similarly, tau can be secreted in an exosome-dependent manner by Neuro2a cells overexpressing tau (Wang et al., 2017), as well as by microglia (Asai et al., 2015). Another vesicular-mediated mechanism involves large extracellular vesicles called exosomes that are directly shed from cells by plasma membrane budding (Théry et al., 2009; **Figure 3**). The third mechanism proposed to mediate tau release and spreading involves formation of thin membranous bridges called tunneling nanotubes (TNTs; Rustom et al., 2004). Moreover, cell depolarization was shown to induce

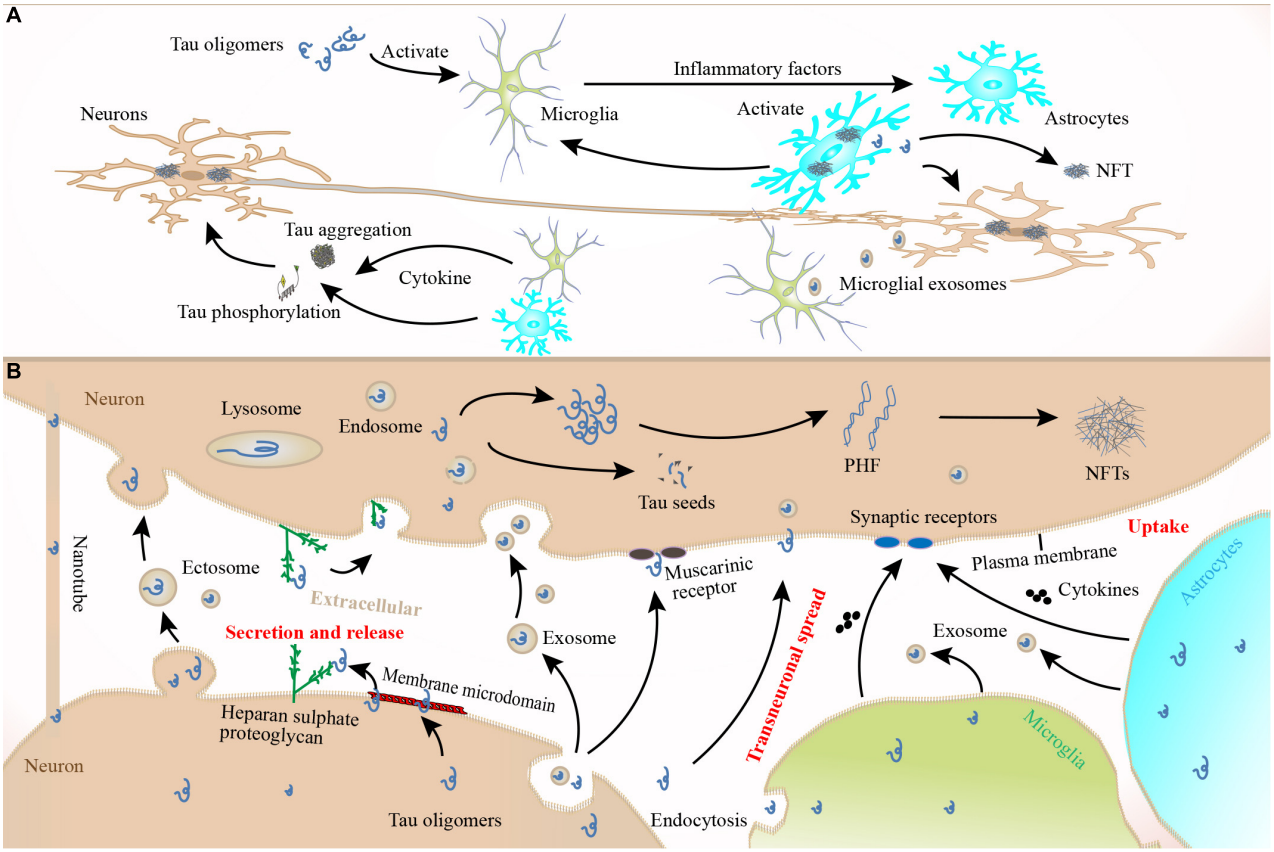

FIGURE 4 | Tau pathology spread. Once released into the extracellular space, tau can be transported to connected cells via exosomes or ectosomes. Tau can also be transported to other cells by binding to muscarinic (M1, M3) receptors or synaptic receptors or via special structures such as membrane microdomains and HSPGs. There may also be nanotubes between cells, which can also spread tau oligomers. The plasma membrane may play a role in tau transmission through endocytosis-mediated uptake of tau oligomers. Microglia can also phagocytose secreted tau oligomers that are then spread to healthy neurons in exosomes, and astrocytes may be involved in this process. Both microglia and astrocytes can secrete cytokines that act on connected neurons, which further accelerates tau pathology. However, the specific mechanisms underlying the roles of microglia and astrocytes in tau pathology spread remain unclear. When tau oligomers or monomers are released by lysosome or ingested by recipient cells, they will misfold and form toxic seeds, PHFs, or NFTs. Once the recipient cells spread the pathological tau fragments to other cells, this perpetuates a vicious cycle that exacerbates AD.

the release of a 20-kDa tau fragment from AD synapses (Sokolow et al., 2015). These four mechanisms appear to be temperature dependent and are likely to be less efficient at low temperatures (Nickel and Rabouille, 2009).

Different forms of tau protein might be secreted through different mechanisms or vectors. Endogenous tau released from primary cortical rat neurons under basal conditions is predominantly full length (Pooler et al., 2013), but truncated species have also been identified (Dujardin et al., 2014a). Tau fragments lacking the proline-rich region are either not secreted or are secreted in a manner different from that of the full-length molecule (Pérez et al., 2016). Monomeric and aggregated tau have been detected in CSF, suggesting that they may be released following axonal degeneration and neuronal death (Hampel et al., 2004). However, other studies found that unstimulated human and rodent neurons only secrete C-terminally truncated forms of endogenous tau (Kanmert et al., 2015). Cell culture studies revealed that tau is released via the unconventional secretory pathway and that tau mutations influence the secretion rate, with 4R tau isoforms less abundant than 3R isoforms (Karch et al., 2012). Moreover, exogenously expressed hyperphosphorylated tau secreted by non-neuronal cells is cleaved at its C-terminus (Plouffe et al., 2012; Croft et al., 2017). For instance, tau cleavage at D421 can increase the secretion rate (Katsinelos et al., 2018). Aberrantly phosphorylated tau is secreted more efficiently than non-phosphorylated tau, at least in cultured cell lines (Plouffe et al., 2012; Katsinelos et al., 2018), possibly because abnormal phosphorylation impairs tau's ability to interact with its partners, therefore altering the protein's normal physiological properties (Yan et al., 2020). Meanwhile, endogenous tau is reportedly released either free and in a full-length, dephosphorylated form (Pooler et al., 2013) or as N-terminally truncated fragments (Bright et al., 2015; Kanmert et al., 2015). A small subset of tau released under these conditions is inside plasma membrane-derived vesicles called ectosomes (Dujardin et al., 2014a). Tau is also released from cells in association with exosomes, particularly when it is exogenously expressed or in a highly phosphorylated and misfolded state

(Plouffe et al., 2012; Saman et al., 2012). One study suggested that tau hyperphosphorylation in AD may induce a vicious circle that amplifies its secretion (Plouffe et al., 2012). In this case, tau hyperphosphorylation would enhance its secretion, which would subsequently increase the level of dephosphorylated tau in the extracellular space. Dephosphorylated extracellular tau would then induce an increase in intracellular Ca^{2+} concentrations, which has been linked with elevated tau hyperphosphorylation (Díaz-Hernández et al., 2010). This vicious circle then promotes tau pathology propagation in the brain and CSF accumulation (Hampel et al., 2010; Plouffe et al., 2012). Golgi dynamics were also proposed to modulate tau secretion from both HeLa cells and primary cortical neurons (Mohamed et al., 2017). Tau cleavage and hyperphosphorylation increase its secretion from HeLa cells. Mitochondrial damage might reduce tau secretion (Shafiei et al., 2017), whereas impaired lysosomal function may increase it (Mohamed et al., 2014). Pathological tau in animal models appears to be more localized to synapses compared to non-pathological tau (Sahara et al., 2014), and synaptosomes isolated from human AD brains were shown to contain more phosphorylated and aggregated tau than those isolated from healthy controls (Tai et al., 2014). In summary, different tau species and isoforms including mutated (Hampel et al., 2004), hyperphosphorylated (Plouffe et al., 2012; Bright et al., 2015), and truncated forms of tau appear to be released via distinct mechanisms (Plouffe et al., 2012).

THE SPREAD OF PATHOLOGICAL TAU PROTEIN

Although the specific routes and mechanisms underlying the spread of pathological tau remain unclear (Braak and Braak, 1991), the propagation of cytosolic tau to connected neurons consists of at least four phases. First, tau must be secreted or released from donor neurons; second, it must undergo aggregation before or after being released; third, tau must be taken up into recipient neurons; and fourth, tau aggregation must be induced in recipient cells (Kanmert et al., 2015). After the release and secretion of tau to the extracellular space following cell death (Simón et al., 2012), stimulation of neuronal activity (Pooler et al., 2013), or other mechanisms (e.g., associated with vesicles, secretory lysosomes, or microvesicle shedding from the plasma membrane) (Nickel and Rabouille, 2009; Saman et al., 2012), pathological tau oligomers, monomers, or aggregates must enter other cells via endocytosis. Subsequently, pathological tau seeds might be degraded, resecreted, or mediate the misfolding of wild-type tau molecules in recipient cells (Wu et al., 2013). Recipient cells appear to favor the uptake of short, low-molecular-weight, tau fibrils over monomers and larger fibrils (Wu et al., 2013). Consequently, the potencies of various tau aggregate species on cellular propagation may be different (Frost et al., 2009). For example, tau uptake is closely related to both the size and conformation of tau aggregates (Kanmert et al., 2015). Intracellular tau accumulation is dependent on the isoform composition of the extracellular tau oligomers (Swanson et al., 2017). However, tau aggregate uptake is not neuron specific; cell-to-cell transfer also occurs between glial cells and neurons. Tau aggregates can transfer between connected cells, induce templated misfolding, and be internalized from the extracellular space by a neighboring cell, which facilitates tauopathy propagation across different brain regions in a prion-like fashion (Jucker and Walker, 2013). Tau oligomers can be internalized by dynamin-dependent bulk endocytosis and are then transported through the endolysosomal pathway in recipient cells (Wu et al., 2013). One study demonstrated that neuronal uptake of α-synuclein and tau aggregate seeds can occur through macropinocytosis, a form of fluid-phase bulk endocytosis that represents the most likely mechanism for tau uptake. This process begins when aggregated proteins bind to HSPGs, a family of core proteins with cell-surface glycosaminoglycan polysaccharides. Interestingly, the internalization process is only initiated by aggregated species, not by monomeric tau (Holmes et al., 2013). Another study also suggested that HSPGs can mediate exosome internalization (Christianson et al., 2013; Fuster-Matanzo et al., 2018). Before internalization via micropinocytosis, tau binds to plasma membrane HSPGs, which promotes membrane rearrangement before endocytosis (Holmes et al., 2013). Tau binding to HSPGs seems to be essential for internalization, and the 6-O-sulfation pattern on heparan sulfate sidechains is an important determinant for tau binding (Rauch et al., 2018; **Figure 4**). However, heparan-like glycosaminoglycan (GAG) mimetics can hide tau's HSPG binding site, which reduces cell-surface tau oligomer binding, uptake, and seeding (Holmes et al., 2013). HSPG-dependent macropinocytosis is instigated by small protein aggregates, and tau trimers were shown to be the smallest size able to initiate this mechanism (Mirbaha et al., 2015; Rauch et al., 2018). The results of a recent study also supported the hypothesis that different tau species could be internalized through different cellular mechanisms (Evans et al., 2018). For example, tau monomers and small oligomers are preferentially taken up by macropinocytosis, while dynamin-dependent endocytosis is the preferred route for larger aggregates. HSPGs and macropinocytosis may also play a role in the uptake of whole exosomes (Christianson et al., 2013), although exosomes are internalized because of this pathway's non-specificity. In short, endocytosis and/or pinocytosis might be favored over direct fusion to the plasma membrane as an exosome internalization route (Tian T. et al., 2013; Polanco et al., 2018). During this process, vesicles can be endocytosed by neighboring cells, which might be involved in the propagation of misfolded or aggregated tau proteins in different neurodegenerative disorders (Goedert et al., 2010; Guo and Lee, 2011). Meanwhile, micropinocytosis might be critical for pathological tau uptake both *in vitro* and *in vivo* (Holmes et al., 2013; Brunello et al., 2016), as well as the uptake of other pathologically misfolded proteins including α-synuclein, TDP-43 (Zeineddine et al., 2015), and PrP (Hooper, 2011). Tau aggregates are reportedly internalized into primary neurons, where they are trafficked anterogradely and retrogradely along axons, and then spread to connected cells (Takeda et al., 2015; Wu et al., 2016; Wang et al., 2017), thereby propagating tau pathology (Calafate et al., 2015; Wu et al., 2016;

Nobuhara et al., 2017). They can also seed the aggregation of native monomers, thereby initiating more aggregates that are then released and spread to neighboring cells (Kundel et al., 2018; Brunello et al., 2020; **Figure 4**). Recent reports found that inoculation of preformed tau fibrils into tau transgenic mice quickly induced an AD-like NFT pathology in connected brain regions (Clavaguera et al., 2013; Ahmed et al., 2014; Boluda et al., 2015). Moreover, misfolded tau proteins spread through anatomically connected neurons, presumably via trans-synaptic tau aggregate transmission (Harris et al., 2012; Liu et al., 2012). However, preformed tau aggregates can also spread by means other than synaptic connections, suggesting the existence of alternative (non-synaptic) propagation pathways (de Calignon et al., 2012; Peeraer et al., 2015).

How neurons release tau that is then transmitted to recipient neurons to instigate tau propagation remains unclear. Although synaptic connections can facilitate tau's transcellular spread, other cellular uptake routes cannot be excluded. Once internalized, tau can be located in both early and late endosomes, which links these tau species to lysosomal vesicles in a retrograde axonal pathway and provides further evidence for a transsynaptic route of transmission (Frost et al., 2009; Wu et al., 2013). Extracellular vesicles play a major role in cellular communication and the transport of pathogenic proteins related to AD (Vingtdeux et al., 2012). Notably, exosomal tau protein levels are elevated in prodromal AD (Fiandaca et al., 2015; Gibbons et al., 2019). Microglia also contribute to tauopathy progression via exosome secretion, such that microglia depletion and inhibition of exosome synthesis can dramatically suppress tau propagation *in vitro* and *in vivo* (Asai et al., 2015). Additionally, astrocytes can internalize both fibrillar and monomeric tau, implying that these cells are also be involved in tau pathology spread (Martini-Stoica et al., 2018; Perea et al., 2019). However, one study found that oligomers and short fibrils that bind to the membrane can be internalized by neuronal cells via a receptor-independent mechanism, while tau monomers, long fibrils, and long filaments cannot (Wu et al., 2013). Thus, these structures (exosomes, ectosomes, or TNTs) mediate neuron-to-neuron transfer of pathological tau protein assemblages, which is considered a fast manner of tau spread that is prion like (Abounit et al., 2016; Tardivel et al., 2016); **Figure 4**). Tau protein modifications can also affect the spread of tau pathology. Tau hyperphosphorylation can enhance spread, while partial dephosphorylation slows it (Alonso et al., 1996). This observation indicates that tau hyperphosphorylation may be a potential target to prevent tau pathology progression in AD and other tauopathies (Hu et al., 2016). Tau fibrils can propagate by incorporating unphosphorylated tau monomers that undergo conformational changes and are then hyperphosphorylated (Goedert et al., 2017). The extracellular domain of the amyloid precursor protein might be involved in tau fibril uptake into cells (Takahashi et al., 2015). It is well known that increasing Aβ42 oligomerization can activate protein kinases (including GSK-3β) that phosphorylate tau (Guo et al., 2013). Aβ aggregation can promote tau hyperphosphorylation, suggesting that Aβ might accelerate the spread of tau pathology (Pérez et al., 2018).

TOXICITY ASSOCIATED WITH THE SPREAD OF TAU PATHOLOGY

Tau is normally enriched on MTs within axons. In tauopathies, tau is hyperphosphorylated and accumulates in the somatodendritic compartment of brain cells, which is one of the pathological hallmarks of AD (Lee et al., 2001). Tau aggregates into insoluble filaments, forming NFTs (Morris et al., 2011) that are associated with cognitive deficits (Braak and Braak, 1991; Bierer et al., 1995; Plouffe et al., 2012). Tau phosphorylation, mislocalization, and conformational changes can alter Ca^{2+} homeostasis, induce dendritic spine loss, impair organelle trafficking (particularly mitochondria), and lead to cell death (Dixit et al., 2008; Zempel et al., 2010; Li et al., 2011; Spires-Jones et al., 2011). These phenotypes represent a pretangle stage, which is widely recognized as an early event in the pathological process of AD (Eckermann et al., 2007; Braak and Del Tredici, 2012). Three hypotheses have been proposed to underlie tau-mediated toxicity. First, insoluble NFTs may be toxic and lead to neuron death and cognitive dysfunction in AD; second, soluble species of misfolded, hyperphosphorylated tau may become toxic when they accumulate in inappropriate cellular compartments, whereas NFTs exert a protective effect by serving as a sink for these toxic species; and in the third view, soluble forms of pathological tau and insoluble NFTs are both toxic to cells in various ways and time scales (Kopeikina et al., 2012). We favor the third view. Neuronal transport disruption is considered an important form of tau toxicity, which is an early phenomenon and underlying cause of neurodegenerative conditions including AD (Lin and Beal, 2006; Morfini et al., 2009; Wang and Schwarz, 2009; Querfurth and LaFerla, 2010; Kopeikina et al., 2012). Recent studies have found that soluble tau species are related to synaptic or neuronal dysfunction (Berger et al., 2007; Polydoro et al., 2009; Hoover et al., 2010; Sydow et al., 2011), with results indicating that tau oligomers—but not monomers or fibrils—act as aggregation seeds in the brains of wild-type mice, leading to mitochondrial dysfunction, synaptic deficits, and memory impairment (Usenovic et al., 2015). Based on these results, the interneuronal spread of these soluble tau species might be involved in the spread of AD pathology through the brain (Braak and Del Tredici, 2012; de Calignon et al., 2012; Clavaguera et al., 2013). Furthermore, neurons can endocytose low-molecular-weight misfolded tau species (but not monomeric tau) that are transported anterogradely and retrogradely, resulting in endogenous tau pathology *in vivo*. However, they cannot endocytose fibrillar tau or brain-derived filamentous tau (Wu et al., 2013). This evidence strongly indicates that tau toxicity may be mediated by the cell-to-cell spread of trimeric and larger oligomeric forms in certain brain regions by endocytosis (Tian H. et al., 2013). Extracellular tau is neurotoxic (Gómez-Ramos et al., 2006) and contributes to the spread of AD pathology. When the extracellular level of free tau exceeds that inside the cell and reaches a critical concentration (Reynolds et al., 2005), tau protein will self-aggregate and induce extracellular toxicity. Paired-helical filament (PHF)-tau is less toxic than free tau. When tau interacts with muscarinic receptors, intracellular Ca^{2+}

levels increase due to Ca^{2+} release from intracellular stores (Gómez-Ramos et al., 2006). Tau seeds can also cause toxicity and cell death via Ca^{2+} dysregulation (Querfurth and LaFerla, 2010; Tian H. et al., 2013; Hallinan et al., 2019); altered intracellular Ca^{2+} homeostasis results in tau phosphorylation, which is related to tau pathology progression in AD (Delacourte et al., 1999). Tau phosphorylation will increase tau detachment from MTs (Avila et al., 2004), increasing free tau levels. Free tau is then released during neurodegeneration or following cell death and binds to muscarinic receptors on surrounding cells, thereby inducing muscarinic toxicity and aggravating tau toxicity and transmission (Gómez-Ramos et al., 2008). In addition, different tau forms or isomers secreted into the extracellular space via different mechanisms may play varied roles in AD pathogenesis. Certain forms of tau released through cell death or neuroactive stimulation may be non-toxic, while misfolded tau fragments or seeds (induced by Aβ, kinases, and hydrolases) exert toxic effects on the extracellular space. Secreted vesicles containing tau protein inhibit tau binding to muscarinic receptors, thus reducing neurotoxicity.

The neurodegenerative consequences of tau hyperphosphorylation include axonal transport impairment (Ittner et al., 2008), tau relocalization to the somatodendritic compartment, and synaptic loss (Di et al., 2016). Synaptic dysfunction can occur both presynaptically, where it can interfere with the transport of phosphorylated tau via synaptic vesicles (Zhou et al., 2017), and postsynaptically via the downregulation of AMPA receptors (Hoover et al., 2010). In the context of the prion hypothesis, tau assemblies that enter the cytoplasm can seed native monomer aggregation, and these species can be released and spread to neighboring cells (Clavaguera et al., 2013; Kundel et al., 2018). Under pathological conditions, aberrant posttranslational modifications such as hyperphosphorylation, truncation, deamidation, and others (Avila et al., 2004) can induce tau detachment from MTs and promote their accumulation in a free form. When neurons degenerate and die, this free tau enters the extracellular space, where it is free to diffuse in every direction (Guo and Lee, 2011; Hu et al., 2016). This is in line with the observation that neuron loss is progressive within brain areas affected by degeneration, and tau species can seed misfolding in human brains without tangles (DeVos et al., 2018). This implies that tau seeds are released from intact neurons prior to neuronal death (Pickett et al., 2017). Another possible explanation of tau pathology patterns in the brains of AD patients is that extracellular NFTs or other substances released by degenerating neurons accumulate in the extracellular space and damage nearby cells (Avila, 2006). These toxic compounds can act like extracellular Aβ peptides (Gómez-Ramos et al., 2006). Thus, both soluble tau species and insoluble NFTs may contribute to the spread of tau toxicity.

CONCLUSION AND PROSPECTS

The mechanism involved in the transcellular propagation of tau in neurodegeneration is still unclear. Studies on the molecular mechanisms underlying the release, propagation, and uptake of tau are needed; improving the ability to detect secreted tau species is also important. Future research should focus on reducing the secretion and generation of extracellular tau in a soluble or aggregated form and inhibiting cell uptake. However, tau aggregate species are diverse, and it is currently unclear if certain species prefer certain secretion pathways. It will be important to clarify whether the physiologic secretion of non-pathological tau from neurons occurs via the same or overlapping mechanisms as those for the pathologic forms. Moreover, both forms of tau secretion are connected to neuronal activity, so blocking synapse-mediated tau propagation and boosting the clearance of tau aggregates that are internalized at the synapse are equally important (Calafate et al., 2015). More attention should also be given to glial cells and the glymphatic system, which might play a role in clearing and propagating pathological protein aggregates. Inhibition of donor cell release and recipient cell uptake are also novel therapeutic directions worthy of consideration. For example, it might be possible to block exosome secretion pathways and apply tau antibodies that can act on pathological tau fragments in the extracellular space and inhibit tau aggregation on membranous structures. Recent studies have shown that anti-tau antibodies can reduce tau hyperphosphorylation and aggregation in the transgenic mouse brain (Yanamandra et al., 2013; Sankaranarayanan et al., 2015). In addition, preventing tau from binding to HSPGs precludes recombinant tau fibrils from inducing intracellular aggregation and blocks transcellular aggregate propagation. *In vivo*, the heparin mimetic F6 prevents neuronal uptake of tau fibrils injected stereotactically (Holmes et al., 2013). Moreover, microglia disseminate tau via exosome secretion, and hampering exosome synthesis significantly reduces tau propagation *in vitro* and *in vivo*, which implies that exosomes and microglia contribute to tauopathy progression. It also suggests that targeting the exosome secretion pathway could be therapeutically useful. Depleting microglia dramatically suppressed tau propagation and reduced excitability in the dentate gyrus in a mouse model of AD (Asai et al., 2015). In summary, tau release mechanics can be explored to develop new treatments for AD and other tauopathies.

AUTHOR CONTRIBUTIONS

HZ wrote the manuscript. YC and LM assisted in the manuscript writing. YW and HL assisted in ideas and modification of the manuscript. All authors contributed to the article and approved the submitted version.

FUNDING

This review was funded by the National Natural Science Foundation of China (No. 81873350), the National Science and Technology Major Project for "Essential new drug research and development" (No. 2019ZX09301114), and the National Natural Science Foundation of China (No. 81904194).

REFERENCES

Abounit, S., Wu, J., Duff, K., Victoria, G., and Zurzolo, C. (2016). Tunneling nanotubes: a possible highway in the spreading of tau and other prion-like proteins in neurodegenerative diseases. *Prion* 10, 344–351. doi: 10.1080/19336896.2016.1223003

Ahmed, Z., Cooper, J., Murray, T., Garn, K., Mcnaughton, E., Clarke, H., et al. (2014). A novel in vivo model of tau propagation with rapid and progressive neurofibrillary tangle pathology: the pattern of spread is determined by connectivity, not proximity. *Acta Neuropathol.* 127, 667–683. doi: 10.1007/s00401-014-1254-6

Al-Bassam, J., Ozer, R., Safer, D., Halpain, S., and Milligan, R. (2002). MAP2 and tau bind longitudinally along the outer ridges of microtubule protofilaments. *J. Cell Biol.* 157, 1187–1196. doi: 10.1083/jcb.200201048

Alonso, A., Grundke-Iqbal, I., and Iqbal, K. (1996). Alzheimer's disease hyperphosphorylated tau sequesters normal tau into tangles of filaments and disassembles microtubules. *Nat. Med.* 2, 783–787. doi: 10.1038/nm0796-783

Alonso, A., Grundke-Iqbal, I., Barra, H., and Iqbal, K. (1997). Abnormal phosphorylation of tau and the mechanism of Alzheimer neurofibrillary degeneration: sequestration of microtubule-associated proteins 1 and 2 and the disassembly of microtubules by the abnormal tau. *Proc. Natl. Acad. Sci. U. S. A.* 94, 298–303. doi: 10.1073/pnas.94.1.298

Asai, H., Ikezu, S., Tsunoda, S., Medalla, M., Luebke, J., Haydar, T., et al. (2015). Depletion of microglia and inhibition of exosome synthesis halt tau propagation. *Nat. Neurosci.* 18, 1584–1593. doi: 10.1038/nn.4132

Augustinack, J., Schneider, A., Mandelkow, E., and Hyman, B. (2002). Specific tau phosphorylation sites correlate with severity of neuronal cytopathology in Alzheimer's disease. *Acta Neuropathol.* 103, 26–35. doi: 10.1007/s004010100423

Avila, J. (2006). Tau phosphorylation and aggregation in Alzheimer's disease pathology. *FEBS Lett.* 580, 2922–2927. doi: 10.1016/j.febslet.2006.02.067

Avila, J., Lucas, J., Perez, M., and Hernandez, F. (2004). Role of tau protein in both physiological and pathological conditions. *Physiol. Rev.* 84, 361–384. doi: 10.1016/j.tcb.2005.02.001

Barten, D., Fanara, P., Andorfer, C., Hoque, N., Wong, P., Husted, K., et al. (2012). Hyperdynamic microtubules, cognitive deficits, and pathology are improved in tau transgenic mice with low doses of the microtubule-stabilizing agent BMS-241027. *J. Neurosci.* 32, 7137–7145. doi: 10.1523/jneurosci.0188-12.2012

Barthélemy, N., Gabelle, A., Hirtz, C., Fenaille, F., Sergeant, N., Schraen-Maschke, S., et al. (2016). Differential Mass Spectrometry Profiles of Tau Protein in the Cerebrospinal Fluid of Patients with Alzheimer's Disease, Progressive Supranuclear Palsy, and Dementia with Lewy Bodies. *J. Alzheimers Dis.* 51, 1033–1043. doi: 10.3233/jad-150962

Barton, A., Harrison, P., Najlerahim, A., Heffernan, J., Mcdonald, B., Robinson, J., et al. (1990). Increased tau messenger RNA in Alzheimer's disease hippocampus. *Am. J. Pathol.* 137, 497–502.

Baudry, M., and Bi, X. (2016). Calpain-1 and Calpain-2: the Yin and Yang of Synaptic Plasticity and Neurodegeneration. *Trends Neurosci.* 39, 235–245. doi: 10.1016/j.tins.2016.01.007

Berger, Z., Roder, H., Hanna, A., Carlson, A., Rangachari, V., Yue, M., et al. (2007). Accumulation of pathological tau species and memory loss in a conditional model of tauopathy. *J. Neurosci.* 27, 3650–3662. doi: 10.1523/jneurosci.0587-07.2007

Bierer, L., Hof, P., Purohit, D., Carlin, L., Schmeidler, J., Davis, K., et al. (1995). Neocortical neurofibrillary tangles correlate with dementia severity in Alzheimer's disease. *Arch. Neurol.* 52, 81–88. doi: 10.1001/archneur.1995.00540250089017

Boluda, S., Iba, M., Zhang, B., Raible, K., Lee, V., and Trojanowski, J. (2015). Differential induction and spread of tau pathology in young PS19 tau transgenic mice following intracerebral injections of pathological tau from Alzheimer's disease or corticobasal degeneration brains. *Acta Neuropathol.* 129, 221–237. doi: 10.1007/s00401-014-1373-0

Bondulich, M., Guo, T., Meehan, C., Manion, J., Rodriguez Martin, T., Mitchell, J., et al. (2016). Tauopathy induced by low level expression of a human brain-derived tau fragment in mice is rescued by phenylbutyrate. *Brain* 139, 2290–2306. doi: 10.1093/brain/aww137

Braak, H., and Braak, E. (1991). Neuropathological stageing of Alzheimer-related changes. *Acta Neuropathol.* 82, 239–259. doi: 10.1007/bf00308809

Braak, H., and Del Tredici, K. (2012). Alzheimer's disease: pathogenesis and prevention. *Alzheimers Dement.* 8, 227–233. doi: 10.1016/j.jalz.2012.01.011

Brandt, R., Léger, J., and Lee, G. (1995). Interaction of tau with the neural plasma membrane mediated by tau's amino-terminal projection domain. *J. Cell Biol.* 131, 1327–1340. doi: 10.1083/jcb.131.5.1327

Bright, J., Hussain, S., Dang, V., Wright, S., Cooper, B., Byun, T., et al. (2015). Human secreted tau increases amyloid-beta production. *Neurobiol. Aging* 36, 693–709. doi: 10.1016/j.neurobiolaging.2014.09.007

Brunello, C., Merezhko, M., Uronen, R., and Huttunen, H. (2020). Mechanisms of secretion and spreading of pathological tau protein. *Cell. Mol. Life Sci.* 77, 1721–1744. doi: 10.1007/s00018-019-03349-1

Brunello, C., Yan, X., and Huttunen, H. (2016). Internalized Tau sensitizes cells to stress by promoting formation and stability of stress granules. *Sci. Rep.* 6:30498. doi: 10.1038/srep30498

Calafate, S., Buist, A., Miskiewicz, K., Vijayan, V., Daneels, G., De Strooper, B., et al. (2015). Synaptic Contacts Enhance Cell-to-Cell Tau Pathology Propagation. *Cell Rep.* 11, 1176–1183. doi: 10.1016/j.celrep.2015.04.043

Chai, X., Dage, J., and Citron, M. (2012). Constitutive secretion of tau protein by an unconventional mechanism. *Neurobiol. Dis.* 48, 356–366. doi: 10.1016/j.nbd.2012.05.021

Chen, X., and Jiang, H. (2019). Tau as a potential therapeutic target for ischemic stroke. *Aging* 11, 12827–12843. doi: 10.18632/aging.102547

Chesser, A., Pritchard, S., and Johnson, G. (2013). Tau clearance mechanisms and their possible role in the pathogenesis of Alzheimer disease. *Front. Neurol.* 4:122. doi: 10.3389/fneur.2013.00122

Christianson, H., Svensson, K., Van Kuppevelt, T., Li, J., and Belting, M. (2013). Cancer cell exosomes depend on cell-surface heparan sulfate proteoglycans for their internalization and functional activity. *Proc. Natl. Acad. Sci. U. S. A.* 110, 17380–17385. doi: 10.1073/pnas.1304266110

Chung, C., Song, Y., Kim, I., Yoon, W., Ryu, B., Jo, D., et al. (2001). Proapoptotic effects of tau cleavage product generated by caspase-3. *Neurobiol. Dis.* 8, 162–172. doi: 10.1006/nbdi.2000.0335

Clavaguera, F., Akatsu, H., Fraser, G., Crowther, R., Frank, S., Hench, J., et al. (2013). Brain homogenates from human tauopathies induce tau inclusions in mouse brain. *Proc. Natl. Acad. Sci. U. S. A.* 110, 9535–9540. doi: 10.1073/pnas.1301175110

Clavaguera, F., Bolmont, T., Crowther, R., Abramowski, D., Frank, S., Probst, A., et al. (2009). Transmission and spreading of tauopathy in transgenic mouse brain. *Nat. Cell Biol.* 11, 909–913. doi: 10.1038/ncb1901

Clavaguera, F., Hench, J., Goedert, M., and Tolnay, M. (2015). Invited review: prion-like transmission and spreading of tau pathology. *Neuropathol. Appl. Neurobiol.* 41, 47–58. doi: 10.1111/nan.12197

Cohen, T., Constance, B., Hwang, A., James, M., and Yuan, C. (2016). Intrinsic Tau Acetylation Is Coupled to Auto-Proteolytic Tau Fragmentation. *PLoS One* 11:e0158470. doi: 10.1371/journal.pone.0158470

Cohen, T., Friedmann, D., Hwang, A., Marmorstein, R., and Lee, V. (2013). The microtubule-associated tau protein has intrinsic acetyltransferase activity. *Nat. Struct. Mol. Biol.* 20, 756–762. doi: 10.1038/nsmb.2555

Cook, C., Carlomagno, Y., Gendron, T., Dunmore, J., Scheffel, K., Stetler, C., et al. (2014). Acetylation of the KXGS motifs in tau is a critical determinant in modulation of tau aggregation and clearance. *Hum. Mol. Genet.* 23, 104–116. doi: 10.1093/hmg/ddt402

Corsetti, V., Amadoro, G., Gentile, A., Capsoni, S., Ciotti, M., Cencioni, M., et al. (2008). Identification of a caspase-derived N-terminal tau fragment in cellular and animal Alzheimer's disease models. *Mol. Cell. Neurosci.* 38, 381–392. doi: 10.1016/j.mcn.2008.03.011

Cras, P., Smith, M., Richey, P., Siedlak, S., Mulvihill, P., and Perry, G. (1995). Extracellular neurofibrillary tangles reflect neuronal loss and provide further evidence of extensive protein cross-linking in Alzheimer disease. *Acta Neuropathol.* 89, 291–295. doi: 10.1007/bf00309621

Croft, C., Wade, M., Kurbatskaya, K., Mastrandreas, P., Hughes, M., Phillips, E., et al. (2017). Membrane association and release of wild-type and pathological tau from organotypic brain slice cultures. *Cell Death Dis.* 8:e2671. doi: 10.1038/cddis.2017.97

de Calignon, A., Fox, L., Pitstick, R., Carlson, G., Bacskai, B., Spires-Jones, T., et al. (2010). Caspase activation precedes and leads to tangles. *Nature* 464, 1201–1204. doi: 10.1038/nature08890

de Calignon, A., Polydoro, M., Suárez-Calvet, M., William, C., Adamowicz, D., Kopeikina, K., et al. (2012). Propagation of tau pathology in a model of early Alzheimer's disease. *Neuron* 73, 685–697. doi: 10.1016/j.neuron.2011.11.033

Delacourte, A., David, J., Sergeant, N., Buée, L., Wattez, A., Vermersch, P., et al. (1999). The biochemical pathway of neurofibrillary degeneration in aging and Alzheimer's disease. *Neurology* 52, 1158–1165. doi: 10.1212/wnl.52.6.1158

DeVos, S., Corjuc, B., Oakley, D., Nobuhara, C., Bannon, R., Chase, A., et al. (2018). Synaptic Tau Seeding Precedes Tau Pathology in Human Alzheimer's Disease Brain. *Front. Neurosci.* 12:267. doi: 10.3389/fnins.2018.00267

Di, J., Cohen, L., Corbo, C., Phillips, G., El Idrissi, A., and Alonso, A. (2016). Abnormal tau induces cognitive impairment through two different mechanisms: synaptic dysfunction and neuronal loss. *Sci. Rep.* 6:20833. doi: 10.1038/srep20833

Díaz-Hernández, M., Gómez-Ramos, A., Rubio, A., Gómez-Villafuertes, R., Naranjo, J., Miras-Portugal, M., et al. (2010). Tissue-nonspecific alkaline phosphatase promotes the neurotoxicity effect of extracellular tau. *J. Biol. Chem.* 285, 32539–32548. doi: 10.1074/jbc.M110.145003

Dickey, C., Kamal, A., Lundgren, K., Klosak, N., Bailey, R., Dunmore, J., et al. (2007). The high-affinity HSP90-CHIP complex recognizes and selectively degrades phosphorylated tau client proteins. *J. Clin. Invest.* 117, 648–658. doi: 10.1172/jci29715

Dixit, R., Ross, J., Goldman, Y., and Holzbaur, E. (2008). Differential regulation of dynein and kinesin motor proteins by tau. *Science* 319, 1086–1089. doi: 10.1126/science.1152993

Dolan, P., and Johnson, G. (2010). A caspase cleaved form of tau is preferentially degraded through the autophagy pathway. *J. Biol. Chem.* 285, 21978–21987. doi: 10.1074/jbc.M110.110940

Dujardin, S., Bégard, S., Caillierez, R., Lachaud, C., Delattre, L., Carrier, S., et al. (2014a). Ectosomes: a new mechanism for non-exosomal secretion of tau protein. *PLoS One* 9:e100760. doi: 10.1371/journal.pone.0100760

Dujardin, S., Lécolle, K., Caillierez, R., Bégard, S., Zommer, N., Lachaud, C., et al. (2014b). Neuron-to-neuron wild-type Tau protein transfer through a trans-synaptic mechanism: relevance to sporadic tauopathies. *Acta Neuropathol. Commun.* 2:14. doi: 10.1186/2051-5960-2-14

Eckermann, K., Mocanu, M., Khlistunova, I., Biernat, J., Nissen, A., Hofmann, A., et al. (2007). The beta-propensity of Tau determines aggregation and synaptic loss in inducible mouse models of tauopathy. *J. Biol. Chem.* 282, 31755–31765. doi: 10.1074/jbc.M705282200

Evans, L., Wassmer, T., Fraser, G., Smith, J., Perkinton, M., Billinton, A., et al. (2018). Extracellular Monomeric and Aggregated Tau Efficiently Enter Human Neurons through Overlapping but Distinct Pathways. *Cell Rep.* 22, 3612–3624. doi: 10.1016/j.celrep.2018.03.021

Fá, M., Puzzo, D., Piacentini, R., Staniszewski, A., Zhang, H., Baltrons, M., et al. (2016). Extracellular Tau Oligomers Produce An Immediate Impairment of LTP and Memory. *Sci. Rep.* 6:19393. doi: 10.1038/srep19393

Fernández-Montoya, J., and Pérez, M. (2015). Cathepsin D in a murine model of frontotemporal dementia with Parkinsonism-linked to chromosome 17. *J. Alzheimers Dis.* 45, 1–14. doi: 10.3233/jad-140456

Fiandaca, M., Kapogiannis, D., Mapstone, M., Boxer, A., Eitan, E., Schwartz, J., et al. (2015). Identification of preclinical Alzheimer's disease by a profile of pathogenic proteins in neurally derived blood exosomes: a case-control study. *Alzheimers Dement.* 11, 600–607.e1. doi: 10.1016/j.jalz.2014.06.008

Fischer, D., Mukrasch, M., Biernat, J., Bibow, S., Blackledge, M., Griesinger, C., et al. (2009). Conformational changes specific for pseudophosphorylation at serine 262 selectively impair binding of tau to microtubules. *Biochemistry* 48, 10047–10055. doi: 10.1021/bi901090m

Fontaine, S., Zheng, D., Sabbagh, J., Martin, M., Chaput, D., Darling, A., et al. (2016). DnaJ/Hsc70 chaperone complexes control the extracellular release of neurodegenerative-associated proteins. *EMBO J.* 35, 1537–1549. doi: 10.15252/embj.201593489

Frost, B., Jacks, R., and Diamond, M. (2009). Propagation of tau misfolding from the outside to the inside of a cell. *J. Biol. Chem.* 284, 12845–12852. doi: 10.1074/jbc.M808759200

Fukutani, Y., Kobayashi, K., Nakamura, I., Watanabe, K., Isaki, K., and Cairns, N. (1995). Neurons, intracellular and extracellular neurofibrillary tangles in subdivisions of the hippocampal cortex in normal ageing and Alzheimer's disease. *Neurosci. Lett.* 200, 57–60. doi: 10.1016/0304-3940(95)12083-g

Fuster-Matanzo, A., Hernández, F., and Ávila, J. (2018). Tau Spreading Mechanisms; Implications for Dysfunctional Tauopathies. *Int. J. Mol. Sci.* 19:645. doi: 10.3390/ijms19030645

Gamblin, T., Chen, F., Zambrano, A., Abraha, A., Lagalwar, S., Guillozet, A., et al. (2003). Caspase cleavage of tau: linking amyloid and neurofibrillary tangles in Alzheimer's disease. *Proc. Natl. Acad. Sci. U. S. A.* 100, 10032–10037. doi: 10.1073/pnas.1630428100

Garcia, M., and Cleveland, D. (2001). Going new places using an old MAP: tau, microtubules and human neurodegenerative disease. *Curr. Opin. Cell Biol.* 13, 41–48. doi: 10.1016/s0955-0674(00)00172-1

García-Sierra, F., Mondragón-Rodríguez, S., and Basurto-Islas, G. (2008). Truncation of tau protein and its pathological significance in Alzheimer's disease. *J. Alzheimers Dis.* 14, 401–409. doi: 10.3233/jad-2008-14407

Garg, S., Timm, T., Mandelkow, E., Mandelkow, E., and Wang, Y. (2011). Cleavage of Tau by calpain in Alzheimer's disease: the quest for the toxic 17 kD fragment. *Neurobiol. Aging* 32, 1–14. doi: 10.1016/j.neurobiolaging.2010.09.008

Gibbons, G., Lee, V., and Trojanowski, J. (2019). Mechanisms of Cell-to-Cell Transmission of Pathological Tau: a Review. *JAMA Neurol.* 76, 101–108. doi: 10.1001/jamaneurol.2018.2505

Goedert, M. (1999). Filamentous nerve cell inclusions in neurodegenerative diseases: tauopathies and alpha-synucleinopathies. *Philos. Trans. R. Soc. Lond. B Biol. Sci.* 354, 1101–1118. doi: 10.1098/rstb.1999.0466

Goedert, M., and Spillantini, M. (2011). Pathogenesis of the tauopathies. *J. Mol. Neurosci.* 45, 425–431. doi: 10.1007/s12031-011-9593-4

Goedert, M., Clavaguera, F., and Tolnay, M. (2010). The propagation of prion-like protein inclusions in neurodegenerative diseases. *Trends Neurosci.* 33, 317–325. doi: 10.1016/j.tins.2010.04.003

Goedert, M., Eisenberg, D., and Crowther, R. (2017). Propagation of Tau Aggregates and Neurodegeneration. *Annu. Rev. Neurosci.* 40, 189–210. doi: 10.1146/annurev-neuro-072116-031153

Goedert, M., Spillantini, M., Jakes, R., Rutherford, D., and Crowther, R. (1989). Multiple isoforms of human microtubule-associated protein tau: sequences and localization in neurofibrillary tangles of Alzheimer's disease. *Neuron* 3, 519–526. doi: 10.1016/0896-6273(89)90210-9

Gómez-Ramos, A., Díaz-Hernández, M., Cuadros, R., Hernández, F., and Avila, J. (2006). Extracellular tau is toxic to neuronal cells. *FEBS Lett.* 580, 4842–4850. doi: 10.1016/j.febslet.2006.07.078

Gómez-Ramos, A., Díaz-Hernández, M., Rubio, A., Miras-Portugal, M., and Avila, J. (2008). Extracellular tau promotes intracellular calcium increase through M1 and M3 muscarinic receptors in neuronal cells. *Mol. Cell. Neurosci.* 37, 673–681. doi: 10.1016/j.mcn.2007.12.010

Guo, J., and Lee, V. (2011). Seeding of normal Tau by pathological Tau conformers drives pathogenesis of Alzheimer-like tangles. *J. Biol. Chem.* 286, 15317–15331. doi: 10.1074/jbc.M110.209296

Guo, J., Covell, D., Daniels, J., Iba, M., Stieber, A., Zhang, B., et al. (2013). Distinct α-synuclein strains differentially promote tau inclusions in neurons. *Cell* 154, 103–117. doi: 10.1016/j.cell.2013.05.057

Guo, T., Noble, W., and Hanger, D. (2017). Roles of tau protein in health and disease. *Acta Neuropathol.* 133, 665–704. doi: 10.1007/s00401-017-1707-9

Gustke, N., Trinczek, B., Biernat, J., Mandelkow, E., and Mandelkow, E. (1994). Domains of tau protein and interactions with microtubules. *Biochemistry* 33, 9511–9522. doi: 10.1021/bi00198a017

Hallinan, G., Vargas-Caballero, M., West, J., and Deinhardt, K. (2019). Tau Misfolding Efficiently Propagates between Individual Intact Hippocampal Neurons. *J. Neurosci.* 39, 9623–9632. doi: 10.1523/jneurosci.1590-19.2019

Hampel, H., Blennow, K., Shaw, L., Hoessler, Y., Zetterberg, H., and Trojanowski, J. (2010). Total and phosphorylated tau protein as biological markers of Alzheimer's disease. *Exp. Gerontol.* 45, 30–40. doi: 10.1016/j.exger.2009.10.010

Hampel, H., Teipel, S., Fuchsberger, T., Andreasen, N., Wiltfang, J., Otto, M., et al. (2004). Value of CSF beta-amyloid1-42 and tau as predictors of Alzheimer's disease in patients with mild cognitive impairment. *Mol. Psychiatry* 9, 705–710. doi: 10.1038/sj.mp.4001473

Hanger, D., Anderton, B., and Noble, W. (2009). Tau phosphorylation: the therapeutic challenge for neurodegenerative disease. *Trends Mol. Med.* 15, 112–119. doi: 10.1016/j.molmed.2009.01.003

Hanger, D., Lau, D., Phillips, E., Bondulich, M., Guo, T., Woodward, B., et al. (2014). Intracellular and extracellular roles for tau in neurodegenerative disease. *J. Alzheimers Dis.* 40, S37–S45. doi: 10.3233/jad-132054

Harris, J., Koyama, A., Maeda, S., Ho, K., Devidze, N., Dubal, D., et al. (2012). Human P301L-mutant tau expression in mouse entorhinal-hippocampal network causes tau aggregation and presynaptic pathology but no cognitive deficits. *PLoS One* 7:e45881. doi: 10.1371/journal.pone.0045881

Holmes, B., DeVos, S., Kfoury, N., Li, M., Jacks, R., Yanamandra, K., et al. (2013). Heparan sulfate proteoglycans mediate internalization and propagation of specific proteopathic seeds. *Proc. Natl. Acad. Sci. U. S. A.* 110, E3138–E3147. doi: 10.1073/pnas.1301440110

Hooper, N. (2011). Glypican-1 facilitates prion conversion in lipid rafts. *J. Neurochem.* 116, 721–725. doi: 10.1111/j.1471-4159.2010.06936.x

Hoover, B., Reed, M., Su, J., Penrod, R., Kotilinek, L., Grant, M., et al. (2010). Tau mislocalization to dendritic spines mediates synaptic dysfunction independently of neurodegeneration. *Neuron* 68, 1067–1081. doi: 10.1016/j.neuron.2010.11.030

Hu, W., Zhang, X., Tung, Y., Xie, S., Liu, F., and Iqbal, K. (2016). Hyperphosphorylation determines both the spread and the morphology of tau pathology. *Alzheimers Dement.* 12, 1066–1077. doi: 10.1016/j.jalz.2016.01.014

Iba, M., Guo, J., Mcbride, J., Zhang, B., Trojanowski, J., and Lee, V. (2013). Synthetic tau fibrils mediate transmission of neurofibrillary tangles in a transgenic mouse model of Alzheimer's-like tauopathy. *J. Neurosci.* 33, 1024–1037. doi: 10.1523/jneurosci.2642-12.2013

Ii, K., Ito, H., Kominami, E., and Hirano, A. (1993). Abnormal distribution of cathepsin proteinases and endogenous inhibitors (cystatins) in the hippocampus of patients with Alzheimer's disease, parkinsonism-dementia complex on Guam, and senile dementia and in the aged. *Virchows Arch. A Pathol. Anat. Histopathol.* 423, 185–194. doi: 10.1007/bf01614769

Iqbal, K., Flory, M., Khatoon, S., Soininen, H., Pirttila, T., Lehtovirta, M., et al. (2005). Subgroups of Alzheimer's disease based on cerebrospinal fluid molecular markers. *Ann. Neurol.* 58, 748–757. doi: 10.1002/ana.20639

Ittner, L., Fath, T., Ke, Y., Bi, M., Van Eersel, J., Li, K., et al. (2008). Parkinsonism and impaired axonal transport in a mouse model of frontotemporal dementia. *Proc. Natl. Acad. Sci. U. S. A.* 105, 15997–16002. doi: 10.1073/pnas.0808084105

Jho, Y., Zhulina, E., Kim, M., and Pincus, P. (2010). Monte carlo simulations of tau proteins: effect of phosphorylation. *Biophys. J.* 99, 2387–2397. doi: 10.1016/j.bpj.2010.06.056

Johnson, G., and Hartigan, J. (1999). Tau protein in normal and Alzheimer's disease brain: an update. *J. Alzheimers Dis.* 1, 329–351. doi: 10.3233/jad-1999-14-512

Johnson, G., and Stoothoff, W. (2004). Tau phosphorylation in neuronal cell function and dysfunction. *J. Cell Sci.* 117, 5721–5729. doi: 10.1242/jcs.01558

Jucker, M., and Walker, L. (2013). Self-propagation of pathogenic protein aggregates in neurodegenerative diseases. *Nature* 501, 45–51. doi: 10.1038/nature12481

Kanmert, D., Cantlon, A., Muratore, C., Jin, M., O'malley, T., Lee, G., et al. (2015). C-Terminally Truncated Forms of Tau, But Not Full-Length Tau or Its C-Terminal Fragments, Are Released from Neurons Independently of Cell Death. *J. Neurosci.* 35, 10851–10865. doi: 10.1523/jneurosci.0387-15.2015

Kar, S., Fan, J., Smith, M., Goedert, M., and Amos, L. (2003). Repeat motifs of tau bind to the insides of microtubules in the absence of taxol. *EMBO J.* 22, 70–77. doi: 10.1093/emboj/cdg001

Karch, C., Jeng, A., and Goate, A. (2012). Extracellular Tau levels are influenced by variability in Tau that is associated with tauopathies. *J. Biol. Chem.* 287, 42751–42762. doi: 10.1074/jbc.M112.380642

Katsinelos, T., Zeitler, M., Dimou, E., Karakatsani, A., Müller, H., Nachman, E., et al. (2018). Unconventional Secretion Mediates the Trans-cellular Spreading of Tau. *Cell Rep.* 23, 2039–2055. doi: 10.1016/j.celrep.2018.04.056

Kenessey, A., Nacharaju, P., Ko, L., and Yen, S. (1997). Degradation of tau by lysosomal enzyme cathepsin D: implication for Alzheimer neurofibrillary degeneration. *J. Neurochem.* 69, 2026–2038. doi: 10.1046/j.1471-4159.1997.69052026.x

Kfoury, N., Holmes, B., Jiang, H., Holtzman, D., and Diamond, M. (2012). Trans-cellular propagation of Tau aggregation by fibrillar species. *J. Biol. Chem.* 287, 19440–19451. doi: 10.1074/jbc.M112.346072

Kim, W., Lee, S., and Hall, G. (2010a). Secretion of human tau fragments resembling CSF-tau in Alzheimer's disease is modulated by the presence of the exon 2 insert. *FEBS Lett.* 584, 3085–3088. doi: 10.1016/j.febslet.2010.05.042

Kim, W., Lee, S., Jung, C., Ahmed, A., Lee, G., and Hall, G. (2010b). Interneuronal transfer of human tau between Lamprey central neurons in situ. *J. Alzheimers Dis.* 19, 647–664. doi: 10.3233/jad-2010-1273

Kopeikina, K., Hyman, B., and Spires-Jones, T. (2012). Soluble forms of tau are toxic in Alzheimer's disease. *Transl. Neurosci.* 3, 223–233. doi: 10.2478/s13380-012-0032-y

Kundel, F., Hong, L., Falcon, B., Mcewan, W., Michaels, T., Meisl, G., et al. (2018). Measurement of Tau Filament Fragmentation Provides Insights into Prion-like Spreading. *ACS Chem. Neurosci.* 9, 1276–1282. doi: 10.1021/acschemneuro.8b00094

Lasagna-Reeves, C., Castillo-Carranza, D., Sengupta, U., Guerrero-Munoz, M., Kiritoshi, T., Neugebauer, V., et al. (2012). Alzheimer brain-derived tau oligomers propagate pathology from endogenous tau. *Sci. Rep.* 2:700. doi: 10.1038/srep00700

Le, M., Kim, W., Lee, S., Mckee, A., and Hall, G. (2012). Multiple mechanisms of extracellular tau spreading in a non-transgenic tauopathy model. *Am. J. Neurodegener. Dis.* 1, 316–333.

Lee, G., Newman, S., Gard, D., Band, H., and Panchamoorthy, G. (1998). Tau interacts with src-family non-receptor tyrosine kinases. *J. Cell Sci.* 111, 3167–3177.

Lee, M., Lee, J., and Rubinsztein, D. (2013). Tau degradation: the ubiquitin-proteasome system versus the autophagy-lysosome system. *Prog. Neurobiol.* 105, 49–59. doi: 10.1016/j.pneurobio.2013.03.001

Lee, V., Goedert, M., and Trojanowski, J. (2001). Neurodegenerative tauopathies. *Annu. Rev. Neurosci.* 24, 1121–1159. doi: 10.1146/annurev.neuro.24.1.1121

Lewis, J., and Dickson, D. (2016). Propagation of tau pathology: hypotheses, discoveries, and yet unresolved questions from experimental and human brain studies. *Acta Neuropathol.* 131, 27–48. doi: 10.1007/s00401-015-1507-z

Li, X., Kumar, Y., Zempel, H., Mandelkow, E., Biernat, J., and Mandelkow, E. (2011). Novel diffusion barrier for axonal retention of Tau in neurons and its failure in neurodegeneration. *EMBO J.* 30, 4825–4837. doi: 10.1038/emboj.2011.376

Lin, M., and Beal, M. (2006). Mitochondrial dysfunction and oxidative stress in neurodegenerative diseases. *Nature* 443, 787–795. doi: 10.1038/nature05292

Liu, L., Drouet, V., Wu, J., Witter, M., Small, S., Clelland, C., et al. (2012). Trans-synaptic spread of tau pathology in vivo. *PLoS One* 7:e31302. doi: 10.1371/journal.pone.0031302

Liu, Y., Wei, W., Yin, J., Liu, G., Wang, Q., Cao, F., et al. (2009). Proteasome inhibition increases tau accumulation independent of phosphorylation. *Neurobiol. Aging* 30, 1949–1961. doi: 10.1016/j.neurobiolaging.2008.02.012

Maas, T., Eidenmüller, J., and Brandt, R. (2000). Interaction of tau with the neural membrane cortex is regulated by phosphorylation at sites that are modified in paired helical filaments. *J. Biol. Chem.* 275, 15733–15740. doi: 10.1074/jbc.M000389200

Martini-Stoica, H., Cole, A., Swartzlander, D., Chen, F., Wan, Y., Bajaj, L., et al. (2018). TFEB enhances astroglial uptake of extracellular tau species and reduces tau spreading. *J. Expe. Med.* 215, 2355–2377. doi: 10.1084/jem.20172158

Matsumoto, S., Motoi, Y., Ishiguro, K., Tabira, T., Kametani, F., Hasegawa, M., et al. (2015). The twenty-four KDa C-terminal tau fragment increases with aging in tauopathy mice: implications of prion-like properties. *Hum. Mol. Genet.* 24, 6403–6416. doi: 10.1093/hmg/ddv351

Min, S., Chen, X., Tracy, T., Li, Y., Zhou, Y., Wang, C., et al. (2015). Critical role of acetylation in tau-mediated neurodegeneration and cognitive deficits. *Nat. Med.* 21, 1154–1162. doi: 10.1038/nm.3951

Min, S., Cho, S., Zhou, Y., Schroeder, S., Haroutunian, V., Seeley, W., et al. (2010). Acetylation of tau inhibits its degradation and contributes to tauopathy. *Neuron* 67, 953–966. doi: 10.1016/j.neuron.2010.08.044

Mirbaha, H., Holmes, B., Sanders, D., Bieschke, J., and Diamond, M. (2015). Tau Trimers Are the Minimal Propagation Unit Spontaneously Internalized to Seed Intracellular Aggregation. *J. Biol. Chem.* 290, 14893–14903. doi: 10.1074/jbc.M115.652693

Mohamed, N., Desjardins, A., and Leclerc, N. (2017). Tau secretion is correlated to an increase of Golgi dynamics. *PLoS One* 12:e0178288. doi: 10.1371/journal.pone.0178288

Mohamed, N., Herrou, T., Plouffe, V., Piperno, N., and Leclerc, N. (2013). Spreading of tau pathology in Alzheimer's disease by cell-to-cell transmission. *Eur. J. Neurosci.* 37, 1939–1948. doi: 10.1111/ejn.12229

Mohamed, N., Plouffe, V., Rémillard-Labrosse, G., Planel, E., and Leclerc, N. (2014). Starvation and inhibition of lysosomal function increased tau secretion by primary cortical neurons. *Sci. Rep.* 4:5715. doi: 10.1038/srep05715

Morfini, G., Burns, M., Binder, L., Kanaan, N., Lapointe, N., Bosco, D., et al. (2009). Axonal transport defects in neurodegenerative diseases. *J. Neurosci.* 29, 12776–12786. doi: 10.1523/jneurosci.3463-09.2009

Morris, M., Maeda, S., Vossel, K., and Mucke, L. (2011). The many faces of tau. *Neuron* 70, 410–426. doi: 10.1016/j.neuron.2011.04.009

Nicholls, S., DeVos, S., Commins, C., Nobuhara, C., Bennett, R., Corjuc, D., et al. (2017). Characterization of TauC3 antibody and demonstration of its potential to block tau propagation. *PLoS One* 12:e0177914. doi: 10.1371/journal.pone.0177914

Nickel, W., and Rabouille, C. (2009). Mechanisms of regulated unconventional protein secretion. *Nat. Rev. Mol. Cell Biol.* 10, 148–155. doi: 10.1038/nrm2617

Nobuhara, C., DeVos, S., Commins, C., Wegmann, S., Moore, B., Roe, A., et al. (2017). Tau Antibody Targeting Pathological Species Blocks Neuronal Uptake and Interneuron Propagation of Tau in Vitro. *Am. J. Pathol.* 187, 1399–1412. doi: 10.1016/j.ajpath.2017.01.022

Park, S., and Ferreira, A. (2005). The generation of a 17 kDa neurotoxic fragment: an alternative mechanism by which tau mediates beta-amyloid-induced neurodegeneration. *J. Neurosci.* 25, 5365–5375. doi: 10.1523/jneurosci.1125-05.2005

Peeraer, E., Bottelbergs, A., Van Kolen, K., Stancu, I., Vasconcelos, B., Mahieu, M., et al. (2015). Intracerebral injection of preformed synthetic tau fibrils initiates widespread tauopathy and neuronal loss in the brains of tau transgenic mice. *Neurobiol. Dis.* 73, 83–95. doi: 10.1016/j.nbd.2014.08.032

Perea, J., López, E., Díez-Ballesteros, J., Ávila, J., Hernández, F., and Bolós, M. (2019). Extracellular Monomeric Tau Is Internalized by Astrocytes. *Front. Neurosci.* 13:442. doi: 10.3389/fnins.2019.00442

Pérez, M., Cuadros, R., Hernández, F., and Avila, J. (2016). Secretion of full-length tau or tau fragments in a cell culture model. *Neurosci. Lett.* 634, 63–69. doi: 10.1016/j.neulet.2016.09.026

Pérez, M., Medina, M., Hernández, F., and Avila, J. (2018). Secretion of full-length Tau or Tau fragments in cell culture models. Propagation of Tau in vivo and in vitro. *Biomol. Concepts* 9, 1–11. doi: 10.1515/bmc-2018-0001

Pickett, E., Henstridge, C., Allison, E., Pitstick, R., Pooler, A., Wegmann, S., et al. (2017). Spread of tau down neural circuits precedes synapse and neuronal loss in the rTgTauEC mouse model of early Alzheimer's disease. *Synapse* 71:e21965. doi: 10.1002/syn.21965

Plouffe, V., Mohamed, N., Rivest-Mcgraw, J., Bertrand, J., Lauzon, M., and Leclerc, N. (2012). Hyperphosphorylation and cleavage at D421 enhance tau secretion. *PLoS One* 7:e36873. doi: 10.1371/journal.pone.0036873

Polanco, J., Li, C., Durisic, N., Sullivan, R., and Götz, J. (2018). Exosomes taken up by neurons hijack the endosomal pathway to spread to interconnected neurons. *Acta Neuropathol. Commun.* 6:10. doi: 10.1186/s40478-018-0514-4

Polanco, J., Scicluna, B., Hill, A., and Götz, J. (2016). Extracellular Vesicles Isolated from the Brains of rTg4510 Mice Seed Tau Protein Aggregation in a Threshold-dependent Manner. *J. Biol. Chem.* 291, 12445–12466. doi: 10.1074/jbc.M115.709485

Polydoro, M., Acker, C., Duff, K., Castillo, P., and Davies, P. (2009). Age-dependent impairment of cognitive and synaptic function in the htau mouse model of tau pathology. *J. Neurosci.* 29, 10741–10749. doi: 10.1523/jneurosci.1065-09.2009

Pooler, A., Phillips, E., Lau, D., Noble, W., and Hanger, D. (2013). Physiological release of endogenous tau is stimulated by neuronal activity. *EMBO Rep.* 14, 389–394. doi: 10.1038/embor.2013.15

Querfurth, H., and LaFerla, F. (2010). Alzheimer's disease. *N. Engl. J. Med.* 362, 329–344. doi: 10.1056/NEJMra0909142

Quinn, J., Corbett, N., Kellett, K., and Hooper, N. (2018). Tau Proteolysis in the Pathogenesis of Tauopathies: neurotoxic Fragments and Novel Biomarkers. *J. Alzheimers Dis.* 63, 13–33. doi: 10.3233/jad-170959

Ramcharitar, J., Albrecht, S., Afonso, V., Kaushal, V., Bennett, D., and Leblanc, A. (2013). Cerebrospinal fluid tau cleaved by caspase-6 reflects brain levels and cognition in aging and Alzheimer disease. *J. Neuropathol. Exp. Neurol.* 72, 824–832. doi: 10.1097/NEN.0b013e3182a0a39f

Rauch, J., Chen, J., Sorum, A., Miller, G., Sharf, T., See, S., et al. (2018). Tau Internalization is Regulated by 6-O Sulfation on Heparan Sulfate Proteoglycans (HSPGs). *Sci. Rep.* 8:6382. doi: 10.1038/s41598-018-24904-z

Reynolds, C., Garwood, C., Wray, S., Price, C., Kellie, S., Perera, T., et al. (2008). Phosphorylation regulates tau interactions with Src homology 3 domains of phosphatidylinositol 3-kinase, phospholipase Cgamma1, Grb2, and Src family kinases. *J. Biol. Chem.* 283, 18177–18186. doi: 10.1074/jbc.M709715200

Reynolds, M., Berry, R., and Binder, L. (2005). Site-specific nitration differentially influences tau assembly in vitro. *Biochemistry* 44, 13997–14009. doi: 10.1021/bi051028w

Riemenschneider, M., Wagenpfeil, S., Vanderstichele, H., Otto, M., Wiltfang, J., Kretzschmar, H., et al. (2003). Phospho-tau/total tau ratio in cerebrospinal fluid discriminates Creutzfeldt-Jakob disease from other dementias. *Mol. Psychiatry* 8, 343–347. doi: 10.1038/sj.mp.4001220

Rustom, A., Saffrich, R., Markovic, I., Walther, P., and Gerdes, H. (2004). Nanotubular highways for intercellular organelle transport. *Science* 303, 1007–1010. doi: 10.1126/science.1093133

Sahara, N., Murayama, M., Higuchi, M., Suhara, T., and Takashima, A. (2014). Biochemical Distribution of Tau Protein in Synaptosomal Fraction of Transgenic Mice Expressing Human P301L Tau. *Front. Neurol.* 5:26. doi: 10.3389/fneur.2014.00026

Saman, S., Kim, W., Raya, M., Visnick, Y., Miro, S., Saman, S., et al. (2012). Exosome-associated tau is secreted in tauopathy models and is selectively phosphorylated in cerebrospinal fluid in early Alzheimer disease. *J. Biol. Chem.* 287, 3842–3849. doi: 10.1074/jbc.M111.277061

Sankaranarayanan, S., Barten, D., Vana, L., Devidze, N., Yang, L., Cadelina, G., et al. (2015). Passive immunization with phospho-tau antibodies reduces tau pathology and functional deficits in two distinct mouse tauopathy models. *PLoS One* 10:e0125614. doi: 10.1371/journal.pone.0125614

Santarella, R., Skiniotis, G., Goldie, K., Tittmann, P., Gross, H., Mandelkow, E., et al. (2004). Surface-decoration of microtubules by human tau. *J. Mol. Biol.* 339, 539–553. doi: 10.1016/j.jmb.2004.04.008

Schmitz, Y., Luccarelli, J., Kim, M., Wang, M., and Sulzer, D. (2009). Glutamate controls growth rate and branching of dopaminergic axons. *J. Neurosci.* 29, 11973–11981. doi: 10.1523/jneurosci.2927-09.2009

Sengupta, S., Horowitz, P., Karsten, S., Jackson, G., Geschwind, D., Fu, Y., et al. (2006). Degradation of tau protein by puromycin-sensitive aminopeptidase in vitro. *Biochemistry* 45, 15111–15119. doi: 10.1021/bi061830d

Shackelford, D., and Yeh, R. (1998). Dephosphorylation of tau during transient forebrain ischemia in the rat. *Mol. Chem. Neuropathol.* 34, 103–120. doi: 10.1007/bf02815073

Shafiei, S., Guerrero-Muñoz, M., and Castillo-Carranza, D. (2017). Tau Oligomers: cytotoxicity, Propagation, and Mitochondrial Damage. *Front. Aging Neurosci.* 9:83. doi: 10.3389/fnagi.2017.00083

Simón, D., García-García, E., Royo, F., Falcón-Pérez, J., and Avila, J. (2012). Proteostasis of tau. Tau overexpression results in its secretion via membrane vesicles. *FEBS Lett.* 586, 47–54. doi: 10.1016/j.febslet.2011.11.022

Sokolow, S., Henkins, K., Bilousova, T., Gonzalez, B., Vinters, H., Miller, C., et al. (2015). Pre-synaptic C-terminal truncated tau is released from cortical synapses in Alzheimer's disease. *J. Neurochem.* 133, 368–379. doi: 10.1111/jnc.12991

Sokolowski, J., Gamage, K., Heffron, D., Leblanc, A., Deppmann, C., and Mandell, J. (2014). Caspase-mediated cleavage of actin and tubulin is a common feature and sensitive marker of axonal degeneration in neural development and injury. *Acta Neuropathol. Commun.* 2:16. doi: 10.1186/2051-5960-2-16

Spires-Jones, T., Kopeikina, K., Koffie, R., de Calignon, A., and Hyman, B. (2011). Are tangles as toxic as they look? *J. Mol. Neurosci.* 45, 438–444. doi: 10.1007/s12031-011-9566-7

Swanson, E., Breckenridge, L., Mcmahon, L., Som, S., Mcconnell, I., and Bloom, G. (2017). Extracellular Tau Oligomers Induce Invasion of Endogenous Tau into the Somatodendritic Compartment and Axonal Transport Dysfunction. *J. Alzheimers Dis.* 58, 803–820. doi: 10.3233/jad-170168

Sydow, A., Van Der Jeugd, A., Zheng, F., Ahmed, T., Balschun, D., Petrova, O., et al. (2011). Tau-induced defects in synaptic plasticity, learning, and memory are reversible in transgenic mice after switching off the toxic Tau mutant. *J. Neurosci.* 31, 2511–2525. doi: 10.1523/jneurosci.5245-10.2011

Tai, H., Wang, B., Serrano-Pozo, A., Frosch, M., Spires-Jones, T., and Hyman, B. (2014). Frequent and symmetric deposition of misfolded tau oligomers within presynaptic and postsynaptic terminals in Alzheimer's disease. *Acta Neuropathol. Commun.* 2:146. doi: 10.1186/s40478-014-0146-2

Takahashi, M., Miyata, H., Kametani, F., Nonaka, T., Akiyama, H., Hisanaga, S., et al. (2015). Extracellular association of APP and tau fibrils induces intracellular aggregate formation of tau. *Acta Neuropathol.* 129, 895–907. doi: 10.1007/s00401-015-1415-2

Takeda, S., Wegmann, S., Cho, H., DeVos, S., Commins, C., Roe, A., et al. (2015). Neuronal uptake and propagation of a rare phosphorylated high-molecular-weight tau derived from Alzheimer's disease brain. *Nat. Commun.* 6:8490. doi: 10.1038/ncomms9490

Tardivel, M., Bégard, S., Bousset, L., Dujardin, S., Coens, A., Melki, R., et al. (2016). Tunneling nanotube (TNT)-mediated neuron-to neuron transfer of pathological Tau protein assemblies. *Acta Neuropathol. Commun.* 4:117. doi: 10.1186/s40478-016-0386-4

Théry, C., Ostrowski, M., and Segura, E. (2009). Membrane vesicles as conveyors of immune responses. *Nat. Rev. Immunol.* 9, 581–593. doi: 10.1038/nri2567

Tian, H., Davidowitz, E., Lopez, P., Emadi, S., Moe, J., and Sierks, M. (2013). Trimeric tau is toxic to human neuronal cells at low nanomolar concentrations. *Int. J. Cell Biol.* 2013:260787. doi: 10.1155/2013/260787

Tian, T., Zhu, Y., Hu, F., Wang, Y., Huang, N., and Xiao, Z. (2013). Dynamics of exosome internalization and trafficking. *J. Cell. Physiol.* 228, 1487–1495. doi: 10.1002/jcp.24304

Usenovic, M., Niroomand, S., Drolet, R., Yao, L., Gaspar, R., Hatcher, N., et al. (2015). Internalized Tau Oligomers Cause Neurodegeneration by Inducing Accumulation of Pathogenic Tau in Human Neurons Derived from Induced Pluripotent Stem Cells. *J. Neurosci.* 35, 14234–14250. doi: 10.1523/jneurosci.1523-15.2015

Vingtdeux, V., Sergeant, N., and Buée, L. (2012). Potential contribution of exosomes to the prion-like propagation of lesions in Alzheimer's disease. *Front. Physiol.* 3:229. doi: 10.3389/fphys.2012.00229

von Bergen, M., Barghorn, S., Biernat, J., Mandelkow, E., and Mandelkow, E. (2005). Tau aggregation is driven by a transition from random coil to beta sheet structure. *Biochim. Biophys. Acta* 1739, 158–166. doi: 10.1016/j.bbadis.2004.09.010

von Bergen, M., Friedhoff, P., Biernat, J., Heberle, J., Mandelkow, E., and Mandelkow, E. (2000). Assembly of tau protein into Alzheimer paired helical filaments depends on a local sequence motif ((306)VQIVYK(311)) forming beta structure. *Proc. Natl. Acad. Sci. U. S. A.* 97, 5129–5134. doi: 10.1073/pnas.97.10.5129

Wang, J., Gao, X., and Wang, Z. (2014). The physiology and pathology of microtubule-associated protein tau. *Essays Biochem.* 56, 111–123. doi: 10.1042/bse0560111

Wang, X., and Schwarz, T. (2009). The mechanism of Ca2+ -dependent regulation of kinesin-mediated mitochondrial motility. *Cell* 136, 163–174. doi: 10.1016/j.cell.2008.11.046

Wang, Y., and Mandelkow, E. (2016). Tau in physiology and pathology. *Nat. Rev. Neurosci.* 17, 5–21. doi: 10.1038/nrn.2015.1

Wang, Y., Balaji, V., Kaniyappan, S., Krüger, L., Irsen, S., Tepper, K., et al. (2017). The release and trans-synaptic transmission of Tau via exosomes. *Mol. Neurodegener.* 12:5. doi: 10.1186/s13024-016-0143-y

Wang, Y., Martinez-Vicente, M., Krüger, U., Kaushik, S., Wong, E., Mandelkow, E., et al. (2009). Tau fragmentation, aggregation and clearance: the dual role of lysosomal processing. *Hum. Mol. Genet.* 18, 4153–4170. doi: 10.1093/hmg/ddp367

Wegmann, S., Eftekharzadeh, B., Tepper, K., Zoltowska, K., Bennett, R., Dujardin, S., et al. (2018). Tau protein liquid-liquid phase separation can initiate tau aggregation. *EMBO J.* 37:e98049. doi: 10.15252/embj.201798049

Wu, J., Herman, M., Liu, L., Simoes, S., Acker, C., Figueroa, H., et al. (2013). Small misfolded Tau species are internalized via bulk endocytosis and anterogradely and retrogradely transported in neurons. *J. Biol. Chem.* 288, 1856–1870. doi: 10.1074/jbc.M112.394528

Wu, J., Hussaini, S., Bastille, I., Rodriguez, G., Mrejeru, A., Rilett, K., et al. (2016). Neuronal activity enhances tau propagation and tau pathology in vivo. *Nat. Neurosci.* 19, 1085–1092. doi: 10.1038/nn.4328

Yamada, K. (2017). Extracellular Tau and Its Potential Role in the Propagation of Tau Pathology. *Front. Neurosci.* 11:667. doi: 10.3389/fnins.2017.00667

Yamada, K., Cirrito, J., Stewart, F., Jiang, H., Finn, M., Holmes, B., et al. (2011). In vivo microdialysis reveals age-dependent decrease of brain interstitial fluid tau levels in P301S human tau transgenic mice. *J. Neurosci.* 31, 13110–13117. doi: 10.1523/jneurosci.2569-11.2011

Yan, X., Uronen, R., and Huttunen, H. (2020). The interaction of α-synuclein and Tau: a molecular conspiracy in neurodegeneration? *Semin. Cell Dev. Biol.* 99, 55–64. doi: 10.1016/j.semcdb.2018.05.005

Yanamandra, K., Kfoury, N., Jiang, H., Mahan, T., Ma, S., Maloney, S., et al. (2013). Anti-tau antibodies that block tau aggregate seeding in vitro markedly decrease pathology and improve cognition in vivo. *Neuron* 80, 402–414. doi: 10.1016/j.neuron.2013.07.046

Yang, L., and Ksiezak-Reding, H. (1995). Calpain-induced proteolysis of normal human tau and tau associated with paired helical filaments. *Eur. J. Biochem.* 233, 9–17. doi: 10.1111/j.1432-1033.1995.009_1.x

Yin, Y., Wang, Y., Gao, D., Ye, J., Wang, X., Fang, L., et al. (2016). Accumulation of human full-length tau induces degradation of nicotinic acetylcholine receptor α4 via activating calpain-2. *Sci. Rep.* 6:27283. doi: 10.1038/srep27283

Zeineddine, R., Pundavela, J., Corcoran, L., Stewart, E., Do-Ha, D., Bax, M., et al. (2015). SOD1 protein aggregates stimulate macropinocytosis in neurons to facilitate their propagation. *Mol. Neurodegener.* 10:57. doi: 10.1186/s13024-015-0053-4

Zempel, H., Thies, E., Mandelkow, E., and Mandelkow, E. (2010). Abeta oligomers cause localized Ca(2+) elevation, missorting of endogenous Tau into dendrites, Tau phosphorylation, and destruction of microtubules and spines. *J. Neurosci.* 30, 11938–11950. doi: 10.1523/jneurosci.2357-10.2010

Zhang, Y., Tian, Q., Zhang, Q., Zhou, X., Liu, S., and Wang, J. (2009). Hyperphosphorylation of microtubule-associated tau protein plays dual role in neurodegeneration and neuroprotection. *Pathophysiology* 16, 311–316. doi: 10.1016/j.pathophys.2009.02.003

Zhang, Z., Song, M., Liu, X., Kang, S., Kwon, I., Duong, D., et al. (2014). Cleavage of tau by asparagine endopeptidase mediates the neurofibrillary pathology in Alzheimer's disease. *Nat. Med.* 20, 1254–1262. doi: 10.1038/nm.3700

Zhao, X., Kotilinek, L., Smith, B., Hlynialuk, C., Zahs, K., Ramsden, M., et al. (2016). Caspase-2 cleavage of tau reversibly impairs memory. *Nat. Med.* 22, 1268–1276. doi: 10.1038/nm.4199

Zhao, Y., Tseng, I., Heyser, C., Rockenstein, E., Mante, M., Adame, A., et al. (2015). Appoptosin-Mediated Caspase Cleavage of Tau Contributes to Progressive Supranuclear Palsy Pathogenesis. *Neuron* 87, 963–975. doi: 10.1016/j.neuron.2015.08.020

Zhou, L., Mcinnes, J., Wierda, K., Holt, M., Herrmann, A., Jackson, R., et al. (2017). Tau association with synaptic vesicles causes presynaptic dysfunction. *Nat. Commun.* 8:15295. doi: 10.1038/ncomms15295

Conflict of Interest: The authors declare that the research was conducted in the absence of any commercial or financial relationships that could be construed as a potential conflict of interest.

Publisher's Note: All claims expressed in this article are solely those of the authors and do not necessarily represent those of their affiliated organizations, or those of the publisher, the editors and the reviewers. Any product that may be evaluated in this article, or claim that may be made by its manufacturer, is not guaranteed or endorsed by the publisher.

frontiers in Cell and Developmental Biology

ORIGINAL RESEARCH
published: 21 October 2021
doi: 10.3389/fcell.2021.733945

Clemastine Ameliorates Myelin Deficits *via* Preventing Senescence of Oligodendrocytes Precursor Cells in Alzheimer's Disease Model Mouse

Yuan-Yuan Xie[1,2,3‡], Ting-Ting Pan[1,2‡], De-en Xu[4‡], Xin Huang[1,2,3], Yong Tang[5,6†], Wenhui Huang[7†], Rui Chen[1], Li Lu[3], Hao Chi[1,2*] and Quan-Hong Ma[1,2*]*

[1] Department of Neurology and Clinical Research Center of Neurological Disease, The Second Affiliated Hospital of Soochow University, Suzhou, China, [2] Jiangsu Key Laboratory of Neuropsychiatric Diseases, Institute of Neuroscience, Soochow University, Suzhou, China, [3] Department of Anatomy, Shanxi Medical University, Taiyuan, China, [4] Wuxi No. 2 People's Hospital, Wuxi, China, [5] International Collaborative Centre on Big Science Plan for Purinergic Signaling, Chengdu University of Traditional Chinese Medicine, Chengdu, China, [6] Acupuncture and Chronobiology Key Laboratory of Sichuan Province, Chengdu, China, [7] Molecular Physiology, Center for Integrative Physiology and Molecular Medicine (CIPMM), University of Saarland, Homburg, Germany

Disrupted myelin and impaired myelin repair have been observed in the brains of patients and various mouse models of Alzheimer's disease (AD). Clemastine, an H1-antihistamine, shows the capability to induce oligodendrocyte precursor cell (OPC) differentiation and myelin formation under different neuropathological conditions featuring demyelination *via* the antagonism of M1 muscarinic receptor. In this study, we investigated if aged APPSwe/PS1dE9 mice, a model of AD, can benefit from chronic clemastine treatment. We found the treatment reduced brain amyloid-beta deposition and rescued the short-term memory deficit of the mice. The densities of OPCs, oligodendrocytes, and myelin were enhanced upon the treatment, whereas the levels of degraded MBP were reduced, a marker for degenerated myelin. In addition, we also suggest the role of clemastine in preventing OPCs from entering the state of cellular senescence, which was shown recently as an essential causal factor in AD pathogenesis. Thus, clemastine exhibits therapeutic potential in AD *via* preventing senescence of OPCs.

Keywords: clemastine, Alzheimer's disease, myelin, oligodendrocyte precursor cells, oligodendrocytes, cellular senescence

OPEN ACCESS

Edited by:
Zhifang Dong,
Chongqing Medical University, China

Reviewed by:
Mengsheng Qiu,
University of Louisville, United States
Chandrasekar Raman,
Joslin Diabetes Center and Harvard Medical School, United States

***Correspondence:**
Li Lu
luli@sxmu.edu.cn
Hao Chi
email@uni.edu
Quan-Hong Ma
maquanhong@suda.edu.cn

†ORCID:
Yong Tang
orcid.org/0000-0002-2543-066X
Wenhui Huang
orcid.org/0000-0001-9865-0375

‡*These authors have contributed equally to this work*

Specialty section:
This article was submitted to Molecular and Cellular Pathology, a section of the journal Frontiers in Cell and Developmental Biology

Received: *30 June 2021*
Accepted: *13 September 2021*
Published: *21 October 2021*

Citation:
Xie Y-Y, Pan T-T, Xu D-e, Huang X, Tang Y, Huang W, Chen R, Lu L, Chi H and Ma Q-H (2021) Clemastine Ameliorates Myelin Deficits via Preventing Senescence of Oligodendrocytes Precursor Cells in Alzheimer's Disease Model Mouse. Front. Cell Dev. Biol. 9:733945. doi: 10.3389/fcell.2021.733945

INTRODUCTION

Clemastine fumarate is a first-generation H1-antihistamine that is mainly used for relieving symptoms of allergic reactions primarily by competing with histamine to bind H1 receptors (Blazsó and Gábor, 1997). In addition to its anti-inflammatory effects, clemastine also shows antimuscarinic type-1 receptors effects. In recent years, it was also found clemastine, among other antimuscarinic compounds, can significantly induce oligodendrocyte precursor cell (OPC) differentiation and myelination (Mei et al., 2014), accelerating the remyelination process in animal models featured

by demyelination (Mei et al., 2014, 2016; Li et al., 2015; Cree et al., 2018). Furthermore, a phase 2 clinical trial on using clemastine for treating multiple sclerosis (MS) showed that remyelination could be achieved during the chronic neurodegeneration process (Green et al., 2017). These studies collectively strongly suggest clemastine is a potent stimulator of myelin formation with a good safety profile. However, the precise mechanisms of clemastine promoting remyelination are still unknown.

Substantial myelin impairment was also observed in Alzheimer's disease (AD) (Dean et al., 2017; Papuć and Rejdak, 2018). A significant reduction of ceramide synthase 2 activity, an enzyme necessary for myelin synthesis, was observed in the early stage of AD, before the appearance of neurofibrillary tangles (Couttas et al., 2016). Even for the patients suffering from amnestic mild cognitive impairment, which is considered as prodromal AD, significant myelin reduction was detected, indicating demyelination is initiated at an early stage during the pathogenesis process (Carmeli et al., 2013). Moreover, focal demyelination was also found to be associated with amyloid-beta (Aβ) plaques (Mitew et al., 2010), which further highlights the association between demyelination and AD. In the etiology of the demyelination, recent studies suggest that the senescence of OPCs is a major contributor to the demyelination for both AD and MS (Nicaise et al., 2019; Zhang et al., 2019). Albeit our understanding of the role of myelin changes in AD is still poor, as to whether it is a critical event in AD is still unclear (Papuć and Rejdak, 2018), clemastine could provide us a new way to study the impact of myelin changes in AD.

In our previous study, we found that chronic treatment of clemastine reduces brain Aβ deposition and rescues the cognitive deficits of 7-month-old APPSwe/PS1dE9 (APP/PS1) mice (Li et al., 2021). Consistent with that, another recent study also shows that chronic treatment of clemastine can improve the memory of young APP/PS1 mice and induces significant myelin formation concomitantly (Chen et al., 2021). In this study, we investigated if chronic treatment of clemastine has therapeutic effects for aged APP/PS1 mice. After 2 months of clemastine treatment for 15-month-old APP/PS1 mice, we found that the Aβ depositions in APP/PS1 mice brain is reduced, and the short-term memory is also rescued. Furthermore, clemastine shows strong protective effects for OPCs, as it spurs the proliferation and differentiation of OPCs and the myelin formation. In addition, our data also indicate that the protective effects could be attributed to its ability to prevent OPCs from entering the state of cellular senescence. Taken together, these results illustrated the therapeutic effects of clemastine for aged APP/PS1 mice, indicating clemastine potentially could provide beneficial effects for AD patients.

MATERIALS AND METHODS

Animals

APP/PS1 transgenic mice (stock number 004462) were purchased from the Jackson Laboratory and maintained by breeding with C57BL/6 mice. Male APP/PS1 transgenic mice and the age-matched wild-type (WT) mice were used in all experiments. Animal care and surgical procedures were approved by the Institutional Animal Care and Use Committee of Soochow University in accordance with international laws.

Drug Treatments

Fifteen-month-old APP/PS1 transgenic mice received a diet of standard laboratory chow supplemented with clemastine (10 mg/kg/day) (sodium salt, Tocris Bioscience) for 2 months (Li et al., 2021). The transgenic mice and the WT mice received the same chow without clemastine.

Immunoblotting

Lysates from the cortex and hippocampus were extracted in lysis buffer [50-mM Tris (pH 7.4), 150-mM sodium chloride, 1% TritonX-100, 1% sodium deoxycholate, 0.1% sodium dodecyl sulfate] containing protease and phosphatase inhibitor cocktail (Roche, Switzerland). Lysates were subjected to sodium dodecyl sulfate-polyacrylamide gel electrophoresis, then transferred to a polyvinylidene fluoride membrane (Millipore, Darmstadt, Germany). The membrane was blocked in 5% bovine serum albumin dissolved in Tris-buffered saline containing Tween 20 (TBST) (20-mM Tris-HCL pH 7.6, 150-mM sodium chloride, and 0.1% Tween 20) for 1 h at room temperature (RT) and then was incubated with the appropriate primary antibodies in 5% bovine serum albumin diluted in TBST for overnight at 4°C. The membranes were washed with TBST and incubated with horseradish peroxidase-conjugated secondary antibodies (Sigma-Aldrich, United States) for 1 h at RT. The immunoreacted proteins were visualized using ECL Western Blotting Detection Reagents (Pierce, United States). Semiquantitative analysis of band density was performed in ImageJ[1] for the protein levels measurement. A list of the primary antibodies used in this study can be found in **Supplementary Table 1**.

Immunostaining

The 17-month-old mice were anesthetized with 1% pentobarbital and perfused with phosphate-buffered saline (PBS), followed by fixation with 4% paraformaldehyde (PFA) overnight. After that, the brain tissues were dehydrated and embedded in an optimal cutting temperature compound. Coronal cryosections of hippocampal tissue and the cortex were collected. In contrast, for the cultured cells, the cells were rinsed with cold PBS before being fixed with 4% PFA for 15 min on ice. In immunostaining, the brain sections or the fixed cells were washed with PBS containing 0.5% Triton and blocked with immunostaining blocking buffer (P0102, Beyotime) for 1 h. Subsequently, the sections are incubated with primary antibodies overnight at 4°C. After rinsing in PBS, the sections are incubated with a secondary antibody for 1 h at RT. The sections are subsequently mounted with the mounting medium containing 4,6-diamidino-2-phenylindole (Vector Laboratories). Images were captured under a Leica confocal microscope LSM700.

Novel Object Recognition Test

A novel object recognition test was performed in a 40 × 40 × 40-cm open arena. The behavior of the mouse was recorded

[1] https://rsb.info.nih.gov/ij

by a camera above and analyzed in the software ANY-maze. Two identical objects were placed on opposite sides in the familiarization phase. In a 10-min time frame, the time of the mice exploring the two objects was recorded. An object preference index is then calculated, which equals the time exploring one of the identical objects/time exploring the identical object pairs × 100%. If the mice show no difference on the object preference index, then one of the objects is replaced with a novel object, and the test phase is carried out. Recognition index is calculated accordingly, which equals the time exploring novel object/(time exploring novel object + time exploring familiar object) × 100%.

Morris Water Maze Test

In the learning phase, the mice took four trials per day for six consecutive days. A different starting position was used on each trial. The duration of one trial was 90 s for the mice to find the platform. Escape latencies (time spent swimming from the start point to the target) and path length (the distance from the start point to the platform), as well as swimming speed, were recorded. The escape latencies in the following training day were analyzed (escape latency in the following day/escape latency in the first day) and labeled as a learning trend. For probe trials, the platform was removed after the last trial of the learning phase. Mice were tested 24 h later to assess memory consolidation. The time spent in the target quadrant within 60 s was recorded. The latency to the first target site was measured, and the numbers of platform-site crossovers were recorded.

Myelin Isolation

The central nervous system myelin isolation method is based on the previous publication (Erwig et al., 2019). Adult Sprague–Dawley rats were perfused with PBS, and the brain was homogenized in 0.32-M sucrose. The brain lysates were laid on 0.85-M sucrose and centrifuged at 75,000 × *g* for 30 min. The crude myelin presented at the interface was harvested and resuspended in dH_2O, then centrifuged at 75,000 × *g* for 30 min. The myelin pellet after the centrifuge is collected and washed once with ddH_2O at 12,000 × *g* for 15 min. The myelin pellet after the centrifuge was resuspended in 0.32-M sucrose, laid on 0.85-M sucrose, and centrifuged at 75,000 × *g* for 30 min. The myelin pellet was collected after the centrifuge and resuspended in ddH_2O. Centrifuged at 75,000 × *g* for 15 min, the purified myelin pellet is collected and resuspended in TBS and stored at −80°C. All the isolation procedures were carried out on ice or at 4°C during the centrifuges.

The oligodendrocyte cell line (OLN) cells were treated with the isolated myelin (10 μg/ml) for 30 min to induce cellular senescence in immunostainings or treated with the isolated myelin (30 μg/ml) for 4 h in Western blot analysis. After that, the cells were treated with 3-μM clemastine (dissolved in dimethyl sulfoxide) for 12 h. The cells treated with dimethyl sulfoxide is served as control. Then, cells were fixed in 4% PFA for 15 min on ice.

Senescence-Associated β-Galactosidase Staining

Senescence-associated β-galactosidase (SA-β-gal) staining was performed for both the fixed cells and the brain cryosections according to the manufacturer's instructions (CellEvent™ Senescence Green Detection Kit, Invitrogen), whereas the sections were subsequently subjected for immunostaining of platelet-derived growth factor-α (PDGFRα). Images were captured under a Leica confocal microscope LSM700.

Statistics Analysis

All the imaging data were processed in Image J and subsequently analyzed in SPSS 25.0 and GraphPad Prism 8.0. All the data are shown as mean ± standard error of the mean. One-way analysis of variance was used to compare the difference between multiple groups. Unpaired Student's *t*-test was used to analyze the difference between the two groups. *P*-value indicates significance, and $P < 0.05$ indicates statistical significance.

To calculate the density of OPCs and oligodendrocytes (OLs) (PDGFRα or CC1 immuno-positive cells per square millimeter), the number of the cells was quantified. Then, it is divided by the surface area of the brain section (square millimeter) to calculate the cell density. The percentage of the Aβ covering area is calculated in a similar way. The Aβ covering area is measured, and then, it is divided by the surface area of the brain section (square millimeter). To quantify the percentage of $PDGFR\alpha^+$ SA-$\beta\text{-gal}^+$ and $PDGFR\alpha^+$ $p21^+$ cells, the number of double-positive cells and the total $PDGFR\alpha^+$ cells were quantified. Then, the number of double-positive cells is divided by the total $PDGFR\alpha^+$ cells to calculate the percentage.

RESULTS

Chronic Treatment of Clemastine Rescues the Short-Term Memory Deficit of Aged APP/PS1 Mice

To investigate if the treatment of clemastine could have a therapeutic effect on aged APP/PS1 mice, clemastine was orally administrated to 15-month-old APP/PS1 mice for 2 months. We first examined the impact of clemastine treatment on cognitive functions to see if it can rescue the cognitive deficits of the 17-month-old APP/PS1 mice. To evaluate the memory of the mice, we performed both a novel object recognition test and Morris water maze. In a novel object recognition test, we confirmed that the age-matched WT mice and APP/PS1 mice treated with or without clemastine show no difference on preference index during the familiarization phase (**Figure 1A**). In contrast, in the test phase, we found that APP/PS1 mice show reduced identification index in comparison with the WT mice (**Figure 1B**), and the treatment of clemastine rescues the index value (**Figure 1B**). This result indicates that the short-term memory deficits of the aged APP/PS1 mice can be rescued by clemastine treatment. In the Morris water maze, the APP/PS1 mice display longer escape latency than the WT mice during the learning phase, indicating that the learning ability is impaired for

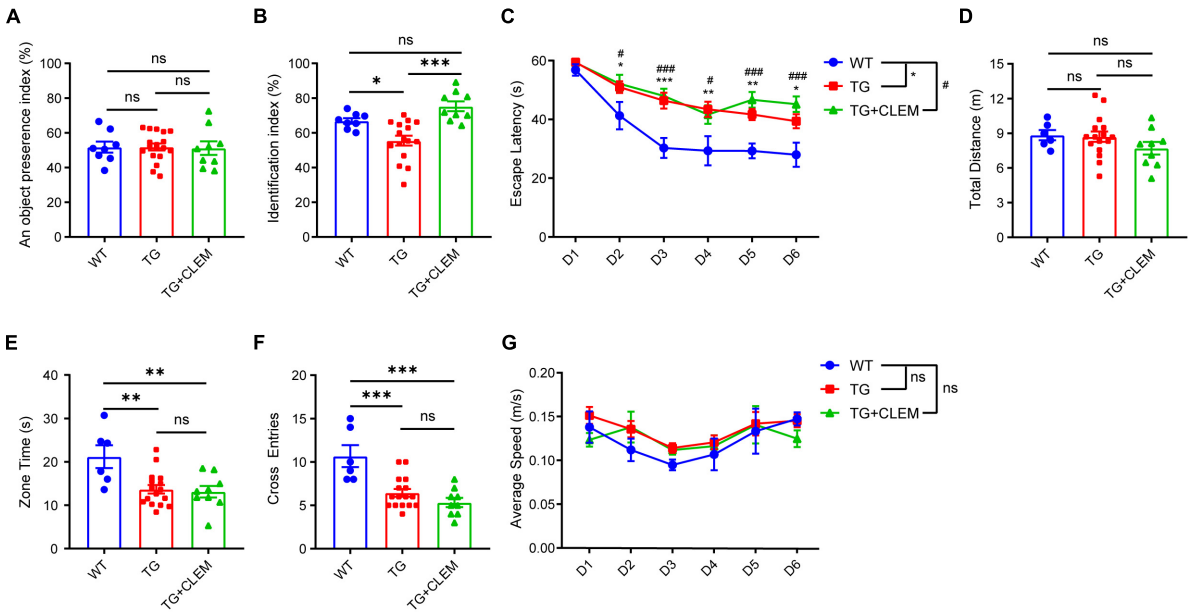

FIGURE 1 | Chronic treatment of clemastine rescues short-term memory deficit of aged APP/PS1 mice. Analyses of mice behavior in novel object recognition test **(A,B)** and Morris water maze **(C–G)**. Index of each analysis includes: **(A)** object preference index, **(B)** identification index, **(C)** escape latency, **(D)** total distance (m), **(E)** zone time and **(F)** cross entries, **(G)** average speed (m/s), should refers to Methods for detail. WT: Wild-type mice. TG: Transgenic mice (APP/PS1). TG + CLEM: Transgenic mice (APP/PS1) treated with clemastine. All tested mice were 17 months old. Values shown represent mean ± SE. $^{*\#}p < 0.05$, $^{**}p < 0.01$, $^{***\#\#\#}p < 0.001$, n = 8–17 mice per group, one-way analysis of variance with Student's t-test.

the APP/PS1 mice (**Figure 1C**). In the probe trial, despite that the swimming distance shows no differences (**Figure 1D**), the APP/PS1 mice spent a shorter time in the target quadrant and swam crossover the target site less often than the WT mice, which indicates the memory retention is impaired for the APP/PS1 mice (**Figures 1E,F**). However, the treatment of clemastine did not alter the performance of the APP/PS1 mice in the trial (**Figures 1C–F**). As all the groups showed no differences in swimming speed, the swimming ability is not a factor affecting the performances of the mice (**Figure 1G**). Together, these data suggest that clemastine treatment can rescue the short-term memory impairment but not the memory retention deficits or learning ability impairment of the aged APP/PS1 mice.

Chronic Treatment of Clemastine Ameliorates the Accumulation of Amyloid-β in the Aged APP/PS1 Mice Brain

Next, we examined the accumulation of Aβ in the brain to evaluate the brain neuropathological burden. A previous study showed that large Aβ plaques were formed in APP/PS1 mice at 10 months of age, which became even larger and covered more area at 17 months of age (Rupp et al., 2011). Consistent with the previous finding, by immunostaining against Aβ of 17-month-old APP/PS1 mice brain, we also observed that large Aβ plaques were formed in both the cortex and hippocampus (**Figure 2A**). In contrast, treatment of clemastine significantly reduced the numbers and the covering areas of Aβ plaques (**Figure 2**). For the cortex, on average, there was over a 50% reduction of the Aβ plaque numbers and the covering area of it (**Figures 2B,C**). In contrast, for the hippocampus, there was approximately 30% reduction of the Aβ plaque numbers and the covering area of it (**Figures 2D,E**). These data show that the brain neuropathological burden was greatly alleviated upon the chronic treatment of clemastine for only 2 months, even at the late stage of the disease.

Chronic Treatment of Clemastine Prevents the Loss of Oligodendrocyte Precursor Cells and Oligodendrocytes in Aged APP/PS1 Mice

To understand the mechanisms of the neurological amelioration effects of clemastine on APP/PS1 mice, we first investigated the impact of clemastine on modulating the proliferation of OPCs. By immunolabeling PDGFRα, a marker of OPCs (Li et al., 2017), we found that there was a significant decline of the PDGFRα immuno-positive($^+$) cells of the APP/PS1 mice in comparison with the WT mice in both the hippocampus and the cortex (**Figures 3A–C**), whereas the treatment of clemastine restored the number of PDGFRα$^+$ cells to the level of WT mice (**Figures 3A–C**). Consistent with that, through Western blot analysis, we also observed an increase of PDGFRα level for the APP/PS1 mice treated with clemastine (**Figures 3D–G**). Therefore, clemastine prevents the loss of OPCs in the brains of aged APP/PS1 mice. By immunolabeling differentiated OLs using the CC1 clone against adenomatous polyposis coli (Bin et al., 2016), we observed an over 50 and 30% decline of CC1$^+$ cells in

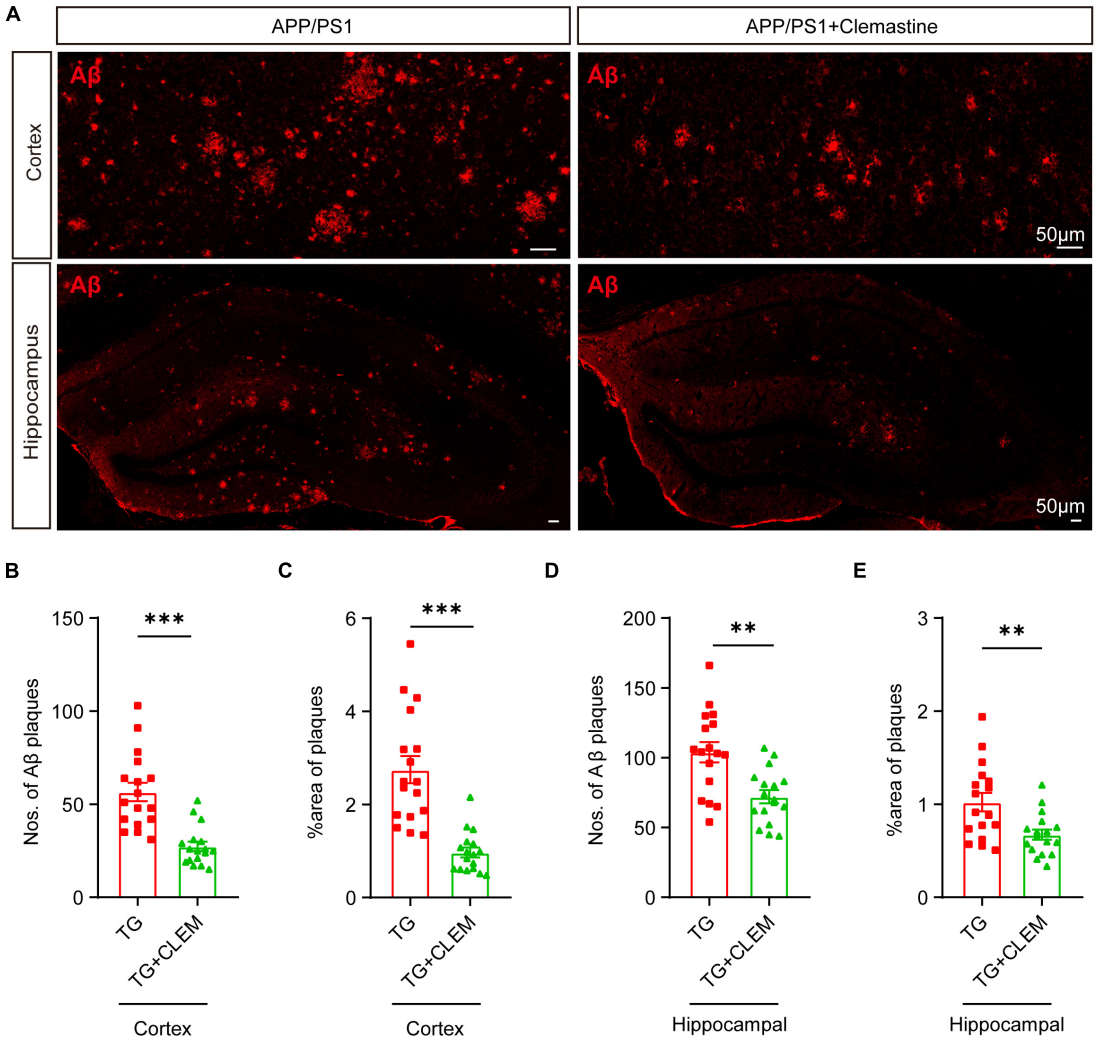

FIGURE 2 | Chronic treatment of clemastine ameliorates accumulation of Aβ in aged APP/PS1 mice brain. **(A)** Confocal images of immunolabeling of Aβ (red) in hippocampus/cortex of APP/PS1 and APP/PS1 mice treated with clemastine. **(B–E)** Quantification of numbers of Aβ plaque and percentage of Aβ plaque covering areas of hippocampus **(B,C)**/cortex **(D,E)** as shown in **(A)**. All brain sections were collected from 17-month-old mice. Values shown represent mean ± SE. $^{**}p < 0.01$, $^{***}p < 0.001$, $n = 4$ mice per group, one-way analysis of variance with Student's *t*-test.

the cortex and hippocampus, respectively, of the APP/PS1 mice in comparison with the WT mice (**Figure 4**), whereas the treatment of clemastine increased the numbers of $CC1^+$ OLs in those two regions (**Figure 4**). Thereby, the clemastine treatment prevents the loss of OPCs and OLs in the brains of the aged APP/PS1 mice.

Chronic Treatment of Clemastine Facilitates the Formation of Myelin, Preventing Its Degeneration in Aged APP/PS1 Mice

We wonder if an increase in myelin formation accompanies the increased numbers of OPCs and OLs. By immunolabeling myelin basic protein (MBP), the main protein component of myelin (Liu et al., 2021), we found that compared with the WT mice, the MBP immunofluorescence intensity was decreased for the APP/PS1 mice (**Figures 5A–C**), which was reverted by the treatment of clemastine (**Figures 5A–C**). Consistently, in Western blot analysis, we also detected the MBP protein level increased upon the treatment of clemastine (**Figures 5D–G**). Thus, the clemastine treatment induced myelin formation in the aged APP/PS1 mice. On the other hand, we evaluated myelin degeneration by immunolabeling degraded myelin basic protein complex (dMBP), which specifically reflects the degenerating myelin (Matsuo et al., 1997). A significant increase of dMBP signal was observed for the APP/PS1 mice in comparison with WT mice in the hippocampus, whereas the clemastine treatment reduced the signal of dMBP (**Figures 5H,I**), indicating the treatment that protected OL MBP from degenerating. Therefore, clemastine treatment enhanced the myelin formation and prevented its degradation in aged APP/PS1 mice.

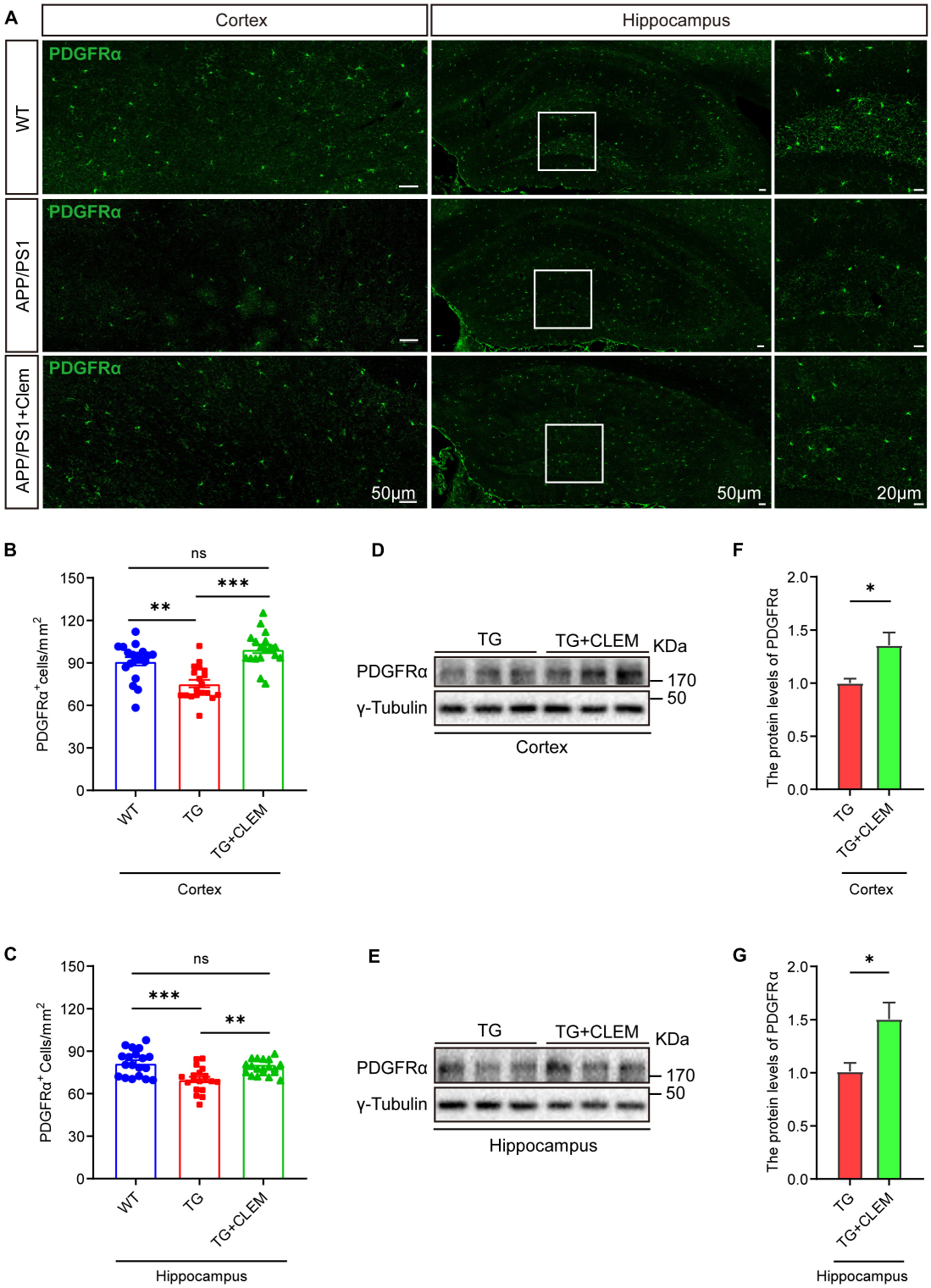

FIGURE 3 | Chronic treatment of clemastine increases number of OPCs in aged APP/PS1 mice brain. **(A)** Confocal images of immunolabeling of PDGFRα (green) in hippocampus/cortex of WT; APP/PS1 and APP/PS1 mice treated with clemastine. White box indicates magnified area of hippocampus. **(B,C)** Quantification of number of PDGFRα$^+$ cells in hippocampus **(B)** and cortex **(C),** respectively. **(D,E)** Western analysis of PDGFRα levels in hippocampus **(D)** or cortex **(E)** of APP/PS1 or APP/PS1 mice treated with clemastine; γ-tubulin was served as loading control. **(F,G)** Quantification of replicated results shown in **(D,E)**, respectively. Ratio values were calculated as "PDGFRα/γ-Tubulin" and normalized to ratio of APP/PS1 mice. Values shown represent mean ± SE. *$p < 0.05$, **$p < 0.01$, ***$p < 0.001$, $n = 4$ mice per group for **(B,C)** and $n = 3$ mice per group for **(F,G)**, one-way analysis of variance with Student's *t*-test.

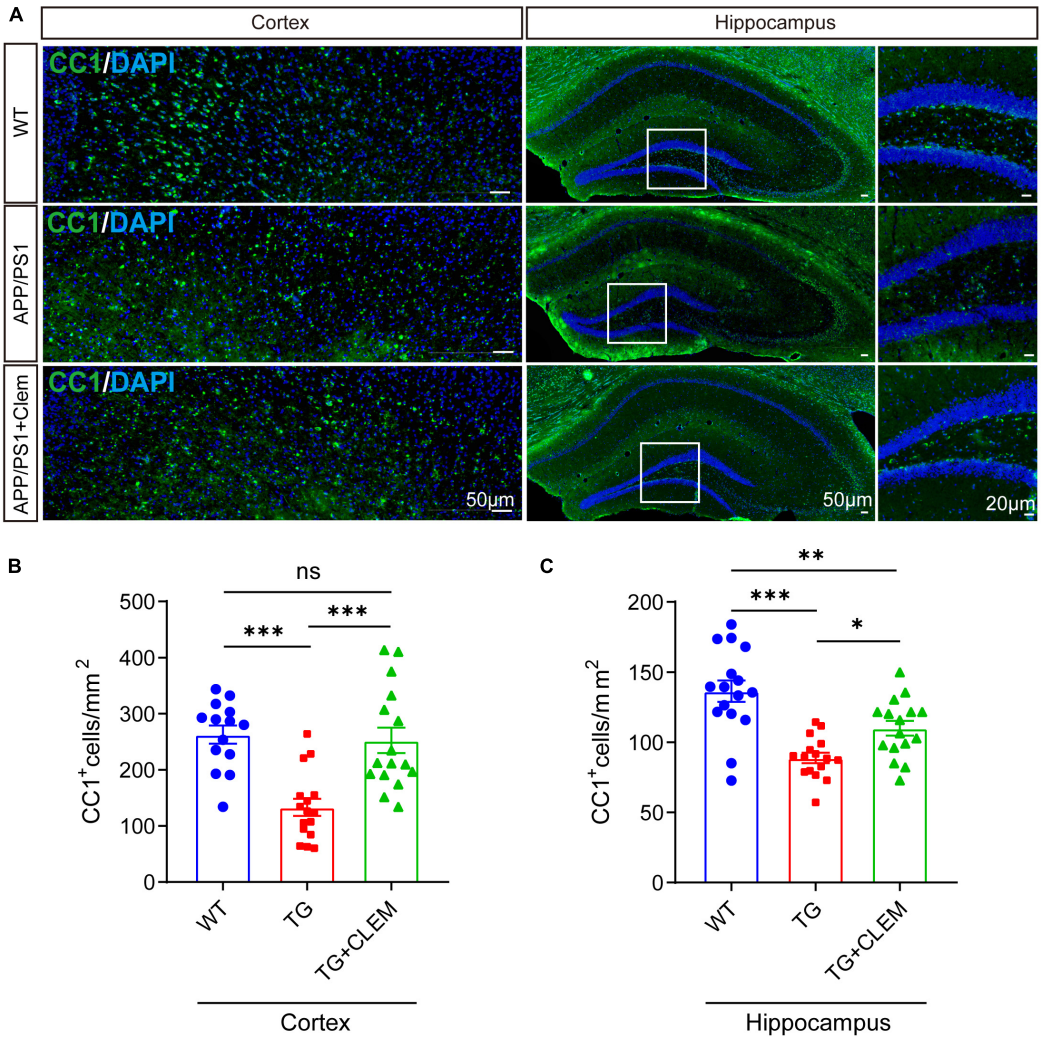

FIGURE 4 | Chronic treatment of clemastine increases number of OLs in aged APP/PS1 mice brain. **(A)** Confocal images of immunolabeling of CC1 (green) and 4,6-diamidino-2-phenylindole (blue) in hippocampus/cortex of WT; APP/PS1 and APP/PS1 mice treated with clemastine. White box indicates magnified area of hippocampus. **(B,C)** Quantification of number of $CC1^+$ cells in hippocampus **(B)** and cortex **(C)**, respectively. Values shown represent mean ± SE. $^*p < 0.05$, $^{**}p < 0.01$, $^{***}p < 0.001$, $n = 4$ mice per group, one-way analysis of variance with Student's *t*-test.

Clemastine Treatment Prevents the Senescence of Oligodendrocyte Precursor Cells

A strong correlation between Aβ plaque and the senescence of OPCs surrounding it was observed in the APP/PS1 mice (Zhang et al., 2019). Selectively removing senescent OPCs reduces the Aβ deposition and ameliorates the cognitive deficits of the mice (Zhang et al., 2019), emphasizing a causal role of senescent OPCs in AD pathogenesis. Therefore, we wonder if the therapeutic effects of clemastine on modulating Aβ deposition and cognition are mediated by preventing the senescence of the glial cells. To directly measure the effects of clemastine on cellular senescence, we used an OLN cell line derived from primary glial cells (Richter-Landsberg and Heinrich, 1996). To induce cellular senescence, we added myelin debris as an external stressor to mimic the overwhelming degradation of myelin under the pathological condition that contributes to the senescence of glial cells (Safaiyan et al., 2016). Also, we measured the activity of the lysosomal enzyme β-galactosidase and the expression of p21, two markers of cellular senescence to detect the senescent cells (Lee et al., 2006; Jurk et al., 2012). The myelin debris induced OLN senescence, as high levels of β-galactosidase activity ($SA\text{-}\beta\text{-}gal^+$) and the accumulation of p21 ($p21^+$) were detected in a portion of the cells (**Figures 6A–D**). Interestingly, the treatment of clemastine significantly reduced both the number of $SA\text{-}\beta\text{-}gal^+$ cells (**Figures 6A,C**) and $p21^+$ cells (**Figures 6B,D**) to a basal level comparable with the non-treated control cells. Thus, clemastine can prevent the senescence of glial cells.

Previously, we reported clemastine enhances autophagy while suppressing the mTOR pathway *in vitro* and *in vivo* (Li et al., 2021), both of which exhibit strong interplay with cellular

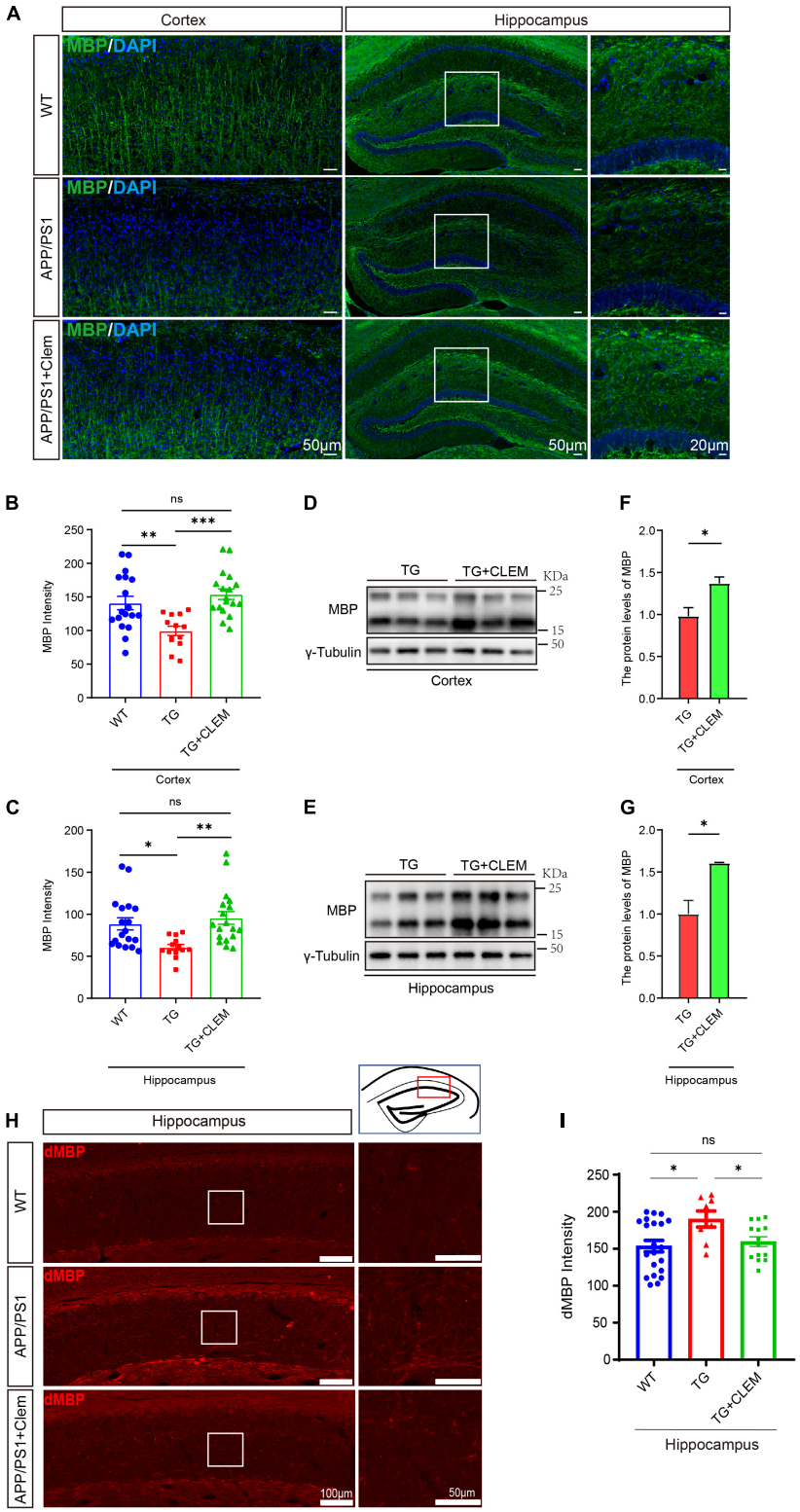

FIGURE 5 | Chronic treatment of clemastine enhances myelin formation in aged APP/PS1 mice brain. **(A)** Confocal images of immunolabeling MBP (green) in hippocampus/cortex of WT; APP/PS1 and APP/PS1 mice treated with clemastine. **(B,C)** Quantification of MBP signal intensity in cortex **(B)** or hippocampus **(C)** from immunostaining. **(D,E)** Western analysis of MBP levels in cortex **(D)** or hippocampus **(E)** of APP/PS1 or APP/PS1 mice treated with clemastine; γ-tubulin was served as loading control. **(F,G)** Quantification of replicated results shown in **(D,E)**, respectively. **(H)** Confocal images of immunolabeling dMBP in hippocampus of WT; APP/PS1 and APP/PS1 mice treated with clemastine. White box indicates magnified area of hippocampus. **(I)** Quantification of dMBP signal intensity shown in **(H)**. Values shown represent mean ± SE. $^{*}p < 0.05$, $^{**}p < 0.01$, $^{***}p < 0.001$, $n = 4$ mice per group for **(B,C,H)** and $n = 3$ mice per group for **(F,G)**, one-way analysis of variance with Student's *t*-test.

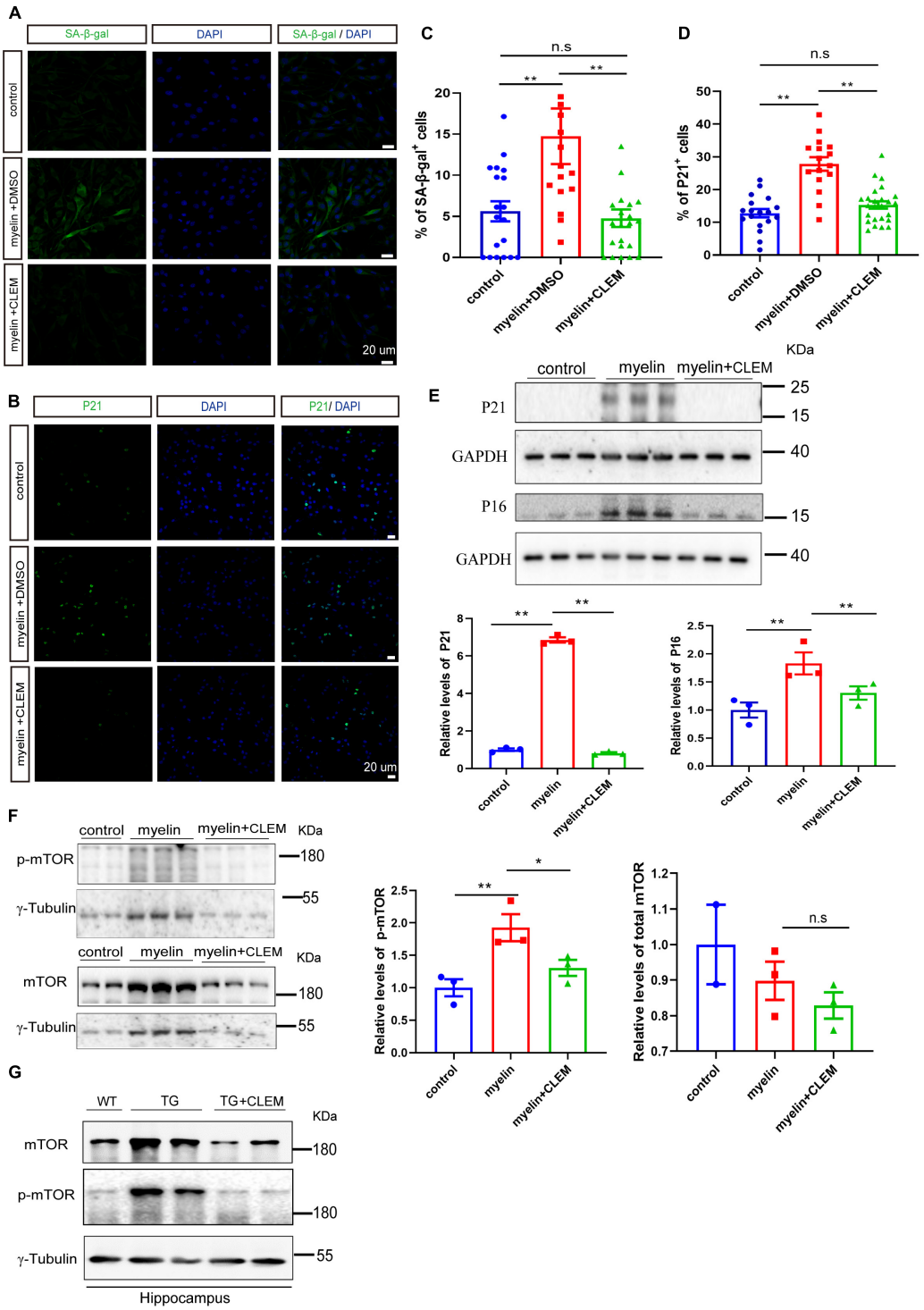

FIGURE 6 | Clemastine treatment prevents senescence of cultured glial cells. **(A,B)** Confocal images of immunolabeling OLN cells with SA-β-gal **(A)** or p21 **(B)** (green) and 4,6-diamidino-2-phenylindole (blue). Cells were either non-treated (control) or treated with myelin and dimethyl sulfoxide (myelin) or treated with myelin and clemastine (myelin + CLEM). **(C,D)** Quantification of numbers of SA-β-gal^{+} cells **(A)** and numbers of p21^{+} cells **(B)**; values shown are mean ± SE from three experiments. $^{**}p < 0.01$, one-way analysis of variance with Student's *t*-test. **(E,F)** Western analysis of protein levels of p16 and p21 **(E)**, mTOR and p-mTOR **(F)** of cells treated with myelin and dimethyl sulfoxide (myelin), or myelin with clemastine (myelin + CLEM) or non-treated (control). GAPDH and γ-tubulin were served as loading controls for **(E,F)**, respectively. Ratio values were calculated as "p16 or p21/GAPDH," "mTOR or p-mTOR/γ-tubulin," and normalized to ratio of control. Values shown represent mean ± SE. $^{*}p < 0.05$, $^{**}p < 0.01$, $n = 3$. **(G)** Western analysis of protein levels of mTOR and p-mTOR in hippocampus of WT; APP/PS1 and APP/PS1 mice treated with clemastine; γ-tubulin was served as loading control.

senescence (Kang et al., 2011; Kwon et al., 2017; Park et al., 2020). Especially, suppression of mTOR plays pivotal roles in preventing cellular senescence in a way either dependent or independent autophagy (Carroll and Korolchuk, 2017; Carroll et al., 2017; Park et al., 2020). Thus, we further examined whether clemastine altered mTOR activity in myelin debris-treated OPCs. Through Western blot analysis, we found myelin debris treatment not only induced the upregulation of p21 and p16, the markers of cellular senescence, but also increased the levels of phosphorylated mTOR (p-mTOR, Ser2448) (**Figures 6E,F**), indicating increased mTOR activity. In contrast, the treatment of clemastine reduced the levels of both p21 and p16, as well as p-mTOR to be comparable with the control **(Figures 6E,F**). Moreover, consistent with the previous observation (Li et al., 2021),we also found that both mTOR and p-mTOR levels were increased in the hippocampus of the APP/PS1 mice, whereas the treatment of clemastine reduced the protein levels to be comparable with the WT mice **(Figure 6G**). Therefore, clemastine prevents the senescence of glial cells and the upregulation of mTOR activity concomitantly.

To further corroborate the senescence prevention effect of clemastine on OPCs, we measured the number of PDGFRα$^+$ OPCs that were positive for SA-β-gal or p21 in the hippocampus of the mice brain. In comparison with the WT mice, there was a significant increase in the percentage of PDGFRα$^+$ OPCs that was positive for SA-β-gal **(Figures 7A,C**) or p21 **(Figures 7B,D**) for the APP/PS1 mice, whereas the treatment of clemastine significantly reduced the percentage of the cells **(Figure 7**). This result indicates that the OPCs in the APP/PS1 mice were more susceptible to be senescent, whereas clemastine can effectively protect the OPCs from senescence. Together, our data suggest that clemastine prevents the senescence of OPCs in the aged APP/PS1 mice, which may contribute to the prevention of Aβ deposition in the aged APP/PS1 mice brain.

DISCUSSION

The discovery of clemastine and other compounds showing muscarinic antagonist properties can induce OPCs differentiation, and myelin formation provided new approaches to tangle with the diseases featuring demyelination, including MS (Mei et al., 2014; Abiraman et al., 2015; Apolloni et al., 2016). The encouraging results from the clinical trial of clemastine for treating MS further substantiated the possibility to enhance remyelination during the neurodegeneration process (Green et al., 2017). Comparing to MS, the degeneration process of AD is rather gradual as prominent brain pathology, and the cognitive deficits commonly appear at the later stages of the disease. In this study, by using aged APP/PS1 mice instead of young mice that were used in the previous studies (Chen et al., 2021; Li et al., 2021), we believe it recaptures the features of AD at a later stage and enables more objective evaluation for the treatment (Huang et al., 2016; Denver et al., 2018). Our finding that chronic treatment of clemastine can enhance myelin formation and prevents myelin degeneration in the aged AD mice indicates that clemastine potentially could induce remyelination process even for the patients with abundant Aβ deposition at the advanced stages.

OPCs can generate mature myelinating OLs in both gray and white matter of the central nervous system throughout life (Huang et al., 2014; Guo et al., 2021). The dynamic changes of myelin are closely associated with cognition during both development stages and the various neurodegeneration conditions (Liu et al., 2016; Papuć and Rejdak, 2018; Bai et al., 2021). Therefore, our finding that the short-term memory is improved upon clemastine treatment is likely to be a direct result of the potentiated remyelination. However, we also found that memory retention and learning ability are not improved upon the treatment, which could be attributed to that the mice are aged. Because the cognitive deficits of APP/PS1 mice begin to manifest when they are 7–8 months old (Reiserer et al., 2007), it might be too late to intervene at this late stage. Supporting evidence comes from our previous study, as we showed that the chronic treatment of clemastine could improve the memory retention and learning ability of 7-month-old APP/PS1 mice (Li et al., 2021).

The enhanced remyelination could be a result of sustained OPCs proliferation and/or enhanced differentiation. In a previous study, it was the number of OLs, but not OPCs, that was increased upon the treatment of clemastine (Liu et al., 2016). In contrast, here we show that both OLs and OPCs were increased upon the treatment. The discrepancy could be attributed to the different models used in the studies, as they used mice that underwent 2 weeks of social isolation, which does not induce the loss of OPCs (Liu et al., 2016). Moreover, a recent study found that in toxin-induced focal demyelination, the proliferation of the migrated OPCs is a requirement for them to differentiate at the lesion site (Foerster et al., 2020). Blocking the cell cycle of OPCs *in vitro* resulted in a significant compromise of the differentiation of the cells (Foerster et al., 2020). Therefore, it is possible that clemastine supports the normal cellular activities of OPCs, including proliferation and differentiation, preventing the loss of the cells rather than enhancing the cellular activities under the neurodegeneration conditions.

Previous studies showed that the effects of clemastine on promoting OPCs differentiation is at least partially due to its antimuscarinic properties (Mei et al., 2016; Chen et al., 2021). However, the downstream effects of antagonizing the receptors that lead to OPC differentiation are still unknown. On the other hand, because OPCs are more susceptible to Aβ deposition associated with cellular senescence than other types of glial cells (Zhang et al., 2019), it is likely that the senescence of OPCs represents a major impediment for them to proliferate and differentiate under the pathological condition. Although our pieces of evidence show that clemastine has a strong effect on preventing the senescence of OPCs, it indicates that clemastine supports the normal activities of OPCs by preventing its senescence.

Previously, we found that clemastine can modulate autophagy in an environment-dependent manner, as it can enhance autophagy by inhibiting mTOR in the APP/PS1 mice but not in the WT mice (Li et al., 2021). The relationship between mTOR signaling, autophagy, and cellular senescence is yet to be examined under the neurodegeneration

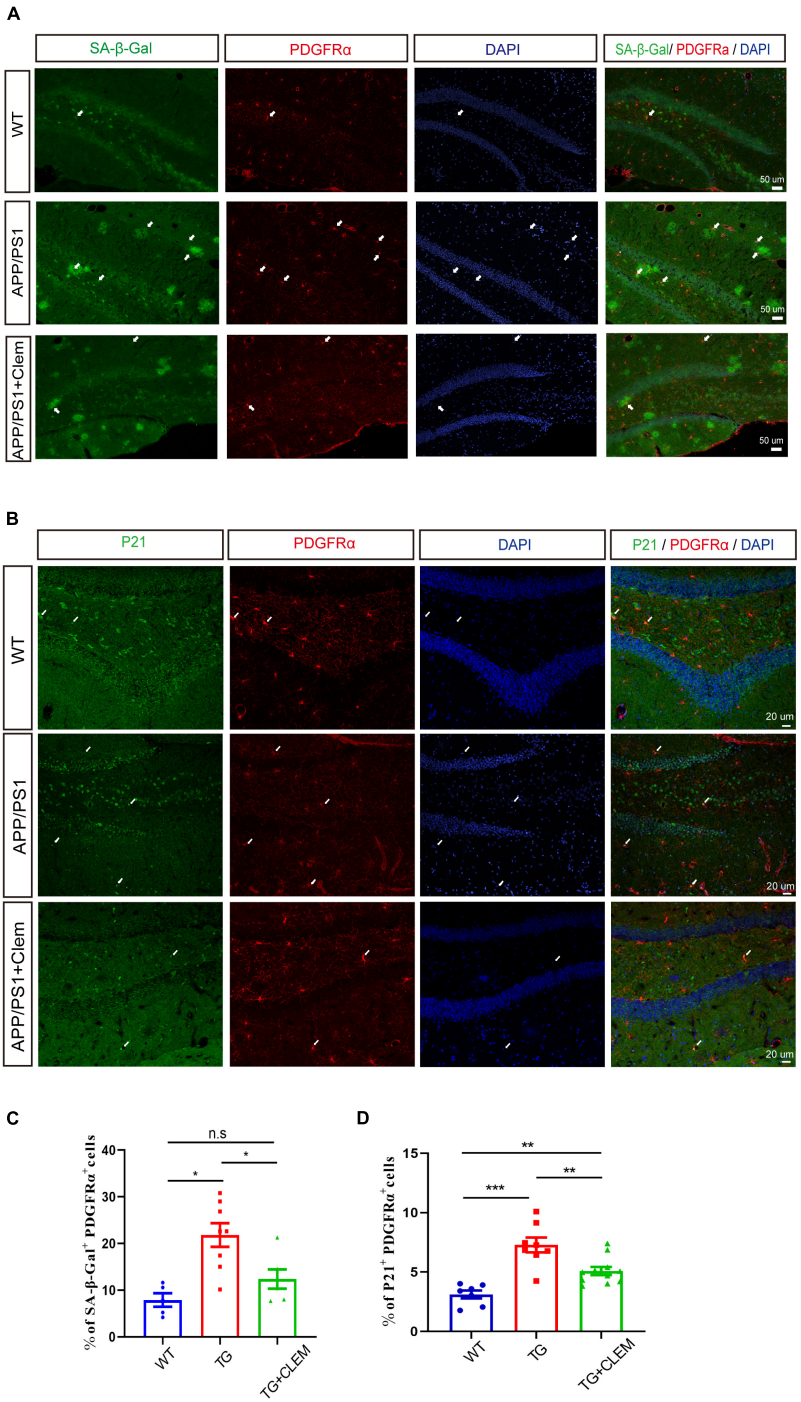

FIGURE 7 | Clemastine treatment prevents senescence of OPCs in aged APP/PS1 mice brain. **(A,B)** Confocal images of immunolabeling hippocampal OPCs with PDGFRα (red) and 4,6-diamidino-2-phenylindole (blue) and SA-β-gal **(A)** or p21 (green) **(B)** in WT; APP/PS1 and APP/PS1 mice treated with clemastine. **(C,D)** Quantification of percentage of SA-β-gal$^+$ PDGFRα$^+$ **(C)** or p21$^+$ PDGFRα$^+$ **(D)** cells. Values shown are mean ± SE. $^*p < 0.05$, $^{**}p < 0.01$, $^{***}p < 0.001$, $n = 3$ mice per group, one-way analysis of variance with Student's *t*-test.

conditions (Kwon et al., 2017; Martínez-Cué and Rueda, 2020). Nevertheless, a large body of evidence suggests that hyperactive mTOR, autophagic impairments, and cellular senescence are involved in the pathogenesis of AD (Li et al., 2010; Jahrling and Laberge, 2015; Uddin et al., 2020; Carreno et al., 2021). In contrast, our pieces of evidence further strengthened the relationship between mTOR activity and the induction of cellular senescence under pathological conditions. Thus, it is

possible that clemastine induces the upregulation of mTOR-mediated autophagy, which contributes to preventing the cellular senescence of OPCs.

Studies have shown that autophagy and cellular senescence are associated with the changes of Aβ deposition (Spilman et al., 2010; Tan et al., 2013; Zhang et al., 2019). Selectively removing the senescent OPCs alleviates the Aβ accumulation in the APP/PS1 mice (Zhang et al., 2019), and inhibiting mTOR signaling also reduces Aβ levels in another AD mice model (Spilman et al., 2010). Herein, we suggest clemastine has a combinational effect of both upregulating autophagic activities and preventing cellular senescence that results in the reduced Aβ plaques. This observation differs from a study that shows Aβ deposition was not altered upon the treatment of clemastine for the 8-month-old APP/PS1 mice (Chen et al., 2021). However, it is consistent with our previous study that shows Aβ deposition is reduced upon the chronic treatment of clemastine for 4 months of 4-month-old APP/PS1 mice (Li et al., 2021). To sum it all, our study provides a new perspective to examine the relationship between mTOR signaling, OPCs senescence, and remyelination under the neurodegeneration conditions featuring protein aggregations.

DATA AVAILABILITY STATEMENT

The original contributions presented in the study are included in the article/**Supplementary Material**, further inquiries can be directed to the corresponding author/s.

ETHICS STATEMENT

The animal study was reviewed and approved by Institutional Animal Care and Use Committee of Soochow University.

AUTHOR CONTRIBUTIONS

Y-YX, D-eX, YT, RC, LL, and Q-HM designed the study. Y-YX, T-TP, and XH performed the experiments and analyzed the data. HC drafted the manuscript. WH and Q-HM revised the manuscript. All authors contributed to the article and approved the submitted version.

FUNDING

This work was supported by the National Natural Science Foundation of China (92049120, 81870897, and 81901296), the Team Innovation Funding Program of Second Affiliated Hospital of Soochow University (XKTJTD202003), Natural the Science Foundation of Jiangsu Province (BK20181436), National Major Scientific and Technological Special Project for "Significant New Drugs Development" (2019zx09301-102), the Guangdong Key Project in "Development of new tools for diagnosis and treatment of Autism" (2018B030335001), the Suzhou Clinical Research Center of Neurological Disease (Szzx201503), the Translational Medicine Fund of WuXi Municipal Health Commission (ZM010), the Priority Academic Program Development of Jiangsu Higher Education Institution (PAPD), the Jiangsu Provincial Medical Key Discipline Project (ZDXKB2016022), and the Jiangsu Key Laboratory of Translational Research and Therapy for Neuro-Psycho-Diseases (BM2013003).

SUPPLEMENTARY MATERIAL

The Supplementary Material for this article can be found online at: https://www.frontiersin.org/articles/10.3389/fcell.2021.733945/full#supplementary-material

REFERENCES

Abiraman, K., Pol, S. U., O'Bara, M. A., Chen, G. D., Khaku, Z. M., Wang, J., et al. (2015). Anti-muscarinic adjunct therapy accelerates functional human oligodendrocyte repair. *J. Neurosci.* 35, 3676–3688. doi: 10.1523/JNEUROSCI.3510-14.2015

Apolloni, S., Fabbrizio, P., Amadio, S., and Volonté, C. (2016). Actions of the antihistaminergic clemastine on presymptomatic SOD1-G93A mice ameliorate ALS disease progression. *J. Neuroinflammation* 13:191. doi: 10.1186/s12974-016-0658-8

Bai, X., Kirchhoff, F., and Scheller, A. (2021). Oligodendroglial GABAergic signaling: more than inhibition! *Neurosci. Bull.* 37, 1039–1050. doi: 10.1007/s12264-021-00693-w

Bin, J. M., Harris, S. N., and Kennedy, F. E. (2016). The oligodendrocyte-specific antibody 'CC1' binds Quaking 7. *J. Neurochem.* 139, 181–186. doi: 10.1111/jnc.13745

Blazsó, G., and Gábor, M. (1997). Evaluation of the anti-oedematous effects of some H1-receptor antagonists and methysergide in rats. *Pharmacol. Res.* 35, 65–71. doi: 10.1006/phrs.1996.0104

Carmeli, C., Donati, A., Antille, V., Viceic, D., Ghika, J., von Gunten, A., et al. (2013). Demyelination in mild cognitive impairment suggests progression path to Alzheimer's disease. *PLoS One* 8:e72759. doi: 10.1371/journal.pone.0072759

Carreno, G., Guiho, R., and Martinez-Barbera, J. P. (2021). Cell senescence in neuropathology: a focus on neurodegeneration and tumours. *Neuropathol. Appl. Neurobiol.* 47, 359–378. doi: 10.1111/nan.12689

Carroll, B., and Korolchuk, V. I. (2017). Dysregulation of mTORC1/autophagy axis in senescence. *Aging* 9, 1851–1852. doi: 10.18632/aging.101277

Carroll, B., Nelson, G., Rabanal-Ruiz, Y., Kucheryavenko, O., Dunhill-Turner, N. A., Chesterman, C. C., et al. (2017). Persistent mTORC1 signaling in cell senescence results from defects in amino acid and growth factor sensing. *J. Cell Biol.* 216, 1949–1957. doi: 10.1083/jcb.201610113

Chen, J. F., Liu, K., Hu, B., Li, R. R., Xin, W., Chen, H., et al. (2021). Enhancing myelin renewal reverses cognitive dysfunction in a murine model of Alzheimer's disease. *Neuron* 109, 2292–2307. doi: 10.1016/j.neuron.2021.05.012

Couttas, T. A., Kain, N., Suchowerska, A. K., Quek, L. E., Turner, N., Fath, T., et al. (2016). Loss of ceramide synthase 2 activity, necessary for myelin biosynthesis, precedes tau pathology in the cortical pathogenesis of Alzheimer's disease. *Neurobiol. Aging* 43, 89–100. doi: 10.1016/j.neurobiolaging.2016.03.027

Cree, B. A. C., Niu, J., Hoi, K. K., Zhao, C., Caganap, S. D., Henry, R. G., et al. (2018). Clemastine rescues myelination defects and promotes functional recovery in hypoxic brain injury. *Brain* 141, 85–98. doi: 10.1093/brain/awx312

Dean, D. C. III, Hurley, S. A., Kecskemeti, S. R., O'Grady, J. P., Canda, C., Davenport-Sis, N. J., et al. (2017). Association of amyloid pathology with myelin alteration in preclinical Alzheimer disease. *JAMA Neurol.* 74, 41–49. doi: 10.1001/jamaneurol.2016.3232

Denver, P., English, A., and McClean, P. L. (2018). Inflammation, insulin signaling and cognitive function in aged APP/PS1 mice. *Brain Behav. Immun.* 70, 423–434. doi: 10.1016/j.bbi.2018.03.032

Erwig, M. S., Hesse, D., Jung, R. B., Uecker, M., Kusch, K., Tenzer, S., et al. (2019). Myelin: methods for purification and proteome analysis. *Methods Mol. Biol.* 1936, 37–63. doi: 10.1007/978-1-4939-9072-6_3

Foerster, S., Neumann, B., McClain, C., Di Canio, L., Chen, C. Z., Reich, D. S., et al. (2020). Proliferation is a requirement for differentiation of oligodendrocyte progenitor cells during CNS remyelination. *BioRxiv* [Preprint] doi: 10.1101/2020.05.21.108373

Green, A. J., Gelfand, J. M., Cree, B. A., Bevan, C., Boscardin, W. J., Mei, F., et al. (2017). Clemastine fumarate as a remyelinating therapy for multiple sclerosis (ReBUILD): a randomised, controlled, double-blind, crossover trial. *Lancet* 390, 2481–2489. doi: 10.1016/S0140-6736(17)32346-2

Guo, Q., Scheller, A., and Huang, W. (2021). Progenies of NG2 glia: what do we learn from transgenic mouse models? *Neural. Regen. Res.* 16, 43–48. doi: 10.4103/1673-5374.286950

Huang, H., Nie, S., Cao, M., Marshall, C., Gao, J., Xiao, N., et al. (2016). Characterization of AD-like phenotype in aged APPSwe/PS1dE9 mice. *Age* 38, 303–322. doi: 10.1007/s11357-016-9929-7

Huang, W., Zhao, N., Bai, X., Karram, K., Trotter, J., Goebbels, S., et al. (2014). Novel NG2-CreERT2 knock-in mice demonstrate heterogeneous differentiation potential of NG2 glia during development. *Glia* 62, 896–913. doi: 10.1002/glia.22648

Jahrling, J. B., and Laberge, R. M. (2015). Age-related neurodegeneration prevention through mtor inhibition: potential mechanisms and remaining questions. *Curr. Top. Med. Chem.* 15, 2139–2151. doi: 10.2174/1568026615666150610125856

Jurk, D., Wang, C., Miwa, S., Maddick, M., Korolchuk, V., Tsolou, A., et al. (2012). Postmitotic neurons develop a p21-dependent senescence-like phenotype driven by a DNA damage response. *Aging Cell* 11, 996–1004. doi: 10.1111/j.1474-9726.2012.00870.x

Kang, H. T., Lee, K. B., Kim, S. Y., Choi, H. R., and Park, S. C. (2011). Autophagy impairment induces premature senescence in primary human fibroblasts. *PLoS One* 6:e23367. doi: 10.1371/journal.pone.0023367

Kwon, Y., Kim, J. W., Jeoung, J. A., Kim, M. S., and Kang, C. (2017). Autophagy is pro-senescence when seen in close-up, but anti-senescence in long-shot. *Mol. Cells* 40, 607–612. doi: 10.14348/molcells.2017.0151

Lee, B. Y., Han, J. A., Im, J. S., Morrone, A., Johung, K., Goodwin, E. C., et al. (2006). Senescence-associated beta-galactosidase is lysosomal beta-galactosidase. *Aging Cell* 5, 187–195. doi: 10.1111/j.1474-9726.2006.00199.x

Li, L., Zhang, X., and Le, W. (2010). Autophagy dysfunction in Alzheimer's disease. *Neurodegener. Dis.* 7, 265–271. doi: 10.1159/000276710

Li, P., Li, H. X., Jiang, H. Y., Zhu, L., Wu, H. Y., Li, J. T., et al. (2017). Expression of NG2 and platelet-derived growth factor receptor alpha in the developing neonatal rat brain. *Neural Regen. Res.* 12, 1843–1852. doi: 10.4103/1673-5374.219045

Li, Z., He, Y., Fan, S., and Sun, B. (2015). Clemastine rescues behavioral changes and enhances remyelination in the cuprizone mouse model of demyelination. *Neurosci. Bull.* 31, 617–625. doi: 10.1007/s12264-015-1555-3

Li, Z. Y., Chen, L. H., Zhao, X. Y., Chen, H., Sun, Y. Y., Lu, M. H., et al. (2021). Clemastine attenuates AD-like pathology in an AD model mouse via enhancing mTOR-mediated autophagy. *Exp. Neurol.* 342:113742. doi: 10.1016/j.expneurol.2021

Liu, J., Dupree, J. L., Gacias, M., Frawley, R., Sikder, T., Naik, P., et al. (2016). Clemastine enhances myelination in the prefrontal cortex and rescues behavioral changes in socially isolated mice. *J. Neurosci.* 36, 957–962. doi: 10.1523/JNEUROSCI.3608-15.2016

Liu, K., Yu, B., Chen, J. F., Li, R. X., Chen, L., Ren, S. Y., et al. (2021). Dicer deletion in astrocytes inhibits oligodendroglial differentiation and myelination. *Neurosci. Bull.* 37, 1135–1146. doi: 10.1007/s12264-021-00705-9

Martínez-Cué, C., and Rueda, N. (2020). Cellular senescence in neurodegenerative diseases. *Front. Cell Neurosci.* 14:16. doi: 10.3389/fncel.2020.00016

Matsuo, A., Lee, G. C., Terai, K., Takami, K., Hickey, W. F., McGeer, E. G., et al. (1997). Unmasking of an unusual myelin basic protein epitope during the process of myelin degeneration in humans: a potential mechanism for the generation of autoantigens. *Am. J. Pathol.* 150, 1253–1266.

Mei, F., Fancy, S. P. J., Shen, Y. A., Niu, J., Zhao, C., Presley, B., et al. (2014). Micropillar arrays as a high-throughput screening platform for therapeutics in multiple sclerosis. *Nat. Med.* 20, 954–960. doi: 10.1038/nm.3618

Mei, F., Lehmann-Horn, K., Shen, Y. A., Rankin, K. A., Stebbins, K. J., Lorrain, D. S., et al. (2016). Accelerated remyelination during inflammatory demyelination prevents axonal loss and improves functional recovery. *Elife* 5:e18246. doi: 10.7554/eLife.18246

Mitew, S., Kirkcaldie, M. T., Halliday, G. M., Shepherd, C. E., Vickers, J. C., and Dickson, T. C. (2010). Focal demyelination in Alzheimer's disease and transgenic mouse models. *Acta Neuropathol.* 119, 567–577. doi: 10.1007/s00401-010-0657-2

Nicaise, A. M., Wagstaff, L. J., Willis, C. M., Paisie, C., Chandok, H., Robson, P., et al. (2019). Cellular senescence in progenitor cells contributes to diminished remyelination potential in progressive multiple sclerosis. *Proc. Natl. Acad. Sci. U.S.A.* 116, 9030–9039. doi: 10.1073/pnas.1818348116

Papuć, E., and Rejdak, K. (2018). The role of myelin damage in Alzheimer's disease pathology. *Arch. Med. Sci.* 16, 345–351. doi: 10.5114/aoms.2018.76863

Park, J. H., Lee, N. K., Lim, H. J., Ji, S. T., Kim, Y. J., Jang, W. B., et al. (2020). Pharmacological inhibition of mTOR attenuates replicative cell senescence and improves cellular function via regulating the STAT3-PIM1 axis in human cardiac progenitor cells. *Exp. Mol. Med.* 52, 615–628. doi: 10.1038/s12276-020-0374-4

Reiserer, R. S., Harrison, F. E., Syverud, D. C., and McDonald, M. P. (2007). Impaired spatial learning in the APPSwe + PSEN1DeltaE9 bigenic mouse model of Alzheimer's disease. *Genes Brain Behav.* 6, 54–65. doi: 10.1111/j.1601-183X.2006.00221.x

Richter-Landsberg, C., and Heinrich, M. (1996). OLN-93: a new permanent oligodendroglia cell line derived from primary rat brain glial cultures. *J. Neurosci. Res.* 45, 161–173. doi: 10.1002/(SICI)1097-4547(19960715)45:2<161::AID-JNR8<3.0.CO;2-8

Rupp, N. J., Wegenast-Braun, B. M., Radde, R., Calhoun, M. E., and Jucker, M. (2011). Early onset amyloid lesions lead to severe neuritic abnormalities and local, but not global neuron loss in APPPS1 transgenic mice. *Neurobiol. Aging* 32, e1–e2324. doi: 10.1016/j.neurobiolaging.2010.08.014

Safaiyan, S., Kannaiyan, N., Snaidero, N., Brioschi, S., Biber, K., and Yona, S. (2016). Age-related myelin degradation burdens the clearance function of microglia during aging. *Nat. Neurosci.* 19, 995–998. doi: 10.1038/nn.4325

Spilman, P., Podlutskaya, N., Hart, M. J., Debnath, J., Gorostiza, O., Bredesen, D., et al. (2010). Inhibition of mTOR by rapamycin abolishes cognitive deficits and reduces amyloid-beta levels in a mouse model of Alzheimer's disease. *PLoS One* 5:e9979. doi: 10.1371/journal.pone.0009979

Tan, C. C., Yu, J. T., Tan, M. S., Jiang, T., Zhu, X. C., and Tan, L. (2013). Autophagy in aging and neurodegenerative diseases: implications for pathogenesis and therapy. *Neurobiol. Aging.* 35, 941–957. doi: 10.1016/j.neurobiolaging.2013.11.019

Uddin, M. S., Rahman, M. A., Kabir, M. T., Behl, T., Mathew, B., Perveen, A., et al. (2020). Multifarious roles of mTOR signaling in cognitive aging and cerebrovascular dysfunction of Alzheimer's disease. *IUBMB Life* 72, 1843–1855. doi: 10.1002/iub.2324

Zhang, P., Kishimoto, Y., Grammatikakis, L., Gottimukkala, K., Cutler, R. G., Zhang, S., et al. (2019). Senolytic therapy alleviates Aβ-associated oligodendrocyte progenitor cell senescence and cognitive deficits in an Alzheimer's disease model. *Nat. Neurosci.* 22, 719–728. doi: 10.1038/s41593-019-0372-9

Conflict of Interest: The authors declare that the research was conducted in the absence of any commercial or financial relationships that could be construed as a potential conflict of interest.

Publisher's Note: All claims expressed in this article are solely those of the authors and do not necessarily represent those of their affiliated organizations, or those of the publisher, the editors and the reviewers. Any product that may be evaluated in this article, or claim that may be made by its manufacturer, is not guaranteed or endorsed by the publisher.

frontiers in Cell and Developmental Biology

ORIGINAL RESEARCH
published: 04 January 2022
doi: 10.3389/fcell.2021.736267

PINK1 Alleviates Cognitive Impairments *via* Attenuating Pathological Tau Aggregation in a Mouse Model of Tauopathy

Xing Jun Jiang[1†], Yan Qing Wu[1†], Rong Ma[2], Yan Min Chang[1], Lu Lu Li[1], Jia Hui Zhu[1], Gong Ping Liu[3,4] and Gang Li[1*]*

[1]Department of Neurology, Union Hospital, Tongji Medical College, Huazhong University of Science and Technology, Wuhan, China, [2]Department of Pharmacology, School of Basic Medicine, Tongji Medical College, Huazhong University of Science and Technology, Wuhan, China, [3]Department of Pathophysiology, School of Basic Medicine and the Collaborative Innovation Center for Brain Science, Key Laboratory of Ministry of Education of China and Hubei Province for Neurological Disorders, Tongji Medical College, Huazhong University of Science and Technology, Wuhan, China, [4]Co-Innovation Center of Neuroregeneration, Nantong University, Nantong, China

OPEN ACCESS

Edited by:
Lei Xue,
Tongji University, China

Reviewed by:
Ranhui Duan,
Central South University, China
Shupeng Li,
Peking University, China

***Correspondence:**
Gong Ping Liu
liugp111@mail.hust.edu.cn
Gang Li
gangli2008@hotmail.com

[†]These authors have contributed equally to this work and share first authorship

Specialty section:
This article was submitted to Molecular and Cellular Pathology, a section of the journal Frontiers in Cell and Developmental Biology

Received: 05 July 2021
Accepted: 25 November 2021
Published: 04 January 2022

Citation:
Jiang XJ, Wu YQ, Ma R, Chang YM, Li LL, Zhu JH, Liu GP and Li G (2022) PINK1 Alleviates Cognitive Impairments via Attenuating Pathological Tau Aggregation in a Mouse Model of Tauopathy. Front. Cell Dev. Biol. 9:736267. doi: 10.3389/fcell.2021.736267

As a primary cause of dementia and death in older people, Alzheimer's disease (AD) has become a common problem and challenge worldwide. Abnormal accumulation of tau proteins in the brain is a hallmark pathology of AD and is closely related to the clinical progression and severity of cognitive deficits. Here, we found that overexpression of phosphatase and tensin homolog (PTEN)-induced kinase 1 (PINK1) effectively promoted the degradation of tau, thereby rescuing neuron loss, synaptic damage, and cognitive impairments in a mouse model of tauopathy with AAV-full-length human Tau (hTau) injected into the hippocampal CA1 area (hTau mice). Overexpression of PINK1 activated autophagy, and chloroquine but not MG132 reversed the PINK1-induced decrease in human Tau levels and cognitive improvement in hTau mice. Furthermore, PINK1 also ameliorated mitochondrial dysfunction induced by hTau. Taken together, our data revealed that PINK1 overexpression promoted degradation of abnormal accumulated tau *via* the autophagy–lysosome pathway, indicating that PINK1 may be a potential target for AD treatment.

Keywords: tau, PINK1, autophagy, memory, Alzheimer's disease

INTRODUCTION

Tauopathies are a group of human neurological disorders, which are pathologically characterized by abnormal accumulation of tau filaments in the brain. Among the tauopathies, Alzheimer's disease (AD) is the most studied (Tapia-Rojas et al., 2019). The main hallmarks of AD pathology are intracellular deposition of tau neurofibrillary tangles and extracellular amyloid-β (Aβ) plaques. Despite being initially considered as a pathological change driven by the toxic effects of amyloid peptide, our understanding of the role that tau plays in AD has been continuously evolving (Götz et al., 2019). Growing evidence indicates that tau pathology can also exert synergistic effects with amyloid peptide and that it correlates more closely to the progression and cognitive impairment of AD than Aβ plaques (Bejanin et al., 2017; Guo et al., 2020). Additionally, given the failure of various clinical Aβ-directed therapies, more efforts have been focused on exploring tau-targeted therapies worldwide in recent years (Congdon and Sigurdsson, 2018).

Phosphatase and tensin homolog (PTEN)-induced kinase 1 (PINK1), a serine/threonine kinase mainly localized to mitochondria, has attracted more and more attention since its mutation was identified in hereditary early-onset Parkinson's disease (PD) (Valente et al., 2004; Rasool and Trempe, 2018). PINK1 is widely distributed across multiple tissues and organs of the human body, with the brain being the region with the highest expression (Fagerberg et al., 2014). Under normal conditions, after being imported to the mitochondrial membrane, PINK1 is cleaved by mitochondrial presenilin-associated rhomboid-like (PARL) protease, after which it is transported into the cytoplasm, where it gets degraded. Upon mitochondrial depolarization, PINK1 is stabilized and activated on the mitochondrial membrane, and can initiate PINK1-Parkin dependent mitophagy (Arena and Valente, 2017). Beyond its originally perceived role as an initiator of mitophagy, PINK1 has also shown to be involved in regulating autophagy–lysosome pathway (ALP), ubiquitin–proteasome system (UPS), neurite outgrowth and neuron survival, inflammation, tumor suppression, and apoptosis (Michiorri et al., 2010; McLelland et al., 2014; Parganlija et al., 2014; Akabane et al., 2016; Arena and Valente, 2017; Sliter et al., 2018). In addition to PD, PINK1 has also been proven to exert neuroprotective effects in other neurodegenerative diseases, including Huntington's disease, amyotrophic lateral sclerosis, and AD (Khalil et al., 2015; Quinn et al., 2020; Baek et al., 2021).

Several studies have reported abnormal expression of PINK1 in patients with AD as well as in cellular and animal models of AD. Among them, most studies showed decreased levels of PINK1 in the context of AD pathology (Choi et al., 2014; Du et al., 2017; Manczak et al., 2018; Reddy et al., 2018; Fang et al., 2019; Ochi et al., 2020; Zhao et al., 2020; Liang et al., 2021), although there are also a minority of studies with opposing conclusions (Mise et al., 2017; Pakpian et al., 2020; Zheng et al., 2020). Researchers showed that the increasing expression of PINK1 lessened Aβ plaques accumulation and rescued cognitive impairments in AD mice. The underlying mechanisms probably included induction of the autophagy pathway, altering APP transcription or secretases, increasing the phagocytosis of Aβ plaques by microglia, promoting mitophagy, and improving mitochondrial function (Du et al., 2017; Fang et al., 2019; Han et al., 2020). However, the specific impact of PINK1 on tau pathology remains largely underexplored and existing relevant and targeted studies are suggestive but inadequate. A previous study showed that activation of mitophagy reduced tau levels, while PINK1 knockdown abolished this effect (Fang et al., 2019). In a different study, G309D PINK1 mutation led to a significant increase in phosphorylated tau (Ser396/404) through inhibition of GSK3β activation in cells (Ye et al., 2015). More efforts are needed to establish the precise role of PINK1 in tau pathology and its possible underlying mechanisms.

Here, using a mouse model of tauopathy injected with AAV2-full-length human TAU into the hippocampus, we showed that upregulation of PINK1 significantly alleviated the deposition of pathological tau, neuron loss, synaptic damage, and cognitive impairments in mice. This occurred through inducing tau degradation *via* ALP, reducing tau accumulation in mitochondria and ameliorating mitochondrial disorders. Taken together, our study supports that PINK1 may be a promising target for AD treatment.

MATERIALS AND METHODS

Animals

Wild-type C57BL/6J mice (male, 8–10 weeks-age, 20–25 g) were acquired from Beijing Vital River Laboratory Animal Technology Co., Ltd. Animals were randomly assigned into cages (4–5 mice per cage), under normative cultured environment: 12-h day–night cycle with freely available food and water. All animal experiments were performed according to the "Policies on the Use of Animals and Humans in Neuroscience Research" revised and approved by the Society for Neuroscience in 1995, the Guidelines for the Care and Use of Laboratory Animals of the Ministry of Science and Technology of the People's Republic of China, and the Institutional Animal Care and Use Committee at Tongji Medical College. The animal study was reviewed and approved by Ethics Committee of Tongji Medical College, Huazhong University of Science and Technology.

Stereotactic Brain Injection and Drug Administration

pAAV-SYN-human Tau-mCherry-3×FLAG-WPRE (1.30×10^{13} vg/ml), pAAV-SYN-PINK1-EGFP-3×FLAG-WPRE (1.35×10^{13} vg/ml), and corresponding vehicles pAAV-SYN-MCS-mCherry-3×FLAG (2.09×10^{13} vg/ml) and pAAV-SYN-MCS-EGFP-3×FLAG (2.84×10^{13} vg/ml) were generated by OBio Tech. Inc. (Shanghai, China). After being fixed on stereotaxic apparatus with adequate anesthesia, mice were injected with 1 μl of virus into the hippocampal CA1 area bilaterally (AP-1.94, ML ± 1.2, DV-1.6). Injection rate was maintained at 100 nl/min, and the needle syringe was kept *in situ* for an additional 10 min after the virus was fully injected. Before putting them back into cages, mice were placed on an electric blanket for revival.

Fourteen days after virus injection, mice were treated with (1) the autophagy inhibitor chloroquine (CQ) (C6628, Sigma-Aldrich) at 50 mg/kg body weight (Campos et al., 2020; Chen et al., 2020), (2) the proteasome inhibitor MG132 (M8699, Sigma-Aldrich) at 0.5 mg/kg body weight (Lu et al., 2017), or (3) the same volume of vehicle daily for 16 days *via* intraperitoneal injection.

Behavior Tests

One month after the stereotactic injection, behavioral experiments were conducted to evaluate the spatial learning and memory capabilities of the mice. The novel object recognition (NOR) test is a learning and memory evaluation method based on the principle that animals are born with a tendency to explore new things. This test was conducted as follows (Hong et al., 2020): 24 h before the test, mice were placed in the arenas (50 cm × 50 cm container)

without objects for a 5-min habituation. The next day, mice were put into the arenas (one sidewall with two identical objects A and A′ separately located on either end) for 5 min. One hour later, object A′ was replaced by a different object, object B, and then the animals were put into the arenas again and allowed to explore both objects for 5 min. A video camera above the arenas logged the experimental behavior. The time that mice spent exploring object A and object B was recorded as TA and TB, respectively. TB/(TA + TB) was set as the recognition index.

The Morris water maze (MWM) test is used to assess the learning and memory abilities of laboratory animals in the context of spatial position and orientation (Morris, 1984). It was performed as follows: during the spatial learning phase, mice were trained to find a concealed platform in a fixed position below the waterline for five consecutive days. The training time was fixed at 12:00 pm-17:00 pm. In each training session, mice were gently put into water from one of the other three quadrants (without target platform), facing the pool wall. If the platform was not sought out within 60 s, mice would be directed to the platform and made to stay in it for another 30 s. On day 7, the platform was removed, and mice were put in the water maze for 60 s to test spatial memory. The motion trails of mice were recorded and analyzed using MWZ-100 system (Techman, China).

Protein Extraction

Hippocampal regions infected with virus were isolated and mechanically homogenized in lysis buffer for Western blotting (P0013, Beyotime). Homogenate was mixed with 8% (wt/vol) SDS buffer and boiled for 10 min. The sample was further disintegrated through sonication and centrifugation at 12,000 ×*g* for 15 min at 4°C. Supernatant was collected as total protein extract.

For preparation of sarkosyl soluble/insoluble fractions (Goedert et al., 1992; Schlegel et al., 2019; Ferrer et al., 2020), the sample was mechanically homogenized in 10 volumes (w/v) of pre-cooling lysis buffer (10 mM Tris-HCl, pH 7.4, 0.8 M NaCl, 1 mM EGTA, 10% sucrose) and then centrifuged at 20,000 ×*g* for 20 min at 4°C. The supernatant (S1) was transferred to a new Eppendorf tube, and the pellet was re-homogenized in 5 volumes (w/v) of lysis buffer and spun at 20,000 ×*g* for 20 min. The supernatant (S2) was mixed with supernatant (S1) and incubated with 1% N-lauroylsarkosynate (w/v) for 1 h at room temperature while shaken. The sample was then spun at 100,000 ×*g* for 1 h at 4°C. The supernatant was transferred to a new Eppendorf tube, designated as the soluble fraction. The pellet was re-suspended (0.2 ml/g) in 50 mM Tris–HCl (pH 7.4) and stored as sarkosyl insoluble fraction.

To separate out mitochondria from cytoplasm, we used the Tissue Mitochondria Isolation Kit (C3606, Beyotime). Following manufacturer's instructions, tissue sample was homogenized in solution A and centrifuged at 1,000 ×*g* for 10 min at 4°C. Supernatant was collected and centrifuged at 11,000 ×*g* for another 10 min at 4°C. Then, supernatant was transferred to a new Eppendorf tube, designated as cytoplasm fraction. The deposit was re-suspended in a lysis buffer supplied by the kit and stored as mitochondrial fraction.

Co-Immunoprecipitation

Hippocampal regions infected with virus were isolated and mechanically homogenized in lysis buffer for immunoprecipitation (IP) (P0013, Beyotime). Then, the homogenate was centrifuged at 3,000 rpm, for 20 min at 4°C. The supernatant was incubated with the primary antibody Tau5 (2 μg/100 μg) (ab80579, Abcam) overnight at 4°C and then Protein A+G Agarose (30 μl/100 μl) (P2012, Beyotime) was added into the sample for 4–6 h. After that, the agarose was washed three times. Proteins attached to the agarose were resuspended in buffer (50 mM Tris-HCl, pH 6.8, 2% SDS, 10% glycerol) and boiled for 10 min. Collected protein sample was analyzed by Western blot.

Western Blot

Via SDS acrylamide gel electrophoresis, protein sample was transferred to nitrocellulose filter membrane (10600002, Whatman) and then blocked in 5% skimmed milk for 1 h. The membrane was then incubated with primary antibodies overnight at 4°C and then incubated with secondary antibody for 1 h. Antibodies used in this study are listed in **Table 1**. Odyssey Infrared Imaging System (LI-COR Biosciences, Lincoln, NE, United States) and ECL Imaging System (610007-8Q, Clinx Science Instruments Co., Ltd.) were used for visualization of protein bands. Quantitative analysis of blots was performed using ImageJ software (Fiji) (Li et al., 2021).

Quantitative Real-Time PCR

Total RNA was isolated from virus-infected mice hippocampal region using Trizol reagent (15596018, Thermo Fisher Scientific). The transcription reagent kit (RR037, Takara) was then used for cDNA synthesis. Quantitative PCR was conducted using the One-Step SYBR PrimeScript PLUS RT-PCR Kit (RR096A, Takara) following the manufacturer's instructions. The PCR system contained 1 μl of forward and reverse primers, 1 μl of cDNA, 3 μl of diethylpyrocarbonate (DEPC H_2O), and 5 μl of SYBR Green PCR master mixes. RT-PCR was performed and analyzed using an ABI Step one plus Real-Time PCR System (Applied Biosystems). Primers for human *TAU* were F: 5′-CGCCAG GAGTTCGAAGTGAT-3′ and R: 5′-TCTTGGTGCATGGTG TAGCC-3′ (Korhonen et al., 2011) and primers for *β-actin* were F: 5′- CAAATGTTGCTTGTCTGGTG-3′ and R: 5′-GTCAGTCGAGTGCACAGTTT-3′ (Wan et al., 2021).

Immunohistochemical and Nissl's Staining

Mice brain slices (paraffin section, 4 μm thick) were baked at 55°C for 1 h and immersed into xylene for 40 min. After being dewaxed, slices were dehydrated through graded ethanol (100%, 100%, 95%, 90%, and 80%) for 5 min each time. Brain slices were immersed into citric acid buffer (pH = 6.0, 10 mM) and heated in a microwave for 10 min to maximize tissue antigen recovery. Then, slices were incubated with 3% H_2O_2 for 30 min and blocked in 5% BSA solution containing 0.5% Triton X-100 for 40 min. Next, slices were incubated with primary antibody (listed in **Table 1**) at 4°C for 24–48 h. After incubation with

TABLE 1 | Antibodies used in this study.

Antibody	Host	Dilution WB	Dilution IHC	Dilution IF	Source
Anti-PINK1	Rabbit	1:500			BC100-494, Novus Biologicals
Anti-PINK1	Rabbit	1:500			ab23707, Abcam
HT7	Mouse	1:1,000	1:100		MN1000, Thermo Fisher Scientific
Tau5	Mouse	1:1,000			ab80579, Abcam
Anti-Tau (pS396)	Rabbit	1:1,000	1:100		11102, Signalway Antibody
Anti-Tau (pS404)	Rabbit	1:1,000	1:100		11112, Signalway Antibody
Anti-Tau (pT205)	Rabbit	1:1,000			11108, Signalway Antibody
Anti-GAPDH	Mouse	1:5,000			60004-1-Ig, Proteintech
Anti-LC3B	Rabbit	1:1,000			ab51520, Abcam
Anti-P62/SQSTM1	Rabbit	1:1,000			18420-1-AP, Proteintech
Anti-LAMP2	Mouse	1:1,000			66301-1-Ig, Proteintech
Anti-Beclin1	Rabbit	1:1,000			11306-1-AP, Proteintech
Anti-Ubiquitin	Mouse	1:1,000			sc-8017, Santa Cruz Biotechnology
Anti-Parkin	Mouse	1:1,000			4211S, Cell Signaling Technology
Anti-COX IV	Rabbit	1:1,000			11242-1-AP, Proteintech
Anti-Caspase 3	Rabbit	1:1,000			9662S, Cell Signaling Technology
Anti-Cleaved caspase 3	Rabbit	1:500			9661S, Cell Signaling Technology
Anti-EGFP	Rabbit			1:100	GB11602, Servicebio
Anti-Iba1	Mouse			1:100	GB12105, Servicebio
Anti-mouse IgG	Goat	1:10,000			A23910, Abbkine
Anti-rabbit IgG	Goat	1:10,000			A23920, Abbkine
Anti-mouse IgG	Goat	1:3,000			A25012, Abbkine
Anti-mouse IgG	Goat	1:5,000			SA00001-1, Proteintech
Anti-rabbit IgG	Goat	1:5,000			SA00001-2, Proteintech
Anti-NeuN	Rabbit		1:200		ab177487, Abcam
Anti-NeuN	Mouse			1:200	ab104224, Abcam
Anti-mouse IgG	Goat		1:200		G1216-3, Servicebio
Anti-rabbit IgG	Goat		1:200		G1215-3, Servicebio
Anti-rabbit IgG	Donkey			1:200	ANT024S, Antgene
Anti-mouse IgG	Donkey			1:200	ANT029S, Antgene

WB, Western blot; IHC, immunohistochemical staining; IF, immunofluorescence staining.

secondary antibody at 37°C for 1 h, slices were stained with DAB reagent (G1212, Servicebio). Then, slices were rehydrated through graded ethanol (80%, 90%, 95%, 100%, and 100%) for 5 min each time, transparentized using xylene for 20 min, and mounted with neutral balsam. For Nissl's staining, after deparaffinage and gradient alcohol dehydration, slices were washed with PBS for 3 × 5 min, and then dyed with 0.5% toluidine blue reagent (G1036, Servicebio) for 2–5 min. If the slice was hyperchromatic, 0.1% glacial acetic acid was used for differentiation. Baked slices were mounted with neutral balsam. A scanning microscope (SV120, OLYMPUS) was used for imaging.

Immunofluorescence Staining

After aforementioned deparaffinage, dehydration, and antigen recovery, mice brain slices were washed with PBS for 3 × 5 min and blocked in 5% donkey serum containing 0.5% Triton X-100 for 40 min. Next, slices were incubated with primary antibody (listed in **Table 1**) at 4°C for 24–48 h. After incubation with secondary antibody at 37°C for 1 h, slices were washed with PBS for 3 × 5 min and stained with DAPI reagent (G1012, Servicebio) for 10 min at room temperature. Slices were sealed with anti-fluorescence quencher (G1401, Servicebio) and imaged using a scanning microscope (SV120, OLYMPUS).

Golgi Staining

FD Rapid GolgiStain™ Kit (FD Neuro Technologies, PK401) was used for Golgi staining. After being deeply anesthetized, the brain of mice was removed and immersed in mixture solution A + B (1:1) for 2–4 weeks. Then, the brain was transferred to solution C for 3–7 days, after which it was placed on an oscillating tissue slicer and cut into slices (100 μm thick). After being air dried in the dark, the slices were stained with a mixture of solution D + E + double distilled water (1:1:2) as per manufacturer's instructions. Images were taken using an optical microscope (Nikon, Japan).

ATP Assay

ATP levels were measured using the ATP bioluminescence detection kit (S0026, Beyotime). Briefly, the hippocampal regions infected with virus was extracted and pyrolyzed with a lysis buffer supplied with the kit. The homogenate was centrifuged at 12,000 ×*g* for 5 min at 4°C. Supernatant was collected for ATP detection. Protein concentration of the supernatant was measured using the BCA Protein Assay Kit (P0012S, Beyotime). Furthermore, 100 μl of supernatant and 100 μl of ATP detection buffer were mixed and the luminescence was measured using a microplate reader. Gradient dilution of the standard solution was conducted to

generate the standard curve (1 nM–1 μM). ATP levels were calculated according to the standard curve and normalized against the standards' protein concentration.

Malondialdehyde Assay

Malondialdehyde (MDA) levels were measured using the Lipid Peroxidation MDA Assay Kit (S0131S, Beyotime). As per manufacturer's instructions, hippocampal regions infected with virus was extracted and pyrolyzed in RIPA lysis buffer (P0013D, Beyotime) and then centrifuged at 12,000 ×*g* for 10 min at 4°C. Supernatant was collected for MDA detection. Protein concentration of the supernatant was measured using a BCA Protein Assay Kit (P0012S, Beyotime). One hundred microliters of supernatant was mixed with 200 μl of MDA detection working buffer containing thiobarbituric acid (TBA) and the MDA-TBA adduct was measured using a microplate reader at 535 nm. Gradient dilution of standard solutions was conducted to generate the standard curve (1–100 μM). MDA levels were calculated according to the standard curve and normalized against the standards' protein concentration, shown as nmol/mg protein.

Statistical Analysis

All data were collected and analyzed in a blinded manner. Data were shown as mean ± SEM or mean ± SD and analyzed using GraphPad Prism (GraphPad Software, Inc., La Jolla, CA, United States). Statistical analyses were conducted using two-tailed unpaired *t*-tests, one-way ANOVA, or two-way repeated measures ANOVA followed by Tukey multiple-comparisons post-hoc tests. $p < 0.05$ was set as the level of statistical significance.

RESULTS

PINK1 Rescues Cognitive Impairments in hTau Mice

We injected pAAV-SYN-human Tau-mCherry-3×FLAG-WPRE into the hippocampal CA1 region of mice for 1 month to mimic Alzheimer-like deposits of tau in the brain (Andorfer et al., 2003; Lasagna-Reeves et al., 2011; Li et al., 2019; Wan et al., 2021). Meanwhile, pAAV-SYN-PINK1-EGFP-3×FLAG-WPRE was also co-injected to explore its effect on tau pathology. SYN is a neuron-specific promoter, which means exogenous PINK1 and hTau would be specifically expressed in neurons. A high transfection efficiency of the virus was confirmed by Western blot, immunofluorescence and immunohistochemistry (**Figures 4A,B,E**; **Supplementary Figure S1**). As core symptoms of AD, cognitive decline and dementia are tightly associated with tau pathology (Bejanin et al., 2017). Thus, we conducted behavioral tests on the mice to assess cognitive function (**Figure 1A**). In contrast with WT mice, human Tau (hTau) mice (injected with pAAV-SYN-human TAU-mCherry-3×FLAG-WPRE) showed obvious learning and memory impairments as evaluated by NOR and MWM tests, while overexpression of PINK1 rescued the cognitive dysfunction. More specifically, in the NOR test, the time that hTau mice spent on exploring novel object was significantly reduced; however, this recognition index was improved by PINK1 overexpression (**Figures 1B–D**). In the MWM test, compared with the WT group, hTau mice had a longer latency period before finding the hidden platform at 3rd–5th days during the training stage. During the test stage, longer latency to reach the place where the platform was previously placed before, less retention time in the target quadrant, and fewer times crossing the platform region were observed in hTau mice, while overexpressing PINK1 attenuated the above learning and memory deficits, as evidenced by decreased time to find the platform during the 4th and 5th day during the training phase, less escape latency, more retention time in the target quadrant, and more times crossing the platform region during the test phase (**Figures 1E–I**). There was no significant difference in swimming speed among the four groups of mice (**Figure 1J**), which excluded defects in motor ability. Overall, our data demonstrated that PINK1 overexpression ameliorates cognitive deficits in hTau mice.

PINK1 ameliorates hTau-Induced Neuron Loss and Synaptic Damage

Growing evidence supports the neurotoxic effects of tau as a primary event for neuron loss and synaptic injury, both of which are common neuropathologic manifestations in AD and closely related to the severity of cognitive disfunction (Iqbal and Grundke-Iqbal, 2002; Giannakopoulos et al., 2003). Especially, neuron loss in the hippocampal CA1 region is a prominent feature of AD (West et al., 1994; Simic et al., 1997). Therefore, we aimed to investigate the underlying mechanisms by which PINK1 ameliorated cognitive deficits in hTau mice. Nissl's staining and immunohistochemical staining were used to observe and compare neuron morphology and number in the hippocampal CA1 area of mice. In WT mice, irrespective of whether injected with PINK1 or not, neurons in the CA1 region had a full and orderly shape and were closely arranged with the Nissl bodies. Meanwhile, hTau mice displayed a reduced number of intact neurons (**Figures 2A,B**). Neurons had abnormal morphology, with an obscure structure and disorganized arrangement (**Figure 2A**). Interestingly, this phenotype was noticeably attenuated following PINK1 overexpression (**Figures 2A,B**). NeuN staining data also supported the finding that PINK1 overexpression ameliorated the neuron loss induced by accumulation of hTau (**Figures 2C,D**). In addition, overexpression of PINK1 attenuated the observed increased levels of cleaved caspase-3 induced by hTau, thus suggesting that PINK1 alleviates hTau-induced cell apoptosis (**Supplementary Figure S2**).

The dendritic spine, functional protrusions on dendrite branches, is the main site of synaptogenesis, and so is closely related to synaptic transmission (Chidambaram et al., 2019).

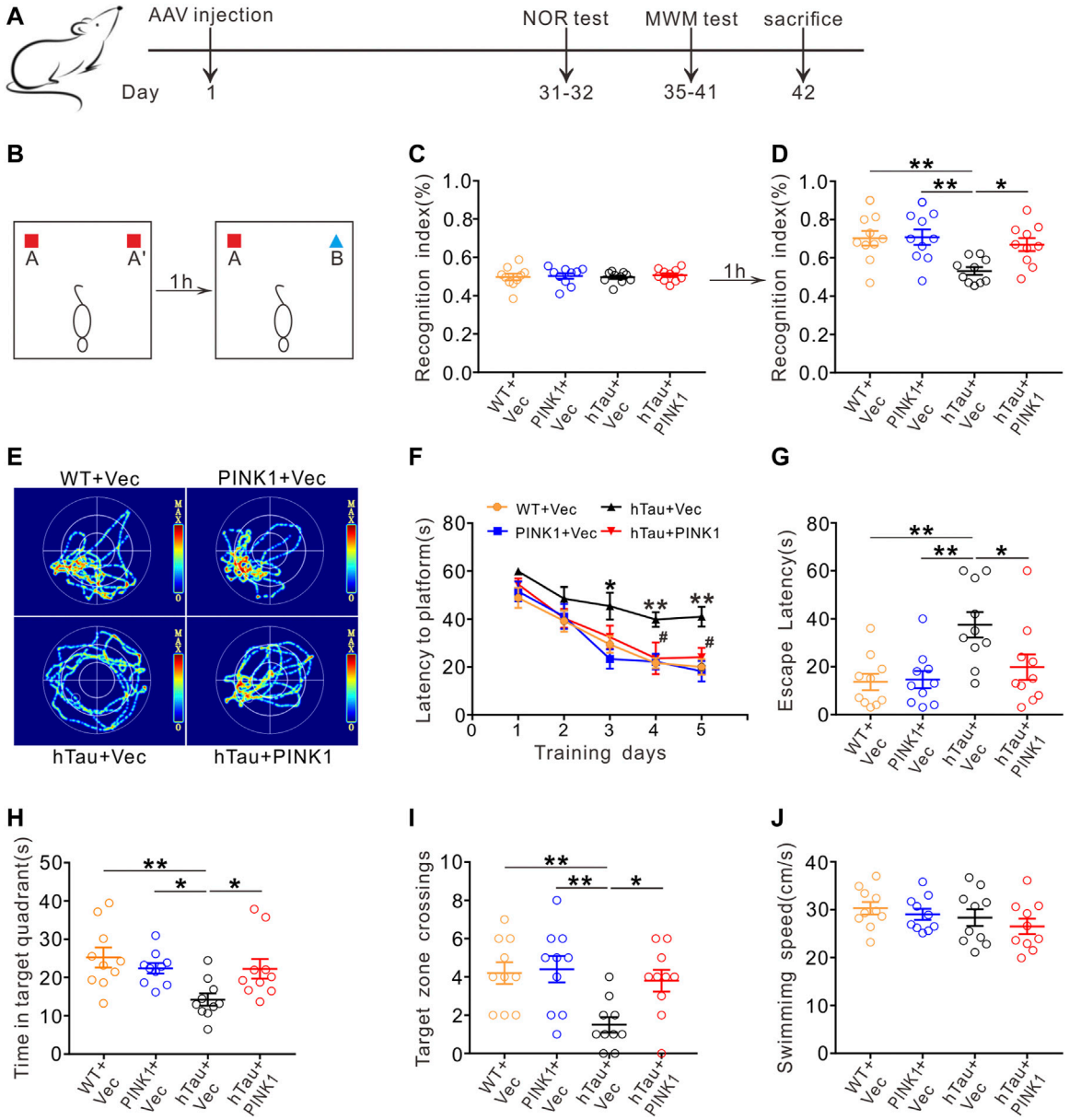

FIGURE 1 | PINK1 ameliorates cognitive impairments in hTau mice. **(A)** Experimental processes of virus injection and behavioral tests. **(B–D)** PINK1 improved cognitive performance of hTau mice in the NOR test shown by elevated recognition index. One-way ANOVA followed by Tukey multiple-comparisons tests. $^{*}p < 0.05$, $^{**}p < 0.01$. **(E)** Representative swimming path of mice in each group during the MWM probe test. **(F)** PINK1 improved learning ability in hTau mice shown by shortened latency to find the hidden platform during training stage in the MMW test. Two-way repeated-measures ANOVA followed by Tukey multiple-comparisons tests. $^{*}p < 0.05$, $^{**}p < 0.01$ vs. WT + Vec; $^{\#}p < 0.05$ vs. hTau + Vec. **(G–I)** PINK1 improved memory ability in hTau mice shown by decreased latency to reach the location of platform **(G)**, longer retention time in the target quadrant **(H)**, and more target zone crossings **(I)** during the MWM probe test. One-way ANOVA followed by Tukey multiple-comparisons tests. $^{*}p < 0.05$, $^{**}p < 0.01$. **(J)** No significant difference in swimming speed was seen among the four groups during the MWM probe test. One-way ANOVA followed by Tukey multiple-comparisons tests. All data were presented as mean ± SEM. $n = 10$ mice for each group.

Here, we identified and quantified dendritic spines in the CA1 region using Golgi staining. Compared with WT mice, dendritic branches were sparser, and the dendritic spine density was significantly reduced in hTau mice (**Figure 3**). Meanwhile, overexpression of PINK1 attenuated such phenotype in hTau mice (**Figure 3**). These data indicated that PINK1 attenuates hTau-mediated neuron loss and synaptic damage.

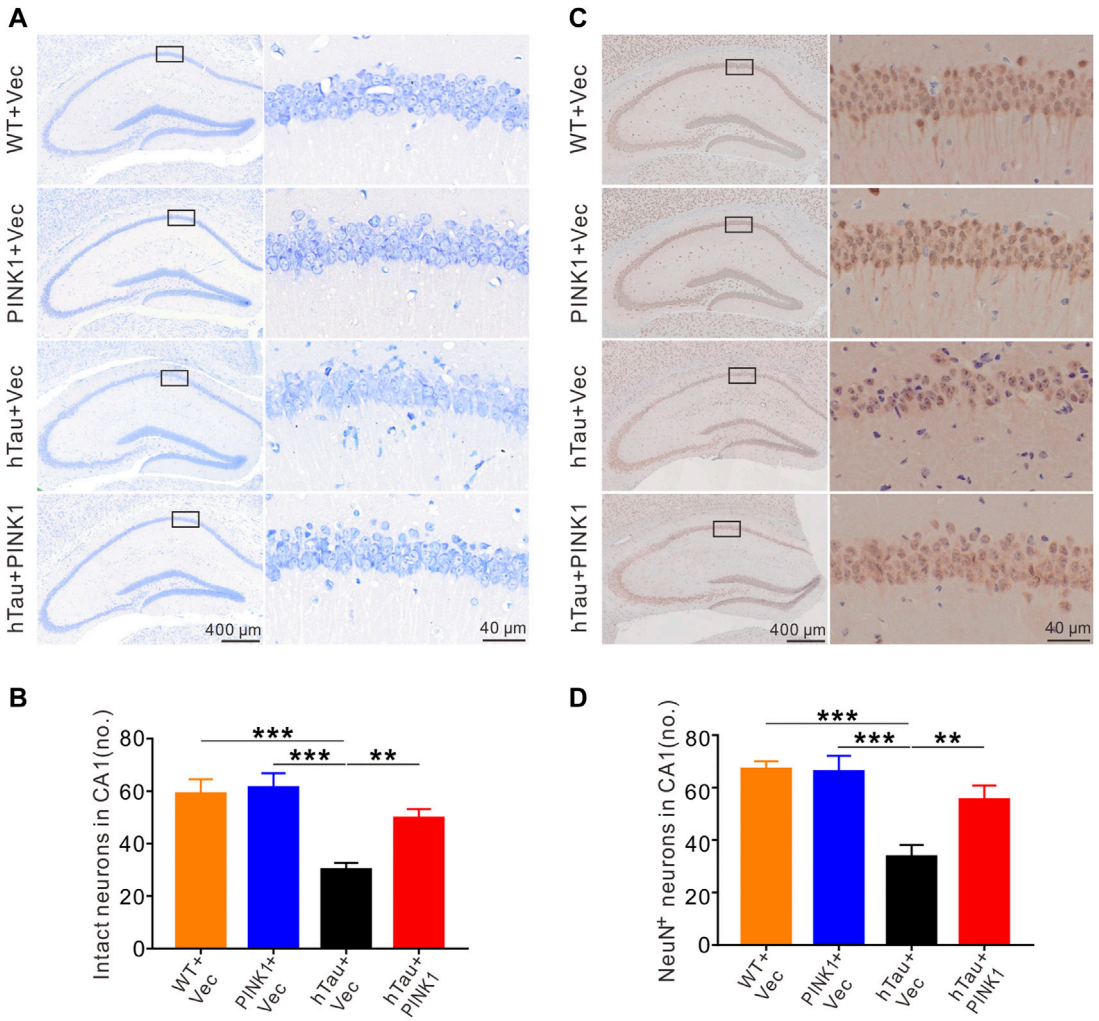

FIGURE 2 | PINK1 alleviates hTau-induced neuronal loss in the hippocampal CA1 region of mice. **(A)** PINK1 ameliorated hippocampal CA1 neuronal loss in hTau mice exhibited by representative images of Nissl staining. **(B)** Quantitative analysis of numbers of intact neurons in area framed within black bordered rectangle. Neurons with visible nuclei, distinctive nucleolus, and cytoplasmic Nissl staining were regarded as intact neurons and counted. One-way ANOVA followed by Tukey multiple-comparisons tests. $^{**}p < 0.01$, $^{***}p < 0.001$. **(C)** Representative images of NeuN immunohistochemical staining. **(D)** Quantitative analysis of numbers of neurons with positive NeuN staining in area framed within black bordered rectangle. One-way ANOVA followed by Tukey multiple-comparisons tests. $^{**}p < 0.01$, $^{***}p < 0.001$. All data were presented as mean ± SD. $n = 3$ mice for each group.

PINK1 Overexpression Reduces Tau Protein Levels in hTau Mice

We observed obvious accumulation of exogenous tau (human Tau) proteins in the hippocampal CA1 region of hTau mice, including total human tau (detected using the HT7 and Tau5 antibodies) and phosphorylated tau at Ser396, Ser404, and Thr205 (**Figures 4A,B,E**), as detected by Western blot or immunohistochemistry. Simultaneously overexpressing PINK1 significantly reduced the levels of exogenous total and phosphorylated tau proteins (**Figures 4A,B,E**). Furthermore, we found that PINK1 overexpression decreased soluble and insoluble exogenous total and phosphorylated tau proteins compared with hTau mice (**Figures 5E–H**, 1–3 lane vs. 4–6 lane). PINK1 did not alter the mRNA levels of hTau (**Figure 4D**), which suggested that overexpressing PINK1 decreased hTau protein levels as a result of an increase in its degradation. Although the endogenous levels of mouse tau displayed a downward trend in the context of PINK1 overexpression, there was no significant difference among the four groups (**Figures 4A,C**). Overall, these data showed that PINK1 decreases the pathological accumulation of tau proteins induced by hTau overexpression.

PINK1 Promotes Clearance of hTau Accumulation *via* the Autophagy–Lysosome Pathway

Given the protective effects of PINK1 against abnormally accumulated tau protein in mice, we sought to find out the

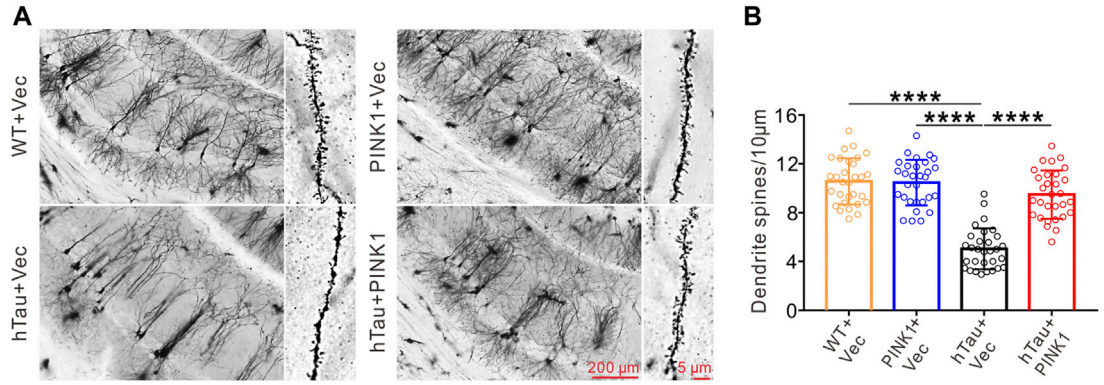

FIGURE 3 | PINK1 reverses the decreased dendritic spine density in the hippocampal CA1 region of hTau mice. **(A)** Representative images of Golgi Staining in the hippocampal CA1 region of mice. **(B)** Quantitative analysis of spine density in the CA1 area of mice. Thirty neurons from each group were analyzed. One-way ANOVA followed by Tukey multiple-comparisons tests. ****$p < 0.0001$. All data were presented as mean ± SD. $n = 3$ mice for each group.

potential underlying mechanism. As PINK1 did not lead to changes in the mRNA levels of hTau (**Figure 4D**), we inferred that PINK1 may affect the degradation pathways of hTau proteins. It has been previously shown that both UPS and ALP contribute to the degradation of tau aggregation in AD (Cheng et al., 2018), and there are also data that indicate the promotive effects of PINK1 on ALP (Michiorri et al., 2010; Parganlija et al., 2014; Du et al., 2017). Therefore, we aimed to detect the expression of autophagic markers (Abdelfatah et al., 2021). As illustrated in **Figures 5A,B**, PINK1 overexpression induced an increase in the expression of LC3 II and lysosomal protein LAMP2, and a decrease in the levels of p62 in the hippocampal CA1 region of hTau mice. The level of Beclin1 was not significantly altered among the four groups. Thus, these results suggest that PINK1 activates ALP in hTau mice.

To further confirm the pathway by which PINK1 induces elimination of abnormal accumulation of tau, MG132, an inhibitor of proteasome pathway, or chloroquine (CQ), an inhibitor of autophagy that blocks the fusion of autophagosome and lysosome, was used to treat the mice overexpressing hTau and PINK1, respectively. We found that CQ (lanes 10–12) but not MG132 treatment (lanes 7–9) reversed the decreased total (Tau5) and phosphorylated tau (pS396, pS404, and pT205) levels induced by PINK1 (**Figures 5C,D**; **Supplementary Figure S3**). Soluble and insoluble proteins were extracted, and total or phosphorylated tau levels were detected by Western blot. The levels of total and phosphorylated tau in the soluble and insoluble fraction of hTau mice were decreased following PINK1 overexpression, while CQ reversed the PINK1-induced reduction of total or phosphorylated tau levels (**Figures 5E–H**, lanes 10–12 vs. lanes 4–6; **Supplementary Figure S3**). MG132 treatment merely induced a small increase in total and phosphorylated tau levels in the soluble fraction, but had no effects in the levels of total or phosphorylated tau in the insoluble fraction (**Figures 5E–H**, lanes 7–9 vs. lanes 4–6; **Supplementary Figure S3**). We also observed that CQ caused an increase in the levels of endogenous tau (**Figures 5E,F**; **Supplementary Figures S4A,B**). All these data suggest that PINK1 decreases the levels of tau through the autophagy pathway.

CQ Reverses the Improved Effects of PINK1 on Cognition

Furthermore, we conducted behavioral experiments to investigate whether the improved cognitive function induced by PINK1 was also reversed by CQ treatment (**Figure 6A**). Unsurprisingly, we found that CQ treatment caused a distinct cognitive decline in hTau and PINK1 overexpressing mice. This was evidenced by a lower recognition index in the NOR test (**Figures 6B,C**), a longer latency period to reach the hidden platform on days 3–5 during the training phase, as well as a longer escape latency, shorter residence time in the target quadrant, and decreased platform zone crossing times during the test phase of the MWM test (**Figures 6D–I**). Treatment with MG132 did not induce significant changes in the cognition of hTau and PINK1 overexpressing mice (**Supplementary Figure S5**).

PINK1 Reduces the Accumulation of hTau in Mitochondria and Improves Mitochondrial Function

Besides our above discovery that PINK1 reduces tau proteins through the autophagy pathway, PINK1 has been widely reported to play vital roles in maintaining mitochondrial homeostasis (Arena and Valente, 2017). Here, we extracted the mitochondrial and cytoplasmic fraction from the hippocampal CA1 region of mice, and found accumulation of hTau in the mitochondrial fraction of hTau mice, which is consistent with our previous study in cells overexpressing hTau (Hu et al., 2016) as well as other previous studies (Lasagna-Reeves et al., 2011; Grassi et al., 2019; Torres et al., 2021), Meanwhile, PINK1 overexpression decreased the levels of hTau in both the mitochondrial and cytoplasmic fraction of hTau mice (**Figures 7A,B**). Furthermore, we

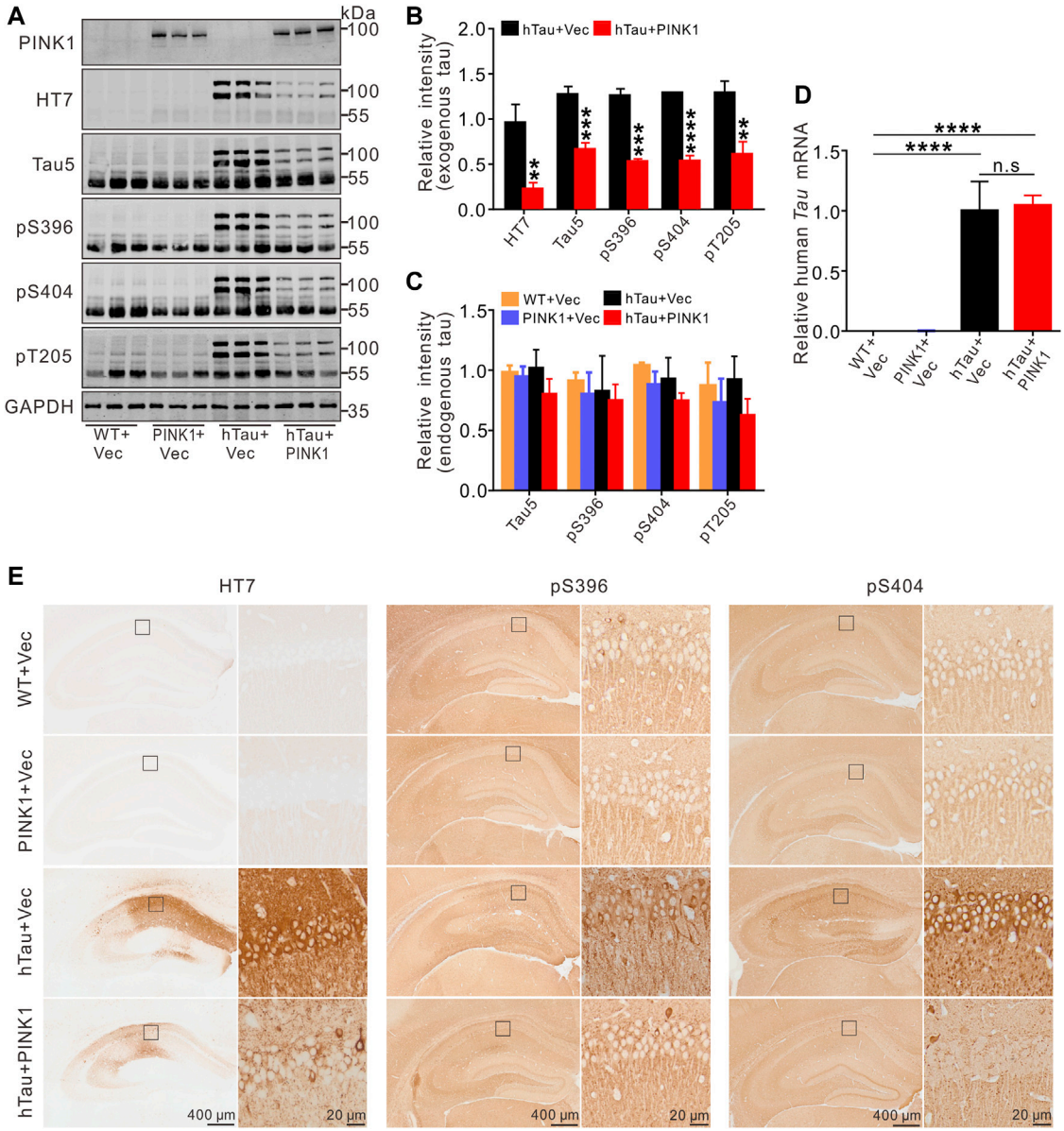

FIGURE 4 | Overexpression of PINK1 decreases tau protein levels in hTau mice. **(A,B)** Representative images and quantitative analysis of Western blot showed overexpression of PINK1 diminished levels of exogenous tau (~106 kDa, human tau), including total tau (HT7, Tau5) and phosphorylated tau (pS396, pS404, and pT205) in the hippocampal CA1 area of hTau mice. Unpaired *t*-tests. $^{**}p < 0.01$, $^{***}p < 0.001$, $^{****}p < 0.0001$. **(C)** Significant alteration of endogenous tau (~55 kDa) was not found among the four groups. One-way ANOVA followed by Tukey multiple-comparisons tests. **(D)** The levels of human *TAU* mRNA had no significant changes with PINK1 overexpression. One-way ANOVA followed by Tukey multiple-comparisons tests. $^{****}p < 0.0001$. **(E)** Representative images of immunohistochemical staining showed PINK1 reduced tau pathology (total tau, phosphorylated tau at Ser396 or Ser404) in the hippocampal CA1 area. HT7 antibody exclusively reacts to human tau proteins. All data were presented as mean ± SD. $n = 3$ mice for each group.

found reduced levels of Parkin in the mitochondrial and cytoplasmic fraction of mice with PINK1 overexpression (**Figures 7A,C**), indicating an activation of Parkin by PINK1 as activation of Parkin would induce its own ubiquitylation and degradation (Zhang et al., 2000; Xiong et al., 2009; McWilliams et al., 2018). In line with previous studies (Li et al., 2016; Guha et al., 2020; Szabo et al., 2020), assessment of mitochondrial function revealed mitochondrial dysfunction in hTau mice, as evidenced by reduced levels of ATP and elevated MDA levels, both of which were reversed in the context of PINK1 overexpression (**Figures 7D,E**).

DISCUSSION

As a primary cause of dementia and death in older people, AD has become a common problem and challenge in an aging

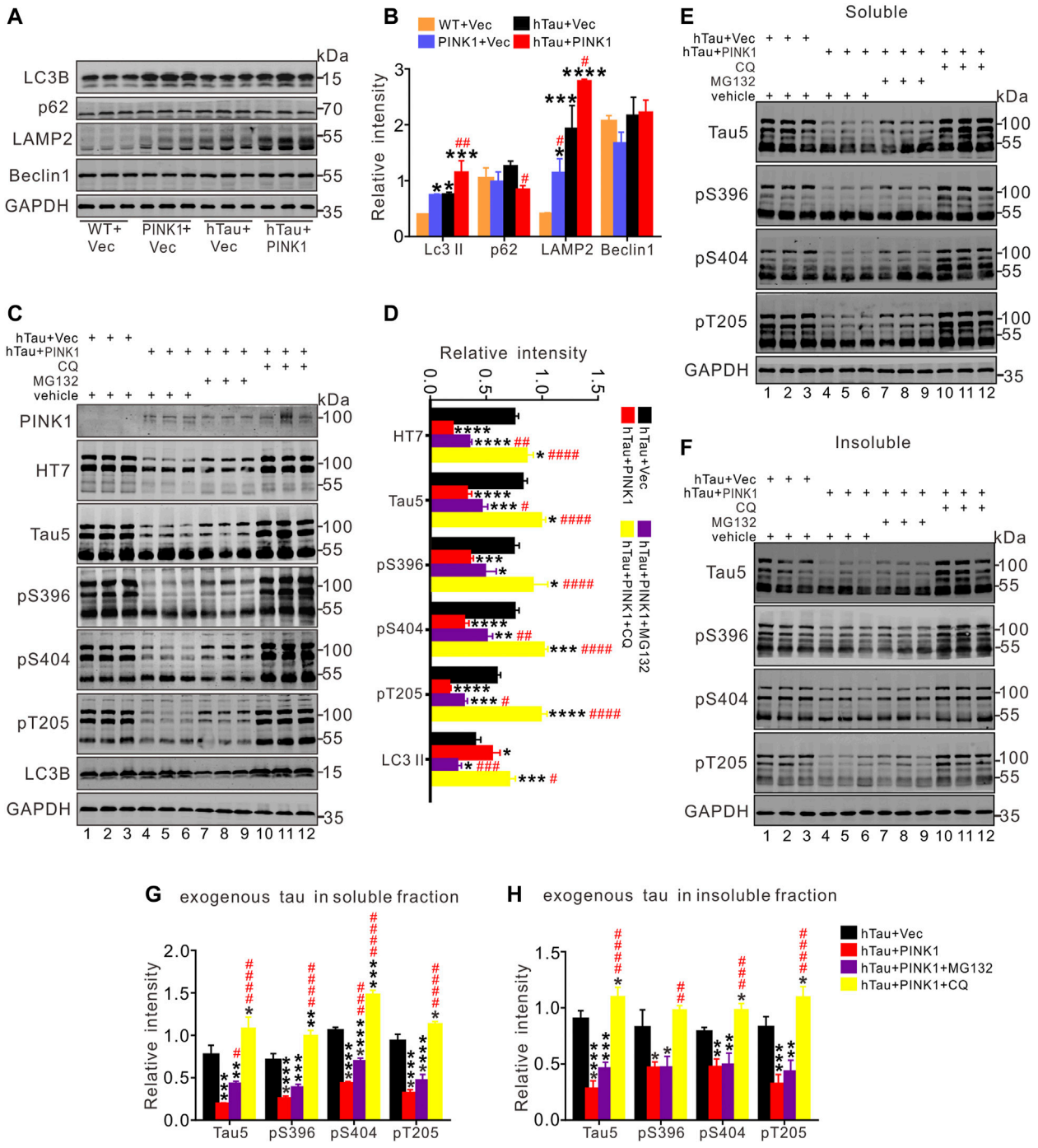

FIGURE 5 | PINK1 promotes clearance of hTau mainly through the autophagy pathway. **(A,B)** PINK1 increased the levels of LC3 II and lysosomal protein *LAMP2*, as well as decreased p62 levels detected by Western blot. One-way ANOVA followed by Tukey multiple-comparisons tests. $^{*}p < 0.05$, $^{**}p < 0.01$, $^{***}p < 0.001$, $^{****}p < 0.0001$ vs. WT + Vec; $^{\#}p < 0.05$, $^{\#\#}p < 0.01$ vs. hTau + Vec. **(C,D)** In total fraction of mice hippocampal CA1, PINK1 diminished the levels of exogenous tau (~106 kDa, human tau: both total and phosphorylated tau), while CQ treatment reversed this reduction shown by Western blot. Treatment with MG132 induced relatively small increase in the levels of hTau proteins in hTau and PINK1 overexpressing mice. **(E–H)** In both the soluble **(E, G)** and insoluble fraction **(F, H)** of mice hippocampal CA1 area, PINK1 decreased the levels of exogenous tau (~106 kDa, human tau: both total and phosphorylated tau) in hTau mice, while CQ treatment reversed the reduction. Treatment with MG132 induced relatively small increase in the levels of hTau proteins in the soluble fraction. One-way ANOVA followed by Tukey multiple-comparisons tests. $^{*}p < 0.05$, $^{**}p < 0.01$, $^{***}p < 0.001$, $^{****}p < 0.0001$ vs. hTau + Vec; $^{\#}p < 0.05$, $^{\#\#}p < 0.01$, $^{\#\#\#}p < 0.001$, $^{\#\#\#\#}p < 0.0001$ vs. hTau + PINK1. All data were presented as mean ± SD. $n = 3$ mice for each group.

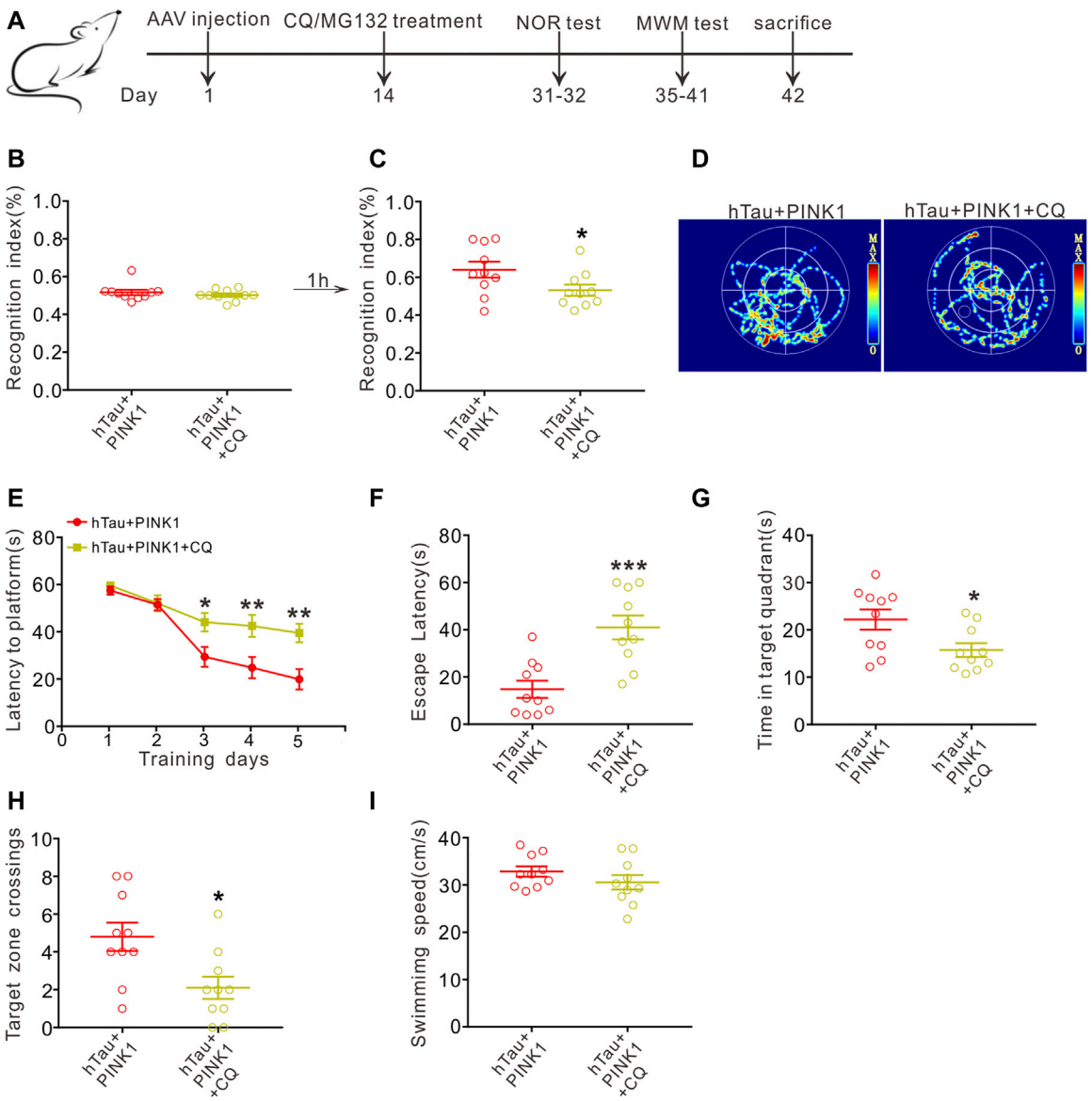

FIGURE 6 | CQ treatment reverses the improved cognition induced by PINK1 overexpression. **(A)** Experimental processes of virus injection, drug treatment, and behavioral tests. **(B,C)** CQ treatment lowered the recognition index of hTau and PINK1 overexpressing mice in the NOR test. Unpaired *t*-tests. $^{*}p < 0.05$. (D) Representative swimming path of mice in each group during the MWM probe test. **(E)** CQ treatment impaired the learning ability of hTau and PINK1 overexpressing mice, shown by prolonged latency to find the hidden platform during training stage in the MWM test. Two-way repeated-measures ANOVA followed by Tukey multiple-comparisons tests. $^{*}p < 0.05$, $^{**}p < 0.01$. **(F–H)** CQ treatment impaired the memory ability of hTau and PINK1 overexpressing mice, shown by longer latency to reach the location of platform **(F)**, shorter retention time in the target quadrant **(G)** and fewer target zone crossings **(H)** during the MWM probe test. Unpaired *t*-tests. $^{*}p < 0.05$, $^{**}p < 0.01$, $^{***}p < 0.001$. **(I)** No significant difference in swimming speed was seen between the two groups during the MWM probe test. Unpaired *t*-tests. All data were presented as mean ± SEM. $n = 10$ mice for each group.

society due to a lack of effective diagnosis and treatment. Here, we injected AAV2-full-length human TAU into the hippocampal CA1 region of mice to mimic Alzheimer-like tau pathology in the brain. We observed an obvious accumulation of tau proteins, neuron loss, synapse injury, mitochondrial function disorders, and cognitive impairments in hTau mice. We also found that overexpression of PINK1 effectively reduced neuropathological accumulation of tau proteins, ameliorated mitochondrial function, attenuated damage to neurons and synapses, and thus rescued cognitive decline in hTau mice.

In our study, overexpression of PINK1 led to activation of ALP, as evidenced by increased LC3 II and lysosomal protein LAMP2, as well as decreased levels of p62. PINK1-induced ALP activation has also been observed in other studies (Michiorri et al., 2010; Parganlija et al., 2014; Du et al., 2017). In transgenic mAPP mice, overexpression of PINK1 increased the expression of LC3 II, lysosome-associated

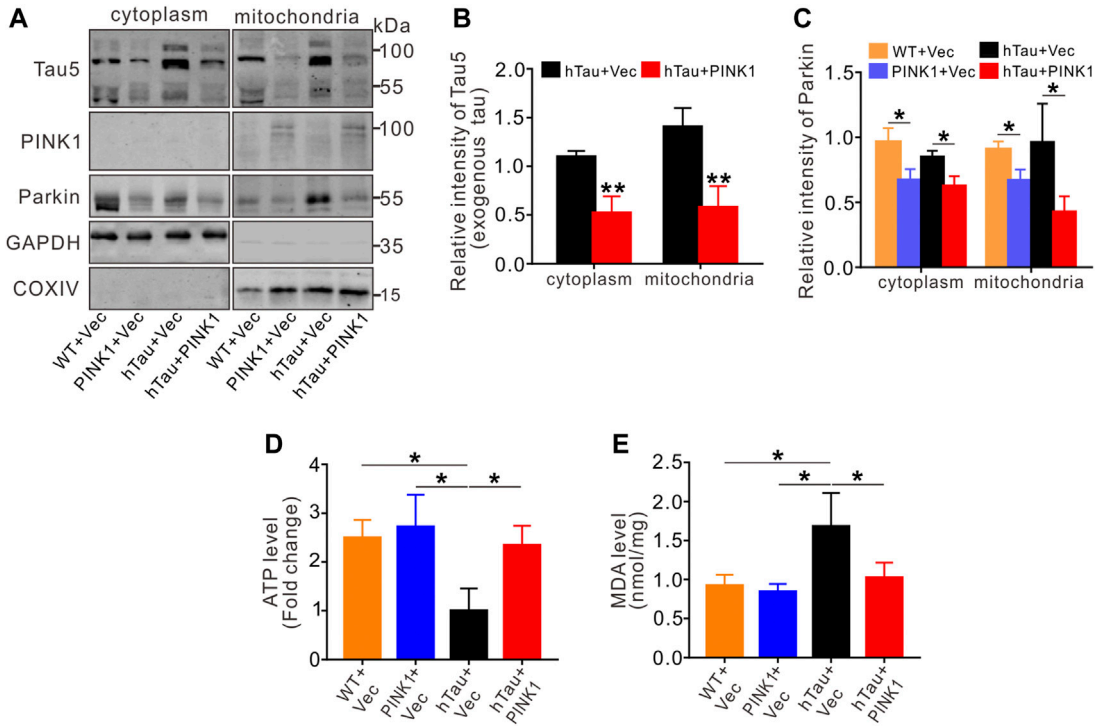

FIGURE 7 | PINK1 reduces tau accumulation in mitochondria and rescues mitochondrial disorders. **(A–C)** The levels of exogenous tau (~106 kDa, human tau) **(A,B)** or Parkin **(A, C)** in both cytoplasm and mitochondria fraction of mice hippocampal CA1 region were detected by Western blot and quantitative analysis. Unpaired t-tests. $^{*}p < 0.05$, $^{**}p < 0.01$. **(D, E)** Overexpression of PINK1 reversed the decreased ATP levels **(D)** or increased MDA levels **(E)** in hTau mice. One-way ANOVA followed by Tukey multiple-comparisons tests. $^{*}p < 0.05$. All data were presented as mean ± SD. $n = 3$ mice for each group.

membrane protein 1 (LAMP1), lysosomal proteases cathepsin D, autophagy receptor OPTN and NDP52, thus leading to the clearance of Aβ plaques (Du et al., 2017). SH-SY5Y cells with PINK1 knockdown showed decreased mRNA levels of *ATG5*, *ATG6*, *ATG7*, *LC3A*, *P62*, *LAMP1*, and *LAMP2* (Parganlija et al., 2014). PINK1 was also reported to directly interact with Beclin1 to promote autophagy (Michiorri et al., 2010). Taken together, our results indicate that PINK1 promotes degradation of tau *via* ALP. After pharmaceutical blockade of the fusion between autophagosome and lysosome by CQ, we found that the decreased hTau proteins in hTau and PINK1-overexpressed mice, including total and phosphorylated tau in whole tissue homogenate, soluble and insoluble portions, were all reversed. In contrast, inhibiting proteasome by MG132 just induced partial increase of hTau proteins in hTau and PINK1-overexpressed mice. This increase was mainly observed in the soluble portion, which is in accord with the idea that the proteasome has a limited ability to deal with oligomeric and aggregated proteins (Kirkin et al., 2009). CQ also reversed the PINK1-induced improvements on cognitive impairment. Overall, the above findings verified that PINK1 relies on ALP to clear abnormal accumulated hTau proteins and ameliorate cognitive deficits. Thus, in future research, we will explore the detailed mechanism by which PINK1 overexpression leads to the degradation of tau *via* ALP.

Previous research has shown that cytosolic PINK1 fragments enhanced Parkin-mediated ubiquitination and degradation of Parkin substrates in neuroblastoma cells and human brain lysates (Xiong et al., 2009), and bioinformatic analysis presented the potential involvement of Parkin in the ubiquitination of tau (Kumar and Kumar, 2019). Researchers have also shown that Parkin brings about Lys63-linked polyubiquitination of misfolded proteins and leads to their clearance *via* the autophagy pathway (Olzmann and Chin, 2008; Khandelwal et al., 2011). In this study, a Co-IP experiment revealed upregulated ubiquitination of tau protein in the hippocampal CA1 region of mice with PINK1 overexpression (**Supplementary Figure S6**).

Our previous studies found that hTau can accumulate in mitochondria, inhibit mitophagy, disrupt mitochondrial dynamics, and induce mitochondrial dysfunction in cellular or animal models overexpressing hTau (Hu et al., 2016; Li et al., 2016), which are considered drivers of synaptic dysfunction and cognitive decline in AD (John and Reddy, 2021; Sharma et al., 2021). In this study, we verified the pathological accumulation of tau in mitochondria, which was reported to induce mitochondrial dysfunction, thus contributing to synaptic impairment and memory deficits in

mice (Torres et al., 2021). PINK1 has been widely reported to play vital roles in maintaining mitochondrial homeostasis (Voigt et al., 2016; Arena and Valente, 2017). Parkin is a cytosolic member of E3 ubiquitin ligase family, and overexpression PINK1 can recruit Parkin to mitochondria and activate it *via* phosphorylation of its UBL domain. Then, Parkin transfers ubiquitin chains to the mitochondrial outer membrane to induce the elimination of mitochondria through mitophagy (Okatsu et al., 2012; Du et al., 2017; Gundogdu et al., 2021). Our study showed that PINK1 reduced hTau accumulation in mitochondria. We observed mitochondrial dysfunction in hTau mice, which was rescued following overexpression of PINK1, possibly because of PINK1-induced reduction of intracellular tau accumulation (Li et al., 2016; Guha et al., 2020; Szabo et al., 2020) and the direct protective effects of PINK1 on mitochondria (Voigt et al., 2016; Arena and Valente, 2017).

It has been extensively reported that tau accumulation induces neuron loss and synaptic impairments, which are closely related to cognitive deficits in AD (Iqbal and Grundke-Iqbal, 2002; Giannakopoulos et al., 2003; Yin et al., 2016). We also found that overexpression of hTau or P301L hTau activated STAT1 and inactivated STAT3 to inhibit the expression of NMDARs, thus inducing dendritic plasticity deficits, including LTP suppression and spine density decrease, and memory deficits (Li et al., 2019; Hong et al., 2020; Wan et al., 2021). In this study, PINK1 overexpression rescued neuron loss and synaptic damage, and ameliorated cognitive impairments by promoting the degradation of accumulated tau in the autophagy pathway, reducing tau accumulation in mitochondria and alleviating mitochondrial disorders. These findings, together with the previous finding that PINK1 decreased Aβ level in transgenic mAPP mice (Du et al., 2017), indicate the potential of PINK1 as a therapeutic target for AD treatment.

DATA AVAILABILITY STATEMENT

The original contributions presented in the study are included in the article/**Supplementary Material**, Further inquiries can be directed to the corresponding authors.

ETHICS STATEMENT

The animal study was reviewed and approved by the Ethics Committee of Tongji Medical College, Huazhong University of Science and Technology.

AUTHOR CONTRIBUTIONS

GL and GPL proposed and designed the research project, and wrote the manuscript. XJ and YW performed most of the experiments, and conducted data analysis and graphics production. RM, YC, LL, and JZ contributed to the experiments. All authors contributed to the article and approved the submitted version.

FUNDING

This work is supported by the grant from the National Natural Science Foundation of China (No. 81974161).

SUPPLEMENTARY MATERIAL

The Supplementary Material for this article can be found online at: https://www.frontiersin.org/articles/10.3389/fcell.2021.736267/full#supplementary-material

REFERENCES

Abdelfatah, S., Abdellatif, M., Abel, S., Ahmed, Z. M., Alves, S., Araki, Y., et al. (2021). Guidelines for the Use and Interpretation of Assays for Monitoring Autophagy (4th Edition)1. *Autophagy* 17 (1), 1–382. doi:10.1080/15548627.2020.1797280

Akabane, S., Matsuzaki, K., Yamashita, S.-I., Arai, K., Okatsu, K., Kanki, T., et al. (2016). Constitutive Activation of PINK1 Protein Leads to Proteasome-Mediated and Non-Apoptotic Cell Death Independently of Mitochondrial Autophagy. *J. Biol. Chem.* 291 (31), 16162–16174. doi:10.1074/jbc.M116.714923

Andorfer, C., Kress, Y., Espinoza, M., De Silva, R., Tucker, K. L., Barde, Y.-A., et al. (2003). Hyperphosphorylation and Aggregation of Tau in Mice Expressing Normal Human Tau Isoforms. *J. Neurochem.* 86 (3), 582–590. doi:10.1046/j.1471-4159.2003.01879.x

Arena, G., and Valente, E. M. (2017). PINK1 in the Limelight: Multiple Functions of an Eclectic Protein in Human Health and Disease. *J. Pathol.* 241 (2), 251–263. doi:10.1002/path.4815

Baek, M., Choe, Y.-J., Bannwarth, S., Kim, J., Maitra, S., Dorn, G. W., et al. (2021). TDP-43 and PINK1 Mediate CHCHD10S59L Mutation-Induced Defects in Drosophila and *In Vitro*. *Nat. Commun.* 12 (1), 1924. doi:10.1038/s41467-021-22145-9

Bejanin, A., Schonhaut, D. R., La Joie, R., Kramer, J. H., Baker, S. L., Sosa, N., et al. (2017). Tau Pathology and Neurodegeneration Contribute to Cognitive Impairment in Alzheimer's Disease. *Brain* 140 (12), 3286–3300. doi:10.1093/brain/awx243

Campos, J. C., Baehr, L. M., Ferreira, N. D., Bozi, L. H. M., Andres, A. M., Ribeiro, M. A. C., et al. (2020). β 2 -Adrenoceptor Activation Improves Skeletal Muscle Autophagy in Neurogenic Myopathy. *FASEB j.* 34 (4), 5628–5641. doi:10.1096/fj.201902305R

Chen, Y., Chen, Y., Zhang, J., Cao, P., Su, W., Deng, Y., et al. (2020). Fusobacterium Nucleatum Promotes Metastasis in Colorectal Cancer by Activating Autophagy Signaling via the Upregulation of CARD3 Expression. *Theranostics* 10 (1), 323–339. doi:10.7150/thno.38870

Cheng, J., North, B. J., Zhang, T., Dai, X., Tao, K., Guo, J., et al. (2018). The Emerging Roles of Protein Homeostasis-Governing Pathways in Alzheimer's Disease. *Aging Cell* 17 (5), e12801. doi:10.1111/acel.12801

Chidambaram, S. B., Rathipriya, A. G., Bolla, S. R., Bhat, A., Ray, B., Mahalakshmi, A. M., et al. (2019). Dendritic Spines: Revisiting the Physiological Role. *Prog. Neuro-Psychopharmacology Biol. Psychiatry* 92, 161–193. doi:10.1016/j.pnpbp.2019.01.005

Choi, J., Ravipati, A., Nimmagadda, V., Schubert, M., Castellani, R. J., and Russell, J. W. (2014). Potential Roles of PINK1 for Increased PGC-1α-Mediated Mitochondrial Fatty Acid Oxidation and Their Associations with Alzheimer Disease and Diabetes. *Mitochondrion* 18, 41–48. doi:10.1016/j.mito.2014.09.005

Congdon, E. E., and Sigurdsson, E. M. (2018). Tau-Targeting Therapies for Alzheimer Disease. *Nat. Rev. Neurol.* 14 (7), 399–415. doi:10.1038/s41582-018-0013-z

Du, F., Yu, Q., Yan, S., Hu, G., Lue, L.-F., Walker, D. G., et al. (2017). PINK1 Signalling Rescues Amyloid Pathology and Mitochondrial Dysfunction in Alzheimer's Disease. *Brain* 140 (12), 3233–3251. doi:10.1093/brain/awx258

Fagerberg, L., Hallström, B. M., Oksvold, P., Kampf, C., Djureinovic, D., Odeberg, J., et al. (2014). Analysis of the Human Tissue-Specific Expression by Genome-Wide Integration of Transcriptomics and Antibody-Based Proteomics. *Mol. Cell Proteomics* 13 (2), 397–406. doi:10.1074/mcp.M113.035600

Fang, E. F., Hou, Y., Palikaras, K., Adriaanse, B. A., Kerr, J. S., Yang, B., et al. (2019). Mitophagy Inhibits Amyloid-β and Tau Pathology and Reverses Cognitive Deficits in Models of Alzheimer's Disease. *Nat. Neurosci.* 22 (3), 401–412. doi:10.1038/s41593-018-0332-9

Ferrer, I., Andrés-Benito, P., Zelaya, M. V., Aguirre, M. E. E., Carmona, M., Ausín, K., et al. (2020). Familial Globular Glial Tauopathy Linked to MAPT Mutations: Molecular Neuropathology and Seeding Capacity of a Prototypical Mixed Neuronal and Glial Tauopathy. *Acta Neuropathol.* 139 (4), 735–771. doi:10.1007/s00401-019-02122-9

Giannakopoulos, P., Herrmann, F. R., Bussiere, T., Bouras, C., Kovari, E., Perl, D. P., et al. (2003). Tangle and Neuron Numbers, but Not Amyloid Load, Predict Cognitive Status in Alzheimer's Disease. *Neurology* 60 (9), 1495–1500. doi:10.1212/01.WNL.0000063311.58879.01

Goedert, M., Spillantini, M. G., Cairns, N. J., and Crowther, R. A. (1992). Tau Proteins of Alzheimer Paired Helical Filaments: Abnormal Phosphorylation of All Six Brain Isoforms. *Neuron* 8 (1), 159–168. doi:10.1016/0896-6273(92)90117-v

Götz, J., Halliday, G., and Nisbet, R. M. (2019). Molecular Pathogenesis of the Tauopathies. *Annu. Rev. Pathol. Mech. Dis.* 14 (1), 239–261. doi:10.1146/annurev-pathmechdis-012418-012936

Grassi, D., Diaz-Perez, N., Volpicelli-Daley, L. A., and Lasmézas, C. I. (2019). Pα-syn* Mitotoxicity Is Linked to MAPK Activation and Involves Tau Phosphorylation and Aggregation at the Mitochondria. *Neurobiol. Dis.* 124, 248–262. doi:10.1016/j.nbd.2018.11.015

Guha, S., Johnson, G. V. W., and Nehrke, K. (2020). The Crosstalk between Pathological Tau Phosphorylation and Mitochondrial Dysfunction as a Key to Understanding and Treating Alzheimer's Disease. *Mol. Neurobiol.* 57 (12), 5103–5120. doi:10.1007/s12035-020-02084-0

Gundogdu, M., Tadayon, R., Salzano, G., Shaw, G. S., and Walden, H. (2021). A Mechanistic Review of Parkin Activation. *Biochim. Biophys. Acta (Bba) - Gen. Subjects* 1865 (6), 129894. doi:10.1016/j.bbagen.2021.129894

Guo, T., Zhang, D., Zeng, Y., Huang, T. Y., Xu, H., and Zhao, Y. (2020). Molecular and Cellular Mechanisms Underlying the Pathogenesis of Alzheimer's Disease. *Mol. Neurodegeneration* 15 (1), 40. doi:10.1186/s13024-020-00391-7

Han, Y., Wang, N., Kang, J., and Fang, Y. (2020). β-Asarone Improves Learning and Memory in Aβ1-42-Induced Alzheimer's Disease Rats by Regulating PINK1-Parkin-Mediated Mitophagy. *Metab. Brain Dis.* 35 (7), 1109–1117. doi:10.1007/s11011-020-00587-2

Hong, X.-Y., Wan, H.-L., Li, T., Zhang, B.-G., Li, X.-G., Wang, X., et al. (2020). STAT3 Ameliorates Cognitive Deficits by Positively Regulating the Expression of NMDARs in a Mouse Model of FTDP-17. *Sig Transduct Target. Ther.* 5 (1), 213–295. doi:10.1038/s41392-020-00290-9

Hu, Y., Li, X.-C., Wang, Z.-H., Luo, Y., Zhang, X., Liu, X.-P., et al. (2016). Tau Accumulation Impairs Mitophagy via Increasing Mitochondrial Membrane Potential and Reducing Mitochondrial Parkin. *Oncotarget* 7 (14), 17356–17368. doi:10.18632/oncotarget.7861

Iqbal, K., and Grundke-Iqbal, I. (2002). Neurofibrillary Pathology Leads to Synaptic Loss and Not the Other Way Around in Alzheimer Disease. *J. Alzheimer's Dis.* 4 (3), 235–238. doi:10.3233/JAD-2002-4313

John, A., and Reddy, P. H. (2021). Synaptic Basis of Alzheimer's Disease: Focus on Synaptic Amyloid Beta, P-Tau and Mitochondria. *Ageing Res. Rev.* 65, 101208. doi:10.1016/j.arr.2020.101208

Khalil, B., El Fissi, N., Aouane, A., Cabirol-Pol, M.-J., Rival, T., and Liévens, J.-C. (2015). PINK1-Induced Mitophagy Promotes Neuroprotection in Huntington's Disease. *Cell Death Dis* 6 (1), e1617. doi:10.1038/cddis.2014.581

Khandelwal, P. J., Herman, A. M., Hoe, H.-S., Rebeck, G. W., and Moussa, C. E. H. (2011). Parkin Mediates Beclin-Dependent Autophagic Clearance of Defective Mitochondria and Ubiquitinated A in AD Models. *Hum. Mol. Genet.* 20 (11), 2091–2102. doi:10.1093/hmg/ddr091

Kirkin, V., McEwan, D. G., Novak, I., and Dikic, I. (2009). A Role for Ubiquitin in Selective Autophagy. *Mol. Cel* 34 (3), 259–269. doi:10.1016/j.molcel.2009.04.026

Korhonen, P., van Groen, T., Thornell, A., Kyrylenko, S., Soininen, M.-L., Ojala, J., et al. (2011). Characterization of a Novel Transgenic Rat Carrying Human Tau with Mutation P301L. *Neurobiol. Aging* 32 (12), 2314–2315. doi:10.1016/j.neurobiolaging.2009.12.022

Kumar, D., and Kumar, P. (2019). Aβ, Tau, and α-Synuclein Aggregation and Integrated Role of PARK2 in the Regulation and Clearance of Toxic Peptides. *Neuropeptides* 78, 101971. doi:10.1016/j.npep.2019.101971

Lasagna-Reeves, C. A., Castillo-Carranza, D. L., Sengupta, U., Clos, A. L., Jackson, G. R., and Kayed, R. (2011). Tau Oligomers Impair Memory and Induce Synaptic and Mitochondrial Dysfunction in Wild-type Mice. *Mol. Neurodegeneration* 6, 39. doi:10.1186/1750-1326-6-39

Li, X.-C., Hu, Y., Wang, Z.-H., Luo, Y., Zhang, Y., Liu, X.-P., et al. (2016). Human Wild-type Full-Length Tau Accumulation Disrupts Mitochondrial Dynamics and the Functions via Increasing Mitofusins. *Sci. Rep.* 6 (1), 24756. doi:10.1038/srep24756

Li, X. G., Hong, X. Y., Wang, Y. L., Zhang, S. J., Zhang, J. F., Li, X. C., et al. (2019). Tau Accumulation Triggers STAT 1-Dependent Memory Deficits by Suppressing NMDA Receptor Expression. *EMBO Rep.* 20 (6), e47202. doi:10.15252/embr.201847202

Li, X, Chen, C., Zhan, X., Li, B., Zhang, Z., Li, S., et al. (2021). R13 Preserves Motor Performance in SOD1(G93A) Mice by Improving Mitochondrial Function. *Theranostics* 11 (15), 7294–7307. doi:10.7150/thno.56070

Liang, C., Mu, Y., Tian, H., Wang, D., Zhang, S., Wang, H., et al. (2021). MicroRNA-140 Silencing Represses the Incidence of Alzheimer's Disease. *Neurosci. Lett.* 758, 135674. doi:10.1016/j.neulet.2021.135674

Lu, H., Liufu, N., Dong, Y., Xu, G., Zhang, Y., Shu, L., et al. (2017). Sevoflurane Acts on Ubiquitination-Proteasome Pathway to Reduce Postsynaptic Density 95 Protein Levels in Young Mice. *Anesthesiology* 127 (6), 961–975. doi:10.1097/ALN.0000000000001889

Manczak, M., Kandimalla, R., Yin, X., and Reddy, P. H. (2018). Hippocampal Mutant APP and Amyloid Beta-Induced Cognitive Decline, Dendritic Spine Loss, Defective Autophagy, Mitophagy and Mitochondrial Abnormalities in a Mouse Model of Alzheimer's Disease. *Hum. Mol. Genet.* 27 (8), 1332–1342. doi:10.1093/hmg/ddy042

McLelland, G.-L., Soubannier, V., Chen, C. X., McBride, H. M., and Fon, E. A. (2014). Parkin and PINK1 Function in a Vesicular Trafficking Pathway Regulating Mitochondrial Quality Control. *EMBO J.* 33 (4), 282–295. doi:10.1002/embj.201385902

McWilliams, T. G., Prescott, A. R., Montava-Garriga, L., Ball, G., Singh, F., Barini, E., et al. (2018). Basal Mitophagy Occurs Independently of PINK1 in Mouse Tissues of High Metabolic Demand. *Cel Metab.* 27 (2), 439–449. doi:10.1016/j.cmet.2017.12.008

Michiorri, S., Gelmetti, V., Giarda, E., Lombardi, F., Romano, F., Marongiu, R., et al. (2010). The Parkinson-Associated Protein PINK1 Interacts with Beclin1 and Promotes Autophagy. *Cell Death Differ* 17 (6), 962–974. doi:10.1038/cdd.2009.200

Mise, A., Yoshino, Y., Yamazaki, K., Ozaki, Y., Sao, T., Yoshida, T., et al. (2017). TOMM40 and APOE Gene Expression and Cognitive Decline in Japanese Alzheimer's Disease Subjects. *J. Alzheimer's Dis.* 60 (3), 1107–1117. doi:10.3233/JAD-170361

Morris, R. (1984). Developments of a Water-Maze Procedure for Studying Spatial Learning in the Rat. *J. Neurosci. Methods* 11 (1), 47–60. doi:10.1016/0165-0270(84)90007-4

Ochi, S., Iga, J.-I., Funahashi, Y., Yoshino, Y., Yamazaki, K., Kumon, H., et al. (2020). Identifying Blood Transcriptome Biomarkers of Alzheimer's Disease Using Transgenic Mice. *Mol. Neurobiol.* 57 (12), 4941–4951. doi:10.1007/s12035-020-02058-2

Okatsu, K., Oka, T., Iguchi, M., Imamura, K., Kosako, H., Tani, N., et al. (2012). PINK1 Autophosphorylation upon Membrane Potential Dissipation Is Essential for Parkin Recruitment to Damaged Mitochondria. *Nat. Commun.* 3 (1), 1016. doi:10.1038/ncomms2016

Olzmann, J. A., and Chin, L.-S. (2008). Parkin-mediated K63-Linked Polyubiquitination: A Signal for Targeting Misfolded Proteins to the Aggresome-Autophagy Pathway. *Autophagy* 4 (1), 85–87. doi:10.4161/auto.5172

Pakpian, N., Phopin, K., Kitidee, K., Govitrapong, P., and Wongchitrat, P. (2020). Alterations in Mitochondrial Dynamic-Related Genes in the Peripheral Blood of Alzheimer's Disease Patients. *Curr. Alzheimer Res.* 17 (7), 616–625. doi:10.2174/1567205017666201006162538

Parganlija, D., Klinkenberg, M., Domínguez-Bautista, J., Hetzel, M., Gispert, S., Chimi, M. A., et al. (2014). Loss of PINK1 Impairs Stress-Induced Autophagy and Cell Survival. *PLoS One* 9 (4), e95288. doi:10.1371/journal.pone.0095288

Quinn, P. M. J., Moreira, P. I., Ambrósio, A. F., and Alves, C. H. (2020). PINK1/PARKIN Signalling in Neurodegeneration and Neuroinflammation. *Acta Neuropathol. Commun.* 8 (1), 189. doi:10.1186/s40478-020-01062-w

Rasool, S., and Trempe, J.-F. (2018). New Insights into the Structure of PINK1 and the Mechanism of Ubiquitin Phosphorylation. *Crit. Rev. Biochem. Mol. Biol.* 53 (5), 515–534. doi:10.1080/10409238.2018.1491525

Reddy, P. H., Yin, X., Manczak, M., Kumar, S., Pradeepkiran, J. A., Vijayan, M., et al. (2018). Mutant APP and Amyloid Beta-Induced Defective Autophagy, Mitophagy, Mitochondrial Structural and Functional Changes and Synaptic Damage in Hippocampal Neurons from Alzheimer's Disease. *Hum. Mol. Genet.* 27 (14), 2502–2516. doi:10.1093/hmg/ddy154

Schlegel, K., Awwad, K., Heym, R. G., Holzinger, D., Doell, A., Barghorn, S., et al. (2019). N368-Tau Fragments Generated by Legumain Are Detected Only in Trace Amount in the Insoluble Tau Aggregates Isolated from AD Brain. *Acta Neuropathol. Commun.* 7 (1), 177. doi:10.1186/s40478-019-0831-2

Sharma, C., Kim, S., Nam, Y., Jung, U. J., and Kim, S. R. (2021). Mitochondrial Dysfunction as a Driver of Cognitive Impairment in Alzheimer's Disease. *Int. J. Mol. Sci.* 22 (9), 4850. doi:10.3390/ijms22094850

Simic, G., Kostovic, I., Winblad, B., and Bogdanovic, N. (1997). Volume and Number of Neurons of the Human Hippocampal Formation in Normal Aging and Alzheimer's Disease. *J. Comp. Neurol.* 379 (4), 482–494. doi:10.1002/(sici)1096-9861(19970324)379:4<482::aid-cne2>3.0.co;2-z

Sliter, D. A., Martinez, J., Hao, L., Chen, X., Sun, N., Fischer, T. D., et al. (2018). Parkin and PINK1 Mitigate STING-Induced Inflammation. *Nature* 561 (7722), 258–262. doi:10.1038/s41586-018-0448-9

Szabo, L., Eckert, A., and Grimm, A. (2020). Insights into Disease-Associated Tau Impact on Mitochondria. *Int. J. Mol. Sci.* 21 (17), 6344. doi:10.3390/ijms21176344

Tapia-Rojas, C., Cabezas-Opazo, F., Deaton, C. A., Vergara, E. H., Johnson, G. V. W., and Quintanilla, R. A. (2019). It's All about Tau. *Prog. Neurobiol.* 175, 54–76. doi:10.1016/j.pneurobio.2018.12.005

Torres, A. K., Jara, C., Olesen, M. A., and Tapia-Rojas, C. (2021). Pathologically Phosphorylated Tau at S396/404 (PHF-1) Is Accumulated inside of Hippocampal Synaptic Mitochondria of Aged Wild-Type Mice. *Sci. Rep.* 11 (1), 4448. doi:10.1038/s41598-021-83910-w

Valente, E. M., Abou-Sleiman, P. M., Caputo, V., Muqit, M. M. K., Harvey, K., Gispert, S., et al. (2004). Hereditary Early-Onset Parkinson's Disease Caused by Mutations in PINK1. *Science* 304 (5674), 1158–1160. doi:10.1126/science.1096284

Voigt, A., Berlemann, L. A., and Winklhofer, K. F. (2016). The Mitochondrial Kinase PINK1: Functions beyond Mitophagy. *J. Neurochem.* 139 (Suppl. 1), 232–239. doi:10.1111/jnc.13655

Wan, H.-L., Hong, X.-Y., Zhao, Z.-H., Li, T., Zhang, B.-G., Liu, Q., et al. (2021). STAT3 Ameliorates Cognitive Deficits via Regulation of NMDAR Expression in an Alzheimer's Disease Animal Model. *Theranostics* 11 (11), 5511–5524. doi:10.7150/thno.56541

West, M. J., Coleman, P. D., Flood, D. G., and Troncoso, J. C. (1994). Differences in the Pattern of Hippocampal Neuronal Loss in normal Ageing and Alzheimer's Disease. *The Lancet* 344 (8925), 769–772. doi:10.1016/S0140-6736(94)92338-8

Xiong, H., Wang, D., Chen, L., Choo, Y. S., Ma, H., Tang, C., et al. (2009). Parkin, PINK1, and DJ-1 Form a Ubiquitin E3 Ligase Complex Promoting Unfolded Protein Degradation. *J. Clin. Invest.* 119 (3), 650–660. doi:10.1172/JCI37617

Ye, M., Zhou, D., Zhou, Y., and Sun, C. (2015). Parkinson's Disease-Associated PINK1G309D Mutation Increases Abnormal Phosphorylation of Tau. *Iubmb Life* 67 (4), 286–290. doi:10.1002/iub.1367

Yin, Y., Gao, D., Wang, Y., Wang, Z.-H., Wang, X., Ye, J., et al. (2016). Tau Accumulation Induces Synaptic Impairment and Memory Deficit by Calcineurin-Mediated Inactivation of Nuclear CaMKIV/CREB Signaling. *Proc. Natl. Acad. Sci. USA* 113 (26), E3773–E3781. doi:10.1073/pnas.1604519113

Zhang, Y., Gao, J., Chung, K. K. K., Huang, H., Dawson, V. L., and Dawson, T. M. (2000). Parkin Functions as an E2-dependent Ubiquitin- Protein Ligase and Promotes the Degradation of the Synaptic Vesicle-Associated Protein, CDCrel-1. *Proc. Natl. Acad. Sci.* 97 (24), 13354–13359. doi:10.1073/pnas.240347797

Zhao, N., Yan, Q.-W., Xia, J., Zhang, X.-L., Li, B.-X., Yin, L.-Y., et al. (2020). Treadmill Exercise Attenuates Aβ-Induced Mitochondrial Dysfunction and Enhances Mitophagy Activity in APP/PS1 Transgenic Mice. *Neurochem. Res.* 45 (5), 1202–1214. doi:10.1007/s11064-020-03003-4

Zheng, J., Akbari, M., Schirmer, C., Reynaert, M.-L., Loyens, A., Lefebvre, B., et al. (2020). Hippocampal Tau Oligomerization Early in Tau Pathology Coincides with a Transient Alteration of Mitochondrial Homeostasis and DNA Repair in a Mouse Model of Tauopathy. *Acta Neuropathol. Commun.* 8 (1), 25. doi:10.1186/s40478-020-00896-8

Conflict of Interest: The authors declare that the research was conducted in the absence of any commercial or financial relationships that could be construed as a potential conflict of interest.

Publisher's Note: All claims expressed in this article are solely those of the authors and do not necessarily represent those of their affiliated organizations, or those of the publisher, the editors, and the reviewers. Any product that may be evaluated in this article, or claim that may be made by its manufacturer, is not guaranteed or endorsed by the publisher.

Advantages of publishing in Frontiers

OPEN ACCESS
Articles are free to read for greatest visibility and readership

FAST PUBLICATION
Around 90 days from submission to decision

HIGH QUALITY PEER-REVIEW
Rigorous, collaborative, and constructive peer-review

TRANSPARENT PEER-REVIEW
Editors and reviewers acknowledged by name on published articles

Frontiers
Avenue du Tribunal-Fédéral 34
1005 Lausanne | Switzerland

Visit us: www.frontiersin.org
Contact us: frontiersin.org/about/contact

REPRODUCIBILITY OF RESEARCH
Support open data and methods to enhance research reproducibility

DIGITAL PUBLISHING
Articles designed for optimal readership across devices

FOLLOW US
@frontiersin

IMPACT METRICS
Advanced article metrics track visibility across digital media

EXTENSIVE PROMOTION
Marketing and promotion of impactful research

LOOP RESEARCH NETWORK
Our network increases your article's readership